IAEA-TECDOC-1356

Emerging nuclear energy and transmutation systems: Core physics and engineering aspects

INTERNATIONAL ATOMIC ENERGY AGENCY IAEA

August 2003

The originating Section of this publication in the IAEA was:

Nuclear Power Technology Development Section
International Atomic Energy Agency
Wagramer Strasse 5
P.O. Box 100
A-1400 Vienna, Austria

EMERGING NUCLEAR ENERGY AND TRANSMUTATION SYSTEMS:
CORE PHYSICS AND ENGINEERING ASPECTS
IAEA, VIENNA, 2003
IAEA-TECDOC-1356
ISBN 92–0–108103–0
ISSN 1011–4289

Printed by the IAEA in Austria
August 2003

FOREWORD

The recycling of plutonium, minor actinides and long-lived fission products in various types of fission reactors, accelerator driven systems (ADS) and molten salt reactors is under investigation in several Member States. The surmised advantages of some of these concepts, e.g. ADS, are intrinsic low waste production, high transmutation capability, enhanced safety characteristics and better long-term resources utilization (e.g. with thorium fuels). Important R&D programmes are being undertaken by various institutions in many Member States to substantiate these claims and advance the basic knowledge in this innovative area of nuclear energy development. For these groups there is the clearly perceived need for coordinating their efforts and also for getting access to information from nationally and internationally coordinated activities.

While long term objectives for developing novel nuclear systems for energy production and transmutation may not be unanimously agreed upon by the different groups participating in this effort, it is clear that the short-term goals are similar. Thus, it is useful to exchange technical information developed in the different approaches and to identify areas of co-operation.

Indications as to the needs of the Member States for co-operation and information exchange in this area emerged from various Agency meetings, and are documented in meeting reports and other publications (e.g., Special Scientific Programme on "Use of High Energy Accelerators for Transmutation of Actinides and Power Production", in conjunction with the 38th IAEA General Conference; Vienna, September 1994; the "Second International Conference on Accelerator-Driven Transmutation Technologies and Applications", Kalmar, Sweden, 1996; The "Eighth International Conference on Emerging Nuclear Energy Systems (ICENES '96)", Obninsk, Russia, June 1996; the "Ninth International Conference on Emerging Nuclear Energy Systems (ICENES '98)", Tel-Aviv, Israel, June-July 1998; and the "Third International Conference on Accelerator-Driven Transmutation Technologies and Applications, Prague, Czech Republic, June 1999.

The Technical Committee Meeting (TCM) on "Core Physics and Engineering Aspects of Emerging Nuclear Energy Systems for Energy Generation and Transmutation" was held from 28 November to 1 December 2000 at Argonne, Illinois, U.S.A. The meeting was hosted by the Argonne National Laboratory, and was convened by the IAEA on the recommendation of its Technical Working Group on Fast Reactors (TWG-FR).

The objectives of this TCM were threefold: to review the status of R&D activities in the area of hybrid systems for energy generation and transmutation, to discuss specific scientific and technical issues covering the different R&D topics of these systems; and to recommend to the IAEA activities that would be specifically targeted to the needs of the Member States performing R&D in this field.

The IAEA would like to express its appreciation to all the participants in the TCM, the chairpersons, and the hosts at Argonne National Laboratory.

The IAEA officer responsible for this publication was A. Stanculescu of the Division of Nuclear Power.

EDITORIAL NOTE

This publication has been prepared from the original material as submitted by the authors. The views expressed do not necessarily reflect those of the IAEA, the governments of the nominating Member States or the nominating organizations.

The use of particular designations of countries or territories does not imply any judgement by the publisher, the IAEA, as to the legal status of such countries or territories, of their authorities and institutions or of the delimitation of their boundaries.

The mention of names of specific companies or products (whether or not indicated as registered) does not imply any intention to infringe proprietary rights, nor should it be construed as an endorsement or recommendation on the part of the IAEA.

The authors are responsible for having obtained the necessary permission for the IAEA to reproduce, translate or use material from sources already protected by copyrights.

CONTENTS

SESSION 4: SUB-CRITICAL BLANKET DEVELOPMENT

SESSION 5: TARGET DEVELOPMENTS

SESSION 6: EXPERIMENTAL STUDIES

SUMMARY

The Technical Committee Meeting (TCM) on Core Physics and Engineering Aspects of Emerging Nuclear Energy Systems for Energy Generation and Transmutation was held 28 November–1 December 2000 at Argonne, Illinois, USA. The meeting was hosted by the Argonne National Laboratory, and was convened by the IAEA on the recommendation of its Technical Working Group on Fast Reactors (TWG-FR).

The objectives of this TCM were threefold: to review the status of R&D activities in the area of hybrid systems for energy generation and transmutation, to discuss specific scientific and technical issues covering the different R&D topics of these systems; and to recommend to the IAEA activities that would be specifically targeted to the needs of the Member States performing R&D in this field.

The TCM had not called for broad overview papers of the various R&D fields. Apart from a rather brief presentation by each delegation of the general issues and the status of the R&D in the respective country, the IAEA had called for in-depth technical papers addressing one or more of the following topics: accelerator driven systems (ADS) concepts, requirements and features of ADS accelerators, target development, experiments and validation, sub-critical core studies, technology of heavy liquid metals, fuel and fuel processes development, and fuel cycle studies.

Forty-five participants from eleven countries and one international organization attended the TCM, and thirty papers were presented.

The status information presented in the delegates' general statements and in some of the papers is as of the time of the TCM. Thus, other later material should also be referenced for more current information. One such source of information is the Web Site of IAEA's project on *Technology Advances in Fast Reactors and Accelerator Driven Systems for Actinide and Long lived Fission Product Transmutation* (http://www.iaea.org/inis/aws/fnss/). However, the technical information provided in the papers, representing the bulk of the information presented, remains valid.

1. GENERAL STATEMENTS

1.1. Belgium

Approximately 60% of Belgium's electricity is from nuclear energy. The nuclear installed capacity is nearly 6 GW(e). The total heavy metal used per year is 114 t UO_2 (with an average enrichment of 4.5%) and 8.4 t MOX (with an average Pu enrichment of 6.4%). For the time being, the interest for ADS development, and for partitioning & transmutation (P&T) in Belgium is driven by waste [minor actinides (MA) and long lived fission products (LLFP)] management considerations. The waste management body (ONDRAF/NIRAS) is considering P&T as an option for waste management that deserves to be studied at an international level, and Belgium should play a role in this activity. The SCK•CEN Board of Directors has agreed on the proposal made by SCK•CEN Management to consider the transmutation as a research topic for the backend of the fuel cycle.

Nearly all the Belgian activities in this area are concerned with the development of the MYRRHA concept, a multi-purpose ADS for R&D. The facility should replace the BR2 reactor for material and fuel research, and radioisotopes production, but will be also useful for

transmutation research and medical applications. The main parameters of the accelerator (H^+ or HH^+ cyclotron) are:
E_p = 350 MeV, I_p = 5 mA. The spallation source is a liquid Pb-Bi windowless target. The sub-critical blanket is made of two zones: an innermost fast spectrum zone made of fast reactor MOX fuel cooled by Pb-Bi, and a thermal spectrum zone made of various in-pile sections located at the fast core periphery.

The ongoing activities are focused on establishing the pre-design of the facility, identifying the R&D needs to support this design, and performing a cost estimate of the project based on the pre-design meeting the scope of application given above. A first evaluation of the overall cost of the facility is around € 100 million (not including the SCK•CEN manpower effort), of which less than half is due to the accelerator. On the basis of a pre-design, SCK•CEN will ask the Belgian Government for funding. SCK•CEN is ready to cover 50% of the project. Other international partners should cover the rest). A more accurate cost estimate of the facility will be available mid 2001.

SCK•CEN participates in the EU 5th Framework Programme (FP5) in activities that are in line with the MYRRHA project (i.e. the projects SPIRE, TECLA, and MUSE, for the time being). Existing collaborations are with CEA (France), PSI (Switzerland), ENEA (Italy), NRC Soreq (Israel), IPUL (Latvia), FZR and FZK (Germany), NRG (Netherlands), IBA, Belgatom, and UCL (Belgium). MYRRHA is not considered to be an ADS demonstration (DEMO) plant, but has its place on the roadmap, as a first step, towards a DEMO.

More specifically, and apart from the activities of SCK•CEN concerning the projects of FP5, the activities related to ADS development presently conducted at SCK•CEN, UCL, IBA, Belgatom and Belgonucléaire are summarized hereafter:

1.1.1. SCK•CEN & UCL

SCK•CEN is willing to design and build an ADS system dedicated to R&D purposes. The applications foreseen in this facility will be on material and fuel research, MA and LLFP transmutation demonstration, ADS technological demonstration, and radioisotope production for medical applications. As complementary applications we foresee neutron and, possibly, proton beam applications for applied physics purposes and also for medical applications. The latter uses depend on establishing collaboration contracts with the academic and medical communities. In support of the MYRRHA project, SCK•CEN is conducting or preparing R&D programmes in the following areas:

- *Basic spallation data:* An experiment is presently conducted at PSI (Switzerland) in collaboration with PSI and NRC Soreq (Israel) consisting in bombarding a solid Pb-Bi target with protons produced by PSI's 590 MeV cyclotron. The parameters to be assessed are the spallation neutron yield (n/p) at 300, 350, 400 and 590 MeV, the spallation neutron energy spectrum, the spallation neutron angular distribution, and the spallation products induced by protons of 300, 350, 400 and 590 MeV.
- *Windowless spallation target design*: An experimental and theoretical programme is presently conducted by SCK•CEN in collaboration with the Department of Thermalhydraulics of the Catholic University of Louvain-la-Neuve (UCL), FZR (Rossendorf, Germany), IPUL (Riga, Latvia), and NRG (Netherlands) aiming at establishing a reliable design of a windowless spallation target made of liquid Pb-Bi. The programme foresees hydraulic experiments with water to simulate the Pb-Bi flow (UCL + FZR) (1999–2000), numerical simulation studies using the FLUENT, FLOW-3D, and STAR-CD CFD (UCL, SCK•CEN, NRG) (1999–2001), confirmation experiments of the MYRRHA windowless spallation module design using a heavy liquid metal (HLM),

namely mercury (SCK•CEN, IPUL, FZR) (2000–2001), and, ultimately, Pb-Bi experiments to be completed in 2001 (SCK•CEN, FZK, ENEA).

- *Validation of the windowless concept in connection with the proton beam vacuum tube*: An experiment called VICE (Vacuum Interface Compatibility Experiment) is presently under preparation at SCK•CEN. The experiment aims at demonstrating the feasibility of connecting a MYRRHA windowless target concept to a vacuum environment compatible with the characteristics of the proton beam delivered by the cyclotron, i.e. the out-gassing of the HLM and the structures, and the assessment of the Pb-Bi evaporation rate in the MYRRHA operating conditions (Pb-Bi at 500°C, vacuum 10^{-6} to 10^{-8} bar).
- *Structural material research*: A research programme is already going on at SCK•CEN based on irradiation in the BR2 MTR, to study the behaviour under high neutron dose irradiation of HT9 (martensitic steel) and EUROFER (reduced activation ferro-martensitic steel, comparable to the F28H Japanese steel) as potential material candidates for MYRRHA structures.
- *THOMOX fuel research*: An R&D proposal in collaboration with TUI (EU) and Belgonucléaire (Belgium) on a comparative study of (Th-Pu)O_2 fuel behaviour as compared to classical MOX or advanced MOX (large grain) is presently under preparation by the partners. The programme foresees fuel fabrication, irradiation in the BR2 MTR under well-characterised conditions (power level, burnup, central temperature, neutron flux), irradiation in stationary and later on in transient conditions, and Post Irradiation Examinations (linear power, burnup, TOP-18 FP, profilometry, SEM, FG punction, gamma scanning, X radiography).

1.1.2. IBA

IBA is a partner of SCK•CEN working on the development of a reliable proton accelerator operating in CW mode and fulfilling the required beam availability specifications for ADS. The present design of the sub-critical core requires the accelerator to deliver a 350 MeV, 5 mA proton beam. This 1.75 MW CW beam has to satisfy a number of requirements, some of which are unique in the world for presently existing accelerators. At this level of power it is compulsory to obtain an extraction efficiency above 99.5% and a very high stability of the beam, but on top of that the ADS application needs a reliability well above that of common accelerators, bringing down the beam trip frequency (trips longer than a few tenths of a second) to below 1 per day. The design principles are based on the following lines of thought:

- Statistics show that the majority of beam trips are due to electric discharges (both from static and RF electric fields). Hence the highest reliability requires minimizing the number of electrostatic devices, which favours a single stage design.
- In order to obtain the very high extraction efficiency, two extraction principles are available: through a septum with well-separated turns, or by stripping.
- The beams are dominated by space charge. Therefore one needs careful transverse and longitudinal matching at injection, and the avoidance of cross talk between adjacent turns (by an enhanced turn separation) if a separated turn structure is required for the extraction mechanism.
- The space charge dominated proton beam needs a 20 mm turn separation at 350 MeV if a septum extraction has to be implemented. This solution requires the combination of a large low-field magnet and of very high RF acceleration voltages for realizing such a large turn separation, and also an electrostatic extraction device.
- In view of what precedes, this solution is not well suited for very high reliability operation. Extraction by stripping does not need separated turns. It may be obtained by the acceleration of H^- ions, but the poor stability of these ions makes them extremely sensitive to electromagnetic stripping (and hence beam loss) during acceleration. The use of H^-

would, therefore, lead to the use of an impracticably large magnetic structure. The other solution is to accelerate 2.5 mA of HH^+ ions up to 700 MeV, where stripping transforms them into 2 protons of 350 MeV each, thus dividing the magnetic rigidity by 2 and thereby allowing extraction. This solution reduces the problems related to space charge since only half the beam current is accelerated. However, the high magnetic rigidity of a 700 MeV HH^+ beam imposes a magnetic structure with a pole radius of almost 7 m, leading to a total diameter of the cyclotron of close to 20 m. The cyclotron would consist of 4 individual magnetic sectors, each of them spanning 45 degrees.

- At the present stage of R&D the last option appears to be the most appropriate one.

1.1.3. BELGATOM

BELGATOM has joined the European Industrial Partnership for developing the ADS DEMO and has expressed its interest in investing some manpower on the ADS topic in the coming years. An implication of BELGATOM in MYRRHA project is expected in the engineering of the auxiliary system and integration of the different components of MYRRHA.

1.1.4. BELGONUCLÉAIRE (BN)

Over the recent years, Belgonucléaire's (BN, Brussels) transmutation activities were mainly concerned with the possibilities of recycling Pu and minor actinides (MA) in presently existing LWRs, either in the homogeneous mode (in an extended MOX fuel) or in the heterogeneous one (MA placed in target pins). A concept was developed, in which target pins loaded with Am, or with Am and Cm, could be put on the corner positions of the MOX assemblies in the core. Attention was paid to the approach to equilibrium in a multiple recycling scheme. The dose rates associated with the fabrication and handling of target pins were determined, and the protections needed were derived. A study considered the incineration of long lived fission products (LLFP), more specifically ^{99}Tc and ^{129}I, in these reactors, but showed that LWRs were not suitable for this. BN also examined, in co-operation with EDF, the multiple recycling of Pu and MA in fast reactors of the EFR (European fast Reactor) type. The following longer term scenario was found to be advantageous: nuclear power plant park consisting of LWRs fuelled with UO_2 (producers of Pu and MA) and of LMFRs of the EFR type without fertile blanket (incinerators of Pu and MA); MA target pins could be loaded on special, moderated positions of the LMFRs, with the objective of reaching 90% burnup, with no further reprocessing of the spent targets. So far, BN did not participate in ADS studies but is intending to participate in the fuel and core design of the MYRRHA project.

1.2. China

The China Institute of Atomic Energy (CIAE) is pursuing a long term scientific and technical project for the development of national, sustainable fission energy, including the construction of an experimental fast reactor (CEFR), the investigation of the MA transmutation capacity of a medium size fast reactor, and basic research in the area of the innovative technical option 'ADS'.

As the first step of the fast reactor engineering development in China, the CEFR is a sodium cooled pool type experimental fast reactor of 65 MW thermal power, matched with a 25 MW turbine generator. By now, the CEFR is just at the beginning of its construction marked by the completion of the reactor building base foundation. It is expected that its first criticality will be at the end of 2005. The second step is to design and build a 300 MW(e) prototype fast breeder reactor (PFBR). It is intended to use the PFBR to burn PWR's MA waste (named

MPFR). With MA content in the fuel of up to 5%, the support ratio of 2 could be reached, provided that acceptable dynamic parameters will be proven.

A five-year programme (Phase 1) of basic research on some physical and technical problems related to ADS is being implemented. A preliminary evaluation of the main performance parameters of the following three ADS has been performed:

- 1 GeV/16 mA accelerator driven fast sub-critical system with a lead spallation target (AD-FBR) could get a support ratio of approximately 4 for the transmutation of MA from PWRs;
- As the previous system, but with a PHWR type sub-critical core (AD-PHWR): the main result is that with the requirement of fissile self-sustainability, U-Pu fuelled sub-critical cores would require a higher beam current compared to the Th-U fuelled case;
- The analysis of a fast-thermal coupled ADS showed that for these systems the required accelerator beam power could be reduced.

Further, some target physics studies have been conducted. The neutron double-differential cross-sections of lead have been measured by irradiating a lead thin target with 1.5 GeV protons at 15°, 30°, 60°, 90°, 120°, and 150°. The theoretical analyses have been performed with the help of the SHIELD code. The results of these calculations agree very well with the experimental data. The neutron yields from lead and tungsten standard thick targets (∅20 cm ×60 cm) have been calculated with both a code based on the Monte Carlo method and the SHIELD code. The results are rather consistent. Further, for the ∅20 cm × 60 cm target as well as for thin targets containing various materials, the proton energy deposition and the irradiation damage cross-sections have been calculated with the help of the SHIELD code. Based on the results of Phase 1, an ADS based on a 300 MeV/3 mA LINAC, using a 0.9 MW lead spallation source driving a uranium-water sub-critical lattice is the proposed design for an ADS verification facility in China. This will be the work scope for Phase 2 of the Chinese ADS R&D programme, planned up to the year 2007.

1.3. Czech Republic

The Czech Republic has been operating PWRs for more than 15 years with the total installed capacity of 1760 MW(e). Just recently (October 2000), the first block (1000 MW(e)) of a new NPP has been started. The regular operation of this block and the startup of the second one (also 1000 MW(e)) has been planned for the year 2001. This means that the amount of spent fuel that is stored in an intermediate storage at the NPP site will be increasing significantly, and, simultaneously, public awareness of the issues linked to spent fuel management will be increasing, too. Therefore, the Czech Republic is very much interested in the development of innovative nuclear energy systems for energy generation and, more importantly, for the transmutation of the accumulated long lived radwaste. The Czech efforts in that direction are focused on a system with liquid fuel, namely in the form of molten fluorides. The developments so far, as well as the current state of the art of this technology are summarized in the following.

After a preparatory study stage in the first half of the 90s, the national consortium TRANSMUTATION has been established at the and of 1996 by four leading institutions in the nuclear R&D field in the country, namely by the Nuclear Research Institute Rez p1c (NRI Rez), the Nuclear Physics Institute of the Academy of Sciences, SKODA Nuclear Machinery Ltd., and the Czech Technical University. The consortium proposed an R&D Programme for the ADS with molten fluorides as liquid fuel that was approved and has been supported by

national governmental authorities since the FY 1998. As of 2000, the first 3-year stage of this R&D Programme has been completed. The main results of this first stage are as follows:

(1) Verification, through computational analyses, of an adopted sub-critical blanket design. Preparation of the basis for the experimental validation of the concept, represented by the experimental reactors LR-O in the NRI Rez and VR-I at the Czech Technical University, as well as a series of technological loops with molten fluorides and the FREGAT pyrochemical line

The theoretical and experimental studies of kinetics of the sub-critical blankets started with different composition of fluorides including fissionable component (UF_4).

(2) A second 3-year stage (2001–2003) was proposed on the basis of the results of the first stage of the R&D Programme. The studies in this second stage will concentrate on experimental verification of the design parameters of a demonstration transmuter with liquid fuel (molten fluorides). The proposal has been approved in September 2000 for financial support by both the Government and the Radwaste Repository Agency.

1.4. Germany

In Germany, 19 Nuclear Power Stations are in operation. One large power station — Mülheim Kärlich — is shut down because of formal reasons. The total capacity is about 22 GW(e). The operation of the power stations is extremely satisfactory. About 5 to 6 of the German power stations are regularly among the worldwide top ten leading stations, with respect to the number of MWh produced per year, and with respect to operational availability. The annual amount of TWh's produced in German nuclear power stations is about 160 TWh/a, i.e. about 1/3 of the total German electricity production.

The present two-party coalition German government is supported by the Socialist Party and the Green Party. The government was elected in late in 1998. From the very beginning, it declared the firm intention to phase out nuclear energy. First attempts to stop reprocessing failed. It soon became very clear that an immediate stop of operation of the German nuclear power plants was to be excluded, both because of technical and legal reasons. Lengthy negotiations between the government and the utilities followed. This lead to a “consensus agreement” in June 2000. The basic elements of this agreement are as follows:

- For each nuclear power plant the amount of electricity which can be produced from 1 January 2000 on is limited. The operation license will cease when this amount of electricity has been produced. In total, 2600 TW(h)'s will be produced (assuming 160 TW(h)/a, this means continuation of nuclear power plant operation in Germany for another 16 years).
- German government and utilities confirm the high safety standard of German nuclear power plants.
- From 2005 on direct disposal — no reprocessing.
- Gorleben is suited to be a final repository. But further evaluations of other sites will be initiated. Evaluation of Gorleben will be interrupted for at least 3, and for a maximum of 10 years.

Taking into account the existence of the “consensus agreement”, it becomes evident that from the government side there is no strong support for the development of new reactor concepts. However, in the “consensus agreement” it is clearly stated that R&D shall not be regulated but shall stay free. In an “evaluation report” which has been prepared by the leading research centers dealing with nuclear and by the federal ministries in charge of nuclear energy related

issues, it is clearly stated that the international development of foreign innovative concepts shall be followed. In particular P&T is mentioned, since it is considered as a possible alternative in the area of waste management. FZK has prepared a limited programme in this area. Because of limited resources, the programme can only be performed within an international cooperation framework, in particular the European cooperation, but also cooperation with the Russian Federation, Japan and the USA. Some important projects FZK is participating in are the CAPRA/CADRA project, the MEGAPIE project, and the MUSE project. The main elements of the programme are:

- Theoretical studies (thermal hydraulics, neutronics, safety, development of new models, new data etc);
- Development of lead / lead-bismuth-technology (KALLA: 3 lead / bismuth loops, maximum capacity 4 MW / 4 m^3/h);
- Target development (participation in the MEGAPIE project, ISTC #559, and international benchmark problems).

All the activities of the FZK programme, as already mentioned, are embedded into international activities, such as the 5th Framework Programme of the EU, or the "Enlarged Technical Working Group" (ETWG), chaired by Professor Rubbia.

1.5. Italy

From 1995 on, a growing interest in ADS concepts has taken place in Italy and has given origin to several basic R&D activities and to an industrial programme involving ENEA (the Italian national research body for energy, environment and new technologies), INFN (the Italian national research institute for nuclear physics), and various industrial partners. Accelerator driven systems, coupling an accelerator with a target and a sub-critical reactor, could simultaneously burn minor actinides and transmute long lived fission products, while producing a consistent amount of electrical energy. As a first step, this interest was confirmed by the national R&D programme TRASCO (Italian acronym standing for waste transmutation – TRAsmutazione SCOrie), funded and started in 1998 under the leadership of INFN for the accelerator, and of ENEA for the sub-critical system. The TRASCO programme was relevant to promote collaboration among groups of different competencies (accelerator, reactor physics, plant design), and will provide important results in support of any related industrial programme. As a matter of fact, parallel to the basic activities of TRASCO, an industrial programme was proposed in two main steps (the first was approved and funded in 1999):

- On-going short term activities in the Italian context to produce a preliminary design of the ADS experimental plant. A reference configuration (named EADF, Energy Amplifier Demonstration Facility, approximately 80 MW(th)) has been proposed and submitted for consideration to the European partners as a contribution to the discussion of the European Road Map for developing an ADS experimental plant. The preliminary design will be completed in the first half of 2001, whilst the main supporting R&D needs were assessed and the realization of the experimental facility CIRCE is in progress, for thermal hydraulic testing of the main subsystems of the experimental plant in lead-bismuth.
- Medium term activities in an European and international context with the aim of performing the detailed engineering design, the realization, and the commissioning of the experimental plant along with all the supporting R&D.

1.6. Japan

In 1988, the Atomic Energy Commission launched the Long Term Programme for Research and Development on Nuclide Partitioning and Transmutation (P&T) Technology (OMEGA Programme). Within the framework of OMEGA, the basic studies and experiments of P&T

concepts have been carried out by the Japan Atomic Energy Research Institute (JAERI), the Japan Nuclear Cycle Development Institute (JNC), and the Central Research Institute of Electric Power Industry (CRIEPI). JAERI is developing concepts of accelerator driven systems (ADS) dedicated to transmutation. The system employs minor actinide (MA)-nitride fuel and lead-bismuth coolant/target. Fabrication and reprocessing technology is being developed for nitride fuel. Development of lead-bismuth coolant/target technology has started recently. Accelerator technology is being developed to construct a powerful proton accelerator under the JAERI-KEK Joint Project. ADS physics and engineering experiments are planned within the framework of the latter. In contrast to JAERI, JNC and CRIEPI are studying transmutation technology using fast breeder reactors (FBRs). JNC is developing a MOX-fuelled sodium cooled FBR. Core design studies, MA-containing MOX fuel fabrication and irradiation experiments are being carried out. Recently, JNC started a feasibility study to evaluate a variety of technology options for commercialized FBR cycle systems. CRIEPI is developing concepts of metal-fuelled sodium cooled FBRs. Fabrication and reprocessing technology is being developed for MA-containing metal fuel.

The Atomic Energy Commission reviewed the progress of the OMEGA Programme in FY 1999. In March 2000, the Commission issued a report entitled Research and Development in Japan on Long Lived Nuclide Partitioning and Transmutation Technology. The review of the status of R&D, the analysis of the effects and significance of P&T technology, and the recommendations for future R&D are contained in this report. It is recommended to continue with the system design work, scenario studies, and basic experiments before embarking on engineering tests for demonstration. It is also recommended to review the progress, to update scenarios, and to reconsider the R&D plans around the year 2005. It must be noted that the importance of active participation in international cooperation projects is underlined in the report.

1.7. Republic of Korea

In the Republic of Korea, an accelerator driven system named HYPER (HYbrid Power Extraction Reactor), is being developed at KAERI within the framework of the national mid and long term nuclear research plan. The basic mission of HYPER is the transmutation of both transuranic elements (TRUs) and long lived fission products (LLFPs). The minimum required sub-criticality of the HYPER core is set to k_{eff}=0.97, and the rated power is 1000 MW(th). Lead-bismuth is used as the coolant due to its benign chemical characteristics. A proton current of 1 GeV impinges on a lead-bismuth target in the core center and generates about 29.3 spallation neutrons per proton. Transmutation of the radioactive nuclides, in general, is based on a closed fuel cycle. Consequently, the related fuel cycle should have a high proliferation-resistance. In HYPER, a simple fuel cycle is assumed, in which spent fuels from commercial reactors are reprocessed with a highly proliferation resistant pyroprocess, such as electro-refining. The TRU fuels contaminated with a significant fraction of lanthanides are incinerated in the HYPER core. The spent fuel of HYPER is also recycled after undergoing a similar proliferation resistant reprocessing. It is claimed that the fuel cycle for the HYPER system has an excellent compatibility with the non-proliferation requirements.

Currently, R&D activities are mainly focused on the core and beam window designs. The HYPER core adopts a hexagonal type fuel array to render the core compact and to achieve a hard neutron energy spectrum. In order to keep the radial power peaking within the design target value of 1.5, the blanket region is divided into three TRU enrichment zones. A low TRU fraction fuel is loaded in the innermost zone and a high TRU fraction fuel in the outermost region. The refueling is to be performed based on the scattered loading with

3 batches for each zone. Target cycle length at the equilibrium state is 1 year with a 75% capacity factor. In order to minimize the reactivity swing of the HYPER core loaded with TRU fuels, two types of burnable absorbers are under investigation, one is B_4C-coated cladding and the other one a mixture of B_4C and ZrH_2. Preliminary studies show that B-10 can be effectively used as a burnable absorber, especially the mixture of B_4C and ZrH_2 can reduce the reactivity swing by a factor of 2, with only a little compromise of the transmutation quality. An important research area is the maximization of the spallation neutron multiplication, in other words, minimization of the proton current. The overall optimization of the core is in progress such that the source multiplication can be maximized.

A unique feature of HYPER is the transmutation of ^{99}Tc and ^{129}I in a locally thermalized neutron spectrum six fission product containing assemblies are loaded in the middle ring of the core in order to make the support ratio of the fission products similar to that of TRU (4–5). In the fission products target region, metallic ^{99}Tc is loaded as a plate in the periphery and NaI or CaI_2 rods are placed in a staggered manner with CaH_2 moderator rods, inside the Tc plate.

Either TRU-Zr metal alloy or (TRU-Zr)-Zr dispersion fuel is being considered as a blanket fuel for the HYPER system. In spite of the successful application of the metal fuel in the conventional LMRs, it is not easy to control the vaporization of americium nuclides in the fabrication process of an alloy type fuel rod. In the case of the dispersion fuel, the particles of TRU-Zr metal alloy are dispersed in the Zr matrix. The cladding material is ferritic-martensitic steel, HT-9. It is expected that the dispersion fuel will generally withstand significantly higher burnup than the alloy fuel.

The proton beam is delivered into the core central region through a beam tube and the target zone is separated by a 2 mm-thick window of 9Cr-2WVTa. Related research work is focused on the lifetime analysis of the window. The target lifetime of window is at least one year. Preliminary results indicate that, as far as the mechanical integrity is concerned, the window seems to withstand 6 mA current of 1 GeV protons. Currently, more detailed analyses are ongoing. In HYPER, a 3-loop heat transport system is adopted in order to keep the coolant speed below the maximum value of 2 m. The p/d (pitch-to-diameter) ratio of the HYPER core is 1.5, and the corresponding Pb-Bi velocity is 1.1 m/s. Instead of wire spacer commonly used for tight lattices, grid spacers are suitable to ensure proper separation of the fuel rod. Thermalhydraulic analyses are being performed with a modified SSC code. In the next phase of R&D, the research will be tuned to the core thermal hydraulic analysis including the target area.

The whole development schedule for the HYPER system is divided into three phases. The basic concept of the system and the key technical issues are identified in Phase 1 (1997–2000). In Phase 2 (2001–2003), core design optimization will be performed to maximize the HYPER economics. Also in phase 2, some experiments will be conducted to confirm the key technical issues. A thermal hydraulic test for Pb-Bi, an irradiation test for the fuel, and a spallation target test are the major experiments that KAERI is considering. In Phase 3 (2004–2007), a conceptual design for the HYPER system will be finished by completing the development of design tools based on the experiments.

1.8. United States of America

In Fiscal Year (FY) 1999, the US Congress directed the Department of Energy (DOE) to develop a “roadmap” to determine the feasibility and life-cycle cost of an accelerator transmutation of waste technology (ATW) system to manage the civilian nuclear spent fuel

from US reactors. The results of this study are published in a report to Congress, "A Roadmap for Developing Accelerator Transmutation of Waste Technology," October 1999. The report addressed issues associated with the question of whether the ATW concept could benefit the waste management system associated with disposing spent fuel from all existing US nuclear plants during their anticipated lifetimes. If successful, the ATW concept transforms plutonium, other long lived actinides, and long lived fission products contained in spent fuel by changing atomic structures. After transmutation, the new less radioactive isotopes can be stored in a permanent repository. By transmutation of long lived radioactive isotopes in spent fuel, the potential exists to: (a) significantly reduce the quantity of fissionable and radioactive material stored in a repository, (b) produce further power from material in spent fuel, and (c) as a result of associated fission product partitioning, permit repository heat management with the potential to significantly enhance the capacity for waste storage in the repository — possibly eliminating the need for additional repositories in the foreseeable future. The US Congress authorized DOE to begin an ATW research programme in FY 2000.

Independent of the ATW research, DOE is also responsible for insuring adequate future tritium production needs of the nation. Although a reactor based option has been chosen as the primary technology to meet the needs, an accelerator production of tritium (APT) backup option exists which to date has developed impressive technology which appears of direct value to demonstrating the ATW objective of benefiting nuclear waste management.

Recognizing the potential synergistic value of ATW and APT, as well as the possibility of supporting the nation's nuclear energy-related education and research infrastructure with an integrated accelerator applications facility, the DOE Office of Nuclear Energy, Science and Technology, under Congressional guidance, established a new Advanced Accelerator Applications (AAA) Programme Office and initiated in FY 2001 an AAA programme whose primary objective will be to conduct scientific and engineering research, development and demonstration to ascertain if cost effective and beneficial transmutation of civilian spent nuclear fuel is possible.

The mission of the AAA programme is to establish a national nuclear technology research capability, a nuclear engineering test bed that can carry out effective transmutation and advanced reactor research and development effort.

The AAA programme will address the following objectives:
- Demonstrate the practical performance of an accelerator driven sub-critical multiplier;
- Demonstrate the viability of transmutation for waste and spent fuel management;
- Enhance the Nation's nuclear science and technology education infrastructure;
- Provide demonstration of a robust backup tritium production capability for national security, if needed.

An accelerator driven test facility (ADTF) would be the key facility for the AAA programme. Existing facilities can support partial completion of the programme objectives, but a new, dedicated facility is required for fully reaching the goals of the AAA programme, which includes demonstrating the safe and efficient coupling of an accelerator, spallation target, and sub-critical multiplier. The ADTF would be designed to perform specific experiments related to the demonstration of waste transmutation, and would have the flexibility to carry out a broad range of experiments for a wide range of advanced nuclear technologies. A target of 2010 has been set as the time frame in which the ADTF would become operational.

This approach will provide the foundation for a new area of nuclear engineering research and technology. AAA research will also contribute to the reinvigoration of nuclear science and

engineering and help train a new generation of nuclear energy experts. Last, this programme will contribute, and support US leadership in advanced nuclear technology through the establishment of a new, first-of-a-kind, world-class research facility.

The research topic areas reflect the fact that the AAA programme integrates the science of spallation-neutron physics with nuclear reactor physics, thermal-hydraulics, heat transfer, and materials into one coupled system that is generally referred to as an accelerator driven sub-critical system. Presently, the research proposed within the AAA programme includes:

- Advanced fuels: R&D on high zirconium/actinide, nitride, mixed oxide, and carbon matrix fuels
- R&D on spent fuel separations (oxide and metal)
- R&D on environmentally acceptable, and cost effective fuel processing (conversion of LWR spent fuel in oxide form to metal fuel for transmutation)
- Sub-critical multiplier neutronics and thermal-hydraulics design
- R&D on coolant compatibility and heat transfer (gas, sodium, and lead/lead-bismuth eutectics)
- Spallation target design, cooling, and the science of coupling spallation neutron sources with sub-critical nuclear lattices
- R&D of new materials which can withstand high energy, high neutron fluence levels, high temperatures, and be compatible with the reference fuel and coolant
- High energy accelerator reliability.

2. SESSION SUMMARIES

2.1. Session 1: Research and development programmes

The research and development session heard papers from the United States of America, Belgium, Italy, Japan, and China. The papers showed a wide variety of concepts, stages of development and mutually interesting basis for potential cooperation.

Presentations from the US gave an overview of a new US Department of Energy Advanced Accelerator Applications (AAA) programme whose research and development plan proposes operation initiation of a 20 to 100 MW proof-of-performance test facility in ten to twelve years.

A Japan Atomic Energy Research Institute representative (JAERI) described current development considerations for ADS under the Japanese OMEGA programme with heavy emphasis on fuels and materials development.

The representative from the China Institute of Atomic Energy described a growing civil-application programme in China with the launching of a joint effort to pursue both fast reactor technology development and ADS basic research.

The Belgium presentation from the SCK•CEN nuclear research center summarized the state of development in their MYRRHA project aimed at having a 20–30 MW ADS facility operational in about eight years utilizing a noteworthy “windowless” target.

The Italian presenter from ENEA, the Italian national research body for energy, the environment, and new technologies, described the parallel efforts of their collaborative TRASCO R&D programme and their national industrial programme supporting the design of an European ADS demonstration plant.

Common themes: country representatives presenting papers in this session appear to have concluded there is sufficient potential value for an ADS to contribute positively to the management of radioactive nuclear waste to warrant recommending enhanced national and international development efforts. Plans were also noted for at least one integrated accelerator/target/multiplier experimental or demonstration facility in the next 8–15 years. Although various combinations of coolant and target material are being considered, lead-bismuth or tungsten targets and some form of liquid metal cooled fast spectrum multiplier facility appear primary in choice for facilities under consideration. In addition, all presenters emphasized the need, and value, for enhancing international collaboration, particularly in the near-term for fuels and materials testing, both in and out-of-pile.

Unique themes: as part of the research and development session, several unique programme features were identified. These include:

- The Belgium paper presented a unique windowless target design concept wherein problems associated with designing a target window to withstand effects associated with intense accelerator beam currents are replaced by problems associated with designing features into the windowless target for required thermal-hydraulic behavior in the presence of spallation products. A significant development and design programme appears underway to firm up the windowless design;
- The Japanese paper identified that serious consideration is now being given in the JAERI programme to use of a nitride based fuel design for the sub-critical multiplier, in which generation of the unwanted ^{14}C isotope is to be suppressed by using nitride fuel enriched with the ^{15}N isotope. Additional reasons given for considering development of nitride fuels include: good thermal conductivity, higher heavy metal density with a resulting harder neutron spectrum than with oxides, as well as other good metallurgical properties. The presenter further noted that the JAERI accelerator driven reference concept includes a dedicated minor actinide consuming reactor system, operating as the second part of a "double-strata, or tier" nuclear fuel cycle system, in which the first strata would be a normal power producing nuclear reactor, utilizing plutonium while producing electricity;
- The Chinese paper noted a major increase in development plans for the Chinese civilian nuclear power programme in which parallel ADS and fast reactor system development programmes are contemplated. Unique to a design under consideration is an accelerator driven sub-critical multiplier system with separate fast and thermal zones incorporated in the single sub-critical assembly;
- US presentations summarized a "multi-mission" ADTF programme being pursued in the US, in which demonstration of tritium backup production capability is included as one of the missions anticipated for the ADTF.

2.2. Session 2: Concept developments

The concept developments session heard papers: (a) on trade studies performed in the US within the frame of the AAA programme to define and compare possible ATW candidates (lead-bismuth eutectic, sodium, and gas cooled systems were considered), (b) on a two-tiered approach based on the incineration of plutonium in LWRs fuelled with fertile-free fuel and on the transmutation of the remaining LWR spent fuel together with the actinides from the spent fertile-free plutonium fuel in an accelerator driven system; and, finally, (c) on economics aspects of the transmutation fuel cycles.

Important assumptions for the liquid metal cooled systems were: fertile-free fuel; no control rods; power of 840 MW(th). Goal of the optimization was to reach a maximum discharge burn up in order to minimize overall losses during multiple recycling. At the same time, the

reactivity loss per cycle was to be minimized, in order to minimize the required increase in accelerator power needed to compensate the loss of reactivity. It turned out that solutions could be found, but the basic assumptions have a significant feedback on the design, and limit design flexibility. In the discussion the question was raised whether the basic assumptions should or could be modified in order to regain more flexibility; e. g. the significant increase in accelerator power at the end of cycle could be avoided, if control rods would be foreseen.

The studies for gas cooled systems assume TRISO (coated particles) as fuel. This fuel allows extremely high burn up values. Therefore it is proposed to limit the number of reprocessing steps. In general it is proposed to have only one reprocessing, irradiate the fuel and put the irradiated fuel into the repository. Different irradiation schemes were investigated. Thermal as well as fast reactors, and critical as well as sub-critical systems are proposed. Because the fuel is not recycled, the burning of the actinides is not as effective as in the case of multiple recycling. Burning of plutonium is nearly complete, most of the MAs, however, stay in the fuel and are not fissioned. It was argued that, because of the excellent long term retention capabilities of the TRISO fuel, this is acceptable.

The paper on the two-tiered approach presented the results of the studies of a strategy that departs from the assumption made in the US roadmap study, published about one year ago, that both the plutonium and the MAs will be burnt in the ATW systems. As a consequence the number of ATWs needed is rather large. In the strategy presented in the paper on the two-tiered approach it is assumed that the plutonium is separated from the MAs. While the MAs will go directly to the ATW, the plutonium will be inserted in LWRs. Special fertile-free plutonium fuel is proposed for this purpose. The burn up is very high. As a consequence, nearly all the fissile plutonium is being burned in the non-fertile fuel LWRs. The remaining spent fuel from the uranium fuelled LWRs together with the residual plutonium and MA from the spent non-fertile fuel are to be burnt in the ATWs. This two-tiered approach results in a significant reduction of the number of ATWs needed to support the cycle. In the discussion doubts were expressed, that the proposed mode of the plutonium irradiation in LWRs is state of the art, as it was claimed in the presentation. Both the fertile-free fuel and the high burn up were mentioned in this respect. Furthermore, it was emphasized that there are also other candidates, in which the plutonium could be burnt efficiently, e.g. gas cooled reactors. In general, however, there was agreement, that this strategy, namely to burn part of the plutonium in existing reactors, seems reasonable.

Economics aspects of transmutation systems were discussed in the last paper. It became evident that fuel cycle costs of these systems are higher than those of existing LWRs. Increase in burn up and other means could improve the situation. Whether fuel cycle cost similar to those of existing LWRs can be reached seems doubtful.

2.3. Session 3: Fuel and fuel cycle

The fuel and fuel cycle session heard four papers (two from the US, and presented by a Czech representative on work performed in the USA in collaboration with the Massachusetts Institute of Technology, and one from Japan).

The first paper in the session presented the current US plans for developing a fuel for the US ATW concept. In general, the functions and requirements for fuel for any of the systems under consideration by the US programme, in system trade studies, are similar to those for reactor fuels. Some specific requirements for operating conditions are now emerging from evaluation of the various system point designs; although those requirements will change as the concepts evolve, the operating requirements are similar to those for reactor systems for the

respective technologies. Of the many uranium-bearing fuel forms that have been utilized or studied in the past, the US has selected four forms that are favored for specific transmuter technologies. Of those, near term R&D work is concentrated to a metallic dispersion fuel and a nitride pellet fuel. Because there is essentially no experience with non-fertile compositions of the types proposed, R&D activities are necessarily directed toward assessing feasibility of the selected forms. Feasibility information must be obtained by 2005 in order to support ATW programme and technology decisions.

The second paper, presented by J. Laidler of ANL (USA) described the baseline technologies under development for the US ATW programme. The presentation opened with the comment that the US would necessarily re-consider current aspects of US non-proliferation policy if an ATW were actually to be deployed — particularly because chemical separations of TRU constituents from irradiated fuel would be necessary to accomplish transmutation. The overall process scheme for ATW fuel processing was described. Because the head end of the process must prepare TRU from a large quantity of spent LWR fuel, a high-through-put process is required. For this reason, a modification of established aqueous processes is proposed (termed "UREX", because it is similar to the PUREX process but modified to produce a relatively pure uranium stream rather than a pure plutonium or TRU stream). The UREX process has been demonstrated with simulated LWR fuel, at laboratory scale, to show that a U product that meets low level waste standards can be produced. (This means that uranium can be disposed in the expensive manner of low level waste rather than as high level waste.) The associated pyrometallurgical processes for separation of TRU from fission products, employed at the head-end and for recycle of ATW fuel, have each been demonstrated with simulated fuel and shown to provide sufficient recovery of TRU from rare earth fission products. Technetium and iodine separation has yet not been demonstrated, however. It was noted that americium follows the TRU constituents in all steps of the process.

The third paper was presented by P. Hejzlar (from the Massachusetts Institute of Technology and representing the Czech Republic), and provided a parametric comparison of various fuel types in a once-through, heavy metal cooled reactor fuel cycle. P. Hejzlar noted that while M. Kazimi's paper, presented in Session 2 (economics paper), addressed one extreme end of the fast reactor fuel cycle (a non-fertile actinide burner employing recycle), his own paper represented the other extreme. Because the analysis in M. Kazimi's paper indicates that reprocessing is not currently economical for fast reactor systems, a once-through fuel cycle warrants consideration. The Hejzlar paper focused on comparative neutronics, radiotoxicity, and proliferation resistance for four fuel types: metal, carbide, nitride and oxide. Uranium only, uranium-plutonium, and uranium-thorium fuels were investigated. The metal fuels were shown to have the internal conversion ratios, indicating that those fuels would allow the longest core lifetime (based on reactivity considerations). An analysis of a model of a streaming fuel assembly fuelled with metal fuel indicated that it is possible to design a core with a small reactivity burn up swing and a negative void coefficient. The model for the streaming assemblies indicated that radiotoxicity and proliferation resistance of spent fuel are important when assessing comparative attributes of fuel forms that would be disposed in a geologic repository. For a given duty, it was found that the metallic uranium only fuel form (U-10Zr), in general, discharged the smallest amount of actinides to the repository, implying the lowest radiotoxicity, radioactivity, and heat load. However, the plutonium that would be converted in the metal fuel cores would have a significantly lower fraction of ^{240}Pu than the other fuel types, with a "plutonium vector" similar to that of weapons grade plutonium. Thus, the author noted that objectives for radiotoxicity reduction and reduction of proliferation threat are seemingly in conflict. It was further noted that the uranium-thorium-bearing fuels eliminated the concerns over generation of weapons grade plutonium, but added concerns

over generation of ^{233}U. The author also noted that the streaming assembly, metal fuel design that might allow a modular, exportable reactor design with a long core life would also provide a good source of weapons-grade plutonium.

The final paper of the session, presented by M. Saito of the Tokyo Institute of Technology, was an assessment of the radiotoxicity concerns associated with long lived spallation products from various target materials. A review of the spallation product yield curves indicated that one group of spallation products includes rare earth isotopes, some of which are alpha emitters of intermediate half life (i.e. 10^6 to 10^8 years). Those isotopes are likely to have maximal radiotoxicity effect, because the alpha emitters induce the most damage in human tissues when ingested, and because some of those rare earth elements would have longer in-body residence times. Yet, it is for that range of atomic numbers for which spallation yield codes are the least accurate — indicating that the amounts of these spallation products present in a target system are probably underestimated. Calculations of equilibrium radiotoxicity indicated that tin targets have lower toxicity than lead targets, which have lower toxicity than tungsten targets. When compared to fission product radiotoxicity, the spallation product radiotoxicity is only slightly lower that for fission products. Incorporation of further transmutation effects reduces both radiotoxicity values, and increases the discrepancy between the two types of species. However, it was noted that the spallation products tend to have higher melting temperatures, and would be more likely to deposit in cooler areas of target cooling loops outside of the active target area — where the nuclides would be less likely to be transmuted. Calculations indicated that radiotoxicity of the alpha-emitting spallation products is similar to that of the ^{210}Po activation product after about 2 years after irradiation. The means available to reduce spallation product radiotoxicity include selection of beam energy, beam type, and target type. The author noted that this work is only preliminary and would be improved by additional analysis. One participant advised that the work is an indication of the importance of considering the radiotoxicity of all activation and spallation products that might be present in an accelerator driven transmutation system — particularly for species that have not been typically part of the source term for previously-assessed reactor systems.

2.4. Session 4: Sub-critical blanket

The sub-critical blanket development session heard seven papers, underscoring the considerable efforts made with respect to all aspects of sub-critical blanket design. Thus, three papers (Y.H. Kim and W.S. Park, C.H.M. Broeders, and S. Taczanowsky and M. Kopec) presented results of neutronics studies (including methods validation); two papers (F.E. Dunn, and B.W. Spencer and J.J. Sienicki) dealt with thermal hydraulics and thermal mechanical issues; and two papers (W. Eriksson et al., and W. Maschek et al.) discussed safety related parameters of sub-critical blanket designs.

The paper by Y.H. Kim and W.S. Park performed a study of the sensitivity of the neutron source efficiency to the main core design characteristics. It was found that the source efficiency is sensitive to the target design (e.g. target designs with a small proton tube result in a source efficiency decrease, while a small buffer zone around the target increases the neutron source efficiency). The study also quantifies the sensitivity of the neutron source efficiency to the number and distribution of parasitic absorptions in the sub-critical blanket (e.g. fixed absorbers around the source can decrease its efficiency significantly).

The paper by C.H.M. Broeders described the methods development and validation work performed at FZK for ADS neutronics analysis. FZK has established a method based on the coupling of spallation codes with deterministic transport codes (KAPROS/KARBUS code

system). Presently, for transient analyses, the coupling of SAS4A with KAPROS/KARBUS and CITATION/VARIANT-K is under way. FZK is using also the code system LCS (combining the high energy code LAHET with the neutron transport code MCNP4), as well as the code MCNPX (a code that combines directly LAHET and MCNP without any interface utilities or files). Validation work for these tools was made on the basis of both OECD/NEA and IAEA benchmarks.

The study presented in the paper by S. Taczanowsky and M. Kopec was also based on MCNP4. The authors' intention was to contribute to a better understanding of the sub-critical neutron multiplication process and its simulation by the code. This increased understanding is essential for a more targeted definition of validation efforts (both experimental and analytical). One of the effects investigated for various targets was the dependence from neutron generation number *i* (or time *t*) of the generation multiplication factor k_i, the number of neutrons, as well as the cumulative energy release. Further, the authors studied the time evolution of the neutron flux and fission rate distributions after a 14 MeV δ-shaped neutron pulse. The results obtained for the relation of the neutron field decay trajectories vs. time and detector position can be explained from physical principles. However, discrepancies observed between the following parameters calculated by MCNP in the KCODE mode: neutron field decay slope, k_{eff}, and life span related to neutron fission (which should be the generation time) could not be fully understood and require further investigations.

The paper by F.E. Dunn presented the results of thermal hydraulics and structural analysis calculations performed on both sodium cooled and lead-bismuth cooled sub-critical blanket designs for which beam interruption transients were assumed. The calculations were performed for base case designs, as well as for designs implementing some mitigation options — either to reduce the strains on the components or to reduce the accelerator trip frequency (e.g. reducing core temperature rise through reduced power or increased coolant flow, reducing the thickness of the subassembly load pads located above core, and assuming two separate accelerators driving the spallation source). The author concludes on allowable beam interruption frequencies for current sodium cooled and lead-bismuth cooled blanket designs. Further, the paper quantifies the effect of design options that could be adopted to accommodate higher beam interruption frequencies.

The paper by B.W. Spencer and J.J. Sienicki[*] presents a sub-critical, lead-bismuth cooled concept with significantly enhanced natural circulation heat transport characteristics. The enhanced natural circulation is attained through the use of ejector (jet) pumps. The jet pumps are driven by two immersed axial flow coolant pumps. During normal operation, 25% of the core flow is assured by the two immersed axial flow coolant pumps, while 75% of the flow follows the natural convection path via the ejector pump diffusers. With a loss of pumping power and simultaneous failure to scram, the core temperature rise would increase to ~390°C (from 140°C during normal operation), and the peak cladding temperature would reach ~850°C (from 565°C under normal operation). The reactor power would passively shut down owing to negative reactivity feedback, and the heat would be rejected passively via the vessel external cooling to air.

The paper by M. Eriksson et al. discusses safety features of a heavy metal cooled accelerator driven waste burning system. The sub-critical blanket is fuelled with plutonium and minor actinides contained in a zirconium-nitride matrix. Transients started by a step increase in the neutron source and by the loss of coolant flow are analyzed with the help of the SAS4A code.

[*] The authors did not submit the full paper.

Special attention is paid to the maximum permissible temperature in the nitride fuel with regard to thermal dissociation mechanisms. In general, the results show that the system copes with protected and unprotected loss of flow scenarios. Peak temperatures in fuel, cladding, and coolant are kept within postulated design criteria. The benign behavior is attributed to large pin pitches that allow for large coolant volume fractions, the use of lead/bismuth as thermal bond between fuel and cladding, and to a primary system designed to maintain large amounts of natural circulation flow. It is found that the system is most sensitive to source transients. An increase in source intensity results in high fuel temperatures and this may jeopardize the stability of the nitride fuel. Safety consequences of source transients depend strongly on the particular assumptions involved in the analysis. Above all, the rate and magnitude of the source disturbance and the effectiveness of the heat removal systems may significantly alter the accident scenario. AN important conclusion is the recognition of the importance for early detection and successful termination of source transients. Finally, the authors discuss the technique used in accelerators to perform emergency shut down of the proton beam, and point out the key features that distinguish accelerator beam shut off from the shut down mechanisms used in critical reactors.

The last paper in the session (by W. Maschek et al.) also discussed the safety features of ADS. The fuel retained by these authors in their study is pure transuranics oxide or nitride fuel ("dedicated fuel" without fertile isotopes). These fuels are still to be developed, and programmes are under way to fabricate, characterize, and investigate these innovative fuels. Analyses show that the use of dedicated fuels for a reactor core leads to a strong deterioration of the safety parameters (e.g. the void worth, the Doppler effect or the kinetics parameters, like the neutron generation time, and β_{eff}). In addition, these cores may contain multiple "critical" fuel masses, resulting in a considerable re-criticality potential. Besides the neutronics aspects, these fertile free fuels may also suffer from deteriorated thermal or thermal-hydraulic features, as reduced melting points, reduced thermal conductivities, or even thermal instabilities. On the basis of the current knowledge on these dedicated fuels it is generally concluded that "critical" reactors may not be feasible, because of the aforementioned safety concerns. However, it is claimed that ADSs, due to the sub-criticality of the system, could accommodate such dedicated fuels. These claims have been supported by quite a number of preliminary ADS safety analyses performed in recent years giving some insight into the system behavior of an ADS and generally showing its promising safety features. However, in most of these studies, the ADS mostly used $^{233}U/^{232}Th$ fuel, thus relying on the overall good safety parameters of fertile isotopes containing fuel. The results presented in this paper, obtained for fertile-free dedicated transmutation fuel, showed possible safety problems, especially in the case of severe transients. The results are compared with those obtained for $^{233}U/^{232}Th$ fuelled ADS, and safety requirements and conditions are formulated which should be fulfilled by cores (critical or sub-critical) fuelled with these innovative dedicated transmutation fuels.

2.5. Session 5: Target developments

The target development session heard three papers.

The first one, entitled MYRRHA: Design of A Windowless Spallation Target for a Prototype ADS, presented by H. Aït Abderrahim (SCK•CEN), addresses the design evolution and simulation studies for the windowless spallation target under development for MYRRHA. The windowless approach is taken because "when you have a feature that you know is going to fail (window), you might as well get rid of it at the start." The approach is an external lead-bismuth loop with a delivery manifold that fills the target tube with the lead-bismuth,

generating a free surface via a hydraulic jump. The beam strikes this free surface. The first design was shown to be too large for practical application in MYRRHA. The current design is 120 mm diameter. Issues included:

- Elimination of vortex which was unstable via anti-swirl member;
- Elimination of recirculation to minimize hotspot temperature;
- Effect of beam interruption;
- Issue of vapor formation and disposition in beam tube vacuum (where tests with lead-bismuth are planned to address this).

One conclusion was that, while computational fluid dynamics (CFD) codes were valuable tools, they need improvement for the windowless target application:

- Free surface tracking/diffusion;
- Combined with heat transfer;
- Turbulence.

The second paper Analysis of Different Design Options for the Beam Target of the Energy Amplifier Demonstrator Facility was presented by S. Buono. Both window target and windowless target options are being examined for the energy amplifier demonstration facility. The window target module has been developed internally; it is 7 m tall, with lead-bismuth target material cooled by natural circulation. The heat exchanger at the top is bayonet type with oil secondary coolant. Beam power is deposited mainly in the coolant funnel beneath the window which measures 140 mm diameter by 300 mm long. Salient issues discussed in this paper are listed below:

- Stresses in the window were analyzed for beam interruptions and were found to be very high, suggesting a rupture failure mode rather than cracking (leakage).
- The natural circulation cooling is said to handle both beam startup and interruptions by introduction of a flow inverter.
- The windowless target is said to be preferred for scaleup to a full size transmuter with high accelerator current.
- Ansaldo has produced a windowless target design that is virtually interchangeable with the window design for the demo facility; it utilizes primary circuit lead-bismuth coolant as the target material.
- There is also a collaboration with the MYRRHA project on a windowless design using a flow of lead-bismuth perpendicular to the beam axis.

The issue of applicability of CFD codes for heavy liquid metal applications is being addressed through a Benchmark Working Group International Collaboration.

The third paper entitled Experimental and Numerical Studies on Thermal-Hydraulics of Spallation Targets was presented by G. Heusener. The Research Center Karlsruhe (FZK) is integrating its laboratory facilities and numerical codes to evaluate spallation target designs, including the ISTC-project #559 design (IPPE), MEGAPIE (PSI), and the ADS-target (FZK). The FZK lead laboratory (KALLA) consists of numerous static facilities plus three separate loops, the technology development loop, thermalhydraulic loop, and corrosion loop for testing of lead and lead-alloy coolants. Water facilities are also available for flow visualization studies. One result of the numerical analyses presented is a proposal for an improved ISTC-project #559 design that is less vulnerable to lateral beam offset.

2.6. Session 6: Experimental studies

The experimental studies session heard four papers.

The first by M. Hron[*] described a planned experimental programme to validate the design of a long lived radwaste transmutation system based on molten fluorides fuel.

The second paper by S.E. Chigrinov et al.[*] presented the "YALINA" experimental setup and the first results of the sub-critical neutronics studies performed at this facility. Experimental ADS validation work using high energy accelerators is expensive. On the other hand, studies have shown that the physics of the coupled target/sub-critical blanket system can be studied simulating the spallation source with the help of a 14 MeV high intensity neutron beam irradiating a lead target. YALINA is the combination of a thermal sub-critical array (10% enriched uranium-polyethylene) with a central neutron source (lead target irradiated by a high intensity (10^{12} ns^{-1}) D-D or D-T continuous or pulsed neutron generator). The author presented first experimental results (reactivity measurements, reaction rate traverses, dynamic characteristics).

The third paper by D.P. Abraham et al. presented the results of an experimental study in which a thermal convection-based test method was used to allow exposure of candidate structural materials (iron-based alloys) to molten lead-bismuth flowing under a temperature gradient. The gradient was deemed essential in evaluating the behavior of the test materials in that should preferential dissolution of components of the test material occur, one would expect dissolution in the hotter regions and deposition in the colder regions, thus promoting material transport. The temperature in the hot leg of the convection harp was ~550°C and the temperature in the cold leg was ~350–425°C. The alloys chosen for the test were AISI S-5, a 2 wt% Si mild steel, and HT-9, a ferritic-martensitic stainless steel. The tests were terminated after sample exposure for ~4500 hours. The authors summarized the results of their studies as follows:

- The AISI S-5 alloy was attacked by the molten lead-bismuth. The depth of intergranular penetration ranged up to 40 μm in the hot leg and up to 5 μm in the cold leg. The test showed that AISI S-5 would not be suitable as a structural material for nuclear reactors using lead-based alloy coolants.
- The HT-9 samples were not attacked by the molten lead-bismuth. The samples appear to have been protected by a stable, adherent, $FeCr_2O_4$-type spinel layer. Close control of oxygen activity was not necessary to form the protective spinel. As long as the oxygen activity is well below that needed to form PbO and above that needed to form the spinel, ample leeway exists to form a protective layer on HT-9.
- A comparison of AISI S-5 and HT-9 corrosion behavior clearly demonstrates the important role of chromium in the passivation of HT-9 and EP-823 alloys exposed to molten lead-bismuth.

The section's last paper by X. He et al described a kinetic model developed to estimate the corrosion/precipitation rate in a non-isothermal liquid lead-bismuth eutectic flow loop. This model provides a useful tool for designing and operating liquid lead-bismuth eutectic cooling systems. The model is based on solving the mass transport equation with the assumptions that convective transport dominates in the longitudinal flow direction, and diffusion dominates in the transverse direction. The species concentration at wall is assumed to be determined either by the solubility of species in the liquid lead-bismuth eutectic in the absence of oxygen, or by

[*] The authors did not submit the full paper.

the reduction reaction of the protective oxide film when active oxygen control is applied. Analyses show that the corrosion/precipitation rate depends on the flow velocity, the species diffusion rate, the oxygen concentration in the liquid lead-bismuth eutectic, as well as the temperature distribution along a loop. Active oxygen control can significantly reduce the corrosion/precipitation of the structural materials. The authors show that the highest corrosion/precipitation does not necessarily locate at places with the highest/lowest temperature. For a material-testing loop being constructed at the Los Alamos National Laboratory, the highest corrosion occurs at the end of the heater zone, while the highest precipitation occurs in the return flow in the recuperator.

3. OVERALL SYNTHESIS, CONCLUSIONS AND RECOMMENDATIONS

High level waste disposal is an element of paramount importance in the discussion of nuclear power generation sustainability. This, and the desire to reduce the quantity of long lived waste material, have stimulated new interest in the transmutation of actinides and some long lived fission products, and in emerging system technologies for energy production with reduced actinide generation. One such system is the combination of a particle accelerator with a subcritical nuclear reactor; another possibility is to reduce the generation of actinides by the introduction of the thorium fuel cycle.

The surmised advantages of accelerator driven systems — apart from their intrinsic low production of long lived radioactive waste, and transmutation capability — are also enhanced safety characteristics and better long term resources utilization (e.g. in connection with thorium fuels). Important R&D programmes are being undertaken by various institutions in many Member States to substantiate these claims and advance the basic knowledge in this innovative area of nuclear energy development.

While long term objectives for developing novel nuclear systems for energy production and transmutation may not be unanimously agreed upon by the different groups participating in this effort, it is clear that the short term goals are similar.

Therefore, quite a few generic R&D areas can be identified that would benefit from international collaboration. The most important technical issues identified and discussed within the framework of the TCM's six sessions were:

- Thermal fatigue (due to beam trips),
- Toxicity of the spallation products,
- The lack of a safety strategy for severe accidents with fertile-free transuranics fuel,
- The lack of data on irradiation damage effects (induced by both proton and neutron irradiation) on the structural properties of the beam window and the adjacent core.

The TCM identified the need and opportunity for collaboration in the following areas:

- Major demonstration facilities, for which international participation should be considered,
- Testing of special effects (e.g. fuels and materials tests, and zero power coupled systems) which offers practical opportunities for dividing up the work, and
- Calculational benchmarks.

Based on the discussions during the TCM, international collaboration was noted several times as being of potential significant value to the various Member States programmes. Potential areas for enhancing collaboration included use of international organizations for coordinating benchmark verification of design analysis codes in areas such as thermal hydraulics and target physics, and for pursuit of establishing criteria for safety related parameters (e.g. sub-

criticality level, fuel composition, reactivity control), and evaluating the design impact of these criteria.

The TCM participants acknowledged the IAEA's role as promoter and facilitator of information exchange and collaborative R&D and encouraged the IAEA to continue using its good offices to promote multi-national collaboration and exchanges. Given the high benefit/cost ratio of data sharing, substantial benefits for the Member States can be achieved through increased IAEA efforts to facilitate the sharing of data. Increased use of dynamic Web-based collaboration and information exchange is considered to be an important means to achieve this goal. It was clearly stated that all the activities in the area of nuclear energy systems for energy generation and transmutation should be tied to the activities of the Technical Working Group on Fast Reactors (TWG-FR).

RESEARCH AND DEVELOPMENT PROGRAMMES

(Session 1)

Chairperson

F. GOLDNER

United States of America

THE ITALIAN R&D AND INDUSTRIAL PROGRAMME FOR AN ACCELERATOR DRIVEN SYSTEM EXPERIMENTAL PLANT

M. CARTA, G. GHERARDI
Ente Nuove Technologie, Energia e Ambiente, Bologna, Italy

S. BUONO
Center for Advanced Studies, Research and Development, Sardinia, Italy

L. CINOTTI
ANSALDO, Genova, Italy

Abstract

Accelerator Driven Systems (ADS), coupling an accelerator with a target and a sub-critical reactor, could simultaneously burn minor actinides and transmute long-lived fission products, while producing a consistent amount of electrical energy. A team of Italian R&D organizations and industries has set up a network of coordinated programs addressed to study the design issues of an 80 MW_{th} Experimental Facility. The present memo focalizes the attention on some results obtained by the R&D activities and by the on-going industrial short term activities aiming at the preparation of the proposed preliminary design, leaving the deal to define the details of the subsequent medium term activities to the expected common program in the European context.

1. INTRODUCTION

Starting from 1995 [1] a growing interest on the Accelerator Driven Systems (ADS) concepts has taken place in Italy and has given origin to several basic R&D activities and to an industrial program involving ENEA (the Italian national research body for energy, environment and new technologies), INFN (the Italian national research institute for nuclear physics) and various industrial partners.

As a first step, this interest was confirmed by the national R&D program TRASCO (Italian acronym standing for waste transmutation – TRAsmutazione SCOrie), funded and started in 1998 under the leadership of INFN for the accelerator and of ENEA for the sub-critical system. The TRASCO program was relevant to promote collaboration among groups of different competencies (accelerator, reactor physics, plant design), which will provide relevant results in support of any related industrial program.

Parallel to the basic activities of TRASCO, an industrial program was proposed in two main steps (the first was approved and funded in 1999):

a) On-going short-term activities in the Italian context to issue preliminary design of the ADS experimental plant. A reference configuration has been proposed [2] (named EADF, Energy Amplifier Demonstration Facility) and submitted to the European partners [3] as a contribution to the discussion of the European Road Map for developing an ADS experimental plant. The preliminary design will be completed in the first half of 2001, while the main supporting R&D needs were assessed and the realization of the experimental facility CIRCE is in progress, for thermal hydraulic testing in PbBi of the main subsystems of the experimental plant.

b) Medium term activities in an European and international context with the aim to perform the detailed engineering design, the realization and the commissioning of the experimental plant along with all the supporting R&D.

2. THE TRASCO PROGRAM

2.1. Introduction

The program, devoted to study the physics and to develop the technologies needed to design an ADS for nuclear waste transmutation, was prepared with close reference to Carlo Rubbia's Energy Amplifier proposal [1]. It consisted of two main parts regarding, respectively, the accelerator and the sub-critical system. The part relative to the sub-critical system, managed by ENEA, was structured through the following topics (in parenthesis the team composition for each topic[a]):

- General safety criteria and classification (ENEA, ANSALDO);
- Nuclear data (ENEA, University of Bologna);
- Neutronics (ENEA, CIRTEN, CRS4);
- Thermal-hydraulics (ENEA, CIRTEN, CRS4, ANSALDO);
- Beam window technology (ENEA, CIRTEN, ANSALDO, INFM);
- Materials technology and compatibility with lead and/or lead-bismuth alloy (ENEA, CIRTEN, CRS4, FN, ANSALDO).

Some outputs from the above topics are summarized in the following section.

2.2. Main results

2.2.1. General safety criteria and classification

The activity was focused on:

a) Set up of rules necessary for the development of EADF design, and
b) Analysis of general safety issues and definition of requirements.

and was shared out in the following four lines.

1) Identification of general safety issues and requirements
   This activity has been finalized to define the safety requirements of the overall process, by emphasizing the peculiarities of an ADS plant, relative to current nuclear power plants. The activity has allowed to define the general safety and functional requirements, against the established objectives for the Italian demonstration plant (EADF). The sole aspects of this type of plant have been shown, for example the sub-critically level in every operational condition and their impact on the design. The criteria about process simplification, use of passive systems, reliability, availability and maintainability of systems and components have been established.

---

[a]ANSALDO Nuclear Division, which also provides the program overall coordination, is the technical coordinator of the subcritical system design activities and is involved in all the main working tasks in order to assure integration and consistency;
CRS4, Center for Advanced Studies, Research and Development in Sardinia, provides support to core/fuel and subcritical system design activities;
CIRTEN: Universities Consortium;
INFM: National Institute for Materials Physics;
FN: Nuclear Fabrications.

The bases for the definition of the design basis accidents, their characterization in terms of probability, the levels of resistance, protection and mitigation toward the accidental situations have been rendered explicit. The requirements against internal, external and special events, caused by human action (for example, impact of a plane, explosions of gas) have been defined. The barriers to the radioactive product release have been redefined in comparison to the classical formulation.

2) Safety classification
   This activity has allowed to associate structures, systems, and components of EADF to the reference standards and codes. According to the previous choices effected on the applicable normative, a first phase of this activity has consisted of to point out the state of the art on the principal methodologies for the classification of systems, structures and components mostly used within the nuclear industry. Among these, the methodology proposed by the EURs, based on the functions of the systems and on the temporal phases, has been examined deeply.

3) Applicable codes and standards
   This activity has been finalized to define the reference regulations to use in the ADS design. These regulations have been established through an in-depth, critical assessment of LWR and LMFBR licensing processes (e.g., by revising existing Regulatory Guides) and of other guides (e.g., industrial standards).

4) Mechanical design criteria
   This activity has carried out to the definition of new criteria for the use of innovative materials, as well as for the operation of nuclear components and structures out of the standard range of applicability.

2.2.2. Nuclear data

The research activity was focused on nucleon induced reactions in the incident energy range from 20 to 150 MeV, above the range of standard nuclear data libraries used in critical reactor calculations and below the pion production threshold.

In the above mentioned energy interval, several pre-equilibrium reaction models, either semiclassical, such as the exciton models and the intranuclear cascade models, or fully quantum mechanical, such as the multistep theories of Feshbach, Kerman and Koonin (FKK) and Tamura, Udagawa and Lenske (TUL), can be applied, with different limitations inherent in their basic assumptions.

In collaboration with researchers of the Institute of Physics and Power Engineering, Obninsk, the hybrid exciton model was used to compute cross sections for production of deuterons, tritons and alpha particles in proton induced reactions on several structural materials and one target material (^{209}Bi) [4], as well as the cross sections of all important channels of neutron induced reactions on ^{238}U [5]. In both cases, the primary nucleon energy ranged from 20 to 150 MeV.

Work is in progress on the improvement of nuclear models of the EMPIRE-II code, which uses the TUL approach to multi-step direct reactions, in collaboration with the author, M. Herman, IAEA Nuclear Data Section, Vienna, in order to extend the range of applicability of the code itself.

As far as nuclear structure data are concerned, a preliminary study of the low-lying discrete levels and of the collective enhancement factor of level densities of even-even thorium isotopes ($^{220-232}$Th) was carried out in the frame of the interacting boson model of collective nuclear excitations [6], with a view to using it in future calculations of neutron cross sections at low and intermediate energies.

The work planned on Th isotopes will benefit from the re-evaluation of neutron data below 20 MeV for ^{232}Th, recently completed within the framework of the same research program by V. Benzi, M. Sumini and co-workers at the DIENCA Department of the University of Bologna, by taking into account the most recent experimental data on total, inelastic and capture cross sections, not yet available at the time of release of the ENDF/B-VI file.

2.2.3. Neutronics

2.2.3.1. Static analyses

In order to investigate the level of accuracy of deterministic calculations (DC) with respect to Monte Carlo calculations (MCC), an intercomparison was launched in the fall of 98 for the EADF configuration. This involved, as well as basic system integral parameters (k_{eff}, K_s), also the spatial – energy characterization of the neutron flux profile inside the sub-critical region. The DC employed an approximate neutron source obtained from the first stage of the MCC starting from the proton source energy until 20 MeV.

The MCC-DC inter-comparison indicated a good agreement between k_{eff} and K_s (differences of around 600 pcm with the same library) and a good reproducibility by the DC of the main reaction rate profiles. In addition, the results validated the approximations employed to generate the neutron source.

2.2.3.2. Development of kinetics and core-dynamics computational tools

The activities were focused on:

- Development of a neutronic model and of a numerical scheme for a two-dimensional system in multigroup diffusion theory.
- Development of consistent quasi-static techniques suitable to treat 3D (multigroup diffusion theory) time-dependent neutronic problems for ADS.
- Study and optimization of numerical algorithms for the time-discretization of the transport equation in source-dominated systems [7, 8].
- Coupling of the single channel - single phase TIESTE thermal-hydraulics code (developed by ENEA) with point kinetics and 2D RZ, multigroup diffusion theory (developed by Politecnico di Torino, Prof. Ravetto team) codes in order to investigate dynamics core behavior [9]. A simplified model of natural convection has been developed to improve the ADS dynamics investigations by considering the mitigation effect relevant to the coolant natural-convection dynamics [10].

2.2.3.3. Kinetics and core-dynamics analyses

The activities were focused on:

— Preliminary analysis of some transient situations.
  A core-dynamics analysis relevant to some typical current-transient events was carried out for the EADF. In particular, fuel and coolant temperature trends relevant to Recovered Beam-Trip and Beam-Jump events were preliminarily investigated [11, 12].

Beam-trip results showed that the drop in temperature of the core-outlet coolant would be appropriately reduced if the beam intensity could be recovered within few seconds. Concerning the current transient "Beam-jump from zero power", it should be recalled that in the EADF design, the primary-loop coolant flow is assured by natural convection and is enhanced by a particular system of cover gas injection into the bottom part of the riser [13]. In the EADF design, the natural convection pull is about 20% of the pull due to the active system based on cover gas injection. Preliminary results confirm that while the active system of cover gas injection is working, the impact of the primary coolant natural convection on Beam-Jump transient behaviors is not significant. On the contrary, the natural convection mitigation of temperature transients becomes clearly significant if the active system of cover gas injection is assumed to be unavailable or to fail.

Moreover, it is well known that ADS respond more benignly than critical systems to reactivity insertions. This ADS characteristic was further analyzed in the EADF case [14, 15]. In particular, possible low feedback reactivity-effects, that mitigate critical system transients induced by reductions in coolant flow, were investigated in the worst hypothetical scenario: i.e., during an unprotected Loss Of Flow accident. Since ADS dynamics are mainly decided by the external source, a parametric study was performed to investigate feedback effects in the EADF, by considering not only different values of the system sub-criticality level, but also different hypotheses on the external-source control-strategy.

- Reactivity monitoring strategies.
  The EADF response to harmonic modulation of the external neutron source intensity was analyzed. The point kinetics approximation was adopted to test the method by numerical simulations. Moreover, spatial effects were theoretically and numerically investigated [16]. Results show that, an absolute "reactimeter" may be conceived.

  In addition, a spatial source-jerk approach was compared with the modulated source method [17]. A numerical simulation of both methods was performed, and results indicated a consistency between the responses by the two methods, although the modulated source method may be considered an on line reactivity measurement. Finally, some indications were derived about the most appropriate positions in the system to monitor the absolute (in dollar units) fundamental reactivity value.

2.2.4. Thermal-hydraulics

The proposed ADS concepts present some peculiar aspects, which require the development of new thermal-hydraulic models, as well as a deep investigation of some fundamental phenomena, at present far from a complete comprehension. In particular, the use of lead or lead-bismuth alloy as a beam target and nuclear coolant, as well as heat removal based on natural convection, has to be carefully studied. Therefore, the activities were focused on[b]:

- Assessment of the limits of applicability of the turbulence models implemented in CFD (Computational Fluid Dynamics) codes for the simulation of liquid-metal flows [18]. In fact, beyond the standard limitations of turbulence models, additional problems can arise, essentially due to the low Prandtl number of liquid metals. A benchmarking activity of

[b] For more details see the CRS4 Energy Amplifier Group web page (http://www.crs4.it/Areas/ea), where a description of the group activities and a list of publications is available.

CFD codes is in progress, in collaboration with other European research centers and with CFD companies, based on experimental measurements in liquid metal flows [19, 20]. Some important results have been already obtained.

- Assessment and development of free-surface-flow algorithms to be used in the design of windowless targets.
- Development of a thermal-hydraulic system codes which can simulate the various reactor transient [21]. Two codes have been developed and their validation is in progress: ANTRASS and RELAP 5. The latter can be used also for 3-D neutronic calculations.
- Structural and thermal-hydraulics analysis of critical components like target, vessel, fuel assemblies [22]. This activity has been performed using through the integrated calculation system described in [23].

2.2.5. Beam window technology

Being subjected to heavy operational conditions, concerning irradiation and corrosion, the beam window is universally considered as a "key" component of a sub-critical system. Advanced materials and technologies have, thus, to be foreseen and developed for this component. Unfortunately, there is a general lack of data on the mechanical properties of these new materials under the synergetic conditions of high neutron and proton fluence and of the interaction with lead or lead-bismuth.

This subprogram aimed to analyze the effects of high fluence proton irradiation, in order to get reliable data on the mechanical properties of candidate materials vs. the irradiation dose. Furthermore, new technologies were investigated for demonstrating the feasibility of windows of actual size.

2.2.6. Materials technology and compatibility with lead and/or lead-bismuth alloy

The program was dedicated to experimental investigations aiming at increasing the know-how on the performance of candidate window materials, structural materials and system components in contact with lead and lead bismuth eutectic alloy at high temperature in stagnant and flowing conditions.

As far as the experimental activity in stagnant lead [24] and lead bismuth [25] is concerned, several tests were done aiming at studying the basic mechanisms and the thermodynamic aspects of the corrosion process for the ADS candidate materials. In particular, a set of tests in stagnant molten lead at 793 K and in lead bismuth alloy at 573 and 673 K were carried out on several materials: mod. F82H martensitic steel, tungsten, mod. F82H martensitic steel hot dip aluminized, MANET II, AISI 316L.

A preliminary experimental investigation in flowing lead bismuth at 573 and 743 K was performed on austenitic and martensitic steels [26] in the framework of a collaboration between ENEA and IPPE-Obninsk (RF). In these experimental campaigns the oxygen content was fixed at the value of $1\text{-}2\times10^{-6}$ wt.% and the duration of the exposition of the steels was 3000 hours.

In order to carry out a more extensive experimental investigation under different operative conditions, two liquid metal loops (LECOR and CHEOPE) have been designed and constructed at the ENEA site of Brasimone.

CHEOPE is a “multitasking” facility, consisting of three parts:

- Section for thermal hydraulics experiments (CHEOPE-1);
- Section for mass transport and chemistry studies (CHEOPE-2);
- Oxygen control and corrosion section (CHEOPE-3).

In particular, CHEOPE-3 is the part of the facility dedicated to the corrosion tests, equipped with an oxygen monitoring and control system. The corrosion tests will be performed at relatively high oxygen content in order to validate the technology of steel protection by in situ oxidation.

The main objective of the experiments to be carried out in LECOR, which is a “figure-of-eight” configuration loop, is the quantitative study of corrosion phenomena and their effects on the mechanical behaviour on beam window candidate materials. The main operative conditions that will be adopted in LECOR can be summarized as follows:

- Temperature range in the test sections: 723-823 K.
- Velocity range in the test sections: 0.5-1 m/s.
- Oxygen content lower than 10^{-8} wt.%.

The experimental device ORE was developed to support the activities to be carried out in LECOR and CHEOPE in the field of oxygen monitoring and control and the conditioning of the liquid metal. For this last aim ORE provided data about the kinetics of lead-bismuth oxides reduction by hydrogen as well as oxygen extraction.

An up-grade of the ORE device, in order to control the oxygen content in molten lead-bismuth, is under design, which will be provided with an oxygen probe, developed in ENEA.

3. THE INDUSTRIAL PROGRAM

3.1. Background and considerations

In Europe a strong industrial interest exists for the ADS technology aimed at the construction of a prototype. Such an interest has been witnessed:

- In the common signature by ANSALDO, FRAMATOME, NNC and SIEMENS of the document “An European Nuclear Industry Interest for the Accelerator Driven Systems Technology to assess an European Reference System Configuration” which has been transmitted 1998 to the European Union;
- By the approval by the EU in the year 2000 of funds for ADS-specific R&D activities;
- By the common application, to be submitted to the EU end this year by leading engineering companies and R&D organizations, for funding within the 5th R&D Program scoping studies aimed at the choice between liquid metal or gas-cooled ADS configuration, to be engineered as Experimental ADS (EADF).

On 1998, the Research Ministers of France, Italy and Spain have established a Technical Working Group (TWG) including R&D organizations and industrial companies in charge of reactor and accelerator studies, in order to identify the crucial technical issues for which R&D is needed. The recommendations of the TWG indicate the needs to design and operate the EADF facility at a sufficiently large scale to become the precursor of the industrial, practical-scale transmuter. Based on the recommendations of the TWG, Italian engineers and scientists of ANSALDO Nucleare, ENEA, CRS4 and INFN, grouped in a team led by ANSALDO,

have anticipated the activity on EADF cooled by Lead-Bismuth Eutectic (LBE). The facility should demonstrate key-features, such as the successful coupling of the sub-critical reactor with the accelerator and the transmutation capability of transuranics and selected fission fragments of concern. With the appropriate selection of main operational parameters, such as a low primary coolant temperature (choice of LBE instead of lead as the coolant) and speed, a low core power density, a proven fuel, and the power removal to the atmosphere, the EADF could be engineered for construction on the basis of information from of a mid-term R&D programme. In particular a large-scale R&D facility, the CIRCE test rig, is scheduled mid 2001 for completion in Italy. The feedback from the operation of the EADF and the answers provided by a long-term R&D programme will be the base, in turn, for the development of the lead-cooled ADS power prototype. The development activity of the Italian team has already made all basic technological choices, illustrated by general arrangement drawings, plot plan and elevation studies, main component data sheets and drawings, Table 1. and Ref. [3]. At present, the purpose of the work is to confirm the main technical features focusing at the following main project topics:

- Overall feasibility;
- Materials exposed to LBE and corrosion protection;
- Fuel type(s);
- Accelerator type and power;
- Target system;
- Primary and secondary coolant, heat transfer equipment, pumping and purification systems;
- R&D needs.

3.2. Status of the industrial program

The results obtained so far, though preliminary and not exhaustive, allow outlining a consistent demonstration prototype configuration, main features of which per plant area are concisely reported in Table 1.

The choice of the power (80 MW_{th}) is motivated by the fact that 80-100 MW_{th} is the minimum consistent with a representative core characterized by annular configuration. Moreover, this power level eases both design and licensing, because the decay heat can be removed passively by the Reactor Vessel Air Cooling System (RVACS) and the Reactor Vessel always operates at loading conditions of negligible creep damage, according to the RCC-MR.

Though the process of selection of the accelerator type for the Demonstration Prototype is continuing at present, the basic scheme assumed is a reasonable extrapolation of the PSI facility and is based on a three-stage system capable to supply a proton beam of a few mA (up to 5-6 mA) at 590 MeV. The first stage, made of the proton source and a small cyclotron, supplies the low energy pre-injection beam (5-6 MeV). The following accelerator stages are provided by two separated-sectors cyclotrons. The intermediate-stage cyclotron provides a low-medium acceleration with extraction at 100 MeV. The final stage cyclotron (the so called “ring cyclotron”) boosts the proton beam to the final energy of 590 MeV. The booster is a 8-sector magnets cyclotron with 6 RF cavities operating at 50 MHz – 1MV.

The target material is molten LBE separated from the reactor coolant. LBE has good spallation efficiency, neutronic properties and low melting temperature. Target eutectic is kept separated from the reactor primary coolant by means of a retrievable target unit. Two target

configuration concepts have been investigated, which differ in the separation barrier adopted at the interface between vacuum pipe and target lead-bismuth eutectic.

The “window” target configuration features a mechanical barrier of a material transparent to the largest possible extent to neutron and proton irradiation and engineered to withstand pressure and thermal loads, the eutectic circulates under natural circulation, cooled in the upper part of the target unit by the diathermic fluid of an auxiliary system.

In the “windowless” target configuration, the proton beam from the accelerator impinges directly on the target eutectic, that circulates driven by a stream of cover gas, according to the same gas lifting principle adopted for the primary system and is cooled by the reactor coolant in the HX located in the bottom part of the target unit.

Coming now to the sub-critical reactor, the basic fuel assembly is similar to that of SPX and, also, the fuel pellets have the same geometry and comparable composition (about 20% of Pu) of the higher enrichment of the SPX core. At the core rated power of 80 MW_{th}, the average fuel power density is 22 W/g·MOX (227 W/cc-MOX), with max radial peaking of 1.32 and axial of 1.13. The core is surrounded by an outer region of four rows of dummy assemblies, which are empty duct structures. This offers a continuous fast-to-thermal neutron flux region, useable for test burning MA and LLFF SA’s.

The core multiplication factor results 0.97 at beginning of life and reduces to 0.94 at end of cycle, at full power. The value k_{eff} = 0.97 is sufficiently low to ensure the safe operation of the reactor without control and shut-down rods. Twelve absorbers radially positioned by means of the refuelling machine, operating without target displacement, can bring the k_{eff} below 0.95 at refuelling conditions (200°C, zero power, target vertically displaced).

Molten Pb-Bi eutectic has been chosen as primary coolant. From the neutronics point of view it behaves like pure lead – which was the first choice of the Energy Amplifier – but it allows lower operating temperature (300°C at the core inlet and 400°C at the core outlet) of the reactor and there is the important experience on its use made by the Russians with the reactors for submarine propulsion.

The reactor has been designed in the pool-type configuration because of the possibility to contain within the main vessel all the primary coolant with the highly active polonium, mainly originated by bismuth, and of the large experience acquired with the design and operation of sodium cooled pool-type reactors. In the EA concept proposed by CERN, the lead coolant operates in natural circulation, driven by the density difference between the riser and the down-comer of the primary circuit. For the Demonstration Prototype the lead-bismuth circulation is enhanced [13] by a flow of about 100 NL/s cover gas, injected into the bottom part of a circular array of 24 identical pipes (0.2 m ID), which make up the riser.

The secondary system is constituted by two safety-related loops, that in normal operation dissipates to the atmosphere the heat generated by the reactor. The thermal cycle temperatures, 320°C for the hot leg, and 280°C for the cold leg, are consistent with the choice of a synthetic diathermic fluid as the coolant, owing to the low vapour pressure of these fluids and the insurance of no fast chemical reactions, in case of leak, with the lead-bismuth eutectic or the air. Each secondary loop is made up of two Intermediate Heat Exchangers (IHX) arranged in parallel, of three Air-fin Heat Exchangers (AHX), of a circulation pump, and of the interconnecting piping. The Air-fin Heat Exchangers (AHX) are arranged in parallel as regard to the air circulation but, on each loop, they are in series as regard to the circulation of

the synthetic diathermic fluid. The system, as it has been designed, could re-use the six AHX's belonging to the RSR circuit of the PEC reactor.

4. PLANNED FUTURE R&D ACTIVITIES AND COLLABORATIONS

In the short term, the following activities are foreseen:

- Preliminary project of the EADF, core section, spallation module and its coupling with the accelerator;
- Realization and operation of the experimental plant CIRCE, execution of the first two test experimental campaigns;
- By means of the experimental facilities at Brasimone (LECOR and CHEOPE), support to the technological development for CIRCE experimental plant and support tests to MEGAPIE and MYRRHA programs;
- Participation to the EU Framework Programme on Partitioning and Transmutation in the following tasks: TECLA (liquid metal technologies), MUSE (physics of the subcritical system), nTOF (nuclear data), PYROREP (pyrochemical reprocessing), Advanced Fuels for ADS, System Analysis (on the EADF);
- Participation to the MEGAPIE project;
- Participation to the bilateral agreement among ENEA and different research institutions (CEA, SCK-CEN, Halden, ITU, ISTC).

In the medium term, the following phases are foreseen:

- Basic researches on accelerator technologies, subcritical system and long-life radioactive species partitioning;
- Finalized researches devoted to the demonstration of the feasibility and economical convenience of particular technical solutions, in the frame of the test support program to the EADF project;
- Project and realization of the EADF.

Afterwards, R&D activities will support the ADS industrial development.

TABLE 1. MAIN EDF DATA BY PLANT AREA

Plant area	Reference solution
Plant power	80 MWth subcritical system controlled by a 590 MeV, 6 mA proton beam
Target/window	Two options: a) Proton window b) Windowless target
Core	0.97 (at beginning of cycle) > k_{eff} > 0.94 (at end of cycle), at full power
Fuel	U and Pu MOX
Primary system	Pool configuration with four integrated IHXs
Primary coolant circulation	Circulation enhanced by gas injection in a natural-circulation reactor configuration
Secondary system	Two low vapour pressure organic diathermic fluid loops rejecting heat by means of air coolers
Thermal cycle	300°C at core inlet, 400°C at core outlet
Reactor roof	Metallic plate
Main vessel and safety vessel	Hung from a cold annular beam
Structural materials	Vessels and internals: 316L target and fuel SAs: 9Cr 1Mo
In-vessel fuel handling	One rotating plug, one fixed arm, one rotor lifting machine
Secondary fuel handling	Flask, encapsulator, canister, lifting and translating equipment, water pool
Nuclear island	Common basemat on antiseismic support
Plant safety	Full passive system

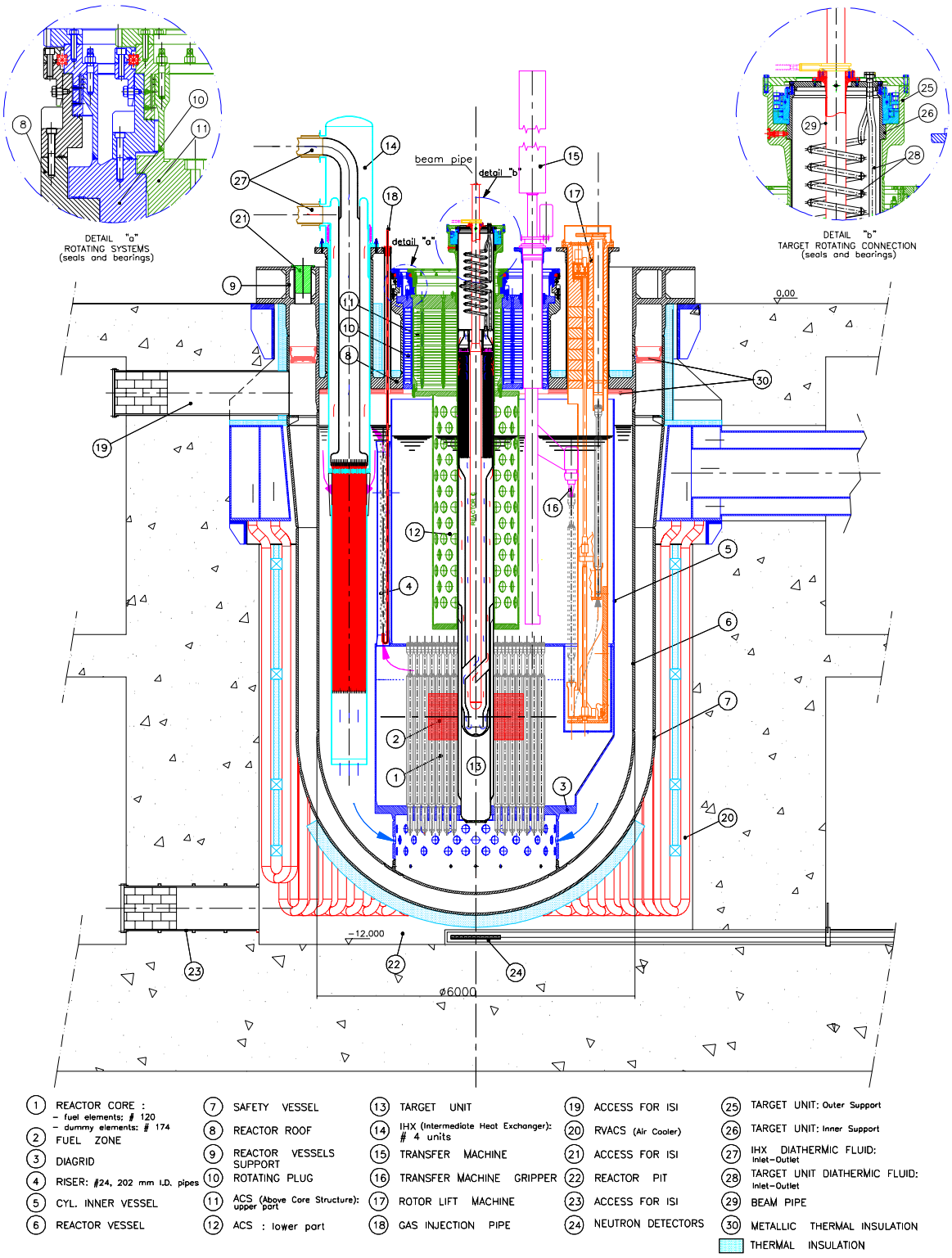

FIG. 1. Energy amplifier demonstration facility.
Reactor assembly drawing of a 80 MWth demonstration facility cooled by Pb-Bi.

REFERENCES

[1] RUBBIA, C., RUBIO, J.A., BUONO, S., CARMINATI, F., FIETIER, N., GALVEZ, J., GELES, C., KADI, Y., KLAPISCH, R., MANDRILLON, P., REVOL, J.P., ROBHE, CH., Conceptual design of a fast neutron operated high power energy amplifier, CERN/AT/95-44 (ET).

[2] CINOTTI, L., et al., Issues Related to the Design of an ADS Cooled by the Pb-Bi Eutectic in Heavy Liquid Metal Coolants in Nuclear Technology, Proc. Conf. on Heavy Liquid Metal Coolants in Nuclear Technology (HMLC'98), 1998, Obninsk, Russia, SSC RF, CRS4, TECH-REP-00/50 (1999).

[3] ANSALDO - Doc EA B0.00 1 200, Rev 0, Summary Report of the EA Demonstration Facility (1999).

[4] LUNEV, V.P., SHUBIN, Yu.N., GRANDI, C., POLI, B., VENTURA, A., The effect of level density and reaction mechanisms on the reaction cross section calculations at intermediate energies, Nuovo Cimento **A112**, 743 (1999).

[5] IGNATYUK, A.V., LUNEV, V.P., SHUBIN, Yu.N., GAI, E.V., TITARENKO, N.N., VENTURA, A., GUDOWSKI, W., Neutron Cross-Section Evaluations for ^{238}U up to 150 MeV, Nucl. Sci. and Eng., **136**, 340 (2000).

[6] CAPOTE, R., KUSNEZOV, D., MENGONI, A., VENTURA, A., Proc. 9th Int. Conf. on Nuclear Reaction Mechanisms, 2000, Varenna, Italy, E. Gadioli (Ed.) Cultura Scientifica ed Educazione Permanente, Special Issue (2000) 125.

[7] RAVETTO, P., LAROSA, A.M., COPPA, G.G.M., LAPENTA, G., CARTA, M., Assessment of numerical methods for time-dependent transport calculations of subcritical systems, Proc. ANS International Conference on Nucl. Science and Techn., Vol. 2, Long Island, NY, USA (1988) 875.

[8] RAVETTO, P., LAROSA, A.M., COPPA, G.G.M., LAPENTA, G., CARTA, M., Analysis and Optimization of Implicit Methods for Time-Dependent Transport Calculations of Source Driven Systems, J. Nucl. Sci. Technol., **37**, 215 (2000).

[9] BIANCHINI, G., CARTA, M., D'ANGELO, A., BOSIO, P., RAVETTO, P., ROSTAGNO, M.M., Dynamics calculations of source driven systems in presence of thermal feedback, Proc. Int. Top. Mtg. On Advances in Reactor Physics and Mathematics and Computation Into the next Millennium (PHYSOR 2000), 7-11 May 2000, Pittsburgh, PA, USA, ANS, ISBN: 0-89448-655-1 (2000) 5303.

[10] D'ANGELO, A., BIANCHINI, G., CARTA, M., BOSIO, P., RAVETTO, P., ROSTAGNO, M.M., A Simple Model to Evaluate the Natural Convection Impact on the Core Transients in Liquid Metal Cooled ADS, Proc. 6th OECD/NEA Information Exchange Meeting on Actinide and Fission Product Partitioning and Transmutation, 11-13 December 2000, Madrid, Spain, NEA, EUR 19783 EN (2000).

[11] D'ANGELO, A., CARTA, M., BIANCHINI, G., Preliminary Analysis of Neutronic Source Transients in a Small ADS Prototype, Proc. 3rd International Conference on Accelerator-Driven Transmutation Technologies and Applications, (ADTTA'99), 7-11 June 1999, Prague, Czech Republic, L M. Hron, V. Lelek (NRI Rez plc), M. Mikisek, M. Sinor, J. Uher, J. Zeman (FNSPE CTU, Prague) (Eds), NRI Rez, Czech Republic (1999), Prague, Czech Republic.

DEVELOPMENT OF ACCELERATORDRIVEN TRANSMUTATION SYSTEM CONCEPT AND RELATED R&D ACTIVITIES AT JAERI

T. TAKIZUKA, T. OSUGI, H. TAKANO
Japan Atomic Energy Research Institute, Japan

Abstract

JAERI has carried out R&D on transmutation of long-lived nuclides with a special emphasis placed on accelerator-driven systems (ADS) under the Japanese OMEGA Program. The ADS is designed to be introduced as a dedicated transmutation system into the second stratum of a double-strata nuclear fuel cycle concept. Early ADS concepts employed sodium coolant and solid tungsten target. A chloride molten-salt system and a molten-alloy system were investigated as advanced options to pursue the possibility of taking full advantages of liquid fuel systems. The current reference ADS design employs eutectic lead-bismuth as spallation target material and coolant. The fuel for the subcritical core is minor-actinide mononitride. The system consists of a 1.5-GeV, 14-mA proton accelerator and an 800-MWt subcritical core with an effective neutron multiplication factor of 0.95. The design incorporates salient features that the coolant inventory is large due to the tank-type configuration, the temperature rise through the core is relatively low, and the power conversion is operated on a saturated steam turbine cycle. These features help mitigate the problems of plant transient during beam interruptions. ADS related R&D is underway in various fields such as scenario study, lead-bismuth technology development, nitride fuel and fuel cycle technology development, nuclear data development, and high-intensity accelerator development. Construction of ADS experimental facilities is planned under the JAERI-KEK Joint Project of a high-power proton accelerator.

1. INTRODUCTION

The Japan Atomic Energy Research Institute (JAERI) has carried out R&D on transmutation of long-lived radioactive nuclides are being carried out at under the Japanese long-term program for research and development on partitioning and transmutation technology (OMEGA Program). An emphasis has been placed on dedicated accelerator-driven systems (ADSs) because of its flexibility in designing a minor-actinide (MA) loaded core and large margin for criticality accidents. Earlier design approach [2] of the ADS had followed that of contemporary sodium cooled fast breeder reactors (FBRs). The major reasons to choose sodium as coolant were its excellent thermal performance, good compatibility with stainless steel, and technology maturity.

Recently, a preliminary design study was started for a heavy liquid-metal cooling option [3, 4] of ADS at JAERI. The main reasons for selecting heavy liquid-metal cooling as the primary design option are improved safety and possible reduction of construction cost of the system, together with prolonged lead-time for an experimental system on tens MW scale.

One technical issue that has recently attracted attention in the ADS area is the negative impact of very frequent beam trips as experienced in existing intense accelerator facilities [5]. Frequent beam trips could cause thermal fatigue problem of ADS component materials, leading to degradation of their structural integrity and reduction of their lifetime. They could also badly erode the availability or the capacity factor of ADS, resulting in poor economics. In the development of accelerators for ADS, it is vitally important to establish technologies to achieve a very high degree of reliability. In parallel, it is also important in the development of ADS to design the plant less sensitive to beam trips and structural components to withstand possible thermal fatigues. The experimental program for development and demonstration of lead-bismuth cooled ADS technology is being planned under the Joint Project with KEK (High Energy Accelerator Research Organization). Conceptual design is being made for the ADS experimental facility.

This paper reviews JAERI development of ADS design concepts, describes design of a lead-bismuth cooled, 800-MWt ADS, and presents an analysis of beam trip transient. The ADS related R&D underway is outlined together with a plan of ADS experimental facilities under the JAERI-KEK Joint Project.

2. DEVELOPMENT OF ADS DESIGN CONCEPT

JAERI has developed several concepts of ADS since late of 1980s. In the proposed system, the subcrital core is driven by a high-intensity proton linear accelerator on a continuous wave (CW) mode. The accelerator delivers a several tens of MW beam power at a proton energy around 1.5 GeV. The amount of MA generated in a light water reactor (LWR) of around 1000 MWe capacity is about 25 to 30 kg/y depending on the fuel burnup and the cooling time. The system design aims at designing an ADS which can burn MA from about 10 units of LWR. This calls for an ADS with about 800-MW thermal power. The system has a power generating system to convert the thermal energy into electricity, the part of which is fed to operate the accelerator.

2.1. Dedicated transmutation system in double-strata nuclear fuel cycle

There are two types of proposals for fuel cycle concept involving partitioning and transmutation (P&T). One is an advanced fuel cycle concept, where commercial FBRs are used for transmutation. Another is a concept of double-strata fuel cycle [6], which combines a P&T fuel cycle (the second stratum) with the conventional fuel cycle for commercial power reactors (the first stratum). Dedicated systems specially designed for transmutation purpose could be introduced in the P&T fuel cycle.

There are several advantages of transmutation with dedicated transmutation systems over recycling MAs to commercial power reactors. Because of much smaller mass flow in the P&T fuel cycle, it could be correspondingly smaller in scale than the main cycle. Its separation from the main cycle together with the small number of units required would allow to apply innovative technologies to fuel fabrication, core design and reprocessing for optimizing the P&T part of the overall fuel cycle system. It would avoid burdening the main cycle with the problems associated with higher radioactivity and decay heat, and reduced safety margins in reactor physics parameters. The P&T cycle could be made very compact by co-locating the entire facilities. This would minimize the transportation of nuclides that are troublesome with respect to waste management, and confine them effectively in the P&T fuel cycle.

A dedicated transmutation system can be either a critical system (burner reactor) or a subcritical system (ADS). A core loaded only with MAs (or with MAs and plutonium) could maximize the transmutation rate and thus the support factor. Systems with very high MA loading, however, pose crucial problems related to reactivity coefficients, and to the small delayed neutron fraction. To mitigate these problems for a critical system, a considerable amount of uranium should be added to the MA based fuel, preferably high-enriched uranium to avoid undesirable accumulation of MAs, but this results in reduced transmutation rate. In an ADS, its subcriticality help to mitigate the problems without adding uranium and thus allows to achieve the maximum transmutation rate. For this reason, it can be concluded that an ADS is the best option for dedicated transmutation device.

A special transmutation system operated with a hard neutron energy spectrum and high neutron flux can be efficient and effective for MA transmutation. In this context, JAERI has been pursuing the strategy of transmutation using dedicated ADSs.

2.2. Early ADS concepts

An early concept of ADS [1] is shown in Fig. 1. A proton beam is horizontally injected through a beam window on to a target area of a subcritical core with a rectangular parallelepiped shape. In this design the target material is MA fuel itself with the aim of higher spallation neutron yield. In order to mitigate the heat load in the target area, the beam is expanded to a rectangular shape of dimensions 1×0.1 m. The subcritical core operates at an effective neutron multiplication factor of around 0.95. The core consists of two alloys (Np-22Pu-20Zr and AmCm-35Pu-5Y) clad with HT-9 tube, following those proposed in the early design study of an ABR [7].

The coolant material is liquid metal; sodium or lead-bismuth eutectic (45-55%).

The nuclear spallation reaction and particle transport process above the cutoff energy of 15 MeV were calculated with NMTC/JAERI code [8]. Thermal hydraulic calculations for the target were carried out to determine the maximum achievable thermal power within maximum allowable temperature limits of fuel and cladding.

The maximum power of 236 MW in the lead-bismuth cooled system is considerably lower than 769 MW in the sodium cooled system mainly due to the lower heat transfer capability of the coolant. Since heat removal performance was a major factor to determine the transmutation rate, sodium was concluded to be a better coolant.

It was also concluded the adoption of fuel material as target material was not a good choice. The fuel in the target area generates significant heat both by spallation and fission and this causes the lower core averaged power density due to the higher power peaking (the peaking factor is around 5).

To avoid the high power peaking, non-fissionable material target systems [9] were designed by both of sodium and lead-bismuth cooled systems. In Table 1, the system parameters are compared for the systems with fuel target and tungsten target. In the fuel target systems, actinide fuel is used as target material whereas the tungsten target systems use tungsten pins in 0.6-m long as the spallation target. Tungsten was chosen because of its high spallation neutron yield and high melting point. In the tungsten target system, the thermal power and hence the transmutation rate were almost doubled. It was concluded that non-fissionable material was preferable for a spallation target.

TABLE 1. MAJOR SYSTEM PARAMETERS OF THE REFERENCE SYSTEMS AND THE TUNGSTEN LOADED SYSTEMS

	Fuel target system		Tungsten target system	
Coolant	Na	Pb-Bi	Na	Pb-Bi
Target	MA/Pu pins		Tungsten pins	
Fuel	MA/Pu alloy		MA/Pu alloy	
Actinide inventory, kg	2020	1285	2290	1610
k_{eff}	0.94	0.95	0.92	0.86
Proton beam, GeV-mA	1.5-18.1	1.5-5.4	1.5-22.6	1.5-9.8
Thermal power, MW	405	163	691	342
Power density, W/cc, max./ave.	776/159	425/83	889/307	510/174
Transmutation rate, kg/y (270 days)	114	42	202	89

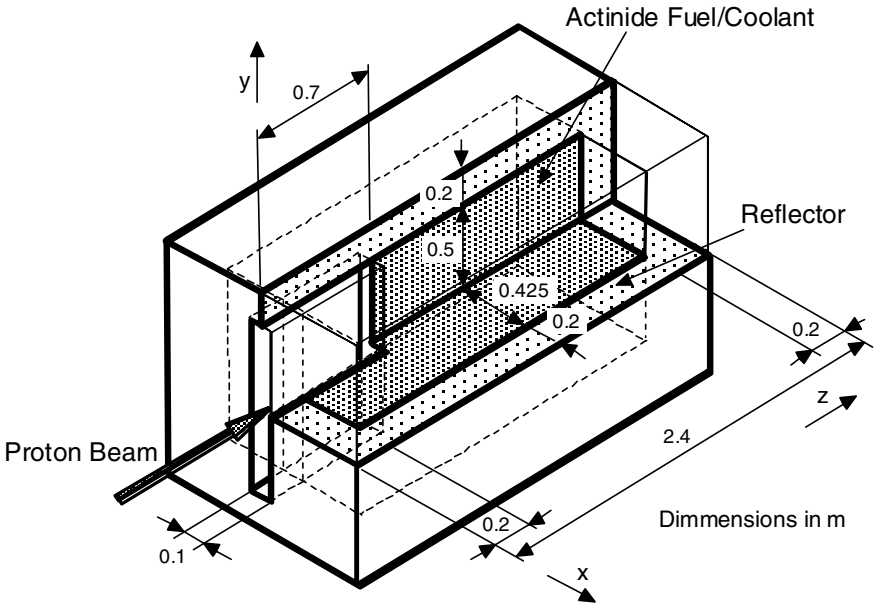

FIG. 1. An early concept of ADS.

2.3. Concept of sodium cooled ADS

Based on the preceding study, sodium cooled ADS was designed to obtain an ADS plant concept. The design follows that of a contemporary LMFBR. A proton beam is injected vertically downward through a beam window into the tungsten target at the center of the subcritical core. Vertical beam injection is preferred to horizontal one particularly for liquid metal cooled systems. The main reasons are safety in case of the window failure, replaceability of the window and the target, flattening of the core power density, and compatibility with the current LMFBR core design. The target is surrounded by the subcritical core loaded with actinide nitride fuel (Fig. 2). The target consisting of multiple layers of tungsten disk with through holes for coolant passage, is designed to maximize the neutron yield and to flatten the axial power distribution. The target and fuel subassemblies are cooled by forced upward flow of primary sodium. The beam window is cooled by impinging coolant flow from the target exit.

In an early design [5], MA metallic alloy was used as fuel for the system. It has been changed to MA mononitride in later designs. Nitride fuel has advantages of excellent thermal property and capability of pyrochemical reprocessing.

With a 1.5 GeV, 33 mA proton beam, the subcritical core having an effective neutron multiplication factor of around 0.95 produces 820-MW thermal power. The net transmutation rate is approximately 10%/y, at a plant load factor of 80%. Heat transport and power conversion systems in the plant design are similar to those for a sodium cooled FBR plant. Electricity of 270 MW is generated through conventional saturated steam turbine. One third of electric power is supplied to its own accelerator. The major parameters of the ADS plant are shown in Table 2.

A wide range of design problems related to the sodium cooled ADS were overviewed [10] with emphasis on target facilities and their interface with accelerators.

TABLE 2. MAJOR PARAMETERS OF THE SODIUM COOLED ADS

Coolant	Na
Target	Tungsten (multi-layered)
Fuel	MA/Pu mononitride
MA/Pu inventory	1950/1300 kg
k_{eff} initial/max./min.	0.93/0.94/0.92
Sodium void reactivity	+4.5% dk/k
Doppler coefficient	-2.2×10^{-4} T dk/dT
Thermal power	820 MW
Transmutation rate	250 kg/y (292 days)
Power density max./ave.	550/380 MW/m^3
Coolant temperature in/out	330/430°C
Coolant velocity max.	8 m/s

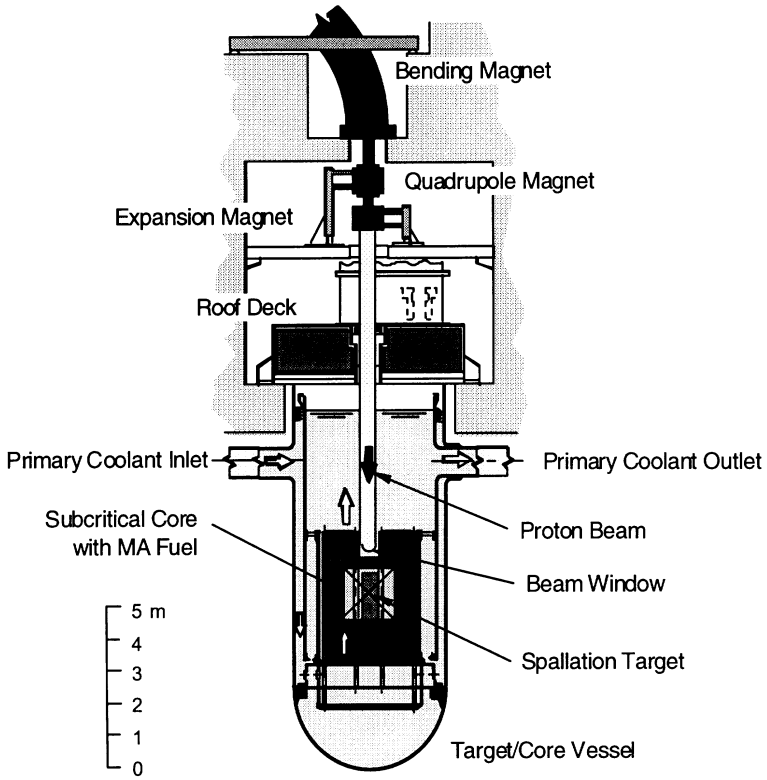

FIG. 2. Conceptual drawing of sodium cooled accelerator-driven transmutation system.

2.4. Molten-salt ADS concept

The molten salt system [11] has been proposed as an advanced option for a dedicated transmutation system in the future. The molten-salt acts both as fuel and as target material, and also serves as coolant. This eliminates the physical and functional separation of target and core, and thus significantly simplifies the target/core configuration as shown in Fig. 3. One of the disadvantages of fluid fuel systems is a large actinide fuel inventory. To reduce the primary molten-salt inventory, main pumps and heat exchangers are contained within a primary vessel.

Chloride salt with a composition of $64NaCl\text{-}5PuCl_3\text{-}31MACl_3$ was chosen for the primary candidate considering actinide solubility, hard neutron energy spectrum and operating temperature. In the 800-MW molten-salt system of an effective multiplication factor of 0.92 with a 1.5-GeV, 25-mA proton beam, the transmutation rate is approximately 250 kg/y, or 4.6% of inventory per year with a load factor of 80%.

Another candidate fuel for a fast-spectrum molten-salt system is $PbCl_2\text{-}AnCl_3$ (An actinide). A preliminary comparative study [12] was made for the sodium-based and lead-based molten-salt systems. Table 3 compares the parameters of the both systems. The difference seems not to be large, but the results are not conclusive due to the lack of reliable property data for these salts. Other major issues of the molten-salt concept are the compatibility of structural material exposed to a high-temperature flowing chloride salt, and the safety concern of reduced defense-in-depth.

TABLE 3. COMPARISON OF SODIUM-BASED SALT AND LEAD-BASED SALT SYSTEMS AVERAGED OVER TARGET/CORE REGION, EXCLUDING IHX REGION

Target/coolant	Molten-chloride-salt	
Salt	$64NaCl\text{-}36AnCl_3$	$70PbCl_2\text{-}30AnCl_3$
k_{eff}	0.93	0.88
Proton beam, GeV	1.5	1.5
Neutrons per proton	37	40
Average neutron energy*, keV	800	768
Power density, keV/cm^3/p, max./ave.	66/27	54/16
Peaking factor	2.5	3.5
Primary system volume, m^3	2.7	3.2
Molten-salt/actinide inventory, kg	10 000/5 400	17 000/4 100

*averaged over target/core region, excluding IHX region.

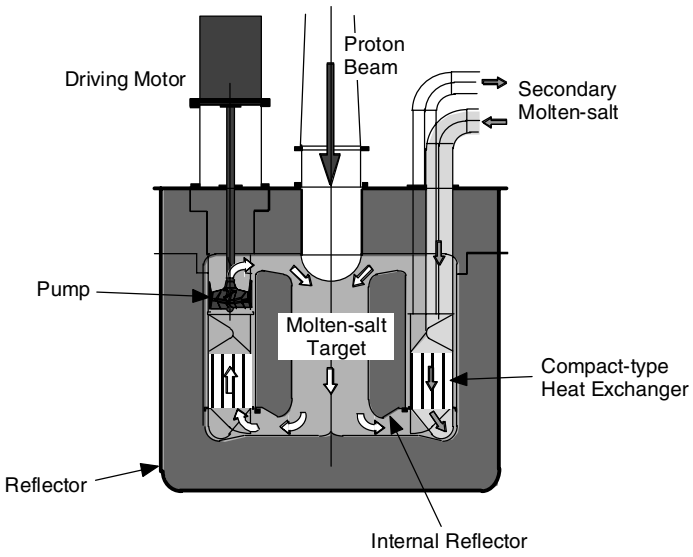

FIG. 3. Concept of molten-salt ADS.

TABLE 4. MAJOR SYSTEM PARAMETERS OF THE PB-BI COOLED ADS

Target/coolant	Pb-Bi
Fuel	MA/Pu mononitride
Fission thermal power	800 MW
Core height/radius	1000/1200 mm
k_{eff} initial/max./min.	0.95/0.95/0.93
Power density max./ave.	310/180 MW/m^3
MA/Pu inventory	2500/1660 kg
Coolant temperature in/out	330/430°C
Coolant velocity max.	2 m/s
Transmutation rate	500 kg/cycle (20%/cycle)

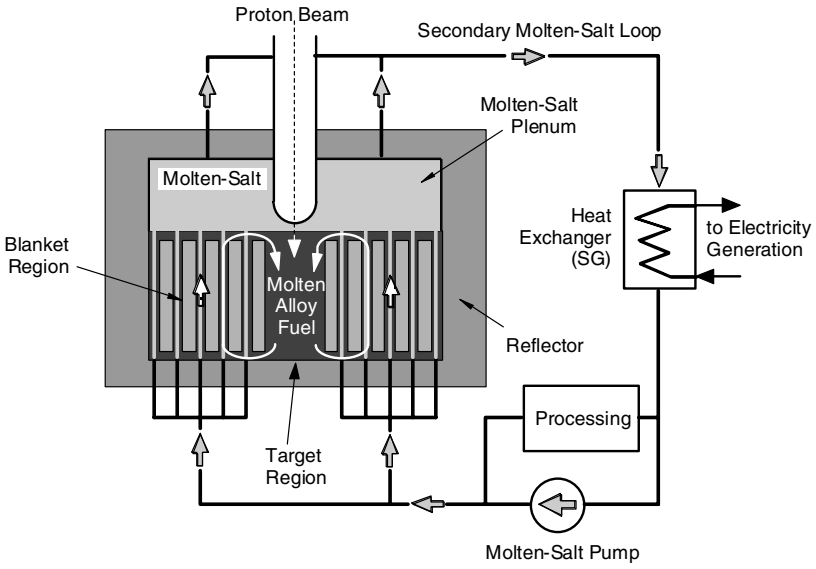

FIG. 4. Concept of molten-alloy ADS.

2.5. Molten-alloy ADS concept

Molten actinide alloy could be another possible liquid target/fuel for a fast neutron system. An evolutionary concept [13] was studied to achieve a minimum inventory with molten-alloy fuel. Figure 4 shows a concept of a molten-alloy ADS. The system is composed of a molten alloy target/fuel, a graphite blanket with vertical coolant channels, and an upper plenum of molten fluoride salt. The preliminary study was performed on the alloy with the composition (11-32.5)Np-(4-12.5)Pu-24Co-(60-30)Ce-Tc.

The secondary molten fluoride salt (Li_2BeF_4) directly contacts with the molten alloy through the vertical channels in the blanket. Efficient heat, mass and momentum transfer is expected at the contact interface between two co-current fluids. This eliminates the need of primary molten-alloy pumps and heat exchanger hardware.

The system with the effective neutron multiplication factor of 0.9 transmutes 145 kg of actinide per year with 1.5-GeV, 16-mA proton beam and produces 455-MW thermal power.

Advantages of the molten-alloy system are a small actinide inventory, and a high transmutation rate, together with the possibility of continuous on-line charging of minor actinides and removing of reaction products. The system, however, poses the problems of material compatibility and safety. The design study of fluid-fuel systems was discontinued due to the lack of data to detail the design and the safety concern of reduced defense-in-depth.

2.6. Lead-bismuth cooled ADS

Conceptual design studies have been carried out on a lead-bismuth cooled ADS [3, 4]. Lead-bismuth is used as both coolant and spallation target material. Lead-bismuth eutectic coolant allows operating the system at about the same temperature level as sodium coolant, much lower than the case of lead coolant. In comparison with sodium, it offers the possibilities to achieve a harder neutron energy spectrum, and to avoid a positive void reactivity. It is also possible to eliminate secondary heat transport loops and associated intermediate heat exchangers because lead-bismuth does not exothermically react with water and air. Technology of lead-bismuth is less mature than that of sodium though Russia has experience of developing lead-bismuth cooled reactors for submarine propulsion.

A conceptual drawing of the lead-bismuth cooled ADS is presented in Fig. 5. An accelerator injects 1.5 GeV proton beam through a beam window into the spallation target region located at the center of the subcritical core. Fuel material of the subcritical core is actinide mono-nitride.

The core is contained within a primary vessel made of steel. All other components of the primary system, including steam generators, main pumps, and auxiliary heat exchangers, are accommodated within the vessel. This tank-type configuration eliminates the need of heavy primary piping. The steam generators are of recirculation, separate type. Separate type steam generators allow the reduction in the depth of the beam window immersed in the lead-bismuth pool compared to integral type steam generators, and thus the reduced pressure load of the beam window. The vessel size and the lead-bismuth inventory of the system with the separate-type steam generators are much larger than those with integral-type steam generators. However, large lead-bismuth inventory slows the temperature transient caused by an accelerator beam trip. Recirculation type steam generators respond much more slowly in beam trip transient compared to one-through type steam generators because of a large heat capacity of steam drums. A disadvantage of recirculation type steam generators is a smaller temperature difference between the lead-bismuth and water/steam sides, resulting in a larger heat transfer area. Dimensions shown in Fig. 5 are based on the four-loop design.

The auxiliary cooling system with lead-bismuth loops is provided as an independent means for decay heat removal, and is also used for preheating of lead-bismuth coolant. The operating temperature range of the primary lead-bismuth is from 330 to 430°C, which is about 100°C lower than those for commercial LMFBR designs. Consequently, the power conversion system operates in a saturated steam turbine cycle used for conventional LWRs with efficiencies around 35% rather than a super-heated steam turbine cycle used for commercial sodium cooled FBRs with efficiencies above 43%. The lead-bismuth temperature rise through the core is 100°C, which is about 50°C lower than those for commercial sodium cooled FBRs. The lower operating temperature is expected to mitigate the material corrosion/erosion problem in lead-bismuth.

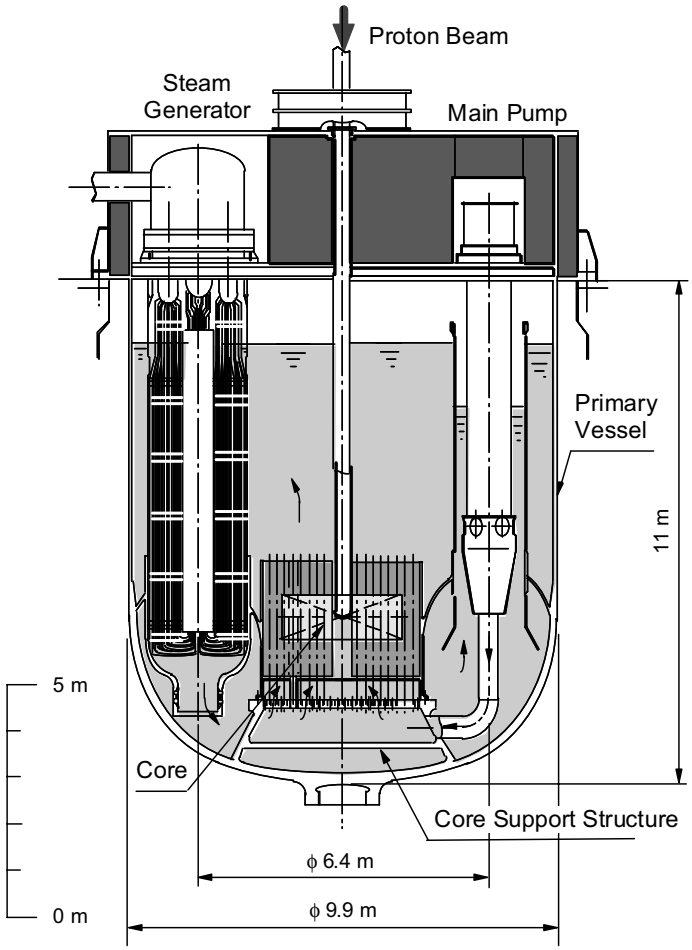

FIG. 5. Concept of Pb-Bi cooled accelerator-driven transmutation system.

TABLE 5. NOMINAL OPERATING PARAMETERS OF THE ADS PLANT

SG Outlet steam pressure	7.0 Mpa
SG Outlet steam temperature	285°C
SG Pressure drop	1.6 Mpa
Recirculation piping pressure drop	0.05 Mpa
Steam piping pressure drop	0.05 Mpa
Recirculation water flow rate	7.88×10^5 kg/h (per loop)
Turbine inlet steam pressure	6.0 Mpa
Turbine inlet steam temperature	275°C
Turbine inlet steam flow rate	1.58×10^6 kg/h
Turbine back pressure	0.005 Mpa
Electric power	280 MW

Corrosion/erosion is one of the major technical issues in lead-bismuth cooled systems. Chromium molybdenum steel (2.25Cr-1Mo steel, 9Cr-1Mo steel, etc.) is a candidate material for structural components in the primary system, as it is expected to have acceptable corrosion resistance, mechanical strength and ductility. The saturated steam turbine cycle is more tolerant in beam trip transients, since the saturated steam turbine is much more resistant to degradation of steam condition than the super-heated one. The lower temperature rise leads to lower temperature swing of the core exit lead-bismuth on beam trip and beam recovery.

The ADS has to be designed to withstand the very frequent beam trip transients that cause frequent thermal cycles of the plant components. In our design, the coolant inventory is large due to the tank-type configuration, relatively low temperature rise through the core, and the saturated steam cycle. The plant response to a beam trip is slow owning to the large coolant inventory and this mitigates the thermal stress problems.

The major system parameters designed are summarized in Table 5. In this design, the system consists of a 1.5-GeV, 14-mA proton accelerator and the 800-MWt subcritical core of the effective neutron multiplication factor of 0.95. The transmutation rate is approximately 250 kg/y when the load factor is 80%. An electric output of 280 MW is obtained at a plant thermal efficiency of 35%.

3. ANALYSIS OF BEAM TRIP TRANSIENT IN ADS

In ADS, a beam trip causes an abrupt drop of core thermal power very similar to the case of a scram in a critical reactor. There are two substantial differences between them from a system design standpoint. Beam trip analyses are reported for LANSCE [14] and for SINQ [15]. One of the differences is the frequency of the event. Beam trips in an ADS would be much more frequent than reactor scrams. The other is the duration of down time. The main source of beam trips occurring at the existing accelerator facilities is failure of RF system. Majority of the beam trips are of short duration, say within few minutes, and the beam recovers from them automatically. For this reason, an ADS has to maintain full flow while awaiting beam recovery.

Figure 6 is a simplified flow diagram of the ADS. Primary lead-bismuth coolant flows upward through the core and exits into the upper plenum. Then, the coolant flow divides equally among four steam generators. The flow through steam generator heat transfer sections enters a lower plenum. The coolant is then returned back to the core by primary main pumps. The water/steam system has four steam drums, four recirculation water pumps, a turbine-generator unit, and a feed water pump. Steam raised in the steam generators is directed to the steam drums. The steam from all the four steam drums combines and drives the turbine-generator unit. The steam is cooled down into water in a condenser at the turbine exit, and the feed water pump returns the water back to the steam drums through a feed water heater not shown in the figure. The recirculation water pump delivers the water from the steam drum to the steam generator.

The analysis dealt with one single loop, under the assumption of the equal operating condition among all the four symmetric loops. The lead-bismuth primary system and the secondary water/steam system were modeled with a simple one-dimensional flow network. The primary system was subdivided into three plenum sections (a core upper plenum, a steam generator inlet plenum, and a core lower plenum) and two components (a core and a steam generator). The primary lead-bismuth coolant was assumed to be fully mixed in the plenums, and the thermal power was given as a boundary condition in the core. In the steam generator, heat transfer was calculated using five empirical equations of heat transfer coefficient: one for the lead-bismuth side and four for the water/steam side (pre-heater region, nucleate boiling region, film boiling region and super-heater region). In the power conversion loop, the recirculation water pump head, the feed water pump flow rate and the turbine back-pressure were given as boundary condition. The steam drum was modeled as a lumped system of saturated water/steam including phase changes. The water in the drum was assumed to be controlled at a constant level. The turbine was modeled using a simple relation among the steam mass flow rate, the inlet pressure, the back-pressure, and the inlet temperature. The

turbine power was assumed proportional to the inlet steam flow rate and the enthalpy difference from the turbine inlet to outlet. The conversion efficiency from thermal to electric power was assumed 35% (constant). The feed water heating was not explicitly simulated in the analysis, but the temperature of the feed water was given as a function of the turbine inlet steam flow rate, neglecting the delay due to steam-to-water heat transfer.

With this flow network model, transient pressures, flow rates, and enthalpies were solved from simultaneous equations of energy conservation, mass conservation, momentum conservation and state. The density, the thermal conductivity, the kinetic viscosity, and the Prandtl number of lead-bismuth were given as functions of temperature [16]. Property of water/steam was based on JSME Steam Tables [17].

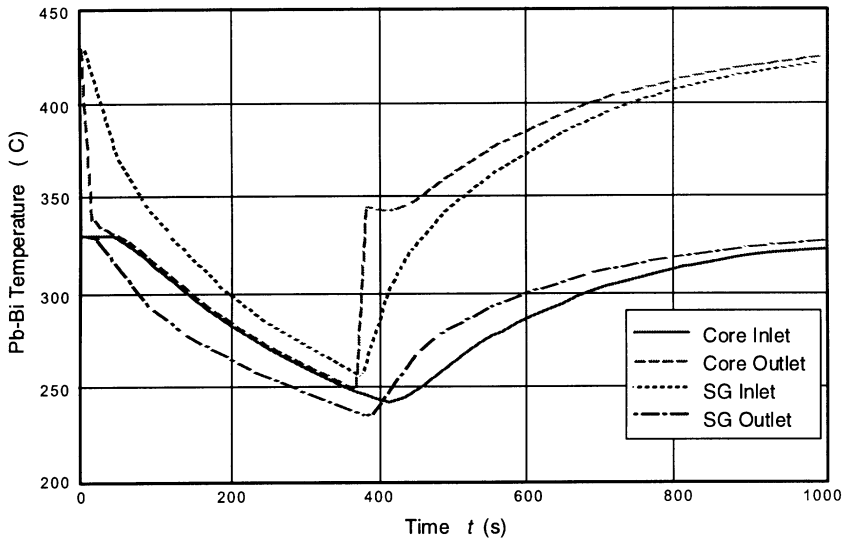

FIG. 7. Temperature change in primary lead-bismuth system during beam trip transient.

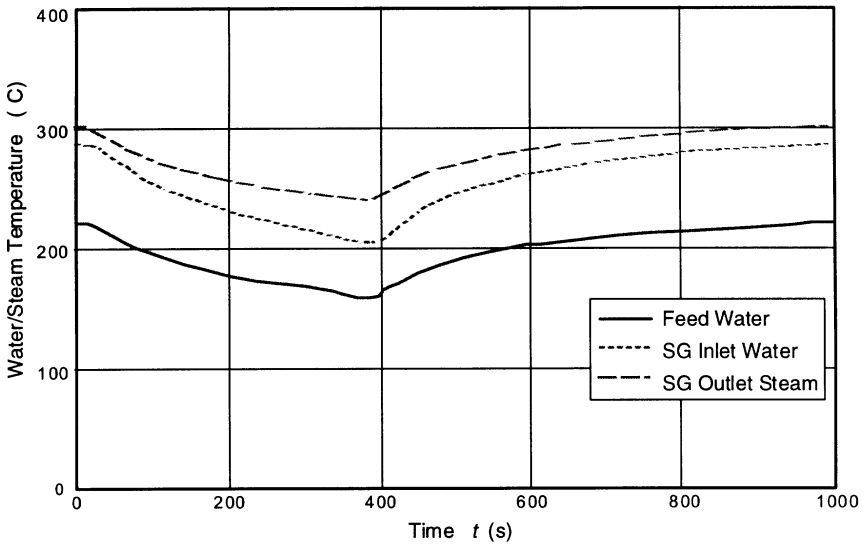

FIG. 8. Temperature change in secondary water/steam during beam trip transient.

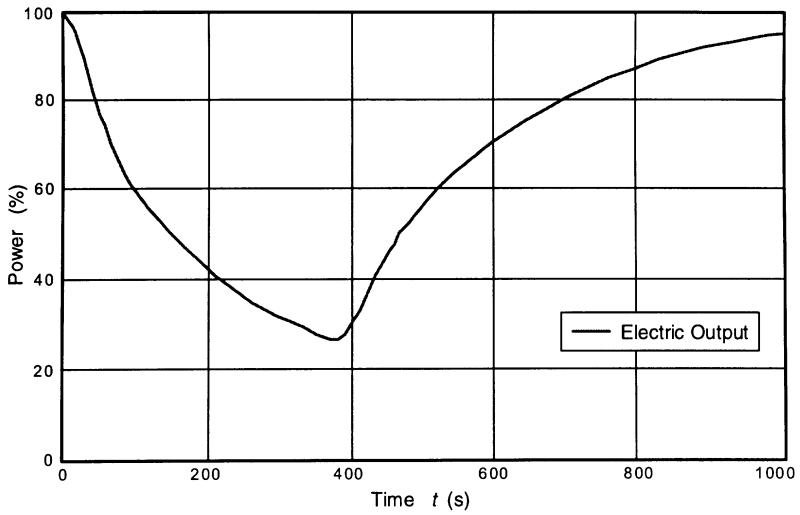

FIG. 9. Electric power generation during beam trip transient.

Results presented here are for the case when the beam is recovered 370 s after the beam trip. A beam down time longer than 380 s requires plant and turbine trips to avoid overcooling. Overcooling could cause damages of primary system components by freezing of lead-bismuth and erosion of the turbine blades from by wetting of steam.

The temperature response of lead-bismuth primary coolant is shown in Fig. 7. On beam trip at t = 0, the core outlet temperature starts to drop rapidly and asymptotically approaches to the core inlet temperature within about 10 s. The coolant temperature at the steam generator inlet responds more slowly because of coolant mixing in the upper plenum. It takes about 120 s for the steam generator inlet temperature to drop down to the initial core inlet temperature. The coolant temperature at the steam generator outlet decreases almost proportionally to that at the steam generator inlet. The temperature change at the core inlet further delays because of coolant mixing in the lower plenum. At t = 370 s when the beam turns on, the core outlet temperature shows a rapid rise from its minimum at 250°C by about 100°C, and then a slight temperature decrease due to the time lag of the core inlet temperature response. The minimums of the steam generator inlet and outlet temperatures occur at about 380 s (10 s after the beam recovery). The core inlet temperature reaches its minimum at about 410 s. The coolant temperatures at the steam generator inlet, the steam generator outlet, and the core inlet increase monotonically from their minimums, and approach to their initial values. It takes around 1000 s after the beam-on before the initial condition is restored. Temperature swings of the primary coolant during the beam trip transient range from 88 to 185°C. The water/steam temperature in the power conversion system is shown in Fig. 8. The water/steam temperatures show similar response to the lead-bismuth temperatures at the steam generator inlet and outlet. The difference between the steam generator inlet temperature and the feed water temperature is kept almost constant at about 80°C. The temperature rise through the steam generator increases as the temperature decreases. This indicates worsening of the steam quality at lower temperatures. Compared to the primary lead-bismuth, the water/steam shows damped temperature swings within 82°C. The electric power generated is shown in Fig. 9. The electric power is nearly proportional to the turbine inlet flow rate, because the enthalpy change of steam at the steam drum outlet is not so large and the enthalpy of the turbine outlet steam is kept constant. The minimum of the electric power is 27% (76 MWe) at about 380 s.

The proposed ADS incorporates several design features to withstand the short beam interruptions that would occur much more frequently than the scrams in a critical reactor.

Transient analysis showed that the plant and the turbine survive beam trip transients shorter than 370 s without trips and special controls. It is concluded that an accelerator-driven system can be designed to alleviate adverse effects of beam trips to acceptable level.

4. ADS RELATED R&D

4.1. Scenario studies [8]

Scenario studies were made to evaluate the effectiveness of ADS introduction into the future fuel cycle for transmutation of MA and iodine. Scenarios assume the nuclear power capacity reaches at a level of 140 GWe in 2100 and levels out thereafter. For a symbiosis system consisting of UO_2/MOX-LWRs, FBRs and ADSs, MA and iodine accumulated become about 150 and 20 tons in 2040, and 900 and 200 tons in 2200, respectively. When the deployment of ADS starts in 2040, MA and iodine become about 250 and 50 tons in 2200.

4.2. Development of partitioning process [19, 20]

A hot verification test of the four-group partitioning process (4-GPP) with concentrated real HLLW was carried out in the Partitioning Test Facility in the hot cell. For the preparation of the concentrated HLLW, about 14 L (11 TBq) of the raffinate from the co-decontamination cycle of Purex Process were first denitrated and then concentrated to about 2.5 L. The raffinate was obtained by two reprocessing tests with about 1 kg of spent fuel burned up to 8 000 MWd/t and with about 1.5 kg of spent fuel burned up to 31 300 MWd/t. Results of the present test well agreed with the either result of previous tests using the unconcentrated real HLLW and the simulated HLLW added with a small amount of real HLLW. More than 99.998% of Am were extracted from the HLLW with the organic solvent containing 0.5M DIDPA-0.1M TBP, and 99.986% of Am were back-extracted with 4M nitric acid. Cadmium showed the same behavior as Am. Neptunium and plutonium were extracted simultaneously in a high yield, and more than 99.9% of them were back-extracted with oxalic acid.

The present 4-GPP necessitates a denitration-filtration step to reduce the acidity of an aqueous feed to a level compatible with DIDPA. It was found that a tridentate diglycolamide (DGA) with an ether oxygen at a center of diamide molecule forms more stable complex with trivalent actinides and lanthanides than that of bidentate malonamides. The effect of chain length of alkyl groups was examined, and a ligand, tetraoctyl 3-oxapentandiamide (TODGA) was selected as the best DGA-extractant. To develop a TODGA-partitioning process, fundamental studies on the extraction behavior and radiolytic degradation were carried out. The results revealed that the TODGA is a satisfactory extractant to be applied to the separation process of actinides and lanthanides (III) in the 4-GPP.

4.3. Fuel fabrication and reprocessing technology [21]

Fabrication of Pu and MA-bearing nitrides and preparation of the thermodynamic database have been carried out besides the irradiation tests of (U,Pu)N fuel up to 4.6 at%. High-purity AmN and (Pu,Cm)N were fabricated by carbothermic reduction of the dioxides. X-ray diffraction patterns showed almost the single phase of NaCl-type structure. PuN pellets containing inert matrix nitrides such as ZrN and TiN were fabricated and characterized. Vapor pressure of Np(g) over NpN, (U,Np)N and (Np,Pu)N was measured by high-temperature mass spectrometry. Measurements of heat capacity and thermal expansion of NpN and PuN are underway. The irradiation of two $(U_{0.8}Pu_{0.2})N$ fuel pins at JOYO was completed in 1999 under the joint research with JNC. The non-destructive and destructive post irradiation examinations are underway and any failure of fuel pins was not observed.

As for pyrochemical process, the electrochemical dissolution behavior of NpN and PuN were measured by cyclic voltammetry and the equilibrium potentials of the nitrides in LiCl-KCl eutectic melt were determined. The electrochemical deposition behavior of Pu at liquid Cd cathode was investigated. In this case the potential of deposition and dissolution shifted positively compared with the case of solid cathode in correspondence with a thermodynamic stabilization by formation of intermetallic compound. The formation of $PuCd_6$ phase was observed at the cathode by microprobe analysis. By adjusting electrochemical parameters such as current density during electrolysis, 10-g scale of Pu was recovered at liquid Cd cathode with high Pu concentration. In addition, the electrochemical deposition behavior of Np at liquid Cd cathode and the phase relationship of Am-Cd binary system were experimentally studied. Nitrogen releasing behavior from NpN and PuN at an anode, and the results of distillation and nitrization of the Cd cathode after the electrolysis were examined. It was proved that the pyrochemical process is fundamentally suitable for N-15 recovery compared with the wet process.

4.4. Lead-bismuth technology

A small-scale lead-bismuth loop with 5-L/s flow-rate was constructed to test the material compatibility with lead-bismuth and to develop oxygen monitor and control technology. Experiments were started for candidate structural materials such as 316L, F82H, F82H ODS, Mo-Cr steel, etc., in the temperature range form 300 to 400°C.

4.5. Nuclear data and file for ADS application [22, 23]

The JENDL Actinides File was developed to supply actinides data for transmutation. The file contains about 90 nuclides from Tl-208 to Fm-255 whose half-life exceeds 1 day. The JENDL High Energy File was developed to supply high energy data for ADS and other accelerator applications. The file includes nuclear data for proton- and neutron-induced reactions up to about 3.0 GeV.

4.6. Development of neutronics design codes [24]

A code system “ATRAS” was developed for neutronics design study of ADS, The code system consists of the nucleon-meson transport code NMTC/JAERI97, the Sn code TWODANT, and the burnup analysis code BURNER. The 73-group cross section library processed from the nuclear data file of JENDL-3.2 is used for transport and burnup calculation. The cross section library contains the data of about 150 nuclides including the actinides from Th-232 to Cf-252 and lumped data for fission products.

4.7. High-intensity proton accelerator development [25-28]

A proton source and a pulsed radio-frequency quadrupole linac (RFQ) were developed as a first step of R&D. The RFQ was designed for 2 MeV-100 mA (peak) beam at 10% duty factor. The maximum RFQ output current achieved was 70 mA at the ion source extraction current of 155 mA at 10% duty facto and 100 mA, at 1% duty factor. A drift tube linac (DTL) hot test model with 9 cells for mock-up of the first part of the DTL was fabricated to study the RF characteristics and the cooling capabilities. Duty factors of 20 and 50% were achieved for field gradients of 2 MV/m and 1.5 MV/m, respectively.

In the superconducting (SC) linac part, the proton velocities β gradually change from 0.43 to 0.92 corresponding to the energy change from 100 MeV and 1.5 GeV. The main concern is the strength of the cavity under the vacuum load for the low β region ($\beta < 0.7$). Mechanical

structure calculations were made to determine cavity shape and electromagnetic parameters. For the development of SC cavities, a test stand equipped with a cryostat 350 cm long and 80 cm diameter and a clean room were constructed. Two sets of single niobium SC test cavities of $\beta = 0.5$ were fabricated by the processes of cold rolling, press of metallic sheet and electron beam welding. The surface was treated by barrel polishing, electro-polishing and high- pressure water rinsing. In so-called vertical tests, the maximum surface peak field of 24 MV/m at 4.2 K and 44 MV/m at 2.1 K were successfully obtained for the second cavity. A single cell cavity of $\beta = 0.89$ and 5-cell cavities of $\beta = 0.5$ and 0.89 were also fabricated and tested successfully.

5. ADS EXPERIMENTAL FACILITY

Experimental programs for ADS developments have been planed within the framework of the JAERI-KEK Joint Project for High-Intensity Proton Accelerators. A full-scale ADS will be driven by a CW proton beam. However, the ADS experimental facilities in the High-Intensity Proton Accelerator Project will be operated on a pulsed mode with a repetition rate of 25 Hz. In the later stage of the development, a CW beam is essential to demonstrate the technology. The experimental facilities will consists of the Reactor Physics Experimental Facility (PEF) and the Engineering Experimental Facility (EEF). The conceptual layout of PEF and EEF is shown in Fig. 10.

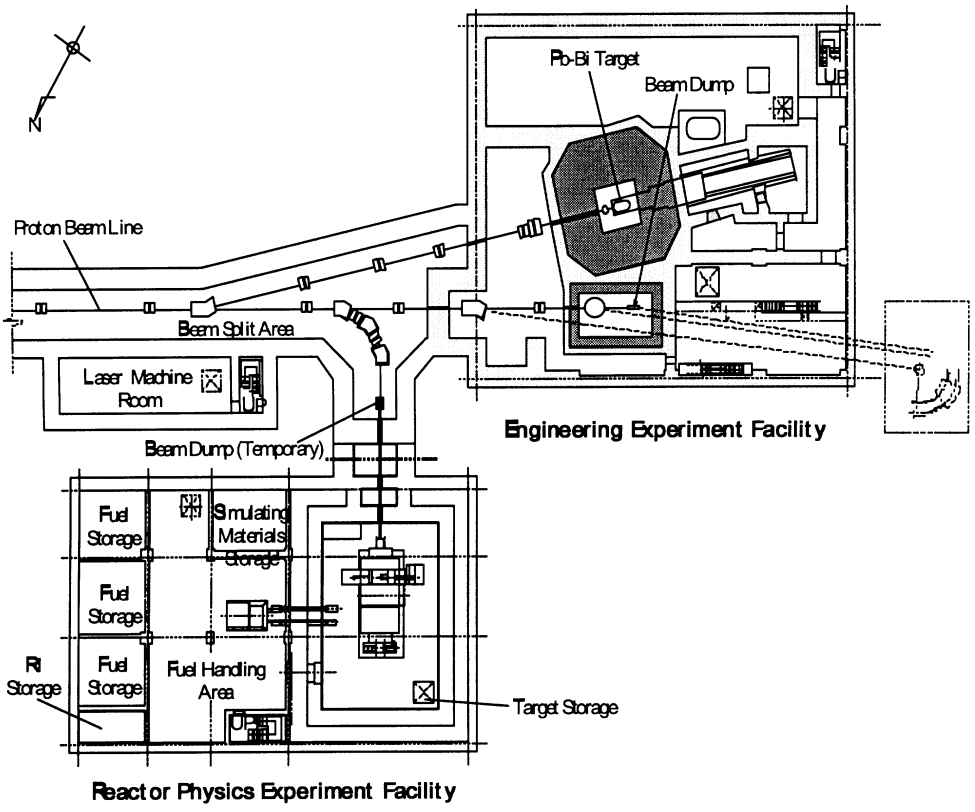

FIG. 10. Conceptual layout of the ADS experimental facilities.

5.1. Reactor physics experiment facility – PEF

Reaction rate ratio and distribution, neutron spectrum, space and time dependent neutron flux, effects of high energy neutron, and the degree of subcriticality are to be measured in reactor physics experiments with a subcritical core. The experimental items relating to system

operation/control are beam-power adjustment, control scheme, beam-trip effects, and restarting procedures after short beam trips.

The design of PEF is based on that of the fast critical assembly FCA of JAERI. Fuel will be 20% enriched uranium oxide and the effective neutron multiplication factor is in the range 0.90-1.0. Experiments at the critical state will be carried out as the step for the precise measurement of reactivity and subcriticality. The maximum proton beam power and core thermal power are limited to 10 and 500 W, respectively. Experiments at the critical state will be also carried out as the step for the precise measurement of reactivity and subcriticality. Reactor physics experiments of the subcritical core and demonstration of the principle of the ADS is to be performed at PEF. The experiments include testing of the instrumentation and the control system.

5.2. Engineering experimental facility - EEF

EEF is designed to test and demonstrate lead-bismuth target technology. The 600-MeV linac delivers 0.3-mA proton beam (200 kW) to EEF. The 200-kW beam power on a lead-bismuth target provides a suitable experimental condition for the material testing and the target system demonstration. In latter phase, the beam power to EEF will be increased up to 2 MW. This upgrade will extend the coverage and volume of experiments.

6. CONCLUSION

Design studies were made on various type of accelerator driven system for nuclear waste transmutation. The current reference design employs lead-bismuth target/coolant and MA nitride fuel cooled ADS. The system consists of a 1.5-GeV, 14-mA proton accelerator and an 800-MWt subcritical core with an effective neutron multiplication factor of 0.95. The transmutation rate of MA is approximately 250 kg/y at 80% load factor. The system incorporates several design features to withstand the short beam interruptions that would occur much more frequently than the scrams in a critical reactor. Transient analysis showed that the plant and the turbine survive beam trip transients shorter than 370 s without trips and special controls. It is concluded that an accelerator-driven system can be designed to alleviate adverse effects of beam trips to acceptable level.

JAERI R&D related to ADS includes scenario studies, development of partitioning process, development of fuel fabrication and reprocessing technology, development of lead-bismuth technology, development of data and codes, and development of high-intensity accelerator.

ADS experimental facilities are planned under the JAERI-KEK Joint Project for High-Intensity Proton Accelerators.

REFERENCES

[1] TAKIZUKA, T., et al., A Study on Incineration Target System, Proc. 5th Int. Conf. On Emerging Nuclear Energy Systems (ICENES'89), 1989, Karlsruhe, Germany, U. von-Moellendorf and B. Goel (Eds), Kernforschungszentrum, Karlsruhe (1989) 70.

[2] TAKIZUKA, T., et al., Conceptual Design of Transmutation Plant, Meeting on Accelerator-Driven Transmutation Technology for Radwaste and Other Applications, Stockholm, 1991, jointly published by LANL, US and SKN, Sweden as LA-12205-C SKN Report No. 54 (1991) 707.

[3] TSUJIMOTO, K., et al., Conceptual Study of the Lead-Bismuth Cooled Accelerator-Driven Transmutation System, Proc. 2nd Int. Topical Mtg. on Nuclear Applications of Accelerator Technology (AccApp'98), 1998, Gatlinburg, Tennessee, USA, ANS, ISBN: 089448-633-0 (1998) 137.
[4] TAKIZUKA, T., et al., Heavy Liquid-Metal Cooling Option of JAERI Accelerator-Driven Transmutation Systems, Proc. Int. Conf. on Heavy Liquid-Metal Coolants in Nuclear Technologies (HLMC'98), 1998, Obninsk, Russian Federation, CRS4, TECH-REP-00/50 (1999) 143.
[5] TAKIZUKA, T., Effects of Accelerator Beam Trips on ADS Components, Proc. OECD/NEA Workshop on Utilization and Reliability of High Power Accelerators, Mito, Japan, 1998, NEA, ISBN: 92-64-17068-5 (1998) 317.
[6] MUKAIYAMA, T., Importance of Double Strata Fuel Cycle for Minor Actinide Transmutation, Proc. 3rd OECD/NEA Information Exchange Meeting on P&T, Cadarache, France, NEA (1994) 30.
[7] MUKAIYAMA, T., et al., Conceptual Study of Actinide Burner Reactors, Proc. International Reactor Physics Conference, Jackson Hole, Wyoming, USA, Vol. 4, ANS (1988) 369.
[8] NAKAHARA, Y., TSUTSUI, T., NMTC/JAERI - A Simulation Code System for High Energy Nuclear Reactions and Nucleon-Meson Transport Process, JAERI-M 82-198 (1982) (in Japanese).
[9] TAKIZUKA, T., et al., A Conceptual Study of Actinide Transmutation System with Proton Accelerator Target Thermal Hydraulics, Proc. 2nd Int. Symposium on Advanced Nuclear Energy Research Evolution by Accelerators, Mito, Japan, 1990, JAERI (1990) 381.
[10] TAKIZUKA, T., Overview on Nuclear Design Problems of Accelerator-Based Transmutation Systems with Emphasis on Target Facilities and Their Interfaces with Accelerators, Proc. OECD/NEA Specialists' Meeting on Accelerator-Based Transmutation, PSI Villigen, Switzerland, NEA (1992) 112.
[11] KATO, Y., et al., Accelerator Molten Salt Target System for Transmutation of Long Lived Nuclides, Proc. OECD/NEA Specialists' Meeting on Accelerator-Based Transmutation, PSI Villigen, Switzerland, NEA (1992) 133.
[12] TAKIZUKA, T., et al., Conceptual Design Study of Accelerator-Driven Systems for Nuclear Waste Transmutation, Proc. 2nd Int. Conf. on Accelerator-Driven Transmutation Technologies and Applications (ADTT'96), 1996, Kalmar, Sweden, H. Condé (Ed.), Uppsala University (1997) 179.
[13] KATSUTA, H., et al., A Concept of Accelerator-Based Incineration System for Transmutation of TRU and FP with Liquid TRU-Alloy Target and Molten-Salt Blanket, Proc. 7th Int. Conf. on Emerging Nuclear Energy Systems (ICENES'93), 20-24 September 1993, Makuhari, Japan, World Scientific Press, ISBN: 981-02-1719-6 (1993) 424.
[14] ERIKSSON, M., PIASZCZYK, C., Reliability Assessment of the LANSCE Accelerator System, Proc. OECD/NEA Workshop on Utilisation and Reliability of High Power Proton Accelerators, Mito, Japan, 1998, NEA, ISBN: 92-64-17068-5 (1999) 183.
[15] BAUER, G., et al., Beam Trips and Target/Subcritical Reactor Problems in Accelerator Driven Systems, Proc. OECD/NEA Workshop on Utilisation and Reliability of High Power Proton Accelerators, Mito, Japan, 1998, NEA, ISBN: 92-64-17068-5 (1999) 355.
[16] JSME Data Book, Heat Transfer, 4th Edition, JSME (1986).
[17] JSME Steam Tables, 4th Edition, JSME (1981).

[18] TAKANO, H., et al Study on a Lead-Bismuth Cooled Accelerator-Driven Transmutation System, paper presented in the 6th OECD/NEA Information Exchange Meeting on Actinide and Fission Product Partitioning and Transmutation, 11-13 December 2000, Madrid, Spain, NEA, EUR 19783 EN (2001).
[19] MORITA, Y. et al., A Demonstration of 4-Group Partitioning Process with Real High-Level Liquid Waste, Proc. Int. Conf. ATALANTE 2000 - Scientific Research on the Back-End of the Fuel Cycle for the 21st Century, 24-26 October 2000, Avignon, France, CEA Cadarache (2000).
[20] SASAKI, Y., et al., Actinide Separation with a Novel Tridentate Ligand, Diglycolic Amide for Application to Partitioning Process, ibid. (2000).
[21] ARAI, Y., OGAWA, T., Research on Nitride Fuel and pyrochemical Process for MA Transmutation, paper presented in the 6th OECD/NEA Information Exchange Meeting on Actinide and Fission Product Partitioning and Transmutation, 11-13 December 2000, Madrid, Spain, NEA, EUR 19783 EN (2001).
[22] NAKAGAWA, T., et al., Japanese Evaluated Nuclear Data Library Version 3 Revision-2: JENDL-3.2, J. Nucl. Sci. Technol., 32, 1259 (1995).
[23] NAKAGAWA, T., et al., Present Status of Minor Actinide Data, International Evaluation Co-operation Report, Vol. 8, OECD/NEA (1999).
[24] SASA, T., et al., Accelerator-driven Transmutation Reactor Analysis Code System -ATRAS-, JAERI-Data/Code 99-007 (1999).
[25] MIZUMOTO, M., et al., A High Intensity Proton Linac Development for JAERI Neutron Science Project, Proc. Conf. LINAC98, Chicago, USA, CERN (1998).
[26] Hasegawa, K., et al., System Design of a Proton Linac for the Neutron Science Project at Japan Atomic Energy Research Institute, Jour. Nucl. Sci. Technol. 36, No. 5 (1999) 451.
[27] KUSANO, J., et al., Development of Superconducting Single Cell Cavity for a Proton Linac in the Neutron Science Project at JAERI, Proc. 6th European Particle Accelerator Conference (EPAC98), 22-26 June 1998, Stockholm, Sweden, Institute of Physics Publishing, Philadelphia, PA, USA, ISBN: 07503 0580 (CD-ROM)(1998).
[28] OUCHI, N., et al., R&D Activities for Superconducting Proton Linac at JAERI, Proc. Int. Conf. on Asian and Pacific Coasts (APAC98), 1998, Tsukuba, Japan, CERN, Geneva (1998).

STATUS OF THE NEW NUCLEAR ENERGY SYSTEMS STUDY IN CIAE

D. DING, Z. LUO, M. XU
China Institute of Atomic Energy, Beijing, China

Abstract

The nuclear energy civil-application has been started in China. To meet the long-term sustainable primary energy supply it could be envisaged that the nuclear power systems will be developed in large scale. Following three key points must be satisfied by the future nuclear energy systems:

- more safer nuclear energy systems than recent those should be developed to decrease the risk of core-melten and unforeseen release of radioactive materials;
- long lived minor actinides and long lived fission products must be safely treated to assure a proper environment;
- uranium resource should be sufficiently utilized.

In order to meet above general requirements, the fast reactor technology development has been launched and the basic researches of Accelerator Driven Subcritical facility (ADS) system has been started in China. The activity of the construction of the China Experimental Fast Reactor and plan for next step, some calculation results on core physics study of ADS, some results on target physics and a proposed verification facility are briefed in the paper.

1. INTRODUCTION

Power supply is a stern issue in China's economic development. Various predictions indicate that the demand on the primary energy resource will reach 4-5 billion tons standard coal, a fact of 4-5 higher than present level, when China steps on the level of the middle-developed country in the middle of the next century. In the constitution of our present primary energy resources, fossil contributes about 90%. About 70% of the total electricity comes from coal burning.

Environment protection is a key link in the sustainable development strategy. The part of the fossil energy resource in the total newly increased power supply should be reduced and the light-pollution energy resources should be developed. Nuclear energy is, of course, a most important and most prospect option. As the fusion energy is now still far away from practicability, in several decades from now on, the nuclear power will be, in all senses, the application of fission energy.

China is speeding up her nuclear power station construction, referring to some estimation (1,2), nuclear power will share about 5% of total national electricity capacity by 2020 and 10 to 20% in the middle of 21st century. That means, the nuclear power capacity will be developed to 30 GWe and 120 to 240 GWe in above mentioned years. Considering this developing scenario, required uranium resource and accumulated spent fuels will be somewhat between 1 to 2 million tons and more then 20 000 tons respectively by the year 2050, if only thermal reactor plants will be developed.

China Institute of Atomic Energy is carrying on a long term scientific and technical project for national sustainable development of fission energy, including construction an experimental fast reactor (CEFR), investigating the MA transmutation capacity by a large size fast reactor and the basic research of the innovative technical option ADS [1]. The activity of the construction of CEFR and plan for next step is described in Section 2, some results of the core physics study of ADS is given in Section 3, some results of the target physics are given in Section 4 and in Section 5 a proposed verification facility is described briefly.

2. FAST REACTOR TECHNOLOGY AND ENGINEERING

The basic researches for fast reactor technology have been carried out in China, which could be divided in to two phases as following:

1. Basic researches from the middle-end of 60's to the year 1987.
   The emphasis were put on fast neutron physics, thermo-hydraulics, materials, sodium technology and some sodium components in small scale. During this period about 12 sodium loops and test facilities have been built up including a fast neutron zero power facility DF-Ⅵcontaining 50 kg U-235.

2. Applied basic researches from the year 1987 to 1993.
   All the research subjects were arranged with a target of 65 MWt experimental fast reactor. The emphasis were put on fast reactor design study, sodium technology, fast reactor safety, fuels and materials and sodium components. About 20 sodium loops and test facilities have been established and tested.

The preliminary strategy study for fast reactor development points out that Chinese fast reactor engineering development will be divided into three steps:

- Step 1: China Experimental Fast Reactor (CEFR) 65 MWt;
- Step 2: Prototype Fast Breeder Reactor (PFBR) 300 Mwe;
- Step 3: Large Fast Breeder Reactor (LFBR) 1000-1500 Mwe.

As the first step, the project in the framework of the National High Technology Programme that was launched in the year 1986 is under execution.
The CEFR is a sodium pool type experimental fast reactor of 65 MW thermal power matched with a 25 MW turbine generator. The main design parameters are given in Table 1 and its schedule is shown in Fig. 1.

The second step will be the Prototype Fast Breeder Reactor (PFBR), which is also as a module of Modular Fast Reactor Power plant, so named again Modular Prototype Fast Reactor (MPFR). Which will be started to design in 2001-2002 and it's envisaged to complete its construction in 2015.

The preliminary study of using MPFR to transmute MA has been conducted [2]. Main design parameters of MPFR reference core and the inference to dynamic parameters due to mixed with 5% MA produced from PWRs to the fuel of reference core are listed in Tables 2 and 3, respectively.

It could be preliminarily concluded that 3×300 MWe MPFRs in the case without any transmutation optimization could transmute MAs from two 1000 MWe PWRs, namely the supporting ration is 2.

TABLE 1. CEFR MAIN DESIGN PARAMETERS

Parameter	Preliminary design
Thermal power, MW	65
Electric power, net, MW	20
Reactor core	
Height, cm	45.0
Diameter equivalent, cm	60.0
Fuel	$(Pu,U)O_2$
Pu, total, kg	141
Pu-239, kg	65.76
U-235 (enrichment), kg	92.33 (36%)
Linear power max., W/cm	430
Neutron flux, n/cm^2s	3.7×10^{15}
Bum-up, target max., MWd/t	100 000
Bum-up, first load max., MWd/t	60 000
Inlet temp. of the core, °C	360
Outlet temp. of the core, °C	530
Diameter of main vessel (outside), m	8 010
Primary circuit	
Number of loops	2
Quantity of sodium, t	260
Flow rate total, t/h	1328.4
Number of IHX per loop	2
Secondary circuit	
Number of loops	2
Quantity of sodium, t	48.2
Flow rate, t/h	986.4
Tertiary circuit	
Steam temperature, °C	480
Steam pressure, MPa	14
Flow rate, t/h	96.2
Plant life, A	30

FIG. 1. CEFR schedule.

TABLE 2. MAIN PARAMETERS OF MPFR REFERENCE CORE

Parameter	Value
Thermal power, MW	840
Electric power, MW	300
Fuel type	MOX
No. of fuel S.A.	
Inner	84
Outer	72
No. of fuel pins in one S.A.	271
Diameter of fuel pin, mm	6.9
Fuel/structure material/sodium, %	36.61/28.43/34.96
Max. linear power, W/cm	326
Fuel cycle, d	300

TABLE 3. DYNAMIC PARAMETER COMPARISON BETWEEN MA 5% CORE AND REFERENCE CORE

Parameter	Reference core	MA 5% core
PuO_2 Contents in fuel		
Inner	21.72%	22.81%
Outer	26.59%	27.12%
Burn-up reactivity lost, Δk/k	3.88%	2.9%
Inner single compensation S.A., Δk/k	1.45%	1.39%
Outer single compensation S.A., Δk/k	0.72%	0.66%
Single safety S.A., Δk/k	1.23%	1.18%
Single regulation S.A., Δk/k	0.176%	0.147%
Doppler constant 530K-633K, Δk/k	-9.26×10^{-3}	-6.07×10^{-3}
β_{eff}, Δk/k	3.67×10^{-3}	3.41×10^{-3}
Neutron life, s	4.05×10^{-7}	3.44×10^{-7}
Na void reactivity		
in fuel, $	2.8	4.9
in whole core, $	2.1	4.3
MA Transmutation, kg/a	-	14.15

3. MAIN RESULTS ON ADS REACTOR PHYSICS CONCEPT STUDY

A five years' program (Phase 1) of basic research on some physical and technical problems related to ADS system is carrying on in recent years. The work package is given in Fig. 2. Some preliminary results of the study on the performance of different blanket illustrate the advantages of ADS in comparing with that of critical one.

3.1. AD-FBR

A medium size sodium cooled fast breeder reactor driven by an accelerator with 1 Gev/16 mA shows its advantages over the ordinary one, such as less Pu inventory required, higher breeding ratio and reasonable transmutation rate (which may support two sets 1000 MWe PWR) at expense of less 15% energy output. The core layout is given in Fig. 3 and the main parameters are given in Table 4. The comparison with ordinary fast breeder with same core layout is listed in Table 3.

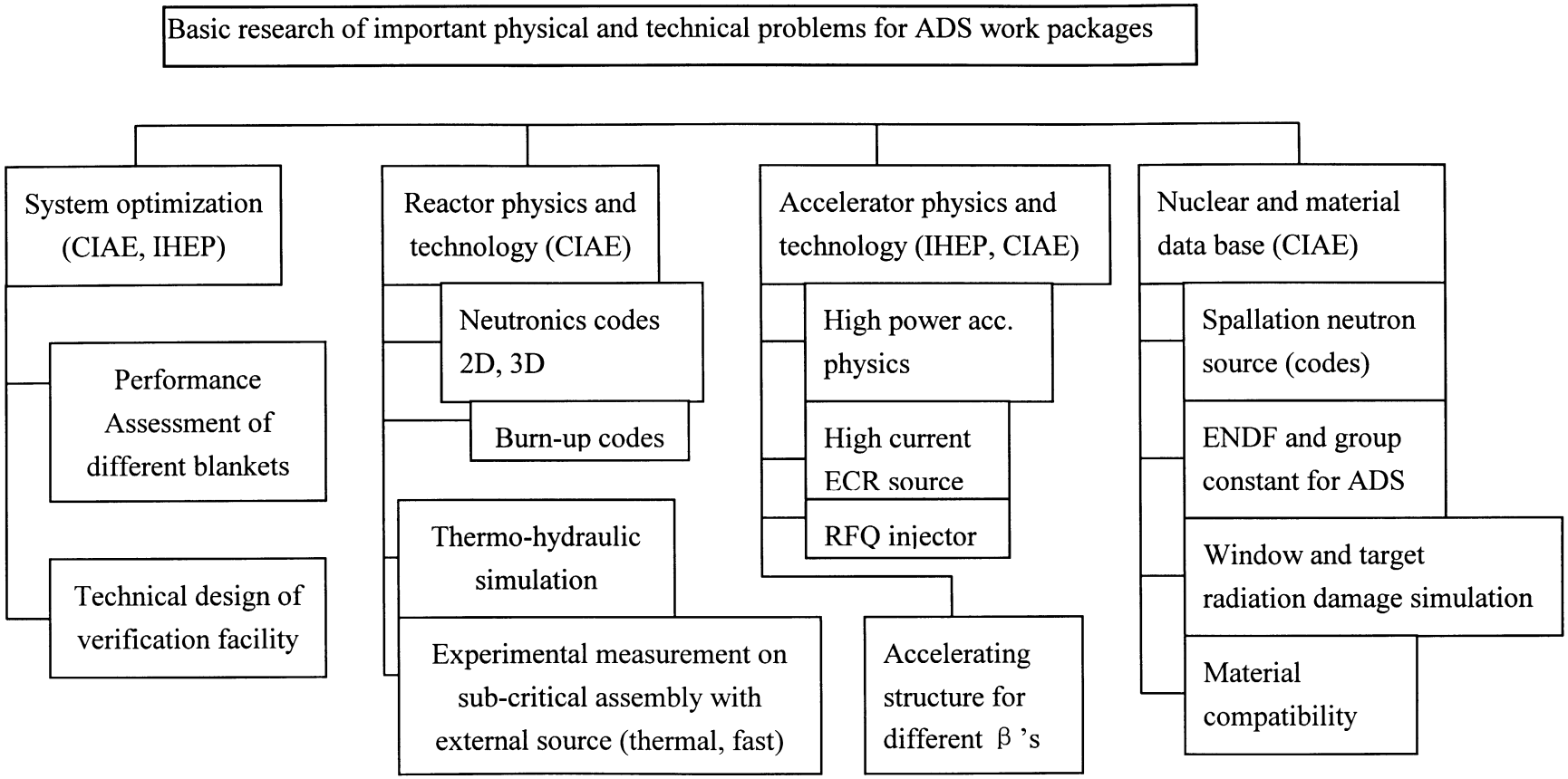

FIG. 2. Work package for ADS research phase 1.

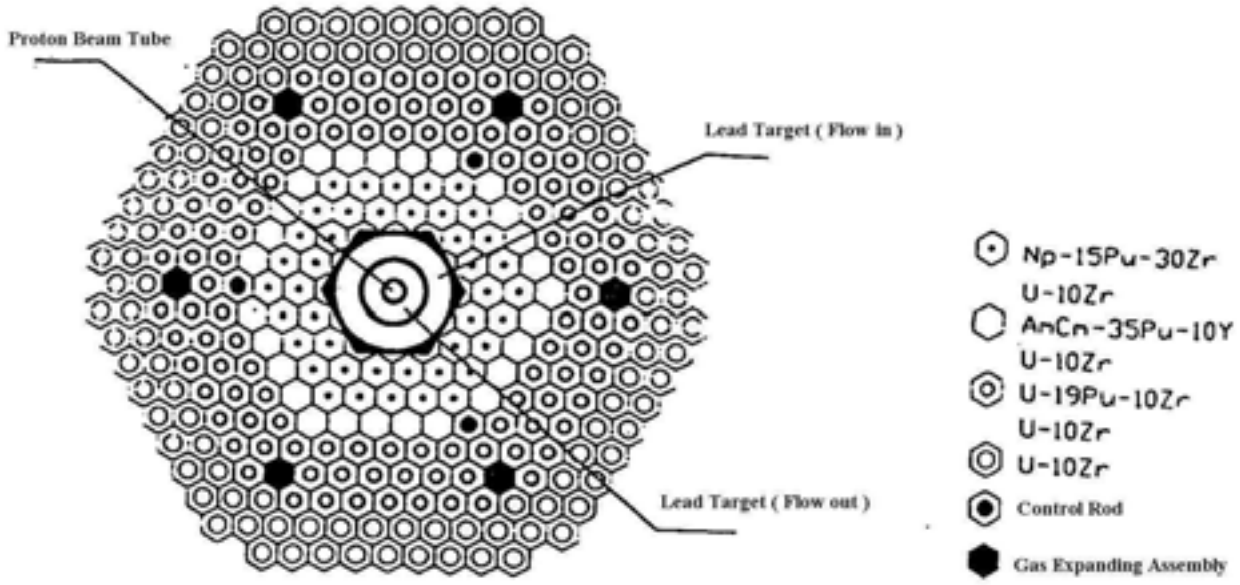

FIG. 3. AD-FBR core configuration.

TABLE 4. SUB-CRITICAL BLANKET FBR

Parameter	Value
Accelerator Ep, GeV	1.0
Ip, mA	16
Target	Pb
Blanket type	Pool
Coolant	Na
k_{eff}	0.971
Energy cain	47.5
Average neutron energy, keV	650
Average neutron flux, $cm^{-2}s^{-1}$	3.87×10^{15}
Maximum neutron flux, $cm^{-2}s^{-1}$	6.47×10^{15}
Average burnup, MWd/t	10^5
MA Inventory, kg	715
Pu Inventory, kg	1187
MA Transmutation rate, kg/y	29.8
MA Production, kg/y	6.4
Support ratio	(Roughly) 4 GWe PWR

TABLE 5. COMPARISON OF AD-FBR WITH FBR

Parameter	AD-FBR	FBR
Power, MWt	760	880
Pu Inventory, kg	1187	1324
BR	1.37	1.27
Doubling time, a	12.5	17.1
k_{eff}	0.97	1.02

This calculation gives us some idea about how the fast sub-critical reactor is in favour of the MA's transmutation and fissile breeding [3].

3.2. AD-PHWR

The pressurized heavy water moderated reactor (CANDU type) was adopted for the analysis both for Th-U and U-Pu fuel cycles. Four central pressurized tubes were substituted by the beam pipe and lead target. The parameters for Th-U fuel and for U-Pu fuel are given in Tables 6 and 7, respectively. It is shown that AD-PHWR is favour to Th-U fuel cycle not only higher burn up, but also with slight breeding capability. While in U-Pu fuel cycle, the fuel may self-sustainable only with relative higher beam current, smaller k value and with a little higher burn up than ordinary CANDU [4].

TABLE 6. SUB-CRITICAL BLANKET AD-PHWR(Th-U)

Parameter	Value
Accelerator Ep, GeV	1.5
Ip, mA	10
Target	Pb
Blanket type	Pressurized tube, D_2O moderator (CANDU type)
k_{eff}	0.985
Fuel composition	UO_2+ThO_2
V_m/V_f	8.93
Burnup, MWd/t	3×10^4
Loading U-233, kg	959
Th-232, kg	64 000
Equilibrium enrichment	1.46%
Breeding ratio	1.01
Power, MWt	1840

TABLE 7. SUB-CRITICAL BLANKET AD-PHWR(U-Pu)

Parameter	Value
Accelerator Ep, GeV	1.5
Ip, mA	46
Target	Pb
Blanket type	Pressurized tube D_2O moderator (CANDU type)
k_{eff}	0.82
Fuel composition	UO_2
V_m/V_f	5.94
Breeding ratio	1.00
Power, MWt	1500

3.3. Fast-thermal coupled system

We consider a system that is consists of an inner core of fast blanket and an outer core of thermal blanket with thermal neutron reflector in between. This means that the thermal neutron cannot diffuse into the inner one while the fast neutron may comes out from the inner one into the outer one. The inner core is a small sized fast blanket, which is used as the transmutor of MA's and to amplify the external neutron number produced in spallation reaction by fission in it. The outer one is, suppose CANDU type one with Th-U or U-Pu fuels. It is used to produce the energy and to transmute the LLFP's.

By using a 44-group constant, the calculation was carried out for a one dimensional (spherical) structure, as shown in Fig. 4. Taking the target volume as a radius 20 cm Pb and a fast blanket of radius 42.5 cm with uniformed mixed 500 kg Np and 5000 kg U-238, the amplifying factor will be 2.3 and 5.1 for k = 0.89 and 0.96, respectively. If the fast blanket with same radius is divided into two layers, first is pure Np of 200 kg and second is uniformly mixed Np and U of 300 kg and 5000 kg, the amplifying factor will be enhanced to 2.5 and 6.1 for the same k value mentioned above [5].

If this system really works, the beneficial effect is to reduce the beam power of accelerator required. This may makes easier life for accelerator specialists.

As the accelerator driven system provides a new technological option for nuclear energy, we may construct the paradigm of fission energy system as in Fig. 5. When one concerns the U-Pu fuel cycle in thermal blanket, one may notice that the requirement of accelerator beam power will be three or four folds higher then other system. This led us to analysis the so-called fast-thermal coupled system.

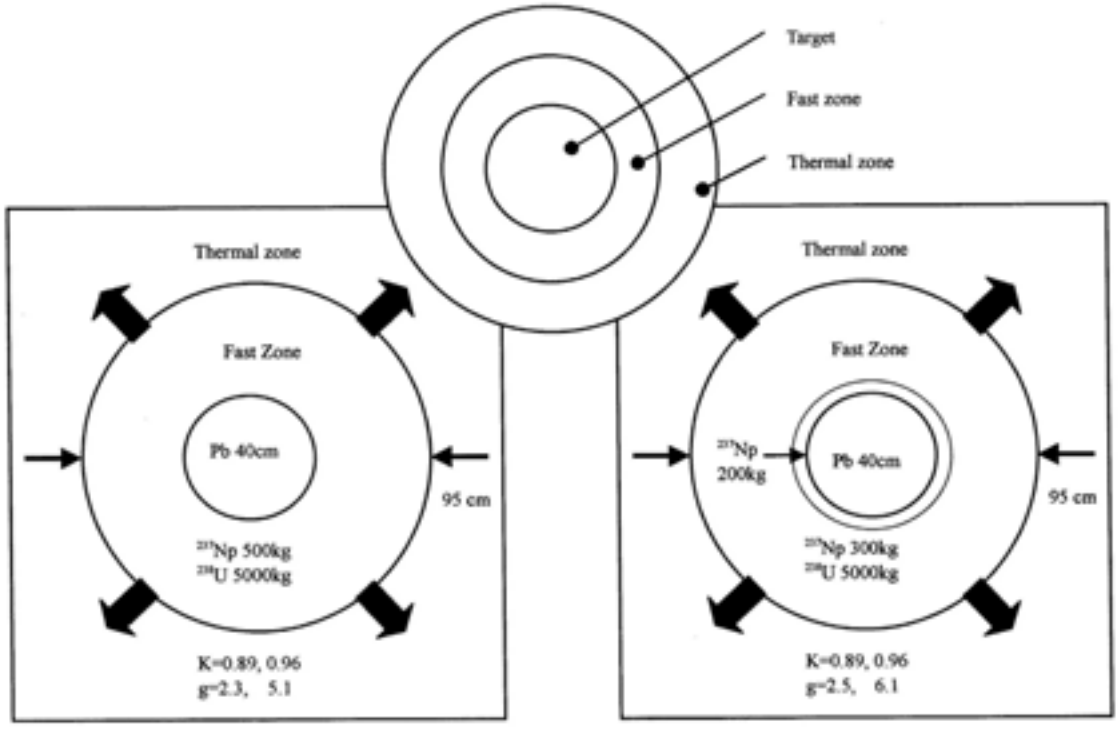

FIG. 4. Fast thermal coupled system.

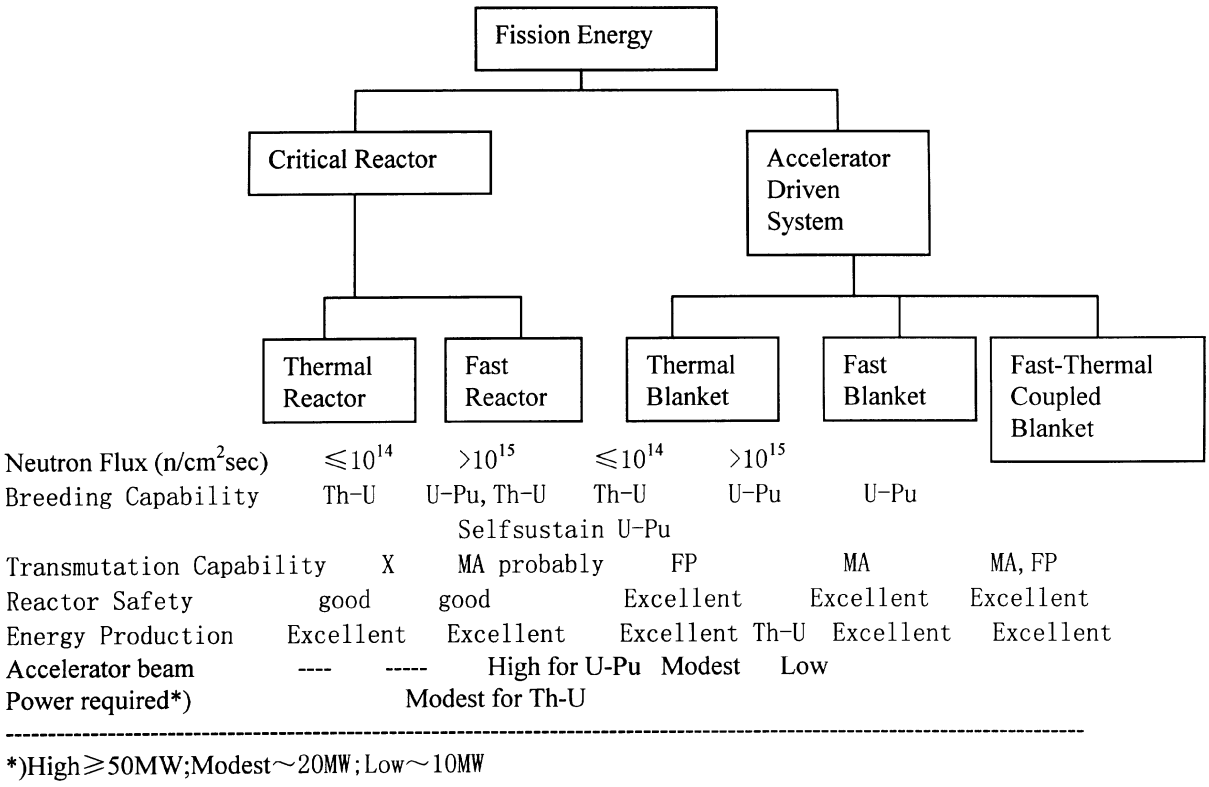

FIG. 5. The paradigm of fission energy system.

4. STUDY ON SPALLATION TARGET PHYSICS

As the proton beam window and the spallation target are the interface of the accelerator and the subcritical reactor, which is the important component of the ADS. From the point of view of the engineering application, the basic problems such as spallation neutron yield, energy deposition, the irradiation damage and radioactivity accumulation are firstly concerned.

The calculation and analysis to the thin target and the standard thick target were made based on the nuclear reactor models in this paper.

4.1. Study on the neutron double differential cross sections of thin target

As a benchmark of the theoretical model used for analysis the comparison of the neutron yield between the calculation results and the measured data of thin target was carried out firstly. Figure 6 shows the comparisons of the neutron double differential cross sections induced by 1500 MeV protons on Pb between the calculated values by SHIELD code [6] and the experimental data [7] at 15°, 30°, 60°, 90°, 120° and 150°, respectively. In summary the predicted neutron double differential cross sections by SHIELD code is better than HETC code.

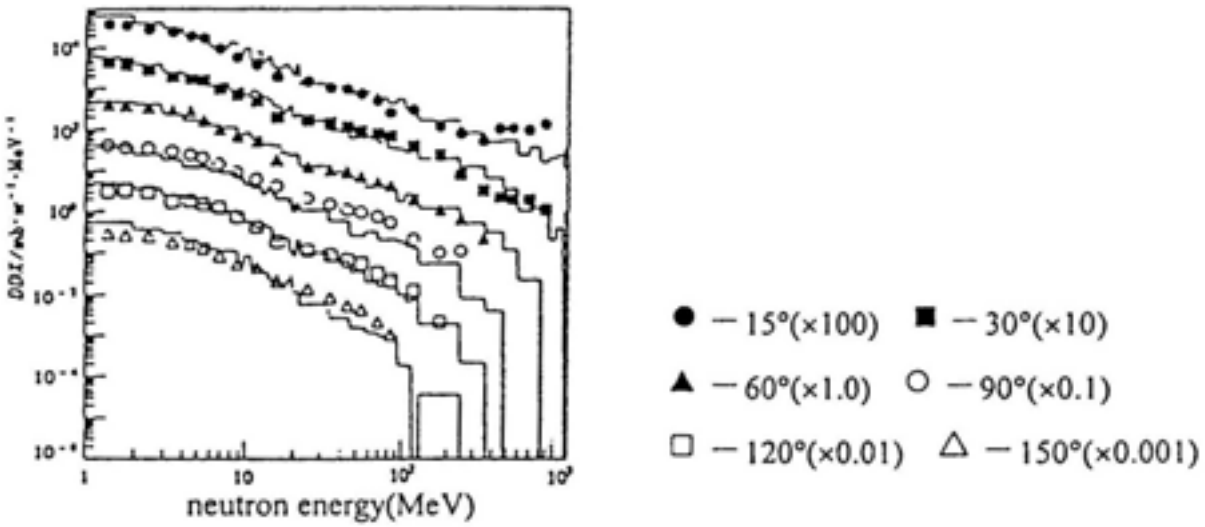

FIG. 6. Double differential cross section of neutron yield from Pb target.

4.1. Study on standard thick target

The size of the standard thick target used in the international code comparison is Φ 20×60 cm cylinder. The neutron yield from lead or tungsten target was calculated by two methods. One is that the particle transport in the target was calculated by the Monte-Carlo method and the nuclear data were taken from the experimental data or the empirical formulas based on experimental data [8, 9], and the second one is by SHIELD code [10]. The results calculated by these two methods differ from 3 to 7% systematically increasing with energy. Our results are compared with experimental data and that quoted from international code comparison in Table 8.

TABLE 8. COMPARISON OF NEUTRON NUMBERS GENERATED PER PROTON FROM Φ 20×60 cm TARGET

Target	Ep, Mev	Average value from int. code comparison	Experimental values		[8]	[9]
W-186	800	19.95 [11]			18.62	
Pb-208	800	17.71 [11]	(16.6+18.9)/2=17.7 [12]	16 [13]	17.72	18.2
Pb-208	1000		19.5 [13]		22.74	24.0
Pb-208	1600		(33.5+37.8)/2=35.65 [12]		35.59	38.3

Figure 7 presents the calculated energy depositions by SHIELD code for six kinds of target materials with 1 GeV protons and Φ 20×60 cm cylinder target. The results were compared with the experimental data [7]. The calculated values agree with the experimental data pretty well for high Z target materials, but fail for low Z materials as poor statistics in these materials for small number of nucleons in light nuclei.

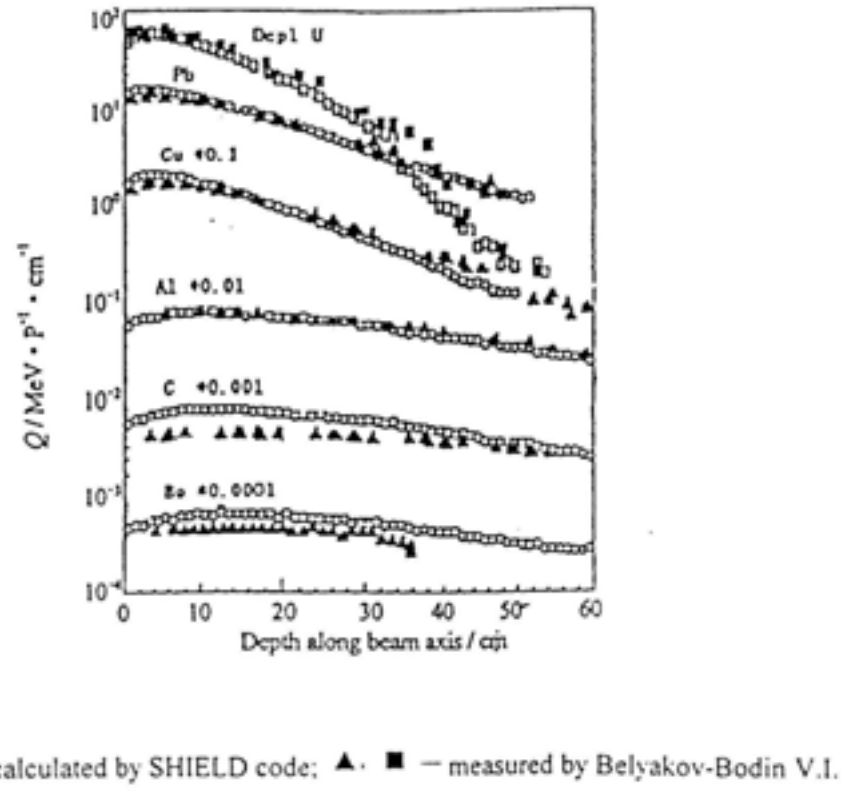

FIG. 7. Comparison of energy deposition in various targets at proton projection.

The irradiation damage of the target and the beam window is the significant issue for the ADS system. The radiation damage induced by the intermediate energy nucleons mainly due to the elastic, inelastic scattering and nuclear reaction, which can lead to atomic displacement in the target material, production of the gas in the light nuclei (mainly H and He) etc. By defining the irradiation damage cross section and the gas production rate, the irradiation damage of the material tungsten and lead was calculated by SHIELD code. In order to compare the various calculated results, the thin target was calculated firstly. Figure 8 shows the comparisons between our results calculated by SHIELD code and the calculated results [10] by HETC code for Ep = 600 MeV as well as the calculated results [14] given by C. Rubbia group for Ep = 800 MeV. As shown in Fig. 8 the irradiation damage cross sections increase basically in a line as the atomic order Z increasing.

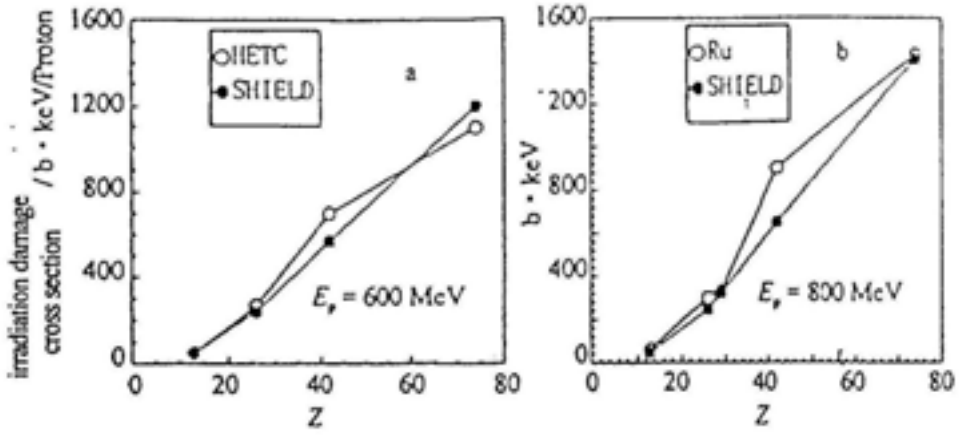

FIG. 8. Irradiation damage cross sections of Al, Fe, Mo and W.
Thin targets induced by incident proton with 600 MeV [10] and 800 MeV [14].

The irradiation damage of the standard W and Fe thick target of Φ 20×60 cm cylinder with 1600 MeV protons was calculated by SHIELD code. Based on the thin target calculations the total irradiation damage induced by the incident protons, secondary protons, secondary neutrons above and below 14.5 MeV is main concentrated in front 30 cm at the target, the irradiation damage in last 30 cm at the target is about 1/8 of the total one. The contribution to the total radiation damage by the secondary neutrons below 14.5 MeV is about 42% that by incident protons is about 30%.

The production rate of the gas is the product of the particle flux and the production cross section σ_i of the gas. The calculated results by SHIELD code show that above 400 MeV protons or neutron bombard, the production cross sections of the helium gas increase rapidly with the incident energy for tungsten target, but slowly for iron target.

The accumulation of the radioactivity in the Pb target by spallation and fast fission was calculated after operation with 30 mA accelerator proton beam for one year. Figure 9 shows the relation of the total, neutron, proton and neutron below 20 MeV radioactivity with time respectively. Figure 10 presents the relation of the total radioactivity and radioactivities of the several typical radioactive nuclides with time. The radioactivity is mainly caused by protons and neutrons (especially above 20 MeV neutrons) for 1600 MeV incident protons. The relation of radioactivity with time is basically accordance with the results [15] for 1600 MeV incident protons.

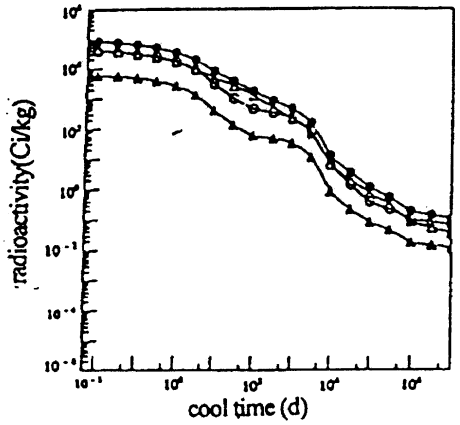

beam flux energy 1600MeV

● total radioactivity;

○ induced by neutron;

Δ induced by proton;

▲ induced by neutron with E<20MeV.

FIG. 9. Changes of total radioactivity and radioactivities induced by neutron,proton and neutron with E < 20MeV.

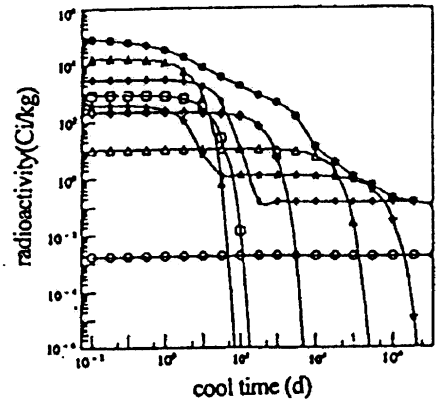

beam flux energy 1600MeV

● total radioactivity; ▲,◇,□,★,✞,△ and ○ raduoactivities from ^{203}Pb 、 ^{202}Pb 、 ^{202}Tl 、 ^{206}Bi 、 ^{194}Au 、 ^{194}Hg 、 ^{193}AU 、 ^{207}Bi and ^{205}Pb

FIG. 10. Changes of total radioactivity and radioactivities from some typical radiation elements.

5. A PROPOSED VERIFICATION FACILITY FOR ADS IN CHINA

ADS is an entirely new approach for the exploitation of the next generation nuclear energy, which including new physics basis, neutronics in high power sub-critical reactor, new technical issues of the reactor system, challenge to the high current medium energy accelerator with high reliability and material problems both for beam extraction window, target system and reactor components etc. All these problems should be solved step by step both individually and integrally. According to present technical status in China, we think a small size multi-purpose verification system is a rational choice. The CIAE and IHEP have proposed such a facility consists of a 150-300 MeV/3mA low energy accelerator, a swimming pool light water sub-critical.

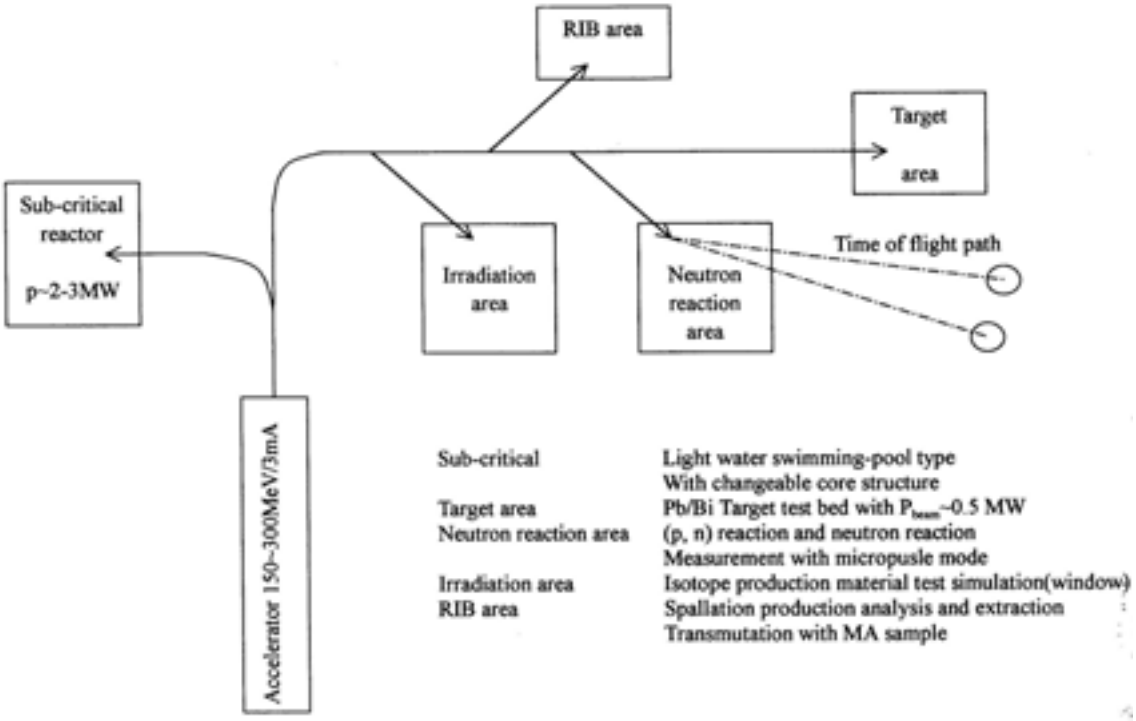

FIG. 11. Conceptual layout of verification facility for AD-RCNPS.

The rational of the parameters of this proposed verification facility and the structure of the accelerator were described in [16, 17]. The core structure and some parameters of this AD-SPR are given in Fig. 12 and Table 9.

The research activity in Phase l and Phase 2 are summarized in Table 10.

The construction of the verification facility is expected in phase 2 until 2007, as shown in Table 10. In phase 1 the technical development will be carried out individually, while in Phase 2 the integral will be undertaken.

On the base of this verification facility we expect that a full scale demonstration experimental facility may be realized in the middle of 2010's.

6. CONCLUSION

For the future nuclear energy supply, FBR and ADS have been considered in China. Up to now their technology developments are all under very early stage. So we have open selections for the future, and we are looking at the development trends and achievement on this field from other countries and welcome to have more international cooperation.

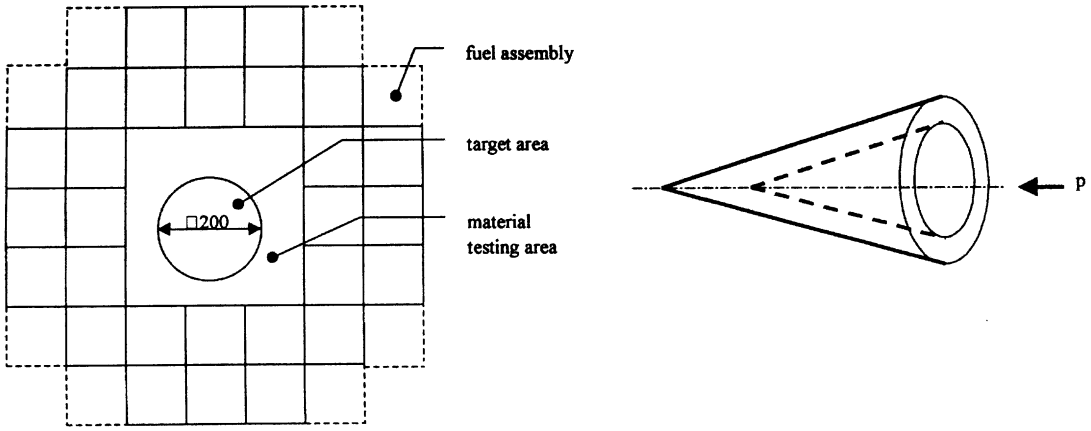

FIG. 12. Layout of AD-SPR.

TABLE 9. SOME PARAMETERS OF AD-SPR

Parameter	Value
Linac	
Proton energy, MeV	300
Beam, MA	3
Target	
Material	Pb/Bi
Target power, MW	≤0.9
Subcritical facility	
Moderator and coolant	H_2O
Power, MW	3
Fuel	U-235 (10%)
Subassembly, mm	68×68
Core height, mm	500
Power peak factor	2.478
Heat flux (average) of fuel element, W/cm^2	36.5
Heat flux (max.) of fuel, W/cm^2	90.4
Doppler coefficient, 10^{-5}/°C	-0.397
Temperature coefficient of moderator, 10^{-5}/°C	-2.475
28 Subassemblies: 2.58 kg U-235	k_{eff} = 0.91
36 Subassemblies: 4.86 kg U-235	k_{eff} = 0.97

TABLE 10. VERIFICATION AND DEMONSTRATION PROJECTS

	Verification facility		Demonstration experimental facility
	2000	2007	
	Phase 1	Phase 2	2008-2015
Accelerator	Key components development - ECR High current source - Ep = 80 KeV, Ip = 60 mA - RFQ injector Ep～5 MeV, Ip～3mA - low β cavity High energy accelerating structure - CCL (normal conductivity and/or super-cond.) accelerator physics - Basic theoretical study of beam dynamics in LINAC and cyclotron	Low energy part of LINAC Pulse mode: Ep = 300 MeV, Ip = 3mA Micropulse mode: Ep = 300 MeV, Ip～10 μA Further study on high energy accelerating structure - SC-CCL - CW-mode operation of LINAC	Full scale accelerator LINAC Ep ≥ 1 GeV Ip ≥ 3 mA
Blanket	- System conception study - Neutronics study using Zero-power sub-critical assembly driven by D-T, Cf external source (both thermal and fast assembly)	LWR sub-critical reactor driven by LINAC $P_{out} \leqslant 3$ MWt - Changeable core structure - Power density flatten - Transmutation simulation	Power output 60 MWt
Material	Pb/Bi test loop W～Na	- Pb/Bi test bed Pb ≤ 0.9 MW - Wsolid state test target Pb ≤ 0.9 MW - Window material test	
Nuclear physics	- Neutron data evaluation - Medium energy nuclear reaction theory - Proton, neutron transport code development	- Spallation neutron source	
Chemistry	Basic research on partitioning process	Techniques on partitioning process	

REFERENCES

[1] ZHAO ZHIXIANG, et al., Selected Papers of the Conceptual Study on Accelerator Driven Radioactive Clean Nuclear Power System, Atomic Energy Press, Beijing (2000).

[2] ZHOU PEIDE, The MA transmutation Analysis With MOX Fuel Modular Fast Reactor, Chinese Journal of Nuclear Science and Engineering, Vol. 22, No. 3 (2002).

[3] ZHANG YUSHAN et al., An Accelerator Driven Modular Fast Reactor, paper presented in the 7th Meeting on Reactor Numerical Calculations and Particle Transport, 4-10 October 1998, Yunan, China, Atomic Energy Press, Beijing (1999).

[4] XU XIAOQIN, Private communication.

[5] LIU GUISHEN, Research on Amplification Multiple of Source Neutron Number for ADS, Selected Papers of the Conceptual Study on Accelerator Driven Radioactive Clean Nuclear Power System, Atomic Energy Press, Beijing (2000) 28-37.

[6] XU CHUNMAO, et al., Preliminary Study on Lead Spallation Target Parameters, High Energy Physics and Nuclear Physics (in Chinese) 23(4): 402 (1999).

[7] BELYAKOV-BODIN, V.I., et al., Caloric measurements of medium-energy protons bombarding beryllium, carbon and aluminium targets, Nuclear Instrum Methods, A314:508 (1992).
[8] SHEN QINGBIO, et al., Calculation of Nuclear Emission and Energy Disposition of Spallation Neutron Sources Induced by Intermediate Energy Protons. Selected Papers of the Conceptual Study on Accelerator Driven Radioactive Clean Nuclear Power System, Atomic Energy Press, Beijing (2000) 231-242.
[9] YU HONGWEI, FAN SHENG, ZHAO ZHIXIANG, et. al., Comparison of the Simulation Results Using Different ADS Spallation Target, J. Nucl. Sci. and Tech., Supplement 2 (2002) 1221-1224.
[10] LEBEDEV, S.G., SMIRNOVA, O.N., SOBOLEVSKY, N.M., RADDAM Code for Simulation damage by High Energy Nucleons, INR-0896/95-16, Moscow (1995).
[11] FILGES, D., et al., International Codes and Model Intercomparison for Intermediate Energy Activation Yields, NEA/NSC/DOC (97) 1 (1997).
[12] VASIKOV, R.G., et al., Proc. International Collaboration on Advanced Neutron Source-XI (ICANS-XI), report KEK-90-25(1990) 340.
[13] LONE, M.A., et al., Total Neutron yields from 100 MeV Protons on Cu, Fe, and Th, Nucl. Instr. Meth In Phys. Research, A265:135 (1987).
[14] RUBBIA, C., et al., Some preliminary considerations on the economical issues of the energy amplifier, CERN/AT/95-45 (ET), Geneva (1995).
[15] SHUBIN, YN.N., et al., The Analysis of Energy Release, Beam Attenuation, Radiation Damage, Gas Product and Accumulation of Long-Lived Activity in Pb and Pb-Bi Target, Proc. 2nd Int. Conf. on Accelerator-Driven Transmutation Technologies and Applications (ADTT'96), 1996, Kalmar, Sweden, H. Condé (Ed.), Uppsala University (1997) 953.
[16] DING DAZHAU, The conceptual Study of Accelerator Driven Radiological Clean Nuclear Power System (AD-RCNPS) in China, Proc. 3rd Workshop on Neutron Science Project, 1998, Japan (JAERI-conf-99-003) 132-140.
[17] GUAN XIALING, LUO ZHANGLIN, Proposal for a verification Facility of ADS in China, paper presented in the OECD/NEA Workshop on Utilization and Reliability of High Power Accelerators, 13-15 October 1998, Mito, Japan, NEA, ISBN: 92-64-17068-5.

MYRRHA: A MULTIPURPOSE ACCELERATOR DRIVEN SYSTEM FOR RESEARCH & DEVELOPMENT

H. AÏT ABDERRAHIM, P. KUPSCHUS, E. MALAMBU, PH. BENOIT,
K. VAN TICHELEN, B. ARIEN, F. VERMEERSCH, P. D'HONDT
Nuclear Research Centre (SCK•CEN), Mol, Belgium

Y. JONGEN, S. TERNIER, D. VANDEPLASSCHE
Ion Beam Applications (IBA), Louvain-la-Neuve, Belgium

Abstract

SCK•CEN, the Belgian Nuclear Research Centre, in partnership with IBA s.a., Ion Beam Applications, is designing an ADS prototype, MYRRHA, and is conducting an associated R&D programme. The project focuses primarily on research on structural materials, nuclear fuel, liquid metals and associated aspects, on sub-critical reactor physics and subsequently on applications such as nuclear waste transmutation, radioisotope production and safety research on sub-critical systems. The MYRRHA system is intended to be a multipurpose R&D facility and is expected to become a new major research infrastructure for the European partners presently involved in the ADS Demo development. Ion Beam Applications is performing the accelerator development. Currently the preliminary conceptual design of the MYRRHA system is under way and an intensive R&D programme is assessing the points of greatest risk in the present design. This work will define the final choice of characteristics of the facility. In this paper we will report on the status of the pre-design study as of June 2000 as well as on the methods and results of the R&D programme.

1. INTRODUCTION

SCK•CEN, the Belgian Nuclear Research Centre, and IBA s.a., Ion Beam Applications, are developing jointly the MYRRHA project, a multipurpose neutron source for R&D applications on the basis of an Accelerator Driven System (ADS). This project is intended to fit into the European strategy towards an ADS Demo facility for nuclear waste transmutation.

The R&D applications that are considered in the future MYRRHA facility can be grouped in three blocs:

i. Continuation, and extension, towards ADS of the ongoing R&D programmes at SCK•CEN in the field of reactor materials, fuel and reactor physics research;
ii. Enhancement and triggering of new R&D activities such as nuclear waste transmutation, ADS technology, liquid metal embrittlement;
iii. Initiation of medical applications such as proton therapy and PET production.

The present MYRRHA concept, as described below, is determined by the versatility of the applications it would allow. Further technical and/or strategic developments of the project might change the present concept.

The design of MYRRHA needs to satisfy a number of specifications such as:

– Achievement of the neutron flux levels required by the different applications considered in MYRRHA:
  $\Phi_{>0.75\ MeV} = 1.0\times10^{15}$ n/cm²s at the locations for minor actinides (MA) transmutation,
  $\Phi_{>1\ MeV} = 1.0\times10^{13}$ to 1.0×10^{14} n/cm²s at the locations for structural material and fuel irradiation,
  $\Phi_{th} = 2.0$ to 3.0×10^{15} n/cm²s at locations for long-lived fission products (LLFP) transmutation or radioisotope production;

- Subcritical core total power: ranging between 20 and 30 MW;
- Safety: $k_{eff} \leq 0.95$ in all conditions, as in a fuel storage, to guarantee inherent safety;
- Operation of the fuel under safe conditions: average fuel pin linear power < 500 W/cm.

2. MYRRHA PRESENT DESIGN STATUS

In its present status of development, the MYRRHA project [1] is based on the coupling of an upgraded commercial proton cyclotron with a liquid Pb-Bi windowless spallation target, surrounded by a subcritical neutron multiplying medium in a pool type configuration (Fig. 1). The spallation target circuit is fully separated from the core coolant as a result of the windowless design presently favoured in order to utilise low energy protons without reducing drastically the core performances.

The core pool contains a fast spectrum core, cooled with liquid Pb-Bi or Pb, and several islands housing thermal spectrum regions located in In-Pile Sections (IPS) at the periphery of the fast core. The fast core is fuelled with typical fast reactor fuel pins with an active length of 600 mm arranged in hexagonal assemblies of 122 mm plate-to-plate. The central hexagon position is left free for housing the spallation module. The core is made of 18 fuel assemblies of which 12 have a Pu content of 30% and 6 have a Pu content of 20% .

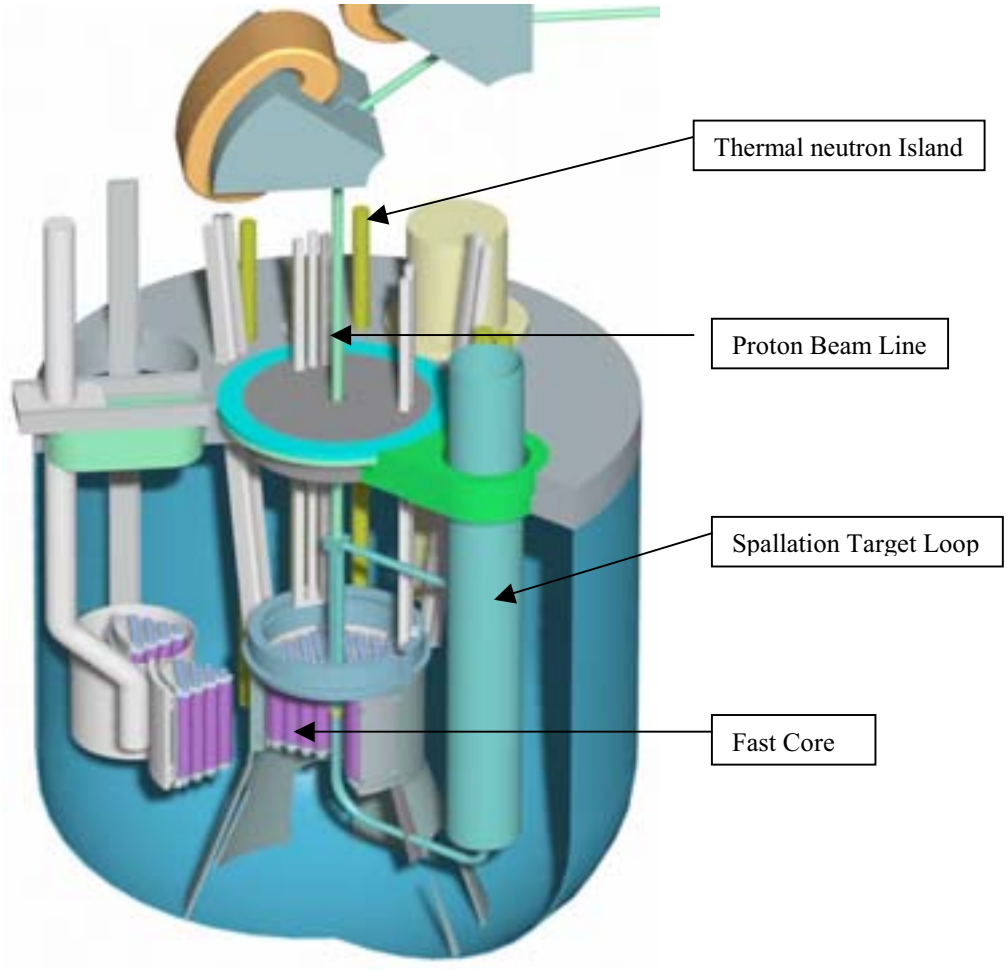

FIG. 1. Global view of the present design of MYRRHA.

The MYRRHA design is determined by the requirement of versatility in applications and the desire to use as much as possible existing technologies. The heat exchangers and the primary pump unit are to be embedded in the reactor pool. The accelerator is to be installed in a confinement building separated from the one housing the sub-critical core and the spallation module. The proton beam will be impinging on the spallation target from the top.

2.1. Accelerator

IBA, a company that has designed the world reference cyclotron for radioisotope production and other machines, is in charge of the design of the accelerator. The accelerator parameters presently considered are 5 mA current at 350 MeV proton energy. The positive ion acceleration technology is envisaged, realised by a two-stage accelerator, with a first cyclotron as injector accelerating protons up to 40 to 70 MeV and a booster further accelerating them up to 350 MeV (Fig. 2). This option is not yet frozen: a trade-off of higher proton energy against current is being explored. Other designs, to go in one step from the ion source energy injection up to the 350 MeV desired energy, or accelerating H_2 molecules with stripping at the final energy stage for beam extraction, are in the assessment phase. For more details, see Section 3.1.

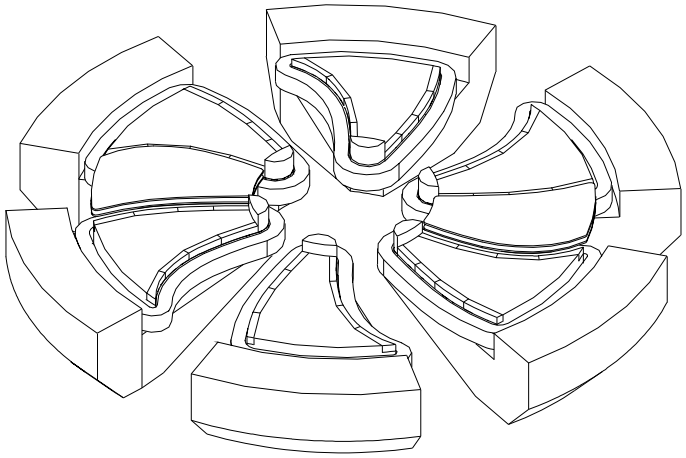

FIG. 2. Lower half of the magnets, with the acceleration electrodes of a 350 MeV MYRRHA booster cyclotron.

2.2. Spallation target

The spallation target is made of liquid Pb-Bi. The Pb-Bi is pumped up to a reservoir from which it descends, through an annular gap ($\varnothing_{outer}$ 130 mm), to the middle of the fast core. Here the flow is directed by a nozzle into a single tube penetrating the fast core ($\varnothing_{outer}$ 80 mm). At about the position of the nozzle a free liquid metal surface is formed, which will be in contact with the vacuum of the proton beam guideline. No conventional window is foreseen between the Pb-Bi free surface and the beam in order to avoid difficulties in engineering this component and to keep the energy losses at a minimum. When the Pb-Bi has left the fast core region, it is cooled and pumped back to the reservoir.

The MYRRHA windowless spallation module is given special attention in the present pre-design phase because of its particular features, as illustrated in [2] and summarized in Section 3.2.

2.3. Subcritical system

The design of the subcritical assembly will have to yield the neutronic performances and provide the irradiation volumes required for the considered applications. In order to meet the goals of material studies, fuel behaviour studies, radioisotope production, transmutation of MA and LLFP, the subcritical core of MYRRHA must include two spectral zones: a fast neutron spectrum zone and a thermal spectrum one.

2.3.1. Fast zone description

The fast core will be placed centrally in a liquid Pb-Bi or Pb pool, leaving a central hexagonal assembly empty for housing the spallation target. It consists of hexagonal assemblies of MOX FR-type fuel pins with a Pu-content, Pu/(Pu+U), ranging from 20 to 30%, arranged in a triangular lattice with a pitch of 10 mm. The fuel pins have an active fuel length of 50 cm (but could be increased to 60 cm to achieve the requested performances) and their cladding consists of 9% Cr martensitic steel. The fuel pins are arranged in typical FR fuel hexagonal assemblies with an assembly dimension of 122 mm plate-to-plate. The fast zone is made of 2 concentric crowns, the first one consisting of 6 highly enriched fuel assemblies (with 30% Pu content) and the second one of 12 fuel assemblies of which 6 are 30% enriched and 6 are 20% enriched.

Neutronic calculations coupling the high energy transport code HETC and the lower energy neutron transport deterministic code DORT have been carried out for simulating typical configurations of the fast core and led to encouraging results showing that the targeted performances could be achieved. Table 1 illustrates the preliminary results we obtained for a particular configuration with an active length of 50 cm but in which the fuel assemblies were not well simulated [3].

TABLE 1. ACHIEVABLE PERFORMANCES IN THE MYRRHA SUBCRITICAL CORE

Spallation Source parameters		E_p = 350 MeV	
		I_p=2 mA	I_p= 5 mA
Source intensity (E<20 MeV) (x 10^{16} n/s)		4.9	12.3
Core parameters	MF = 1 / (1 - K)	19.15	19.15
	K	0.948	0.948
	Thermal Power (MW)	10.0	25.0
	Avg Power density (W/cm^3)	87	218
	Peak linear Power (W/cm)	191	477
	Max Flux >0.75 MeV (x 10^{14})	4.5	11.2
	# fuel pins (MOX 30% & 15%)	2646	2646
	MOX-30%- zone ID (cm)	12.8	12.8
	MOX-15%- zone ID (cm)	34.2	35.2
	Fast Core OD (cm)	55.5	55.5

2.3.2. Thermal zone description

The initial design, with a water pool surrounding the fast core zone and housing the thermal neutron core zone, has been completely changed for evident safety reasons (water penetration into the fast zone). In the present approach the thermal zone will be kept at the fast core periphery, but it will consist of various In-Pile Sections (IPS) to be inserted in the Pb-Bi liquid metal pool from the top of the reactor cover. Each IPS will contain a solid matrix made of moderating material (Be, C, $^{11}B_4C$) on which a total leakage flux of $1\text{-}3\times10^{15}$ n/cm²s will impinge. Local boosters made of fissile materials can be considered depending on the particular performance needed in the thermal neutron IPS. Black absorbers settled around the IPS could ensure the neutronic de-coupling of the thermal islands from the fast core.

In addition to the spallation target, the fast core and the thermal islands, the pool will contain other components of a classical reactor such as heat exchangers, circulation pumps, fuel loading and handling machines, and emergency-cooling provisions.

2.4. Confinement building

Parallel to the core and the spallation module design, attention is given to the confinement building where the MYRRHA subcritical reactor including the spallation module will be located. The accelerator will be kept in a separate confinement building to facilitate the maintenance and inspection procedures.

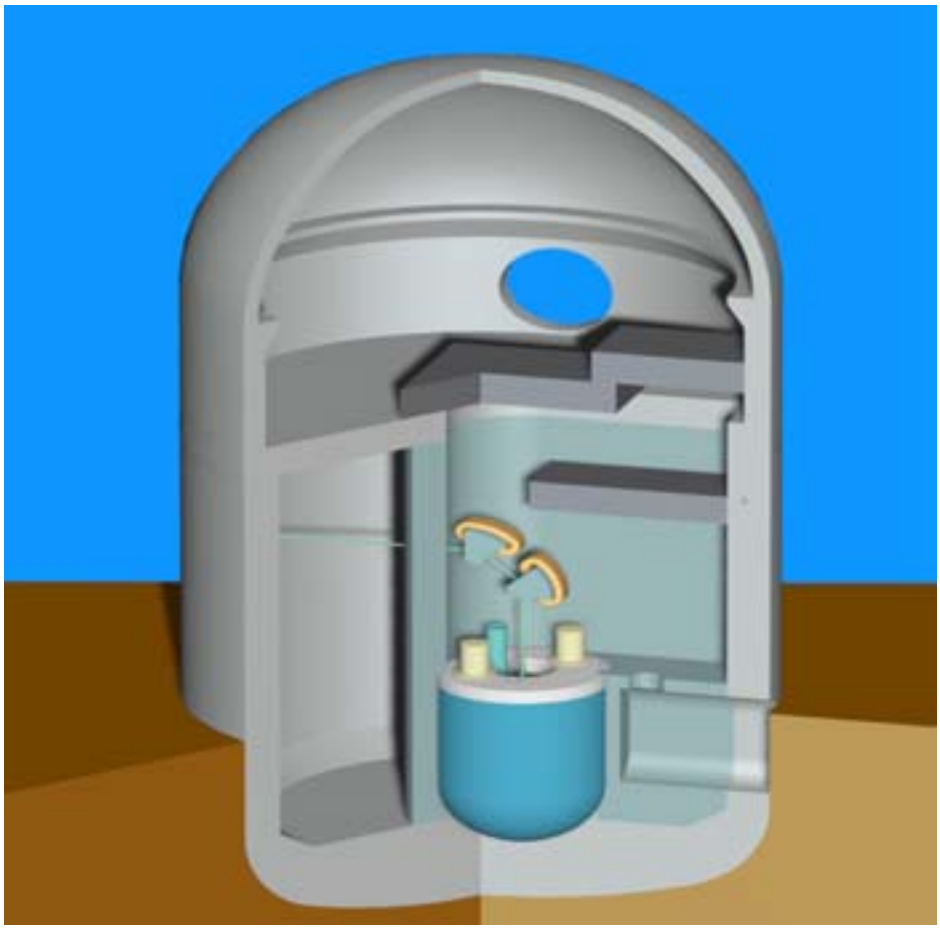

FIG. 3. MYRRHA in an inaccessible confinement building, during operation.

For the sub-critical reactor building, three options are being assessed:

- Re-using an existing confinement building where the operators are not allowed to enter during the operation of the system, as illustrated in Fig. 3.
- Re-using an existing confinement building where the operators are allowed to enter during the operation of the system, which means that the dose exposure is less than 10 μSv/h. A preliminary assessment showed that lateral shielding of 1 m steel followed by 2 m heavy concrete would be necessary for achieving such a radiation level due to the very high neutron leakage. These preliminary estimates are based on analytical estimates as well as on MCNP modelling [4].
- Designing a completely new building with the 2 options considered above.

3. MYRRHA ASSOCIATED R&D PROGRAMME

For the period 1999-2000 the MYRRHA project team is performing a detailed conceptual design and is completing the needed R&D effort to assess the main technical risks of this design for the accelerator and the spallation source, the most important parts of the system, as outlined below.

3.1. Accelerator

IBA is conducting preliminary design studies on the accelerator required for MYRRHA.

The present design of the subcritical core requires the accelerator to deliver a 350 MeV, 5 mA proton beam. This 1.75 MW CW beam has to satisfy a number of requirements, some of which are unique in the world of accelerators up to now. At this level of power it is compulsory to obtain an extraction efficiency above 99.5% and a very high stability of the beam, but on top of that the ADS application needs a reliability well above that of common accelerators, bringing down the beam trip frequency (trips longer than a few tenths of a second) to below 1 per day. The design principles are based on the following lines of thought:

- Statistics show that the majority of beam trips is due to electric discharges (both from static and RF electric fields). Hence the highest reliability requires to minimize the number of electrostatic devices, which favours a single stage design.
- In order to obtain the very high extraction efficiency, two extraction principles are available: through a septum with well separated turns, or by stripping.
- The beams are dominated by space charge. Therefore one needs careful transverse and longitudinal matching at injection, and avoiding of cross talk between adjacent turns (by an enhanced turn separation) if a separated turn structure is required for the extraction mechanism.

The space charge dominated proton beam needs a 20 mm turn separation at 350 MeV if a septum extraction has to be implemented. This solution requires the combination of a large low-field magnet and of very high RF acceleration voltages for realizing such a large turn separation, and also an electrostatic extraction device. In view of what precedes, this solution is not well suited for very high reliability operation. Extraction by stripping does not need separated turns. It may be obtained by the acceleration of H^- ions, but the poor stability of these ions makes them extremely sensitive to electromagnetic stripping (and hence beam loss) during acceleration. The use of H^- would, therefore, lead to the use of an impractically large magnetic structure. The other solution is to accelerate 2.5 mA of HH^+ ions up to 700 MeV, where stripping transforms them into 2 protons of 350 MeV each, thus dividing the magnetic rigidity by 2 and thereby allowing to extract. This solution reduces the problems related to space charge since only half the beam

current is accelerated. However, the high magnetic rigidity of a 700 MeV HH^+ beam imposes a magnetic structure with a pole radius of almost 7 m, leading to a total diameter of the cyclotron of close to 20 m. The cyclotron would consist of 4 individual magnetic sectors, each of them spanning 45 degrees. At the present stage of R&D the last option appears to be the most appropriate one.

3.2. Spallation source

The choice of a windowless design was influenced by the following considerations:

- At about 350 MeV, an incident proton delivers 7 MeV kinetic energy per spallation neutron. Almost 85% of the incident energy exits the target in the form of "evaporation" energy of the nuclei. The addition of a window would diminish the fraction of the incident energy delivered to the spallation neutrons [5].
- A windowless design avoids vulnerable parts in the concept, increasing its reliability and avoiding a very difficult engineering task.
- Because of the very high proton current density (> 130 μA/cm²) and the low energy proton beam we intend to use, a window in the MYRRHA spallation module would undergo severe embrittlement.

The project team has identified three main risks to be assessed for this windowless design:

1) Need for basic spallation data

   Since the flux characteristics in an ADS are determined by the spallation neutron intensity and since there is a lack of experimental spallation data in the proton energy range considered, SCK•CEN is assessing, in collaboration with Paul Scherrer Institute (PSI-Switzerland) and Nuclear Research Centre Soreq (NRC-Soreq, Israel), basic spallation reaction data when bombarding a thick Pb-Bi target with protons at energies close to the values that are considered for MYRRHA (E_p = 350 to 590 MeV). A joint team from the three institutes conducts the experimental programme at the PSI proton irradiation facility (PIF). The programme started in December 1998 and is due to finish by the end of May 2000 for the experimental part. The analysis of the data is still going on and expected to be finalised by the end of 2000. The expected data from this programme are:
   - neutron yield or amount of spallation neutrons per incident proton (n/p yield);
   - spallation neutron energy spectrum;
   - spallation neutron angular distribution;
   - spallation products created in the Pb-Bi target

2. Feasibility of the windowless design

   The design of the windowless target is very challenging: a stable and controllable free surface needs to be formed within the small space available in the fast core ($\varnothing_{outer}$ 140 mm). This free surface will be bombarded with protons, giving rise to a large and concentrated heat deposition (1.75 MW) dispersed over a 15 cm depth starting from the surface for a proton energy of 350 MeV. This heat needs to be removed to avoid overheating and possible evaporation of the liquid metal.

   To gain confidence and expertise in the possibility of creating a stable free surface, SCK•CEN is conducting an R&D program in collaboration with the thermal-hydraulics department of the Université Catholique Louvain-la-Neuve (UCL, Belgium). Within this R&D program, water

experiments on a one-to-one scale are performed. Water is used because of its good fluid-dynamic similarity with Pb-Bi. This programme has been complemented by velocity field measurements in collaboration with Forschungszentrum Rossendorf (FZR, Germany) using ultrasonic velocity profile and hot-wire techniques. Currently, the design of the spallation target is being fine-tuned and adapted to the latest geometrical constraints imposed by the neutronics of the fast core.

A confirmation experimental programme making use of Hg as a fluid is in progress at the Institute of Physics at the University of Latvia (IPUL) at Riga. As a final confirmation, we will run experiments with the real fluid at the actual temperatures in collaboration with Forschungszentrum Karlsruhe (FZK, Germany) where the MYRRHA spallation target head will be inserted in their KALLA Pb-Bi-loop, which has a working temperature of about 250°C.

In parallel with the experiments, numerical simulations using Computational Fluid Dynamics codes are performed, aimed both at reproducing the existing experimental results and giving input for the optimisation of the head geometry in the experiments. The CFD calculations will also be used to investigate the flow pattern and temperature profile in the presence of the proton beam, which cannot be simulated experimentally at this stage. At SCK•CEN the CFD modelling is performed with the FLOW-3D code which is specialised for free surface and low Prandtl number flow. This effort is being backed up at Université Catholique Louvain-la-Neuve (UCL, Belgium) using the Fluent code. Moreover, a collaboration agreement with Nuclear Research Group - Petten (NRG, The Netherlands) is set up for more CFD calculations with the Star-CD code. Details on this R&D associated programme can be found in [2].

3. Compatibility of the windowless free surface with the proton beam line vacuum

As the free surface of the liquid metal spallation source will be in contact with the vacuum of the proton beam line, SCK•CEN is concerned about the quantitative assessment of emanations from the liquid metal. These can lead to the release of volatile spallation products, Pb and Bi vapours and of Po, which will be formed by activation of Bi. These radioactive and heavy metal vapours can contaminate the proton beam line and finally the accelerator, making the maintenance of the machine very difficult or at least very demanding in terms of manpower exposure.

In order to assess the feasibility of the coupling between the liquid metal of the target and the vacuum of the beam line and to assess the types and quantities of emanations, SCK•CEN is preparing the VICE experiment (Vacuum-Interface Compatibility Experiment), studying the coupling of a vacuum stainless steel vessel containing 130 kg Pb-Bi, heated up to 500°C, with a vacuum tube (10^{-4} ~ 10^{-6} Torr) simulating the proton beam line. A mass spectrometer will measure the initial and final out-gassing of light gasses and the metal vapour migration. To protect the vessel from liquid metal corrosion, the possibility of Mo and W coating is currently being investigated. The full experiment will be commissioned during the third quarter of 2000. First results are expected in early 2001.

4. MYRRHA INTERNATIONAL COLLABORATIONS

The MYRRHA project, in its design phase, during its construction and also in its future operational stage, is an international collaboration project. Agreements have already been signed and collaborations are in progress with:

- Nuclear Research Centre (NRC, Israel): basic spallation data;
- Paul Scherrer Institute (PSI, Switzerland): basic spallation data, MEGAPIE;
- Ente per le Nuove tecnologie, l'Energia e l'Ambiente (ENEA, Italy): spallation source thermal hydraulics, core dynamics;
- Université Catholique de Louvain-la-Neuve (UCL, Belgium): spallation source design;
- Ion Beam Applications (IBA, Belgium): cyclotron design and construction;
- Forschungzentrum Rossendorf (FZR, Germany): instrumentation for the spallation target;
- Forschungzentrum Karlsruhe (FZK, Germany): spallation source testing with Pb-Bi;
- Nuclear Research Group (NRG, The Netherlands): CFD modelling and system safety assessment;
- Commissariat à l'Energie Atomique (CEA, France): subcritical core design, MUSE experiments, system studies and window design for the spallation target;
- Institute of Physics of University of Latvia, Riga (IPUL, Latvia): spallation source testing with Hg.

Contacts that may lead to additional collaborations exist with:

- RIT, Sweden: participation in MYRRHA;
- International Science and Technology Centre (ISTC), Contact Expert Group of the Project 559, IPPE Obninsk, Russia: PbBi target design;
- LANL et al., USA: Accelerator Transmutation of Waste (ATW) project;
- AEKI, Hungarian Nuclear Energy Institute: modelling of the spallation source;
- Belgonucleaire (Belgium): fuel and core design, fuel loading policy and fuel procurement;
- Tractebel Energy Engineering (Belgium): confinement building and auxiliary systems.

5. FUNDING SOURCES FOR THE MYRRHA PROJECT

An accurate evaluation of the needed investment to build MYRRHA and an analysis of the potential sources of funding is expected to be completed by the end of the pre-design phase end-2000 – mid-2001. Since the MYRRHA project is likely to be attractive for several types of scientific and industrial groups at the regional, national and international level, SCK•CEN and IBA will explore funding possibilities such as:

- Nuclear waste management agencies and producers of long-lived radioactive waste (at the Belgian level: NIRAS/ONDRAF and the electric utilities).
- Governmental authorities at the regional, national and international level in charge of scientific policy, energy policy or industrial development. Since MYRRHA is proposed as a first technical step in the development of a large scale demonstration model for the transmutation of radioactive waste in Europe, proposals for support of MYRRHA will be submitted to the European Union or to specific member states.
- Industrial partners, in particular engineering companies challenged by innovative technologies, for which participation in the development of MYRRHA can be an important reference. These industrial opportunities may also attract public and private venture capital.

6. CONCLUSIONS

Accelerator Driven Systems can become an essential and very viable solution to the major remaining problems of nuclear energy production. The MYRRHA system would provide the indispensable first ADS step towards a European ATW installation without forcing to freeze all options of ADS (liquid Pb-Bi versus gas, pool versus loop, sub-criticality level, mitigating tools for reactivity effects, etc).

MYRRHA is an innovative project that will trigger different research and industrial activities in fields such as accelerator reliability, nuclear waste management (transmutation), development of new materials, environmental medicine, structural material corrosion and embrittlement, and safety of nuclear installations. Increasing knowledge and know-how in these fields will contribute to aspects of sustainable development and offer a potential for industrially applicable spin-offs.

REFERENCES

[1] AÏT ABDERRAHIM, H., KUPSCHUS, P., JONGEN, Y., TERNIER, S., A multi-purpose ADS for first step towards waste transmutation – curent status of the project, SCK•CEN Report, BLG 841 (2000).

[2] VAN TICHELEN, K., KUPSCHUS, P., AÏT ABDERRAHIM, H., SEYNHAEVE, J.M., WINCKELMANS, G., JEANMART, H., Proc. 10th Int. Conf. on Emerging Nuclear Energy Systems (ICENES 2000), Petten, Netherlands, H. van Dam, J.C. Kuijper (Eds), Uitgave: NRG, Petten, ISBN: 90-805906-2-2 (2000) 130-142.

[3] MALAMBU, E., A multi-purpose ADS for first step towards waste transmutation – curent status of the project, SCK•CEN Report, R-3438 (2000).

[4] COECK, M., AOUST, Th., VERMEERSCH, F., AÏT ABDERRAHIM, H., Shielding assessment of the MYRRHA accelerator driven systems using the MCNP code, submitted for publishing in Proc. MC2000 Conference – Advanced Monte Carlo for Radiation Physics, Particle Transport Simulation and Applications, 23-26 October 2000, Lisbon, Portugal.

[5] WACQUIER, W., Determination of the Neutronic Gain of a Spallation Source: Application to ADONIS Concept, Master Degree Dissertation, Universiteit Gent/Katholieke Universiteit Leuven, Belgium (1997).

CONCEPT DEVELOPMENTS

(Session 2)

Chairperson

G. HEUSENER

Germany

NEUTRONICS DESIGN STUDIES OF AN LBE COOLED ATW BLANKET

W.S. YANG, H.S. KHALIL
Argonne National Laboratory, Argonne, Illinois, United States of America

Abstract

As part of the Advanced Accelerator Application (AAA) program in the US, preliminary trade studies have been performed at Argonne National Laboratory (ANL) and Los Alamos National Laboratory (LANL) to define and compare candidate Accelerator Transmutation of Waste (ATW) systems. The studies at ANL have focused primarily on the blanket component of the overall system, because the choice of blanket technologies is among the most important technical decisions faced in developing an ATW system. A wide range of potential transmuter designs has been investigated for lead-bismuth eutectic (LBE), sodium, and gas cooled systems. This paper summarizes the results of neutronic design studies of an LBE cooled ATW blanket. These studies have been focused primarily on achieving high discharge burnup while simultaneously achieving low burnup reactivity loss over an operating cycle. A fission-power level of 840 MWt is targeted, the same power level previously adopted for the PRISM Advanced Liquid Metal Reactor (ALMR). The blanket is assumed to be fueled with a non-uranium metallic dispersion fuel; pyrochemical techniques are used for recycle of residual transuranic actinides (TRU) in this fuel after irradiation. The key system objective of high discharge burnup is shown to be achievable in a configuration with comparatively high power density and relatively low burnup reactivity loss. System design and operating characteristics that satisfy these goals while meeting key thermal-hydraulic and materials-related design constraints have been preliminarily developed. Results of the performance evaluations indicate that an average discharge burnup of ~26% is achieved with a four year fuel residence time. Reactivity loss over the half-year cycle is 4.7%Δk. The peak fast fluence value at discharge, the TRU fraction in the charged fuel, and the peak coolant velocity are well within the assumed design limits. Owing to its use of non-uranium fuel, this proposed LBE cooled system can consume Light Water Reactor (LWR) discharge TRU at the maximum rate achievable per unit of fission energy produced (~1.0 g/MWd).

1. INTRODUCTION

Trade and system studies were initiated in the US in FY 2000 to evaluate the efficacy of the various technical options for ATW system configuration [1]. The studies at ANL have focused primarily on the blanket component of the overall system, because the choice of blanket technologies is among the most important technical decisions faced in developing an ATW system. LBE, sodium, and gas-cooled systems are among the blanket technology options currently under consideration. In this paper, we present the results of preliminary neutronics design studies aimed at defining a LBE cooled ATW system.

The primary objective of the LBE system development studies has been to define the characteristics of a system that effectively consumes TRU separated from LWR spent fuel and minimizes TRU losses to the waste streams. The blanket is assumed to be fueled with a non-uranium metallic dispersion fuel; pyrochemical techniques are used for recycle of residual TRU in this fuel after irradiation. Blanket development studies were focused primarily on achieving two important and somewhat contradictory performance objectives: 1) maximizing discharge burnup, so as to minimize number of successive recycle stages and associated recycle losses, and 2) minimizing burnup reactivity loss over an operating cycle, to minimize reduction of source multiplication with burnup. A wide range of potential transmuter designs was investigated for an assumed transmuter fission-power level of 840 MWt, the same power level previously adopted for the PRISM ALMR.

In order to develop a blanket design satisfying these contradictory objectives, two-step parametric studies were previously performed. The discharge burnup was first maximized by varying the fuel pin diameter and pitch, fuel height, and blanket geometry under key thermal-hydraulic and material-related design constraints [2]. These design constraints include the maximum coolant velocity, the peak linear power and maximum TRU fraction for fuel, and the

peak fast fluence limit for structure material. Two possible approaches to reducing the burnup reactivity loss while simultaneously achieving high discharge burnup were subsequently investigated [3]. One option is to design for low specific-power by employing a large blanket and incorporating absorbing materials. This option yields a comparatively low reactivity loss rate and thus permits relatively long cycle duration. The alternative approach is to design for high blanket specific-power and to employ more frequent refueling to limit burnup reactivity loss. Based on the results of these parametric studies, an LBE system point design (LBE-SPD) was developed to satisfy the aforementioned design goals while meeting key thermal-hydraulic and materials-related design constraints [4].

One of these design constraints considered in these studies was the maximum volumetric fraction of fuel particles (assumed to be TRU-10wt%Zr) in the dispersion fuel. Specifically, a fuel particle volume fraction limit of 50% was employed; and the highest fuel particle fraction in the charged fuel was 36.5% for the LBE-SPD. Subsequent investigations on metallic dispersion fuel indicate that lower volume fractions are preferred [5]. Thus, additional design studies were pursued to reduce the fuel particle volume fraction to 25% while still achieving the targeted high discharge burnup. Any reduction of TRU fraction in the fuel results in a reduced multiplication factor. Thus, in order to keep the same subcriticality level at the beginning of equilibrium cycle (BOEC), it is necessary to increase the fuel volume fraction or the blanket size. The fuel volume fraction and the blanket size (i.e., power rating) are closely interrelated through the constraints on the maximum coolant velocity and the peak linear power. Since any increase of blanket size has adverse economic consequences, systematic parametric studies were performed to find the optimum fuel volume fraction satisfying all the design constraints for a minimum blanket size. Based on these parametric studies, a high power-density, low TRU-fraction blanket design was developed.

The results of these parametric studies and the design and performance characteristics of the low TRU-fraction blanket design are summarized in this paper. Design objectives are first described in Section 2, and then results of parametric studies are discussed along with the key thermal-hydraulic and material-related design constraints in Section 3. The design and performance characteristics for the low TRU-fraction blanket design are presented in Section 4. Section 5 summarizes conclusions and future works.

2. DESIGN OBJECTIVES

The main purpose of the ATW system is to facilitate spent fuel disposal by removing TRU elements and long-lived fission products (LLFP) from the spent fuel and transmuting these constituents in the ATW blanket. Accordingly, one practical measure for the performance of the ATW system is the fraction of the initial TRU inventory that is not transmuted and lost to the waste stream; minimization of this fraction is obviously desirable. Denoting the TRU mass charged per pass as C, the fractional TRU discharge burnup as B_d, and the fraction of TRU lost in recycle/refabrication as f, then the amount of TRU converted into energy by fission is $B_d C$ and the amount of TRU lost to the waste stream is given by $(1 - B_d) fC$. As a result, the fractional loss of the initial TRU inventory is represented as

$$l_w = (1 - B_d) f / [(1 - B_d) f + B_d] \quad (1)$$

Therefore, in order to minimize this fractional loss, it is necessary to maximize the fractional discharge burnup and minimize the fractional loss in recycle/refabrication.

The incentive to minimize burnup reactivity loss can be illustrated by noting that the fission power produced by the subcritical blanket varies with subcriticality level (i.e., static reactivity) ρ as

$$P_{fission} \propto SI_s /(-\rho) \tag{2}$$

where S is the spallation neutron source intensity and I_s is the source importance factor [6] The subcriticality level ρ is related to the effective multiplication factor k ($k<1$) of the equivalent homogeneous system as $\rho = 1 - 1/k$. As TRU isotopes are depleted over an irradiation cycle, k decreases and ρ becomes more negative. Thus, absent compensating measures, the fission power declines with fuel depletion, making it difficult to design an economic heat removal system and, if the system produces electricity, reducing the generation of electric power whose sale is intended to reduce net system cost.

Burnup reactivity loss over an operating cycle $\delta\rho_c$ can be expressed as the product of an average reactivity loss rate and the irradiation time per cycle T_{ci} (T_{ci} is the product of the capacity factor and the cycle duration T_c). Analogously, discharge burnup B_d is proportional to the product of the specific power P_s and the *total* fuel irradiation time nT_{ci}, where n is the number of irradiation cycles. The reactivity loss over a cycle $\delta\rho_c$ is roughly proportional to the cycle burnup B_c, i.e.,

$$\delta\rho_c \propto B_c = B_d / n \propto P_s T_{ci} \tag{3}$$

Therefore, in order to attain a *high* discharge burnup B_d and *low* burnup reactivity loss $\delta\rho_c$ simultaneously, a sufficiently large number of irradiation cycles n is required to limit the cycle burnup B_c.

Equation (3) also shows that a low burnup reactivity loss can be attained by design for a low specific power or a short irradiation cycle time. The low specific-power approach requires a low power density and high TRU inventory, as well as a large number of irradiation cycles (and fuel management batches) to achieve the targeted high discharge burnup. The short irradiation-cycle approach, which permits a blanket with higher power density and specific power, requires more frequent refueling. According to a recent study, [3] the latter approach is preferred at the present time because it employs a more compact (economical) blanket and because the more frequent refueling may not adversely impact system availability given the likely need for periodic shutdown for maintenance or replacement of accelerator, beam delivery and spallation target components. By adopting this latter approach, the present study focused on optimizing the blanket configuration and material volume fractions to maximize the discharge burnup under key thermal-hydraulic and material-related design constraints; the burnup reactivity loss over an operating cycle was reduced within a reasonable limit by adjusting the cycle length.

3. DESIGN CONSTRAINTS AND PARAMETRIC STUDIES

Denoting the average power density (in W/cc) as q_v, the total fuel residence time (in days) in the blanket as T_R, and the fuel volume fraction as v_f, the discharge burnup B_d (in atom %) can be represented as:

$$B_d = cT_R q_v / v_f \rho_{tru} \tag{4}$$

where ρ_{tru} is the TRU density in fuel and c is a constant. This relation suggest that the discharge burnup can be maximized by designing for the maximum power density and fuel residence time and the minimum fuel volume fraction and TRU mass loading in the fuel. However, these design parameters are interrelated and limited by various design constraints.

- With lead-based coolant, corrosion and erosive wear of core structural materials are intensified as coolant velocity increases, and hence the coolant velocity must be limited [7]. This limitation constrains the allowable values of volumetric power density and coolant fraction. For a specified maximum coolant velocity, the minimum coolant volume fraction required for adequate cooling increases as the power density increases.

- The peak linear power is constrained by the need to limit peak fuel centerline temperature. The minimum fuel volume fraction required to satisfy the specified constraint on peak linear power increases as the power density increases, and hence by volume conservation the maximum coolant volume fraction decreases.

- The TRU mass per unit of fuel volume (ρ_{tru}) is determined such that the desired sub-criticality level at BOEC is achieved for the selected blanket configuration and fuel management scheme. This quantity is constrained by the maximum volumetric fraction of fuel particles (assumed here to be TRU-10wt%Zr) in the dispersion fuel. In the previous study, [2], this maximum volume fraction was assumed to be 50%, and the highest fuel particle fraction in the charged fuel was 36.5%. Subsequent assessments of constraints on the metallic dispersion fuel indicated that a reduction of the fuel particle volume fraction to 25% should be targeted.

- The peak fast fluence and the discharge burnup are limited by the need to ensure the fuel pin integrity. In the proposed dispersion fuel, fission products are retained within the fuel particles, which are contained within the matrix. As a result, a higher burnup can be achieved compared to the conventional metallic fuel, and thus the discharge burnup is not likely to constrain the design. On the other hand, there is likely a fast fluence limit for the core structural material (assumed to be a low-swelling stainless steel alloy similar to HT-9), and the peak fast fluence limit is assumed to be $\sim 4.0\times10^{23}$ n/cm^2. This peak fluence limit on the blanket structural material constrains the fuel residence time.

Previous parametric studies showed that, for fixed fuel residence time and cycle duration, the discharge burnup increases monotonically as the fuel volume fraction and the core size decrease [2, 4]. This indicates that there is no extreme point, and hence the maximum discharge burnup is determined by the imposed constraints. In addition, these studies showed that the burnup reactivity loss becomes slightly higher with the poison material when based on the same number of fuel management batches and discharge burnup. (To achieve the same discharge burnup with the same number of irradiation cycles, the blanket with the poison material re-

quires a higher power density or a longer cycle length). Therefore, the present study focused on determining the minimum blanket size and material volume fractions under the above design constraints. Specifically, since any increase of blanket size has adverse economic consequences, it was tried to find the optimum fuel volume fraction satisfying all the design constraints for a minimum blanket size.

In order to find the optimal fuel volume fraction, the feasible domain in the two-dimensional phase space composed of the fuel volume fraction and the blanket size (i.e., number of fuel assemblies) was investigated for each design constraint. In determining the feasible domains for the constraints on the maximum coolant velocity and the peak linear power, analytic formulas based on simple heat transfer calculations were employed. For each limiting value, a simple inequality was developed using typical peaking factors. However, since the TRU content in the fuel to keep the subcriticality level at BOEC to the specified level (e.g., 0.97) is a strong function of the fuel volume fraction and the blanket configuration, the feasible domain for the constraint on the maximum fuel particle fraction was determined by performing equilibrium cycle analyses for various blanket configurations. For each blanket configuration, the fuel volume fraction was searched such that the TRU-10Zr particle fraction in fuel required to achieve the desired subcriticality level is 25 volume percent. These parametric studies were performed with the fuel residence time and cycle duration fixed; a fuel residence time of four years at 75% capacity factor was assumed with a cycle length of one half year.

Equilibrium cycle performance characteristics were calculated using the REBUS-3 fuel cycle analysis code [8, 9]. (The equilibrium state results from repeated recycles of discharged fuel, with LWR-discharge TRU supplied as make-up for TRU consumed by fission.) Region-dependent multi-group cross sections used in the neutronics analyses are based on ENDF/B-V.2 basic data and were generated for a 21-group energy structure using the MC^2-2 [10] and SDX [11] processing codes. REBUS-3 flux calculations can be performed using a variety of neutronics solution options, including the finite-difference diffusion [12], nodal diffusion [13], variational nodal transport [14], and discrete ordinate transport [15] options. Previous studies showed that the global performance parameters computed with different flux calculation methods are essentially the same [4]. Thus, for computational convenience, homogeneous (eigenvalue) calculations were performed for each blanket configuration modeled in RZ geometry. (For the detailed analyses of the proposed system point design, inhomogeneous source problems were solved using a "generic" spallation neutron source distribution generated for a 1 GeV proton beam and a prototypic LBE target [16]).

The feasible domain of the fuel volume fraction and number of fuel assemblies for various design constraints are summarized in Fig. 1. The minimum fuel volume fraction required to satisfy the specified constraint on peak linear power increases as the power density increases, and hence the minimum blanket size for a fixed power level (e.g., 840 MWt) decreases as the fuel volume fraction increases. On the other hand, for a specified maximum coolant velocity, the maximum power density adequately removed by the LBE coolant decreases as the coolant volume fraction decreases, and hence by volume conservation the minimum blanket size increases as the fuel volume fraction increases. For a fixed TRU fraction in fuel (e.g., 25%), the neutron leakage probability decreases as the fuel volume fraction increases, and hence the desired subcriticality level at BOEC can be achieved with a reduced blanket size. As a result, the minimum blanket size for which the desired subcriticality at BOEC can be achieved with the specified TRU fraction in fuel decreases as the fuel volume fraction decreases. Each curve in Fig. 1 represents the minimum blanket size required to satisfy the given constraint as a function of fuel volume fraction, and the feasible domain for the corresponding constraint is the region above the curve. For example, the region above the solid curve represents the region

where the maximum fuel particle volume-fraction limit of 25% is satisfied. In this figure, the constraint on the maximum coolant velocity is shown for two limit values, and the peak linear power constraint is shown for two different fuel pin diameters. Peak linear power limits of 30 kW/m and 32 kW/m (derived on the basis of simple heat transfer calculations) are assumed for the 6.35 and 5.80 mm pins, respectively.

It can be seen from Fig. 1 that the maximum fuel particle volume-fraction limit of 25% is much more demanding than the peak linear power constraint. If the maximum coolant velocity limit is 2.0 m/s, then the shaded region in Fig. 1 is the feasible domain where all three constraints are satisfied. Therefore, for the maximum coolant velocity limit of 2.0 m/s, the optimum fuel volume fraction satisfying all three design constraints with a minimum number of fuel assemblies is ~0.21. In this case, the corresponding minimum number of fuel assemblies is ~230. If the maximum coolant velocity limit is reduced to 1.5 m/s, then the optimum fuel volume fraction is reduced to ~0.19, and the minimum number of assemblies is increased to ~280. In this study, the maximum coolant velocity limit of 2.0 m/s was assumed.

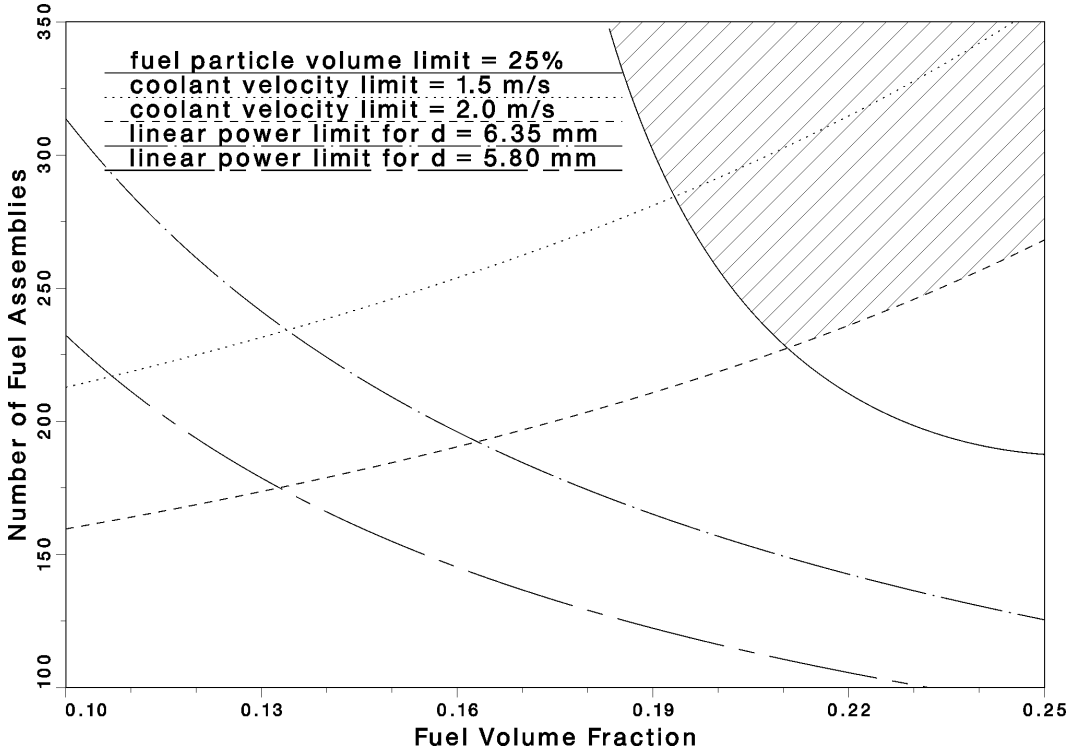

FIG. 1. Feasible domain of fuel volume fraction and number of fuel assemblies satisfying key design constraints.

4. LOW TRU-FRACTION DESIGN

Based on the results of the above parametric studies, a high power-density, low TRU-fraction design was developed. As discussed above, if we determine the pin diameter and pitch such that the fuel volume fraction is ~0.21, all three constraints on the maximum coolant velocity, the peak linear power, and the maximum fuel particle fraction in dispersion fuel can be satisfied by a blanket configuration of ~230 fuel assemblies. The blanket power distribution was flattened by optimizing the split of the TRU loading among concentric planar zones of blanket. Three

different blanket zones differing in the TRU fraction of the fuel (i.e., in "enrichment") were employed, and the zone sizes and enrichments were determined such that the peak linear powers of the three zones are close to each other. The number of fuel assemblies of 230 is 11% larger than the previous LBE-SPD design where the highest fuel particle fraction is 36.5% [4]. As a result, the average power density and flux level would be reduced considerably, and hence the peak fast fluence would be reduced for a fixed fuel residence time. Based on this observation, the fuel residence time was increased by one half-year cycle compared to the LBE-SPD design. That is, an 8-batch fuel management scheme was adopted while limiting the fuel residence time in the innermost zone to seven cycles. The fuel residence time in the innermost zone was limited to 7 cycles to limit the peak fast fluence.

While keeping the total number of fuel assemblies as close to 230 as possible, the blanket configuration was specified such that the number of assemblies in each blanket zone is an integer multiple of the corresponding number of fuel batches. The low TRU-fraction blanket layout is shown in Fig. 2, it consists of 19 hexagonal lattice positions containing the LBE target/buffer and 234 fuel assemblies. The blanket is surrounded by two hexagonal rows of steel reflector assemblies and one row of B_4C shield assemblies. In order to increase the fuel volume fraction from 0.142 of the LBE-SPD design to ~0.21, the pin diameter was increased from 0.580 to 0.675 cm. With this new pin diameter, the fuel volume fraction is increased to 0.209. While this reduces the coolant volume fraction from 0.682 to 0.570, no violation of thermal-hydraulic design constraints is expected because the volume fractions were determined to satisfy all three design constraints. The principal design parameters of the lower TRU-fraction design are compared with those of the LBE-SPD design in Table 1.

TABLE 1. COMPARISON OF DESIGN PARAMETERS OF THE LBE-SPD AND LOW TRU-FRACTION DESIGNS

Parameter	LBE-SPD	Low TRU-fraction
Pin diameter (cm)	0.580	0.675
Cladding thickness (cm)	0.070	0.070
Pitch-to-diameter ratio	1.691	1.453
Number of pins per assembly	271	271
Fuel smear density (%)	85	85
Volume fraction at operating temp. (fuel/structure/coolant)	0.142/0.138/0.682	0.209/0.165/0.570
Hexagonal assembly pitch (cm)	16.142	16.142
TRU fraction split factor (outer/ middle/inner zone)	1.45/1.28/1.00	1.45/1.28/1.00
Active fuel height (cm)	106.68	106.68
Equivalent fuel region outer diameter (cm)	253.12	269.61
Maximum blanket diameter (cm)	359.98	376.95
Cycle irradiation time (day)	137	137

The equilibrium-cycle neutronics performance of the low TRU-fraction design was analyzed using the REBUS-3 code. The inhomogeneous flux calculations were performed with the triangular-z finite difference option of DIF3D using a generic spallation neutron source distribution generated for a 1 GeV proton beam and a prototypic LBE target. A medium burnup (33 000 MWd/MT) PWR assembly with 25-year cooling time was used to specify a composition of the LWR-discharge feed stream. Computed equilibrium cycle performance parameters of the low TRU-fraction design are compared to those of the LBE-SPD in Table 2. Compared to the performance of LBE-SPD, the TRU inventory at BOEC is increased by ~12% because of the increased number of assemblies. Consequently, the average discharge burnup and the

burnup reactivity loss are reduced slightly. An average discharge burnup of ~26% is achieved with a 4-year fuel residence time; this discharge burnup would increase to ~28%, while staying within the peak fast fluence constraint, if the capacity factor were increased from the assumed 75 to 81%. (The discharge burnup of 28% within the peak fast fluence limit is the same to that of LBE-SPD; this indicates that the achievable discharge burnup is constrained primarily by the fast fluence limit.) The burnup reactivity loss for the point design is 4.7% with the assumed half-year cycle. The highest fuel particle fraction in the charged fuel (i.e., the outermost zone enrichment) is 25.6vol.%, which is slightly larger than the design limit of 25%. Increasing the fuel volume fraction slightly can further reduce this value, since there are sufficient margins to thermal-hydraulic design limits as discussed below.

The adopted enrichment zoning results in similar power peaking factors of 1.44 at BOEC and 1.56 at the end of equilibrium cycle (EOEC). At BOEC, the peak linear power (21.0 kW/m) occurs in the outer fuel zone. Because of the increased spallation source intensity and non-uniform TRU depletion, the peak power location moves to the inner fuel zone (22.8 kW/m) at EOEC. The resulting peak linear powers in the three blanket zones are very close to each other as desired, and they are well within the limiting value of 30 kW/m. The peak fast fluence value of 3.69×10^{23} n/cm^2 occurs in the inner blanket zone, and is well within the assumed fast fluence limit of 4.0×10^{23} n/cm^2. The batch-averaged fission power produced by each fuel assembly and the fission power densities at the blanket mid-plane are shown in Figs 3 and 4, respectively. The highest assembly power of 4.42 MW occurs in one of the middle zone assemblies at EOEC. The coolant velocity required to remove this heat load is 1.54 m/s for a coolant temperature rise of 150 K, which is well within the assumed velocity limit of 2.0 m/s.

TABLE 2. COMPARISON OF PERFORMANCE CHARACTERISTICS OF THE LB-SPD AND LOW TRU-FRACTION DESIGN

Parameter		LBE-SPD	Low TRU-fraction
TRU fraction in fuel (TRU-10Zr volume %)	Inner zone	25.2	17.7
	Middle zone	32.3	22.6
	Outer zone	36.5	25.6
Burnup reactivity loss (%Δk)		5.3	4.7
Core-average power density (kW/L)		156.3	136.4
Power peaking factor (BOEC/EOEC)		1.46/1.51	1.44/1.56
Peak linear power (kW/m)	Inner zone	25.0 (at EOEC)	22.8 (at EOEC)
	Middle zone	26.1 (at EOEC)	22.5 (at EOEC)
	Outer zone	24.5 (at BOEC)	21.0 (at BOEC)
Average discharge burnup (atom %)		26.7	25.7
Peak fast fluence (10^{23} n/cm^2)		3.88	3.69
Net TRU consumption rate (kg/year)		237	237
Equilibrium loading (kg/year)	LWR TRU	237	237
	Recycled TRU	649	682
	Total TRU	886	919
BOEC heavy metal inventory (kg)		2661	3170

5. CONCLUSIONS

Parametric studies have been performed to optimize the LBE-cooled ATW system's performance for a reduced value of the maximum volumetric fraction of fuel particles in the dispersion fuel. Based on the results of these studies, a high power-density, low TRU-fraction blanket design has been developed under key thermal-hydraulic and materials-related design constraints. The key system objective of high ATW fuel discharge burnup was shown to be achievable in a configuration with comparatively high power density (enabling small system size and potentially favorable economics) and relatively low burnup reactivity loss. Perhaps more significantly, a systematic approach was devised for meeting these key objectives subject to the assumed constraints. This approach should greatly facilitate future efforts to optimize the system's performance, e.g., for further updated values of the constraining variables or taking a broader set of performance objectives into consideration.

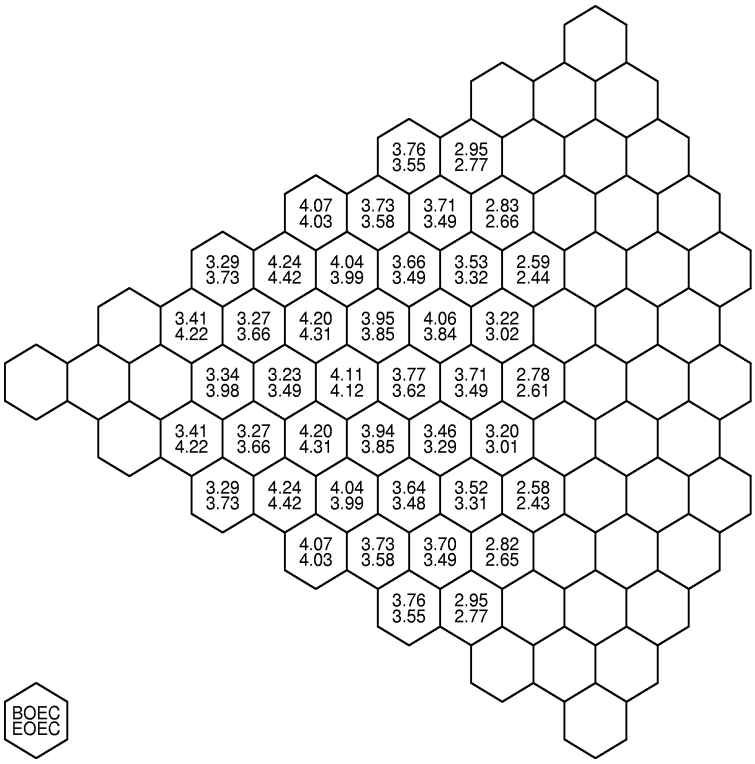

FIG. 3. Total assembly fission power (MWt) for the low TRU-fraction LBE-cooled blanket design.

Two key assumptions made in developing the proposed point design are the power level of the transmutation system (840 MWt) and its minimum subcriticality level (k_{eff} = 0.97 at the start of cycle); both parameters strongly affect system characteristics and directly impact the accelerator beam power required per transmuter. The choice of transmuter (fission) power level is based largely on the recent design experience with the PRISM ALMR, which indicates that favorable economics and safety performance can be achieved with the 840 MWt system size. The applicability of this experience to the LBE cooled ATW transmuter should be examined in future studies. With respect to degree of subcriticality, the assumed level is believed to be a good compromise between the competing objectives of minimizing accelerator power (favors

high k_{eff}) and precluding the potential for criticality as a result of operational or accidental reactivity insertions (favors low k_{eff}). However, explicit dynamic and safety analyses will be required to optimize the choice of subcriticality level.

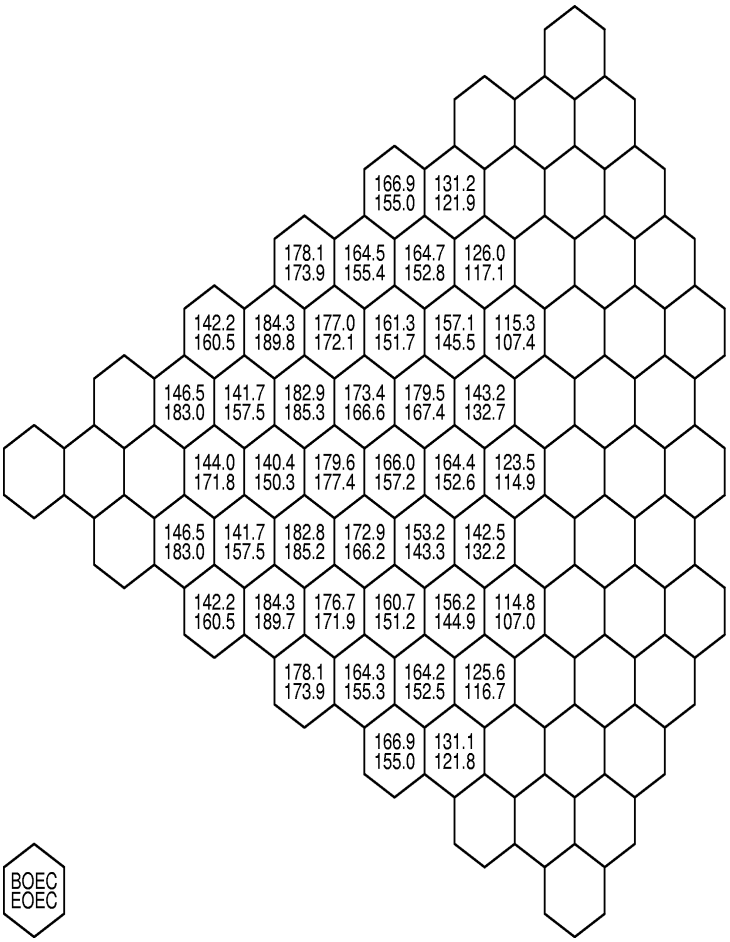

FIG. 4. Fission power density (W/cc) at midplane of low TRU-fraction LBE-cooled blanket design.

With respect to transmutation performance, the current study has focused on the equilibrium-cycle mass flows, assuming that TRU losses during recycle are negligible. Future studies are needed to assess the impact of non-zero TRU losses on the fuel cycle mass flows in general (including fuel composition effects) and the waste streams in particular. Moreover, a blanket management/control strategy should be developed for accommodating with the evolution of fuel composition (and reactivity) during the transition to the equilibrium, as well as for variations in the LWR feedstock composition and other deviations from the equilibrium conditions.

REFERENCES

[1] A Roadmap for developing Accelerator Transmutation of Waste (ATW) Technology; A Report to Congress, DOE/RW-0519, US Department of Energy (1999).

[2] YANG, W.S., NABEREJNEV, D.G., KHALIL, H.S., Physics Design Studies of an LBE Cooled ATW System, Trans. Am. Nucl. Soc., **83**, 328 (2000).

[3] YANG, W.S., KHALIL, H.S., Reduction of Burnup Reactivity Loss in Accelerator Driven Transmutation Systems, Proc. 4th Topical Meeting on Nuclear Applications of Accelerator Technology, 13-15 November 2000, Washington DC.
[4] YANG, W., KHALIL, H., Blanket Design Studies of an LBE Cooled Accelerator Transmutation of Waste System, to be published in Nuclear Technology.
[5] CRAWFORD, D.C., HAYES, S.L., MEYER, M.K., Current U.S. Plans for Development of Fuels for Accelerator Transmutation of Waste, paper presented in the IAEA Technical Committee Meeting on Core Physics and Engineering Aspects of Emerging Nuclear Energy Systems for Energy Generation and Transmutation, 28 November-1 December 2000, Argonne National Laboratory.
[6] SALVATORES, M., SLESSAREV, I., TCHISTIAKOV, A., RITTER, G., The Potential of Accelerator-Driven Systems for Transmutation or Power Production Using Thorium or Uranium Fuel Cycles, Nucl. Sci. Eng., **126**, 333 (1997).
[7] FOMITCHENKO, P.A., Physics of Lead-Cooled Reactors, Proc. The 1998 Frédéric Joliot Summer School in Reactor Physics, 17-26 August 1998, Cadarache, France.
[8] TOPPEL, B.J., A User's Guide to the REBUS-3 Fuel Cycle Analysis Capability, ANL-83-2, Argonne National Laboratory (1983).
[9] YANG, W.S., KHALIL, H.S., Analysis of the ATW Fuel Cycle Using the REBUS-3 Code System, Trans. Am. Nucl. Soc., **81**, 277 (1999).
[10] HENRYSON II, H., TOPPEL, B.J., STENBERG, C.G., MC^2-2: A Code to Calculate Fast Neutron Spectra and Multigroup Cross Stions, ANL-8144, Argonne National Laboratory (1976).
[11] STACEY, Jr., W.M., et al., A New Space-Dependent Fast-Neutron Multigroup Cross-Stion Preparation Capability, Trans. Am. Nucl. Soc., **15**, 292 (1972).
[12] DERSTINE, K.L., DIF3D: A Code to Solve One-, Two-, and Three-Dimensional Finite-Difference Diffusion Theory Problems, ANL-82-64, Argonne National Laboratory (1984).
[13] LAWRENCE, R.D., The DIF3D Nodal Neutronics Option for Two- and Three-Dimensional Diffusion Theory Calculations in Hexagonal Geometry, ANL-83-1, Argonne National Laboratory (1983).
[14] PALMIOTTI, G., LEWIS, E.E., CARRICO, C.B., VARIANT: Variational Anisotropic Nodal Transport for Multidimensional Cartesian and Hexagonal Geometry Calculation, ANL-95/40, Argonne National Laboratory (1995).
[15] ALCOUFFE, R.E., BRINKLEY, F.W., MARR, D.R., O'DELL, R.D., User's Guide for TWODANT: A Code Package for Two-Dimensional, Diffusion-Accelerated, Neutral-Particle Transport, LA-10049-M, Los Alamos National Laboratory (1990).
[16] NA, B.C., WYDLER, P., TAKANO, H., OECD/NEA Comparison Calculations for an Accelerator-Driven Minor Actinide Burner: Analysis of Preliminary Results, paper presented in the 2nd Workshop on Utilization and Reliability of High Power Proton Accelerators, OECD/NEA, 22-24 November 1999, Aix-en-Provence, France, NEA, ISBN: 92-64-18749-9 (2001).

PHYSICS STUDIES FOR SODIUM COOLED ATW BLANKET

R.N. HILL, H.S. KHALIL
Argonne National Laboratory, Argonne, Illinois, United States of America

Abstract

Because the choice of blanket technologies is among the most important technical decisions faced in the Accelerator Transmutation of Waste (ATW) program, extensive system studies have been pursued on blanket design. A wide range of potential transmuter configurations and fuel cycle scenarios have been investigated using sodium, lead-bismuth eutectic (LBE), and gas as coolant. The primary objective has been to define the characteristics of a system that effectively consumes transuranics (TRU) separated from LWR spent fuel and minimizes TRU losses to the waste stream. For the liquid-metal cooled design studies, a fission-power level of 840 MWt was targeted, the same level previously adopted for the PRISM Advanced Liquid Metal Reactor (ALMR). The blanket is fueled with a non-uranium metallic dispersion fuel; pyrochemical techniques are used for recycle of residual TRU in this fuel after irradiation. Parametric studies were performed to optimize the sizing of the sodium cooled transmuter blanket, to mitigate the power peaking problems near the source region, and to assess startup core performance; results are summarized in this paper. Performance evaluations indicate that an average discharge burnup of 275 MWd/kg (29.5 atom%) is achieved with a 3.5 to 4 year fuel residence time. Reactivity loss over the half-year cycle is 4.9%Δk. The sodium coolant allows a compact core design with the volume reduced by ~1/3 compared to LBE cooled ATW blanket designs.

1. INTRODUCTION

Trade and system studies were initiated in the US in FY 2000 to evaluate the efficacy of various technical options for ATW system configuration [1]. The studies at ANL have so far focused primarily on the blanket component of the overall system, because the choice of blanket technologies is among the most important technical decisions faced in the ATW program. Both the basic technology and the particular features of the blanket design strongly impact transmutation performance and requirements on other ATW sub-systems (spallation target, accelerator, chemical separations). The sodium-cooled concept developed here is one of several blanket technology options currently under consideration in the ATW program. It is planned to conduct screening evaluations leading to the selection of two or three of the candidate concepts for further development, and later to select a single preferred technology from among those retained in the initial screening process.

A discussion of the issues associated with the use of alternative coolants for ATW can be found in the reports of the ATW roadmap working groups [2,3]. An in-depth summary of the key neutronic, thermal hydraulic, material compatibility, coolant chemistry, and coolant activation characteristics of various liquid metal coolants is provided in Reference 4. The sodium-cooled blanket design study builds on previous analyses conducted for an LBE cooled system [5]; similar design objectives and analysis techniques are utilized in this work.

In Section 2, the basic objectives and system assumptions for the sodium-cooled blanket design studies are described. The specific performance objectives and design constraints are identified in Section 3; the calculation methods are briefly described in Section 4. Parametric studies conducted to evaluate tradeoffs associated with adoption of various design parameters are presented in Section 5. The primary focus of these studies is development of a compact core and mitigation of power peaking problems inherent to the source driven configuration. In Section 6, the performance of startup and recycle fuel management scenarios is compared. Section 7 summarizes key conclusions.

2. OBJECTIVES AND SYSTEM ASSUMPTIONS

The primary objective of the system development efforts at ANL has been to achieve efficient transmutation of the transuranic actinides (TRU) separated from LWR spent fuel. It is generally recognized that a fast neutron energy spectrum is needed to accomplish the transmutation of minor actinides efficiently, because the fission-to-capture ratio for several key TRU nuclides is significantly greater in a fast spectrum [6]. The higher capture probability per incident neutron in a thermal spectrum causes build-up of the higher actinide fraction in the proportion of the TRU loading not consumed by fission, which adversely impacts neutron balance at high burnup and complicates recycle if the burnup is incomplete. On the other hand, the higher TRU inventory of fast systems for a given power level implies a lower specific power and a correspondingly lower burnup rate. Moreover, the fuel irradiation time in a fast spectrum is limited by radiation damage to structural materials caused by the large flux of high-energy neutrons. Consequently, fuel burnup in a fast system is generally incomplete in one pass through the transmutation blanket, and recycle of discharged fuel is required to achieve an acceptably low TRU content in the waste stream. It is assumed in the point design for the sodium-cooled system that fuel recycle is performed using pyrochemical techniques referred to as "PYRO-B" in the ATW roadmap [1].

The major assumptions made in developing the sodium system point design are similar to those employed in the ATW roadmap as a basis for estimating ATW system costs and analyzing deployment scenarios; they can be summarized as follows:

1. A high-power linear accelerator generates a beam of energetic (~1 GeV) protons for delivery to target/blanket "transmuter" system; the proton beam impinges on a spallation target and produces a source of neutrons that drives the subcritical blanket.
2. Beam delivery to the target is in the vertical direction. Several target options are under consideration for use in conjunction with the sodium-cooled blanket; these options include a liquid lead-bismuth eutectic (LBE) target, a sodium cooled tungsten target, and a gas cooled tungsten target. For this study, the LBE target is assumed.
3. The blanket is fueled with solid, uranium-free fuel clad with a low-swelling stainless steel alloy similar to the HT9 alloy developed in the U.S. Advanced Liquid Metal Reactor Program [7,8]. The fission power level of each transmuter module is 840 MWt -- consistent with the ALMR power level selected on the basis of favorable economics (through modular fabrication and installation) and excellent safety (passive removal of decay heat using ambient air as an inexhaustible heat sink).
4. Chemical separations required to extract uranium and fission products from the LWR discharge fuel are performed with the UREX process [1], and the TRU-containing output stream from this process is treated with a subsequent pyrochemical process "PYRO-A" [1] to produce metallic TRU feed for use in ATW fuel fabrication. Recovery of the TRU remaining in the ATW fuel after irradiation in the ATW blanket is performed using the "PYRO-B" [1] process.
5. Key long-lived fission products (I-129 and Tc-99) are separately recovered during the LWR spent fuel pre-treatment steps. It has not yet been decided whether to immobilize these species in suitable waste forms or to transmute them in the ATW blanket; thus, initial system development efforts have focused on transmutation of TRU only.

The central objective of the system development studies conducted to date has been to define the characteristics of a transmutation system that minimizes transuranic losses to the waste streams. It should be emphasized that neither the feasibility nor optimality of the system developed with this objective has been demonstrated; for example, alternative systems may exhibit superior economic or safety performance.

As shown in Section 3, the objective of minimizing TRU losses to the waste stream is accomplished by maximizing the discharge burnup of ATW fuel (to minimize the number of recycle passes) and minimizing the fractional TRU loss per pass in recycle and refabrication. The achievable discharge burnup is likely constrained primarily by the fast-neutron irradiation damage to the cladding (fast fluence limit). The discharge burnup value currently targeted (~30 atom%) is high for conventional LMR fuels and remains to be demonstrated for the metallic dispersion fuel currently identified as the reference fuel. However, this burnup appears to be a reasonable development goal for the dispersion fuel type, particularly uranium-free fuels employing a non-fissioning matrix (e.g., zirconium or molybdenum); at a fixed heavy atom (fractional) burnup, the fission product density is much lower with a non-fissioning matrix than with a uranium matrix. Thus to the extent achievable fuel burnup is governed by fission product accumulation, higher burnup fractions can be targeted for non-uranium fuels.

3. PERFORMANCE OBJECTIVES AND CONSTRAINTS

In this study, full advantage is taken of the parametric studies performed as part of the lead bismuth eutectic (LBE) cooled ATW transmuter study [9]. In particular, the zirconium matrix metallic-dispersion fuel form developed for the LBE system is employed. In addition, the performance objectives reflect the general trends observed in the LBE cooled ATW trade studies (e.g., a preference for low inventory transmuter options).

The main purpose of the ATW system is to facilitate spent fuel disposal by removing the transuranic (TRU) elements and possibly long-lived fission products (LLFP) from the spent fuel and transmuting these constituents in the ATW blanket. Accordingly, the overriding performance objective for the ATW system is to minimize the fraction of the initial TRU inventory that is not transmuted and lost to the waste stream. Because there is a fraction of the TRU inventory lost every time the material is processed, developing high efficiency processing technology and limiting the number of processing operations required are design targets. From the viewpoint of transmuter design, the key design goal is to maximize the discharge burnup; this implies the fewest number of recycle/refabrication campaigns to destroy a given amount of material.

The primary design goal to eliminate TRU from the final waste stream is also the reason for utilizing uranium-free fuel forms. This prevents the generation of new TRU by in-reactor transmutation of uranium into plutonium. Because all current reactors operate on uranium-based fuel forms, a fuel development program will be required for this waste transmutation mission; accommodation of high burnup is a primary development goal for this new fuel form. For this application, a dispersion fuel where TRU-10Zr fuel particles are dispersed in a zirconium metal matrix has been proposed [1]. Extensive experience with U-10Zr and U/Pu-10Zr fuels in the EBR-II fuel development program demonstrated the compatibility of similar fuel forms with sodium coolant; sodium was also utilized as a bond material within the pin. The dispersion fuel will be designed so that the fission products are contained within the fuel particles, which are contained within the matrix. Thus, this fuel form is expected to have superior irradiation performance (much less swelling than metal plutonium alloys) and there is no conceptual limit to the burnup.

Given the design goal of high discharge burnup, the required fuel irradiation time will be roughly proportional to the TRU inventory of the transmuter blanket. Low inventory options offer several advantages from a global fuel cycle perspective. Although the total amount of material destroyed is dictated solely by the power level, with low inventory of TRU a higher rate of burnup accumulation (MWd/kg per year or atom%/year) is achieved. In addition, low inventory transmuters require less of the TRU inventory targeted for transmutation to run a

single system; thus, additional transmuters can be started from the same initial inventory, increasing the overall destruction rate. Low inventory systems also have a smaller final discharge (un-transmuted) inventory at the end of their operation campaign.

Conversely, design options with high inventory offer several improvements to the performance of the transmuter blanket. One of the major problems associated with utilization of uranium-free fuel is the complete loss of internal conversion of the uranium matrix, which creates fissile material (Pu-239) with fuel burnup. This leads to magnified reactivity losses with fuel burnup compared to conventional systems. For the "pure burner" design [6] developed for the ALMR for weapons plutonium disposition, reactivity loss rates were reduced by maximizing the TRU inventory; this was done by increasing the core volume and adding a fixed poison. Since the TRU loss rate is determined solely by the system power level, this effectively increases the ratio of end-of-cycle TRU mass to beginning-of-cycle TRU mass for a given cycle length, leading to smaller reactivity loss rates. In general, high inventory designs will be larger than low inventory options. The associated reduction of power density may be desirable to reduce the heat loads for the unproven non-uranium fuel forms. On the other hand, there will be economic penalties associated with any blanket size increase.

The relative performance of high and low inventory ATW design options was evaluated in Ref. [5] for the LBE-cooled ATW system. Results indicate that reactivity losses can be kept reasonably small through the use of sufficiently short cycle lengths (e.g., 3 to 6 months). The resulting reactivity losses can be compensated by a combination of increased source strength or potential reactivity insertion. Therefore, low TRU inventory has been adopted as a preferred option for the sodium-cooled transmuter studies. This approach will result in compact (low cost) design options with superior fuel cycle performance.

For conventional fast reactor systems, fuel pin integrity is ensured by imposing discharge burnup limits for the fuel matrix and peak fast fluence limits for the cladding material. Typically, the fuel lifetime is constrained to 4-5 years at which point the irradiated fuel is near both limits. For the zirconium matrix dispersion fuel employed here, there is no conceptual burnup limit. Therefore, the fuel lifetime will be constained only by damage considerations for the structural materials. For this analysis, a peak fast fluence limit of 4.0×10^{23} n/cm^2 is assumed; this value is based on data for low-swelling ferritic alloy (HT-9) developed in the ALMR program [7,8].

The TRU fraction in the fuel is determined such that the effective multiplication factor at the beginning of cycle is 0.97. The reactivity loss and declining source multiplication during the operating cycle are assumed in the current design analyses to be compensated by increased source strength. To prevent a need for accelerator capacity to increase by more than a factor of three, the end of cycle effective multiplication factor must be at least 0.91; this limit effectively constrains the cycle length for a given reactivity loss rate.

A maximum volume fraction of 50% TRU-Zr fuel particles in the proposed dispersion fuel is assumed. However, the dispersion fuel will be easier to fabricate and likely have improved irradiation performance at much lower fuel volume fractions. Thus, design options that result in reduced fuel volume fraction within the dispersion matrix are preferred.

Finally, the power density of the transmuter blanket is constrained by fuel heat load and heat transfer considerations. In particular, the peak linear power is constrained by the need to limit peak fuel centerline temperatures to prevent fuel melting. Estimates of the peak linear power limit for the proposed fuel form and for ternary (U-Pu-10Zr) metallic alloy fuel, which was the reference fuel form in the PRISM ALMR [7], are derived in Table 1.

TABLE 1. ESTIMATION OF PEAK LINEAR POWER FOR ATW DISPERSION FUEL (U-10Zr/Zr) AND ALMR METALLIC ALLOY FUEL (U-27Pu-10Zr)

Parameter	ALMR Metal fuel sodium coolant	ATW Dispersion fuel sodium coolant	ATW Dispersion fuel LBE coolant
Coolant film heat transfer coefficient, W/m^2K	1.42E5	1.42E5	3.77E4
Clad thermal conductivity, W/mK	26.8	26.8	26.8
Fuel solidus temperature, ^oC	990	840	840
Fuel thermal conductivity, W/mK	15.3	13.8	13.8
Matrix thermal conductivity, W/mK	-	22.2	22.2
Fuel volume fraction, %	100	~40	~30
Irradiation decrease in fuel conductivity, %	50	50	50
Effective fuel matrix thermal conductivity, W/mK	7.65	16.1	17.6
Peak linear power estimate, W/cm	374	454	332

The TRU-10Zr composition of the fuel particles in the ATW dispersion fuel has a significantly lower (~150^{o}C) solidus temperature compared to the ternary metal fuel alloy. However, the thermal conductivity of the dispersion (composite) fuel is significantly improved because the zirconium matrix is highly conductive and its thermal properties are not expected to degrade with irradiation as observed for fuel alloys. The net result is an estimated increase in the allowable peak linear power from 375 to 450 W/cm. Note that the peak linear power limit is lower with LBE coolant because of a much larger temperature rise in the coolant itself. This difference is attributed primarily to higher coolant flow rate and improved thermal conductivity in the sodium. Given the large uncertainties associated with thermal properties of the non-uranium dispersion fuel, it was considered prudent to impose a conservative design constraint. Thus, a peak linear power limit of 400 W/cm was assumed in these parametric studies.

4. COMPUTATIONAL METHODS AND TECHNIQUES

Analyses of the sodium-cooled system point design have so far focused primarily on the equilibrium fuel cycle, because system performance under equilibrium conditions is believed to be a good basis for design optimization (startup cycle performance is compared to the equilibrium results in Section 6). Equilibrium cycle performance characteristics were calculated using the REBUS-3 fuel cycle analysis code [10,11]. The region-dependent multigroup cross sections used in the neutronic analyses were originally generated for the ALMR pure burner design as described in Ref. [7]; they are based on ENDF/B-V.2 basic data processed using the MC^2-2 [12] and SDX [13] codes for a 21-group energy structure.

In the equilibrium fuel cycle model, the charged fuel contains the transuranics recovered via recycle from the discharged ATW fuel, supplemented by LWR-discharge TRU to make up for the TRU consumed by fission. Determination of the equilibrium composition neglected the very small proportion of TRU lost during recycle and refabrication, and assumed 5% of rare-earth fission products carried over by the recycled ATW TRU. The TRU mass loading in the fuel which meets the targeted subcriticality level at BOEC was determined using the REBUS-3 enrichment search techniques. REBUS-3 also computes both batch-dependent and batch-averaged compositions at BOEC and EOEC for each specified depletion region. In this study, five (equal length) axial depletion zones were consistently used; in the planar dimension, depletion zones consisted of individual fuel assemblies or groups of neighboring assemblies with similar reaction rates. Irradiation swelling of the fuel was modeled in the depletion calculations as a uniform 5% axial expansion of the fresh fuel, based on IFR experiments for U-Pu-Zr ternary metal fuel, even though the proposed dispersion fuel is expected to exhibit less irradiation swelling.

Preliminary sensitivity studies of the effect of various flux computational options available in REBUS-3 were performed as part of the LBE cooled ATW blanket design studies [9]. Both the inhomogeneous source problem and the corresponding homogeneous eigenvalue problem (i.e., a system without the spallation source made artificially critical by use of an eigenvalue to scale neutron production) were considered. These sensitivity studies demonstrated that the global performance parameters are very similar for different flux calculation methods. In addition, the integral parameters estimated with the eigenvalue calculations were found to agree well with the results of the corresponding inhomogeneous source calculations; peak flux and power were not as accurately predicted by the eigenvalue calculations. Thus, for computational convenience, homogeneous (eigenvalue) neutronic calculations performed using the hexagonal-Z nodal diffusion option of DIF3D were employed as a basis for optimizing the global design parameters (e.g., system size) of the sodium-cooled ATW blanket as described in Section 5.1.

The increase in source strength required to compensate the lower EOEC neutron multiplication leads to large increases in flux in the vicinity of the source region, which creates flux and power peaking problems. In Section 5.2, design options to mitigate the power peaking inherent to the source-driven configuration are investigated. For this analysis, inhomogeneous source problems were solved using a “generic” spallation neutron source distribution generated for a 1 GeV proton beam and a prototypic LBE target [14]. Even though the spallation neutron source distributions need to be generated for specific transmuter (target/blanket) configurations, inhomogeneous source analyses can be performed with sufficient accuracy using generic source distributions appropriate to the accelerator beam proton energy and the spallation target material and geometry. For these analyses, the flux calculation method was switched to the triangular-Z finite difference option of DIF3D [15] to estimate the peak values more accurately.

5. PARAMETRIC DESIGN STUDIES

5.1. Core sizing study

A preliminary 840 MW (thermal) LBE cooled ATW transmuter design was used as the starting point for developing the sodium cooled system. This LBE configuration employs the seven central assembly locations for the LBE target and buffer as shown in Fig. 1.

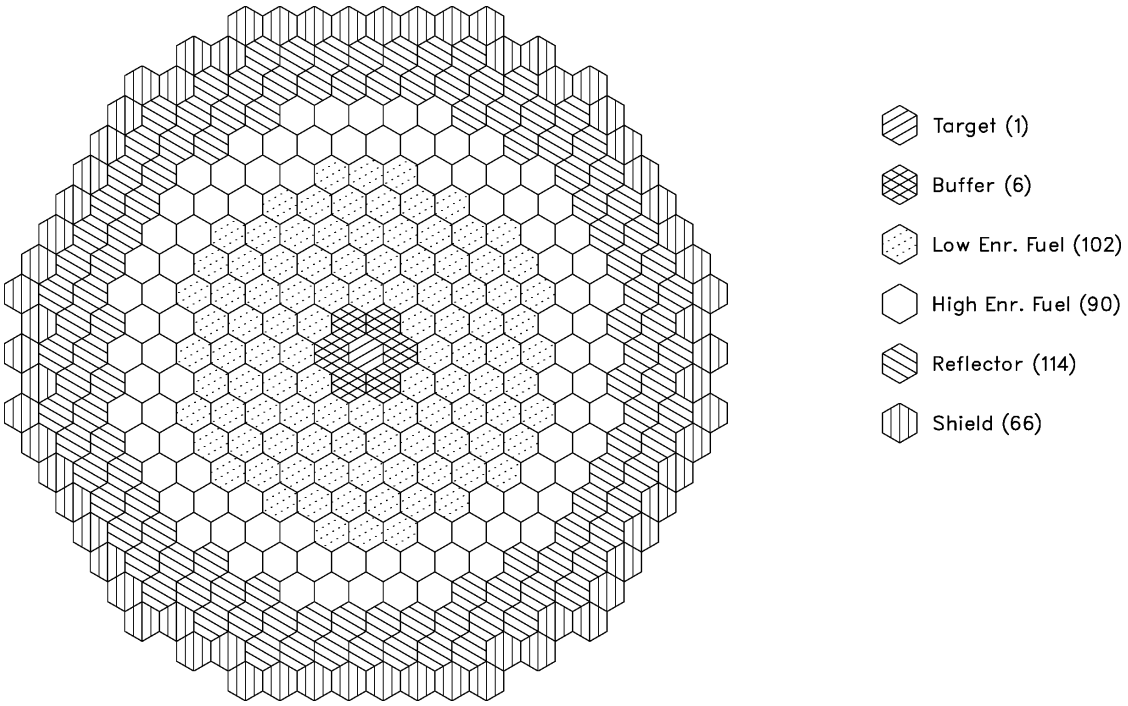

FIG. 1. LBE cooled ATW blanket configuration.

The preliminary LBE-cooled blanket is composed of 192 fuel assemblies in two "enrichment" zones. The enrichment is varied by using a higher volume fraction of the TRU-10Zr fuel particles within the zirconium matrix in the outer region; an enrichment split of 1.2 was assumed.

For the LBE coolant, the lattice design is quite loose with a pitch-to-diameter (P/D) ratio of 1.73 resulting in a coolant volume fraction of nearly 70%. This high coolant volume fraction is necessary to achieve the low coolant velocity required for the heavy liquid metal coolant. In addition, several dummy structural pins were employed for holding down the assembly; this hold-down mechanism is required with the heavy liquid metal coolant but not with sodium coolant. The net result is a low fuel volume fraction of only 20% as compared to a smeared fuel volume fraction of 38% in the ALMR design [7].

First, the performance effects were evaluated for a direct replacement simple exchange of LBE coolant with sodium, using the loose (LBE) lattice design. In addition, the fuel cycleparameters of the LBE system were retained, i.e., a fuel residence time of six 145-day cycles was assumed. This evaluation illustrates the impact of sodium coolant (relative to LBE) on the reactor performance. Performance results are compared for the two coolants in Table 2. From a reactor physics viewpoint, the main difference between the sodium and LBE coolant is increased scattering (without moderation) in the LBE. Thus, the LBE reduces neutron escape from the interior regions of the blanket and provides superior reflection for neutrons that leak out of the active zone. Thus, a much higher (~30%) TRU inventory is required to achieve the beginning-of-equilibrium-cycle (BOEC) multiplication target of 0.97 when sodium coolant is used. For a fixed fuel lifetime, a corresponding decrease in the average discharge burnup (by 20%) is observed. As identified in Section 3, the high inventory has a favorable impact of reducing the reactivity loss rate. In addition, the power peaking factors are lower in the sodium system because the LBE coolant retains more neutrons in the peak power regions. The low fast fluence for the sodium case (2.5 vs. 4.0×10^{23} n/cm^2 for the LBE case) indicates that fuel lifetime can be

extended. A scoping study indicated that the fuel lifetime can be extended from 6×145 = 870 effective full-power days (efpd) to 1400 efpd before the fluence limit is exceeded for the sodium cooled case. Results calculated for a fuel management scheme of eight 175-day irradiation intervals (1400 efpd fuel lifetime) are also given in Table 2.

TABLE 2. PERFORMANCE PARAMETERS OF LBE CONFIGURATION WITH LBE AND SODIUM COOLANT

LBE configuration and assembly design		LBE-cooled	Sodium substitution	Extended fuel lifetime
Number of fuel batches		6	6	8
Cycle irradiation time (days)		145	145	175
Fuel particle fraction (volume % in matrix)	Inner zone	27.5	34.2	38.2
	Outer zone	33.5	41.8	46.8
Multiplication factor	BOEC	0.970	0.970	0.969
	EOEC	0.912	0.928	0.922
Burnup reactivity loss (% Δk)		5.80	4.17	4.69
Peak linear power (W/cm)		317	287	311
Discharge burnup (MWd/kgHM)		272	218	314
Peak fast fluence (10^{23} n/cm^2)		3.96	2.55	4.03
BOEC Heavy metal inventory (kg)		2256	2899	3024

A corresponding increase in average burnup from 218 to 314 MWd/kg is observed. Because the average burnup of the blanket also increases, a 4% increase in the TRU inventory is required to maintain the BOEC multiplication factor. An important result is that the sodium-cooled design achieves a higher average discharge burnup than the LBE-cooled design (314 vs. 272 MWd/kg) at the same discharge fluence level. This difference is attributed to the moderating effect of the sodium coolant. The neutron energy spectrum is harder when the LBE coolant is utilized, resulting in a higher fast fluence to total flux ratio. This difference is particularly pronounced for lattice designs such as the LBE cooled ATW configuration where the coolant volume fraction is quite high.

One drawback of the design where sodium is simply substituted in the LBE configuration is that the volume fraction of fuel particles (47% in the outer zone) is close to the 50% limit. Moreover, the resulting configuration does not take advantage of the possibility of designing a more compact system (reduced coolant volume fraction at higher flow rate) with sodium coolant. Thus, modifications to the assembly design which increase the fuel volume fraction were investigated; these changes effectively allocate additional space for zirconium matrix material. The most significant change was to switch from the loose lattice (P/D ~1.7) LBE design to a conventional tight lattice (P/D ~1.2) design. The assembly design proposed for the sodium-cooled ALMR [7] was utilized. This change nearly doubles the fuel matrix volume as the smeared fuel volume fraction increases from 20% to 38. Furthermore, the smear density of the fuel was increased from 75 to 85%. Significant swelling of the dispersion fuel is not expected; thus, the large gaps required to accommodate fuel swelling in the ALMR ternary metal fuel design can be reduced.

Using this assembly design, the fuel particle fraction decreased to ~20%, roughly half the volume fraction required for the loose lattice assembly design. The exchange of coolant for fuel matrix material and additional structural material lead to a 10% increase in the required TRU inventory as a result of increased leakage and parasitic capture in the structural materials. The higher inventory decreases the average discharge burnup to 285 MWd/kg. However, the fast fluence did *not* decrease despite the reduction in discharge burnup. This is attributed to spectral hardening associated with the decreased coolant volume fraction in the tight lattice design. The tight lattice sodium design exhibited performance characteristics similar to the LBE cooled configuration with a 50% higher TRU inventory for the same net TRU consumption rate. The specific TRU consumption rate of the LBE design was 10.5% per year as compared to 7% per year for this sodium-cooled option. Therefore, design options to reduce the TRU inventory of the sodium-cooled design were explored next.

The ALMR tight lattice design introduces an additional row of pins within an assembly of the same physical dimensions. This reduces the peak linear power from 311 to 260 W/cm despite larger power peaking factors in the tight lattice case. There remains significant margin to the peak linear power limit of 400 W/cm derived in Section 3. Thus, more compact configurations using the tight lattice design were evaluated. In addition to lowering the TRU inventory requirements, reductions in the core volume provide the economic benefit of reducing the system size and blanket hardware requirements (e.g., fewer fuel assemblies).

For this evaluation, the core height and assembly design were retained, and fuel assemblies were progressively eliminated from the periphery of the ATW configuration. Results are given in Table 3 for cases where the number of fuel assemblies was reduced from 192 to 132, and 120 assemblies.

TABLE 3. PERFORMANCE PARAMETERS OF COMPACT SODIUM COOLED CONFIGURATIONS

		192 Fuel assemblies	132 Fuel assemblies	120 Fuel assemblies
Number of fuel batches		8	6	6
Cycle irradiation time (days)		175	175	175
Fuel particle fraction (volume % in matrix)	Inner zone	19.6	21.6	21.4
	Outer zone	23.7	26.2	25.9
Multiplication Factor	BOEC	0.970	0.970	0.970
	EOEC	0.912	0.913	0.905
Burnup reactivity loss (% Δk)		4.51	5.68	6.48
Peak linear power (W/cm)		260	372	419
Discharge burnup (MWd/kgHM)		286	281	310
Peak fast fluence (10^{23} n/cm^2)		4.00	3.83	4.45
BOEC Heavy metal inventory (kg)		3373	2602	2320

To avoid exceeding the assumed fluence limit, the fuel residence time must be decreased roughly in proportion to the volume decrease. For both revised configurations, a six cycle management scheme was utilized with the 175 day cycle length retained. The 120 assembly case has a peak linear power of 419 W/cm which exceeds the design limit as well as a peak fast fluence of 4.45×10^{23} n/cm^2. Thus, the 132 assembly configuration shown in Fig. 2 was identified as a favorable size for the sodium-cooled blanket configuration. The number of fuel assemblies is reduced by ~30% compared to the LBE cooled blanket. The specific consumption rate increases to 9.5% per year. The 372 W/cm peak linear power and 3.83×10^{23} n/cm^2 leave some margin to the design limits to accommodate increased flux and power peaking when the inhomogeneous source is modeled as evaluated in Section 5.2.

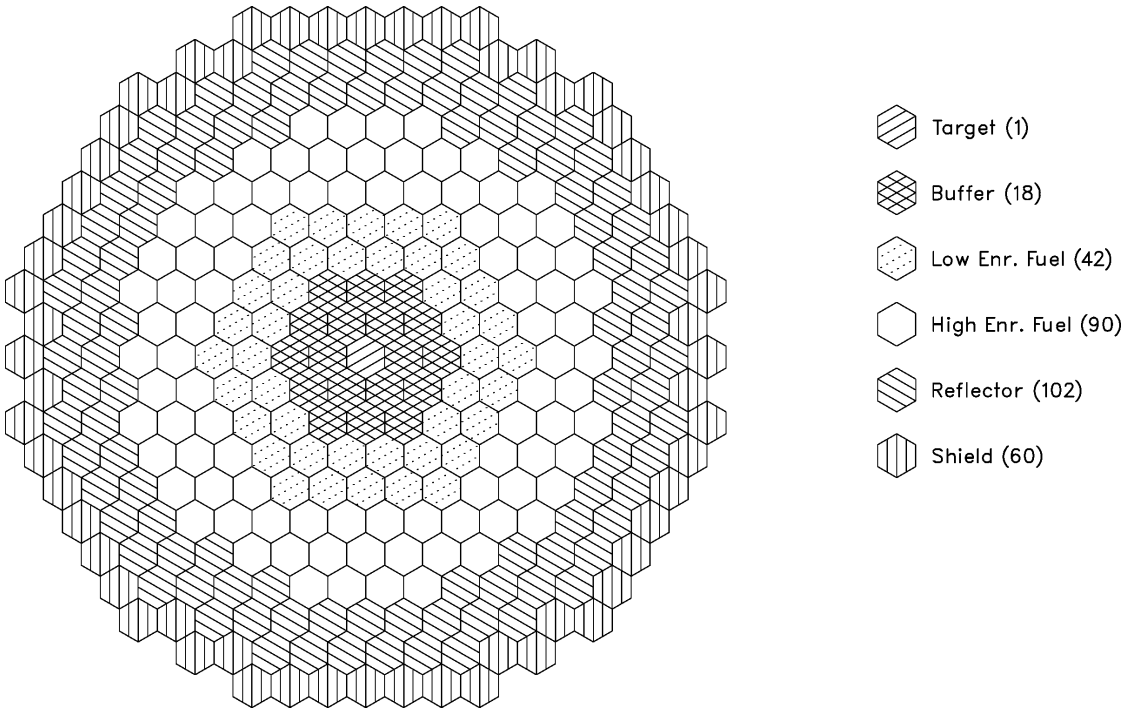

FIG. 2. Sodium-cooled ATW blanket configuration.

5.2. Power peaking study

In this section, design options to enhance the flux and power peaking performance of the sodium-cooled ATW blanket are evaluated. For this investigation, it is important to consider the impact of the inhomogeneous source on the flux and power distributions. Performance results for the eigenvalue neutronics computation and the inhomogeneous source model are compared in Table 4. The fuel enrichment requirements and mass flows are very close; the TRU inventory is ~1% greater for the source-driven computation. These results confirm that the eigenvalue calculation adequately predicts the global performance parameters for the modest subcriticality levels of interest. However, significant differences are observed in the EOEC power peaking. Because the multiplication factor is lower at EOEC, the required neutron source strength increases by roughly a factor of three (if no other reactivity control techniques are used) to maintain the power output. This leads to a large flux peak in the interior fuel assemblies close to the spallation target. This phenomenon can also lead to a power peak in the innermost row of assemblies (increases from 372 to 459 W/cm). In addition, the fast fluence in this innermost row increases to 4.83×10^{23} n/cm^2.

Several design options can be conceived to mitigate this peaking behavior:

- The enrichment zoning of the blanket can be tailored to suppress the peak.
- The cycle length can be shortened to reduce the decline in multiplication factor between BOEC and EOEC.
- The blanket size can be increased to reduce the power density and specific power; the reduced cycle burnup also mitigates the multiplication factor decline.
- Fuel shuffling can be employed to preferentially place high burnup assemblies and limit exposure time in the inner locations of the blanket near the source.
- Fewer irradiation cycles can be employed for the innermost fuel assemblies. This does not reduce the flux or power peaking itself but does reduce the discharge fast fluence for the limiting (interior) fuel assemblies.

Increased blanket size is an undesirable option because the TRU inventory would increase as shown in the previous subsection. Fuel shuffling could be utilized to accommodate the power peak, but in-residence fuel movement complicates fuel handling. The final option (decreased inner region residence) is also not favored because it penalizes the discharge burnup of the inner region fuel. Thus, the current parametric studies have focused on the first two options (enrichment zoning and reduction of cycle duration). Furthermore, a tentative limit of two enrichment zones was imposed for this study. Additional enrichment zones could be employed to better flatten the power shape, but utilization of numerous enrichments (different fuel particle volume fractions within the dispersion matrix) complicates both fuel fabrication and fuel handling.

First, alternate allocations of the assemblies to high and low enrichment zones were investigated with the inner-to-outer blanket zone enrichment split of 1.2 retained. The most favorable performance was observed when the low enrichment zone was sized at two rows thickness; this results in only 42 low enrichment assemblies, as shown in Fig. 2. The large number of high enrichment assemblies leads to a lower power level in the low enrichment zone with a compensating power increase in the high enrichment. The power peaking factor decreases from 1.71 to 1.625; however, the flux does not decrease in the interior region because the EOEC multiplication factor is not significantly affected; thus, the peak fast fluence is not significantly reduced.

To reduce flux peaking, the EOEC multiplication factor can be increased by using a fuel management strategy with a shorter cycle length. Thus, conversion to an eight-batch scheme with the cycle length reduced from 175 to 135 days (roughly conserving fuel lifetime) was evaluated; results are given in Table 4.

The EOEC multiplication factor increases from 0.906 to 0.921; this implies a ~20% decrease in source intensity. Since the source is centrally located, this further reduces the inner row peaking factor from 1.71 to 1.57 with a peak linear power of 427 W/cm (close to the 400 W/cm limit). The reduced source strength also decreases the flux in the interior assemblies; thus, a slight decrease in the peak fast fluence is observed in this case.

TABLE 4. SELECTED POWER PEAKING STUDY PERFORMANCE RESULTS

Type of computation		Evalue	Source	Source	Source
# of High enrichment assemblies		66	66	42	42
Number of fuel batches		6	6	8	8
Cycle irradiation time		175	175	135	135
Enrichment split		1.2	1.2	1.2	1.3
Fuel particle fraction (volume % in matrix)	Inner zone	21.6	21.7	21.2	20.2
	Outer zone	26.2	26.3	25.7	26.6
BOEC Heavy metal inventory (kg)		2602	2623	2617	2638
Multiplication factor	BOEC	0.970	0.970	0.970	0.971
	EOEC	0.913	0.907	0.921	0.921
Burnup reactivity loss (% Δk)		5.68	6.31	4.92	4.95
Power peaking factor	BOEC	1.467	1.470	1.478	1.508
	EOEC	1.447	1.708	1.566	1.515
Peak linear power (W/cm)		372	459	427	399
Discharge burnup (MWd/kgHM)		281	280	285	283
Peak fast fluence (10^{23} n/cm^2)		3.83	4.83	4.71	4.55

Finally, variations in enrichment split between the high and low enrichment zones were evaluated. Using the blanket configuration shown in Fig. 2, the enrichment split was varied between 1.2 and 1.8. As the enrichment split is increased, the BOEC power peaking factor increases because the power peak is located in the outer core. Conversely, the EOEC power peak initially decreases because it is located in the inner core region. At an enrichment split of roughly 1.3 the peak EOEC power in the inner and outer zones are roughly equal, and the lowest peaking factor of 1.515 is obtained. At higher enrichment splits, the EOEC power peak is located in the outer core, thus peaking becomes more severe with increasing outer zone enrichment. Parametric results show that the peak fast fluence also decreases with increasing enrichment split. The fluence peak is located in the inner (low enrichment) zone, and shifting of the TRU loading (and fission rate) into the outer region reduces the inner zone flux. Based on these results, an enrichment split of 1.3 was specified for the sodium-cooled system point design. This is the only split that meets the peak linear power limit of 400 W/cm. Since the peak discharge fast fluence exceeds the assumed limit for all cases, a modified fuel cycle is required. In the final recommended point design, the fuel lifetime for the inner (low enrichment) fuel assemblies is reduced from eight to seven cycles; this results in discharge fast fluence within the design limit with only a slight penalty in the TRU burnup performance.

6. COMPARISON OF STARTUP AND RECYCLE SCENARIOS

In this section, the performance of the sodium-cooled ATW design operating on a startup cycle (i.e., using LWR-discharge transuranics for the ATW feed stream) is contrasted to the base equilibrium (with recycle) case. For the startup case, an equilibrium REBUS-3 calculation is performed with processed LWR transuranics as the sole source of fuel material (no recycled feed). This computation roughly models the behavior of the ATW blanket in its initial core loadings and the condition of the fuel material for its first pass through the transmutation system. The comparison of startup and equilibrium cycle performance was performed for the blanket configuration developed in Section 5 (Fig. 2) with an enrichment split of 1.3. The cycle length of 135 days (~1/2 year at a 75% capacity factor) was retained. An eight-batch fuel management strategy was employed for the high enrichment fuel assemblies and a seven-batch strategy for the interior low enrichment fuel assemblies. Performance results for the startup case are compared to the recycle case in Table 5.

TABLE 5. PERFORMANCE CHARACTERISTICS FOR STARTUP AND RECYCLE SCENARIOS

		Recycle	Startup
Fuel particle fraction (volume % in matrix)	Inner zone	19.9	16.0
	Outer zone	26.2	21.0
Multiplication factor	BOEC	0.970	0.971
	EOEC	0.920	0.909
Burnup reactivity loss (% Δk)		4.94	6.13
Power peaking factor	BOEC	1.501	1.453
	EOEC	1.508	1.559
Peak linear power (W/cm)		397	449
Discharge burnup (MWd/kg)		275	340
Peak fast fluence (10^{23} n/cm^2)		4.06	4.26
BOEC Heavy metal inventory (kg)		2620	2025

The TRU volume fraction and TRU inventory for the startup case are ~20% lower than the equilibrium recycle; this is attributed to changes in the TRU isotopics as discussed below. The reduced inventory leads to a greater reactivity loss over the burnup, which in turn exacerbates the EOEC power peak. It appears a higher enrichment split and/or shorter cycle lengths are desirable to reduce the power peaking in the initial (low inventory) loadings. On the positive side, the reduced inventory yields a proportional increase in the average discharge burnup with associated fuel cycle performance benefits.

The evolution of the TRU isotopics in the ATW fuel cycle is illustrated in Table 6 where the charge and discharge compositions for the startup and recycle cases are compared. After the initial in-core residence, the Pu-239 fraction has decreased from 53 to 34%. The proportion of Pu-239 and other fissile nuclides is reduced relative to the fertile transuranics that tend to concentrate due to their lower cross sections. This phenomenon is the cause of the lower TRU enrichment requirements for the startup core where the fissile fraction is highest. The isotopics

change significantly during the first irradiation campaign. The Pu-240 has already increased to nearly its equilibrium level (~33%). It takes longer for the higher capture products Pu-242, Am-243, and Cm-244 to reach their equilibrium concentration. The Am-241 fraction actually decreases because the initial feed has a much longer post-irradiation cooling time, yielding additional Pu-241 decay, than the ATW discharge and recycle compositions. The evolution of isotopic fractions displayed in Table 6 suggests a fairly rapid and smooth transition from the startup cycle performance to the equilibrium recycle performance.

TABLE 6. EVOLUTION OF TRU ISOTOPICS (WEIGHT %) IN THE ATW FUEL CYCLE

Isotope	Startup cycle		Equilibrium recycle		
	Initial feed (LWR TRU)[a]	Once-through discharge	Equilibrium feed[b]	Equilibrium discharge	0.8y Cooled eq. discharge
U-234	0.000	0.080	0.468	0.580	0.621
U-235	0.004	0.012	0.110	0.153	0.154
U-236	0.002	0.013	0.149	0.204	0.207
U-238	0.478	0.642	1.022	1.249	1.249
Np-237	5.023	3.541	2.896	1.990	1.997
Pu-238	1.272	5.773	5.039	6.226	6.552
Pu-239	53.196	34.254	28.729	18.499	18.502
Pu-240	21.533	31.800	31.492	35.437	35.548
Pu-241	3.782	5.683	5.523	6.780	6.525
Pu-242	4.686	7.285	10.555	13.005	13.007
Am-241	8.967	6.831	6.850	5.068	5.316
Am-242m	0.014	0.565	0.340	0.480	0.478
Am-243	0.926	1.800	3.404	4.440	4.440
Cm-242	0.000	0.771	0.030	0.519	0.147
Cm-243	0.002	0.066	0.039	0.057	0.056
Cm-244	0.104	0.763	2.471	3.682	3.570

[a]Processed transuranics from medium burnup PWR at 25 years cooling [16].
[b]Equilibrium feed is a mixture of recycled ATW transuranics and processed LWR transuranics as required for makeup

7. CONCLUSIONS

Parametric studies have been performed to optimize the sizing of the sodium cooled transmuter blanket, to mitigate power peaking problems near the source regions, and to assess startup core performance. In these studies, a wide range of potential transmuter configurations and fuel cycle scenarios were investigated for an assumed fission-power level of 840 MWt, typical size of modular fast reactor designs such as the ALMR.

Compared to ATW systems employing lead-bismuth eutectic (LBE) coolant, sodium cooled blankets require a higher TRU inventory because of increased neutron leakage. However, much higher flow rates can be used with sodium coolant that allows a significant reduction in the coolant volume fraction; for this study, the ALMR tight lattice (pitch-to-diameter ratio of ~1.2) fuel assembly design was employed. The associated increase in fuel volume fraction allows considerable compaction of the blanket (~30% compared to the LBE cooled design) with associated economic benefits. The extent of this size reduction is constrained by the peak linear power limit that was estimated to be 400 W/cm for the non-uranium metallic dispersion fuel in a sodium cooled environment.

Design options to enhance the flux and power peaking performance of the sodium cooled ATW blanket were also investigated. The increased source strength at end-of-cycle (EOC) can lead to severe flux and power peaks in the blanket near the source. Refined allocations of the assemblies to high and low enrichment zones were developed to reduce the power peaking factors. Parametric studies indicate that an enrichment split of 1.3 gives the most favorable performance. In addition, the cycle length was shortened to 135 days (half a year at 75% capacity factor) to reduce the decline in multiplication factor. Even with improved power peaking behavior, high flux levels in the inner blanket require a somewhat shorter fuel lifetime (compared to the outer blanket) for the same discharge fast fluence level.

The performance of the sodium cooled ATW blanket system point design operating on a startup cycle was contrasted to the equilibrium cycle results. The main performance difference is that the transuranic inventory is ~20% lower for the startup cycle because of the higher fissile content of the LWR discharge feed. The evolution of the transuranic isotopics suggests a fairly rapid and smooth transition from the startup cycle performance to the equilibrium cycle performance.

If successfully developed, the proposed sodium cooled system would consume LWR-discharge TRU at the maximum rate achievable per unit of fission energy produced (~0.9 g/MWtd). The overriding design objective of high discharge burnup was shown to be achievable in a configuration with high power density (enabling small system size and potentially favorable economics) and relatively low burnup reactivity loss (to reduce requirements for reactivity and/or source control). System design and operating characteristics that satisfy these goals while meeting key thermal-hydraulic and materials-related design constraints were preliminarily developed.

REFERENCES

[1] A Roadmap for developing Accelerator Transmutation of Waste (ATW) Technology; A Report to Congress, DOE/RW-0519, US Department of Energy (1999).

[2] HILL, D.J., et al., A Roadmap for Developing ATW Technology: Systems Scenarios and Integration, Argonne National Laboratory Report, ANL/RE-99/16 (1999).

[3] VENNERI, F., et al., Roadmap for the Development of Accelerator Transmutation of Waste: Target and Blanket System, Los Alamos National Laboratory Report, LA-UR-99-3022 (1999).

[4] SPENCER, B.W., The Rush to Heavy Liquid Metal Reactor Coolants – Gimmick or Reasoned, Proc. 8th Int. Conf. on Nuclear Engineering (ICONE-8), 2000, Baltimore, MD, USA, American Society of Mechanical Engineers (ASME), New York (2000).

[5] YANG, W.S., NABEREJNEV, D.G., KHALIL, H.S., Physics Design Studies of an LBE Cooled ATW System, Trans. Am. Nucl. Soc., **83**, 328 (2000).

[6] HILL, R.N., et al., Physics Studies of Weapons Plutonium Disposition in the Integral Fast Reactor Closed Fuel Cycle, Nucl. Sci. Eng., **121**, 17 (1995).
[7] GLUECKER, E.L., U.S. Advanced Liquid Metal Reactor (ALMR), Prog. In Nucl. Energy, **31**, 43 (1997).
[8] LEGETT, R.D., WALTERS, L.C., Status of LMR Fuel Development in the United States, J. Nucl. Matls., **204**, 23 (1993).
[9] YANG, W.S., KHALIL, H.S., Neutronics Design Studies of an LBE Cooled ATW Blanket, paper presented in the IAEA Technical Meeting on Emerging Nuclear Energy Systems, 27-29 November 2000, Argonne, Illinois, USA, to be published as IAEA-TECDOC.
[10] TOPPEL, B.J., A User's Guide to the REBUS-3 Fuel Cycle Analysis Capability, ANL-83-2, Argonne National Laboratory (1983).
[11] YANG, W.S., KHALIL, H.S., Analysis of the ATW Fuel Cycle Using the REBUS-3 Code System, Trans. Am. Nucl. Soc., **81**, 277 (1999).
[12] HENRYSON, II, H., TOPPEL, B.J., STENBERG, C.G., MC^2-2: A Code to Calculate Fast Neutron Spectra and Multigroup Cross Sections, ANL-8144, Argonne National Laboratory (1976).
[13] STACEY, Jr., W.M., et al., A New Space-Dependent Fast-Neutron Multigroup Cross-Section Preparation Capability, Trans. Am. Nucl. Soc., **15**, 292 (1972).
[14] NA, B.C., WYDLER, P., TAKANO, H., OECD/NEA Comparison Calculations for an Accelerator-Driven Minor Actinide Burner: Analysis of Preliminary Results, paper presented in the Second Workshop on Utilization and Reliability of High Power Proton Accelerators, OECD/NEA, 22-24 November 1999, Aix-en-Provence, France, NEA, ISBN: 92-64-18749-9 (2001).
[15] DERSTINE, K.L., DIF3D: A Code to Solve One-, Two-, and Three-Dimensional Finite-Difference Diffusion Theory Problems, ANL-82-64, Argonne National Laboratory (1984).
[16] LUDWIG, S.B., RENIER, J.P., Standard- and Extended-Burnup PWR and BWR Reactor Models for ORIGEN2 Computer Code, ORNL/TM-11018, Oak Ridge National Laboratory (1989).

TWO-TIERED APPROACH FOR LIGHTWATERREACTOR WASTE DISPOSITION USING EXISTING LIGHTWATER REACTORS AND A MINOR ACTINIDE BURNER

H.R. TRELLUE, E.J. PITCHER, P. CHODAK III, D. BENNETT
Los Alamos National Laboratory, Los Alamos, New Mexico, United States of America

Abstract

One approach being explored for the disposition of light-water reactor (LWR) spent, low-enriched uranium fuel (LEUF) is a two-tiered scheme in which the plutonium is separated from LWR transuranic waste and returned to existing LWRs as nonfertile fuel (NFF) and minor actinides are sent to an accelerator-driven system. Preliminary studies have shown that significant portions of LWR cores can be replaced by this NFF using existing safety envelopes without reactor modification. Substantial burnup of ^{239}Pu and total plutonium can be achieved using NFF in existing LWRs. An accelerator-driven subcritical burner is used to burn remaining isotopes directly from the LWR-spent LEUF combined with the residual actinide from the spent NFF assemblies. The use of a fission product target outside the main blanket of transuranic material is also discussed.

1. INTRODUCTION

One of the main goals of the Accelerator Transmutation of Waste (ATW) project has been to study target and blanket materials (spallation neutron source, claddings, coolants, etc.) to determine their performance under various operating conditions [in terms of spallation neutron production, flux/power distribution in the blanket, minor actinide (MA) and fission product transmutation efficiency, etc.]. Some of the target materials that were examined include lead-bismuth eutectic (LBE), sodium-cooled tungsten, and gas-cooled tungsten. The main blanket examined consisted primarily of zirconium/transuranic (TRU) fuel surrounded by a stainless-steel cladding and lead-bismuth or sodium coolant. Alternate options for blankets included a molten salt/graphite/actinide mixture or dispersion fuels in a gas-cooled matrix. For these analyses, it has been assumed that all TRU isotopes (plutonium plus MAs) were transmuted in an accelerator-driven system (ADS). However, one of the only ways to make an ATW system economically feasible is to assume that it will provide power to the electricity grid. Current accelerator systems are subject to beam trips and power interruptions and may not provide a reliable means of power production. Although fissions in the blanket provide a majority of the neutrons (the fraction k_{eff}) for a chain reaction to be maintained, the remaining fraction ($1-k_{eff}$) must be provided by spallation neutrons from the proton beam. One of the other concerns in an ADS is the change in beam power over a cycle. The goal at the beginning of a cycle is to start with a k_{eff} of ~0.97, decreasing to no less than 0.90 at the end of cycle. Using all TRU isotopes from spent light-water-reactor (LWR) fuel, this process occurs at ~6 months. However, the beam current (and thus power) over this 6 months must increase ~3.5 times to account for the change in reactivity [see Eq. (1)]. Thus, establishing methods to minimize this reactivity swing are highly desirable.

$$I = \frac{\upsilon \times P \times 1.602 \times 10^{-19} C/p}{S \times k_{eff}/(1-k_{eff}) \times Q_{ave}} \quad (1)$$

where

I = the beam current (amps),
υ = the number of neutrons produced/fission (~2.9 in a fast spectrum),
P = the power defined by user for each material,
S = the number of neutrons leaking from the target into the blanket (~30 spallation neutrons/source proton),

k_{eff} = the effective multiplication factor obtained by the Monte Carlo neutron and photon transport code (MCNP),

$k_{eff}/(1-k_{eff})$ = the ratio of the number of fission neutrons to the number of spallation neutrons because the number of fission neutrons + the number of spallation neutrons must = 1.0,

Q_{ave} = the average recoverable energy released per fission (~200 MeV, or 3.2×10^{-11} J).

The best method of increasing the reliability of power generation is to use a reactor to produce consistent power augmented by an ADS to burn what cannot be efficiently transmuted in a reactor. Plutonium (Pu) burns well in a thermal spectrum, and existing LWRs could be used for this purpose, while providing a reliable source of electricity. The extent of licensing modifications that would be required for this is not yet known but would presumably be less than that required to license a new reactor, which is the other option for this two-tiered approach.

However, the rest of the MAs [in particular, curium (Cm)] are more efficiently transmuted in a fast spectrum, where the fission-to-capture ratio is larger and the buildup of higher actinides smaller. (Note: Neptunium and americium can burn in a thermal spectrum, but this process leads to the production of more ^{238}Pu, Cm, and higher isotopes.) Thus, MAs would be transmuted more effectively if sent directly to an accelerator-driven system with a fast neutron spectrum while plutonium was sent to a reactor. Scoping studies of this two-tiered system were thus performed and are described in Section 2. However, the separation of MAs from plutonium raises some proliferation concerns (the plutonium is more attractive if combined with less attractive materials, such as MAs).

Additionally, transmutation of long-lived fission products (LLFPs) (^{99}Tc and ^{129}I) is not addressed in Section 2 because it is assumed that they will be located in a separate region outside the main TRU blanket. The presence of this fission product target region is discussed briefly in Section 3.

2. TWO-TIER APPROACH

Burning reactor-grade plutonium from LWR spent fuel in LWRs certainly offers the advantages of transmuting the plutonium and producing reliable electricity at the same time. One of the most popular fuels used for plutonium consumption in LWRs is mixed oxide (MOX) fuel, which is a combination of UO_2 and PuO_2 (usually ~5 to 10% PuO_2 and depleted or natural uranium oxide). Unfortunately, the presence of uranium offsets the efficiency of burning just the plutonium (fissions will occur in the uranium as well as the plutonium, thus decreasing the percentage of plutonium transmuted, and captures also will occur in the uranium, which could lead to the production of additional plutonium). Therefore, plutonium would be burned more efficiently in a uranium-free matrix so that a majority of the neutron interactions destroy the plutonium, not produce it. One type of uranium-free fuel is nonfertile and consists of plutonium stabilized in an inert matrix (such as ZrO_2). The fact that partial MOX-fueled cores are already licensed may make them faster to implement than a new fuel type, but the burnup rate of plutonium and MAs in MOX fuel is only 30 to 40% compared to the 70 to 80% obtainable with uranium-free cores [1]. More information on nonfertile fuel (NFF) is given in Section 2.1. Burning only MAs in an ADS also has advantages in that the reactivity no longer decreases significantly with burnup. These and other differences are discussed in Section 2.2. Figure 1 shows a flow chart for the proposed two-tiered system.

2.1. Nonfertile fuel

NFF is a revolutionary new fuel type that has been proposed within the last decade [2-5]. It is a uranium-free fuel in the form of an inert matrix with both plutonium and burnable poison (most commonly erbium) to control reactivity and power peaking. The most common inert (neutronically) materials typically considered are ZrO_2, CeO_2, MgO, Al_2O_3, and even ThO_2 (which is fertile and leads to the breeding of uranium, which is undesirable in this application). In the past, one-third MOX-fueled cores with <10% plutonium have been licensed within safety boundaries, and similar core load fractions would be expected for NFFs. Studies with NFF have ranged from a one-eighth core to a full-core loading, and preliminary safety issues are not a concern in either case if a sufficient amount of burnable poison is used.

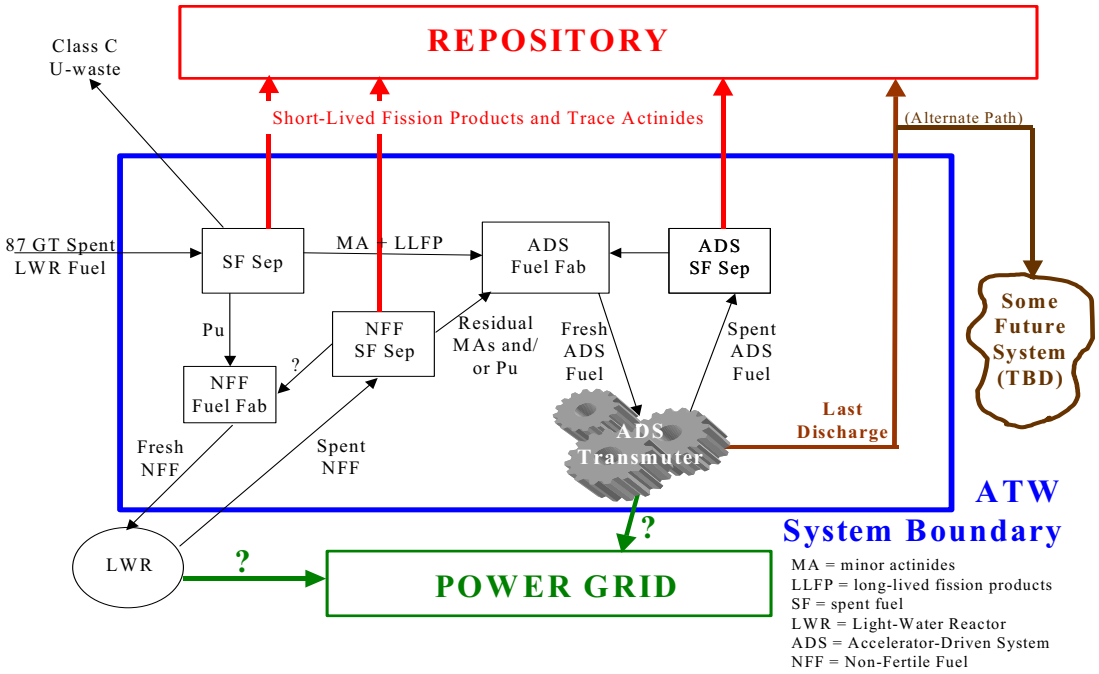

FIG. 1. Flow chart of material for proposed two-tiered system.

Several different options are available for NFF burning. When studies on the two-tiered approach were initiated, it was assumed that the plutonium would be sent to an LWR and that MAs would still go to an ADS. Results from a preliminary run show that the burnup efficiency (amount burned relative to that put into the system) increases little as a function of time beyond 80%, so results for that case are given here. Also displayed are results for a case in which only the plutonium is recycled as NFF and a case in which both the plutonium and MAs are recycled and put back into the system. Results are given for burnup efficiencies of ~80%, even though higher ones are possible (but probably not beneficial because the power density in NFF after that point is fairly small). Each case involved the same number of LWR cycles, and fluence limitations on the cladding and/or fuel were not applied at this time. It was hypothesized that higher plutonium burnups were possible when only plutonium was used and/or recycled, as opposed to plutonium plus MAs. In the recycle cases, individual fuel rods were removed after shorter burnups (i.e., shorter residence times), resulting in fewer variations in power density and flux and a decrease in material damage concerns. However, separating the spent NFF fuel at regular intervals would be expensive and would pose additional proliferation risks (especially when separating only the plutonium).

Another option for using NFF and LWRs is to not separate the spent LWR plutonium and MAs at all and send both streams to be transmuted in the LWR as NFF. This is advantageous from a proliferation standpoint because keeping the MAs mixed with the plutonium makes it more difficult to divert the plutonium for nonpeaceful purposes. However, the effect on the accelerator is more pronounced because the fission-to-capture ratio of the NFF discharge is higher than that of MA from spent LWR fuel, which causes the reactivity swing in the accelerator to decrease (this will be discussed further in Section 2.2). A comparison of ending vs beginning compositions for these straight-burn (no recycle) cases is given in Table 1. These preliminary NFF calculations also show a negative Doppler coefficient for the system examined (see Fig. 2). Comparisons of several system parameters for each case are given in Table 2 (no control rod movement was considered, and thus, reactivity did not stay critical), and Fig. 3 shows the amount of material burned for each given constant irradiation times.

TABLE 1. BEGINNING AND ENDING ISOTOPICS FOR NFF BURNING

	Straight Pu burn		MA + Pu burn	
	BOL	EOL	BOL	EOL
^{237}Np		0.001	5.023	0.178
^{238}Pu	1.500	0.403	1.269	2.671
^{239}Pu	62.917	0.116	53.196	0.669
^{240}Pu	25.417	2.046	21.507	3.402
^{241}Pu	4.500	1.679	3.790	2.489
^{242}Pu	5.542	7.958	4.680	6.347
^{241}Am		0.034	8.950	0.063
^{242m}Am		0.001	0.016	0.003
^{243}Am		0.871	0.922	0.541
^{242}Cm		0.120	0.000	0.130
^{243}Cm		0.006	0.000	0.010
^{244}Cm		4.417	0.103	4.041
^{245}Cm		0.296	0.011	0.454
^{246}Cm		0.275	0.000	0.311
Total Pu		12.2		15.6
Total MA		6.02		5.73

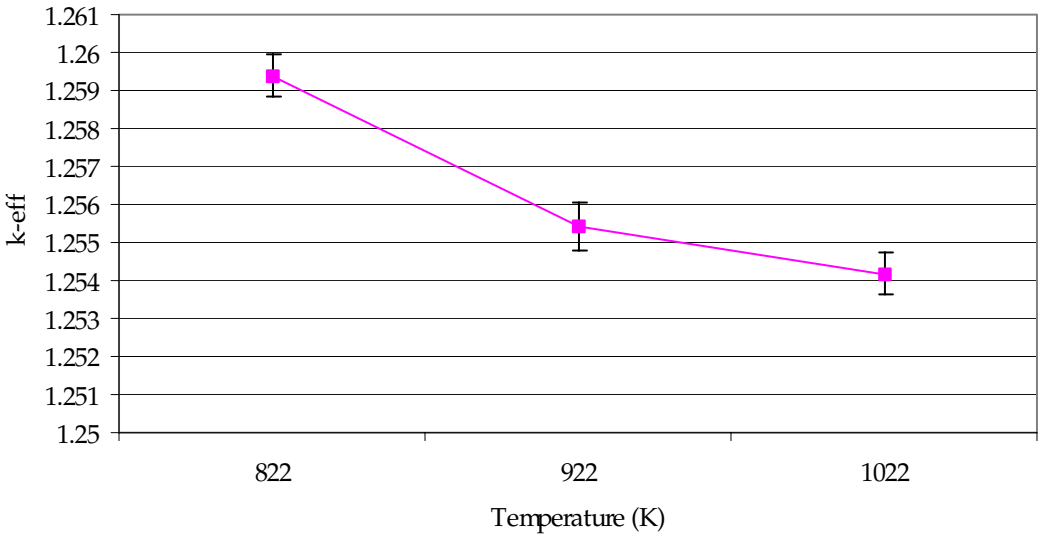

FIG. 2. Doppler coefficients for NFF case in LWR – one-ninth core loading.

TABLE 2. COMPARISON OF NFF RUNS

Parameter	Pu feed/ no recycle	Pu feed/ no Pu removal	Pu feed/Pu & MA recycle	Pu & MA feed/ no recycle
Δk_{eff}	0.09	0.1	0.1	0.07
Flux – NFF region (n/cm^2 –s)	1.6 to 1.0×10^{14}	1.6 to 1.3×10^{14}	1.6 to 1.3×10^{14}	1.3 to 1.0×10^{14}
Power density NFF region (W/cm^3)	150 to 30	160 to 60	150 to 80	110 to 70
Flux – UO_2 region (n/cm^2 –s)	1.5 to 2.2×10^{14}	1.4 to 1.7×10^{14}	1.4 to 1.7×10^{14}	1.5 to 2.0×10^{14}
Power density UO_2 region (W/cm^3)	120 to 220	110 to 180	110 to 180	120 to 220
Actinide burnup	81%	83%	75%	65%

From Fig. 3, it is observed that the fissile plutonium and actinide destruction is greatest when recycling occurs (because material is added at regular intervals, fluxes and power densities remain higher in the NFF region throughout the burn, making the irradiation more efficient), but so is the buildup of ^{242}Pu. It is evident that the amounts of ^{237}Np and ^{241}Am are greatest when they are used either initially (the plutonium plus MA straight-burn case) or recycled, but the buildup of higher curium isotopes (such as ^{244}Cm, which has a < 20-year half-life) is also more predominant for these cases. Overall actinide burnup is higher when only plutonium is initially used (instead of Pu + MAs) because the fission-to-capture ratio of the fuel is larger, causing less buildup of MAs.

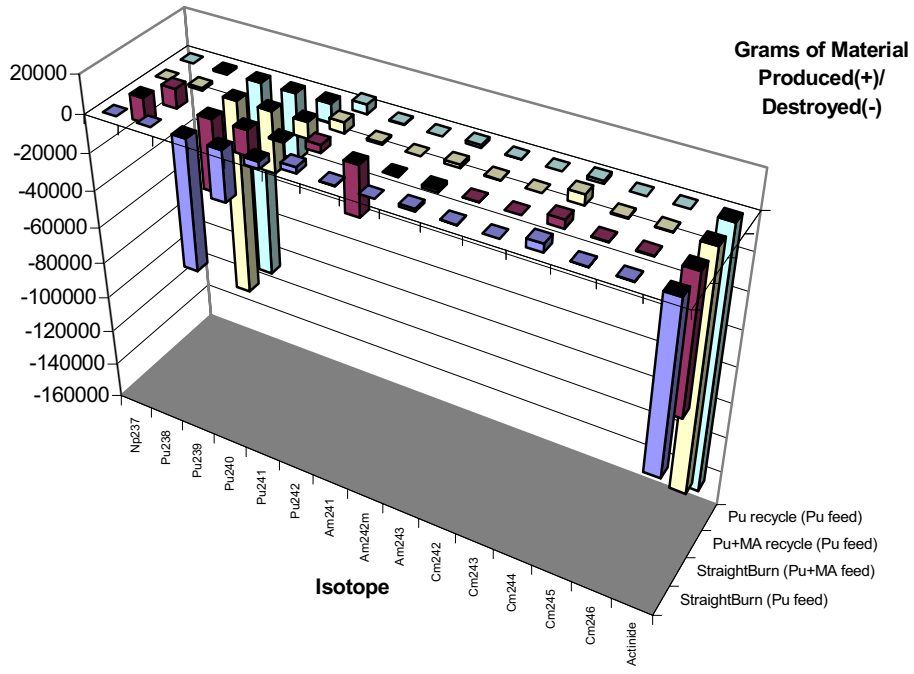

FIG. 3. Comparison of amount of material produced (burned if negative) using different feeds.

The model used to perform these calculations consisted of nine assemblies infinitely reflected to provide symmetry (see Fig. 4). Because the model is simply an infinitely reflected set of assemblies, no pressure vessel or radial/axial leakage effects were considered, but the spectrum should be similar to that seen if such a combination were actually placed in an LWR core. Burnup calculations were performed using the code Monteburns [1]. Future NFF studies will involve a more accurate geometry (such as a one-eighth core model with NFF assemblies placed in the periphery positions). In addition, the possibility of using MOX- or thorium-based fuel will be explored. The composition of NFF used in this study was ~28wt% oxygen, 56wt% zirconium, 5wt% calcium, 1wt% erbium (all three of these are in the form of oxide), and 9wt% actinide.

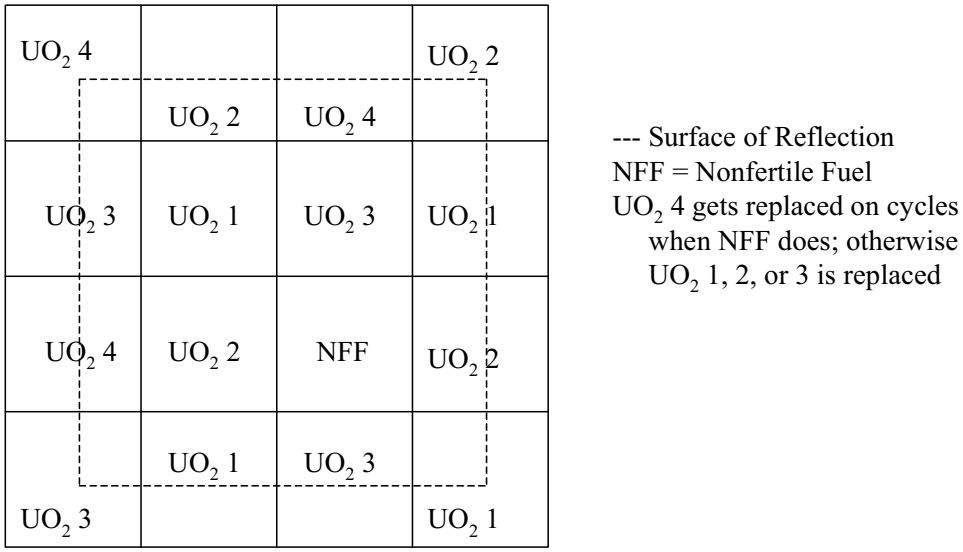

FIG. 4. Assembly layout of a one-ninth core NFF with UO_2 fuel in an LWR.

2.2. MA ADS

One of the benefits of the two-tiered option to the ADS is that less material would be sent to an ADS and the reactivity swing in the ADS will probably be smaller (if not negligible). The weight percentage of MAs in spent LWR fuel is assumed to be ~15%. If it is assumed that the remaining 85% is plutonium and is sent to an LWR and that 90% of that plutonium can be burned, the material stream going to the ADS can be reduced by 70% (this includes the MAs that are built up in the spent NFF). In addition, when MAs are used solely to fuel an ADS system, instead of decreasing, the reactivity swing actually increases as fissile plutonium is built up in the system. When enough plutonium finally exists, k_{eff} finally will start to decrease (see Fig. 5). Without any initial plutonium, it will take ~8 years in the fast-spectrum systems currently being examined before k_{eff} starts decreasing. By adding a certain amount of plutonium from LWR spent fuel and/or spent NFF discharge to the starting ATW MA system, fairly constant reactivity can be maintained for the first 2.5 years. After that, enough plutonium exists in the system that k_{eff} decreases. To offset this, a large quantity of MA must again be added to keep reactivity constant for cycles at steady state (the beginning of cycle actinide fission-to-capture ratio must be ~0.8 to maintain constant reactivity over a 2.5-year cycle). The MA from LWR spent fuel is better for this purpose because it has a lower fission-to-capture ratio than MAs from spent NFF. If a feed stream of half-spent LWR MA and half-spent NFF MA is used, a portion of the fuel in the ADS at the end of each cycle actually must be removed to be able to get the starting fission-to-capture ratio to ~0.8 without so much feed being added that k_{eff} becomes >0.97. The quantity of actinide that must be removed varies on

the exact feed being input, but it also can be used as feed at a later time. Without removal of some fraction of the material in the system, the reactivity swing over a 2.5-year cycle will decrease a little instead of remaining constant (but not as much as if all spent LWR fuel were sent to the ADS), or the cycle length at steady state can be decreased to limit the reactivity swing to desired values.

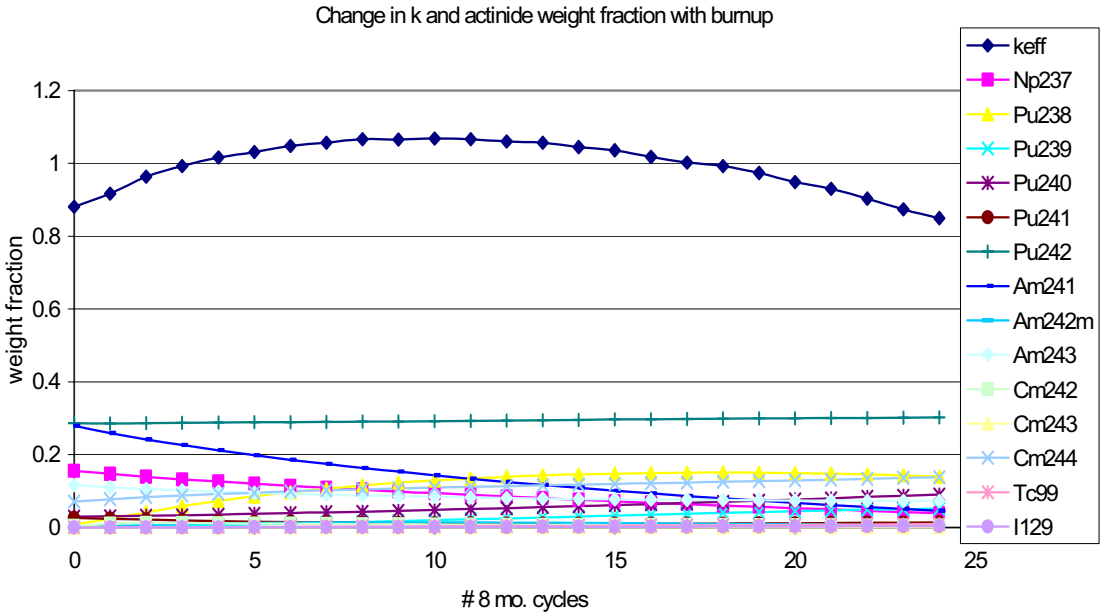

FIG. 5. Change in reactivity and weight fraction of TRU isotopes with number of cycles.

Preliminary runs show that initially keeping ~10% of the plutonium from LWR-spent fuel that would otherwise be fabricated to NFF for LWRs and sending it to the ADS instead would maintain constant reactivity for the first cycle. Alternatively, instead of using plutonium from spent LWR fuel to keep reactivity from significantly increasing the first cycle, another option would be to take plutonium from the spent NFF discharge. By using a combination of 15wt%-spent NFF plutonium, 42.5wt%-spent NFF MA, and 42.5wt%-spent LWR MA at the beginning of life and using spent LWR MAs as feed every 2.5 years, the reactivity remains fairly constant with burnup. The extent of the NFF burn will influence what isotopes need to be burned in the ADS; what was presented here was merely optimal for maintaining a small or negligible reactivity swing in the accelerator and short cycle lengths. The smaller the reactivity swing, the smaller the cost of the accelerator, and the larger the cycle length, the smaller the cost of overall separations (it would be done less often) and the less time spent removing and/or reshuffling the fuel rods. The traditional ADS examined with both plutonium and MA feed has a cycle length of only 6 months before k_{eff} goes below 0.90. If plutonium and MAs are kept together and burned in an LWR as NFF, the discharge would still have to be transmuted by an ADS, but the cycle length could be a little longer before reactivity dropped (but still probably under a year). Separating the plutonium and MAs either before or during LWR NFF burning allows cycle times in the ADS to be as long as 2.5 to 3 years (at which point fluence limitations are met). Thus, the most cost-effective option for the ADS would be to use a purely MA feed stream after the first cycle; however, any mix certainly could be accommodated.

The model used to perform the calculations presented here contains three homogeneous fuel regions (the blanket), each with varying actinide-to-zirconium fuel fraction loadings to keep the flux/power profile as flat as possible. Actinide feed is added to each region at the end of

each cycle to lower the fission-to-capture ratio and raise/maintain k_{eff}. The LBE target is located in the center, with an incoming proton beam to produce spallation neutrons for the subcritical blanket regions (see Fig. 6). Zirconium-based fuel used here is surrounded by stainless-steel cladding and sodium coolant (a fast spectrum). Beginning and ending steady-state-cycle isotopes are given in Table 3. The homogeneous mixture in each region consisted of 36.6vol% of sodium coolant and 25.7vol% of cladding and the remainder is zirconium fuel with 15 to 24vol% of actinide. Initial studies show that a slightly positive fuel Doppler coefficient could be an issue in this ADS, but with proper burnable poison addition or fuel composition, this could easily be eliminated.

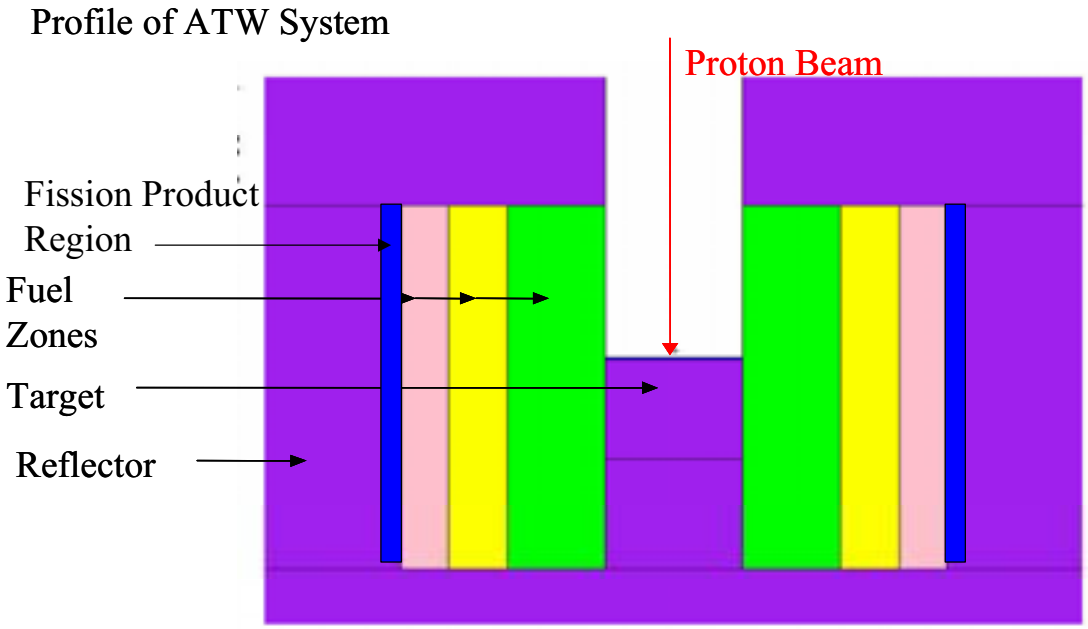

FIG. 6. Profile of ADS system used in two-tier calculations.

TABLE 3. COMPARISON OF STEADY-STATE ISOTOPIC DISCHARGE COMPOSITIONS

Isotope	Ending isotopics in MA ATW	Col. 1 weighted appropriately to reduction of material going to ATW	Ending isotopics in Pu/MA ATW
^{237}Np	13.492	4.048	3.134
^{238}Pu	26.602	7.981	6.552
^{239}Pu	7.039	2.112	25.089
^{240}Pu	4.612	1.384	35.196
^{241}Pu	0.840	0.252	6.409
^{242}Pu	7.934	2.380	10.868
^{241}Am	19.474	5.842	4.906
^{242m}Am	1.638	0.491	0.331
^{243}Am	3.157	0.947	2.550
^{242}Cm	3.292	0.988	0.780
^{243}Cm	0.316	0.095	0.087
^{244}Cm	6.283	1.885	2.936

From this table, it appears that the concentrations of neptunium and americium are much greater when purely MAs are used in the ADS as opposed to all spent LWR fuel with plutonium and MAs. However, the amount of material going to ADSs is reduced by 70%, so there will be 70% less discharge. To verify this, the steady-state actinide loadings were compared for each case, and they were indeed similar (~2000 kg for each case). Even though the ^{237}Np and ^{241}Am concentrations look significantly higher for the MA-only case, the actual amount of those isotopes going to the repository is only about four-thirds times greater, and the amount of fissile plutonium going to the repository is reduced by more than a factor of eight. This is a huge advantage for proliferation concerns.

3. LLFP TARGETS

Another development in the ATW program has been to look at LLFP (^{99}Tc and ^{129}I) transmutation and examine whether these fission products are transmuted better when fabricated as part of the TRU fuel in the blanket or in a separate fission-product target region outside the blanket. The benefit of having a separate fission-product region outside the blanket is that instead of acting as a poison within the TRU fuel and absorbing neutrons that would be used for actinide transmutation, fission-product targets would instead take advantage of neutrons that would otherwise leak from the blanket and leave the system. The cross-sections of technetium and iodine are greater in a thermal neutron spectrum than in a fast one, so another factor that benefits the transmutation of LLFPs in the system is a graphite-containing thermalizer region outside the fission product region that slows neutrons down and reflects them back into the fission product region. However, if these thermal neutrons are not absorbed in the fission product region, they can be reflected back into the blanket with TRU fuel, causing thermal fission and increasing the k_{eff} of the system. With ~2 cm of fission-product targets and 12 cm of thermalizer radially, this effect is minimized and the most efficient transmutation of LLFPs occurs. Preliminary studies show that approximately twice the quantity of LLFP can be transmuted using a fission-product blanket vs mixing them with the TRU blanket (assuming the same system design) over 15 to 20 years. Further studies must be performed with exact system geometries and materials before a definitive design can be proposed. If a larger quantity of fission products needs to be burned, then a larger thickness of the fission-product region can be used effectively as well. The initial fission-product target examined consisted of a homogeneous mixture of 33vol% sodium coolant and 15vol% stainless-steel cladding, with the remainder being technetium and iodine in the percentage in which they exist in spent LWR fuel. The thermalizer region consisted of 85wt% carbon and 15wt% sodium. Further studies on various materials (such as yttrium-hydride for the thermalizer) may optimize this even further.

4. CONCLUSIONS

Preliminary calculations show that a two-tiered approach to spent fuel transmutation is indeed a viable option for reducing the hazard of spent nuclear fuel in a repository and should be pursued further. The proposed two-tiered system involves burning plutonium in an LWR, MAs in an ADS, and LLFPs in a separate fission-product region within the ADS. The two-tiered system proposed suggests the use of (1) LWRs because LWRs are already built and (2) NFF because it allows a higher burnup than MOX fuel without additional reprocessing. The use of this type of fuel is still in the basic research phases, but it would prove highly beneficial for the transmutation of waste.

The optimum accelerator system would take some feed from the spent NFF in the LWR, but it would primarily use the MAs from spent LWR fuel that were separated from plutonium. Using this combination could provide a fairly constant reactivity swing for an ADS cycle of 2 to 3 years, which would reduce demands on the accelerator to produce the remainder of neutrons (if k_{eff} is 0.97, the accelerator must generate spallation neutrons to account for 3% of the neutrons in the system).

The use of a separate fission-product target region would also greatly benefit the transmutation of LLFPs (^{99}Tc and ^{129}I) by using neutrons already leaking from the core, thermalizing them, and sending them back into a fission product target region to be absorbed.

REFERENCES

[1] STERBENTZ, J.W., Neutronic Evaluation of a Non-Fertile Fuel for the Disposition of Weapons-Grade Plutonium in a Boiling Water Reactor, Idaho National Engineering Laboratory report INEL-94/0079 (1994).

[2] AKIE, H., et al., A New Fuel Material for Once-Through Weapons Plutonium Burning, Nuclear Technology, Vol. 107, No. 2 (1994) 182-191.

[3] OLSON, C.S., Non-Fertile Fuel Development for Plutonium and High-Enriched Uranium Dispositioning in Water Cooled Reactors, Idaho National Engineering Laboratory report INEL-95/0038 (1994).

[4] EATON, S.L., et al., Development of Nonfertile and Evolutionary Mixed Oxide Nuclear Fuels for Use in Existing Water Reactors, Los Alamos National Laboratory report LA-UR-97-1359 (1997).

[5] SHELLEY, A., et al., Parametric Studies on Plutonium Transmutation Using Uranium-Free Fuels in Light Water Reactors, Nuclear Technology, Vol. 131 (2000) 197-209.

[6] POSTON, D.I., TRELLUE, H.R., User's Manual, Version 2.0, for Monteburns, Version 1.0, Los Alamos National Laboratory document LA-UR-99-4999 (1999).

CORE PHYSICS PERFORMANCE OF RECYCLED LWR DISCHARGE TRU OXIDE FUEL IN A GT/AD-MHR

T.A. TAIWO, Y. GOHAR, P.J. FINCK
Argonne National Laboratory, Argonne, Illinois, United States of America

Abstract

The core physics performance of recycled LWR-discharge-transuranic (TRU) oxide fuel in a gas-cooled and accelerator driven (GT/AD-MHR) system has been assessed for the U.S. DOE accelerator transmutation of waste (ATW) program. This activity is part of preliminary design studies being performed at ANL and LANL to define and compare candidate ATW systems. The studies have focused primarily on the blanket component of the overall system, since the choice of blanket technologies is an important technical decision faced in designing an ATW system.

The gas-cooled system point design is a 600 MWt hybrid system operated in the critical mode for three cycles and in a subcritical accelerator-driven mode for a subsequent single cycle. The transmuter contains both thermal and fast spectrum transmutation zones. The thermal zone is fueled with the "fresh" LWR-discharge TRU oxide fuel (encapsulated as TRISO-coated particles); the fast zone is fueled with TRU-oxide fuel that has been burned in the thermal region for three critical cycles and one additional accelerator-driven cycle. The fuel loaded into the fast zone is irradiated for four additional cycles. This design ensures the high consumption of the high thermal-neutron-cross-section Pu isotopes in the thermal spectrum zone, and the relatively enhanced consumption of minor actinides in the fast-spectrum zone.

Single batch and three-batch fuel loading schemes for the GT/AD-MHR system have been evaluated using Monte Carlo and deterministic codes to determine the feasibility of achieving high consumption levels without exceeding reactivity and power density limits. The studies revealed the potential for high consumption of Pu-239 (97%), total Pu (71%), and total TRU (64%) in the system. These consumption levels are however lower than values obtained in previous studies in which weapons-grade plutonium is employed as fuel, because the latter fuel is more reactive and hence permits a longer cycle length at the same operating power. The higher consumption levels in the gas-cooled system, relative to say a fast system is due to the relatively lower fuel inventory required in the gas-cooled system. Our evaluation also confirmed the need for burnable absorber, most likely Er-167, for both suppressing the initial excess reactivity and ensuring a negative temperature coefficient under all operating conditions. Additionally, current results suggest that it may be preferable to use a double strata thermal critical system and fast subcritical system to achieve nearly complete destruction of the TRU oxide fuel.

1. INTRODUCTION

Various blanket options for the multiplication of neutrons produced from a spallation process have been proposed under the U.S. DOE Accelerator Transmutation of Waste [ATW] Program [1]. The Argonne National Laboratory (ANL) has proposed and designed fast neutron blankets using either liquid metal lead-bismuth-eutectic or sodium as coolant [2]. A gas-cooled, coupled thermal-and-fast blanket that is designed for operation in both critical and subcritical modes has been proposed by General Atomics (GA) [3]. Design studies of these ATW systems are currently being performed at both Argonne and the Los Alamos National Laboratory (LANL) to assess the performance of these blankets and evaluate their potential for incorporation into the ATW system. These activities are crucial since the choice of blanket technologies is an important technical decision faced in designing an ATW system. The purpose of this paper is to present the preliminary results of the assessment of the GA gas-cooled and accelerator driven (GT/AD-MHR) system performed by Argonne. The inclusion of the gas-cooled system in the ATW study arises from the potentially high destruction of transuranics possible in such systems without additional reprocessing and recycling. GA has demonstrated this item for the plutonium content of weapons-grade transuranic (TRU) oxide fuel [4]. The current study focuses on the performance of the GT/AD-MHR when recycled LWR-discharge-TRU oxide is used as fuel in the blanket.

The primary objectives of the GT/AD-MHR system are grouped into three areas:

- Achieve very high burnup of the initial loading of plutonium and minor actinides.
- Maintain fuel particle integrity throughout the fuel cycle and into disposal, thus avoiding the need for intermediate reprocessing.
- Maintain high operating temperatures needed to achieve a high net thermal efficiency.

The GT/AD-MHR design used in the current Argonne study remains relatively close to the design database developed by GA over so many years. This implies that the GA fuel block and core dimensions, lattice and block pitches, core power, and temperatures were retained in the current study. It is anticipated that future studies will include significant flexibility in the selection of these parameters. Nevertheless, the effects of several other design parameters on the system performance were studied. These include the initial heavy metal and burnable poison loadings, which are expected to have effects on the initial reactivity, cycle length, temperature coefficient, and achievable burnup. The effects of the variations in the particle (fuel and erbium) dimensions and fuel management schemes were also additionally studied.

In Section 2, a general description of the GT/AD-MHR system is provided. The reactor physics codes and models used for the neutronic evaluation of the core are discussed in Section 3. The various code verification studies in which the deterministic results are compared to the Monte Carlo results are also discussed in this section. The results of fuel block and whole-core parametric studies, used for understanding the physics trends of the GT/AD-MHR system are presented in Sections 4 and 5 respectively. In Section 6, results are presented for the GT/AD-MHR system point design employing single-batch and three-batch loading schemes. The summary and conclusions from this work are given in Section 7.

2. GT/AD-MHR SYSTEM DESCRIPTION

Figures 1 and 2 provide a general description of the system proposed by GA. The transmuter consists of a steel vessel housing, containing an annular transmutation region operating in a thermal neutron spectrum. This annular region contains the “fresh” TRU separated from the LWR spent fuel. The TRU is contained in TRISO-coated particles. These spherical particles consist of a 200 μm diameter $TRUO_{17}$ fuel kernel surrounded by layers of graphite buffer, inner pyrolitic graphite, silicon carbide, and outer pyrolitic graphite, having thicknesses of 100 μm, 35 μm, 35 μm, and 40 μm, respectively. The buffer zone is designed to absorb gaseous fission products, while the silicon carbide layer serves as a stable barrier and pressure vessel. These particles are mixed with graphite powder and packed into cylindrical compacts. The compacts are loaded into cylindrical channels within hexagonal graphite blocks. The blocks also have channels for helium coolant flow and channels for introducing erbium burnable poison (BP) into the system. The blocks are 36 cm flat-to-flat, and contain 202 fuel channels, 108 coolant channels and 14 burnable poison channels, all arranged on a 1.88-cm triangular pitch. Each block has a height of 79.3 cm. The active core comprises ten of these blocks stacked vertically, at a given radial location.

Fuel blocks are loaded into the fifth, sixth, and seventh radial rings of a hexagonal core (see Fig. 2). Three rings of graphite reflector are arranged both inside and outside of this thermal region. The innermost layer is filled with fast fuel assemblies, composed of the TRU material that has undergone four years of burning in the thermal region. The fast assemblies have not yet been designed, and for the purpose of this study it is assumed that they are similar to the Gas Cooled Fast Reactor (GCFR) design developed in the 1970’s and early 1980’s. At the

center of the core is the location for a spallation target used during the period of subcritical operation.

The transmuter is cooled by helium heated to an outlet temperature of 850°C. Helium is carried to a direct-cycle gas-turbine-generator system. The high operating temperatures and the characteristics of the direct Brayton power conversion system allow electric generation with a high net thermal efficiency of approximately 47%.

The GT/AD-MHR transmuter operates in the critical mode for approximately three years, which corresponds to 75% of its cycle length. In this mode, the fission process is driven by the thermal region and limited transmutation events are expected in the fast region. After these three years, the core becomes subcritical and is driven by the spallation target during a fourth year. The local multiplication of spallation neutrons in the fast region might produce a significant fast flux thus helping the transmutation of the minor actinides. The GT/AD-MHR plant would comprise four 600 MWt transmuters, sharing one 15 MW beam accelerator.

3. CODES AND MODELS FOR REACTOR PHYSICS CALCULATIONS

The GT/AD-MHR design includes several levels of heterogeneity that require proper treatment in order to obtain accurate physics predictions for the core. At the compact level, there are particle heterogeneity effects arising from the application of the multi-layer ceramic-coated fuel or BP particles dispersed in a graphite matrix. Fuel block heterogeneity from the heterogeneous arrangement of fuel, BP and coolant channels in the block, also exists in this design. Core level heterogeneity is also present because of the annular core layout that employs inner and outer reflector zones and the two afore-mentioned fueled core zones. The reactor physics of the GT/AD-MHR is additionally complicated by the presence of the low-energy-lying plutonium and Er-167 resonances (0.2-1.1 eV) and by the fact that the neutron spectrum has a low-energy peak about this energy range. This peak can change depending on the core state or material loading. The location of the peak and the direction of the spectral shift greatly affect both the resonance fission and capture rates and dictate the core or block criticality state and the magnitude and sign of reactivity coefficients.

Two complementary computational paths have been implemented at Argonne for accurate predictions of the GT/AD-MHR core reactivity states and power distributions. The first is a deterministic path based on the DRAGON [5], DIF3D [6], and REBUS-3 codes [7] while the second is a stochastic path based on the MONK [8] Monte Carlo code. The DRAGON lattice code was selected because it can handle the dispersed fuel design of the GT/AD-MHR. Whole-core neutronics calculations are performed using the DIF3D code, which solves the multigroup transport equations or approximations of the equations. The DIF3D code is also the computational engine of the REBUS-3 fuel-cycle analysis package [6]. Most of the design evaluations have been performed with the deterministic codes because of the exorbitant time requirements of the high-fidelity Monte Carlo codes, particularly as the total number of core states to be analyzed becomes large or when the magnitude of the reactivity worth of interest is small. While the deterministic path promises fast running times and allows for multiple perturbation calculations, it however relies on a series of energetic and spatial homogenization steps that might limit its accuracy. It was therefore necessary to find an independent path for verifying the core predictions obtained with the deterministic path. The MONK Monte Carlo code provides this alternate path, and has been used to verify the results of homogeneous-cell, pin-cell, fuel-lattice, and whole-core calculations performed with the deterministic codes.

3.1. Deterministic model

Burnup-dependent, block-average microscopic cross-sections were calculated with the DRAGON lattice code, using ENDF/B-VI based 69-group library; a 172-group library that could be used with DRAGON is also available at Argonne. The DRAGON code was selected because it handles accurately the dispersion fuel in a graphite matrix design of the GT/AD-MHR block and permits full-block calculations using the collision probability method. Resonance self-shielding and depletion calculations in the particles are possible because DRAGON allows explicit representations of the multi-layer fuel and BP particles, the matrix graphite and the block graphite of the GT/AD-MHR design. For each burnup state, the DRAGON model solves a half block problem and produces the group cross sections for the block. The code is also used to generate the cross sections for the non-core zones.

The deterministic, three-dimensional core physics model is based on the DIF3D code, which solves the multigroup transport equations or approximations of the equations by either nodal or finite difference approaches. Both the eigenvalue and external source problems that are pertinent to the GT/AD-MHR system analysis are solved by the code. The DIF3D-nodal diffusion theory model is used for calculating both the power distributions and reactivity states of the GT/AD-MHR core. A 23 neutron-energy group structure is currently used in the model. This detailed group structure was selected to give a good representation of the Pu and Er resonances in the 0.2 to 1.1 eV energy range. The DIF3D model is a detailed representation of the GT/AD-MHR core. The model represents 11 rings of hexagonal-prismatic assemblies, resulting in 331 radial computational nodes. Axially, the whole length of the active core (about 793 cm), and additional lower and upper graphite reflector zones (100 cm each), are modeled. Forty axial computational nodes (30 in the active core) are employed in the model. A void boundary condition is imposed on all external surfaces.

The REBUS-3 depletion model uses the DIF3D-nodal model discussed above for its neutronics calculations. The 23-group, microscopic cross sections obtained from the DRAGON block depletion calculations are used in the REBUS-3 model. The REBUS-3 code capability that permits the fitting of both capture and fission cross sections of the active isotopes is employed in the calculations. This approach approximately accounts for cross section variations due to changes in the neutron spectrum as a function of the depletion. Seventeen heavy-metal nuclides are tracked in the 3-D depletion calculations; these are all Pu, Np, Am, Cm and U isotopes. Additionally, 35 fission-product (FP) and one lumped-fission-product nuclides are employed in the REBUS-3 model. The 35 FP nuclides account for about 95% or so of the overall reactivity effect attributable to fission products, and this model is quite adequate for the current study. The heavy-metal isotopes, FP nuclides, and two erbium isotopes (Er-166 and Er-167) are specified as depletable isotopes in the REBUS-3 model.

3.2. Stochastic model

Core heterogeneities have been evaluated using the MONK Monte Carlo code, which employs the JEF2.2 nuclear data library. MONK has the capability to explicitly model the geometry under consideration and to perform criticality and burnup analyses in an integrated manner. In the current model, the fuel and burnable poison particles, compacts, fuel blocks and core regions, are explicitly represented. The particles in a compact are represented as a close-packed hexagonal lattice of spheres. Each layer of a particle is also explicitly represented.

The MONK criticality calculations are performed with quasi-continuous energy or multigroup datasets. The quasi-continuous energy dataset is processed into a fine energy mesh structure

(13193 or 8220 groups). The multigroup libraries are processed in a much coarser set (172 or 69 groups). MONK burnup calculations however currently use the coarser multigroup datasets [8].

3.3. Verification calculations for the deterministic models

Preliminary verification of the physics predictions obtained with the deterministic codes has been performed using the MONK results as reference. Additionally, the need for the very detailed lattice models has also been assessed. To evaluate the importance of the explicit representation of the fuel and burnable poison particles, three different models of the fuel or burnable poison compacts in the fuel block were developed. These are:

- Explicit modeling of the block including the multi-layer fuel or burnable poison particles inside the compacts.
- Block model using a homogeneous mix of the particle layers inside the compact (homogenized particles).
- Block model employing a homogeneous mix of particle layers and matrix graphite (homogenized compact).

The difference in the block k-infinity, between case (a) and case (b) or (c) provides an estimate of the heterogeneity effect due to the particles in the compact. Table I summarizes the MONK results for the fuel compact modeling assumptions for a case employing a heavy-metal loading of 771 grams per block; there are 1020 blocks per core. In the MONK analysis, it was assumed that the fuel block is loaded with fuel compacts and helium coolant channels, without erbium poison compacts and the fuel-handling hole. The MONK results show a strong heterogeneity effect (14%). The DRAGON model similarly predicted this effect to be 14% $\Delta k/k$. MONK studies of the various models for representing the BP compact also show a compact heterogeneity effect. The homogenized-compact approximation for the BP was found to underpredict the block k-infinity by 2.2% $\Delta k/k$ in this case. The homogenized-region models (without additional recipe) give inaccurate k-infinities because they significantly underpredict the self-shielding of the strong absorption resonances in plutonium isotopes (particularly Pu-240) contained in the fuel compact and Er-167 in the BP compact. This is caused by the fact that the fuel or BP particle dimension is relatively large compared to the mean free path of neutrons in the low-energy-lying resonances of these isotopes. Because of this the inner zone of the particle is shielded from neutrons by the outer zone and simple homogenization of cross sections does not account correctly for the self-shielding effect. For both the fuel and BP compact cases, the heterogeneity effect was found to be dependent on the particle composition and the packing fraction. The difference in k-infinity between the homogenized-region and explicit models decreases as the packing fraction increases or as the particle radius decreases.

Fuel block power distributions predicted by MONK and DRAGON have also been compared. Such comparison for a fuel block containing 14 BP compacts and at the cold state (293 K) indicated that DRAGON accurately predicts the power distribution in the block. The difference in the maximum compact power predicted by the codes is about 1.1%. The maximum power in this case occurs in a fuel compact located close to the block boundary because of the extra (non-cell) graphite present in this zone, which acts to provide a softer spectrum. The maximum compact power difference is about 2.9% and occurs for a compact operating close to the average block power and also neighboring a coolant channel and a BP compact.

In summary, the DRAGON and MONK codes give consistent results on a series of calculations from simple compact cells to full block analyses. These results provide confidence in the validity of the deterministic calculations, with respect to a high-fidelity method. The strong double heterogeneity effects observed for the fuel and erbium particles imply that a very detailed modeling of these particles is required.

The DRAGON depletion model has also been verified by comparing results for GT/AD-MHR compact-cell (fuel compact and surrounding graphite) cases to those obtained with the British WIMS8 [9] lattice code. The compact-cell calculations were done primarily to check the performance of DRAGON compared to another deterministic code, which also employs a different base cross-section library (JEF-2.2 versus ENDF/B-VI used in DRAGON). The WIMS8 code has been used for evaluating high-temperature gas-cooled reactor systems employing particulate fuel in graphite matrix, and hence is adequate for the comparison. The two codes predicted very similar k-infinities for an at-power case in which the fuel particles and matrix graphite were explicitly represented and another case in which they were smeared together into a single composition. The codes also gave very similar trend of k-infinity with burnup for a constant-flux depletion case. For this case, the codes predicted practically the same time evolutions of the number densities of the primary nuclides. The slight differences in the time evolutions of the number densities of Pu-238 and Pu-242 were attributed to the differences in the depletion chains.

Core power distributions predicted by MONK and DIF3D have been compared for a fresh core state having a heavy metal loading of 787 kg and an Er-167 loading of 27.7 kg. The results indicated that the deterministic approach provides a very accurate model of the whole-core. The DIF3D model using block-average cross sections generated by DRAGON (but currently with no additional block homogenization factors) gave a maximum block power that is different by 0.4% from the MONK value. The maximum difference in block power is 2.5%.

The results so far obtained in the verification calculations indicate that the deterministic models currently being employed by Argonne for assessing the GT/AD-MHR design give accurate predictions of core performance parameters when compared to MONK results. Further effort is required and ongoing to validate the burnup predictions.

4. PARAMETRIC STUDIES OF FUEL BLOCK NEUTRONICS

Parametric calculations were performed for a fuel block to gain understanding of the dependence of the block reactivity on fuel kernel diameter and packing fraction, erbium loading, and operating temperature. Results for two of these parametric studies will be presented here.

Figure 3 shows the variation of the block k-infinity as a function of the fuel-particle packing fraction for three different BP-particle packing fractions, at the hot operating state. These results were obtained with the DRAGON model. The variation of k-infinity versus the packing fraction shows a peak below 0.05 packing fraction. The primary reason for the trend is the shift in the neutron spectrum with the packing fraction. Above a packing fraction of 0.05 and as the packing fraction decreases, the carbon-to-heavy-metal ratio increases and leads to an increase in the thermalization of neutrons, causing the neutron spectrum to become softer. There are also competing effects arising from the decrease in the particle self-shielding with packing fraction. The relatively improved utilization of neutrons (relative increase in Pu-239 absorption rate), resulting from the softer spectrum however dominates and results in the k-infinity increasing as the packing fraction decreases. The increase in k-infinity with

packing fraction, below the peak, is due to the fact that increase in the fissile content dominates. The packing fraction corresponding to the highest k-infinity differs for the three curves because as the BP loading increases, the spectrum hardens (increasing the relative absorption in Pu-240 and Er-167) and requires more fuel to achieve the same k-infinity.

Calculations were also performed to determine the effect of the fuel kernel diameter on the block k-infinity, for a block with a BP-particle packing fraction of 0.10. Results for three fuel diameters (base diameter, double the base diameter, and half the base diameter) were obtained with the DRAGON model and compared. In these calculations, the thickness of the other particle layers was kept constant. The results show that for a given heavy-metal mass, the block k-infinity increases as the particle diameter increases. An increase in the fuel kernel diameter leads to a decrease in the packing fraction and an increase in the distance between kernels. This causes a relative increase in the thermalization of neutrons and leads to a softer spectrum. Additionally, the larger diameter increases the self-shielding of the resonance absorbers (particularly Pu-240). Note that the Pu-239 resonance fission cross-section is also reduced by the self-shielding effect. However, the reduction of the Pu-240 absorption cross section is the predominant effect.

5. RESULTS FOR WHOLE-CORE PARAMETRIC STUDIES

Whole-core parametric studies were performed with the DIF3D/REBUS-3 model in order to evaluate the feasibility of achieving very high Pu-239 and total plutonium burnup in the GT/AD-MHR system. These preliminary calculations employed no fast-core zone, and were for the critical mode operation. The findings from this study are:

- The initial core k_{eff} increases as the initial mass of heavy metal decreases, for a given burnable poison loading. This is consistent with the trend observed for the fuel block (see Section 4).
- The relatively low heavy metal loading of the gas-cooled blanket ensures a high burnup of the heavy metals for a given power level. The lower the initial mass however, the lower the cycle length.
- Adequate quantity of burnable poison is required at the end of cycle to ensure a negative isothermal temperature coefficient below 300°C; the operating temperature is about 770°C.
- The plutonium burnup increases as the burnable poison loading decreases. This results primarily because of the softening of the neutron spectrum as the initial Er-167 mass decreases. The Er-167 loading cannot however be arbitrarily small because Er-167 provides a strong negative component for the ITC. Additionally, the Er-167 is also used to control the initial excess reactivity at the beginning of cycle.
- By using a 3-batch loading scheme (versus 1-batch loading), the initial excess reactivity can be greatly reduced. This reduction depends on the fuel and burnable poison loading, and typical values from our study varied from 3.5-6.5%$\Delta k/k$.

Parametric studies were also done to compare the performance of weapons-grade-Pu oxide fuel to the LWR-discharge-TRU oxide fuel used in the current study. The weapons-grade composition employed is 94% Pu-239 and 6% Pu-240. A core with an initial heavy-metal loading of 790 kg and initial Er-167 loading of 28 kg was used in the study. Table 2 is a summary of some pertinent performance parameters. The results show that the initial k_{eff} of the core using weapons-grade-Pu oxide fuel is much higher than that for the LWR-discharge-TRU oxide fuel. This is because the weapons-grade-Pu oxide fuel contains a higher fraction of fissile Pu-239 and lower fraction of Pu-240 than the LWR-discharge-TRU

oxide fuel. The significantly higher k_{eff} for weapons-grade fuel would require additional strategy for holding down the excess reactivity. This could be done by using three or more batches of different burnups and/or by initially operating with control rod absorbers in the core. A higher erbium poison loading could also be used; this would however degrade the consumption levels. The higher reactivity of the weapons-grade Pu fuel results in a longer cycle length, which (at a fixed power level) gives a higher burnup and consumption of Pu-239. Much higher consumption levels of total Pu and heavy-metal are also obtained for the weapons-grade fuel.

6. RESULTS FOR A SYSTEM POINT DESIGN

The General Atomics (GA) "Teledial" concept aims to run a transmuter island containing four transmuters operating concurrently, with three units running in the critical mode, and the fourth running in the accelerator (source) driven mode. It is therefore expected that the cycle length of both the critical and accelerator-driven modes would be the same, if no unit were to be idle for a long time. The preliminary GA proposal specifies a cycle length of a year. A design using this latter requirement was therefore used in the evaluations for a system point design. Two sets of calculations were performed, one for a single-batch loading scheme, and the other for a three-batch loading scheme.

Figure 4, displays the schematics of a transmuter fuel cycle in the teledial concept, for the three-batch loading scheme. The recycled LWR-discharge-TRU oxide fuel is loaded into the outer thermal spectrum zone of the GT/AD-MHR for burning in the critical mode for about three years. Previously burned fuel is in a central fast zone. In the fourth year, the same unit is configured as an accelerator-driven system, containing a centrally located spallation target. The three-year, thermal-zone burned fuel and the inner fast-zone fuel from the critical mode operation are used in this subcritical cycle, and remain in their respective zones. At the end of this one-year subcritical irradiation, the outer thermal-zone fuel is reconstituted and used as fast-zone fuel in another critical mode operation. As the fuel in the fast-zone has reached its end of life it is discharged, with very low transuranics content. The critical mode operation is staggered, and each GT/AD-MHR unit undergoes the subcritical burn in one out of four year. The difference between the three-batch and single-batch loading schemes is that in the three-batch scheme, the critical operation has a cycle length of about a year and hence undergoes fractional-core fuel loading three times during this stage of the system. On the other hand, in the single-batch-loading scheme, the fuel is loaded once, at the beginning of the three-year critical operation.

Obtaining the mass flow in the coupled critical/subcritical mode system requires iterations between the critical mode and subcritical mode calculations. This is necessary because the fuel is interchanged between the two modes of operation, and it is necessary to ensure that the masses discharged from one mode and charged into the other mode have converged. This issue is significant because our current fuel cycle code does not have the capability to model both critical and subcritical sub-cycles in the same run.

Table 3 contains the summary of core performance parameters for the three-batch and single-batch cases, for an initial heavy metal loading of 1054 kg. Initial Er-167 (burnable poison) loading is specified in the Table. The Er-167 amount used in these calculations is lower than that likely to be used in the final design, but correspond to the value that gives a critical mode duration of about three years. Additionally, in the results in Table 3, the subcriticality level of the single batch core was realized by adding more burnable poison prior to the start of the accelerator-driven-mode calculation. It should also be note that these results were obtained

using a representative neutron source spectrum and distribution. No extensive effort has been devoted to this issue at the current time.

As evident from Table 3, very high consumption levels of both Pu-239 and the heavy nuclides were obtained in these cores. The consumption amounts reported here are however generally lower than the values previously reported by GA and surely less than what would have been obtained if weapons-grade Pu fuel is used. The higher heavy nuclide consumption for the three-batch core relative to the single-batch core is due to the longer discharge cycle length (see Table 3). The single-batch core has a higher initial k-effective in the critical cycle because fresh fuel blocks are used. A combination of control rods and burnable poison would be employed to control the excess reactivity in the initial stages of the cycles. The multiplication factor of the accelerator-driven cycle for the three-batch core varies from 0.963 to 0.732, implying a seven-fold increase in the source strength over the cycle, to keep the power level constant. A five-fold increase is indicated for the single-batch core. The low ending-state multiplication factor (0.732 or 0.827) is probably lower than would be permitted in actual operation of the core, since this would imply a high beam power and would make the accelerator cost prohibitive. The low multiplication factor resulted because the sub-critical mode cycle length was set to that for the critical mode in this study.

The power fractions of the fast and thermal zones are fairly constant during the critical operation cycle in both the single-batch and three-batch cores. The fast-zone accounts for about 3-5% of the total power in both of these cores. The power fraction of the fast–zone increases however with burnup in the accelerator-driven cycle, for both the single-batch and three-batch cores. The system becomes more subcritical as fissile content (and neutron multiplication) of the thermal-zone decreases with burnup, causing the flux to shift towards the center of the core.

The core radial and axial power distributions were also investigated for both the critical and accelerator-driven cycles. It was found that the critical operation power distributions are relatively flat and the peak is within acceptable limits. The power peaking is more pronounced in the accelerator-driven cycle than in the critical operation cycle. The highest power densities were observed in the fast-zone of the accelerator-driven cycle, and they increase with irradiation time. Additionally, the axial power profile of the fast-zone peaks significantly at the center, because this is the level that the external source is located. Because the fast zone sees about 3-5% of the total power during the critical operation cycle, the plutonium and heavy-metal consumption rates of the fuel residing in this zone is quite small. Additionally, since the fast zone also sees about 10 to 40% power during its stay in the accelerator-driven cycle, the overall consumption of fuel in this zone is limited.

Finally, while high burnups have been calculated for the discharge fuel, it was also observed that the final burning stage in the fast region was not very effective due to the relatively soft spectrum in the central fast region (this softening is due to the return of moderated neutron from the graphite reflector). Adding thermal absorbers (such as boron, cadmium, or certain long-lived fission products) in the graphite blocks around the fast region could probably prevent return of these neutrons; the density of the graphite between the fast and thermal zones could also be reduced to achieve the same result. Nevertheless, this would not raise the fast flux in the central region, necessary for effective transmutation of the higher minor actinides. More efficient solutions have been discussed between ANL, GA, and LANL. One straightforward solution would be to adopt a double strata system, where a thermal (accelerator-driven or not) gas-cooled transmuter would be used to burn as much plutonium as possible. The fuel would then be reconstituted (potentially after an intermediate reprocessing

step) and introduced into an accelerator driven gas-cooled fast reactor for deep burning of the minor actinides. Separation of the fast and thermal burning functions, while less elegant than the proposed GA approach, might avoid complex engineering issues. Another solution is to redesign the fast region within the proposed concept to make it a better neutron multiplier, thus generating its own sustained fast flux; this could be achieved by enlarging it and providing it with more fissile material for example from partially burned fuel.

7. SUMMARY AND CONCLUSIONS

The physics performance of the General Atomics GT/AD-MHR design has been evaluated using independent deterministic (DRAGON/DIF3D/REBUS-3) and Monte Carlo (MONK) codes. Comparisons of the deterministic and Monte Carlo results indicate that the deterministic models give very accurate predictions of the core performance parameters. Additional comparisons are still required in this area, particularly for the whole-core depletion calculations.

Fuel block and whole core calculations were performed to gain understanding of the physics behavior of the GT/AD-MHR core. These calculations included parametric studies of the effect of fuel and burnable poison loading on the fuel block and core performance. The effects of using different fuel kernel diameter and fuel form (weapons-grade-Pu versus LWR-discharge-TRU) were also studied. Better system performance would however be obtained by either using weapons-grade-Pu fuel or larger fuel kernel diameter. The application of the weapons-grade fuel would however increase control requirements of the system.

The system point design confirmed the feasibility of very high burnup of Pu-239, total Pu, and heavy metal in this system. The level of burnup obtained in the current evaluations using LWR-discharge-TRU oxide fuel is however still lower than expect; higher burnup would be required to eliminate the need for fuel recycling. If this trend persists following further improvements in the design, the double strata approach may be needed to achieve the very high burnup required for this fuel type. Power peaking however does not appear to be a problem in the current design, particularly for the thermal zone. While significant peaking are observed for the fast zone, during the subcritical mode operation, the power density in this zone is however still low (compared to a LWR pin). Preliminary analysis suggests that it is feasible to cool this zone without adverse effect on the fuel performance. Attention must however be given during system design to the coolant flow requirements for this zone.

Several paths have been identified for increasing the performance of the thermal region: for example lower inventories and larger particle sizes might result in deeper burnups, though the resulting shorter cycle lengths and potential power peaking might be an operational issue. Also, larger core outer diameters might result in higher performances, but at the cost of having to significantly improve the shielding characteristics of the outer reflector.

Control issues also need to be addressed: means to contain the initial excess reactivity need to be developed. Additionally, methods for controlling the system reactivity or the accelerator beam intensity during the subcritical stage also require further study. As much as possible, it seems desirable to obtain a flat reactivity profile during operations (in order to avoid excessive power peaking): this would give the preference to cores with large fissile inventories and elaborate fuel management schemes (for example, a long-life core with several fuel batches).

No attempt has yet been made to find suitable modes for incinerating Long-Lived Fission Products (LLFP). Positions in the inner or outer reflector seem ideally suited for these tasks. Burning rates will need to be estimated and LLFP target design will need to be optimized.

TABLE 1. FUEL COMPACT HETEROGENEITY EFFECT

Case	k-infinity	Δk/k (%)
Explicit Modeling	1.2764	--
Homogeneous layers	1.1101	-13.0
Homogeneous Compact	1.0928	-14.4

TABLE 2. COMPARISON OF WEAPONS-GRADE-PU AND LWR-DISCHARGE-TRU OXIDE FUELS

Parameter	Oxide fuel type	
	LWR-discharge-TRU	Weapons-grade
Beginning of cycle k_{eff}	1.0924	1.4232
Cycle length, (EFPD)	405	810
Cycle consumption, %		
Pu-239	69	91
Total Pu	34	67
Total heavy-metal	32	66

TABLE 3. PERFORMANCE PARAMETERS FOR THREE-BATCH AND SINGLE-BATCH CORES

Parameter		Core	
		Three-batch	Single-batch
Total fresh heavy metal loading, kg		1054	1054
Total initial erbium-167 loading, kg		0.62	0.62
Cycle length, effective full power days			
Critical cycle		270	720
Accelerator-driven cycle		270	240
Initial critical mode k-effective		1.074	1.137
Accelerator-driven cycle multiplication factor	Beginning state	0.963	0.963
	Ending state	0.732	0.827
Fast-zone discharge consumption levels			
Pu-239 consumption, %		97	94
Net plutonium consumption, %		71	61
Net heavy metal consumption, %		64	56
Fractional power contributed by fast-zone			
During critical operation, %		3	4
During accelerator-driven operation, %		10-40	10-40

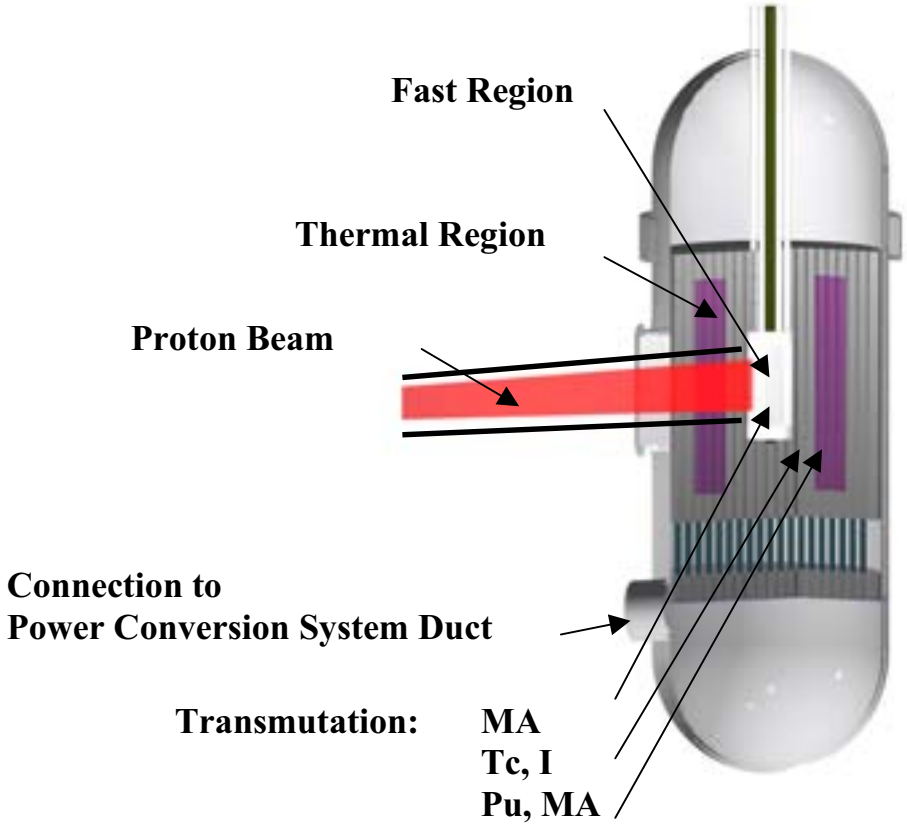

FIG. 1. General Atomics (GA) thermal-fast transmuter.

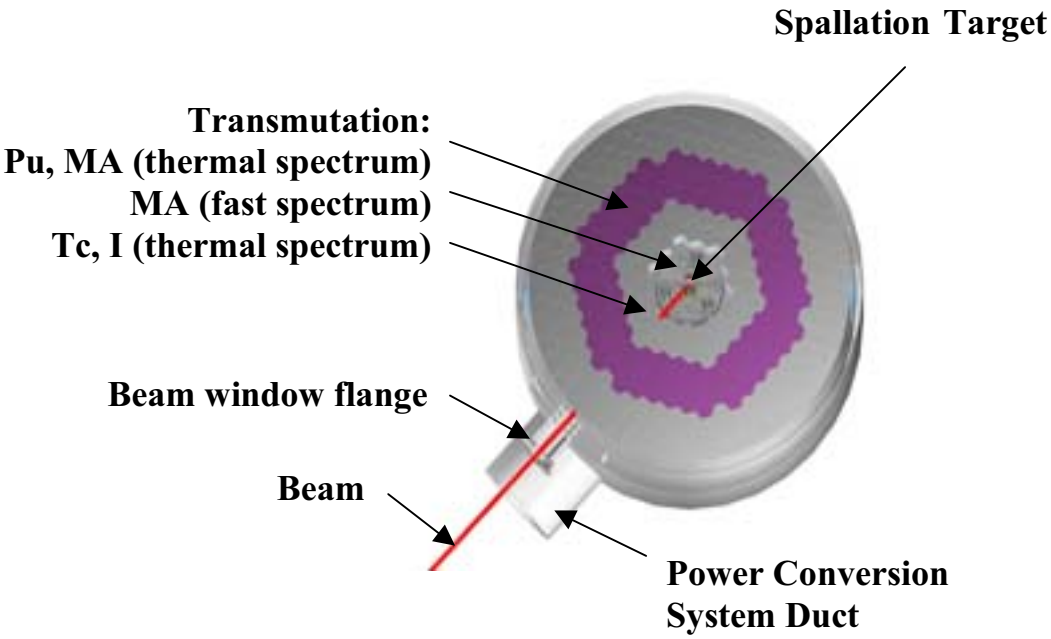

FIG. 2. GA Thermal-fast transmuter cross section.

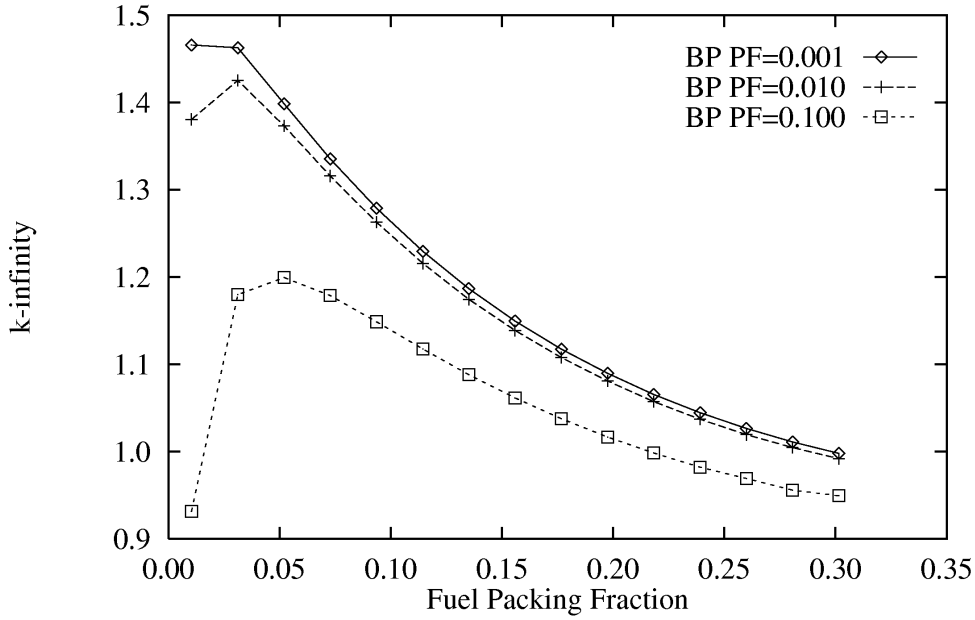

FIG. 3. Unit block k-infinity as a function of packing fraction.

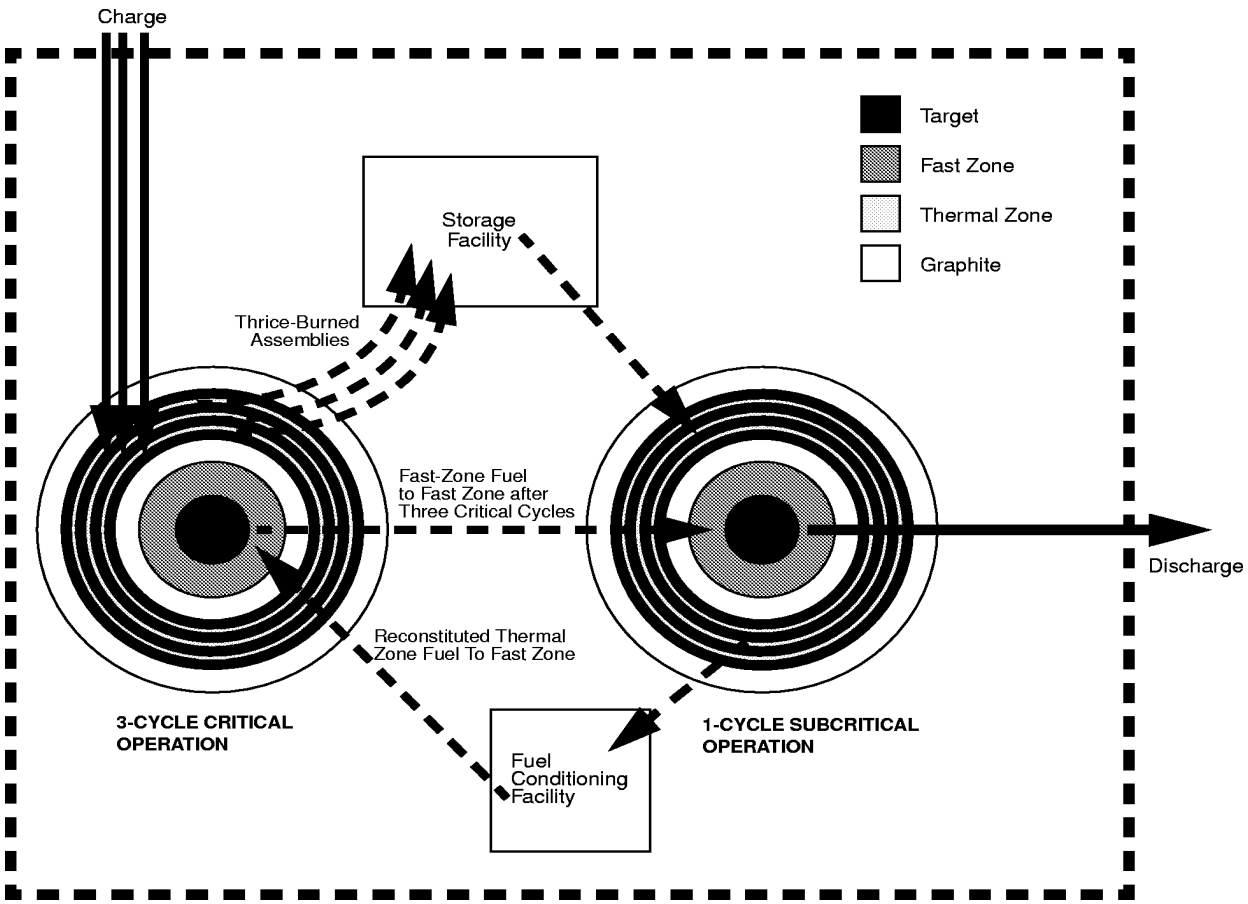

FIG. 4. GT/AD-MHR hybrid cycle.

REFERENCES

[1] A Roadmap for Developing Accelerator Transmutation of Waste (ATW) Technology, DOE/RE-0519, US Department of Energy (1999).

[2] YANG, W.S., NABEREJNEV, D.G., KHALIL, H.S., Physics Design Optimization of an LBE-Cooled ATW Blanket, Trans. Am. Nucl. Soc., **83** (2000).

[3] RODRIGUEZ, C., et al., Transmutation of Nuclear Waste Using Thermal and Fast Neutron Energy Spectra, Proc. 8th Int. Conf. on Nuclear Engineering (ICONE-8), 2000, Baltimore, MD, USA, American Society of Mechanical Engineers (ASME), New York (2000).

[4] BAXTER, A.M., et al., Combining a Gas Turbine Modular Helium Reactor and an Accelerator for Near Total Destruction of Weapons Grade Plutonium, American Institute of Physics (1995).

[5] MARLEAU, G., et al., A User's Guide for DRAGON, IGE-174, Rev. 3, Ecole Polytechnique de Montreal (1997).

[6] DERSTINE, K.L., DIF3D: A Code to Solve One-, Two-, and Three-Dimensional Diffusion Theory Problems, ANL-82-64, Argonne National Laboratory (1984).

[7] YANG, W.S., KHALIL, H., Analysis of the ATW Fuel Cycle Using the REBUS-3 Code System, Trans. Am. Nucl. Soc., **81**, 277 (1999).

[8] The ANSWERS Software Package, MONK - A Monte Carlo Program for Nuclear Criticality Safety and Reactor Physics Analyses, User Guide for Version 8, ANSWERS/MONK (98) 6, AEA Technology, UK.

[9] The ANSWERS Software Package, WIMS - A Modular Scheme for Neutronics Calculations, User Guide for Version 8, ANSWERS/WIMS (99) 9, AEA Technology, UK.

THE ECONOMICS OF TRANSMUTATION FUEL CYCLES

D. KIM, M.S. KAZIMI, M.J. DRISCOLL, N.E. TODREAS
Massachusetts Institute of Technology, Cambridge, Massachusetts, United States of America

Abstract

The fuel cycle cost of any transmutation system is one of the major components of the total cost of electricity generated by that system. The fuel cycle cost was estimated for an 1800 MWth actinide burning reactor (ABR) design developed by MIT and INEEL. The fuel is of metallic material composed of 25-30% of TRU and 70-75% Zr. The cost calculations were based on the cost estimates of fuel reprocessing and manufacturing facilities similar to those discussed in the ATW road-mapping effort. An assumption was made that 10 ABRs will be serviced by the fuel separations and manufacturing facilities, and that the fuel will be discharged at a burnup of 70 MWD/kg of total metal (TRU + Zr). A nominal capacity factor of 80% was assumed for operations of the reactor and electric plant system. An analysis was performed to examine the sensitivity of the fuel cycle cost to key factors, specifically to the unit costs of the front-end components of the fuel cycle and the reactor capacity factor (in effect fuel burnup).

The results show that the fuel cycle cost of the reference ABR will be about 11 Mills/kWhe, much higher than that of existing LWR nuclear power plants at around 6 Mills/kWhe. The fuel cycle cost has small (< 14%) sensitivity to a ±15% variation in each of the following unit costs: LWR fuel reprocessing, ABR fuel reprocessing and ABR fuel fabrication. The variation of fuel cycle cost is found to be 3 Mills/kWhe for capacity factor variation from 70 to 95%. Therefore, means to reduce the fuel cycle cost would be needed to improve the economic competitiveness of the ABR compared to other electricity generation systems.

This work suggests two possible ways to reduce the fuel cycle cost. One is scaling up the production capacity of the fuel separation and manufacturing facilities, perhaps to service 15 ABRs. The second is increasing the discharge burnup, perhaps to 100 ~ 125 MWD/kg of total metal, which will cut the cost down proportionally. Additionally, the cost of the fuel cycle can be tolerated if the capital cost of the system can be made lower than the other electricity generation systems.

1. INTRODUCTION

Actinide burning systems can be divided into two types: a sub-critical burner driven by a proton accelerator and a critical burner reactor without accelerator. Both can be deployed for the purpose of reducing long term high level radioactive materials from LWR spent fuel or from dismantling of nuclear weapons. The critical Actinide Burner Reactor (ABR) is one of several advanced power plant concepts currently under development worldwide.

One measure of the attractiveness of a new concept is its economic competitiveness. Since proposed actinide burning systems are still at the development stage, it is worthwhile to assess the design direction that may best serve to enhance the economics of the fuel cycle. In this work, the fuel cost, one of the major components of total electricity cost, is estimated using three fuel cost models:

- An ORNL (Oak Ridge National Laboratory) model [4];
- The FBR (Fast Breeder Reactor) model in the book by Waltar and Reynolds [13]; and
- A Simple model used in MIT fuel cycle classes [7].

Since several components of the estimated cost are uncertain due to lack of sufficient development of processes and the scale that can be adopted for facilities, a parametric analysis is performed to elucidate the effect of reasonably expected variations in these cost components on the cost of electricity production.

The present ABR fuel cost estimation is based on scaling of available ATW reference plant and fuel facilities data [1]. The ATW system (Accelerator Transmutation of Waste) is selected as the reference plant in this work because the ATW and the ABR fuel cycles are similar. In particular, the fuel materials, and fuel separation processes of the two systems are

nearly identical, except for small differences in material mass fractions. Therefore the fuel cost parametric work of this paper is expected to encompass a range of reasonably estimated values. Furthermore, the use of ATW unit cost estimates as a base provides the means to maintain consistency between the ABR and ATW fuel cost estimates. Note that this paper covers only the fuel cycle cost of the ABR. The details of the analysis reported here can be found in Ref. [1].

2. BASIC PARAMETERS

2.1. Fuel

The function of the subject fuel is to burn actinides and long-lived fission products from spent LWR fuel. Thus the ABR should have a small conversion ratio to prevent production of higher transuranics. This requirement can be satisfied with fuels that have a matrix free of fertile isotopes such as U238 or Th 232 since these fertile isotopes create higher actinides by neutron capture reactions during reactor operation.

There are three fuel types available for this application:

- Metal fuels,
- Oxide fuels, and
- Nitride fuels.

Among these three types of fuel, metal fuels having a zirconium matrix can provide the largest reactivity excess because of the low absorption rate in the zirconium matrix and the hardest neutron spectrum due to the absence of strong moderating materials. The superior reactivity performance of metal fuel was demonstrated when the reactivity of oxide, nitride fuel with N^{15} and metal fuel with zirconium in fast neutron spectrum reactors was compared [14]. Therefore the metal type fuel with a zirconium matrix but in which fertile isotopes have been excluded is selected for the ABR to maximize the actinide burning rate and to minimize conversion from fertile isotopes. This type of fuel has the considerable advantage of being almost identical with that considered for the ATW program, the cost estimates of which are used in this work. In addition, it is similar to the metal fuel used in the IFR program and its associated reprocessing process.

TABLE 1. THE ABR FUEL COMPOSITION

Isotope	Weight percent
Zr	74%
Pu + MAs	26%
Pu composition	20.8% total
Pu238	2% of total plutonium
Pu239	58% of total plutonium
Pu240	26% of total plutonium
Pu241	10% of total plutonium
Pu242	4% of total plutonium
MA composition	5.2% total
Np237	43% of total MA
Am241	45% of total MA
Am242	0% of total MA
Am243	9% of total MA
Cm244	3% of total MA

The fuel of present interest has the form of a metallic alloy composed of zirconium matrix, plutonium and minor actinides. The composition of plutonium corresponds to that of LWR discharged spent fuel. The minor actinide composition also corresponds to that in LWR discharged spent fuel. The heavy metal (plutonium plus minor actinides) weight percentage has been varied from 20 to 30% in neutronic studies; the representative material composition of 26 weight percent of heavy metal and 74 weight percent of zirconium in Table 1 is selected for this economic study.

2.2. System

The ABR characteristics needed for fuel economic analysis are shown in Table 2. The fuel cycle is assumed to involve 2 batches and a 1.5 year refueling interval, resulting in 3 years in-core fuel residence time. Detailed system descriptions can be found in Refs [3, 8].

TABLE 2. ACTINIDE BURNER REACTOR CHARACTERISTICS FOR ECONOMIC ANALYSIS

Thermal power (MWth)	1 800
Electric power (MWe)	600
System thermodynamic efficiency (%)	33.3
Capacity factor (%)	80
Plant lifetime (years)	60
Fuel inventory (MTTRU)	5.742
No. of fuel batches	2
Refueling interval (years)	1.5
Fuel residence time in core (years)	3
Discharge burnup (MWD/MTHM)	275 000
Discharge burnup (MWD/MTFM)	71 400

HM = Heavy Metal (i.e., transuranics)
FM = Fuel Metal (HM+Zr)

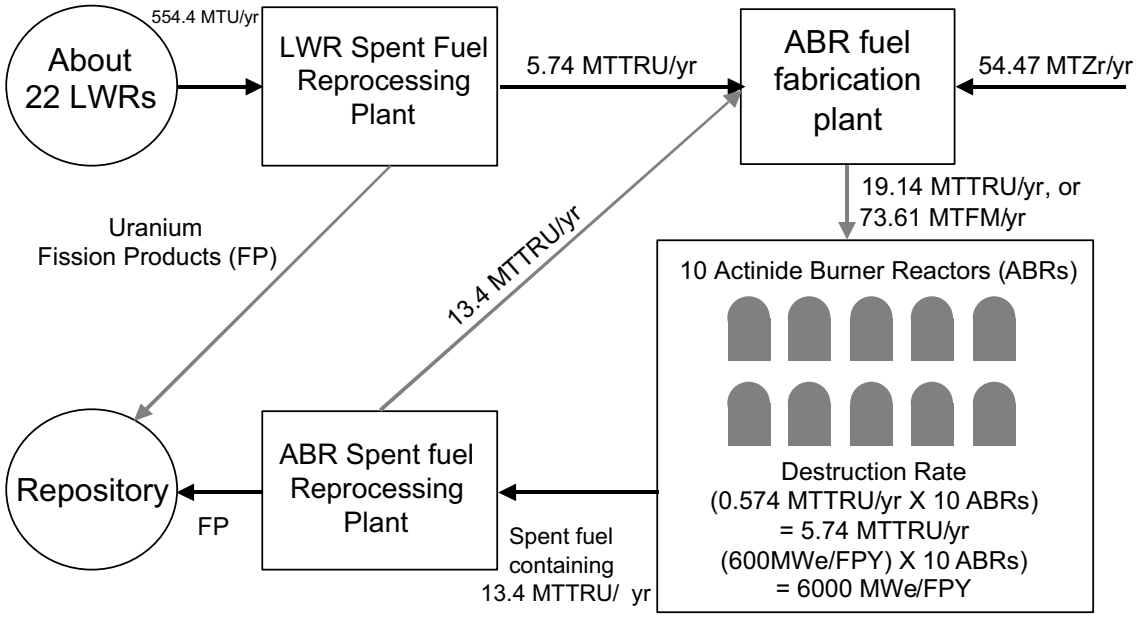

FIG. 1. Front-end of fuel cycle for one fuel processing facility. (serving 10 actinide burner reactors)

The mass balance for one fuel facility which can serve 10 typical Actinide Burner Reactors (ABRs) is shown in Fig. 1. This fuel facility will process about 554.4 MT/yr of uranium from LWR spent fuel; this means that a total of 33 264 MT of uranium will be processed during the entire system life time, 60 years. At steady state, this 554.4 MTU/yr corresponds to about 22 LWRs. The mass of discharged fuel from a PWR varies from 20~30 MTU/yr depending on core inventory, fraction refueled per cycle and cycle length. A discharged mass of 25 MTU/yr per LWR is chosen in this report. The LWR spent fuel processing plant has the functions of separating the fission products and actinides from the LWR spent fuel and of preparing the plutonium, minor actinide isotopes and some other isotopes for subsequent fabrication into actinide burner reactor fuel assemblies. A total of 5.74 MT/yr of transuranics will be extracted in the LWR spent fuel reprocessing plant for 10 ABRs.

The spent fuel from the ABRs will contain 13.4 MT of transuranics mixed with zirconium and fission products. These transuranics are extracted in the ABR spent fuel reprocessing plant and sent to the ABR fuel fabrication plant. The reprocessing plant has two functions; 1) separate the actinide isotopes removed from actinide burner reactor spent fuel, 2) mix these recycled actinides with new actinide materials from the LWR spent fuel reprocessing plant. The fuel fabrication plant will blend the 5.74 MTTRU/yr of plutonium plus minor actinides (TRU) from the LWR spent fuel reprocessing plant and 13.4 MTTRU/yr from the ABR reprocessing plant with zirconium, (54.47 MTZr/yr) to create one year's worth of fuel for 10 ABRs. This annually needed quantity of fuel contains 19.14 MT of TRU or 73.61 MT of fuel metal (TRU plus zirconium). The burning of 5.74 MTTRU/yr in 10 ABRs generates 18 000 MWth-yr per full power-year which corresponds to 6000 MWe-yr/FPY (system thermodynamic efficiency = 33.3%). However the annual electric power generation depends on the annual capacity factor which is assumed to be 80% in this study. Note that the initial ABR fuel load comes from the LWR spent fuel reprocessing plant alone.

2.3. Finance

Table 3 shows the key financial parameters employed in this fuel cost estimation. They are applicable to utility ownership. Any on-site fuel cycle facilities which are integral to the ABR are assumed to be utility owned and subject to utility financial assumptions. But if the fuel facilities were off-site, such as a central fuel cycle facility and any module factories, they could be assumed to be industry-owned and subject to typical industrial financial parameters. In this work, on-site fuel cycle facilities are assumed, therefore the financial parameters for utility ownership are used. These financial parameters for utility ownership are taken from the DOE NECDB (Nuclear Energy Cost Data Base) [4].

TABLE 3. KEY FINANCIAL PARAMETERS [4]

Parameter	Symbol	Value (utility owned)
Capitalization (%)		
Debt	b	50
Preferred stock	p	10
Common equity	c	40
Interest rate (%/yr)		
Debt	i_b	9.7
Preferred stock	i_p	9.0
Common equity	i_c	14.0
Average cost of money (%/yr)	d	11.35
Ratio of cost of debt/average cost of money		0.427
Inflation rate (%/yr)	i	5.0
Tax rate (%)	τ	36.63
Real (inflation adjusted) cost of money (%/yr)	d_0	6.05

The average cost of money (effective interest rate) can be computed by the following expression.

$$d = (i_b \times b) + (i_p \times p) + (i_c \times c) \quad (2\text{-}1)$$

where

b : bond fraction
i_b : bond interest rate
p : preferred stock fraction
i_p : preferred stock interest rate
c : common equity fraction
i_c : common equity interest rate

The real inflation adjusted cost of money can be computed from the average cost of money using the following expression.

$$d_0 = \frac{(1+d)}{(1+i)} - 1 \quad (2\text{-}2)$$

In this economic work, the following assumptions are used:

- Escalation during the design and construction period is occurring at the same rate as inflation, which means there is no real cost escalation during this period.
- The annual carrying charge rate (ϕ) from the financial parameters in Table 3 is used to obtain the annual capital cost of each fuel facility. The following expression gives the annual carrying charge rate value as 0.15/yr (assuming very long facility lifetime and no net salvage or decommissioning cost).

$$\phi = (b \times i_b) + (\frac{1-b}{1-\tau}) i_s \quad (2\text{-}3)$$

where

b : bond fraction
i_b : bond interest rate
i_s : equity interest rate
τ : tax rate

Note that ϕ is a current market rate including both the effect of inflation and taxes.

- It should be noted that the Tax Reform Act of 1986 no longer allows bond interest rate to be expensed (i.e., allowed as a tax deduction) during construction, but requires that it be fully capitalized. Thus the average and not the tax-adjusted cost of money must be used in calculating interest during the construction period [4].

3. FRONT AND BACK END COSTS

3.1. Front end unit cost

3.1.1. Zirconium purchase

Two zirconium price quotes (year 1999) were obtained for this study; 1) nuclear grade ingot type zirconium, \$12/lbm or \$26/kg from Wahchang, the US supplier, 2) sponge type

zirconium, $16/lbm or $35/kg from CEZUS, the French supplier. Therefore the zirconium price used in this fuel cost study is taken to be $30/kg.

3.1.2. LWR spent fuel reprocessing

The LWR spent fuel reprocessing plant processes the LWR spent fuel assemblies into a transuranic (TRU) stream for actinide burner fuel, a uranium stream for storage or disposal, a fission product stream for treatment or disposal and an irradiated metal waste stream for disposal. The reference costs for design, construction and operation for the LWR reprocessing plant are based on the ATW cost reports [1]. The base costs for the ABR are then estimated using the learning curve and production capacity scaling techniques. The LWR spent fuel reprocessing plant for the ABR in this study is assumed to have the same functions but a different processing capacity that is 554.4 MTU/yr. For the base case, it will be assumed that the cost of LWR processing per unit of heavy metal is the same for U and TRU. This is equivalent to charging only 1% of the fuel reprocessing cost to the TRUs, assuming that the cost is mostly associated with the either the disposal of U or its use by other reactors.

3.1.3. Spent fuel from ABR reprocessing plant

This reprocessing plant has the functions (1) of separating the TRUs from spent fuel discharged from the actinide burning system and mixing them with the fresh TRUs from the LWR reprocessing plant to make new actinide burner fuel and (2) of recycling technetium and iodine. This reprocessing plant is assumed to begin reprocessing irradiated actinide burning system fuel assemblies several years following startup of the first transmuter and to provide the recycled transuranics needed for subsequent transmuter core loading. Also this reprocessing plant will continue operation until some period after the last transmuter shutdown for reprocessing and recycling of spent fuel assemblies from the last transmuter.

3.1.4. Fuel fabrication plant

ATW's fuel fabrication plant has the function of preparing two kinds of fuel; 1) new ATW fuel assemblies fabricated from the transuranics removed from LWR spent fuel and ATW spent fuel, 2) target assemblies fabricated from technetium and iodine. At this stage of ABR system assessment, only the first of these functions is being addressed. Fission product transmutation in special, moderated radial blanket assemblies or in LWRs is reserved for future work.

3.1.5. Front end unit costs

The basic cost numbers shown in Table 4 are for the LWR reprocessing plant, spent fuel reprocessing plant costs and fuel fabrication plant costs in this study for their [1] stated capacity, without learning curve adjustments, but including a 25% contingency in both design and construction costs. The capacity and cost numbers for ATW come from the roadmap report [1]. The front end unit costs are estimated using the cost numbers scaled by the learning effect and by the production capacity effect and using the annual carrying charge rate (ϕ) as specified in Section 2.3 for both the ATW and ABR as in the following expressions. It is assumed that there will be no applicable design cost for the NOAK plant. Note that the cost per kg TRU is assumed to be the same as per kg total heavy metal in LWR reprocessing plant, which in effect assigns the largest part of the reprocessing cost to the recovered uranium and fission products. Thus the cost of TRU recovery used in what follows may be a low estimate.

LWR spent fuel reprocessing

$$\$/kgU = \frac{(Design \times \phi) + (Contruction \times \phi) + (O\ \&\ M)}{(Capacity)} \quad (3\text{-}1)$$

Spent fuel from ABR reprocessing plant

$$\$/kgTRU = \frac{(Design \times \phi) + (Contruction \times \phi) + (O\ \&\ M)}{(Capacity)} \quad (3\text{-}2)$$

Fuel fabrication plant

$$\$/kgFM = \frac{(Design \times \phi) + (Contruction \times \phi) + (O\ \&\ M)}{(Capacity)} \quad (3\text{-}3)$$

TABLE 4. ESTIMATED FUEL FACILITY COSTS FOR ATW AND ABR FUEL FACILITIES (CONSTANT 1999 $)

Reference plant	ATW*	ABR-1**	ABR-2***
LWR Fuel reprocessing			
Capacity (MTU/yr)	210	554.4	554.4
Design (M$)	73.7	131.96	
Construction (M$)	663.6	1188.14	1128.74
O&M (M$/yr)	56.25	100.71	100.71
ATW/ABR Fuel reprocessing			
Capacity (MTTRU/yr)	6.514	13.4	13.4
Design (M$)	64.2	98.97	
Construction (M$)	577.5	890.24	845.73
O&M (M$/yr)	27.6	42.55	42.55
ATW/ABR Fuel fabrication			
Capacity (MTFM/yr)	41.67	73.6	73.6
Design (M$)	36.3	51.07	
Construction (M$)	326.6	459.46	436.49
O&M (M$/yr)	80.7	113.53	113.53

* Ref. [12].
** First of a kind ABR.
*** The 2nd of a kind ABR, assuming construction cost reduction of about 5% due to experience.

Using the above expressions (3-1), (3-2), and (3-3) and the fuel facility costs of Table 4, the unit mass costs of the three front end fuel processing steps have been estimated. These unit costs turn out to be of very high value in comparison with LWR front end processing costs. Therefore a parametric variation of unit costs as a function of the number of ABRs served by one fuel facility is performed. Figure 2 shows the results of this parametric variation.

These costs are based on the second N-th Of A Kind (NOAK-2) plant and an annual carrying charge rate of 0.15/yr. The NOAK-2 plant costs, such as construction and O&M, are evaluated with a 95% learning effect for construction and using a production capacity scaling to the power 0.6. Note that the unit costs (i.e., costs per kg processed) in the most recent ATW system cost estimate report [12] are given as 30~50% lower than the ATW unit costs cited in Fig. 2. This is in part because calculations are based on a real (i.e., inflation free) discount rate of only 3% per year [12].

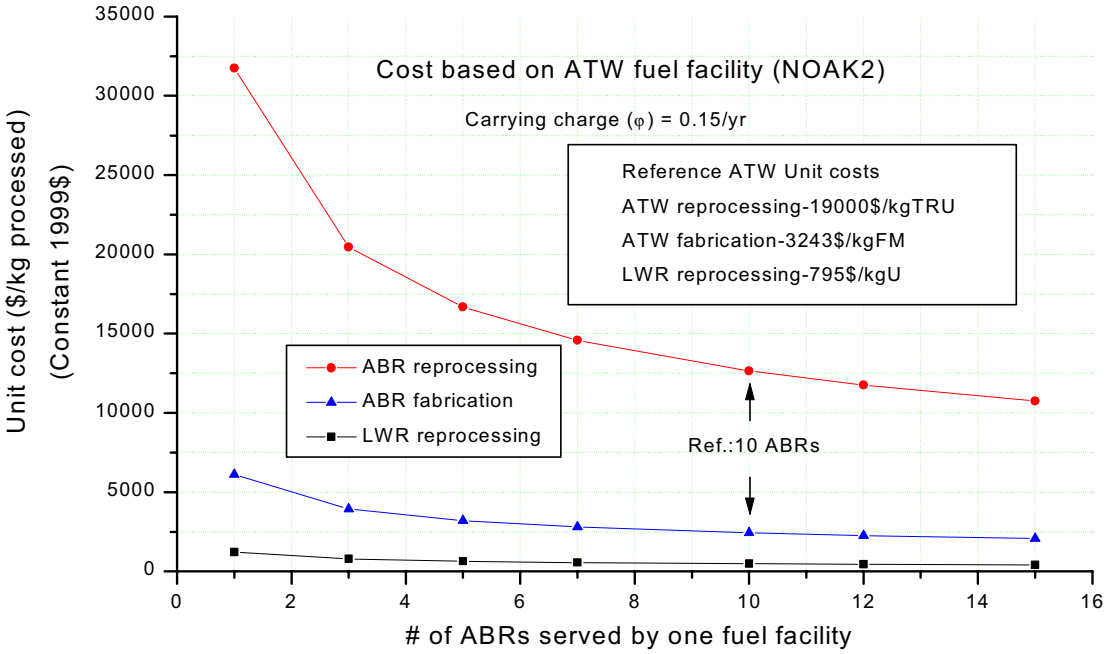

FIG. 2. Unit costs of ABR front end processing.

3.2. Back end cost

Long-term storage followed by direct disposal is considered in this study because there are discharged materials from both the reprocessing plants and the fuel fabrication plant. Given the lack of specific cost information, the back-end cost of this part of the fuel cycle is assumed to be the 1 Mill/kWhe, Federal Waste Disposal Fee. This assumption may be conservative if one considers the possibility of sending only a small fraction (say 1%) of the TRUs to the repository.

4. FUEL COST ESTIMATION AND SENSITIVITY ANALYSIS

4.1. Fuel cost estimation

Figure 3 shows the fuel cost estimation using the three models. The ORNL model and the FBR model, give very close fuel costs. However, the cost values from the Simple model are 0.5~1 Mill/kWhe lower than those of the other two models. Figure 3 shows the results in comparison to the current ATW fuel cost and a value quoted for the ALMR fuel cost [2, 9]. In comparison, current LWR one-through fuel costs are around 6 Mills/kWhe [11].

Costs in Fig. 3 are based on the Second Of A Kind fuel processing facility. Hence the fuel costs will be somewhat higher for the First Of A Kind fuel processing facility. The ATW fuel cost (18.5 Mills/kWhe) in Fig. 3 is the mean value of the three ATW fuel cost estimations by the three fuel cost models using the ATW information in Table 4. It is close to the results obtained earlier using a much simpler approach [5]. In that study the carrying charges were assumed to be 0.1, but more of the cost of LWR processing was assigned to the ATW cycle. The ALMR fuel cost (12.4 Mills/kWhe) in Fig. 3 is taken directly from Ref. [2]. This paper does not give detailed cost information, but only the final fuel cost. Thus, the basis for this calculation is likely to be somewhat different from the basis used in this ABR cost estimation. Furthermore, cost escalation to our reference year 1999 was not applied.

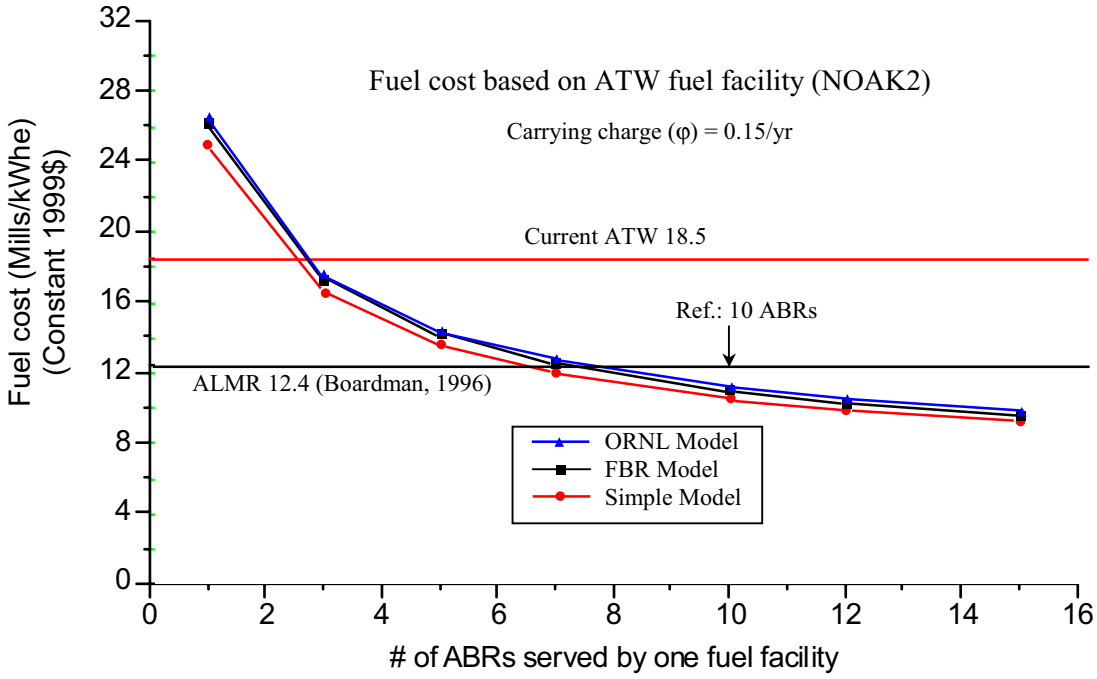

FIG. 3. Fuel costs for the ABR given by the three models applied in this study.

4.2. Sensitivity analysis

The purpose of this study is to estimate the fuel cost of an ABR and to identify the key factors affecting fuel cost. Hence a sensitivity analysis of the effect on fuel cost of key factors such as the unit cost of each major process in the fuel facility and the capacity factor (which implies changing the discharged fuel burnup) has been performed. It is assumed that the number of ABRs served by one fuel facility is 10, as noted in an earlier section

4.2.1. Unit costs

The four elements of unit cost which exist for the front end of the ABR fuel which are: zirconium purchase, LWR spent fuel reprocessing, spent fuel from ABR reprocessing and ABR fuel fabrication, have been addressed in previous sections. Among them, the zirconium purchase unit cost is excluded in this sensitivity study because there is no significant uncertainty in zirconium cost and the cost itself is very small in comparison with the other three front end process unit costs.

The range of unit cost variation for LWR spent fuel reprocessing and ABR spent fuel reprocessing is taken to be –15% to +15%. The variation of the unit cost of the ABR fuel fabrication process is taken as –15% to +30%, a higher upper bound because there is the possibility of high fuel fabrication unit cost due to the high melting point of zirconium. (The high melting point of our zirconium rich alloy may make it difficult to fabricate the fuel). The results of the parametric study are given in Figs 4 - 6.

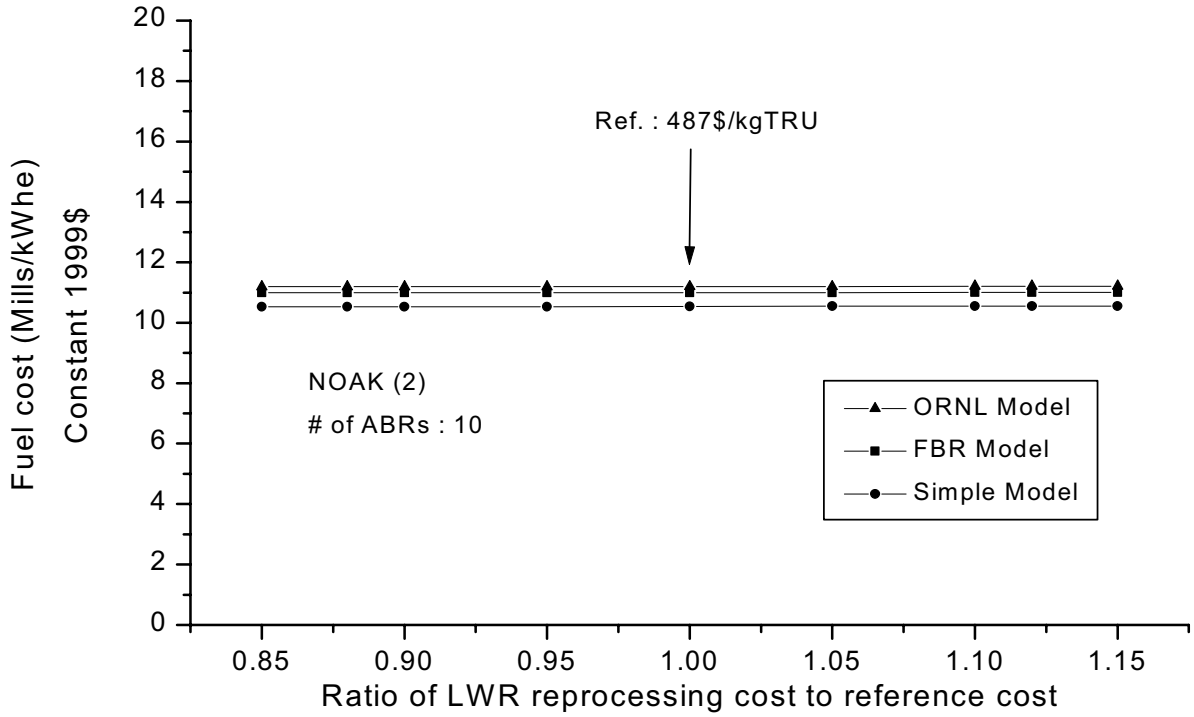

FIG. 4. Fuel cost vs. LWR reprocessing unit cost.

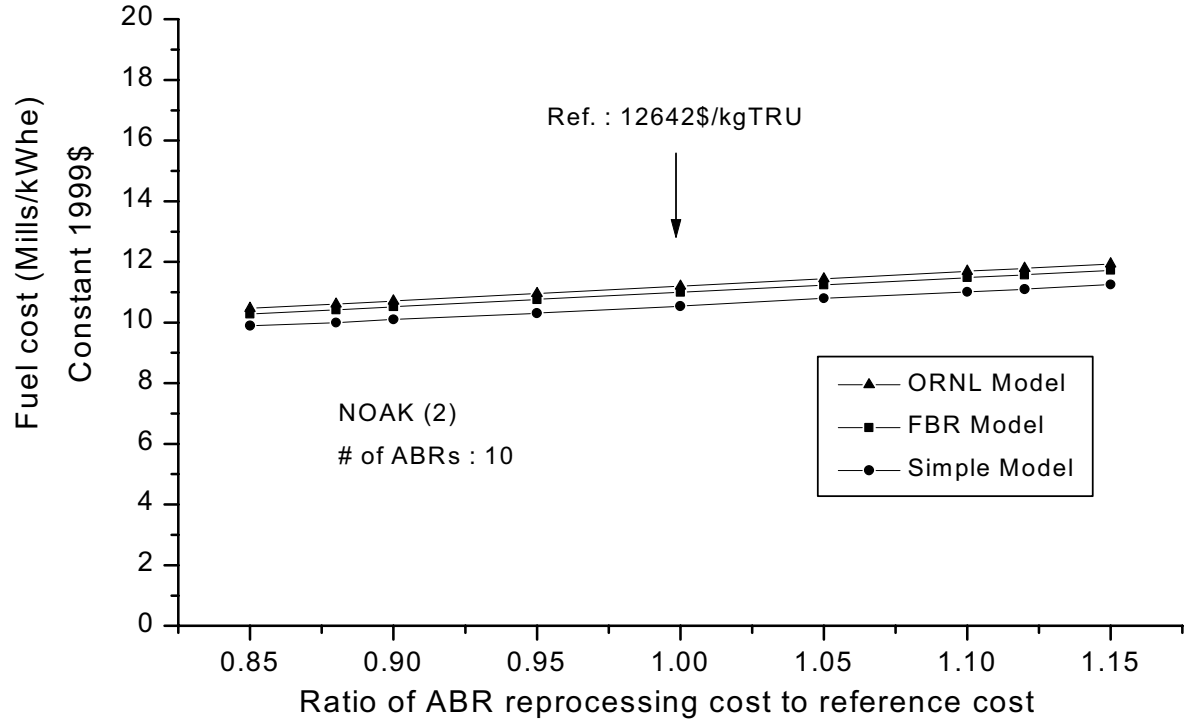

FIG. 5. Fuel cost vs. ABR reprocessing unit cost.

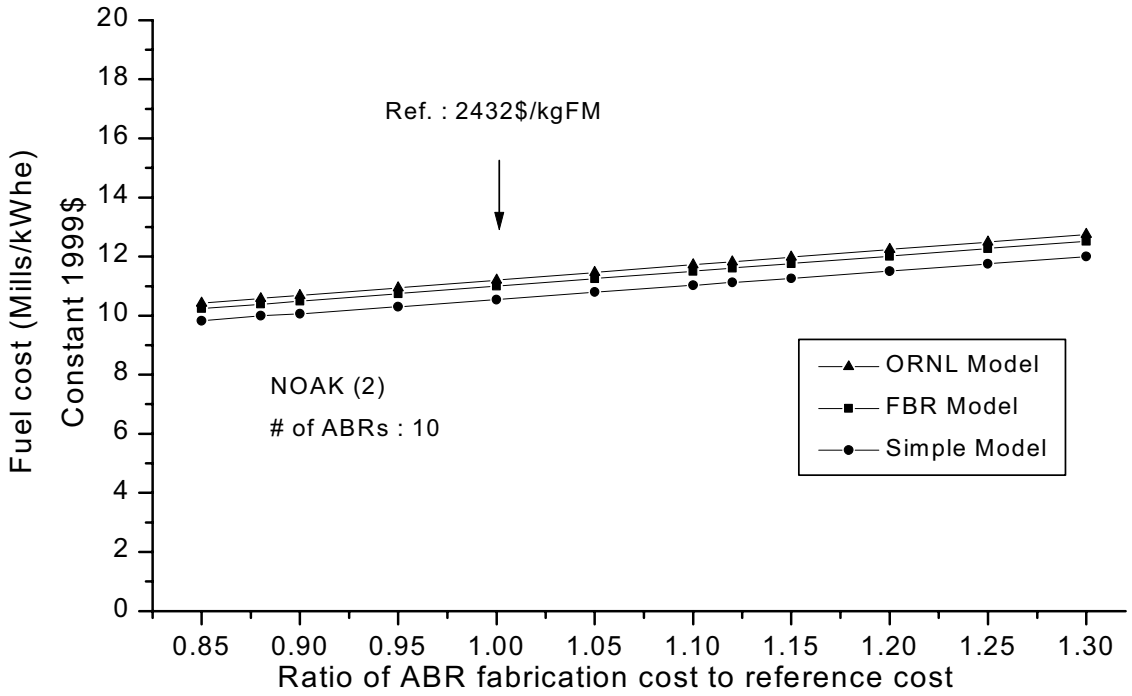

FIG. 6. Fuel cost vs. ABR fuel fabrication unit cost.

The LWR reprocessing unit cost has the least effect on fuel cost because of its smaller unit cost value. The sensitivity of fuel cost to the other two front end steps is nearly the same. The sensitivities to the ABR reprocessing unit cost and fuel fabrication unit cost are similar despite the large difference of total mass of material processed in these two steps. ABR reprocessing has the largest unit cost but has a much smaller mass throughput (TRU) processed than that of FM (TRU + zirconium) in the fuel fabrication step. Therefore the total cost in these two process steps has nearly the same effect on fuel cost.

As mentioned in Section 3.1, the LWR reprocessing unit cost per kg TRU is assumed to be the same as the cost per kg U processed. However this assumption is extremely optimistic and results in negligible sensitivity of fuel cost to LWR reprocessing unit cost, as seen in Fig. 4. Therefore a parametric study is performed with two more realistic LWR reprocessing unit cost cases: (1) assigns 50% of the reprocessing cost to the recovered uranium and fission products (i.e., 50% of the cost is assigned to TRU recovery cost) and (2) assigns 0% to the uranium and fission products (i.e., 100% of the cost is assigned to TRU recovery cost). The results are given in Figs 7 and 8.

The fuel cost variations for LWR reprocessing unit cost in Figs 7 and 8 are larger than those in Fig. 4. This is due to increasing the cost value of LWR fuel reprocessing. Nevertheless these fuel cost variations due to different LWR reprocessing cost options are of the same magnitude as those of the other two front-end components because the mass of processed material (TRU) in the LWR reprocessing is smaller than those of the other two front end components. Note that the LWR reprocessing unit cost per kg TRU is assumed to be the same as $/kgU processed through all this report, except these two cases above (i.e., 50% and 100% cases).

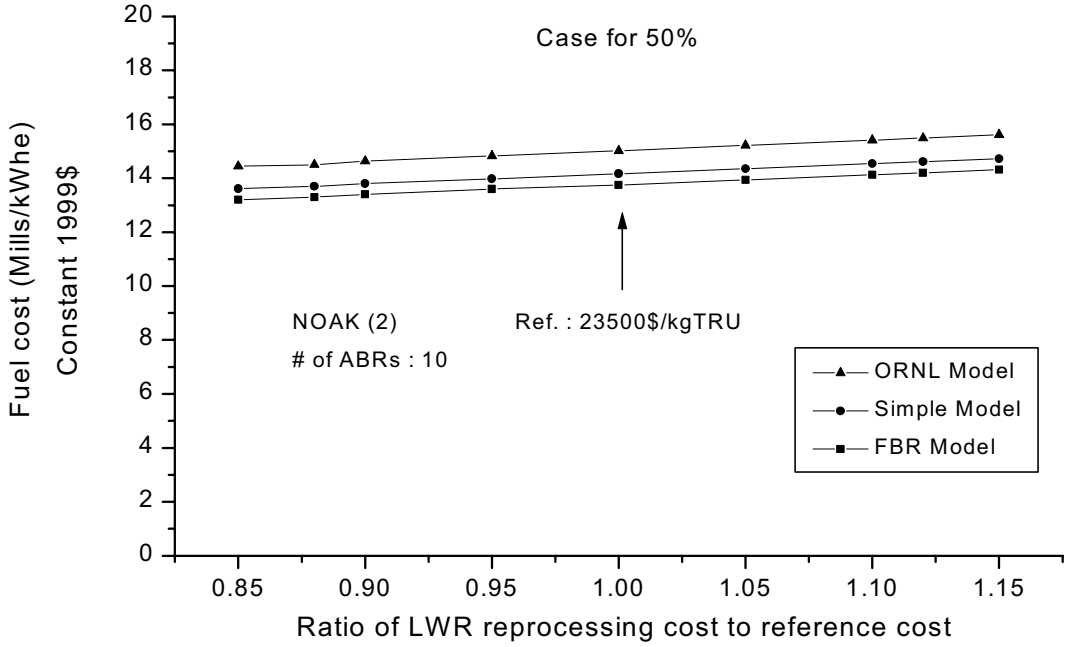

FIG. 7. Fuel cost vs. LWR reprocessing unit cost for 50% case.

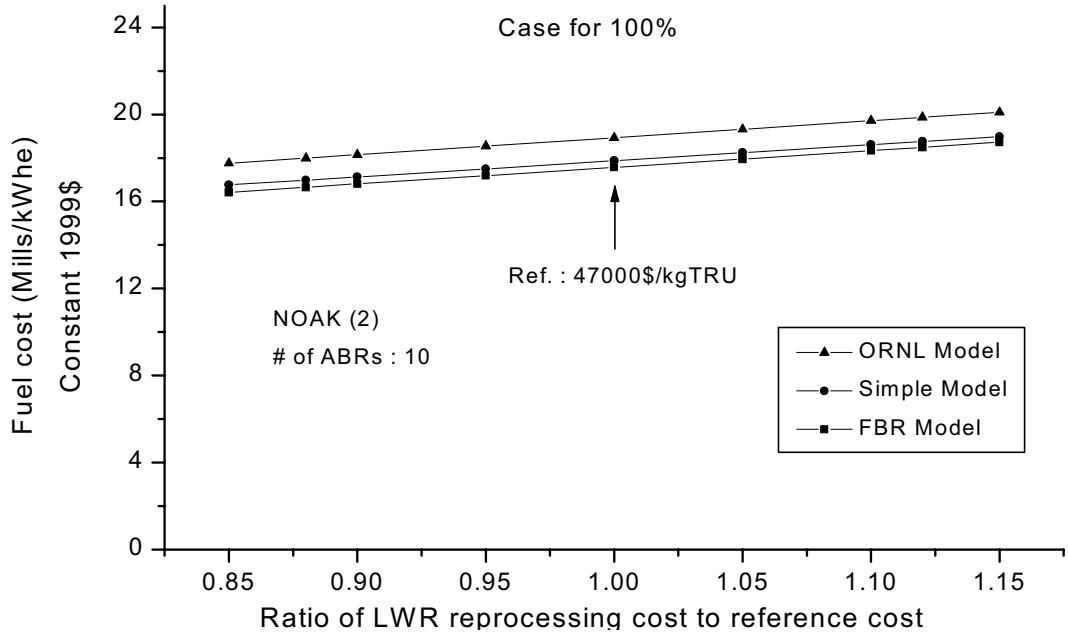

FIG. 8. Fuel cost vs. LWR reprocessing unit cost for 100% case.

4.2.2. Capacity factor

The capacity factor of the power plant and its associated fuel processing system are an important factor from the economic point of view. A higher capacity factor (i.e., higher burnup per pass) can give better economics, not just in the fuel cost but also in entire system cost. An 80% capacity factor (ABR) is assumed for the ABR (not the fuel facility) in this study. Since there is the possibility of increasing this capacity factor, a parametric study

varying capacity factor has been performed. The variation range is 70 to 95%. Fixed fuel core residence time and reload fuel enrichment (plutonium plus minor actinides) are assumed in this parametric study. Consequently discharged fuel will have different remaining transuranic quantities after irradiation in core, which would change the makeup of quantities of transuranics from the LWR spent fuel reprocessing plant. Thus the possibility of a change in the unit cost of LWR spent fuel reprocessing exists. However this possibility is neglected since the LWR reprocessing unit cost change effect is very small as seen in Fig. 4.

Figure 9 exhibits a variation of around 25% of the total fuel cost for a reasonable capacity factor range. According to the ALMR report [9], a capacity factor of 86% was used in the ALMR cost estimation. There is also the possibility of enhancing the capacity factor with development of advanced technology. Note that all results in this report except for the parametric study of capacity factor are based on an 80% ABR capacity factor. Therefore capacity factor enhancement together with increasing spent fuel burnup offer an effective possibility for reducing the fuel cost of ABRs. On the other hand, this potential is much less certain for the ATW, because of relatively high frequency of interruption of the proton beam in current high-power accelerators and because of the smaller availability of the tandem accelerator-reactor, i.e., the availability of the two systems working in series is the product of the availabilities of each individual system [6].

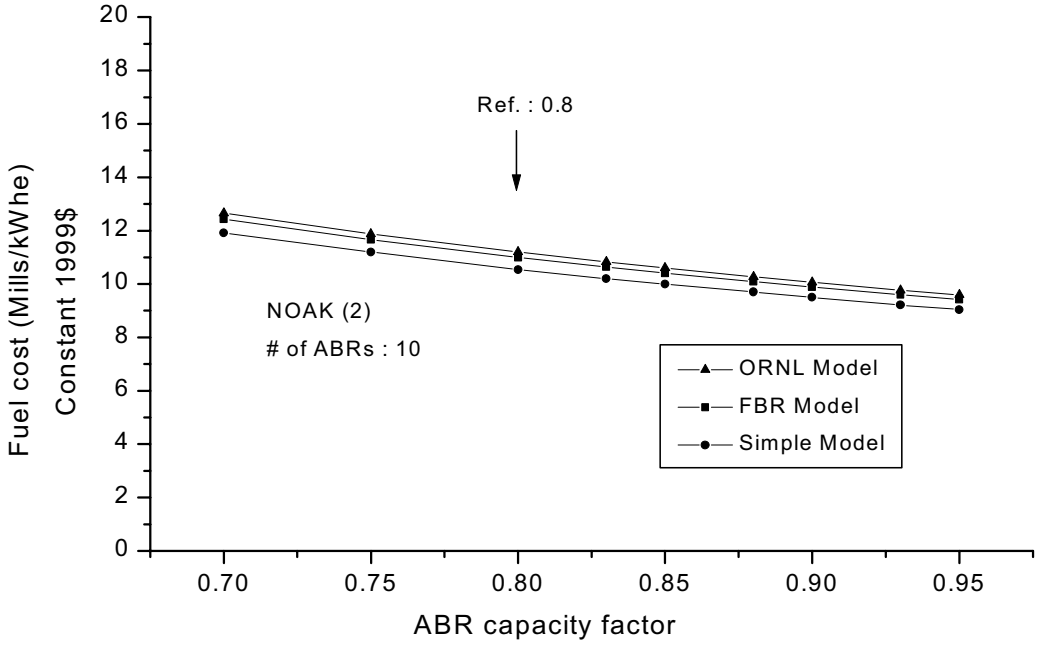

FIG. 9. Fuel cost vs. ABR capacity factor.

5. CONCLUSION

Fuel cost is an important factor in the cost of electricity generated by a nuclear power plant. In this study, the fuel costs for a actinide burner reactor were estimated using three models:

1. ORNL model,
2. FBR model, and
3. Simple model.

The fuel cost of the ABR is found to be considerably higher than the 6 Mills/kWhe characteristic of existing LWR nuclear power plants. Unless there can be reductions in other cost factors (for example, reactor capital cost or O&M cost) or in the fuel cycle itself, society may need to grant credits to the ABR to make its electricity generating costs comparable to alternative generation means. This study suggests several possible ways to reduce the fuel cost. For example, by enlarging the production capacity of the fuel facility. To handle 800 MTU/yr of LWR fuel, as in the existing French and UK facilities, which would serve 14 ABRs, and the other needed processes also had the capacity for serving 14 ABRs, the fuel cost could be cut from 11 Mills/kWhe to about 9.6 Mills/kWhe. Also, by increasing the discharge burnup of the fuel and/or increasing the capacity factor, the fuel cycle costs can be considerably reduced. To first order, if the burnup is raised by 10%, the fuel cycle cost will be decreased by 10%. Furthermore, it might be possible to design a simpler fuel recycle approach to minimize the costs.

REFERENCES

[1] ATW A Roadmap for Developing Accelerator Transmutation of Waste (ATW) Technology, DOE/RW-0519, US Department of Energy (1999).

[2] BOARDMAN, C.E., et al., Integrating ALWR and ALMR Fuel Cycles, Proc. Int. Conf. on Nuclear Engineering (ICONE-4), 1996, New Orleans, LA, American Society of Nuclear Engineers (ASME), New York, NY, USA (1996) 211-214.

[3] BUONGIORNO, J., TODREAS, N.E., KAZIMI, M., Thermal Design of Lead-Bismuth Cooled Reactor for Actinide Burning and Power Production, MIT-ANP-TR-066 (1999).

[4] DELENE, J.G., HUDSON II, C.R., Cost Estimate Guidelines for Advanced Nuclear Power Technologies, ORNL/TM-10071/R3 (1993).

[5] DRISCOLL, M.J. KIM, DOH YOUNG, The Need for Actinide Burner Reactor Fuel Cycle Cost Reduction, Trans. Am. Nucl. Soc., (2000).

[6] ERIKSSON, M., PIASZCZYK, C., Reliability Assessment of the LANSCE Accelerator System, paper presented in the NEA/OECD Workshop on Utilization and Reliability of High Power, 13-15 October 1998, Mito, Japan, NEA, ISBN: 92-64-17068-5.

[7] HANDWERK, C.S., DRISCOLL, M.J., TODREAS, N.E., McMAHON, M.V., Economic Analysis of Extended Operating Cycles in Existing LWRs, MIT-NFC-TR-007 (1998).

[8] HEJZLAR, P., DRISCOLL, M., KAZIMI, M., Void Reactivity Performance in Lead-Bismuth-Cooled Reactor for Actinide Transmutation, MIT-ANP-TR-068, (1999).

[9] HUTCHINS, B., PAVIENCO, G., BABKA, P., 1991 ALMR Power Plant Capital and Busbar Cost Estimates, GEFR-00900 (1991).

[10] KIM, D., KAZIMI, M.S., TODREAS, N.E., DRISCOLL, M.J., Economic Analysis of the Fuel Cycle of Actinide Burning Systems, MIT-NFC-TR-019, MIT Nuclear Engineering Dept., (2000).

[11] NEA, The Economics of the Nuclear Fuel Cycle, Nuclear Energy Agency (1994).

[12] SMITH, R.I., et. al., Estimated Cost of an ATW System, PNNL-13018 (1999).

[13] WALTAR, A.E., REYNOLDS, A.B., Fast Breeder Reactors, Pergamon Press (1981).

[14] SEKIMOTO, H., MIZUTANI, A., NEMOTO, A., Improvement of Fast Reactor Performance in the Future Nuclear Equilibrium State, Proc. 9th Int. Conf. on Emerging Nuclear Energy Systems (ICENES 98), 1998, Herzliya, Israel, Y. Ronen, L. Tepper, E. Elias (Eds.), Knassim Ltd., Tel Aviv, Israel (1998) 569-577.

FUEL AND FUEL CYCLE

(Session 3)

Chairperson

D. CRAWFORD

United States of America

CURRENT US PLANS FOR DEVELOPMENT OF FUELS FOR ACCELERATOR TRANSMUTATION OF WASTE

D.C. CRAWFORD, S.L. HAYES, M.K. MEYER
Argonne National Laboratory, Idaho Falls, Idaho, United States of America

Abstract

The United States is currently investigating the feasibility of proposed technologies for the Accelerator Transmutation of Waste (ATW) concept, which is funded as part of the U.S. Department of Energy's Advanced Accelerator Applications (AAA) Program. The ATW concept is proposed as a means to transmute transuranic isotopes and, perhaps, long-lived fission products removed from light water reactor spent fuel to shorter-lived fission products. To attain maximum possible transmutation rates, no fertile material (i.e., U-238 or Th-232) is to be incorporated into the fuel. Fuel forms currently proposed for ATW application include non-fertile dispersions of metal alloy or nitride fuel particles in a metal matrix, a non-fertile metal alloy, or non-fertile nitride pellets for a fast-spectrum, liquid metal-cooled transmuter, and non-fertile TRISO-coated particles dispersed in graphite compacts for a thermal-spectrum, gas-cooled transmuter. There is little or no experience with these non-fertile fuels, so an extensive fuel development program is envisioned. Current plans call for initial effort to demonstrate feasibility of the proposed fuel forms by the end of 2005, consistent with AAA program decision milestones. Feasibility research and development will consist of the following:

- Development of fabrication processes to demonstrate fabricability of the proposed fuel forms;
- Simple irradiation tests to screen samples of each fuel type for unexpected or poor performance; and
- Determination of intrinsic properties or characteristics (e.g., out-of pile interdiffusion behavior of fuel and constituents and thermophysical properties).

If the decision is made to continue development of the ATW concept beyond 2005, then of the successful candidate forms, one or two will be selected for further development, with more extensive irradiation testing and fuel property characterization.

1. INTRODUCTION

The Accelerator Transmutation of Waste (ATW) concept has been proposed as a means to reduce or eliminate transuranic elements from commercial high-level nuclear waste in the U.S. As envisioned, the concept consists of a transmuter in which transmutation by fission (or by neutron capture in long-lived fission products, or LLFPs) is accomplished in a neutron flux, provided by an accelerator-driven neutron source and multiplied through a subcritical blanket containing actinides [1].

The transmuter is designed as a spallation neutron source-driven, subcritical blanket, with an environment similar to those of nuclear reactor cores. Therefore, much of the transmuter design would be based on technology already developed for nuclear reactors, including design of heat-exchange systems, configuration of transuranic-bearing blanket fuel into coolant channels, and design of blanket fuel rods, target rods and assemblies. Although the candidate technology options for an ATW system are based on reasonably-mature reactor technologies, the stated features of the system require fuel types with which there is little or no experience. Specifically, the ATW concept calls for use of non-fertile (i.e., non-uranium-bearing) fuels to allow the system to achieve maximum transuranic destruction rates. Because much of the development of reactor fuel over the past several decades was motivated by the desire for sustainable energy generation, the great majority of relevant fuel experience is with uranium-bearing fuel. The proposed transmutation system thus requires that a new and unproven fuel be developed, characterized, and qualified. This paper summarizes the current U.S. R&D plans to develop blanket fuel for an ATW transmuter, with emphasis on establishing by the end of fiscal year 2005 the feasibility of the fuel forms considered.[*] The approach reported here is described more fully in a yet-unpublished document entitled

[*] Although technologies proposed for consideration for an ATW concept include liquid-fueled concepts as well as solid-fueled concepts, at the time of this writing, solid fuel technology options are considered more viable.

"Accelerator Transmutation of Waste: Fuel and LLFP Target Development Plan for FY'01 through FY'05". Upon successful completion of the described activities, sufficient information will have been obtained to support decisions regarding the feasibility of proposed ATW fuel technologies. Although a parallel development of several fuel types is underway, down-selection to a reference and an alternative fuel type will be necessary upon completion of the feasibility R&D phase, if not sooner.

2. TRANSMUTER REQUIREMENTS FOR FUEL

2.1. General fuel requirements

Specific requirements for blanket fuel performance will be derived from the requirements for ATW system performance, such as actinide destruction rates, safety requirements, and fuel processing. However, some general fuel requirements can now be identified and are listed as follows:

- ATW fuel must be fabricable using remote processes. The majority of the head-end processes being considered to prepare LWR spent fuel for transmutation and the processes being considered for recycle of transuranics back into the transmuter would leave residual fission products in the blanket fuel feed. Therefore, fuel fabrication will likely be conducted in a hot cell environment, demanding that fabrication processes be amenable to remotization.
- ATW fuel must be compatible with the fuel recycle process. If transuranics are to be recycled back into the ATW transmuter, then some type of chemical or mechanical processing of the irradiated blanket fuel will be required.
- The blanket fuel must maintain the fissile material in a predictable configuration and location in the transmuter.
- The blanket fuel must provide robust containment for fission products and radionuclides, as a first barrier for safety, during normal operations; i.e., cladding failure with leakage of fission products must be a low-probability event.
- The blanket fuel must retain a coolable geometry during normal operations and all design basis accidents.

2.2. Emerging specific requirements

Two primary types of transmuters have been proposed for ATW application [1]. One type of system is a fast-spectrum system, cooled by either sodium or a eutectic composition of lead-bismuth alloy. Two proposed fast-spectrum systems are loosely based on the U.S. concept for the sodium-cooled Advanced Liquid Metal Reactor (ALMR), developed by General Electric using Integral Fast Reactor technology [2, 3], and the Russian lead-cooled BREST reactor system [4]. Another proposed fast spectrum-system would be cooled by helium and would be similar to the Gas Cooled Fast Reactor concept (e.g., [5]).

Furthermore, technical issues requiring resolution for solid and for liquid fuels are quite different in nature, and therefore necessitate separate treatment. Therefore, efforts to address liquid fuel R&D have been deferred until an appropriate time.

The second type of system is a gas-cooled, thermal-spectrum system proposed by General Atomics (GA) in the U.S.

Although these system types are not described here, requirements for fuel for some of the transmuter concepts are listed in Table 1. Many of the requirements are tentative, based on assumptions used for calculations to support the evaluation of system point designs. Such requirements are likely to change or evolve as limits to fuel characteristics (e.g., fissile loading) or performance (e.g., operating temperature or burnup) are determined or as the tramsmuter concepts evolve.

TABLE 1. EMERGING REQUIREMENTS OR DESIRED CAPABILITIES OF PROPOSED ATW TRANSMUTER CONCEPTS

Sodium-cooled transmuter fuel requirements [6]	
Burnup potential:	> 30% desired
Linear heat generation rate:	400 W/cm, possibly up to 500 W/cm
Fuel TRU density:	3.2 to 4.2 g/cm^3 in fuel slug as described
	2.7 to 3.5 g Pu/cm^3 inside cladding I.D. of 0.632 cm
	2.0 to 2.5 g/cm^3 within fuel pin of O.D. 0.744 cm
Lead-bismuth-cooled transmuter fuel requirements [7]	
Burnup potential:	> 30% desired
Linear heat generation rate:	300 W/cm
Fuel TRU density:	3.2 to 4.6 g/cm^3 in fuel slug as described
	2.7 to 3.9 g Pu/cm^3 inside cladding I.D. of 0.440 cm
	1.5 to 2.2 g/cm^3 within fuel pin of O.D. 0.580 cm
Gas-cooled, thermal-spectrum transmuter fuel requirements [8]	
Achieve very high burnup of the initial loading of plutonium and minor actinides.	
Maintain fuel particle integrity throughout the fuel cycle and into disposal, if possible, avoiding the need for intermediate reprocessing.	
Maintain high operating temperatures needed to achieve a high net thermal efficiency.	

3. SELECTION OF CANDIDATE FUEL FORMS

Development of new, non-fertile fuel forms is best initiated with consideration of non-fertile analogues to more-familiar uranium-bearing fuel forms. A varied experience base exists with several chemical and physical forms, which are listed in Table 2. Considerable effort will be required to establish feasibility by 2005 for any of the potential fuel types. Technical judgement and experience provide the basis for limiting the fuel candidates to those that appear most attractive and are most likely to be successful.

TABLE 2. PREVIOUSLY-INVESTIGATED CHEMICAL AND PHYSICAL FUEL FORMS

Chemical forms	Familiar examples
Metallic (usually alloy)	U-Fs, U-Zr, U-Pu-Zr
Oxide	UO_2, $(U,Pu)O_2$
Nitride	UN, (U,Pu)N
Carbide	UC, (U,Pu)C
Intermetallic compound	UAlx, Uranium silicides
Physical forms	**Familiar examples**
Monolithic	
Metal alloy slug	Na-bonded U-Zr for EBR-II
Pressed pellets	UO_2 for LWRs
Particulate	- Vipac - Sphere-pac
Dispersion (with metal or ceramic matrix, with metallic or compound fuel dispersant)	- UAl_x in AL matrix for research reactors - Coated UO_2 particles in graphite compacts used for gas-cooled reactors

The advantages and disadvantages of each of the fuel option is not addressed here; however, some rationale for selection of candidate fuel forms for development is provided. Some of the available fuel options were chosen as candidates based on programmatic considerations. For example, oxide fuel, including oxide fuel particles in a dispersion fuel, is not a candidate fuel form because of considerations related to chemical processing. (Pyroprocessing techniques – though feasible – are more complicated for oxide fuel than for other fuel types). Aqueous recycle processes that are currently established for oxide fuel are considered undesirable for ATW due to proliferation concerns. Carbide and nitride fuels are equally attractive in terms of properties. Although a more extensive database exists for carbide fuels than for nitride fuels, of the two, only nitride fuels are considered for ATW due to compatibility with the pyroprocess and due to interest in nitrides in Japan, Europe, and Russia. Particulate fuel types, such as vi-pac, are not considered because it is unlikely that the cost associated with development of a fuel type with which the U.S. has little experience could be supported by the ATW budget. The selected fuel forms are described in the following subsections, which include a description of current fuel element design and issues to be addressed by R&D.

3.1. Metallic and ceramic dispersions

A dispersion of TRU-Zr alloy fuel particles in a zirconium matrix has been proposed for application to a liquid metal-cooled transmuter. The TRU-Zr alloy is proposed based on experience with alloy fuel from the Integral Fast Reactor (IFR) program. Zirconium was selected as the alloying element because of the fabrication, reprocessing, and irradiation experience obtained with U-Zr and U-Pu-Zr fuel during the IFR program. Zirconium is the component of the U-Pu-Zr fuel alloy that raises the alloy solidus temperature and provides resistance against fuel-cladding chemical interaction [9] and dimensional stability during irradiation [10]. Cubic phases are stable in the Pu-Zr system at reactor temperatures for compositions of interest for ATW fuel. Although the behaviour of multi-element alloys is not known, TRU-Zr alloys may also form alloys with cubic crystal structures that are likely to be more stable against growth under irradiation.

If successful, this fuel form would combine the performance advantages of a dispersion fuel (including high-burnup potential, low fuel temperature, and retention of fission gas) with a low temperature fabrication route that will minimize the amount of volatile actinide loss

during fabrication. Using metallic fuel particles in a metal matrix will also impart favorable neutronic safety characteristics to the fuel that are typical of metal fuel. These include high thermal expansion, which provides substantial negative reactivity feedback as fuel temperatures rise during transient events, and low heat capacity, which reduces the amount of stored energy in the core that must be dissipated in the event of a loss-of-flow accident. A metallic dispersion is expected to be compatible with pyrometallurgical processing concepts now being considered for recycle of ATW blanket fuel.

To minimize the potential for fuel-cladding chemical interaction, it is proposed that the compacted fuel "meat" (i.e., the Zr-matrix rod bearing the fuel particles) be placed inside of an enclosing Zr sheath. The Zr-enclosed fuel slug would then be co-extruded inside an enclosing cladding tube, which would ensure good thermal contact between the fuel slug and cladding. The fuel slug could be either a rod or a shorter "pellet." If irradiation testing indicates that the Zr-matrix fuel swells sufficiently to stress the co-extruded cladding, then a radial gap inside the cladding can be incorporated as a backup option. The Zr-enclosed fuel slug would then be bonded to the cladding using a liquid-metal bonding alloy similar to that used for the metal alloy fuel. The fuel would be clad in a ferritic-martensitic stainless steel, and the fuel rods would be loaded in hexagonal-shaped subassemblies similar to those used in Experiment Breeder Reactor-II and the Fast Flux Test Facility.

A (TRU)N (i.e., nitrides of TRU elements) fuel particle in a Zr matrix is proposed as an alternative to the metallic dispersion. This nitride offers a higher fuel-particle margin to melting combined with the thermal and neutronic advantages of the metal matrix. Nitride compounds are currently being investigated as fuels by researchers in Japan, Europe and Russia (including some work with non-fertile nitrides). Additional complexity associated with fabricating a nitride dispersion might be balanced against the advantages of mitigating problems of americium volatility (americium nitride is less volatile than americium metal).

Alternative matrix metals will be considered as required to provide chemical stability with the fuel phase, with an emphasis on identifying candidates based on compatibility with ATW recycle processes, acceptable irradiation performance characteristics, fabricability, high temperature strength, and compatibility with potential coolants. Another design variant that could be considered is a coating on the fuel particle, which may enhance the ability of the fuel particle to retain fission products and reduce interdiffusion of fuel constituents and matrix constituents. Fabrication of other design characteristics will also be considered, including means for placing a barrier the fuel slug and cladding.

A number of issues must be investigated to establish feasibility for this fuel type:

- What is the optimum particle loading that balances competing requirements for fabricability and low fuel swelling against the desire for a relatively high fissile density?
- Which fuel alloy composition best balances fissile density with fuel performance?
- Will fuel co-extruded with cladding (with no fuel-cladding gap) perform acceptably, or must a radial gap be incorporated into the design?
- If co-extruded cladding is used, will unacceptable stresses be induced in the cladding due to thermal expansion of the fuel upon startup and shutdown or accelerator transients?
- If a gap is required, what is a suitable bond metal?
- Can the fuel slugs be fabricated as long rods, or must shorter pellets be used?
- Can the fuel be fabricated using remotely-adaptable methods?
- Can the fuel be fabricated with sufficient fissile density to satisfy transmuter performance requirements or goals?

- Do the fuel particles remain intact during the irradiation, or do fuel constituents interdiffuse with the matrix?
- Is a matrix material other than Zr required?
- Does the fuel retain integrity and dimensions during irradiation?
- Do metal fuel particles melt during overpower transients, and what are the consequences?
- What is the behavior of high-burnup ceramic fuel particles during overpower transients?
- Will a Zr matrix dissolve at unacceptable rates upon contact with lead-bismuth coolant (e.g., during failed-fuel operation)?
- Is a barrier between the fuel "meat" and cladding required to limit fuel-cladding chemical interaction?
- Must fuel particles be coated to achieve desired performance?
- Can alternative matrix metals that are more compatible with lead-bismuth be identified?

3.2. Metal alloy

A TRU-Zr alloy fuel has been proposed as an alternative, based on experience with metal alloy fuel during the Integral Fast Reactor (IFR) program. This fuel form would consist of a slug of TRU-Zr alloy similar to the metallic fuel alloy envisioned for use in the dispersion fuel option, but with a higher Zr content.

The fuel rod design proposed is the same as that employed most recently for the IFR concept. A fuel smear density of 75% and a plenum-to-fuel volume ratio of 1.4 are proposed to accommodate radial swelling and fission gas release, respectively. Experience with metal fuel performance has demonstrated that accommodation of radial swelling and fission gas release from the fuel into the fuel-cladding plenum enables relatively high-burnup. The fuel would be clad in a ferritic-martensitic stainless steel, and fuel rods would be loaded in hexagonal-shaped subassemblies similar to those used in Experiment Breeder Reactor-II and the Fast Flux Test Facility.

Use of a liquid metal bond (selected to be compatible with fuel, cladding and coolant) would be required to ensure adequate heat transfer from the fuel to the cladding, in a manner similar to the Na bond used for previous fast reactor metal fuel designs. For the Na-cooled transmuter, Na would be used as the bond metal. It is not clear that Na is suitable as a bond metal for the lead-bismuth transmuter; interactions between Na and both lead and bismuth must be investigated to understand implications for failed-fuel operation.

Assessment of feasibility for this fuel will require investigation of the following:

- Can the fuel be fabricated without unacceptable loss of volatile transuranics?
- Are volatile actinide recovery techniques necessary and feasible?
- Is irradiation performance of TRU-Zr alloy fuel similar to that of U-Pu-Zr?
- What constituents diffuse to the fuel-cladding interface and is fuel-cladding chemical interdiffusion of consequence?
- Can fuel-cladding chemical interaction be mitigated?
- What is the dissolution behavior of TRU-Zr alloy in lead-bismuth, and what are the implications for failed fuel operation?
- Can a bond metal for the fuel-cladding gap be identified which will be compatible with fuel, cladding and lead-bismuth coolant.
- Can alloying elements be identified as potential alternatives to Zr?

3.3. Nitride

A non-fertile nitride fuel is proposed for application in fast-spectrum, liquid metal-cooled or gas-cooled transmuters based on prior experience with uranium nitride and mixed nitride fuels. Although, for the present time, a diluent in the fuel is assumed necessary, it is not clear which element(s) would be best suited for that purpose. (TRU,Zr)N is proposed initially, because Zr is compatible with the pyroprocess and would have small impact on neutron economy. An initial investigation of the Pu-Zr-N system indicates that PuN and ZrN are soluble, so that fabrication of an acceptable fuel mixture appears feasible. Although there is no irradiation performance experience with this fuel, non-fertile nitrides are being considered for actinide destruction in R&D programs in Japan and Europe. Therefore, international collaboration will be important for consideration of this fuel form.

The fuel rod designs proposed are those studied for (U,Pu)N fuels previously developed and tested in the U.S. Those designs consisted of pellets stacked and loaded into cladding tubes with either a gas or Na bond; gas-bonded and Na-bonded designs were each determined to perform acceptably. For ATW application, it is believed that a lead-bismuth bond could be used for a lead-bismuth-cooled transmuter, because Russian work indicates that (U,Pu)N is compatible with a lead-bismuth bond. A liquid metal bond provides for lower fuel operating temperatures, which was helpful to reduce fuel fracturing for (U,Pu)N. As stated for the other fast-spectrum fuel candidates, fuel rods would be loaded into hexagonal subassemblies in a manner consistent with U.S. fast reactor experience.

Neutron irradiation of the N-14 isotope leads to formation of C-14 through the $N^{14}(n,p)C^{14}$ reaction. For the purposes of this document, it will be assumed that enrichment of N-15 in the nitrogen will be employed for fabrication of the (TRU,Zr)N fuel. Therefore, N-15 collection and recycle techniques must be developed.

Assessment of feasibility for this fuel will require investigation of the following:

- Can (TRU,Zr)N be easily fabricated as a solid solution in the desired composition using feed material from the ATW recycle process?
- Will (TRU,Zr)N retain fission gas and resist cracking at moderate temperatures in a manner similar to that of (U,Pu)N?
- How do TRU nitrides behave in the fuel matrix while under irradiation?
- How severely do nitride fuels fragment during overpower transients, and is the fragmentation of any consequence?
- Do any issues emerge for failed fuel operation (e.g., due to interaction of (TRU,Zr)N with lead-bismuth)?
- Is a gas bond or liquid metal bond preferable?
- Is N-15 enrichment required to avoid C-14 generation issues?

3.4. TRISO-coated particles

Recently proposed concepts for thermal-spectrum, gas-cooled systems (critical or subcritical) call for the use of TRISO-coated oxides of uranium and/or plutonium. “TRISO” is an acronym that designates the coating configuration around the central fuel particle. Specifically, the fuel kernel is surrounded by a lower-density, pyrolytic carbon “buffer layer”, then a dense pyrolytic carbon layer and a silicon carbide layer, with an pyrolytic carbon layer. The coated fuel kernels are dispersed in graphite compacts, which are placed in arrays in graphite blocks, referred to as fuel elements. These fuels appear capable of sustaining very high burnup values, but experience has demonstrated that proper fuel design and fabrication

quality are essential for good irradiation performance. Some work performed by General Atomics and ORNL in the early 1970s indicates that TRISO-coated PuO_2 fuel kernels can achieve burnup values as high as 75at.% [11].

Experience with the New Production Reactor (NPR) program conducted in the U.S. during the late 1980's and 1990's indicates that uranium oxycarbide fuel kernels performed better than UO_2 fuel kernels. Furthermore, considering that oxygen stoichiometry was determined to be an important parameter for achieving high-burnup performance of PuO_2 kernels, the multiple valences of TRU oxides might have some effect on the fabrication or performance of those fuel kernels. Use of oxycarbide fuel kernels would eliminate the variance of oxidation states for the TRU elements, perhaps simplifying fabrication or aiding fuel performance. Therefore, it is proposed that TRU oxycarbide [(TRU)OC] be considered as a fuel kernel option for thermal-spectrum gas-cooled transmuter fuel in addition to TRU oxide $(TRU_x)O_y$. Programs in the U.S., Russia, South Africa and France are currently considering gas-cooled reactor systems and/or accelerator-driven systems for a variety of applications; therefore, potential exists for effective international collaboration in developing this fuel form.

Current proposals from General Atomics, an industrial developer and designer of thermal gas-cooled reactors, call for using SiC layers in the TRISO coatings. However, recent work with ZrC coatings in Japan indicates that the ZrC coatings may have better resistance to failure and to palladium corrosion than the SiC coatings. Therefore, ZrC will be considered as an alternative to SiC as a pressure-restraining coating.

Fabrication and irradiation performance for this fuel type must be demonstrated, using bench-top scale samples, to establish feasibility. There is no known experience with TRU oxycarbide TRISO-coated fuel, so fabrication techniques must be developed and irradiation performance investigated. Some specific feasibility issues include:

- Can transuranic fuel particles be synthesized and coated with acceptable loss (or no loss) of volatile actinides?
- Is either $(TRU_x)O_y$ or TRU(OC) a superior fuel kernel material?
- Do the multiple oxide valences of TRU elements effect fabrication or performance of $(TRU_x)O_y$ fuel kernels?
- Will TRISO-coated TRU fuel perform with acceptable failure rates?
- Is SiC the best pressure-bearing coating, or is ZrC better?
- Can the bonding strength between coating layers and the layer thickness be optimized for better high-burnup performance?
- What is the overpower transient response of high-burnup TRISO-coated particles?
- Is post-failure behavior of TRISO-coated TRU fuel acceptable?

4. R&D DESCRIPTION

The R&D described in this plan is intended to determine feasibility of the proposed fuel concepts in support of ATW technology decisions. General feasibility issues are best categorized into four areas of R&D:

- Fabrication;
- Property measurement and out-of-pile experiments;
- Irradiation performance;
- Modeling of behavior and phenomena.

4.1. Fabrication development

Fabrication development activities will address the two primary needs of the ATW program. These are:

1) fabrication of specimens suitable for screening irradiation tests in the ATR and for fast flux irradiation testing, and
2) identification and development of fabrication processes that can be successfully deployed for large scale ATW fuel manufacturing.

Initially, small representative fuel specimens will be fabricated for use in ATR irradiation testing. Fabrication techniques employed to make these specimens may be chosen for expedience rather than being representative of a large-scale fabrication process, facilitating an aggressive irradiation testing schedule. Experience gained during fabrication of small specimens will be applied to production of more prototypic fuel rods for fast flux irradiation testing and to the conceptual design of a large-scale fabrication process.

An important consideration for all fuel types is volatilization of americium, leading to loss or redistribution during fabrication. It is partially for this reason that dispersion fuels were chosen as a candidate fuel form. Dispersion fuels are fabricated using powder metallurgical processes that are well developed and currently used for the production of research reactor fuel elements. Powder metallurgical processes allow for lower fabrication temperatures than melt processing, providing an opportunity to reduce americium volatilization during fabrication. These same techniques could also be applied to the production of monolithic metal fuel. The advantages of powder processing come at the expense of the need to remotely handle powder. This issue is of equal or greater concern for a nitride pellet fuel.

Fuel particles required for a dispersion can be fabricated by any number of methods. However, the metal feed from the reference electrorefining process fits well with both hydride-dehydride (-nitride) and mechanical powder production techniques. The ability to perform the hydride-dehydride process may depend on the purity of actinide metal feed. Thermo-mechanical consolidation of fuel meat compacts into clad, rod-shaped dispersion fuels by swaging, drawing, and extrusion will be evaluated. Methods to characterize the integrity of the core to clad bond will be developed.

At present, little is known about non-fertile nitride fuels. The R&D program for this fuel type will include fabrication of (TRU,Zr)N pellets and characterization of their microstructures, as well as preparation of specimens for irradiation testing. Both hydride/dehydride/nitride and carbothermic reduction processes are possible routes to production of nitride fuel powder. The inert element might be incorporated in an alloy or oxide precursor, or by solid state reaction of nitride powders to produce either homogeneous or heterogeneous fuel microstructures. Powder will likely be sintered using conventional techniques to produce pellets appropriate for irradiation testing.

4.2. Property measurements and out-of-pile experiments

Given that the non-fertile compositions proposed for use as an ATW blanket fuel have only recently begun to be seriously considered as nuclear fuels, little to no experimental data exist on the thermophysical properties of most of these materials. During the first phase of the ATW program undertaken to demonstrate the feasibility of the proposed fuel forms, an experimental program has been initiated to characterized the candidate fuels and measure important material properties. This effort is being undertaken to support the analysis and design of upcoming irradiation experiments, support fuel modeling efforts and aid in the

ultimate evaluation and selection of the final ATW blanket fuel. In general, the property testing program will include investigation of: the thermal conductivity, specific heat and thermal expansion characteristics of each fuel composition; the thermal equilibria for each fuel type; and the materials compatibility of each fuel-cladding-coolant system. In each case, the existing literature is reviewed and evaluated, followed by actual experimental measurements where needed.

For both the metallic and ceramic dispersion fuels, properties to be measured or characterized include:

- Thermal conductivity and specific heat;
- Thermal expansion;
- Phase equilibria and interdiffusion behavior of TRU-Zr and matrix alloy system, including melting temperature determination;
- Compatibility and dissolution kinetics of dispersion fuel and individual fuel constituents in Pb-Bi eutectic; and
- Fuel particle-cladding interdiffusion behavior.

For the metal alloy candidate fuel, properties to be measured or characterized include:

- Thermal conductivity and specific heat;
- Interdiffusion behavior of fuel alloy constituents;
- Phase stability and presence in as-fabricated fuel alloy and evolution with time at elevated temperatures;
- Fuel-cladding interdiffusion behavior; and
- Compatibility and dissolution kinetics of the fuel alloy in Pb-Bi eutectic and bond metals.

For the nitride candidate fuel, properties to be measured or characterized include:

- Thermal conductivity and specific heat;
- High-temperature dissociation behavior;
- Phase stability and presence in as-fabricated fuel pellet and evolution with time at elevated temperatures;
- Fuel-cladding interdiffusion behavior; and
- Compatibility with cladding and with Pb-Bi eutectic.

For the TRISO-coated particle fuel option, properties of non-fertile, TRISO-coated fuel particles in graphite compacts may be more readily determined from data from similar fuels (e.g., from well characterized TRISO-coated UOC fuel particles) than for the other fuel options. New property measurements for TRU oxycarbides and oxides of ATW–relevant compositions would be required for the following:

- Thermal conductivity and specific heat; and
- High temperature phase stability.

4.3. Irradiation performance

Irradiation testing needs are very similar for each of the fuel types under consideration. Since no irradiation performance data exist for these non-fertile, plutonium-based and minor actinide-laced fuel forms, the approach undertaken consists of initially simple steady-state irradiation tests to identify potential irradiation performance behavior that may limit use of the fuels; these tests will serve as quick screening tests performed simultaneously on all the

candidate fuel forms. Follow-on irradiation tests will narrow the variety of fuels being tested and demonstrate behavior characteristics under expected nominal irradiation conditions.

The initial steady state irradiation tests will be performed in the Advanced Test Reactor (ATR), located at the Idaho National Engineering and Environmental Laboratory. Although the neutronic conditions available in the ATR will not be prototypic of fast-spectrum transmuters, prototypic fission rates and fuel temperatures can be attained. This will allow a timely and qualitative assessment of key phenomena such as fuel swelling, fission gas release, and fuel constituent interdiffusion. Some phenomena cannot be evaluated in a thermal spectrum test, such as the matrix swelling and creep behavior of dispersion fuels and cladding performance for fuel designs intended for fast-spectrum transmuters. Therefore, subsequent irradiation tests will be conducted at conditions that are representative of those expected in particular transmuter designs, which will require irradiation in fast-spectrum test reactors; the identity of the fast-spectrum test reactor to be used remains unknown. Other tests may be required to better investigate specific phenomena, as identified in initial irradiation tests or out-of-pile characterization, such as irradiations at higher-than-nominal temperatures or power levels. ATR can provide prototypic conditions for irradiation of the TRISO-coated particle fuel proposed for use in a thermal-spectrum, gas-cooled transmuter. Eventually, transient testing of both as-fabricated and pre-irradiated fuel samples could be performed in the Transient Reactor Test Facility (TREAT) located at the ANL-West site, depending on the availability of this facility.

Post-irradiation examination of domestically irradiated test fuel will be performed at hot cell facilities such as the Hot Fuel Examination Facility (HFEF) at ANL-West or the Alpha-Gamma Hot Cell Facility (AGHCF) at ANL-East. Examination of test fuel that might be irradiated in non-U.S. fast flux test reactors would likely be performed in the country where the test reactor resides, dependent upon negotiation.

Currently, at least three irradiation tests are envisioned for the FY'01 to FY'05 time period. Irradiation test ATW-1 has as its objective an assessment of irradiation performance characteristics of fuel forms proposed for Pb-Bi-cooled and Na-cooled fast-spectrum transmuters. ATW-1 will include samples of the dispersion, metal alloy, and nitride fuels irradiated in the ATR. This initial test is intended to be a quick-turnaround, inexpensive screening test including a large variety of fuel samples.

Irradiation test ATW-2 has as its objective an assessment of irradiation performance characteristics of non-fertile TRISO-coated fuel compacts and particles under conditions prototypic of a gas-cooled, thermal-spectrum transmuter. ATW-2 will incorporate fuel particles, both loose and in graphite compacts, fabricated with ATW-representative TRU contents, irradiated in the ATR. SiC and ZrC coatings will be employed and various coating thicknesses will be evaluated.

Irradiation test ATW-3 has as its objective an assessment of irradiation performance characteristics of fuel forms proposed for Pb-Bi-cooled and Na-cooled fast-spectrum transmuters under representative spectrum and temperature conditions. ATW-3 will incorporate prototypic fuel rods of metallic and ceramic dispersions, metal alloys, and/or nitrides, depending on which of those forms emerge from ATW-1 and out-of-pile experiments as promising candidates, with compositions and fabrication variables to be determined. It will be desirable to irradiate samples with representative quantities of minor actinides, as well as samples that are primarily Pu-bearing, to allow reference to the samples

from ATW-1 expected to have low quantities of minor actinides. The irradiation test will be performed in a fast-spectrum test reactor.

4.4. Modeling of behavior and phenomena

Modeling to support the ATW blanket fuel development effort will focus on applying (or developing, as needed) mechanistic models of key phenomena that are observed in irradiation tests. During the initial feasibility phase of the program, modeling work will emphasize developing an understanding of observed phenomena; gaining a predictive capability through development of mechanistic models will take place outside the framework of an all-encompassing fuel performance code, since such a code is generally quite fuel system-specific.

Initially, existing and applicable fuel behavior data, models or correlations for each fuel type will be identified from the literature. Although it is most desirable to employ models based on mechanistic understanding of phenomena, development of such models can require considerable effort over long periods of time. Therefore, a set of empirical correlations that can be used in initial fuel performance calculations will be prepared, and existing models will be used as appropriate. It is anticipated that empirical correlations and models based on uranium fuel analogues (or Pu, where available) to the ATW fuel systems will be used initially, with subsequent work to refine these models to describe non-fertile TRU fuel systems. Finally, longer-term work will begin to develop mechanistic models for these fuel phenomena from theoretical considerations, data from the literature and results of PIE from the irradiation test program.

For TRISO-coated particle fuel, the models developed by General Atomics and the Idaho National Engineering and Environmental Laboratory as part of the New Production Reactor program will be employed. Those models are reasonably mature and will provide a suitable beginning to ATW-related model development.

5. EXPECTED RESULTS

At the end of FY'05, it is expected that feasibility will be established for one reference fuel form and one alternate (resources permitting) for each ATW transmuter system remaining under consideration. Establishing feasibility will require that acceptable irradiation performance be demonstrated (at least to moderate burnup values) under nominal, representative conditions and that other potential problems have reasonable engineered solutions to allow implementation (e.g., cladding liners to address incompatibility between fuel or target materials and cladding). In addition, key property measurements will be documented, having sufficient quality to support safety analyses for more extensive irradiation testing and licensing of a potential test transmuter unit.

REFERENCES

[1] A Roadmap for Developing Accelerator Transmutation of Waste (ATW) Technology, report no. DOE/RE-0519, US Department of Energy (1999).

[2] QUINN, J.E., BOARDMAN, C.E., The Advanced Liquid Metal Reactor (ALMR - A Multiple Missions Power Source, Proc. ANS/ASME Nuclear Energy Conference, Foundations for the Future - Safe and Reliable Performance, 1992, San Diego California, ANS (1992) 131-137.

[3] TILL, C.E., CHANG, Y.I., HANNUM, W.H, The Integral Fast Reactor – An Overview, Progress in Nuclear Energy, 31 (1997) 3-12.
[4] ADAMOV, E.O., ORLOV, V.V., FILIN, A.I., TSIKUNOV, V.S., SILA-NOVITSKY, A.G., SMIRNOV, V.S., LEONOV, V.N., Conceptual Design of Brest-300 Lead-Cooled Fast Reactor, Proc. Int. Top. Mtg. on Advanced Reactors Safety, 17-21 April 1994, Pittsburgh, Pennsylvania, American Nuclear Society, ISBN: 0-89448-193-12 (1994) 509-515.
[5] MELESE-D'HOSPITAL G., SIMON, R.H., Status of Gas-Cooled Fast Breeder Reactor Programs, Nuclear Engineering and Design, 40 (1977) 5-12.
[6] HILL, R.N., Private Communication, Argonne National Laboratory, 2000.
[7] YANG, W.S., NABEREJNEV, D.G., KHALIL, H.S., Physics Design Optimization of an LBE-Cooled ATW Blanket, Trans. Am. Nucl. Soc., 83 (2000) 328-330.
[8] TAIWO, T.A., GOHAR, Y., FINCK, P.J., Assessment of the Teledial Gas-Cooled Transmuter Concept, Trans. Am. Nucl. Soc., 83 (2000) 330-331.
[9] PAHL, R.G., PORTER, D.L., LAHM, C.E., HOFMAN, G.L., Experimental Studies of U-Pu-Zr Fast Reactor Fuel Pins in the Experimental Breeder Reactor-II, Met. Trans. A, 21A (1990) 1863-1870.
[10] HOFMAN, G.L., WALTERS, L.C., Metallic Fast Reactor Fuels, in Materials Science and Technology: A Comprehensive Treatment, Vol. 10A, B.R.T. Frost (Ed.), VCH Publishers Inc. New York (1994) 1-43.
[11] SANDERS, C.F., CEASE, J.D., Fabrication and Characterization of Plutonium Test element FTE-13: An HTGR Test Element Containing PuO_{2-x}, $Th_{0.75}Pu_{0.25}O_{2-x}$, and ThO_2, Oak Ridge National Laboratory report, No. ORNL-TM-4207 (1973).

CHEMICAL SEPARATIONS TECHNOLOGIES FOR THE US ACCELERATOR TRANSMUTATION OF WASTE PROGRAMME

J.J. LAIDLER
Argonne National Laboratory, Argonne, Illinois, United States of America

Abstract

Management of the spent nuclear fuel generated by the operating commercial reactors in the United States is entering a new phase because it is clear that the continued rate of accumulation of spent fuel is such that the spent fuel inventory will soon exceed the legislated capacity of the proposed Yucca Mountain repository. An integrated chemical separations system has been conceived for the partitioning of this fuel preparatory to transmutation of transuranic elements and long-lived fission products in an accelerator-driven transmuter reactor. A hybrid aqueous/pyrochemical separations system is being developed, with the initial separation done with an aqueous solvent extraction process called UREX. The UREX process extracts uranium, technetium and iodine and directs the transuranic elements and other fission products to the liquid waste stream. The uranium is sufficiently pure that it can be disposed as a low-level waste, while the technetium and iodine are converted into targets for transmutation to stable isotopes. The liquid waste stream containing the transuranics is converted to solid oxide form and the transuranics are separated from the fission products by electrorefining after having been converted to the metallic state. Demonstrations of the process with actual LWR spent fuel are in progress.

1. INTRODUCTION

The nearly 100 operating commercial nuclear power stations in the United States generate about 2000 tonnes of spent fuel each year. Presently, this spent fuel is being stored in water basins or dry cask storage areas at the reactor sites; some spent fuel has been transferred to offsite independent spent fuel storage installations. Because the spent fuel has been accumulating for decades, the total inventory will soon reach a level that exceeds the legislated limit (around 63 000 tonnes of spent nuclear fuel) for the proposed Yucca Mountain deep geologic repository.

The U.S. Accelerator Transmutation of Waste (ATW) program is directed toward the development of an alternative approach to high-level waste management. This program would provide an integrated partitioning and transmutation system for the fissioning of transuranic elements and the transmutation of environmentally-important long-lived fission products. Efficient elimination of these radionuclides would greatly reduce the radiotoxicity of the material to be disposed in the repository and thereby the cumulative risk to the public. By removal of the long-lived radionuclides of concern to public health over periods of several hundred thousand years, the regulatory lifetime of the repository could be reduced to time periods that are well within the realm of recorded human history and hence amenable to credible performance predictions. If properly designed, the chemical separations technologies employed for partitioning might be capable of reducing the volume of high-level waste to be disposed, thus extending the capacity of the repository and possibly precluding the need for a second repository in the near term. All of these advantages of partitioning and transmutation can lead to an optimized nuclear waste management strategy that can be expected to receive favorable public reception and reduce opposition to the construction and operation of a high-level waste repository.

2. SEPARATIONS REQUIREMENTS

Conceptual design of the ATW chemical separations system is proceeding on the basis of a requirement to process 1500-2000 tonnes (heavy metal) of commercial spent fuel per year. This is taken to be a virtually homogeneous feed of zircaloy-clad oxide fuel with burnups ranging from 20 to 70 gigawatt-days per tonne and with cooling periods of at least 10 years

and possible more that 25 years. A number of target performance requirements have been established for the processing of this fuel. Principal among these is a requirement to separate uranium as a pure product, sufficiently pure that it will meet present regulations for disposal of low-level waste in greater confinement disposal (GCD) sites. Among other limitations, this requires that the total transuranic content be less than 100 nanocuries per gram of uranium. Other target requirements pertain to the efficiency of recovery of specific nuclides: over 99.9% recovery for the transuranic elements, and over 95% recovery for the long-lived fission products ^{129}I and ^{99}Tc. In a more general sense, a guideline for minimization of process waste generation has been adopted for all process design evaluations.

2.1. Separations system concept

The overall chemical separations scheme that has been selected for initial study in the ATW program is shown in Fig. 1. An aqueous separations method was chosen for the extraction of uranium; this process has been named the UREX process. Iodine is removed in the dissolution step and technetium is co-extracted with uranium and subsequently separated. The UREX liquid waste stream contains the transuranic elements and all of the remaining fission products. This liquid stream is denitrated and converted to dry oxide powder. The oxide product is sent to the PYRO-A process, a pyrochemical process in which the fission products and transuranics are efficiently separated. The transuranics are recovered as metals that are then sent to the transmuter reactor fuel fabrication step.

After irradiation in the accelerator-driven transmuter reactor to burnups as high as 30 atom percent, the discharged transmuter fuel will be processed to recover the unburned transuranics for recycle and to extract the newly-generated iodine and technetium for transmutation. The process for accomplishing these separations has been given the generic name PYRO-B. The PYRO-B process must deal with fuel that has been cooled for only a short period (about 2 years, to minimize further storage requirements and reduce plant costs) and that contains a significant concentration of fissionable transuranic isotopes. The quantity of fuel that must be processed in one year is much less than in the case of the LWR spent fuel (perhaps 30 tonnes per year vs. 1500-2000 tonnes for LWR spent fuel). These considerations led to the selection of a pyrochemical process for treatment of the transmuter fuel, which has been assumed to have zero uranium content (i.e., a non-fertile fuel). Pyrochemical systems, being free of a water moderator, can accommodate larger masses of fissile isotopes. The molten salts used in these processes operate at elevated temperatures and are stable against alpha and gamma radiation damage, so short fuel cooling periods are feasible.

The only process high-level waste streams arising in the overall separations system come from the pyrochemical processes (PYRO-A and PYRO-B). The similarity of these processes is such that the waste streams are virtually identical. The transition metal fission products accumulate in metallic form and are combined with decontaminated cladding hulls to form a metal alloy waste form. The alkali metal and alkaline earth fission products are initially concentrated in process salts and then absorbed in zeolite that is subsequently transformed to the mineral sodalite; in the process of sodalite synthesis, the sodalite particles are encapsulated in borosilicate glass, yielding a glass-ceramic composite with good leach resistance.

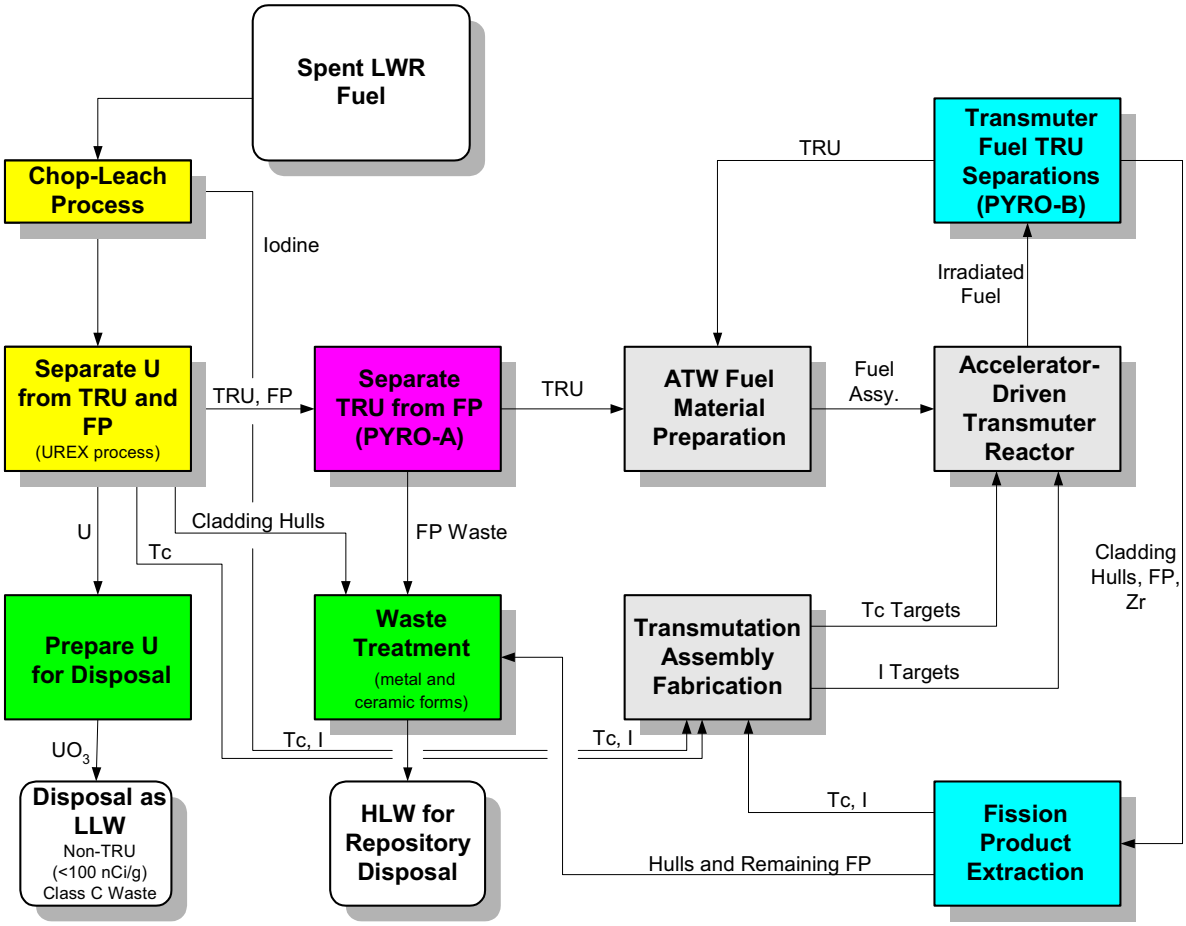

FIG. 1. Overall chemical separations scheme for the single-tier accelerator transmutation of waste (ATW) system. (FP = fission product; TRU = transuranic element; HLW =high-level waste; LLW = (low-level waste); LWR = light water reactor).

2.2. LWR spent fuel processing

The aqueous solvent extraction process (UREX) was selected as the baseline process for LWR spent fuel processing because a similar process (PUREX) is a mature technology that is well understood and fully capable of meeting the throughput requirements of the ATW system. The UREX process is a special modification of PUREX that permits efficient extraction of uranium, at high decontamination levels, in one extraction cycle. The distinguishing feature of the UREX process is the addition of a reductant/complexant, acetohydroxamic acid (AHA), to the dissolver solution. The addition of AHA results in the suppression of plutonium extraction and in the retention of certain problematic fission products (e.g., Mo, Zr, and Ru) that would otherwise contaminate the uranium and technetium product streams.

The UREX liquid waste stream contains all of the transuranic elements and all of the fission products except technetium, iodine, xenon and krypton. In order to limit the volume of waste produced, this stream is to be evaporated to near-dryness and then calcined to convert the transuranics and fission products to their oxides. These oxides are sent to the PYRO-A process where they are reduced to the metallic state in a molten CaO-$CaCl_2$ bath by a direct electrochemical reduction process. The collection of metals is then transferred to an electrorefiner, where the transuranics are separated from the fission products. Minor contamination of the transuranics with lanthanides occurs in the electrorefining step. There is no separation of plutonium from the minor actinides in this process, thus enhancing the

proliferation resistance of the system. The collection of transuranics is sent directly to the transmuter fuel fabrication step.

2.3. ATW transmuter fuel processing

At the present time, a final selection of the fuel type for the transmuter reactor has not been made. It is assumed for now that the fuel is a metallic alloy of transuranics in zirconium, with a composition in the range 40-50 weight percent transuranics and a target burnup of 20-30 atom percent. The initial concept for treatment of this fuel utilized a chloride volatility process whereby the zirconium matrix was digested by formation of volatile $ZrCl_4$. The transuranics were then to be extracted by electrowinning from the chloride salt containing transuranics and fission products. While this process may be appropriate for a dispersion of TRU-Zr particles in a zirconium matrix, recent fuel properties evaluations tend to favor a homogeneous TRU-Zr alloy. In this case direct electrorefining of the TRU-Zr fuel appears to be a better option. There is a precedent for this process in the treatment of EBR-II spent fuel, where the fuel composition for a portion of the fuel to be treated is (U,TRU)-10Zr.

2.4. Status of chemical separations technology development

The UREX process flowsheet has been demonstrated with simulated LWR spent fuel. The extraction of transuranics was completely inhibited by the AHA complexant/reductant; consequently, the decontamination of uranium was well below the 100 nanocuries per gram level. The recovery efficiency for uranium and transuranics exceeded 99.999%. Technetium was not extracted in these initial experiments because the acid concentration was not optimized. A complete demonstration of the UREX flowsheet, modified for technetium extraction, will be carried out with a bank of 33 centrifugal contactors in the latter half of 2001. A demonstration of the full process for LWR spent fuel treatment, from UREX separations to denitration and TRU recovery in the PYRO-A process, will be conducted with actual spent fuel beginning in October 2001 and continuing through 2003.

The PYRO-B process for irradiated transmuter fuel is at an earlier stage of development, but will benefit from experience with EBR-II spent fuel treatment. Fuel types other than metal alloy are under consideration, and conceptual flowsheets have been developed for the processing of non-fertile oxide fuel with a ceramic matrix (cercer fuel), TRU nitrides in a ZrN matrix, and TRU oxide and nitride in a metal matrix (cermet fuel). Extensive (and expensive) demonstrations with the transmuter fuel will be deferred until the preferred fuel type is selected.

3. CONCLUSIONS

The chemical separations technology development described in this paper pertains to a single-tier transmutation system in which the transuranics and long-lived fission products from LWR spent fuel are sent to an accelerator-driven fast spectrum system for transmutation. There is increasing interest in the U.S., however, in a multi-tier system. In such a system, the existing infrastructure of commercial light water reactors is supported by new advanced thermal reactors (Tier 1) that can be used as efficient burners of plutonium in a close-coupled system. The unburned minor transuranics in the advanced thermal reactor spent fuel would be directed to a fast spectrum reactor (Tier 2), either critical or accelerator-driven subcritical, where the minor actinides can be destroyed. This multi-tier system would clearly impose different requirements on the associated chemical separations technologies, and the separations processes that would be needed are now being evaluated.

IMPACT OF FUEL CHOICES ON SPENT FUEL CHARACTERISTICS FOR ONCE-THROUGH HEAVY METAL COOLED REACTORS[1]

P. HEJZLAR, M.J. DRISCOLL, N.E. TODREAS
Massachusetts Institute of Technology, Cambridge, Massachusetts, United States of America

Abstract

Recently, heavy metal cooled reactors have been studied, either as potential candidates for burning of actinides from LWR spent fuel or as a promising power generation source for long term deployment. This study investigates a lead-bismuth-cooled core in a once-through fuel cycle that does not require expensive fuel reprocessing and strives for long core life while maintaining low reactivity swing. Contrary to earlier studies, our systematic scoping study, while for cores with acceptable operating and safety characteristics, is focused primarily on the spent fuel inventory, toxicity and proliferation resistance.

Oxide, carbide, nitride and metallic fuels with U-238 and Th-232 as fertile materials and U-235 and Pu drivers have been investigated in a systematic manner. Metallic fuels were found to provide the best conversion ratio, followed by carbide fuels, nitride fuels and finally the oxides. Within one chemical form, Pu fuels exhibited the smallest reactivity decrease with burnup, U235-driven fuels were the next best and the fuels containing Th showed the largest decrease. Fuels driven by U-235 and having U-238 as fertile material were found to discharge fuel with the smallest waste inventory, decay heat, radioactivity and ingestion hazard. The Pu based fuels show significantly higher ingestion hazard and curie inventory. Fuels with fertile Th-232 produce less plutonium, nevertheless, their fuel toxicity is slightly higher than that of the U-238 fuels due to the activity of polonium, radon, and radium from the thorium decay chain.

UZr and PuUZr fuels have been identified as the most promising alternatives for long life core concept design. They show the best potential to achieve small reactivity swing over the long core life and at the same time permit a relatively large core having a negative coolant density reactivity coefficient. Moreover, the UZr discharged fuel exhibits the smallest radiotoxicity, waste inventory, decay heat and radioactivity of all the fuels investigated. The key drawback is proliferation concern due to the high content of bred-in fissile material with an isotopic composition comparable to weapons grade plutonium. This is a key challenge to be overcome for this fuel type and all uranium-driven fuels in hard spectrum reactors. On the other hand, the Pu-driven fuels, among them UPuZr, exhibit the largest radiotoxicity, waste inventory, decay heat and radioactivity, but less proliferation threat.

1. INTRODUCTION

In the past decade, increased attention has been paid to heavy metals, in particular lead-bismuth eutectic (LBE) and lead, to replace sodium as coolant in fast reactors. This shift has been motivated partially by the new openness of the Russian nuclear program that made available information from their extensive development of LBE coolant for alpha-class submarine reactors [HLMC, 1998] and from the current development of a lead cooled fast reactor [1], partially by R&D on accelerator driven transmutation systems, where lead is considered as a beam target and most importantly by safety benefits and an enhanced potential to achieve new objectives established for nuclear power plants into the 21st century[2]. Safety benefits involve primarily chemical inertness that eliminates concerns with the exothermic reaction of sodium coolant with water and very high boiling temperature (1670°C for LBE versus 892°C for Na) that substantially increases margin to boiling and practically eliminates concerns with reactivity increase from coolant boiling. Moreover, lead-based coolants have a higher scattering cross section that results

[1]This work is supported by Idaho National Engineering and Environmental Laboratory

[2]These criteria involve [21]: 1) minimization of proliferation vulnerability, 2) the achievement of extremely high levels of inherent/passive safety, 3) minimization of waste and environmental impact, and 4) promotion of public understanding of the need, benefits, and safety of atomic energy. Most importantly, the new systems must be economically competitive with other alternatives for energy generation.

in smaller neutron leakage and thus better neutron economy and reduced requirements for burnup reactivity to compensate for the cycle reactivity swing. The ancillary benefit of high scattering cross section is a larger rate of neutron leakage upon coolant voiding, which together with the smaller absorption cross section of LBE gives smaller coolant void worth than in sodium cooled reactors. A detailed review of heavy metal coolants versus sodium is given in [15].

Due to very hard spectrum and small neutron leakage, fast reactors with heavy metal coolant can operate with modest burnup compensation without need for refueling for a substantial time period. The small absorption cross section of the fission products in a hard spectrum reactor further enhances the reactivity-limited refueling cycle length because the fraction of parasitic absorptions in the growing fission product inventory remains small even for high burnups. These aspects in combination with high burnups achievable with fast reactor fuels make heavy metal cooled reactors promising candidates for a sustainable energy source that effectively utilizes abundant U-238 and Th-232 resources. A fast spectrum heavy metal cooled reactor is thus capable of very high utilization of the nuclear fuel resource in a once-through fuel cycle. In addition, it can attain long reactor lifetime without refueling (once-for life fueled reactor) offering potentially better economy and reducing proliferation threat by eliminating fuel manipulation and access to fuel during reactor operation.

In response to the new top-level criteria for successful reemergence of nuclear energy in the 21st century, and considering the advantages of heavy metal coolants as well as availability of information from Russian work [16], a number of lead and lead based cooled reactor concepts as a potential generation source for long-term deployment have recently appeared in the literature. [17] proposed a conceptual design of a small 150MWth reactor that could be transported to the site and operated for 12 years without refueling while maintaining burnup reactivity swing less than 0.1%Δk and negative coolant void reactivity over the entire burnup period. The potential of these small reactors to consume most of the self-generated transuranium species and long-lived fission products by operating in a so called radioactive waste confining equilibrium closed reactor fuel cycle was also shown [13]. Systematic comparison of sodium- and LBE-cooled small, low-power-density, long-life cores (100 MWe) [10] confirmed the benefits of smaller coolant void worth and reactivity swing for LBE-cooled units in comparison to sodium-cooled systems, but cautioned that burnup reactivity losses rather than fluence or burnup limits will be the limiting performance attribute. In the Ref. [6] it was proposed the design of a small modular lead cooled and reflected core (125 or 250 MWth) and established the range of core design variables that allow reactor operation for 15 effective full power years (EFPY) with nearly zero reactivity swing without any fuel handling and reshuffling using Pu-U-Zr(10%) or U-Zr(10%) fuel [18].

Heavy metals are also attractive coolants for fast spectrum actinide burning systems due to the high fission to capture cross section ratio achievable in hard neutron spectrum in these systems. Although most of the research and activity on actinide burning has been done for subcritical accelerator driven systems, several studies of LBE- or lead-cooled critical actinide burners have recently appeared [7, 12, 19]. Critical actinide burners have to overcome several safety and control challenges, in particular positive coolant void worth, small Doppler effect, small effective delayed neutron fraction and large reactivity swing. Investigations performed at MIT addressed these challenges and confirmed the feasibility of an LBE-cooled critical actinide burner, which has a TRU destruction rate comparable to that of an accelerator driven subcritical system, such as ATW, while maintaining acceptable safety characteristics [7, 8]. However, the projected fuel

cycle cost of this recycling-mode system was found to be two to four times larger than the direct cost of LWR fuel today [4]. Although there appear to be viable options to significantly reduce the fuel cycle cost of transmutation systems, it may take decades before economical concepts with recycling can be implemented. Therefore, the potential of an economic electricity production system with a long life core and a once-through fuel cycle that does not require expensive fuel reprocessing, similar to that proposed in Ref. [20], has been explored.

The objective of this study was to evaluate a conceptual design of a high conversion LBE-cooled reactor of appreciable power output that:

- Operates in a once through cycle,
- Needs no reprocessing,
- Has very long refueling period (up to 15 years),
- Discharges a minimum amount of waste,
- Is proliferation resistant, and
- Achieves excellent safety characteristics with emphasis on inherent and passive safety.

Most of the aforementioned earlier investigations of small long-life cores strove for a small reactivity swing and excellent safety characteristics with emphasis on the attainment of neutronic feedbacks that would allow passive or inherent plant response to reactivity perturbations. Thus these investigations primarily reflect the requirement of Shlyakhter's (see footnote) second criterion for new generation plants. This systematic scoping study, while for cores with acceptable operating and safety characteristics, is focused primarily on the waste inventory, toxicity and proliferation resistance of the discharged fuel, i.e., the primary thrust will be directed on the first and third criteria as listed in the footnote. In addition, to minimize the capital cost per installed kW and reduce fuel cycle cost in compliance with the requirements of economic competitiveness of future nuclear plants, the study is not limited to small cores, as was earlier work on long-life cores, and assumes a once-through fuel cycle, to capitalize on the advantages of economy of scale and fuel cycle cost reduction by elimination of expensive reprocessing. In the area of safety, this paper does not cover all the neutronics aspects. The key challenge addressed is the attainment of long-core life at small reactivity swing while maintaining acceptable coolant temperature coefficient.

2. ANALYSIS TOOLS

Reactor physics analysis generally requires several successive steps involving few-group cross section preparation for a homogenized cell and then a dehomogenization procedure to reconstruct the pin by pin power distribution from the homogeneous solution. All these steps can be accomplished in one comprehensive step with the Monte Carlo Method. In addition, the Monte Carlo Method provides a 3-D transport solution that is more accurate than finite difference multigroup methods. Therefore, the Monte Carlo Neutron Photon Transport (MCNP) code MCNP4A [2], developed at Los Alamos National Laboratory, was selected as the main tool for neutron physics analysis, due to its availability, versatility and extensive verification for a variety of applications including heterogeneous lattices for fast reactors. One of the MCNP limitations is its inability to calculate core depletion. To perform the burnup calculations, the ORIGEN2.1 code [3], developed at Oak Ridge National Laboratory (ORNL), has been chosen. The coupling between MCNP and ORIGEN2.1 has been attained through the set of coupling utility programs assembled in the MOCUP code [14].

TABLE 1. FISSION PRODUCTS CARRIED IN MOCUP BURNUP CALCULATIONS

KR 83	RU102	AG109	CS134	ND144	SM151
ZR 93	RU103	CD111	CS135	ND145	SM152
ZR 95	RH103	CD113	CS137	ND146	EU153
MO 95	RU104	IN115	LA139	ND147	EU154
ZR 96	PD104	I127	BA140	PM147	EU155
MO 97	RH105	I129	LA140	SM147	GD156
MO 98	PD105	XE131	CE141	ND148	GD157
MO 99	RU106	XE132	PR141	PM148	
TC 99	PD106	XE133	CE143	PM149	
MO100	PD107	CS133	ND143	SM149	
RU101	PD108	XE134	PR143	ND150	

TABLE 2. LIST OF ACTINIDES INCLUDED IN MOCUP BURNUP CALCULATIONS

TH232	U237	NP237	PU241	CM242	CM248
TH233	U238	NP238	PU242	CM243	BK249
PA231	U239	PU237	PU243	CM244	CF249
U233	U240	PU238	AM241	CM245	CF250
U234	NP235	PU239	AM242M	CM246	CF251
U235	NP236	PU240	AM243	CM247	CF252
U236					

Sixty-two fission products accounting for 95% of the absorptions of all the fission products and 37 actinides, as listed in Tables 1 and 2, respectively were tracked in all MOCUP calculations.

3. EVALUATION OF NEUTRONIC MERITS FOR VARIOUS FUEL FORMS

First a systematic scoping study was performed on the infinite unit cell (see Fig. 1) to explore the theoretical potential for internal conversion achievable for various fuel types and other characteristics of interest to the above goals. Fuels considered in the study are summarized in Table 3. In each fuel category alternative drivers were considered using Pu from LWR spent fuel (without minor actinides), weapons-grade plutonium or U-235. To explore the possible benefits of thorium as a fertile material, variants with Th were also explored. Thorium based fuels employed depleted U238 to denature bred-in U233, except for Pu-Th-Zr fuel, which was examined to assess the potential of pure thorium fuel. Uranium dioxide was taken as a reference fuel against which the alternative fuel types are compared. The mononitride UN and monocarbide UC fuel are also proven nonmetallic fuel types, although developed to a much less extent than UO2. In the metallic fuel category, the proven IFR fuel U-Zr was selected for study. Each of these specific fuels are U235-enriched. The initial enrichment was found by iterative MCNP runs to achieve an approximately critical state in the modeled unit cell.

Table 4 shows the density and reactor-physics characteristics of interest for each fuel type. The densities were either taken from tables of properties (where available) or calculated as 95% of theoretical density using the weight fractions of nuclides present in a given fuel. The comparison of the internal conversion ratios (ICR) at BOL shows that metallic fuels provide the best conversion potential. They are followed by carbide fuels, nitride fuels and finally the oxides. Within a fuel category, Pu fuels exhibit the largest ICR, U235-driven fuels are the next and the fuels containing Th show the smallest ICR.

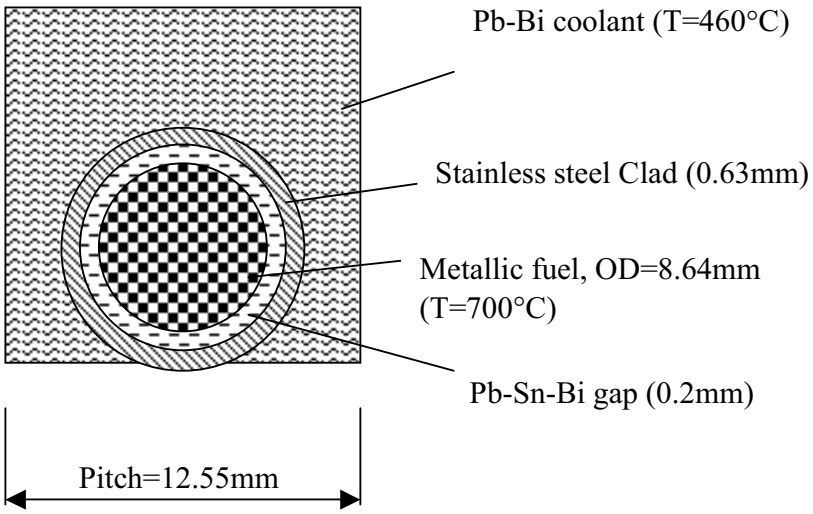

FIG. 1. Unit cell of an infinite Pb-Bi cooled square lattice.

The discharge burnup after 15 years of fuel residence time is shown in the 4th column. It is defined per initial heavy metal mass and was calculated from the average pin linear heat rate of 120 W/cm. This derated linear power (about one third that of the typical values of 370 W/cm for fast reactor cores) was selected in such manner that the discharge burnup is close to 100 MWd/kg – the maximum average burnup demonstrated for IFR metallic fuel. The same linear power was used for all fuel types, although it is to be noted that not all the fuels under investigation will necessarily withstand such high burnup because of mechanical and pellet cladding interaction constraints. For the fixed burnup limit, lower discharge burnup (for constant exposure time) indicates a possibility to increase power rating, provided that mechanical limits are not exceeded.

TABLE 3. LIST OF CONSIDERED FUEL TYPES

Fuel type	Composition		k_{inf} at BOL
	Driver component	Balance (in wt% in HM)	
Oxides			
UO_2 (reference)	11.1 wt% U235*	88.9 wt% U238	1.000±0.001
Nitrides			
U-N	10.2 wt% U235	89.8 wt% U238	1.001±0.001
U-Pu-N	9 wt% Pu**	91 wt% U+	1.001±0.001
U-Th-N	30 wt%U (16.6 wt% U235)	70 wt% Th232	1.003±0.001
Carbides			
U-C	9.8 wt% U235	90.2 wt% U238	1.006±0.002
U-Pu-C	9.7 wt% Pu	90.3 wt% U+	1.002±0.001
U-Th-C	30 wt%U (16.0 wt% U235)	70 wt% Th232	1.000±0.001
Metallic			
U-Zr	90 wt%U (8.7 wt% U235)	10 wt% Zr	1.004±0.001
U-Pu-Zr	7.2 wt% Pu*	82.8 wt% U+, 10 wt% Zr	1.007±0.001
U-Th-Zr	30 wt% U(15 wt% U235)	60% Th, 10 wt% Zr	1.006±0.001
Pu-Th-Zr	10.2 wt% Pu*	79.8 wt% Th232, 10 wt% Zr	1.007±0.001

* The enrichment or Pu weight fraction was adjusted to attain a critical unit cell in an infinite lattice. i.e., k_{inf}~1.
** Pu vector for all Pu-driven fuels = Pu238/Pu239/Pu240/Pu241/Pu242=2/58/26/10/4wt%.
+ Depleted uranium with 0.2 wt% U235.

Columns 5 and 6 show one-group effective cross sections of major fissile isotopes for fission and capture, respectively and column 7 lists capture cross sections for fertile isotopes. U-233 exhibits the largest fission and the smallest capture cross section. U-235 has the largest fission cross section in the UO_2 fuel form and the smallest one in the metallic fuel form. This is consistent with the trend that the harder the spectrum the smaller the cross section. A similar trend can be observed for capture cross sections, but the decrease of capture cross section with spectrum hardening is more pronounced than the changes of fission cross section. Thus the fission to capture cross section ratio increases when moving to metallic fuel resulting in higher reactivity for fixed enrichment or lower enrichment requirement for fixed reactivity. Also, the ICR is the largest for metallic fuels due to a higher content of fertile nuclides that can be loaded in these fuels with lower enrichment as well as due to a higher cross section ratio of capture in fertile to absorption in fissile nuclides.

TABLE 4. SELECTED NEUTRONICS CHARACTERISTICS OF INDIVIDUAL FUEL TYPES

Fuel type	Density (g/cm^3)	ICR*	B_d (MWd/ kgHM)	σ_f (b) fissile**	σ_c (b) fissile**	σ_c (b) fertile+	Equil. $N_{fissile}/N_{fertile}$	EOL $\frac{N_{23}+N_{25}}{N_U}$
Oxides								
UO_2 (reference)	10.42	0.967	116	1.835	0.536	0.289	0.122	
Nitrides								
U-N	13.61	0.988	87	1.697	0.459	0.246	0.114	
U-Pu-N	13.65	1.572	87	1.768	0.445	0.264	0.119	
U-Th-N	11.98	0.914	99	2.472/ 1.710	0.230/ 0.368	0.278/ 0.244	0.103/ 0.117	0.110
Carbides								
U-C	12.95	1.067	91	1.718	0.475	0.258	0.118	
U-Pu-C	12.98	1.692	91	1.754	0.451	0.276	0.125	
U-Th-C	11.45	0.976	103	2.502/ 1.705	0.480/ 0.384	0.291/ 0.257	0.098/ 0.123	0.106
Metallic								
U-Zr	15.2	1.114	82	1.495	0.364	0.200	0.108	
U-Pu-Zr	15.2	1.849	82	1.636	0.282	0.214	0.112	
U-Th-Zr	13.1	1.015	95	2.263/ 1.624	0.200/ 0.253	0.230/ 0.199	0.09/ 0.106	0.103
Pu-Th-Zr	10.7	1.519	116	2.311/ 1.634	0.210/ 0.281	0.242	0.096	0.914

* Internal conversion ratio at BOL is defined as $\frac{\phi\left(\Sigma_c^{28}+\Sigma_c^{02}+\Sigma_c^{40}\right)}{\phi\left(\Sigma_a^{25}+\Sigma_a^{49}+\Sigma_a^{41}\right)}$.

** U235 for systems without Pu, Pu239 for systems with Pu and U233/Pu239 for systems with Th.

+ U238 for U-Pu systems and Th232/U238 for U-Th systems.

The next column shows the equilibrium ratio of fissile to fertile number densities. This characteristic was obtained by equating production to destruction. Note that U-233 exhibits a smaller fissile to fertile nuclide ratio than U-235 or Pu-239. Therefore, there is significantly less U-233 bred in thorium fuels than Pu-239 in fuels with U-238 fertile material. In addition, U-233 has a lower η value than Pu-239. Thus, the thorium-uranium systems have less promising

potential for internal conversion and achievement of long core life. In addition, the proliferation resistance criterion requires that the ratio of U-233+U-235 nuclides to total number of uranium nuclides is less than 12% [5]. Therefore, Th-232 must be loaded together with U-238 to denature U-233, which strictly limits the benefits of Th. The last column, which shows the above ratio for individual thorium fuels at the EOL (after 15 EFPYs of irradiation), indicates that for the initial Th weight fraction of 30wt%, the proliferation limit of the discharged fuel is satisfied. However, the margin is relatively small and further increase of thorium fraction in the fuel is very limited, especially in case of nitride fuels where this limit is almost reached at 30wt% of thorium. If thorium only is used as fertile material, almost pure U-233 is present in discharged fuel, as the last line of Table 4 indicates.

The development of k_{inf} as a function of burnup is shown in Fig. 2. The Pb-Bi coolant provides a hard neutron spectrum, which results in a significant contribution of fissions of even nuclides and thus an increase of fuel quality resulting in a reactivity rise with exposure time for all fuels* considered. Clearly, metallic fuels provide the best potential to attain long core life through internal conversion of fertile to fissile material. They are followed by carbide fuels, nitride fuels and finally the oxides. Within each fuel category, Pu fuels exhibit the largest reactivity increase, U235-driven fuels are the next and the fuels containing Th (hence U-233) show the smallest reactivity rise. Note that larger reactivity increases are desirable since higher reactivity excess provides more option space to counteract the coolant void worth challenge through enhanced leakage while still maintaining enough neutrons for internal conversion.

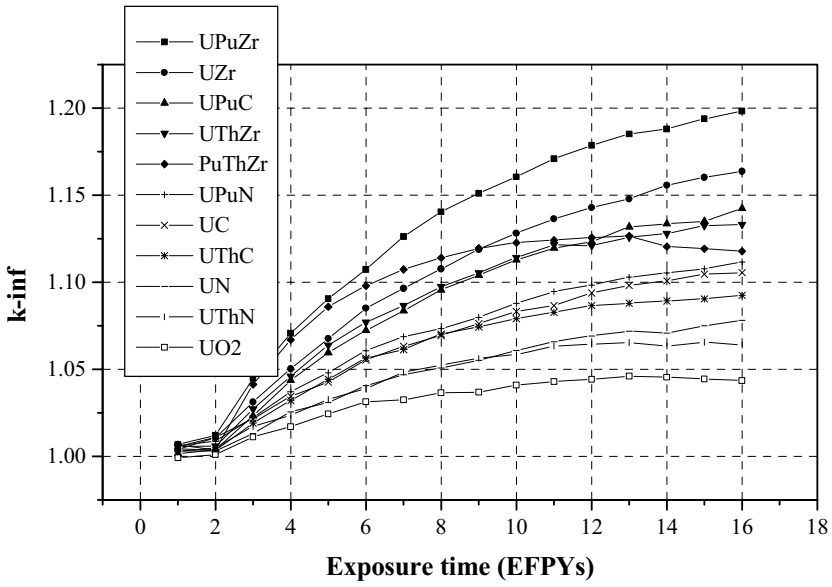

FIG. 2. Development of k_{inf} in a unit cell of an infinite lattice for various fuel types.

* This increase is valid for an infinite unit cell, but does not necessarily mean that the same trend will be observed for a real system where more neutrons are consumed in parasitic absorptions and leak out of the core. Therefore, less neutrons are available for breeding, resulting in a reactivity reduction with burnup for low-ICR fuels.

4. THE CHALLENGE OF BALANCING ICR AND COOLANT DENSITY REACTIVITY COEFFICIENT

Large cores of fast reactors exhibit positive coolant temperature coefficient and design measures must be incorporated to make it negative or limit it to small values so that the other negative reactivity feedbacks render the overall reactivity response negative under all circumstances. However, it is difficult to design a large core with negative coolant temperature coefficient and at the same time with high ICR because the design direction for cores with negative coolant void worth is high leakage while that for high-ICR cores is small leakage – a contradictory requirement

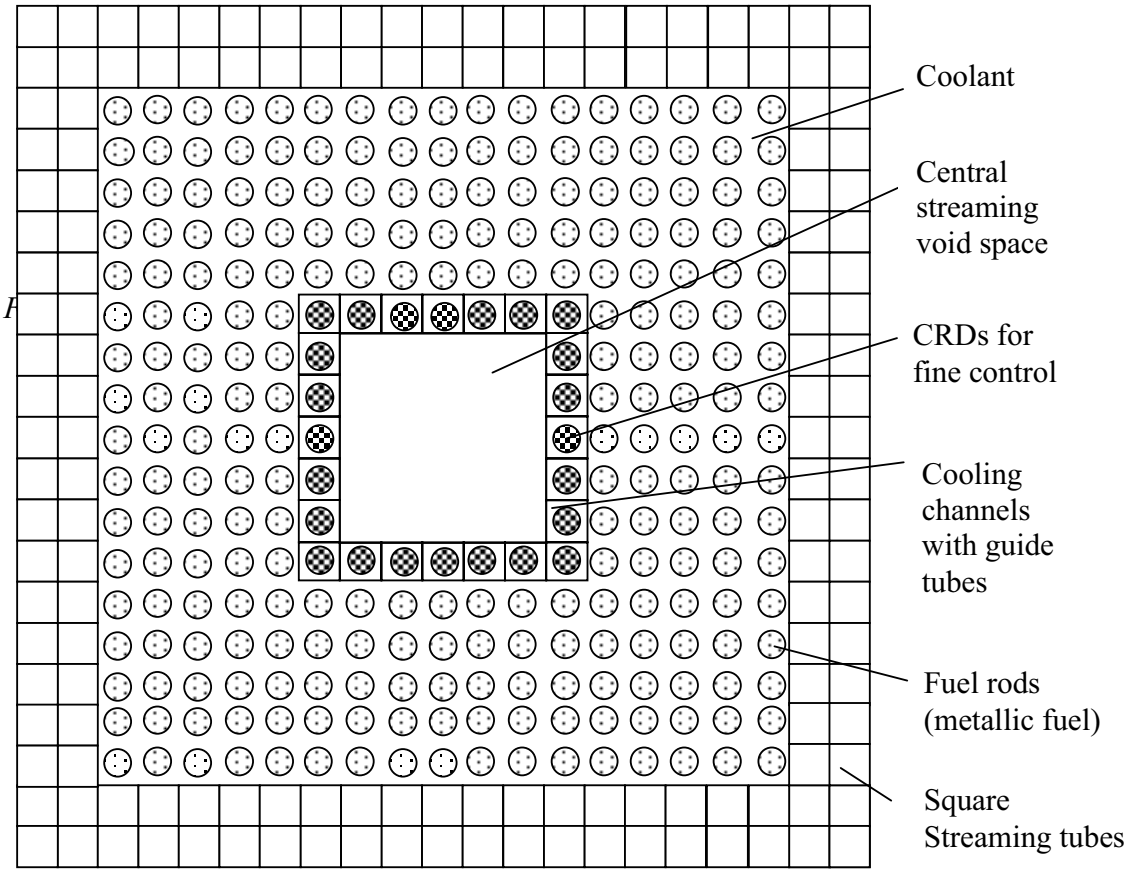

FIG. 3. Streaming fuel assembly with cooled CRDs.

Reactivity response to coolant density changes was investigated on a full-core model for the fuels with the largest ICR, i.e., UZr and UPuZr. These fuels were loaded into a core having 157 fuel assemblies in a 17×17 square array, CRDs were fully withdrawn and the enrichment was increased in comparison with the unit cell model to reach an approximately critical state. The core layout was identical as for PWR cores with 157 FAs. The core active height and the height of the gas plenum were assumed 130 and 100 cm, respectively. Two fuel assembly designs were investigated – the regular 17×17 fuel assembly and a 21×21 streaming fuel assembly proposed for the critical actinide burner design [8], shown in Fig. 3. The 21×21 positions assembly

contains 240 fuel rods, 152 square streaming tubes arranged in two rows at the FA periphery and 7×7 positions in the FA center. The streaming tubes are filled with gas and sealed.

The simulation assumed changes of coolant average density in the core and gas plenum region between the reference value of 10.25 g/cm^3 and zero while the coolant in the reactor vessel including the lead-bismuth eutectic reflector around the core was kept at original density*. The results, plotted in Figs 4 and 5 for UZr and UPuZr fuels in the regular core respectively, show reactivity increase upon coolant density reduction from the reference density, i.e., positive coolant temperature coefficient. If this fuel, albeit at a slightly higher enrichment to reach criticality, is loaded into the same core with streaming fuel assemblies, the coolant temperature coefficient can be made negative for UZr fuel and negative (below a coolant density of 6 g/cm^3) or slightly positive for higher densities (maximum reactivity rise of +0.0028Δk is attained at a density of 8 g/cm^3) for UpuZr fuel. Therefore, the streaming FAs are very effective in overcoming the coolant reactivity void worth challenge**.

TABLE 5. ICRS FOR THE FULL CORE MODELS OF THE ONCE-THROUGH CONCEPT

Case	ICR at BOL
Regular core, UZr fuel, 10.8wt% U235	0.862
Streaming core, UZr fuel, 14.1wt% U235	0.669
Regular core, PuUZr fuel, 9.5wt% Pu	1.352
Streaming core, PuUZr fuel, 10.5wt% Pu	1.228

However, there is a penalty on achievable ICR due to the higher enrichment. Table 5 shows these penalties for both fuels. Pu-fueled cores have a less tight neutron balance and the ICR at BOL remains well above 1.0 in a streaming core. The ICR for UZr fuel exhibits a substantial reduction upon replacement of regular fuel assemblies with the streaming bundles, resulting in a relatively large reactivity swing over core life. This is shown in Fig. 6, which was generated from burnup calculations of the full-core MOCUP model. On the other hand, the Pu driven core can maintain relatively flat reactivity over a long core life due to achievement of ICR above unity. Note that power density in these full core burnup runs was doubled in comparison with the unit cell runs to increase burnups to the high fuel burnups of 170 MWd/kgHM expected to be attainable for metallic fuels. These results indicate that the design of a large LBE-cooled long life core having a small reactivity swing and plausible coolant void worth is feasible for the Pu-driven cores, but more difficult for UZr fuel because of the smaller reactivity excess that requires higher enrichment. On the other hand, UZr fuel exhibits better void reactivity performance.

* The approach of voiding the whole core but not the out-of-core coolant is typically used to evaluate coolant void worth. In LBE or lead cooled cores, this type of voiding is highly hypothetical since the high boiling point of these coolants (~1700°C) virtually eliminates the possibility of boiling in a core with stable geometry. Moreover, complete voiding may not give conservative results, because small coolant density changes from heating, which are more likely to occur in real situations, may yield a reactivity increase. Therefore, the reactivity curve along the entire coolant density space was calculated in this work to ensure that reactivity changes remain acceptable under any coolant conditions.

** Note that even for the small core (rating 250 MWth, core OD = 53cm, H = 400 cm) of the Pb-cooled, Pu-fueled ENHS (Encapsulated Nuclear Heat Source) concept proposed in Ref. [6] coolant void worth is positive at +0.025Δk for comparable P/D in the scenario of voiding the whole core (equivalent to zero density point in Fig. 5. This compares to -0.038Δk for the large streaming core studied here (rating 1800 MWt, core OD = 370 cm, H = 130 cm).

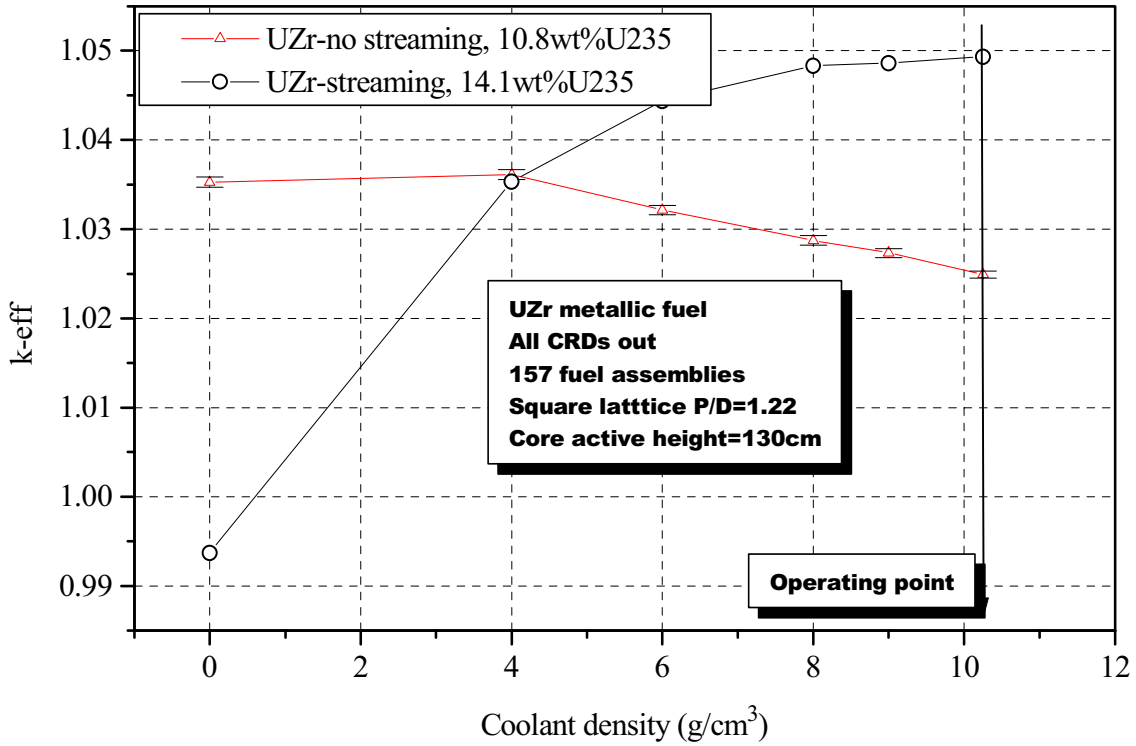

FIG. 4. Reactivity changes with coolant density for UZr fuel in regular and streaming core.

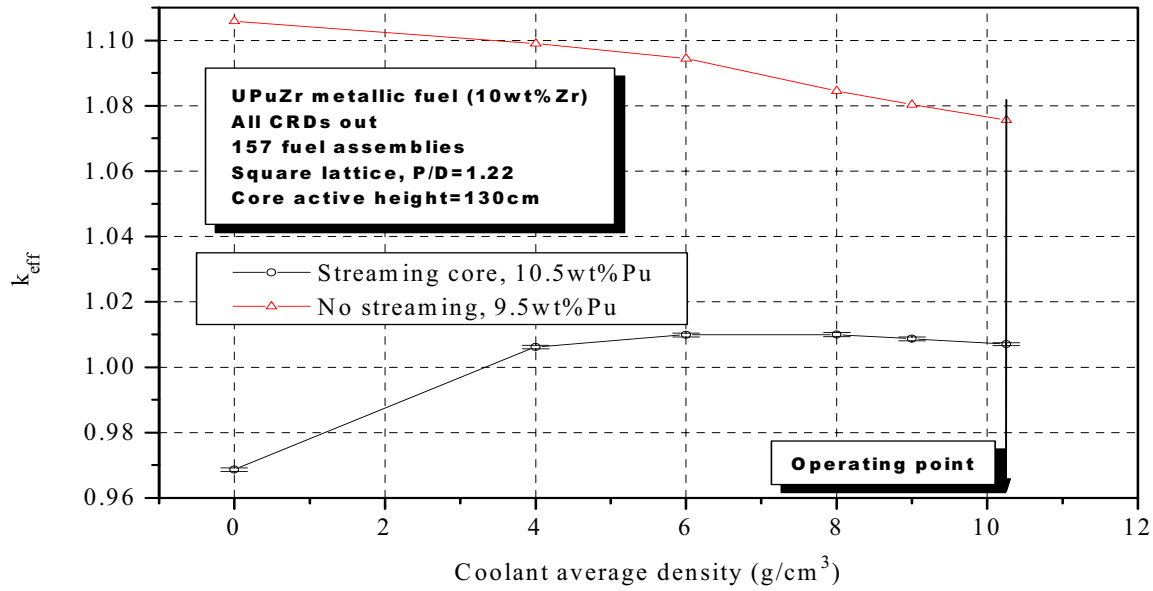

FIG. 5. Reactivity changes with coolant density for PuUZr fuel in regular and streaming core.

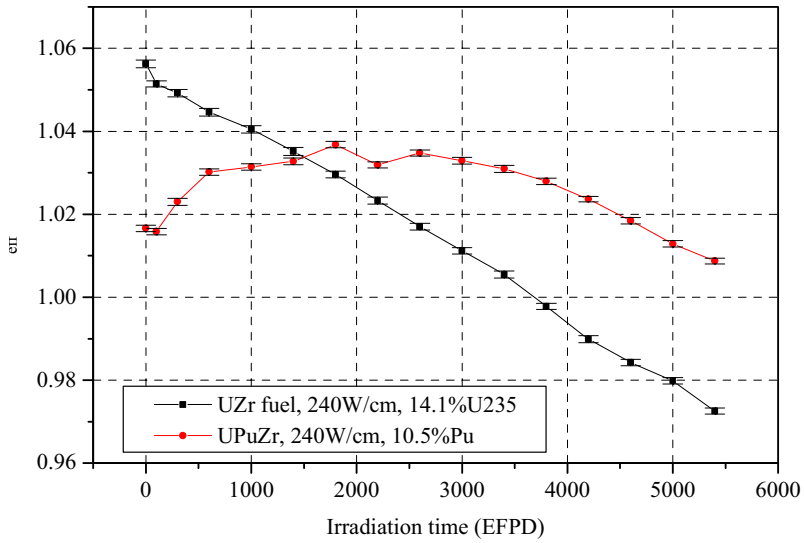

FIG. 6. Burnup curves for UZr and UPuZr fuels in a full core with streaming fuel assemblies.

5. SPENT FUEL CHARACTERISTICS

The characteristics of interest for the spent fuel, obtained from the unit cell model, are given in Table 6. The calculations assumed that the reactor was operated at full power at an average pin linear heat rate of 120 W/cm for 15 EFPYs, the discharged fuel went through 50 years of cooldown period (10 years in the pools at the NPP and 40 years in dry storage) before being deposited in the permanent repository.

The total mass of discharged actinides deposited in the permanent repository is roughly comparable for individual fuels. However, the amount of actinides, excluding the naturally occurring isotopes, per 1 MT of disposed fuel is appreciably higher for Pu-driven fuels. Metallic fuels have the most favorable heavy metal inventory per 1 MT of disposed fuel. Comparison of the discharged actinide mass inventory with a typical UO_2-fueled PWR (assuming a power output of 1142 MWe, plant efficiency 33.5%, fuel inventory 101 tonnes of UO_2, burnup of 33 GWd/t, 3 cycles with the replacement of 1/3rd of the core inventory once a year) showed that the high conversion concept with UZr fuel would discharge approximately 3 times less actinides per year per MWt-hr than a typical PWR. Increasing the burnup of metallic fuel to 170 MWd/kg further reduces this indicator to 4.5 times less.

UZr fuel exhibits the smallest radioactivity and ingestion hazard. The carbide fuels tend to have a larger hazard than the nitride fuels but less than oxide fuel. All fuel types containing Pu in the initial loading have, by almost an order of magnitude, higher toxicity than other fuel forms. In the thorium-based fuels, the activity of polonium, radon, radium and other isotopes from the thorium decay chain provides a significant contribution to the overall fuel activity, which degrades the benefits of thorium fuels. Similar trends can be observed for thermal power. The decay heat is by far the smallest for UZr fuel and significantly larger than any other fuel types (by an order of magnitude) in Pu fuels. High decay heat levels in Pu fuels are the consequence of a high content of Pu-238 and Am-241, which are strong alpha emitters with half-life of 87.7 and 432.7 years, respectively.

TABLE 6. TOTAL MASS, ACTIVITY, THERMAL POWER AND RADIOACTIVE INGESTION HAZARD PER 1 MT OF FUEL AFTER 15 EFPY OF OPERATION AND 50 YEARS AFTER DISCHARGE FROM REACTOR

Fuel	Actinide mass (kg)	Actinides-U,Th* (kg)	Activity (Ci)	Thermal power (W)	Ingestion hazard in m^3 of water
UO_2	793	82.06	2.24E+04	5.17E+02	3.36E+09
UN	879	77.71	1.14E+04	2.86E+02	1.85E+09
UPuN	875	121.36	8.91E+04	1.70E+03	1.15E+10
UThN	872	80.89	1.34E+04	3.66E+02	2.00E+09
UC	887	81.13	1.21E+04	3.01E+02	1.95E+09
UPuC	883	124.28	8.88E+04	1.70E+03	1.15E+10
UThC	876	86.51	1.50E+04	4.04E+02	2.24E+09
UZr	840	66.84	8.28E+03	2.16E+02	1.40E+09
UPuZr	837	98.85	6.28E+04	1.23E+03	8.32E+09
UThZr	833	70.23	1.12E+04	3.15E+02	1.64E+09
PuThZr	810	113.04	8.84E+04	1.86E+03	1.10E+10

* Actinides excluding naturally occurring actinides, such as Th-232, U-238, and U-235.

TABLE 7. PU PROLIFERATION CHARACTERISTICS OF THE FUEL AFTER 15 EFPY OF OPERATION AND 50 YEARS AFTER DISCHARGE FROM REACTOR

Fuel	Pu mass (kg/1 MT of fuel)	Spontaneous neutron production of Pu (n/kg-s)	Pu isotopics $Pu^{38}/Pu^{39}/Pu^{40}/Pu^{41}/Pu^{42}$ (wt%)
UO_2	79.82	1.44E+05	0.51/86.72/12.62/0.08/0.07
UN	64.71	1.02E+05	0.28/91.23/8.43/0.04/0.02
UPuN	115.82	2.24E+05	0.92/70.49/24.84/0.29/3.46
UThN	43.86	1.29E+05	0.45/90.88/8.61/0.04/0.02
UC	68.23	1.01E+05	0.27/91.06/8.60/0.04/0.02
UPuC	118.79	2.19E+05	0.89/71.13/24.36/0.28/3.34
UThC	47.78	1.35E+05	0.48/90.20/9.25/0.04/0.03
UZr	57.05	8.81E+04	0.21/93.06/6.70/0.03/0.01
UPuZr	94.80	2.00E+05	0.22/74.68/21.73/0.24/3.13
UThZr	36.89	1.15E+05	0.38/92.46/7.12/0.03/0.02
PuThZr	42.83	4.66E+05	2.22/36.68/50.72/0.63/9.75
UO_2-PWR*	-	3.72E+05	2.40/54.20/22.30/14.90/6.20
Weapons grade	-	5.35E+04	0.012/93.80/5.80/0.35/0.022

*UO2 fuel, burnup 45MWD/kg [9].

The key challenge for the heavy metal cooled long-life cores, which has not been pointed out in earlier studies of these systems, appears to be their failure to attain a discharged fuel composition that would be at least as proliferation resistant as current LWR spent fuel (Table 7). In particular, metallic fuels with U-235 fissile driver produce a very clean Pu vector, comparable to that of weapons-grade Pu due to relatively high Pu-239 production rate ($\sigma_c^{28} / \sigma_a^{29}$ an order of magnitude higher than in PWR cores) and the relatively low Pu-239 transmutation rate to higher isotopes ($\sigma_c^{29} / \sigma_a^{29}$ three times smaller than in a PWR). Even when a Pu vector from PWR spent fuel is used as a driver, the Pu composition of the spent fuel from the PbBi-cooled reactor is less

proliferation resistant than the original Pu vector. Replacing U-238 with Th-232 limits the Th-232 fraction to about 30-40wt% in a U-238/Th-232 mixture to keep the content of bred U-233 in the discharged fuel below the 12wt% proliferation constraint (Table 4). Thus, the benefits of thorium with respect to Pu generation cannot be fully realized and the main benefit is just the reduction of Pu mass in the spent fuel, which still contains a very high fraction of Pu-239.

It needs to be pointed out that the results obtained from the infinite unit cell model in this scoping study yield higher Pu mass in the discharged fuel because in the real core higher enrichment is needed to compensate for leakage and parasitic absorptions. To investigate these effects, UZr fuel was irradiated in the core with streaming assemblies to 170 MWd/kgHM and the Pu composition in the discharged fuel after 50 years of cooling was compared to that from the unit cell model of the same burnup. The higher burnup (pin linear heat rate was increased from the reference value of 120 to 240 W/cm) was selected to evaluate the effect of increased burnup on the composition of the Pu vector. The results are compared in Table 8. Doubling discharge burnup from 82 to 170 MWd/kgHM increased the mass of discharged Pu per 1 MT of fuel by 40% (but discharged Pu mass per energy produced was decreased by about 32%) and reduced the fraction of odd Pu isotopes (compare the first and second rows), but not enough to dilute the Pu vector to a level comparable with the Pu vector in spent LWR fuel. The comparison of the results from unit cell and full core model shows about 10% smaller Pu mass in the full core model and slightly higher mass ratio of Pu239 to Pu240. The latter result is at first surprising considering the fact that the spectrum in the full core model is slightly softer. Examination of the results revealed that although Pu239 generation was smaller in the full core model than in a unit cell simulation due to a smaller capture cross section of U238 and higher absorption cross section of Pu239, an appreciably higher absorption cross section of Pu240 in the full core model led to a faster removal rate of Pu240. Nevertheless, the differences between the unit cell and full core model are relatively small and unit cell results of discharged fuel indicators can be considered sufficient for this systematic scoping study.

TABLE 8. COMPARISON OF PU VECTORS FOR UZR FUEL AFTER 50 YEARS OF COOLING AT MEDIUM AND HIGH DISCHARGE BURNUPS AND THE DIFFERENCES BETWEEN UNIT CELL AND FULL CORE MODEL

	Pu238	Pu239	Pu240	Pu241	Pu243	Total Pu (kg/1 MT)
Unit cell, B_d=82MWd/kgHM	0.21	93.06	6.70	0.03	0.01	57.05
Unit cell, B_d=170MWd/kgHM	0.57	86.71	12.55	0.08	0.09	78.4
Full core, B_d=170MWd/kgHM	0.68	88.41	10.79	0.06	0.06	70.4

In addition to an increase of burnup, the strategy of softening the neutron spectrum was explored in an effort to reduce the fraction of odd Pu nuclides in the spent fuel. But even in the most extreme hypothetical case, where UZr fuel after an exposure of 120 MWd/kgHM in the Pb-Bi-cooled core was irradiated for additional 50 MWd/kgHM in a light water cooled lattice of identical geometry, the Pu vector in the spent fuel still contained a higher Pu-239 fraction than that of spent LWR fuel.

TABLE 9. CONSEQUENCES OF HARD SPECTRUM Pb-Bi FUEL CHOICES

FISSILE	FERTILE	PRO	CON
U-235 @ ≤ 20 w/o enrichment	U-238	• Fresh core fuel is not weapons usable • Lowest radioactivity, decay heat and radioactive ingestion hazard of spent fuel • The smallest mass of spent fuel • Very high conversion ratio	• Produces weapons grade Pu
	Th-232	• U-233 is denatured by U-238 • Less Pu production • Spent fuel toxicity only slightly higher	• Limited to ≤ 30 w/o Th because of enrichment limit on U-233 • Lowest conversion ratio • Highest initial enrichment • Lowest heavy metal loading
	None	Option not feasible due to U-235 enrichment limit	
Pu: LWR spent fuel weapons surplus; with or without minor actinides	U-238	• Highest conversion ratio • Smallest initial fissile enrichment	• Fresh core is an inventory of weapons-usable Pu • Even more so is spent fuel • High neutron flux, hence high dpa due to low fissile loading • High radioactivity, decay heat and radioactive ingestion hazard of spent fuel
	Th-232	• High Pu destruction rate • Appreciable U-232 production	• Produces weapons grade U-233 • Highest neutron flux and dpa • High radioactivity, decay heat and radioactive ingestion hazard of spent fuel
	None (Pu and/or MA burner)	• High Pu/MA destruction rate • Spent fuel not weapons usable	• Large cycle Δk, small β and Doppler Δk—especially if MA-only

Ranking of performance characteristics

Characteristic	Rank with chemical fuel form	Rank with fissile/fertile isotope
Conversion ratio	Metal (Zr) > Carbide>Nitride>Oxide	Pu>>U-235; U-238>Th-232
Reactivity gain	Metal (Zr) > Carbide>Nitride>Oxide	Pu>>U-235; U-238>>Th-232
Discharged TRU inventory	Oxide > Carbide >Nitride >Metal(Zr)	Pu>>U-235; Th-232>U-238
Curie inventory	Oxide > Carbide >Nitride >Metal(Zr)	Pu >>U-235; Th-232>U-238
Thermal decay power	Oxide > Carbide >Nitride >Metal(Zr)	Pu >>U-235; Th-232>U-238
Ingestion hazard	Oxide > Carbide >Nitride >Metal(Zr)	Pu >>U-235; Th-232>U-238
Discharged Pu inventory	Oxide > Carbide >Nitride >Metal(Zr)	Pu >>U-235; U-238>>Th-232
% Pu-239 in Pu	Metal (Zr)> Nitride ≈ Carbide >Oxide	U-235>Pu; U-238>>Th-232

6. CONCLUSION

Heavy metal cooled reactors with metallic zirconium based fuels can achieve long core life without refueling at very small reactivity swing. In addition, the designs of relatively large cores having negative coolant void worth for whole core voiding as well as negative coolant (or very small positive) temperature reactivity coefficient were found to be feasible. For the once-through reactor concept, an important consideration must be given to spent fuel. The consequences of fuel

choices in a hard spectrum Pb-Bi cooled reactor are summarized in Table 9. Fuels driven by U-235 and having U-238 as fertile material exhibit high conversion ratios and reactivity gain and have the smallest ingestion hazard, waste inventory, decay heat and radioactivity of discharged fuel. On the other hand they pose the worst proliferation threat since the bred-in Pu has a high content of Pu-239. Among these candidates metallic UZr fuel has the best reactivity and waste indicators, but the worst proliferation aspect with a Pu vector close to that of weapon grade Pu. Generally it can be stated that with respect to curie and TRU discharge inventory and ingestion hazard, chemical fuel forms can be ranked from metallic fuels (lowest) to nitrides, carbides and oxides with highest values. The difference between the nitride and carbide fuels is small. The fuels that have Pu as fissile exhibit significantly higher ingestion hazard and curie inventory. Fuels with Th-232 as fertile produce less plutonium, nevertheless, their fuel toxicity is slightly higher than that of the U-238 fuels.

Fuels driven by U-235 and having U-238 as fertile material were found to exhibit high conversion ratios and reactivity gain and the smallest ingestion hazard, waste inventory, decay heat and radioactivity of discharged fuel. The fuels that have Pu as the fissile isotope show significantly higher ingestion hazard and curie inventory. Fuels with fertile Th-232 produce less plutonium, nevertheless, their fuel toxicity is slightly higher than that of the U-238 fuels due to the activity of polonium, radon, and radium from the thorium decay chain. Note, however, that our hazard assessment does not account for differences in transportability of the various chemical species from repository to an exposed populace. In terms of discharged waste mass inventory, the long-life core generates 3 times less waste than a typical PWR at 33 GWd/t if a burnup limit of 100 MWd/kg is employed, but doubling the burnup to 170 MWd/kgHM, which is still feasible with metallic fuels increases this benefit by an additional 50%.

The key challenge for once-through Pb-Bi cooled reactors is to minimize the proliferation threat, in particular for fuels driven by enriched uranium. The demands of proliferation resistant fuel are contradictory to other requirements, such as low Curie inventory and ingestion hazard, because safeguards favor high radioactivity to hinder manipulation of the fuel, while for waste stream materials the least radiotoxicity is desirable. A solution to the spent fuel issue can be provided through reprocessing, i.e., extracting the actinides and recycling them back, but this shifts the proliferation problem to reprocessing site and fuel transport routes. It has been also proposed that the long-life cores that do not need refueling during their lifetime and are sealed preventing access to fuel provide enhanced proliferation resistance and thus could be exported to third world countries. However, in view of the above results, these claims may be questioned for cores with very hard spectrum where over most of the core life a large quantity of weapons grade plutonium resides in the core and it is difficult to assure that persons with malicious intentions do not break into the core to recover this material. International proliferation resistance criteria need to be defined to provide transparent rules for reactor design, operation and spent fuel characteristics including reprocessing guidelines to ensure a reasonably low proliferation threat and at the same time allow some freedom for the design of economical and safe generation four reactors.

REFERENCES

[1] ADAMOV, E., ORLOV, V., FILIN, A., LEONOV, V., SILA-NOVITSKI, A., SMIRNOV, V., TSIKUNOV, V., Next Generation of Fast Reactors, Nuclear Eng. Design, Vol. 173 (1997) 143-150.

[2] BRIESMEISTER, J. F., Ed., MCNP - A General Monte Carlo Code for Neutron, Photon and Electron Transport, Version 3A/3B/4A/4B, Los Alamos National Laboratory Rep. LA-7396-M, 1986, Revised in 1988, 1991, and 1997.

[3] CROFF, A.G., A User's Manual for the ORIGEN2 Computer Code, Oak Ridge National Laboratory Rep., ORNL/TM-7175 (1980).

[4] DRISCOLL, M.J., KIM, D., The Need for Actinide Burner Reactor Fuel Cycle Cost Reduction, Trans. Am. Nucl. Soc., Vol. 82 (2000).

[5] FORSBERG, C.W., HOPPER, C.M., VANTINE, H.C., What is Nonweapons-Usable U-233?, Trans. Am. Nucl. Soc., Vol. 81, Long Beach, California (1999) 62.

[6] GREENSPAN, E., SHIMADA, H., WANG, K., Long-Life Cores with Small Burnup Reactivity Swing, Proc. Int. Top. Mtg. on Advances in Reactor Physics and Mathematics and Computation Into the Next Millenium, (PHYSOR 2000), 7-11 May 2000, Pittsburgh, USA, ANS, ISBN: 0-89448-655-1 (2000).

[7] HEJZLAR, P., DRISCOLL, M.J., KAZIMI, M.S., Neutronic Design for a Pb-Bi Cooled Actinide Burner Fast Reactor**,** Trans. Am. Nucl. Soc., Vol. 81, Long Beach, California (1999) 271.

[8] HEJZLAR, P., DRISCOLL, M.J., KAZIMI, M.S., Conceptual Reactor Physics Design of a Lead-Bismuth-Cooled Critical Actinide Burner, Topical Report MIT-ANP-TR-069, Massachusetts Institute of Technology, Dep. of Nuclear Eng., (2000).

[9] HERRING, J.S., MAC DONALD P.E., Low Cost, Proliferation Resistant, Uranium-Thorium Dioxide Fuels for Light Water Reactors, Trans. ANS, Vol. 80 (1999).

[10] HILL, R.N., CAHALAN, J.E., KHALIL, H.S., WADE, D.C., Development of Small, Fast Reactor Core Design Using Lead-Based Coolant, Proc. Int. Conf. on Future Nuclear Systems, (Global '99), 1999, Jackson Hole, WY, USA, ANS, ISBN: 0-89448-641-1 (1999).

[11] VERHODKO, S.Z., ZAMUKOV, V.V., The Experience of Designing, Using and Utilizing the Nuclear Power Installations with Lead-Bismuth Liquid Metal Coolant for the "Alpha" Type Nuclear Submarine, paper presented in the Heavy Liquid Metal Conference (HLMC), 5-8 October 1998, Obninsk, Russia, CRS4, TECH-REP-00/50 (1999).

[12] KHORASOV, G.L., IVANOV, A.P., KOROBEINIKOV, V.V., Lead Coolant for Fast Reactor Burner with Hard Neutron Spectrum, Proc. Int. Top. Mtg. on Advances in Reactor Physics and Mathematics and Computation Into the Next Millenium (PHYSOR 2000), 7-11 May 2000, Pittsburgh, USA, ANS, ISBN: 0-89448-655-1 (2000).

[13] KUZNETSOV, V.V., SEKIMOTO, H., Radioactive Waste Transmutation and Safety Potentials of the Lead Cooled Fast Reactor in the Equilibrium State, J. Nucl. Sci. Tech., 32 (1995) 507-516.

[14] MOORE, R.L., SCHNITZLER, B.G., WEMPLE, C.A., BABCOCK, R.S., WESSOL, D.E., MOCUP: MCNP-ORIGEN2 Coupled Utility Program, INEL-95/0523, Idaho National Engineering Laboratory (1995).

[15] SPENCER, B.W., The Rush to Liquid Heavy Metal Reactor Coolants – Gimmick or Reasoned, Proc. 8th Int. Conf. on Nuclear Engineering (ICONE-8), 2000, Baltimore, MD, USA, American Society of Mechanical Engineers (ASME), New York (2000).
[16] SUBBOTIN, V.I., MATVEEV, V.I., TOSHINSKI, G.I., Lead-Bismuth Cooled Fast Reactors in Nuclear Power of the Future, Proc. Int. Top. Mtg. on Advanced Reactor Safety (ARS'94), 17-21 April 1994, Pittsburgh, USA, ANS, ISBN: 0-89448-193-2 (1994) 516-520.
[17] SU'UD, Z., SEKIMOTO, H., Design Study of Lead – and Lead-Bismuth-Cooled Small Long-Life Nuclear Power Reactors Using Metallic and Nitride Fuel, Nuclear Technology, 109 (1995).
[18] SHIMADA, H., GREENSPAN, E., STONE, N., WANG, S., Long-Life Lead-Cooled Core Fueled with Enriched Uranium, Trans. Am. Nucl. Soc., Vol. 80, Boston (1999) 199.
[19] TOMMASI, J., MASSARA, S., L.M.F.R. Dedicated Cores for Transmutation: Critical versus Subcritical Systems Comparison, Proc. Int. Conf. on Future Nuclear Systems (Global'99), 1999, Jackson Hole, WY, USA, ANS, ISBN: 0-89448-641-1 (1999).
[20] TOSHINSKY, G.I., LMFBR Operation in the Nuclear Cycle Without Fuel Reprocessing, Proc. Int. Topical Meeting on Advanced Reactors Safety (ARS'97), 1-5 June 1997, Orlando, FL, USA, Vol. 1., ANS, ISBN: 0-89448-624-1 (1997) 39-44.
[21] U.S. Department of Energy, Generation IV: Looking to the Future of Nuclear Power, Office of Nuclear Energy, Science and Technology, http://gen-iv.ne.doe.gov/ (2000).

RADIOLOGICAL HAZARD OF LONG LIVED SPALLATION PRODUCTS IN ACCELERATOR DRIVEN SYSTEM

M. SAITO, V. ARTISYUK, A. STANKOVSKII
Tokyo Institute of Technology, Japan

Abstract

The present paper focuses on analysis of radiological hazard of spallation products that appears to be an important factor that might affect the choice of beam/target performance in designing the accelerator-driven systems. The analysis is done in terms of toxicity expressed in units of annual limits on intake (ALI). It reveals the significant contribution of alpha emitting rare earths (^{146}Sm, ^{148}Gd, ^{150}Gd, ^{154}Dy) into overall toxicity of spallation targets.

1. INTRODUCTION

Accelerator-Driven System (ADS) often assumes a clean image compared to conventional critical reactors. Emotionally it relates to the fact that ADS is considered as a promising candidate for waste transmutation. Scientifically it is based on the subcritical operation mode that gives a chance of more safe incineration of the transuranics whose fission releases more neutrons than conventional fuel, other terms being equal. Such a safe fissioning in turn heavily relies on neutron supply initiated through spallation reaction triggered by high energy ions in so-called spallation target. Because of non-fission origin, these external neutrons being normalized to one hypothetical fission give a clear advantage of ADS in terms of available neutron excess relatively to the critical systems. That is very much attractive for transmutation of fission products (FP). Systematic analysis of neutron excess generation in ADS for FP transmutation has been already done in several studies [9, 10], while radiological burden of spallation products (SP) associated with this excess received less attention so far. Up till now, the most concern was given to alpha emitting ^{210}Po ($T_{1/2}$ =138 d) whose accumulation through neutron capture reactions in lead and lead-bismuth spallation targets is broadly discussed. However, some rare earth (RE) elements presented among SP (samarium, gadolinium, and dysprosium) have the isotopes unstable to alpha decay with half-lives ranging from several decades (^{148}Gd, $T_{1/2}$ =74.6 yr) to million years (^{146}Sm, $T_{1/2}$=1.03×10^{8} yr). There is not enough information to qualify these SP and that is the main incentive force to make their analysis.

Being scarcely presented in the waste stream of fission and fusion technologies alpha emitting RE are rather unique for nuclear engineering community. Because of their small mass number they cannot be transmuted through fission reaction in the same manner as alpha emitting transuranics. So, they are definitely the nuclear ash and their radiological burden is important to compare with that of FP and activation products (like ^{210}Po). In view of lack of data on RE accumulation, their yields obtained by means of computer simulation remains to be an important source of information. That is why the authors of the present paper did some careful validation of high-energy transport code CASCADE/INPE [1, 7] that is the main tool behind the present paper. Radiological burden of various spallation targets was estimated in terms of toxicity (units of Annual Limit on Intake). It reveal significant contribution of RE into overall toxicity of spallation targets that, in the case of Pb and Pb-Bi targets is comparable with polonium toxicity. The ways to reduce their accumulation without compromising the neutron production in ADS are also discussed.

2. SIMULATION OF SPALLATION PRODUCTS YIELDS IN VARIOUS TARGETS

Up till now quite a few experiments have been done to simultaneously cover the range of SP nuclides from light (atomic number is about 20) to initial target isotopes (W, Pb, U). That is why the experimental data are very welcome by ADS community for validation of computer codes engaged in ADS analysis. The validation usually goes through comparison of theoretical and experimental data for all the list of nuclides available from the experiment. Various modifications of mean square deviation criteria weighted over the all the SP nuclides serve to illustrate the code's predictive power, the logarithmic scale being often employed in order to level out the order-of-magnitude difference commonly observed in such a long list of data [13]. An important analysis of predictive power was done in Ref. [14] in terms of the following coincidence criterion:

$$F = 10^{\sqrt{\langle f \rangle}}$$

where $f = \lg(\sigma_{cal,i} / \sigma_{\exp,i})^2$; $\sigma_{j,i}$ -production cross-section of *i*-type nuclide in spallation target derived from the experiment and calculated by computer code. Table 1 lists the *F*-values inherent in several well famous computer codes applied to simulation of the experiment with irradiation of thin lead foil by 1 GeV protons [14]. As one can see, the predictable power of CASCADE/INPE code seems to be rather high.

TABLE 1. DEVIATION OF CALCULATED SPALLATION PRODUCTS' YIELDS FROM EXPERIMENTAL RESULTS*

Computer code	Reference	*F*-value
LAHET (ISABEL)	[15]	1.92
CEM2k	[16]	1.62
CASCADE	[17]	2.18
YIELDX	[18]	2.76
INUCL	[19]	2.89
CASCADE/INPE	[20]	1.85

* *F*-value for the codes and code references were taken from Ref. [14].

However, the low *F*-value does not prove the feasibility of the code for simulation of the yields for some particular class of SP, so, in this paper it is essential to prove the feasibility of the code to estimate yield of rare earths. Shown in Table 2 are the cumulative yields of some of them whose experimental yields were obtained in the experiment with irradiation of uranium foils by proton of various energies [13].

The table makes a stress on the fact that obvious underestimation in ^{155}Dy accumulation, would probably lead to underestimating the contribution of alpha emitting RE into the overall spallation target toxicity. Note, that this effect is about one order of magnitude. In other words, RE toxicity referred to in the present paper gives the only lower bound of what must be reasonably expected. Another important issue drawn from the Table 2 is that both additional experimental studies as well as elaboration on the theoretical models incorporated in the computer codes are requested with the stress on accumulation of SP with neutron number close to magic number 82.

TABLE 2. EXPERIMENTAL AND CALCULATED YIELDS OF RARE EARTHS IN $^{nat}U^{*}$

Nuclide	$T_{1/2}$	Proton energy (GeV)					
		0.8		1.2		1.6	
		Exp.	Calc.	Exp.	Calc.	Exp.	Calc.
^{171}Lu	8.24 d			2.30±0.26	1.34	6.77±0.62	6.26
^{169}Lu	34.06 h					4.34±0.41	5.33
^{166}Yb	56.7 h					3.51±0.40	4.18
^{160}Er	28.58 h					4.69±0.41	2.01
^{155}Dy	9.9 h	1.03±0.13	0.054	1.97±0.20	0.083	4.02±0.38	0.63

* Experimental data taken from Ref. [13].

Figure 1 gives more generic representation of SP accumulation in four different types of spallation target. Natural uranium, lead, tungsten and tin are selected to encompass the targets under consideration in various ADS projects [2, 6, 8, 12] as well as a wide variation of SP. Their independent yields were obtained with the help of CASCADE/INPE code. Three classes of SP might be identified from the shown distributions. One is represented by sharp peak of the light products dominated by tritium. The second comprises a wide list of intermediate products resulted from either fission and evaporation (in the case of heavy targets) or only evaporation (in the case of tungsten and tin) and the third is formed by extended range of nuclides sharply peaked at the mass numbers of initial target nuclei.

Figure 1 may shed light on the mechanism of RE accumulation. Their yield is obviously tends to increase for target material with mass numbers declining to rare earths. Even in uranium targets, where fission process could contribute in RE accumulation, their yield is obviously inferior to Pb and W targets. That gives strong evidence that the basic mechanism of their generation is evaporation process following the intranuclear cascade reaction. Needless to say that in tin target there is no RE among the SP, that is simply because the mass number of initial target material is less than RE.

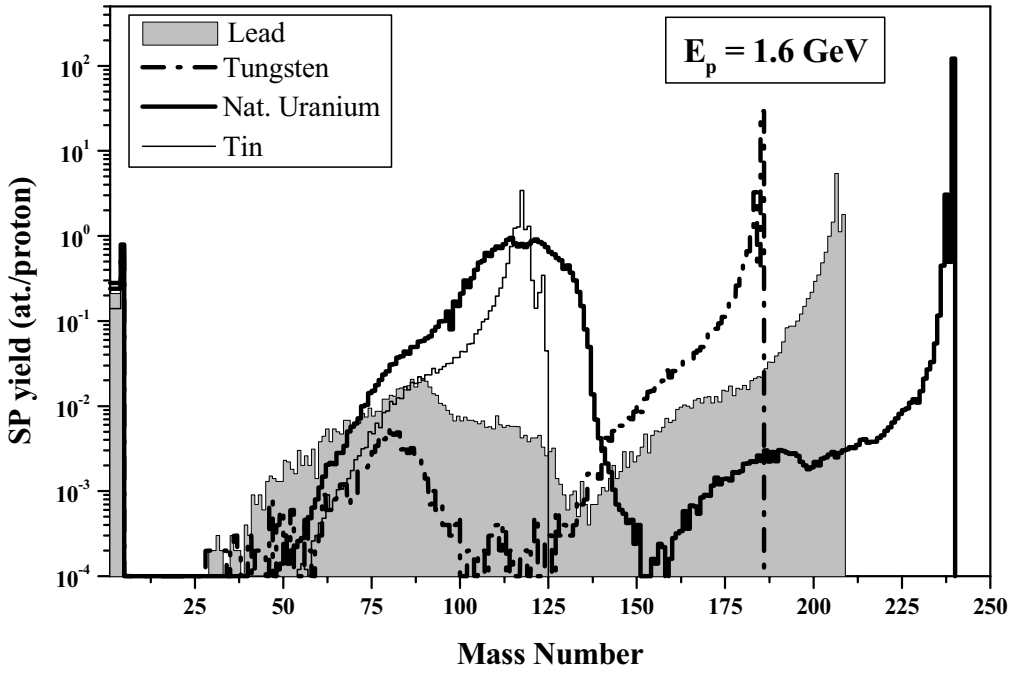

FIG. 1. Mass distribution of spallation products in various targets irradiated by 1.6 GeV protons.

3. TOXICITY ANALYSIS OF SPALLATION PRODUCTS IN VARIOUS TARGETS

Potential biological hazard from radionuclides is a technically best explained in terms of toxicity. By general definition toxicity is a ratio of amount of radioactivity to specified radioactivity guide [4]. Basically two kinds of toxicity are referred to in transmutation studies. One involves the concept of dose coefficient (DC) that is the committed effective dose resulting from unit intake (Sv/g). Given the amount of material in mass units, its normalization to inverse of DC gives the toxicity expressed in Sv. The other one is based upon the concept of Annual Limit of Intake (ALI) which is the smaller value of intake (Bq) in a year by the reference man that would result in a relevant committed dose limits. Taken the amount in activity units (Bq) and ALI as a radioactivity guide, the toxicity is simply treated in ALI units. DC are available from the International Commission on Radiological Protection [5] and ALI from The Code of Federal Regulations [3]. Characteristically enough, alpha emitting RE are poorly presented in both sources giving no data for ^{150}Gd and ^{154}Dy. These isotopes are the heaviest among the key RE and, therefore, their accumulation rate is expected to exceed that for ^{146}Sm and ^{148}Gd. For this reason it is quite important to make a reasonable assumption of their dose standards and that is the subject of this section.

Both concepts DC and ALI focus on the committed dose that, by definition, represents the dose received (by individual, organs or tissue) during some period of time following the intake (usually 50 yr for adult). So, to estimate the radioactivity guide one should take into consideration decay energy and energy deposition (both determining the dose) as well as half-life and characteristics of retention in the body (both reflecting the dose accumulation after intake). The authors of the present paper got used to refer ALI as a radioactivity guide and henceforth all the points concerning toxicity analysis will be discussed in ALI units. Note that ALI values are specified for different types of intake (inhalation, ingestion), different ranges of clearance half-times (day, week, year), different chemical compounds and might be differently normalized (whole body, critical organs). To avoid an ambiguity, in the present paper the minimum ALI value was selected for each particular nuclide. This resembles the approach in reactor safety analysis that deals with potentially severe accidents of extremely low probability postulated just to provide the limits for system designing.

Table III gives a general picture of minimum ALI values derived from [3], Part 20 for several classes of nuclides important in ADS analysis: MA and Pu (accelerator-driven transmuters are designed for); Pb, Bi and Po isotopes (activation products of especial concern in spallation target designs); several FP (some of them, like Tc and I are the candidates for transmutation in ADS), RE (with known ALI); uranium and tritium being presented merely for comparison. Also included in Table III are retention characteristics taken from Ref. [5], Publication 68 in terms of gut transfer factor – proportion of the intake transferred to body fluids in the gut. The information presented in Table 3 helps to make an assumption of ALI for ^{150}Gd and ^{154}Dy absent in the referred data sources.

TABLE 3. CHARACTERISTICS OF RADIOLOGICAL TOXICITY

Element	Isotope	Decay mode	Decay energy (MeV)	Half-life	ALI (Bq)*	Gut Transfer Factor**
Cm	244	α	5.9	18.1 yr	3.7×10^{2}	5.0×10^{-4}
	245	α	5.6	8.5×10^{3} yr	2.2×10^{2}	
Am	240	β	1.38	2.12 d	7.4×10^{7}	5.0×10^{-4}
	241	α	5.6	432.2	2.2×10^{2}	
Pu	239	α	5.25	2.41×10^{4} yr	3.7×10^{2}	5.0×10^{-4}
	241	β	0.02	14.4 yr	1.1×10^{4}	
Np	237	α	4.96	2.14×10^{6} yr	1.5×10^{2}	5.0×10^{-4}
	238	β	1.3	2.12 d	2.2×10^{5}	
U	235	α	4.7	7.04×10^{8} yr	1.5×10^{3}	0.02
	237	β	0.52	6.75 d	7.4×10^{7}	
	238	α	4.3	4.47×10^{9} yr	1.5×10^{3}	
Po	207	β	2.9	5.80 h	1.1×10^{8}	0.1
	210	α	5.4	138 d	2.2×10^{4}	
Bi	210m	α	5.3	3.0×10^{6} yr	2.6×10^{4}	0.05
	210	β	1.16	5.01 d	1.1×10^{5}	
Pb	210	β	0.064	22.3 yr	1.5×10^{4}	0.02
	205	β	0.051	1.43×10^{7} yr	3.7×10^{7}	
	202	β	0.05	5.25×10^{4} yr	1.9×10^{5}	
Hg	194	β	0.04	520 yr	7.4×10^{5}	0.02
Gd	148	α	3.3	74.6 yr	1.1×10^{3}	5.0×10^{-4}
Sm	146	α	2.53	1.0×10^{8} yr	2.2×10^{3}	5.0×10^{-4}
I	129	β	0.194	5.7×10^{6} yr	1.9×10^{5}	1***
Tc	99	β	0.3	2.1×10^{5} yr	2.6×10^{7}	0.8
Sn	126	β	0.38	$\sim10^{5}$ yr	2.2×10^{6}	0.02
	117m	β	0.315	13.6 d	3.7×10^{7}	
	119m	β	0.09	293.1 d	3.7×10^{7}	
	121m	β	0.006	55 yr	1.9×10^{7}	
H	3	β	0.019	12.33 yr	3.0×10^{9}	1.0

* Derived from Ref. [3], Part 20.
** Taken from Ref. [5], Publication 68.
*** Data for fast consumption through inhalation.

A cursory glance at the table shows that ALI for alpha-emitters are generally 2-5 orders of magnitude lower than for beta emitters. It is very important that gut transfer factors of transuranics and RE are the same and minimal among the nuclides presented in Table 3. It is worth to estimate the energy deposition during 50 yr after intake for ^{150}Gd and ^{154}Dy and compare this with MA. It could help to make an assumption of their ALI values. This approach reveals that such an energy deposition for nuclides in question is similar to that of ^{244}Cm. It gives strong evidence that expected ALI values for them are in the range between 2.2×10^{3} (the same as for ^{146}Sm that is maximum among alpha emitting RE) and 3.7×10^{2} (data for ^{244}Cm). In the present section for ^{150}Gd and ^{154}Dy ALI = 2.2×10^{3} was assumed to specify the lower bound of toxicity.

The toxicity analysis starts from differential equation for the time behavior of radioactive species:

$$\frac{dN_i}{dt} = I\ Y_i - \left(\lambda\ + \sigma\varphi\right)_i N_i = 0 \tag{1}$$

where the first term on the right side stands for SP accumulation rate associated with beam current I and the last term stands for depletion rate through both natural and artificial transmutation (herein the only neutron induced transmutation is envisioned). The yield of each particular nuclide per one proton (Y_i) might be translated to ***generated toxicity***.

$$T_i = \left(\frac{\lambda Y}{ALI}\right)_i \tag{2}$$

thus giving an image of toxicity weight of each nuclide produced by one proton at every time moment. Another characteristic is an ***equilibrium toxicity*** that makes a stress on natural trend of radionuclide to approach saturation. With assumption of no artificial transmutation, equilibrium toxicity derived from Eq. (1) looks like follows:

$$T_i^{eq} = I\left(\frac{Y}{ALI}\right)_i \quad . \tag{3}$$

Both characteristics enable to make a preliminary but important analysis: being largely governed by activity, T_i highlights the short-lived nuclides, while T_i^{eq} addresses the interplay between yield and specific radioactivity guide (that is ALI in the case).

Figure 2 [11] shows T_i and T_i^{eq} for three targets: lead, tungsten and tin irradiated by 1.6 GeV protons (maximum energy being discussed in ADS projects). Wide range of nuclides with half-lives in-between 12.3 yr (tritium) and 4.47×10^9 yr (^{238}U) was taken into consideration. The beam current of 1 mA was assumed as a reference in equilibrium analysis. It appears that RE alpha-emitters provide 90% contribution to generated toxicity in tungsten. In lead target it is dominated by relatively short-lived isotopes ^{60}Co and ^{90}Sr (effect of high activity) and ^{194}Hg (large yield), though the contribution of alpha emitting RE is also quite appreciable being about 10% (Fig. 2a). The impressive is their role in equilibrium state. They contribute the most into both lead and tungsten targets' toxicity (Fig. 2b). It is interesting to note that exclusively the presence of RE makes the tungsten target more toxic than lead in a long-term perspective.

Though equilibrium toxicity being considered here ignores the SP burnup in situ it might be used for feasibility analysis especially in the case of liquid targets. As known, rare earths are characterized by rather high melting point (1310, 1070, and 1425°C correspondingly for Gd, Sm and Dy) and they might precipitate in the structures of heat exchangers outside the neutron field. From this standpoint toxicity estimates given in this section represent the upper limiting values for liquid lead and tin targets with strong evidence in favor of tin.

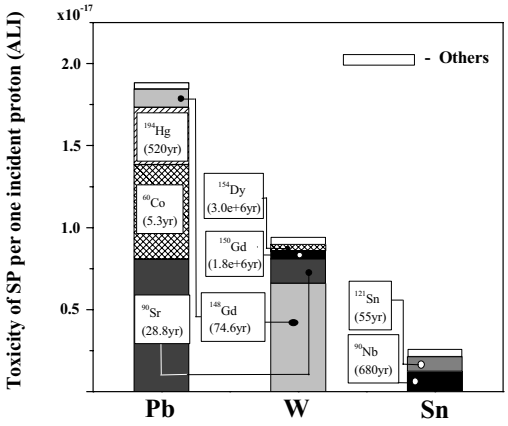

a) Generated toxicity.

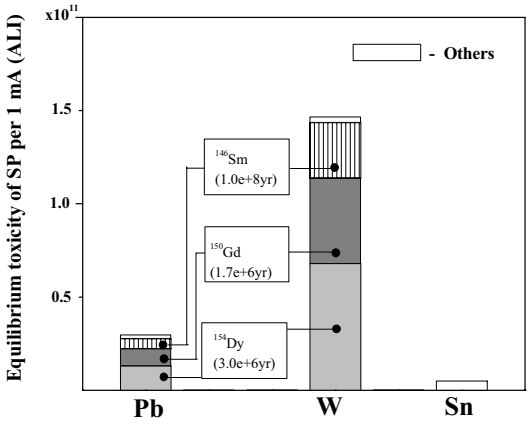

b) Equilibrium toxicity (beam current is 1 mA).

FIG. 2. Generated and equilibrium toxicities in various targets irradiated with 1.6 GeV protons.

4. TOXICITY OF SPALLATION, FISSION AND ACTIVATION PRODUCTS

This section deals with comparison of RE toxicity in Pb-Bi target with that of fission products in the blanket. It seems to be interesting in view of the fact that neutron excess available in ADS almost in each project is advertised for transmutation of long-lived ^{99}Tc ($T_{1/2}$ = 2.11×10^5 yr) and ^{129}I ($T_{1/2}$ = 1.57×10^7 yr). Another important topic is alpha emitting activation product ^{210}Po ($T_{1/2}$ = 138 days) which is the main concern and continuous issue of contention in discussing the pro and contra of heavy liquid coolants like lead and lead-bismuth eutectic for advanced fast reactor. The same concern appears in discussing the pro and contra of various spallation targets.

4.1. Alpha emitting rear earths against long-lived fission products

As it was mentioned before, along with fissioning the transuranics, neutronics of ADS blankets is considered with respect to transmutation of long-lived FP such as ^{99}Tc and ^{129}I, which are the most problematic nuclides because of their high mobility in geological structure. Final goal of artificial transmutation is to approach the equilibrium inventories which are manageable within the fuel cycle, thus to avoid uncontrolled underground storage. For this reason it is the equilibrium toxicities of fission and spallation products that are being compared in this paper. Artificial transmutation of SP should not be neglected and in view of Eq. (1) the expression for SP equilibrium toxicity turns to

$$T_i^{eq} = I\left(\frac{Y}{ALI\times(1+\sigma\varphi/\lambda)}\right)_i. \qquad (4)$$

Fission neutrons from the blanket will effect the neutronics in the target. In the present analysis assumed blanket power is 1 GWt that reveals flux of 10^{15} n/(cm^{2}s) that is typical for fast spectrum facilities. Having assumed this value, total flux in the target derived from the target neutronic simulation is 2.4×10^{15} n/(cm^{2}s). Corresponding beam current of 1.6 GeV protons is about 20 mA. Summary of the important neutronics characteristics is given in Table 4. Not surprisingly, because of low neutron absorption in the target, flux in the target is higher than in the blanket. At this neutronics conditions the lifetimes of selected SP in the target are 27.6, 5.42 and 1.82 yr for ^{146}Sm, ^{150}Gd and ^{154}Dy, respectively. It means that they easy approach their equilibrium state under neutron irradiation.

TABLE 4. CHARACTERISTICS OF SELECTED ISOTOPES IN FAST NEUTRONICS ENVIRONMENT INHERENT IN ADS

	Spectra in spallation target		Blanket spectrum
	Bare target	Target with blanket	
Average energy (keV)	1428	342	367
One group cross-sections (b)			
^{146}Sm	0.10	0.43	0.39
^{150}Gd	0.29	2.44	1.73
^{154}Dy	0.75	7.26	4.25
^{99}Tc	-	-	3.15
^{129}I	-	-	0.82
Typical flux (n/cm^{2}s)	(*)	2.4×10^{15}	1×10^{15}

* Total flux in the target is governed exclusively by beam current.

Figure 3 represents the equilibrium toxicities for selected SP and FP. Note, that for ^{154}Dy and ^{150}Gd maximum ALI was assumed (ALI = 2.2×10^3) to show the lower boundary of SP toxicity (in the reality with other terms being equal, the SP toxicity might be higher than that of comprised in Fig. 3). Case 1 does not account for transmutation of any nuclide. It is matter of fact that SP and FP demonstrate quite comparable equilibrium toxicity. Transmutation in situ reveals intensive SP transmutation that results in their equilibrium toxicity being in three orders of magnitude less compared to FP (Case 2). However this is a limiting case since being circulated with liquid lead, SP will escape neutron irradiation and, as was stressed before, might precipitate and be kept outside the target region. So, it is worth to consider the limiting situation when the FP are transmuted in the blanket but SP remain unaffected (corresponding data are presented by left column of Case 2 and right column of the Case 1 in Fig. 3). This gives the caution about advantages of ^{99}Tc and ^{129}I transmutation in ADS. The benefit of their transmutation might be counterbalanced or even outweighed by accumulation of alpha-emitting RE if the last are not treated properly.

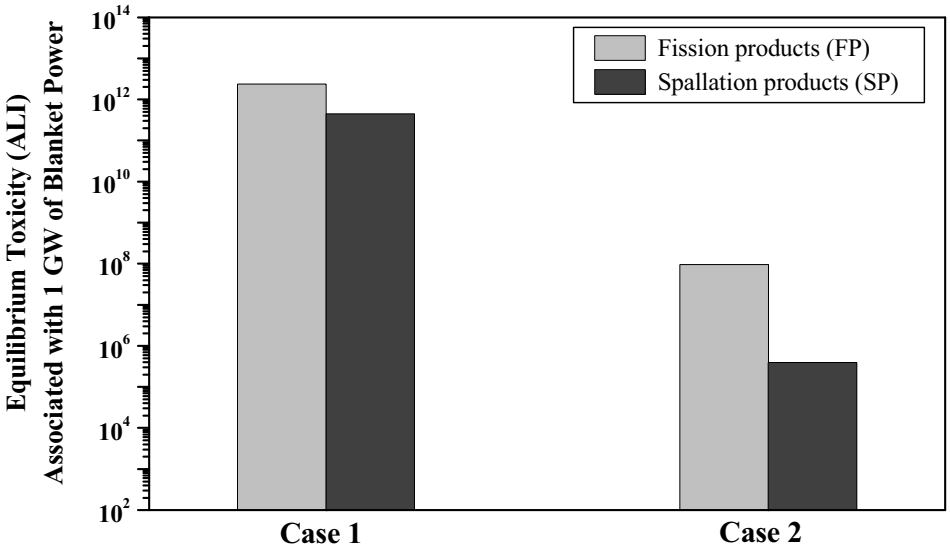

FIG. 3. Equilibrium toxicities of selected fission (^{99}Tc, ^{129}I) and spallation products (^{146}Sm, ^{150}Gd and ^{154}Dy).

Case 1: No transmutation applied.
Case 2: Transmutation in situ (FP in the blanket, SP in the target).

4.2. Alpha emitting rare earths against polonium activation products

Reference model for analysis of polonium accumulation is the same as assumed in the previous section: beam current is 20 mA, total flux in the target is 2.4×10^{15} n/(cm^{2}s), neutron spectrum was obtained trough CASCADE/INPE code. The results are presented in Fig. 4 as a time behavior of toxicities of the key alpha emitters (polonium and RE) in the course of ADS performance.

In reactor coolants, accumulation of ^{210}Po goes mainly through neutron capture in ^{209}Bi, thus giving the possibility of one-step production reaction in the eutectic, and, at least two-step reaction in pure lead that starts from neutron capture in double-magic nucleus of ^{208}Pb. In the case of spallation target, in addition to neutron-induced activation, proton capture and (*p, xn*) reactions feed the bismuth component and yields the light polonium isotopes ^{208}Po ($T_{1/2}$ = 2.9 yr), ^{209}Po ($T_{1/2}$ =102 yr) as well. That is why at the early stages of irradiation the toxicities of light polonium isotopes exceed that of ^{210}Po.

Interesting result is that ^{210}Po toxicity converges in the area of uncertainties of ^{154}Dy toxicity after two years irradiation. One could reasonably expect that polonium and RE toxicities are quite comparable. It means that after shutdown of ADS, toxicity of spallation target would be governed by RE alpha emitters for a quite long time. This fact should not be ignored in designing the ADS.

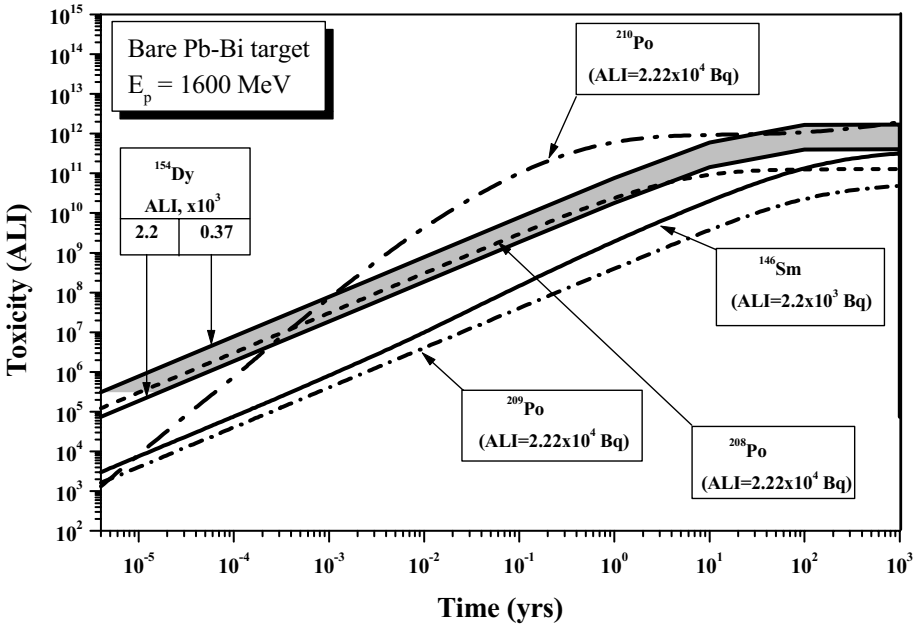

FIG. 4. Time behavior of toxicities for alpha emitters in Pb-Bi spallation target.

5. WAYS TO REDUCE RE ACCUMULATION IN LEAD TARGET

Changing the target material from lead to tin is a rather straightforward approach. The technology of liquid tin is less known that that of lead-based alloys. That is why it is worth to consider the ways of reducing the RE accumulation in lead target. At first consider the beam energy. It is illustrated by Fig. 5 that shows SP yields in lead target irradiated by protons with energy 0.8, 1, and 1.6 GeV [11]. Especially prominent is reduction of nuclides with atom numbers around 150. However this effect will confront with the overall decrease in neutron production. Another approach to reduce the RE accumulation is to apply the deuteron beam. It is well known fact that at the same initial energy, deuteron generates more neutrons than

proton. Increase in neutron production is about 10% as follows from Fig. 6a that comprises the energy dependent neutron production in spallation targets bombarded by protons and deuterons.

Pure outcome from energy adjustment might be seen in terms of total equilibrium toxicity ($\sum_i T_i^{eq}$) related to one neutron shown for tin and Pb-Bi targets in Fig. 6b. Below 0.8 GeV total equilibrium of lead target is largely determined by ^{194}Hg and two long-lived isotopes ^{202}Pb ($T_{1/2}$ = 5.25×10^{4}yr) and ^{205}Pb ($T_{1/2}$ = 1.53×10^{7}yr) and, though contribution of alpha-emitters vanishes, lead remains to be inferior to tin. This is the main result that might be obtained from energy adjustment for both proton and deuteron beams.

Change of the beam type from proton to deuteron especially effective for Pb-Bi target. That is the pure effect of suppressing in RE accumulation. In the case of deuteron, the reference energy might be translated to the 800 MeV per one nucleon at which RE accumulation significantly less than at 1.6 GeV (Fig. 6). This results in toxicity reduction by factor 5 at reference energy of 1.6 GeV.

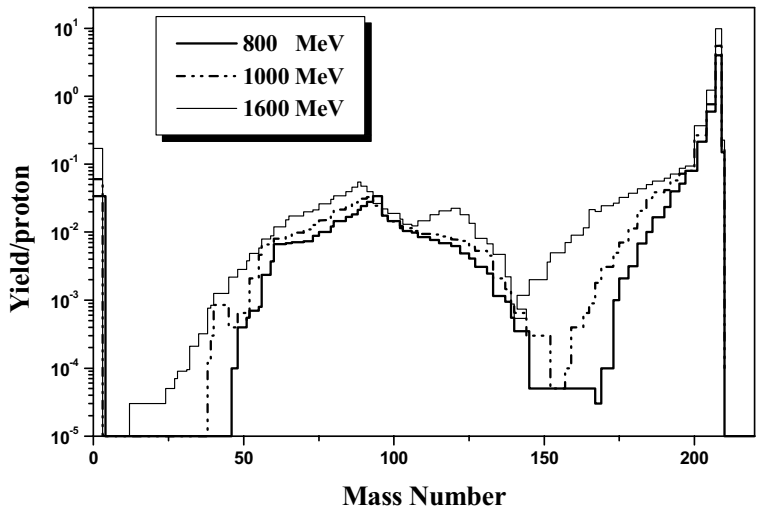

FIG. 5. Yield of spallation products in lead target irradiated by 0.8, 1.0, and 1.6 GeV protons.

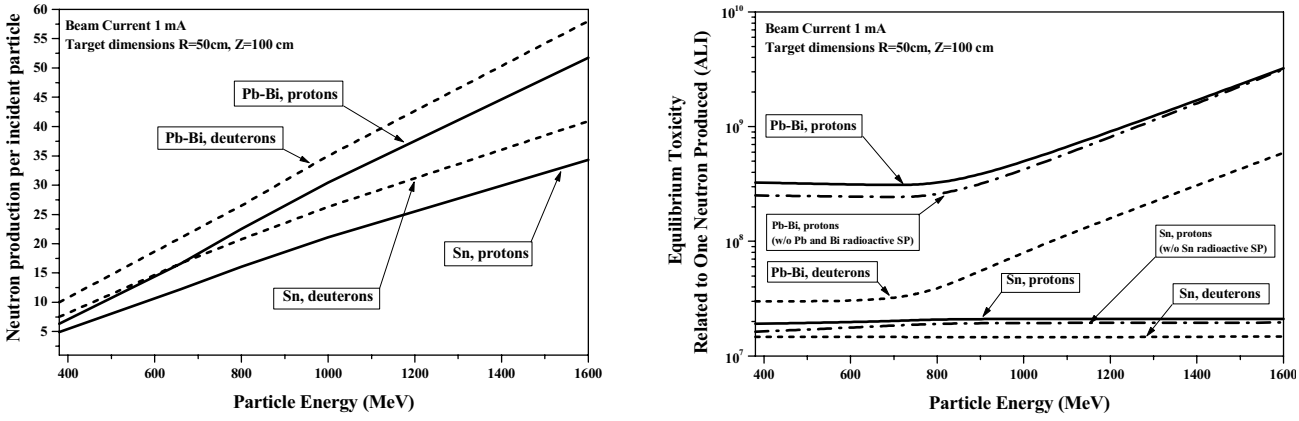

a) Neutron production per one incident particle.

b) Equilibrium toxicity normalized to one neutron produced.

FIG. 6. Effect of beam characteristics on neutron production and equilibrium toxicity in Pb-Bi and Sn spallation targets.

6. CONCLUSIONS

The main outcome of the present paper is toxicity analysis of radionuclides accumulated in various spallation targets that reveals an important role of alpha-emitting rare earths ^{146}Sm, ^{148}Gd, ^{150}Gd and ^{154}Dy. These nuclides give a significant contribution into overall toxicity of spallation targets with exception of tin, which is free from alpha-emitters. This seems to be an important factor to make a design choice of accelerator-driven neutron source. Spallation products transmutation in situ in lead target was studied for alpha-emitting rare earths against transmutation of ^{99}Tc and ^{129}I advocated in current projects of accelerator-driven cores. The results obtained give a caution about benefits of ^{99}Tc and ^{129}I transmutation without proper treatment of ^{146}Sm, ^{150}Gd and ^{154}Dy. The toxicity of rare earths is rather prominent in comparison with that of polonium. This preliminary result is very important and will be carefully elaborated on in the future studies.

REFERENCES

[1] BARASHENKOV, V.S., et al., CASCADE/INPE. Code System, Atomnaya Energiya, 87 (1999) 283 (in Russian).

[2] CAPPIELLO, M.W., The Fluidized Bed Spallation Target, Proc. 3rd Int. Embedded Top. Mtg. on Nuclear Applications of Accelerator Technology (AccApp99), 14-18 November 1999, Long Beach, CA ANS, ISBN: 0-89448-643-8 (1999) 53-58.

[3] CFR, The Code of Federal Regulations, Part 20: Standards for Protection Against Radiation Appendix B (1991).

[4] HEBEL, L.C., et al., Report to the American Physical Society by the Study Group on Nuclear Fuel Cycles, Rev. Mod. Phys., 50, No 1, Part II (1987).

[5] ICRP, International Commission on Radiological Protection, Publication 68, 72, Inhalation and Ingestion Data for Workers (1994).

[6] KHORASANOV, G.L., et al., Lead and Tin Targets for Reducing Polonium Waste, Proc. 3rd Int. Conf. on Accelerator-Driven Transmutation Technologies and Applications (ADTTA'99), 7-11 June 1999, Prague, Czech Republic, Eds: L M. Hron, V. Lelek (NRI Rez plc), M. Mikisek, M. Sinor, J. Uher, J. Zeman (FNSPE CTU, Prague), NRI Rez, Czech Republic (1999).

[7] KONOBEEV, A.Yu., et al., Study of Accelerator-Driven Reactor System, Kerntechnik 64, 127 (1999).

[8] RUBBIA, C., Conceptual Design of a Fast Operated High Power Energy Amplifier, CERN/AT/95-44(ET), Geneva (1995).

[9] SAITO, M., et al., Contribution of External Neutron Sources in Excess Neutron Generation for SCNES, Progress in Nuclear Energy, Vol. 32 (1997) 697-705.

[10] SALVATORES, M., et al., A Global Physics Approach to Transmutation of Radioactive Nuclei, Nucl. Sci. Eng., 116 (1994) 1-18.

[11] STANKOVSKII, A., et al, Accumulation and Transmutation of Spallation Products in the Target of Accelerator-Driven Systems, submitted for publishing in Journal of Nuclear Science and Technology in 2000.

[12] TAKIZUKA, T., et al., Pathways for Fission Energy Supply Infrastructures of 21st Century. A systems Viewpoint, Proc. Int. Conf. on Future Nuclear Systems, (Global'99), 1999, Jackson Hole, Wyoming, USA, ANS, ISBN: 0-89448-641-1 (1999) 422-427.

[13] TITARENKO, Yu.E., et al., Experimental and Computer Simulation Study of Radionuclide Production in Heavy Materials Irradiated by Intermediate Energy Protons, Embedded Top. Mtg. on Nuclear Applications of Accelerator Technology (AccApp99), 14-18 November 1999, Long Beach, CA, ANS, ISBN: 0-89448-643-8 (1999) 212-221.
[14] TITARENKO, Yu.E., et al., Cross sections for nuclide production in 1 GeV proton-irradiated ^{208}Pb, Phys. Rev. C 65 064610 (2002).
[15] PRAEL, R.E., LICHTENSTEIN, H., User Guide to LCS: The LAHET Code System, LANL Report LA-UR-89-3014 (1989).
[16] MASHNIK, S.G., et al., Improved Cascade-Excitation Model of Nuclear Reactions, Proc. 5th Int. Workshop on Simulating Accelerator Radiation Environments, 17-18 July 2000, OECD Headquarters, Paris, France, NEA (2000).
[17] BARASHENKOV, V.S., et al., High-Energy Transport Code CASCADE, JINR, R2-85-173, Dubna, Russia (1985).
[18] SILBERBERG, R., et al., Partial Cross Sections of Nucleus-Nucleus Reactions, Astrophys. J., 501, 911 (1998).
[19] LOBOV, G.A., et al., Cascade-excitation model analysis of proton spallation from 10 MeV to 5 GeV, ITEP Preprint ITEP-91, Moscow, Russia (1983).
[20] BARASHENKOV, V.S., et al., CASCADE/INPE. Code System, Atomnaya Energiya, 87, 283 (1999) (in Russian).

SUB-CRITICAL BLANKET DEVELOPMENT

(Session 4)

Chairperson

H.A. ABDERRAHIM

Belgium

SOURCE NEUTRON MULTIPLICATION IN SUBCRITICAL REACTORS: ITS DEPENDENCY ON CORE DESIGN

Y.H. KIM, W.S. PARK, T.Y. SONG
Korea Atomic Energy Research Institute, Republic of Korea

Abstract

The effectiveness of the external neutron source has been evaluated in terms of its multiplication in subcritical reactors. Mathematical formulas for the source neutron multiplication are reviewed and their implications are addressed. In order to identify dependency of the spallation neutron multiplication on the core design features, numerical experiments are performed with a Monte Carlo code for an accelerator-driven system, HYPER (HYbrid Power Extraction Reactor). For various core conditions, the actual source multiplication factors are compared with the conventional critical mode expectation. Sensitivity of the multiplication factor to the radial power distribution is investigated to find an optimum radial power distribution from the point of the spallation neutron multiplication. Also, impacts of neutron absorbers on the source multiplication are considered in this work. In addition, the efficiency of external spallation neutrons is evaluated for proton target designs.

1. INTRODUCTION

Recently, the accelerator-driven system (ADS) has been actively studied over the world, with a new paradigm of the nuclear energy, due to its enhanced safety and greater potential of transmutation of the radioactive nuclear waste [1-3]. In ADS, the reactor core is subcritical and produces a constant power with external spallation neutron sources generated by high power proton accelerators. The basic principle of ADS is that spallation neutrons, which are produced in a target zone, are multiplied in the fuel blanket via fission reactions. In general, the smaller subcriticality is, the higher is the multiplication.

ADS is usually designed to have sufficient subcriticality, $k_{eff} = 0.90 - 0.98$, to guarantee its surmised advantages. In such a highly subcritical core, effective multiplication of spallation neutrons is crucial for economics. A report for the ATW (Accelerator Transmutation of Waste) system shows that the multiplication of source neutrons should be at least larger than 20 for economic operations [4]. Concerning the neutron multiplication, in ADS-related works, the effective neutron multiplication factor, k_{eff}, is frequently used as a measure of the source multiplication without any concrete explanation: a spallation neutron is multiplied by a factor of $1/(1-k_{eff})$ in the fuel blanket. Based on the critical mode expectation, the authors of Ref. [4] concluded that k_{eff} of the ATW core should be greater than 0.95.

As is well known, $1/(1-k_{eff})$ represents, on the average sense, the multiplication of a fission source neutron in subcritical reactors, not the external spallation neutron. In practical ADS, the spallation neutrons are generated in a local target zone, where no fission source is generated, and also the energy spectrum of spallation neutrons is far from that of the fission neutrons. As a result, the two neutrons have different importance and the fission neutron distribution is much different from that obtained with a critical mode calculation. Therefore, multiplication of the spallation neutron is generally different from that of the fission neutron. Thus, using the simple formula, $1/(1-k_{eff})$, for an ADS may lead to serious misunderstanding of the subcritical system and the related results can be invalid. It should be noted that, when it comes to the spallation neutron multiplication, ADSs with the same subcriticality may have quite different values, depending on the core design features.

The objective of this work is to address the basic phenomena of the spallation neutron multiplication in the ADS system. The fundamental physics of subcritical reactors is briefly reviewed from the viewpoint of the source neutron multiplication. Also, various numerical experiments are performed for an ADS with a Monte Carlo code, MCNAP [5], to investigate the dependency of the source multiplication on fuel blanket and target designs.

2. THEORETICAL ANALYSIS

Let us consider a stationary subcritical system described by the neutron transport theory. Letting $S(r,\Omega,E)$ be the external spallation neutron source, a subcritical system can be written, in an operator form,

$$(F - M)\phi + S = 0, \tag{1}$$

where F and M denote the appropriate fission and neutron removal operators, respectively, and ϕ is the angular flux. For simplicity, detail expressions for F and M are not given here.

In this paper, the source multiplication factor (M_s) for the system of Eq. (1) is defined by 1 plus fission neutron gains. The fission neutron gain is the number of fission neutrons produced by a source neutron in the fuel blanket. Then, M_s can be written as

$$M_s = \frac{\hat{S}_{tot}}{\hat{S}} \tag{2a}$$

$$\hat{S} = <1, S> \tag{2b}$$

$$\hat{S}_{tot} = <1, F\phi + S> \tag{2c}$$

where $<\cdot>$ means the inner product.

Following the definition, the static reactivity of the subcritical system (ρ_{st}) can be written as

$$\rho_{st} = \frac{<\Phi_\lambda^*, [F - M]\phi>}{<\Phi_\lambda^*, F\phi>}, \tag{3}$$

where the weighting function Φ_λ^* is the so-called adjoint λ –mode flux satisfying

$$(M^* - \lambda F^*)\Phi_\lambda^* = 0, \tag{4}$$

where F^* and M^* are the adjoint operators of F and M , respectively.

As is well known, the adjoint operator cannot be defined uniquely for a subcritical system. Conventionally, the λ–mode equation, Eq. (3), is used for consistency with the critical reactor system. It is obvious that the fundamental eigenvalue of Eq. (4) is equal to the inverse of the effective multiplication factor, i.e., $1/k_{eff}$ for the corresponding critical system. In other words, the static reactivity of Eq. (3) can be rewritten as

$$\rho_{st} = 1 - \lambda = 1 - \frac{1}{k_{eff}}, \tag{5}$$

where $1/k_{eff}$ is the eigenvalue of the following critical system

$$(M - \frac{1}{k_{eff}} F)\varphi = 0. \tag{6}$$

Using Eqs (1) and (3), one can get a static adjoint-weighted source multiplication formua for the subcritical system of Eq. (1):

$$< \Phi_{\lambda}^{*}, [F\phi + S] >= \frac{1}{1 - k_{eff}} < \Phi_{\lambda}^{*}, S > . \tag{7}$$

Equation (7) shows that the source multiplication factor in subcritical reactor cannot be determined by only the k_{eff} value, instead the critical mode expectation is only a adjoint-weighted value. This implies that an accurate calculation of the source multiplication factor can only be done by directly solving the inhomogeneous problem in Eq. (1). The λ-mode adjoint flux generally depends on the core design and is a highly space-dependent function. Consequently, the source multiplication is tightly linked to all the core design features such as source distribution, fuel composition, geometry of the core, etc.

In Eq. (7), setting Φ_{λ}^{*} to be unity, we get an approximate source multiplication, M_s^{apx},

$$M_s^{apx} = \frac{1}{1 - k_{eff}} \tag{8}$$

M_s^{apx} is just the frequently-used expression for the external source multiplication in ADS. In other words, the simple critical mode expectation for M_s is an unweighted inaccurate source multiplication. Thus, it is clear a critical-mode analysis of a subcritical system can only provide an approximate source multiplication factor given by Eq. (8).

Equations (7) and (8) say that there can be a big discrepancy between the actual source multiplication and the approximate one. One example would make the point very clear. Let us assume that a localized independent source is located in the core center and the source is surrounded by a black absorber. Even in this situation, it is possible to make the core slightly

subcritical, e.g., $k_{eff} = 0.99$. For this system, M_s^{apx} gives a source multiplication factor of 100. However, the actual source multiplication factor M_s is obviously 1.0, i.e., no multiplication, since the source neutron cannot produce any fission neutrons.

The difference between M_s and M_s^{apx} would be clear for the case of a point neutron source with particular values of r_0, Ω_0, and E_0: $S = S_0(r_0, \Omega_0, E_0)$, where δ is the delta function. In this case, the source multiplication factor can be written as

$$M_s = \frac{1}{1-k_{eff}} \frac{<1, [F\phi + S]>}{<\frac{\Phi_\lambda^*}{\Phi_\lambda^*(r_0, \Omega_0, E_0)}, [F\phi + S]>}. \quad (9)$$

In Eq. (9), one can see that the source multiplication depends on the ratio of Φ_λ^* to the source neutron importance $\Phi_\lambda^*(r_0, \Omega_0, E_0)$. Clearly, increasing $\Phi_\lambda^*(r_0, \Omega_0, E_0)$ results in more efficient source neutron multiplication and small $\Phi_\lambda^*(r_0, \Omega_0, E_0)$ gives ineffective multiplication of the source neutron. It should be noted that M_s is maximized and is greater than M_s^{apx}, if the source neutron is located at the point of the maximum neutron importance, i.e., $\Phi_\lambda^*(r_0, \Omega_0, E_0) = \max \Phi_\lambda^*$. Unfortunately, the optimal source neutron cannot be realized in practical subcritical reactor due to the resulting unacceptably high power peaking at the source point. Therefore, the source position is usually compromised within the constraints of core designs.

3. NUMERICAL EXPERIMENTS

3.1. The HYPER core

In order to address the limitation of the approximate source multiplication factor and to investigate the impact of core design features on the source multiplication, various numerical experiments are performed for the HYPER (HYbrid Power Extraction Reactor) [6]. The HYPER system is a Pb-Bi-cooled ADS under development at KAERI, with the aim of transmuting both TRUs (transuranic elements) and fission products (FPs) such as Tc-99 and I-129. The thermal power of HYER is 1000 MWth and its minimum required subcriticality is $k_{eff} = 0.97$.

Figure 1 shows a schematic configuration of the evolving HYPER core. As shown in Fig. 1, the fuel blanket is divided into 3 TRU enrichment zones to flatten the radial power distribution. In HYPER, a proton beam of 1 GeV impinges on the Pb-Bi target in the core central region, generating spallation neutrons. A unique feature of the HYPER core is the transmutation of Tc-99 and I-129 in specially designed FP assemblies. A study on the FP transmutation can be found in [7].

The pitch of the HYPER fuel assembly is 19.96 cm and each fuel assembly has 331 fuel rods with diameter of 0.334 cm. A fairly open lattice (pitch-to-diameter ratio = 1.5) is adopted in HYPER. Currently, two fuel types are considered for HYPER, one is the TRU-Zr metal and the

other one is TRU-Zr dispersion fuel, where TRU-Zr particles are dispersed in Zr matrix. In this work, the dispersion fuel is assumed. PWR spent fuels of 33 GWD/MTU burnup, after 30-year cooling time, are reprocessed with the pyrochemical processing and then recycled into the HYPER core. Consequently, uranium in the spent fuel cannot be completely removed. In this work, a uranium removal rate of 99.9%, is used and Table 1 contains the isotope composition of the feed fuel.

TABLE 1. FUEL COMPOSITION IN WEIGHT PERCENT, w/o
(3.3 w/o UO_2, 33 GWD/MTU, 30-year cooling)

Isotope	Weight percent (w/o)
U-233	0.1710E-3
U-234	0.2000E-2
U-235	0.7894E-1
U-236	0.3840E-1
U-238	0.8920E+1
Np-237	0.4449E+1
Pu-238	0.9909E+0
Pu-239	0.4756E+2
Pu-240	0.2168E+2
Pu-241	0.2689E+1
Pu-242	0.4101E+1
Am-241	0.8649E+1
Am-242m	0.3868E-2
Am-243	0.7591E+0
Cm-243	0.1207E-2
Cm-244	0.6604E-1
Cm-245	0.7321E-1
Cm-246	0.8515E-3

3.2. Spallation neutron source

The proton beam, accelerated up to 1 GeV by a high power linear accelerator, is delivered to the central region of the core through a beam tube to maximize the source neutron importance and also to obtain favorable axial power distribution. The spallation neutron distribution highly depends on the beam width and the shape. We have considered two types of proton beams, one is with the width of 20 cm and the other with 10 cm width. In both cases, a parabolic beam shape is assumed:

$$I(r) = \frac{2I}{\pi R^4}(R^2 - r^2), \tag{10}$$

where R is the beam width and I is the total current, and r is the distance from the beam center.

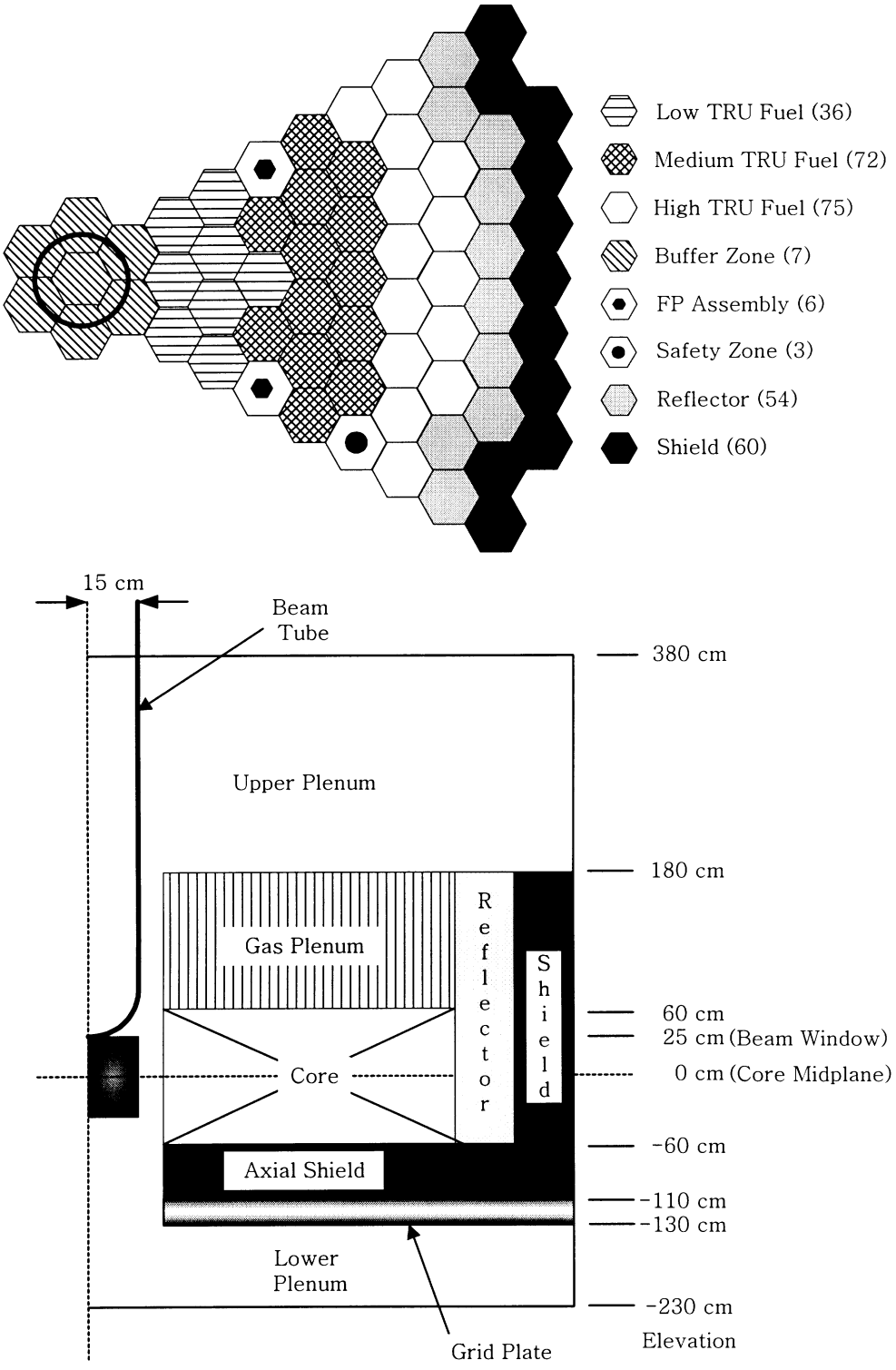

FIG. 1. Schematic configuration of the Pb-Bi-cooled HYPER core (183 fuel assemblies).

In the HYPER system, 9Cr-2WVT is used as the beam tube and window material, and the thickness is 2 mm. Assuming a Pb-Bi target zone of 50 cm diameter and 50 cm height, Monte Carlo simulations, with the LAHET code [8] were performed to calculate the spallation neutron distributions. Figure 2 shows the radial and axial distributions of the spallation neutrons generated in the target zone. In Fig. 3, the energy spectrum of the spallation neutrons is given, where 20 cm beam diameter and the window position of 25 cm are used. The total number of spallation neutrons was 29.32 (20 cm beam diameter) and 29.19 (10 cm beam diameter), respectively. In the subsequent calculations, the average value, 29.26, is used as the number of spallation neutrons produced by a proton.

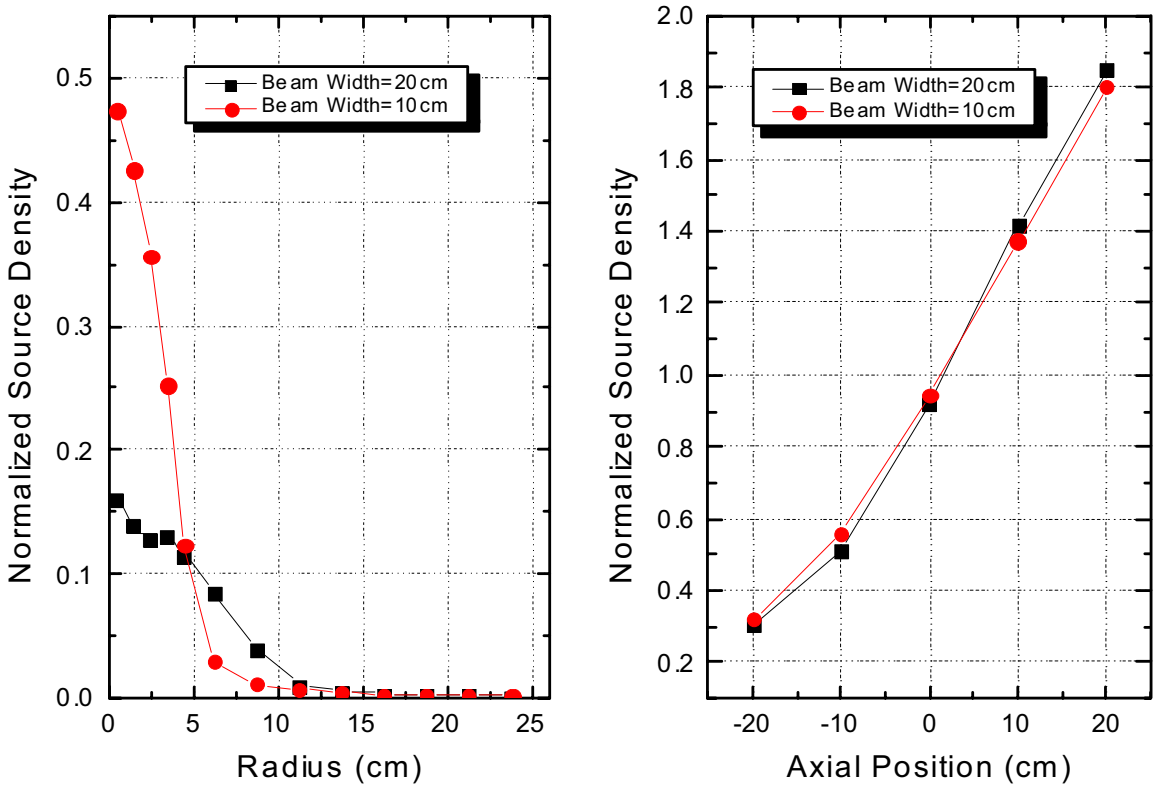

FIG. 2. Radial and axial distributions of spallation neutrons.

For the radial source distributions, it is observed that most spallation neutrons are produced in the central cylinder and the distribution is sensitive to the beam width. In the axial distribution, the source density is highly top-skewed, thus most neutrons are produced in the upper half of the target zone. As is expected, axial source distributions were almost identical for the two types of proton beams. Concerning the energy spectrum, one can note that the spectrum is relatively wide and some spallation neutrons are born with very high energy, e.g., more than 20 MeV. These results are used as inputs for the core calculations in the following sections.

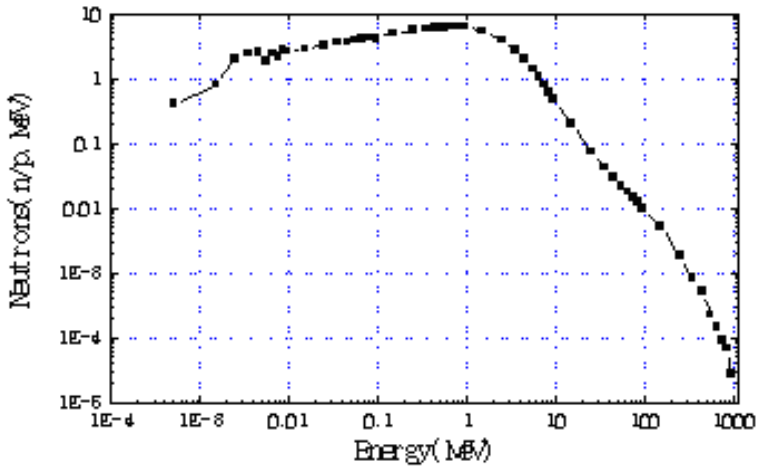

FIG. 3. Energy spectrum of spallation neutrons generated in the target.

3.3. Impacts of blanket design

Seven Monte Carlo experiments were conducted on the multiplication of spallation neutrons in the initial HYPER core loaded with fresh TRU fuels. The 3-dimensional HYPER core (Fig. 1) was analyzed in both critical and subcritical modes with the MCNAP using the continuous energy ENDF/B-VI cross section libraries. Each homogenized fuel assembly was modeled as an independent cell and the active core was divided into 6 axial segments. In this paper, the spallation neutron source is assumed to be isotropic. We believe that the isotropic assumption does not invalidate the results since most spallation neutrons are produced isotropically. Table 2 shows majors features of the seven experiments.

TABLE 2. CLASSIFICATION OF NUMERICAL EXPERIMENTS

Experiment	Enrichment zone* (TRU w/o)	Tc-loading
Case 1	Single zone (24.295)	0
Case 2	L (19.31), M (24.72), H (30.50)	0
Case 3	LL (19.0), L (19.31), M (24.72), H (30.50)	0
Case 4	LL (18.0), L (19.31), M (24.72), H (30.50)	0
Case 5	L (19.80), M (29.40), H (31.50)	856.1 kg
Case 6	Single zone (26.60)	856.1 kg
Case 7	L (19.80), M (26.30), H (35.00)	856.1 kg

* LL = inner-most ring of fuel assemblies, L=Low, M=Medium, H=High

In all the experiments, the beam diameter is 20 cm and the diameter of the beam tube is 30 cm. The objective of Case 1 ~ 4 is to assess the effects of the radial power distributions on the source multiplication. Case 3 and 4 are different from Case 2 in the TRU enrichment of the inner-most fuel assembly ring; 19.0 w/o for Case 3 and 18.0 w/o for Case 4. Case 5 ~ 6 are considered to identify the impacts of the FP-loading in the core. In Case 5 ~ 7, Tc-99 of 856.1 kg was loaded in the FP assembly; 30% of the FP assembly volume was occupied by the Tc-99 metal and the

remaining 70% by the coolant. Case 1 ~ 5 is have the same FP assembly location, as shown in Fig.1, while the FP assembly is placed in the inner-most assembly in Case 6 and Tc-99 is loaded in the interface region between the middle and outer zones of the core in Case 7.

An objective of this work is to assess the spallation neutron multiplication, relative to the conventional critical mode expectation. So, a measure of the source neutron efficiency (S_{eff}) is introduced. S_{eff} is defined by

$$S_{eff} = 100 \times \frac{M_s}{M_s^{apx}} (\%) \tag{11}$$

Basically, introduction of S_{eff} is based on the observation that M_s^{apx} is hardly achievable in practical ADSs. In an ADS like HYPER, the proton beam should be delivered to the core central region through a vacuum tube. Thus, some fraction of the produced spallation neutrons directly leaks into the upper plenum without multiplication in the blanket regime. Especially, the neutron importance of the target zone is generally lower than that of the surrounding fuel regions, even when the target is placed in the core center. Thus, in the practical situations, the actual source multiplication is usually smaller than the critical mode expectation, M_s^{apx}.

Table 3 compares the seven numerical experiments in terms of M_s, S_{eff}, P_n, and I_P. In Table 3, P_n is the fission power generated by a spallation neutron in the system and I_P means the proton current required for 1 GWth power. The radial power distributions are depicted in Figs. 4-6 for each case. Given M_s and P_n, the beam current can be calculated by Eq. (12):

$$I_P = 1.6021 x 10^{-16} \frac{P_{sys}}{n_{sp} P_n} [mA]. \tag{12}$$

where n_{sp} is the number of spallation neutrons produced by a 1 GeV proton (n_{sp} =29.26) and P_{sys} is the system fission power (P_{sys} =1 GWth). The beam current for $k_{eff} = 0.97$ was estimated using a linear relationship between k_{eff} and M_s.

Given a fixed source distribution, the source multiplication would mostly depend on the material composition and distribution in the blanket region. Table 3 shows that the source efficiency S_{eff} does not exceed 82% in all cases considered. As is expected, Case 1 provides the largest efficiency because the power distribution is highly inner-skewed. However, Case 1 using the homogeneous TRU loading cannot be accepted due to its unacceptably large peaking factor, 1.859, as shown in Fig. 4. In the HYPER core, the allowable maximum radial peaking factor is set to 1.5.

TABLE 3. SUMMARY OF MONTE CARLO EXPERIMENTS
(beam width = 20 cm, diameter of beam tube = 30 cm)

Experiment	k_{eff}	M_s	S_{eff} (%)	P_n (J/n)	I_P (mA)	Power peaking
Case 1	0.97002 (0.0010)[1)]	27.291 (0.038)[1)]	81.82	0.454E-9	12.05 (12.05)[2)]	1.859
Case 2	0.97032 (0.0010)[1)]	24.819 (0.040)[1)]	73.66	0.410E-9	13.36 (13.51)[2)]	1.273
Case 3	0.96849 (0.0010)[1)]	25.622 (0.045)[1)]	80.73	0.423E-9	12.94 (12.32)[2)]	1.263
Case 4	0.97084 (0.0009)[1)]	22.926 (0.042)[1)]	66.85	0.377E-9	14.52 (14.93)[2)]	1.270
Case 5	0.96814 (0.0010)[1)]	18.129 (0.038)[1)]	57.76	0.294E-9	18.94 (17.55)[2)]	1.223
Case 6	0.96726 (0.0010)[1)]	12.45 (0.050)[1)]	40.76	0.195E-9	28.06 (25.71)[2)]	1.327
Case 7	0.96737 (0.0011)[1)]	21.599 (0.038)[1)]	70.48	0.354E-9	15.47 (14.22)[2)]	1.289

[1)] standard deviation

[2)] beam current for $k_{eff} = 0.97$

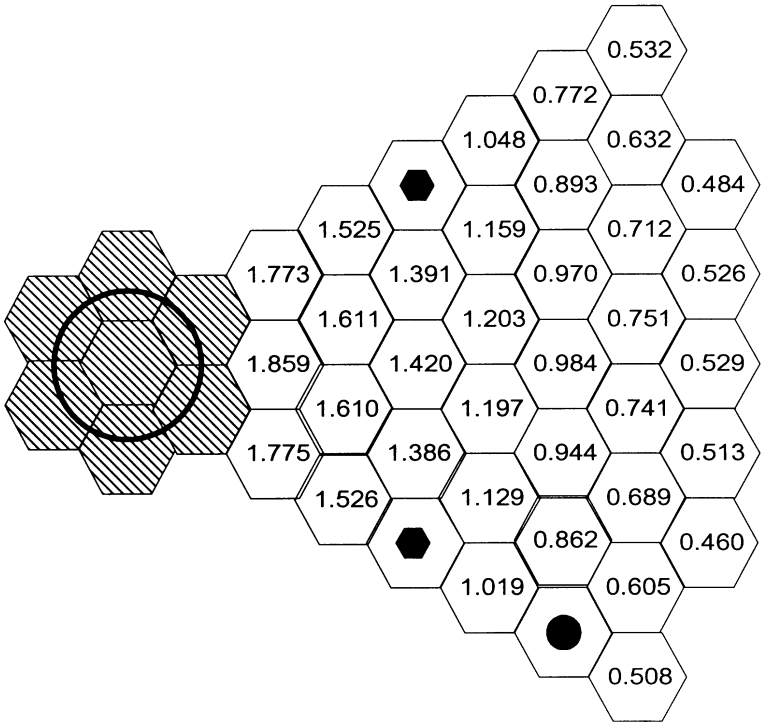

FIG. 4. Radial power distribution for Case 1.

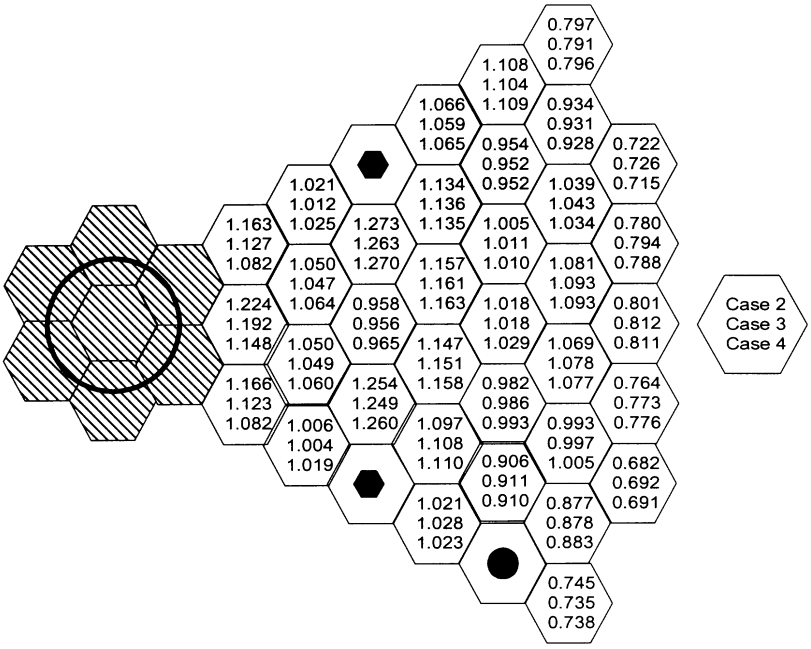

FIG. 5. Radial power distributions for Case 2 ~ 4.

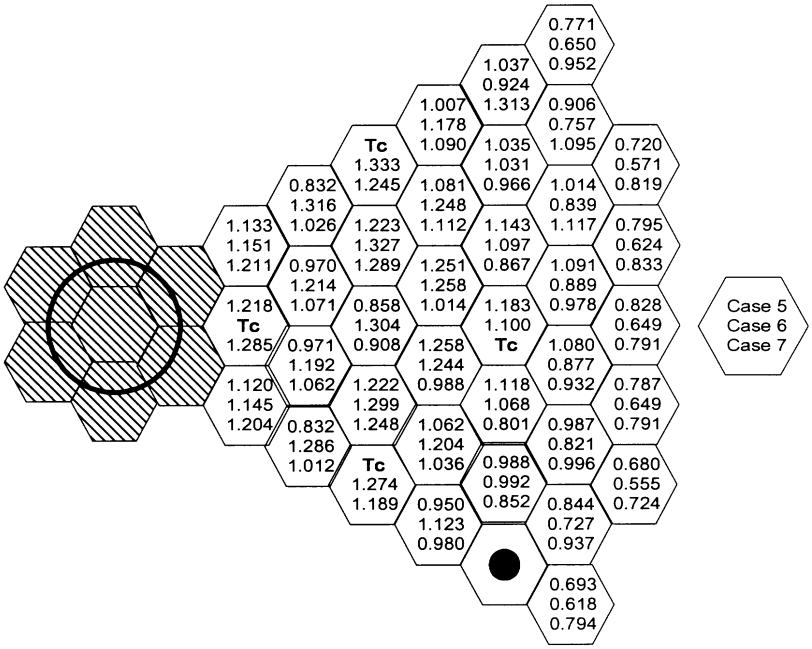

FIG. 6. Radial power distributions for Case 5 ~ 7.

In Case 2 ~ 4, radial power distributions were flattened with TRU enrichment zoning and the inner zone power was significantly decreased, providing reasonable power peaking factors. It is observed that S_{eff} of Case 2 also significantly decreased, compared with Case 1. Reduced source efficiency in Case 2 is mainly because the inner zone power is considerably decreased in Case 2 (see Fig. 5). Interestingly, one can see that S_{eff} of Case 3, where TRU enrichment of the inner-most ring is 19 w/o, is almost comparable to that of Case 1. On the other hand, further reduction of the TRU enrichment in the inner-most ring resulted in the worst source efficiency among Case 2, 3, 4. These results indicate that the source efficiency is sensitive the power distribution in the inner zone and there exists an optimum inner zone power distribution providing a maximum source multiplication. It is important to note that the inner-most ring should be treated separately in order to get a high source multiplication. Case 2 ~ 4 reveals that high power peaking in the inner-most fuel ring does not always lead to best source efficiency. These characteristics of source multiplication can be ascribed to the following feature of the HYPER core. In the conventional critical cores, neutrons in the core center have the highest importance. However, in HYPER, the central buffer zone is filled with the coolant, furthermore, the target zone is linked with the upper plenum with a vacuum tube. Consequently, fission neutrons produced in the inner-most fuel rings have a relatively high leakage probability.

Table 3 shows that loading of Tc-99 has a relatively large impact on the source multiplication. Especially, placing Tc-99 beside the source region as in Case 6 gives very low source neutron efficiency. The ineffective multiplication in Case 6 is because a significant fraction of the source neutrons is parasitically absorbed by Tc-99, without giving birth to fission neutrons in the fuel blanket. One the one hand, S_{eff} of Case 7 is comparable to that of Case 2, since there exists sufficient buffer zones between source position and the Tc-99 zone. One the other hand, Case 5 with FP assembly in the middle zone has S_{eff} comparable to the average of Case 6 and Case 7. Although Case 7 has a relatively high S_{eff}, neutron flux in the FP assembly is relatively low, leading to ineffective transmutation of Tc-99. Therefore, the position of the FP assembly should be determined by considering the accelerator power and the transmutation efficiency of FPs.

The proton beam current required for 1 GWth power is inversely proportional to the source neutron multiplication. Also, the larger source efficiency, the smaller current would be necessary to produce the same fission power. Table 3 indicates that the HYPER core with $k_{eff} = 0.97$ would need a beam current of 12 ~ 18 mA at beginning of cycle of the initial core, depending on the TRU zoning and FP-loading.

In this work, we have neglected high energy source neutrons above 20 MeV. Although the fraction of the high energy neutrons is fairly small (~1.0%), the effect would not be negligible. In addition to the assumption, another point we have neglected is the secondary protons, which are generated by spallation reactions. Thus more accurate source efficiency and corresponding beam current could be determined with more detail core modeling and more reliable computer codes.

3.4. Impacts of beam and target designs

The impacts of the beam and target designs on the source multiplication are evaluated in terms of beam width and window position. First, the beam diameter is changed from 20 to 10 cm and the

results are compared with those of Case1 of the previous section. In this case, a homogeneous TRU loading is adopted and the diameter of the beam tube is decreased to 16 cm in virtue of the smaller beam diameter. However, the window position is the same, i.e., 25 cm, as in Case 1. Results are summarized in Table 4 and the radial power distribution is given in Fig. 8.

TABLE 4. IMPACTS OF SMALLER BEAM WIDTH AND BEAM TUBE
(beam width = 10 cm, diameter of beam tube = 16 cm)

k_{eff}	M_s	S_{eff} (%)	P_n (J/n)	I_P (mA)	Power peaking
0.96933 (0.0012)[1)]	28.745 (0.041)[1)]	88.16	0.479E-9	12.05 (11.18)[2)]	1.896

[1)] standard deviation

[2)] beam current for $k_{eff} = 0.97$

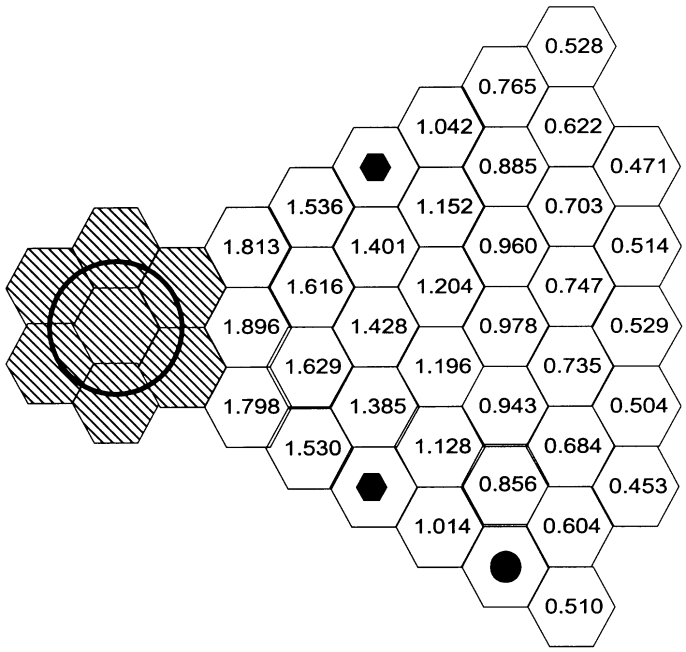

FIG. 8. Radial power distribution for smaller beam diameter and beam tube.

Comparing with Case 1 with 20 cm beam diameter, we observe that the source efficiency increased significantly and, as a result, the required proton current decreased by about 7%. This better performance of the smaller beam diameter is mainly because the void area became smaller and the direct leakage of spallation neutrons through the beam tube decreased. In other words, more spallation neutrons contribute to the fission reactions in the fuel blanket. Regarding the radial power distribution, the inner zone power slightly increased, relative to Case 1, since more spallation neutrons are available in the central target zone. These results indicate that smaller beam diameter is desirable for better source efficiency. However, too small beam diameter may cause the concern for the window integrity. Therefore, an optimum beam and tube diameters should be determined by considering the overall performance of the associated designs.

Second, assuming the 20 cm beam width, the source neutron efficiency is calculated for several window positions. In all cases, fuel is loaded homogeneously and the TRU enrichment was adjusted to get $k_{eff} = 0.97$. It is worthwhile to note that the coolant voiding in the core center results in a reactivity decrease in the HYPER core. Therefore, the reactivity decreases a little as the beam window position is lowered. Figure 9 shows the efficiency of spallation neutrons as a function of the window position.

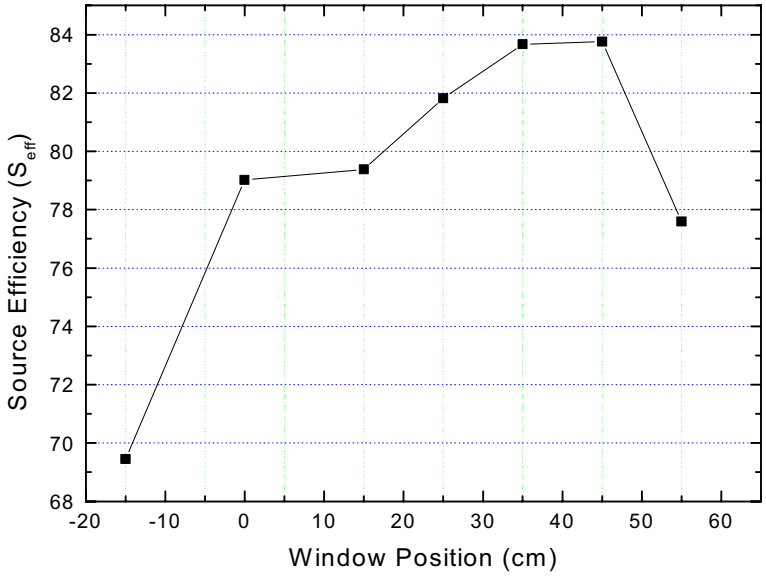

FIG. 9. Source neutron efficiency as a function of the window position.

Figure 9 clearly shows that the optimal window position is above the core mid plane. This is mainly because the axial profile of the source density is top-skewed and the beam window is in the vacuum condition. One can observe that the optimal window position, in terms of the source neutron multiplication, is within the range 30 ~ 45 cm. As the window position gets higher, the axial leakage probability of spallation neutrons would increase. If the window position is within 30 ~ 45 cm, most spallation neutrons are produced in the upper half region of the target zone and the axial leakage would be fairly higher than that of a low window position, e.g., 10 cm. Nevertheless, the source multiplication is maximized when the window position is relatively high. This phenomenon has much to do with axial power distributions of the core.

Figure 10 compares the core-averaged axial power distributions for several window positions. It is seen that the maximum source efficiency occurs when the axial power distribution is slightly top-skewed and the axial power distribution is almost symmetric when the window placed in the neighborhood of 25 cm. If the window position is below 25 cm, the axial power distribution becomes bottom-skewed and the efficiency starts decreasing. Generally, the axial leakage of neutrons is minimized when the axial power distribution is symmetric with respect to the core midplane. This explains the fairly high source efficiency for the window position of 25 cm. Meanwhile, a little higher source efficiency for the window position of 35 ~ 45 cm is due to the

asymmetric configuration of the HYPER core. As shown in Fig. 1, a gas plenum is located above the core and below the core is the HT-9 shield. Consequently, neutrons leaking to the shield region have lower probability to reenter the fuel blanket than in the upper gas plenum. This leads to the maximum source multiplication at the window position of 35 ~ 45 cm.

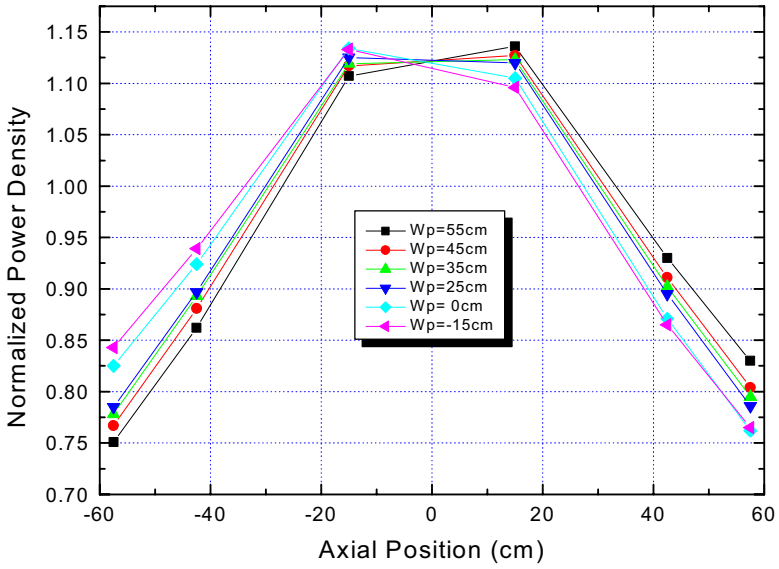

FIG. 10. Core-averaged axial power distributions for several window positions.

The optimum window position should be determined by taking into account both the source efficiency and the axial power distribution, since asymmetric power distribution increases the power peaking factor. At this point, a window position within 20 ~ 35 cm is desirable for HYPER. In the present work, we have assumed an isotropic spallation neutron source. However, the actual spallation neutrons are known to have some anisotropicity. Therefore, a more detail evaluation should be performed to determine the final window position.

4. CONCLUSIONS

The theoretical background for the source multiplication was reviewed and various Monte Carlo simulations were conducted for the TRU-loaded HYPER to evaluate effectiveness of the spallation neutron.

It is found that there can be very a large discrepancy between the actual source multiplication and the conventional multiplication factor based on the critical mode analysis, i.e., $1/(1-k_{eff})$. Numerical experiments reveal that the actual source multiplication is far below the critical mode expectation, depending on the core design. The critical mode expectation is hardly achievable in practical ADSs loaded with the TRU fuel.

We have found that the source neutron multiplication is fairly sensitive to core characteristics such as power distribution, fuel composition, absorbers, etc. Concerning the power distribution, it

is desirable that the power sharing of the central region is maximized. However, optimization of the inner-zone power distribution is required for best performance. Absorbing material such as Tc-99 around the source can significantly reduce the source neutron multiplication. A narrow beam tube is desirable to minimize the axial leakage of the source and for efficient source multiplication. Regarding the window position, the best source efficiency can be obtained when the axial power distribution is well balanced. This means that the beam window should be placed in the middle of the upper half core.

As a concluding remark, the core design should be optimized such that the importance of the external neutron source can be maximized as much as possible for better competitiveness of the ADS.

REFEENCES

[1] A Roadmap for Developing Accelerator Transmutation of Waste (ATW) Technology, DOE/RW-0519, US Department of Energy (1999).

[2] SALVATORES, M., French Perspective and Activities on ADS, Proc. 4th Accelerator and Transmutation Technology Workshop, KAERI/GP-146/2000 (2000) 24-26.

[3] INTERNATIONAL ATOMIC ENERGY AGENCY, Accelerator-Driven Systems: Energy generation and transmutation of nuclear waste, Status report, IAEA-TECDOC-985, Vienna (1997).

[4] KRAKOWSKI, R.A., Accelerator Transmutation of Waste Economics, Nuclear Technology, **110** (1995) 295.

[5] SHIM, H. J., et al., Monte Carlo Depletion Analysis of a PWR with the MCNAP, M&C 99, Proc. Int. Conf. on Mathematics and Computation, Reactor Physics and Environmental Analysis in Nuclear Applications, 27-30 September 1999, Madrid, Spain, **2** Senda Editorial, SA. Madrid (1999) 1026-1035.

[6] PARK, W.S., et al., HYPER (Hybrid Power Extraction Reactor): A system for clean nuclear energy, Nuclear Engineering and Design, **199** (2000) 155.

[7] PARK, W.S., et al., Fission Product Target Design for HYPER System, paper presented in the 6th Information Exchange Meeting on Actinide and Fission Product Partitioning and Transmutation, 11-13 December 2000, Madrid, Spain, NEA, EUR 19783 EN (2001).

[8] PRAEL, R.E., et al., Users Guide to LCS: The LAHET code System, LA-UR-89-3014, Los Alamos National Lab., (1989).

DEVELOPMENT AND VALIDATION OF CALCULATION PROCEDURES FOR THE NEUTRON PHYSICS INVESTIGATION OF ACCELERATOR DRIVEN SUB-CRITICAL SYSTEMS

C.H.M. BROEDERS, I. BROEDERS
Forschungszentrum Karlsruhe, Germany

Abstract

After an overview of the development and validation work at FZK for the neutron physics investigations of accelerator driven systems, some results related to the IAEA Coordinated Research Program are presented.

1. INTRODUCTION

Neutron physics investigations for accelerator driven sub-critical systems are in progress at the Forschungszentrum Karlsruhe (FZK) since the early nineties. The first step of these efforts was the implementation and qualification of suitable calculation methods and codes, especially for the description of the spallation processes and for the coupling of the external neutron source with the transport calculations for the sub-critical reactor system. For the qualification of the calculation tools participation to several international benchmark investigations was very helpful. The applied high-energy codes could be validated by the participation to the NEA international code comparison of intermediate energy nuclear data [14]. For the validation of the calculation of sub-critical reactor systems with strong external neutron sources, the IAEA ADS neutronic benchmark for lead cooled thorium/^{233}U fuel was a successful undertaking [17, 28]. The potential of nuclear waste incineration by the transmutation of long-lived minor actinides and fission products was already studied in an early stage [7, 27]. In this contribution only some application investigations related to an IAEA Coordinated Research Program for ADS are presented.

2. DEVELOPMENT OF CODES AND LIBRARIES

For the analysis of accelerator driven systems (ADS) the whole energy spectrum from several GeV down to thermal energies has to be covered. The traditional calculation tools for fission reactors only describe the energy range up to about 10 MeV for 26- and 69-group libraries at FZK [6]. Other multi-group libraries and also the special libraries for Monte Carlo calculations (e.g., MCNP) apply energies in the range of the evaluated data libraries like ENDF/B, usually being 20 MeV. For the higher energies special methods, data and codes had to be adapted from other research areas, e.g., from high-energy accelerator investigations. In Fig. 1 the basic flowchart for our ADS investigations is shown. Three main components may be identified:

- Calculation of the neutron source with high energy transport codes;
- Calculation of the steady state reactor with deterministic or Monte Carlo transport codes;
- Burn-up or depletion calculations.

In the following sections these components will be discussed in some detail.

2.1. Preparation of codes

In connection with the ADS investigations, a number of developments have been accomplished for the different calculation stages.

2.1.1. High energy spallation calculations

The investigations started with the implementation and qualification of the HETC and MORSE modules from the HERMES code system from the Jülich research center [12]. The MORSE module was soon replaced by the more modern MCNP code [5]. Later on, the LAHET code system LCS [18] from Los Alamos, being an improved coupling of LAHET and MCNP4B was adopted and applied. Moreover, FZK is beta-tester of the new MCNPX [29] code system, in development at Los Alamos for ADS applications. In the meantime most calculations are performed with MCNPX. All codes mentioned before are based on Monte Carlo simulations, both in the energy region for spallation and in the lower energy region for neutron transport.

2.1.2. Transport calculations

At FZK a strong effort was devoted to the qualification of the discrete ordinate code TWODANT [1] for the transport calculations below a cutoff energy of 10 to 50 MeV, in order to save significant amounts of computing times for simplified geometrical models. In Fig. 2 a comparison of TWODANT and MCNP results is shown for the radial power density distributions in two axial positions of the IAEA ADS benchmark (see Section 4). The TWODANT results were obtained on an IBM RS6000 workstation in about two hours of computing time, whereas the MCNP code needed several days on the same workstation. The very good agreement shows that for simplified geometrical models it is advantageous to apply deterministic codes.

2.1.3. Depletion calculations

After the development of the PROSDOR system, a first semi-automated coupling of the codes HERMES, MCNP and KORIGEN [26], a fully automated coupling of the depletion calculations with the KAPROS/KARBUS [6] code system, developed for critical fast, epithermal and thermal reactors, with the codes HETC/LAHET and MCNP/ TWODANT was implemented and validated. The KAPROS [3 code system has been developed at FZK since many years. It is a very flexible fully modular system consisting of a controller program and a large number of independent application modules. Important features are the very flexible data-management on different storage levels (fast memory, hard-disc and tapes), the standardized interfaces (e.g., for cross sections, spectra, etc.) and the very powerful archiving and restart options. The system has been developed on an IBM mainframe computer and the first versions utilized the specific features of the mainframe computer environment at FZK with as a consequence, that transferring to other computer environments was very problematic. In the past 10 years a portable version for workstations with UNIX operating systems has been redesigned and realized. The first KAPROS applications were related to fast breeder reactors. In connection with investigations for tight light water reactors the treatment of up-scatter in the thermal energy region and of the resonance absorption in the epithermal region has been significantly improved. For fuel cycle studies a special module KARBUS was developed. The main tasks of KARBUS are [6]

- Preparation of multi-group cross section data, using the most adequate methods for the problem under investigation from options for fast, thermal and epithermal spectrum solutions. FZK has developed own formats for the storage of multi-group cross section data on direct access files. The data structures are optimized for application in all types of reactor spectra and combine characteristics of typical applications for thermal and fast reactors, e.g., up-scatter matrices, isotope-dependent fission spectrum matrices, separate treatment of elastic, inelastic, (n,2n), (n,3n) processes.

- Preparation and performing of multi-group reactor calculations. A number of alternative flux calculation codes may be selected with one- to three dimensions for the geometry and finite differences and nodal solutions for the transport or diffusion approximation of the Boltzman equation. Some of the earlier codes developed at FZK have a strong coupling with KAPROS; others are only loosely coupled by common interface files.
- Best estimate preparation of zone-dependent one-group cross sections for use in the depletion module BURNUP. The module BURNUP is a KAPROS implementation of the program KORIGEN [15] the well-known FZK depletion program developed from the ORIGEN code [4]. As in ORIGEN, BURNUP treats all isotopes for which data is stored on the code-own libraries for one-group depletion calculations (in the meantime for up to about 3000 isotopes). If data for isotopes is available on the applied multi-group library the required one-group cross sections are provided by KARBUS, using selectable best-estimate weighting formalisms.

2.1.4. Coupling of the calculation steps

Figure 3 shows a more detailed overview of an actual KAPROS procedure, as applied for the solution of the IAEA ADS benchmark [17, 28]. However, it should be mentioned that the new MCNPX code combines LAHET and MCNP in one code. The application of MCNPX also may lead to some simplifications in the calculation scheme of Fig. 3. In general the code system KAPROS in conjunction with the powerful script languages of the UNIX operating systems are very flexible tools for the coupling of advanced computer codes.

2.2 Development of libraries

For the ADS investigations at FZK usually 69 group cross section libraries with the well-known WIMS [2] energy group structure are applied. The upper energy boundary of these libraries is 10 MeV. As a consequence the ADS investigations utilize the formalisms of the high-energy codes above 10 MeV. These formalisms are not well qualified in the energy range up to about 300 MeV. In order to be able to study the influences of these approximations with multi-group calculations, an extended library with energies up to 50 MeV and 6 additional groups above 10 MeV of the WIMS structure has been established. First comparisons for the IAEA ADS benchmark show good agreement for the results of 69- and 75-group calculations [9, 16].

2.2.1. Validation investigations

The validation of calculation tools for accelerator driven sub-critical systems is a challenging task because no real experience is available with such systems where the proton beam of a powerful accelerator has to be guided into a high power spallation target within a sub-critical reactor system. Several aspects have to be verified:

- Impact of a strong neutron source in a sub-critical reactor system.
- Characteristics of the spallation target.
- Coupling of the spallation target and the sub-critical reactor system.

At present projects related to these three aspects are in progress.

2.2.1.1. Impact of a strong neutron source in a sub-critical system

Two complementary experiments for the investigation of the effects of a neutron source in a sub-critical system are in progress:

- In the ISTC project B70, performed in Minsk/Sosny, Belarus [11], a powerful neutron generator with 14 MeV neutrons is coupled with a low-power sub-critical thermal reactor system with the objective to study the behaviour of the sub-critical system and to perform integral cross section measurements for important isotopes of the back-end of the nuclear fuel cycle. FZK is collaborator in this project. Furthermore, the IAEA has included this project in its on-going ADS Coordinated Research Program (see Section 4). The first experimental results for the sub-critical core show good agreement with MCNP calculations for a detailed core-model [17].

- In the MUSE program [19] the effects of neutron sources with increasing strength in different positions of the experimental low-power fast reactor MASURCA at CEA, Cadarache, France, are investigated. FZK is participating in the MUSE project within the 5-th framework program of the European Community. One of the first steps in this project was the definition of benchmark models for the MASURCA reactor. Actually, this experimental reactor has some features not yet intensively investigated with KAPROS/KARBUS. The composition of the large reflectors leads to very strong self-shielding effects in structural materials, especially in iron. To investigate these effects, a very strongly simplified benchmark model was proposed by CEA [22]. First calculations at FZK showed large discrepancies between the k_{eff} results of continuous energy MCNP calculations and of KAPROS/KARBUS multi-group calculations with 26- and 69-group constant libraries. After this observation a number of isotopes of structural materials were recalculated for the 69-group library. In Table 1 some of the FZK results are summarized.

TABLE 1. FZK RESULTS FOR MUSE SIMPLIFIED BENCHMARK 2

Multi-group library/comments	k_{eff} S_8 transport 69 groups
G69P1UX3 Old standard library	1.0796
G69P1UD2 Extended library, minor corrections	1.0854
G69P1UD2 + Fe and Cr from JEF2.2	1.0470
G69P1UD3 JEF2.2 for nearly all materials	1.0159
G69P1UD3 + Alternative shielding approximation	1.0193
MCNP4C FZK solution (ENDF/B-VI)	1.0184

We may observe a strong overestimation of k_{eff} for the old standard library for this simplified model of an experimental reactor system. Updating with new JEF2.2 [20] based group cross sections leads to comparable results of 69-group calculations and of MCNP4C and is in accordance with results of other participants to the MUSE project [22]. More detailed investigations showed that nearly all newly calculated isotopes contributed to a reactivity change into the same decreasing direction. It may be concluded that the participation of the MUSE project already has improved the 69-group constant library significantly.

2.2.1.2. Investigations for a high power spallation target

Typical ADS design proposals for energy production or spent fuel incineration apply proton beams with energies around 1 GeV and currents larger than 1 mA, sometimes even larger than 100 mA. For the target materials usually heavy metals like tungsten, lead, bismuth are

selected. The construction of such a high power device is a challenging task and several aspects like material behaviour, window cooling, and impact of spallation products have to be considered carefully. Most of the input data for these investigations must be provided by the physics calculations. As a step towards the construction of a spallation target for ADS, the MEGAPIE initiative of FZK, CEA and PSI, Switzerland, plans to construct a lead-bismuth eutectic (PBE) target as replacement in the existing SINQ accelerator at Villigen, Switzerland [25]. The proton beam at the SINQ target amounts about 575 MeV at 1.74 mA (≈1 MW). In order to gain confidence in the results of the physics calculations for such a target, a MEGAPIE benchmark investigation was initiated with participation of CEA, PSI, FZK, CNRS (France) and ENEA (Italy) [21]. Parameters to be investigated are: heat deposition in structural materials, decay heat and activation, neutron flux distribution, spallation product yields, damages in structural materials and neutron leakage. Preparatory investigations are presented in [10]. First comparisons of the preliminary results show that our solutions usually are in satisfactory agreement with those of the other benchmark participants.

2.2.1.3. Coupling of a spallation target and a sub-critical reactor

A real irradiation of a slightly sub-critical system with a proton beam in order to investigate the generic problems with such a coupling is planned at JINR, Dubna, Russia. The proton beam of an existing accelerator with 600 MeV, few μA, will be guided into a small sub-critical fast spectrum reactor core with MOX fuel, surrounded by a thick lead reflector. The sub-criticality level will be about $k_{eff} \approx 0.95$ leading to a system-power around 25 W. FZK supports this proposal and has recommended the realization as an ISTC project. The FZK cooperation within this project also resulted in an improvement of the multi-group data libraries of the KAPROS/KARBUS system. The Russian colleagues proposed to utilize Russian critical experiments with fast spectrum fuel with lead reflectors of increasing thickness as a benchmark investigation [23]. In Table 2 a summary of the specification of the Russian critical assemblies is given.

TABLE 2. SPECIFICATION OF THE RUSSIAN CRITICAL ASSEMBLY DATA FOR LEAD BENCHMARK

Exp.	Critical core radius (cm)	Core critical mass (g)	Internal void radius (cm)	Thickness lead reflector (cm)	External assembly radius (cm)	k_{eff}
B1	6.668	18773	-	-	-	1.000±0.0025
B2	6.000	13739	1.00	3.04	9.04	1.000±0.0040
B3	5.350	9722	1.00	28.45	33.80	1.000±0.0040

Fuel composition: Pu^{239} 95.30%, Pu^{240} 1.75%, Ni 1.28%, Ga 1.67%

During the evaluation of these critical experiments an error on the standard 69-group library was detected: the group constants for the Pb-isotopes were not complete, but contained only data for depletion calculations. Table 3 shows the results with 2 libraries discussed in Table 1. We may observe, that for the old library G69P1UX3 the results with Pb isotopes are completely wrong. The updated library G69P1UD3 gives satisfactory results. If we compare multi-group and MCNP4C results, we may observe the same trends: increasing k_{eff} values with increasing Pb-reflector. However, the MCNP4C results are somewhat higher.

TABLE 3. RESULTS FOR RUSSIAN CRITICALITY BENCHMARKS

Exp.	Case	G69P1UX3	G69P1UD3	MCNP4C
B1	M1	0.9892	0.9935	0.9960
	M2	0.9898	0.9880	
B2	M1 M4	0.9094	0.9921	1.0121
	M1 M5	1.0001	1.0017	
	M2 M4	0.9094	0.9877	
	M2 M5	1.0000	0.9973	
B3	M1 M4	0.8179	1.0007	1.0284
	M1 M5	1.0195	1.0185	
	M2 M4	0.8179	0.9975	
	M2 M5	1.0195	1.0153	

Experimental values: $k_{eff} = 1.000$
M1: Ni isotopes in calculation
M2: Ni element in calculation
M4: Pb isotopes in calculation
M5: Pb element in calculation

2.2.1.4. Selected applications

A number of application investigations have been performed, e.g., preliminary analysis for Pu-incineration in ADS [7, 10] and power flattening with multiple-beam designs for large ADS. [10, 13, 16]. In the next sections some investigations related to the international IAEA Coordinated Research Program (CRP) "Use of Th-based fuel cycle in accelerator-driven systems (ADS) to incinerate Pu and reduce long-term waste toxicities" are discussed.

2.2.1.5. IAEA ADS Bemchmark for a TH-U^{233} based energy amplifier

In 1996 the IAEA initiated in the framework of an IAEA CRP an international ADS benchmark based on a proposal of Rubbia et al. [24] for an energy amplifier with a power of 1500 MW_{th} and based on Th-^{233}U fuel and lead coolant. For three values of the "beam shut-off" criticality (0.94, 0.96 and 0.98) the ^{233}U-enrichment had to be determined and a number of parameters had to be calculated. For the FZK contribution [8] the calculations of the neutron-flux density spectra and of reaction rates (total fission reaction rate, fission reaction rates for individual isotopes) have been carried out with the transport code TWODANT in S_4/P_1 approximation, using the actual 69-group constant library. The neutron source provided with the benchmark data has been transformed to our energy group structure in such a way that the number of neutrons per eV was conserved for each energy group.

3. BURNUP BEHAVIOUR

An important objective of the IAEA ADS benchmark was the determination of the time-dependence of the reactivity of the sub-critical reactor system. In the benchmark specifications the power-level and the time-steps are specified in detail. The cylindrical geometry model-specification contains 5 zones: lead, inner core, outer core, radial reflector and axial reflector. For our burn-up calculations each fuel zone was subdivided into 3 radial and 3 axial sub-zones, leading to a TWODANT (R-Z)-model with 22 zones. During the analysis of the results it pointed out that some other benchmark solutions were based on burn-up calculations without sub-division of the fuel zones. For that reason a comparison calculation without sub-division was carried out, leading to a TWODANT (R-Z)-model with

7 zones. In Fig. 4 FZK results for the time-dependence of the reactivity is shown. These results are in satisfactory agreement with solutions of other participants. We may observe that for the case $k_{eff} = 0.96$ the influence of the sub-division of the fuel zones is remarkable.

4. POWER DISTRIBUTIONS

The technical feasibility of ADS is strongly influenced by the power density distribution in the system. So, another important issue of the IAEA ADS benchmark investigation was the comparison of the radial power distributions for the different sub-criticality levels. In general the agreement between the solutions of the participants was good. In Fig. 5 our radial power density distribution in the mid-plane of the reactor system is shown. Also the radial form-factors, defined as maximum-to-mean power density ratio, are given. We may observe that the form-factor strongly increases with decreasing reactivity of the system. Such values are not acceptable in large power systems. As a consequence of these observations at FZK a considerable effort was devoted to improve the power-density distribution [13, 16].

5. IAEA ADS BENCHMARK STAGE 3.1

In the course of the IAEA CRP a number of cases were defined in order to study specific problems related to ADS with thorium fuel. In stage 3.1 of the CRP the characteristics of plutonium incineration in ADS with thorium-based fuel was investigated. For this purpose, FZK has prepared the detailed input data for the fuel. The other benchmark specifications were unchanged. In figure 6 first preliminary results for k_{eff} are shown of solutions from five participants: IPPE Obninsk, Russia; NRG Petten, Netherlands; CIEMAT Madrid, Spain; and FZK. We may observe very large discrepancies between these solutions. The burn-up results of Monte Carlo calculations of CIEMAT and NRG are 4-5% higher than the results of the deterministic codes from IPPE and FZK. Moreover, the strong influence of the lead cross sections may be observed for the FZK solutions. In Fig. 7 some influences of the applied cross section data on FZK-solutions is given. Generally, a strong increase of k_{eff} may be observed during burn-up, mainly caused by the build-up of U^{233} and the good conversion ratio in the Pu. The discrepancies of Fig. 6 are not yet clarified and there is a strong need for a third type of solution, e.g., with alternative Monte Carlo burn-up programs.

6. SUMMARY

Development and validation of calculation procedures for the neutron physics investigation of accelerator driven sub-critical systems (ADS) at FZK are discussed in some detail. For the three steps in such investigations, determination of the neutron source from the spallation processes, of the steady state neutron transport in the reactor system and of the long-term burn-up and depletion, adequate tools have been made available and coupled. For this coupling the modular code system KAPROS/KARBUS, developed at FZK, plays an important role. Extensive validation work has been performed. Some of the recent improvements of the applied multi-group libraries are explained in more detail. Selected applications, related to the IAEA CRP on the use of thorium fuel in ADS are presented. Large discrepancies in the results for ADS with Th/Pu fuel and lead coolant still have to be clarified.

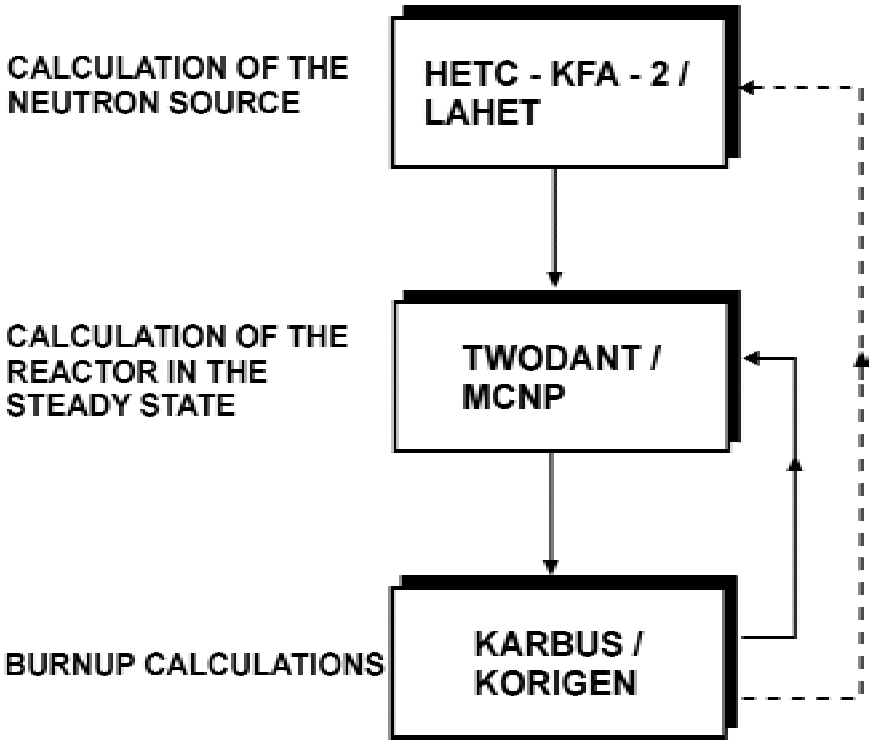

FIG. 1. Simplified flowchart for a complete ADS calculation.

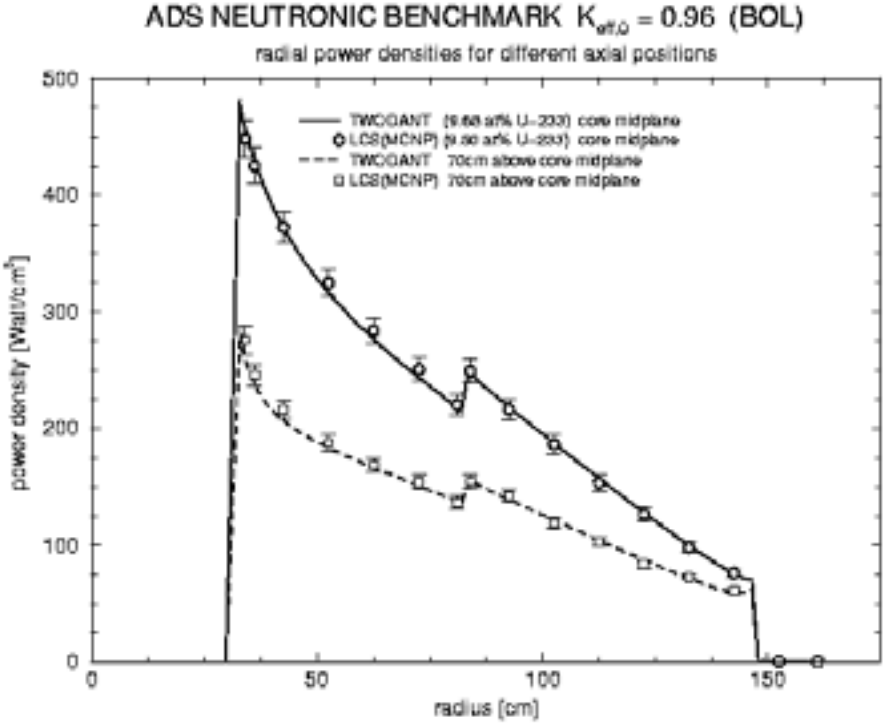

FIG. 2. Comparison of radial power density distributions for the IAEA benchmark from TWODANT and MCNP calculations.

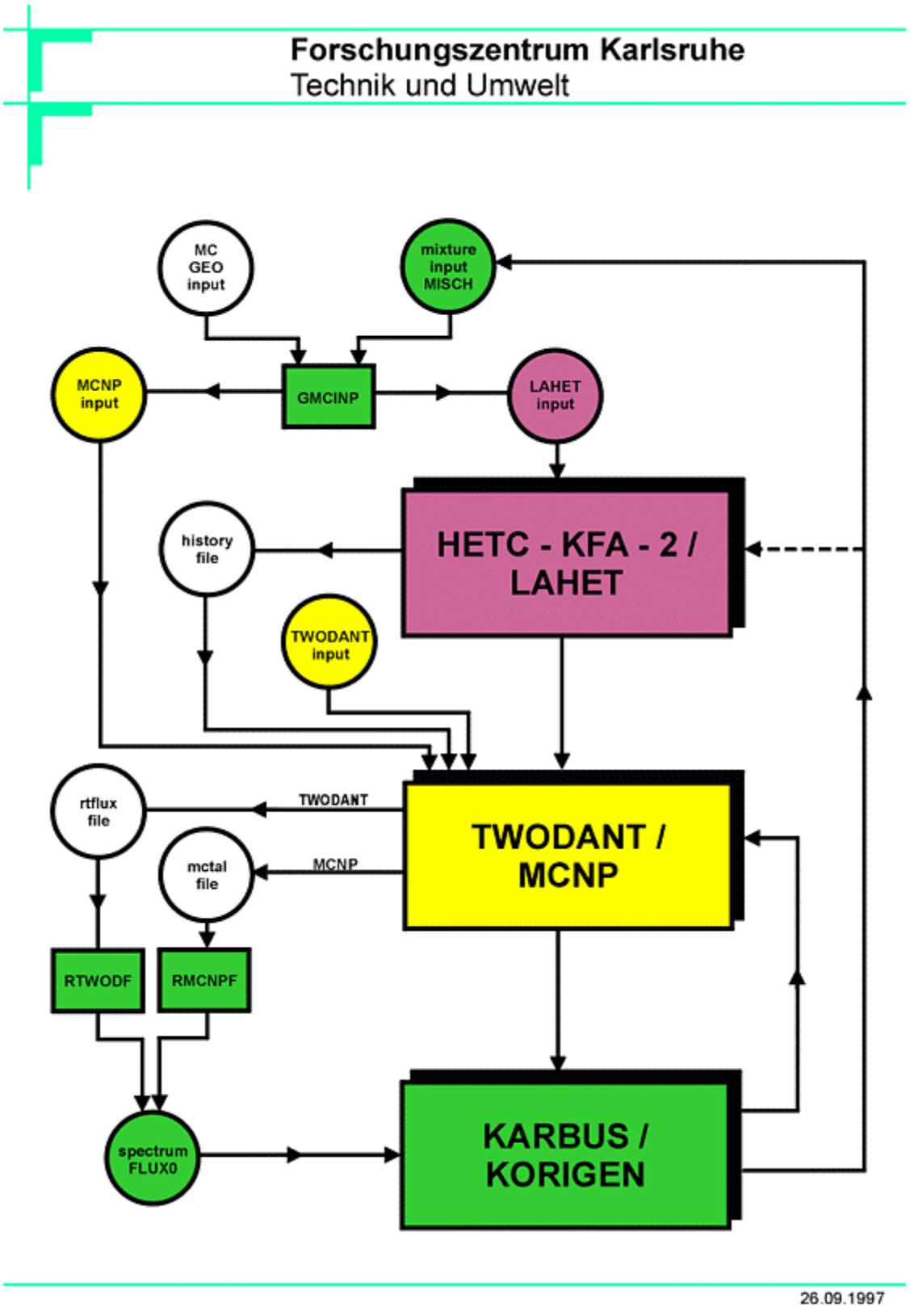

FIG. 3. Detailed flowchart for a complete ADS calculation at FZK.

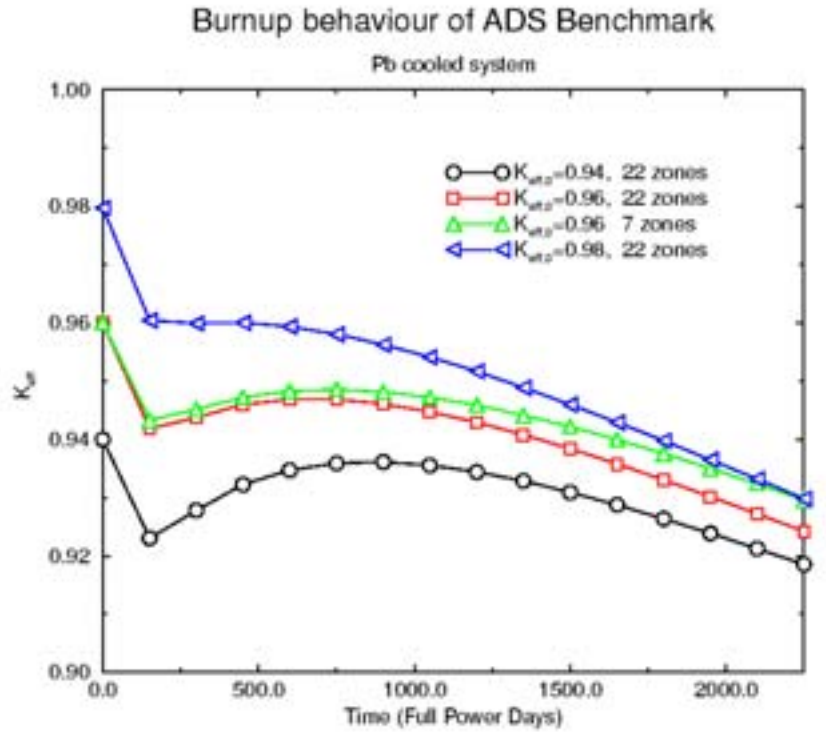

FIG. 4. Reactivity of the IAEA ADS benchmark as a function of full power days.

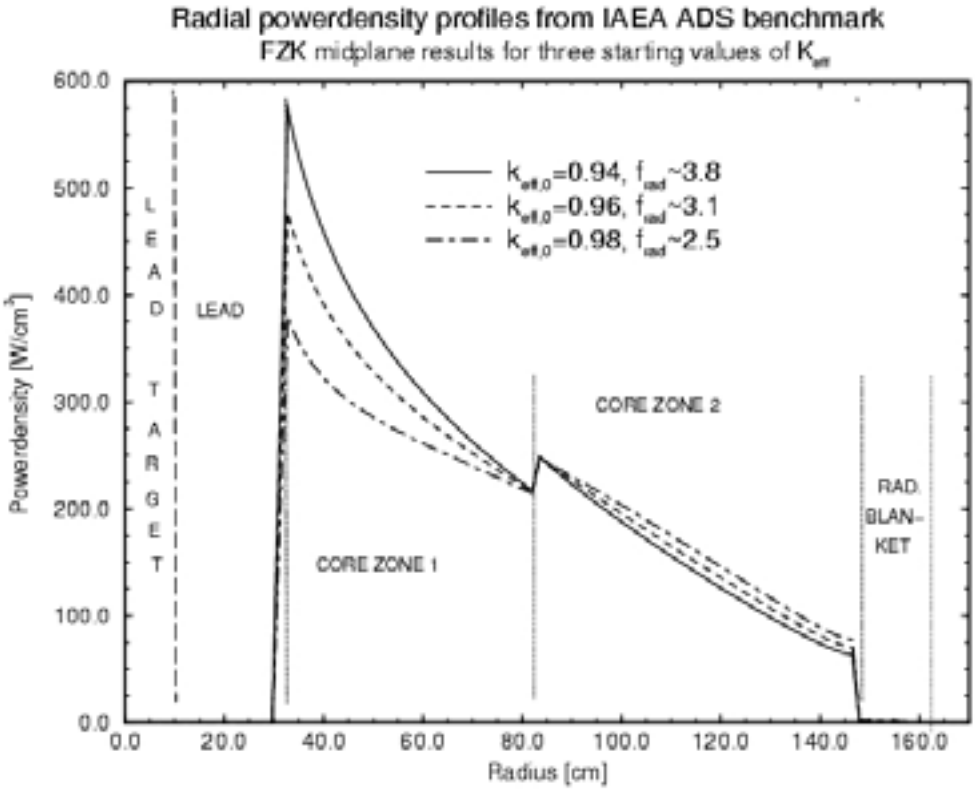

FIG. 5. Radial power-density profiles for different levels of k_{eff} in ADS.

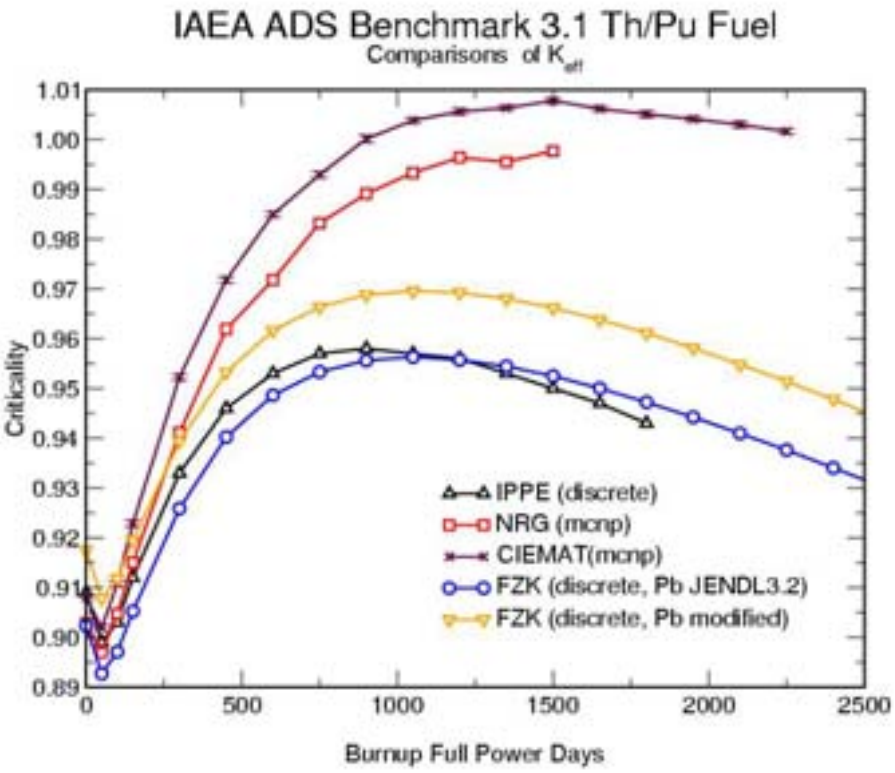

FIG. 6. k_{eff} as a function of burn-up for IAEA ADS benchmark stage 3.1 (Th/Pu) fuel.

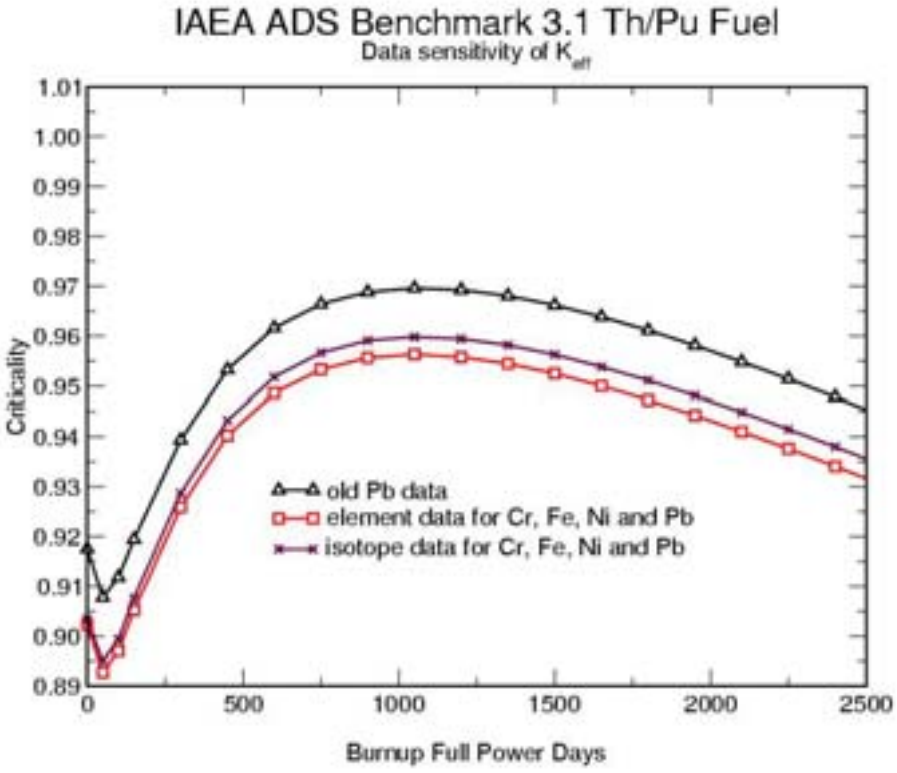

FIG. 7. k_{eff} as a function of burn-up for IAEA ADS benchmark stage 3.1 (Th/Pu) fuel.

REFERENCES

[1] ALCOUFFE, E., BRINKLEY, F.W., MARR, D.R., O'DELL, R.D., Users Guide for TWODANT: A Code-Package for Two-Dimensional, Diffusion-Accelerated, Neutral Particle Transport, LA-10049-M, Rev. 1, Manual (1984) Revised February 1990.

[2] ASKEW, J.R., FAYERS, F.J., KEMSHELL, P.B., A General Description of the Lattice Code WIMS, Journal of British Nuclear Energy Society, 5, 564 (1966).

[3] BACHMANN, H., BUCKEL, G., HOEBEL, W., KLEINHEINS, S., The Modular System KAPROS for Efficient Management of Complex Reactor Calculations, Proc. Conf. Computational Methods in Nuclear Energy, Charleston, USA., CONF-750413 (1975).

[4] BELL, M.J., ORIGEN- The ORNL Isotope Generation and Depletion Code, ORNL-4628 UC-32 (1973).

[5] BRIESMEISTER, J.F., MCNP - A General Monte Carlo N-Particle Transport Code, Version 4B, Report LA-12625-M (1997), Los Alamos National Laboratory (1997).

[6] BROEDERS, C.H.M., Entwicklungsarbeiten für die neutronernphysikalische Auslegung von Fortschrittlichen Druckwasserreaktoren (FDWR) mit kompakten Dreiecksgittern in hexagonalen Brennelementen, KfK 5072 (1992).

[7] BROEDERS, I., BROEDERS, C.H.M., Implementation, Development, Validation and First Applications of Different Code Chains for the Investigation of Accelerator-Driven Transmutation, Proc. Conf. on Emerging Nuclear Energy Systmes (ICENES'96), 1996, Obninsk, Russia, P. Nagel, R.D. Neef (Eds), CERN (1996).

[8] BROEDERS, C., BROEDERS, I., Calculations for the IAEA coordinated ADS neutronic benchmark, FZKA 5963 (1997).

[9] BROEDERS, C., BROEDERS, I., Generation of a Group Constant Library for Neutron Energy until 50 MeV, Tests and Applications, FZKA 6126 (1998).

[10] BROEDERS, C.H.M., BROEDERS, I., Neutron physics analyses of accelerator-driven sub-critical assemblies, Nuclear Energy and Design, 202 (2000).

[11] CHIGRINOV, S.E., KIEVITKAYA, A.I., RAKHNO, I.I., SERAFIMOVICH, I.G., RUTKOVSKAIA, C.K., KHILMANOVICH, A.M., MARSTINKEVITCH, B.A., Experimental and Theoretical Research on Transmutation of Long-Lived Fission Products and Minor Actinides in a Sub-Critical Assembly Driven by a Neutron Generator, paper presented in the 3rd Int. Conf. on Accelerator-Driven Transmutation Technologies and Applications, (ADTTA'99), 7-11 June 1999, Prague, Czech Republic, Eds: L M. Hron, V. Lelek (NRI Rez plc), M. Mikisek, M. Sinor, J. Uher, J. Zeman (FNSPE CTU, Prague), NRI Rez, Czech Republic (1999), Prague, Czech Republic.

[12] CLOTH, P., FILGES, D., NEEF, R.D., STERZENBACH, G., REUL, CH., ARMSTRONG, T.W., COLBORN, B.L., ANDERS, B., BRÜCKMANN, H., HERMES-A Monte Carlo Program System for Beam-Materials Interaction Studies, Jül-2203 (1988).

[13] DAGAN, R., BROEDERS, C.H.M., STRUWE, D., Modifications of the Code SAS3A for Simulation of ADS Designs, FZKA 6334 (2000).

[14] FILGES, D., NAGEL, P., NEEF, R.D., (Eds), OECD Thick Target Benchmark for Lead and Tungsten, Report NSC/DOC(95)2 (1995).

[15] FISCHER, U., WIESE, H.W., Verbesserte konsistente Berechnung des nuklearen Inventars abgebrannter DWR-Brennstoffe auf der Basis von Zell-Abbrand-Verfahrenmit KORIGEN, KfK 3014 (1983).

[16] GUDOWSKI, W., (Ed.), Impact of accelerator-based technologies on nuclear fission safety, IABAT project, EUR 19608 EN (2000).

[17] GUDOWSKI, W., BROEDERS, C., CHIGRINOV, S., KADI, Y., KIEVITSKAYA, A., KLIPPEL, H., SLESSAREV, I., STANCULESCU, A., IAEA Benchmark on Accelerator Driven System, paper presented in the Accelerator Applications/Accelerator Driven Transmutation Technology And Applications '01 (AccApp/ADTTA'01), 2001, Reno, USA, ANS, ISBN: 0-89448-633-0 (2001).
[18] HUGHES, H.G., ADAMS, K.J., CHADWICK, M.B., COMLY, J.C., FRANKLE, S.C., HENDRICKS, J.S., LITTLE, R.C., PRAEL, R.E., WATERS, L.S. YOUNG, P.G., Jr., Status of the MCNP™ / LCS™ Merger Project, Proc. The Radiation Protection and Shielding Topical Conference, „Technologies for the New Century", 19-23 April 1998, Nashville, Tennessee, USA, ANS, ISBN: 0-89448-637-3 (1998).
[19] LEBRAT, J.F., et al., Experimental investigation of multiplying subcritical media in presence of an external source operating in pulsed or continuous mode: The MUSE - 3 Experiment, Proc. 3rd Int. Conf. on Accelerator-Driven Transmutation Technologies and Applications (ADTTA'99), 7-11 June 1999, Prague, Czech Republic, Eds: L M. Hron, V. Lelek (NRI Rez plc), M. Mikisek, M. Sinor, J. Uher, J. Zeman (FNSPE CTU, Prague), NRI Rez, Czech Republic (1999), Prague, Czech Republic.
[20] NEA Data Bank, The JEF-2.2 Nuclear Data Library, JEFF Report 17 (2000).
[21] POITEVIN, Y., ENDERLE, R., LEHMANN, E., Specifications for a Neutronic Benchmark on the MEGAPIE Spallation Target, SERMA/LCA/RT/00-2862/A (2001).
[22] RIMPAULT, G., Private communication, 2000.
[23] ROGOV, A., Private communication, 2000.
[24] RUBBIA, C., RUBIO, J.A., BUONO, S., CARMINATI, F., FIETIER, N., GALVEZ, J., GELES, C., KADI, Y., KLAPISCH, R., MANDRILLON, P., REVOL, J.P., ROCHE, CH., Conceptual Design of a Fast Neutron Operated High Power Energy Amplifier, CERN/AT/95-44(ET), Geneva (1995).
[25] SALVATORES, M., BAUER, G.S., HEUSENER, G., The MEGAPIE initiative, PSI Bericht Nr. 00-05, PSI Villigen (2000).
[26] SEGEV, M., PROSDOR – An IBM-3090 Based Semi-Automated Procedure Linking HERMES MCNPand KORIGEN for the Burnup Analysis of Accelerator Driven Cores, KfK-5328 (1994).
[27] SEGEV, M., KÜSTERS, H,. PELLONI, S., Transmutation of Long-Lived Minor Actinides and Fission Products by Accelerated Protons, KfK-5384 (1994).
[28] SLESSAREV, I., TSCHISTIAKOV, A., IAEA-ADS BENCHMARK (Stage 1), RESULTS and ANALYSIS, paper presented in the Technical Committee Meeting on Feasibility and motivation for hybrid concepts for nuclear energy generation and transmutation, 17-19 September 1997, Madrid, Spain, IAEA-TC-903.3, Ciemat, Spain (1998).
[29] WATERS, L.S., Ed., MCNPX USERS'MANUAL, TPO-E83-G-UG-X-00001 (1999).

INVESTIGATIONS OF NEUTRONICS OF SUBCRITICAL SYSTEMS WITH THE USE OF MCNP CODE

S. TACZANOWSKI, M. KOPEĆ
University of Mining & Metallurgy, Krakow, Poland

Abstract

As the tool particularly appropriate for investigations of neutronics of subcritical systems, the MCNP code (4b version) has been chosen in view of its great advantages of universality and wide spread. Two simplified models of the systems have been assumed in calculations - a full-scale spherical assembly and a smaller cylindrical experimental one. The neutron multiplication process has been examined in subcritical systems with various targets while following the generation dependent: neutron multiplication factor k_i, number of neutrons and cumulative energy release. This has provided indications for right selection of the active cycles in the MCNP code for correct estimation of the k_{eff}. Then, the spatial distribution of fissioning (i.e., approximately that of heating) has been simulated. E.g., within a uniform system of k_{eff} amounting to 0.962, the span in specific fissioning has been found larger than in similar, exactly critical systems even by over 3 orders of magnitude, thus proving a drawback of the former. Finally, the time evolution of fissioning have been studied in detail - among others also the development of the neutron spectrum in the subcritical system after a 14 MeV neutron δ-shaped pulse. The particularities of neutron field trajectories according to the place of detector and time proved explainable. Instead, discrepancies between the provided neutron lifetimes by the MCNP in the KCODE and Fixed Source modes require further studies. In conclusion, we can state that the performed study has illustrated some properties of subcritical systems, contributed to their better understanding and of the used tool the MCNP code, thus allowing for better design and reliability of the respective validation experiments.

1. INTRODUCTION

Though the physics of critical systems has been intensively explored since ca. 6 decades, during the same time the field of closely related subcritical systems has been drawing incomparably less attention. It is comprehensible in view of lack until now of such large-scale assemblies. Consequently, the properties of subcritical i.e., external source driven systems have not been sufficiently investigated. At present, however, the demand for safe incineration of nuclear waste has arisen and much interest in subcritical systems (esp. accelerator-driven ones) has emerged. In particular the significance of the source, its influence etc., still require more research. One of the most common, universal and efficient research tools in the field of neutron transport is the MCNP code [1]. The present study attempts to contribute to better understanding of these systems and of the applied research instrument.

The difference between critical and subcritical systems may seem lesser when one perceives the critical system as a prompt subcritical one driven by a (momentarily) independent source which is just the delayed neutron component. The spatial distribution of its precursors strictly follows the local decay weighted integral (over last several minutes) of fissioning whereas the spectrum is much softer than that of prompt neutrons that sometimes may much reduce the fraction of delayed neutrons to the effective value β_{eff} [3]. In steady state, the shape of this distribution is determined by the asymptotic distribution of fissioning.

Instead, in the true subcritical systems (i.e., prompt + delayed), generally the space-time-energy distribution of the external neutron source is significantly different from the above one. Usually neutron sources are localised in a small volume, e.g. in accelerator targets, thus one can hardly imagine an independent external source distributed over the whole system exactly eigenstate-like and having the same fission spectrum. The spatial distribution of transmutations is determined by the neutron flux, hence its reliable evaluation is crucial for the burnup calculations.

Theoretically, the problem of calculating flux in the presence of an external neutron source lies in solving the inhomogeneous differential or integral equation [9]. The solution of such equations is composed of the sum of both the special and homogenous solutions. Yet, it should be noticed that when k_{eff} is low (i.e., in case of a deep subcriticality operation) the eigenstate may not be reached at all because of too early fading of the neutron field [10]. Then in subcritical reactors the source component is preponderant and determining the peaking factor of heat production distribution and the importance function of the neutrons of a number early generations. In that case, a confining to the fundamental mode distribution instead of the one obtained with consideration of the source may be well misleading. On the other hand, for safety of the system its distance from supercriticality is essential, thus making the exact and reliable evaluation of the k_{eff} most important.

The MCNP code may serve as a very pertinent instrument of investigation of subcritical systems provided its operation is well understood. Generally, the flux distribution can be calculated with the use of this code in the source mode, whereas the asymptotic distribution is calculated in the KCODE mode, when having skipped a number of initial cycles dominated by the source neutrons and a number of the immediate generations. A question may appear how many cycles should be skipped in order to obtain a correct fundamental mode and a reliable evaluation of its parameters.
The other objective of the present study is to show a possibility of use of the above computing tool for experimental validation. For instance, the kinetic properties of subcritical reactors are experimentally studied [2]. Thus, the distributions of fissioning vs. time in subcritical assemblies will be also investigated as serving to both purposes, i.e., to a better knowledge of these systems and of the code.

The calculations with the MCNP4B code have been performed in two modes: 1) in the Fixed Source one, i.e. with consideration of the source and 2) without in – in the KCODE mode. Since the considered systems have been rather simple, except of the cases regarding detailed studies of the time distributions, the computation time required for having a satisfactory precision of results need not to be longer in the Fixed Source mode calculations than in the KCODE runs (500-1000 minutes on a work station). On the other hand, one should admit that a correct initial guess of the source distribution can shorten the KCODE mode calculations.

2. NEUTRON MULTIPLICATION

The calculations have been done for two configurations with homogenised media, spherical fast and thermal ones ($k_{eff} \geq 0.96$), for simplicity and saving computer time, as allowing for presentation of the effects vs. one dimension fully describing the system (Fig. 1a). A smaller cylindrical 14 MeV neutron driven experimental assembly ($k_{eff} \sim 0.99$) shown in the Fig. 1b.

Since the spherical symmetry may seem inappropriate the source neutrons distribution has been sketched in the Fig. 2. Then, in Fig. 3, the evolution of neutron multiplication process in successive generations is presented.

One can see in Fig. 2. that the forward anisotropy of input neutrons is not particularly exposed, thus the assumption of isotropy seems acceptable, particularly for larger, industrial scale systems. In turn, on the basis of the Fig. 3 one may see when the generation dependent neutron multiplication factor k_i and thus the multiplication process seem “stabilised” [8]. In the above cases, one could apparently (as it will be shown later) safely declare that since 10-20 generation the asymptotic value of k_i, slightly below 0.97, is attained. However, the requirements concerning the estimations of the k_{eff} are much more rigorous, therefore a further pursuit, this time rather of the number of neutrons in the system than of its k_i, has been carried out and is illustrated in the Fig. 4a-c.

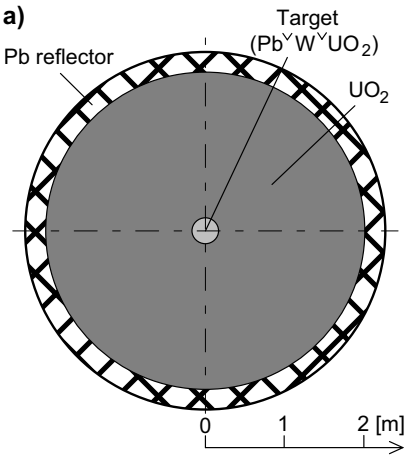

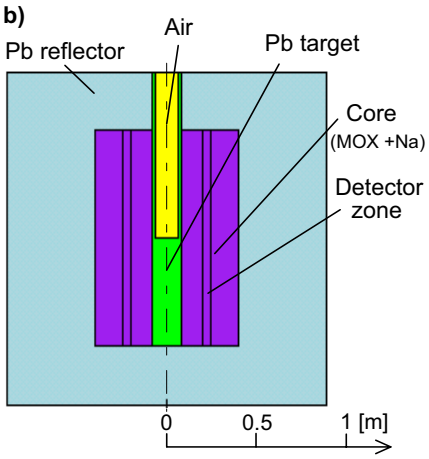

a) Full scale spherical assembly. *b) Cylindrical research one.*

FIG. 1a-b. Models of the systems to be investigated.

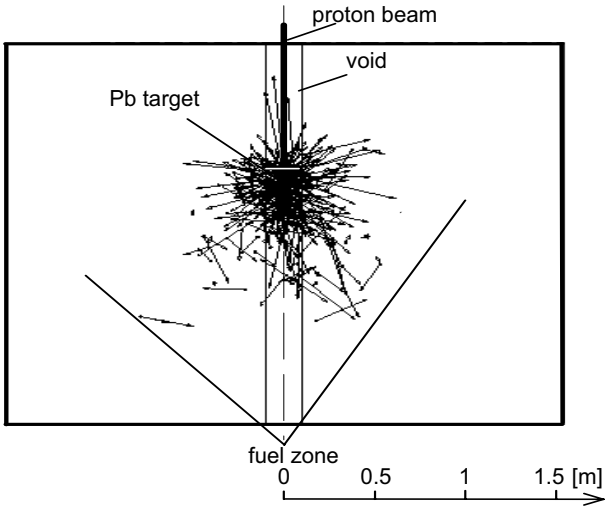

FIG. 2. A picture of space-angular distribution of input neutrons for MCNP calculations [7]/ (obtained from the LAHET code [4] for <20 MeV).

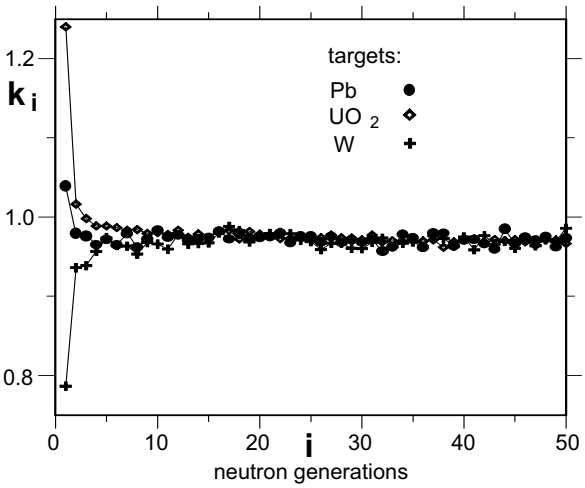

*FIG. 3. Generation dependent neutron multiplication factor k_i vs. generation number **i.***

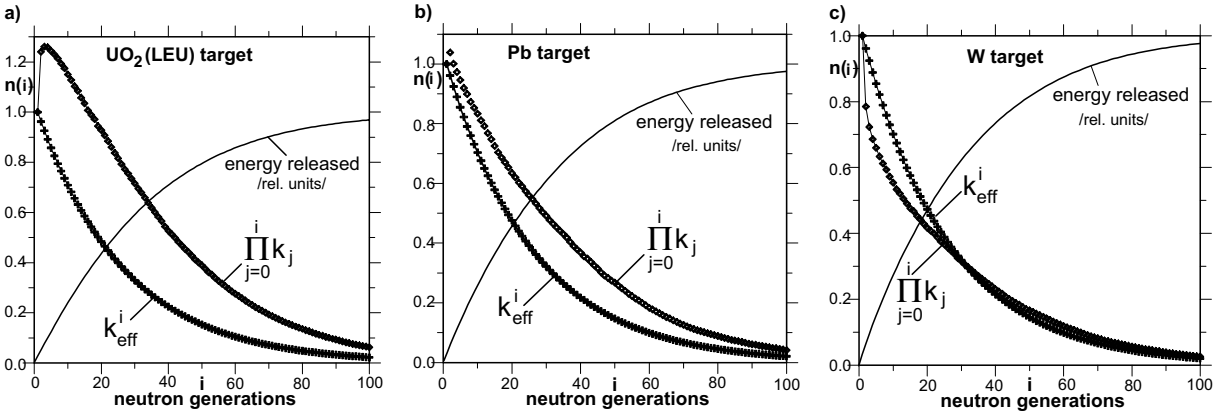

FIG. 4a-c. Number of neutrons and cumulative energy release in subcritical systems with various targets vs. generation number.

One of the most spectacular effects seen in the Fig. 4a-c. is the influence of the target material on the number of neutrons in not only the first but also in all the next generations [6, 8]. Thus, W as a strong absorbent is "sucking" the source neutrons, making the first generation significantly weaker. In contrast, the LEU target is supplying neutrons in extra fissioning, whereas, in this view, the Pb target proves neutral. Consequently,
the total number of neutrons in the system, i.e. the sum $\sum_{i=1}^{\infty}(\prod_{j=0}^{i} k_j)$ over all generations can be either much higher (for fissile material in the source zone) or, to the contrary, much lower (for W target), than the sum $\sum_{i=1}^{\infty}(k_{eff})^i$ equal to $1/(1 - k_{eff})$.

In Fig. 4a-c a much finer effect can be noticed, namely a non-uniformity of the neutron multiplication. For systems with the Pb and (still more) W targets a higher multiplication than the asymptotic one takes place in the ca. 20-70 i.e., the "medium" generations. Simultaneously, one sees that in all the above cases i.e. for given values of k_{eff} most of the energy (much more than 90%) is released in the transient phase of the multiplication process. The answer after which generation the k_i becomes constant is given in Fig. 5.

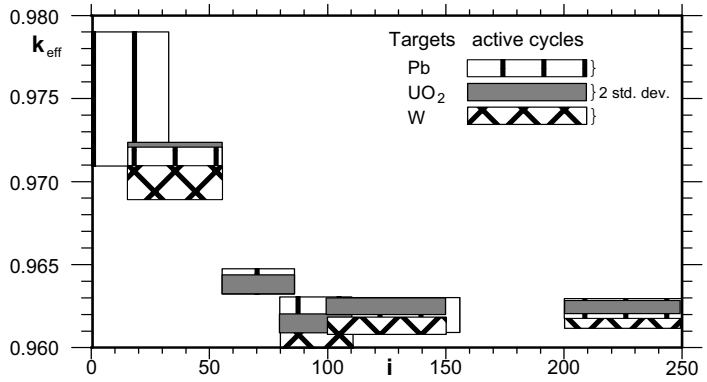

FIG. 5. Values of the k_{eff} vs. the selected active cycles.

On this basis (Fig. 5), one can conclude that in the given circumstances only after 80-100 generations (to be skipped in the KCODE mode calculations) the asymptotic state is attained. All this gives rise to a need for further investigations.

3. MODELING AND ANALYSIS OF FISSIONING DISTRIBUTIONS

Most demonstrative seems presentation of the neutron field in the 3-dimensional form as a function of space (system radius) and (approximately) time, as a generation number (Fig. 6 a,b). Instead of the neutron flux (of variable spectrum, see below) the fissioning has been chosen in belief that the heating distribution is much more meaningful.

In both the above pictures one sees how the birthplaces of successive neutron generations in external source-driven subcritical systems gradually spread out away from the source. Having seen this (particularly well in the Fig. 6a) one can explain the fine evolution of the values of k_i corresponding to successive generations related to different spatial distributions. Around half-way from the source to the outside of system the influence (either positive or negative) of the target on the number of neutrons disappears, while the leakage from the system still remains insignificant, thus making the respective values of k_i higher than the ultimate (asymptotic) ones. However, the "neutron wave" must at last reach the system edge, make the leakage larger and finally bring the k_i to its asymptotic i.e., eigenvalue. This explains the higher values of k_i in the respective generations.

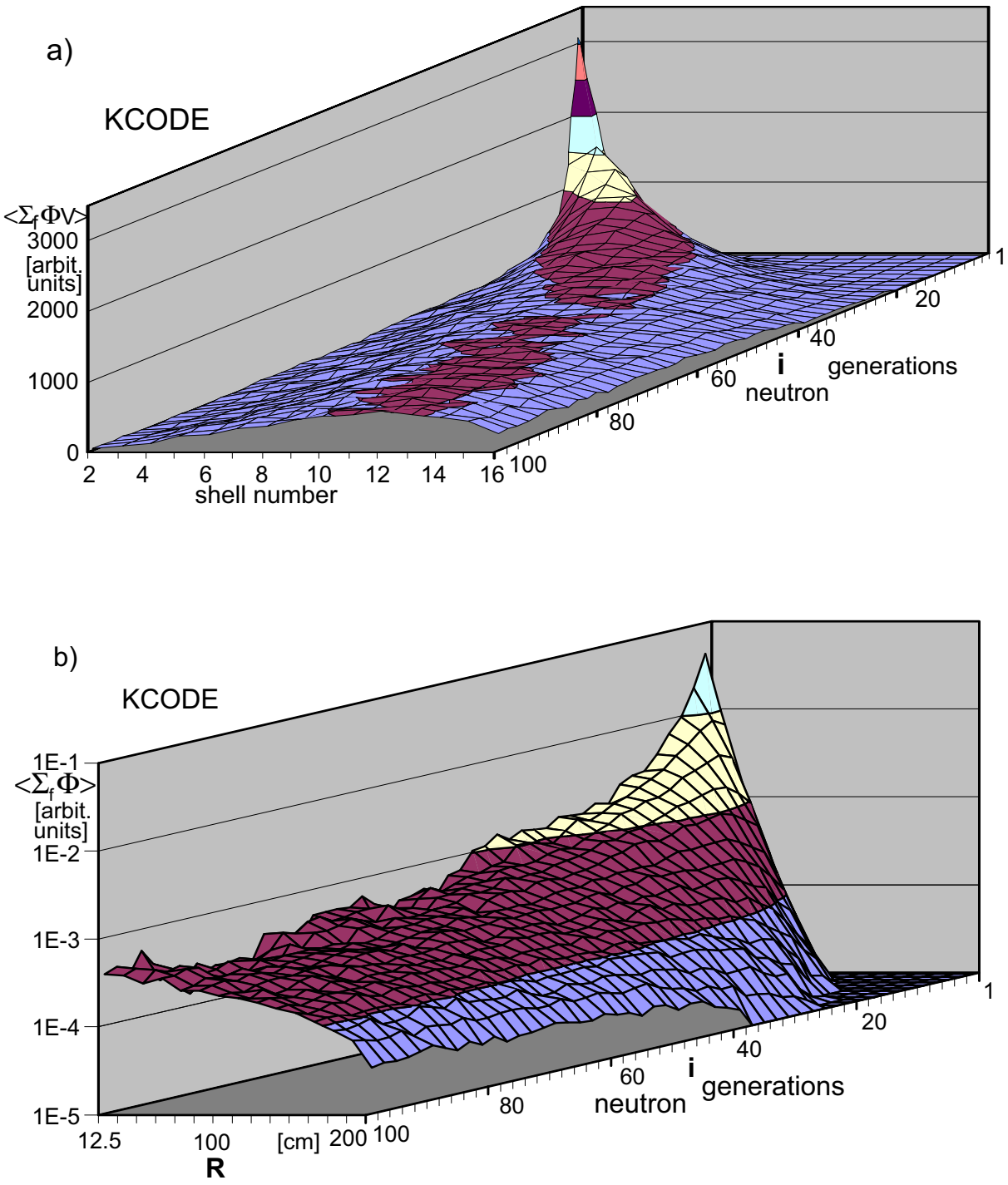

*FIG. 6a-b. Spatial distribution of fissioning vs. generation number **i** in a subcritical system.*

It should be reminded here, that although the neutron generation time remains approximately constant over generations, the x-axis representing the sequence of neutron generations only approximately corresponds to the time, thus giving rise to a need for illustration of fissioning dependence on time (see Section 3.1).

Now, the effective fissioning distribution within the system is to be analysed (Fig. 7a-d).

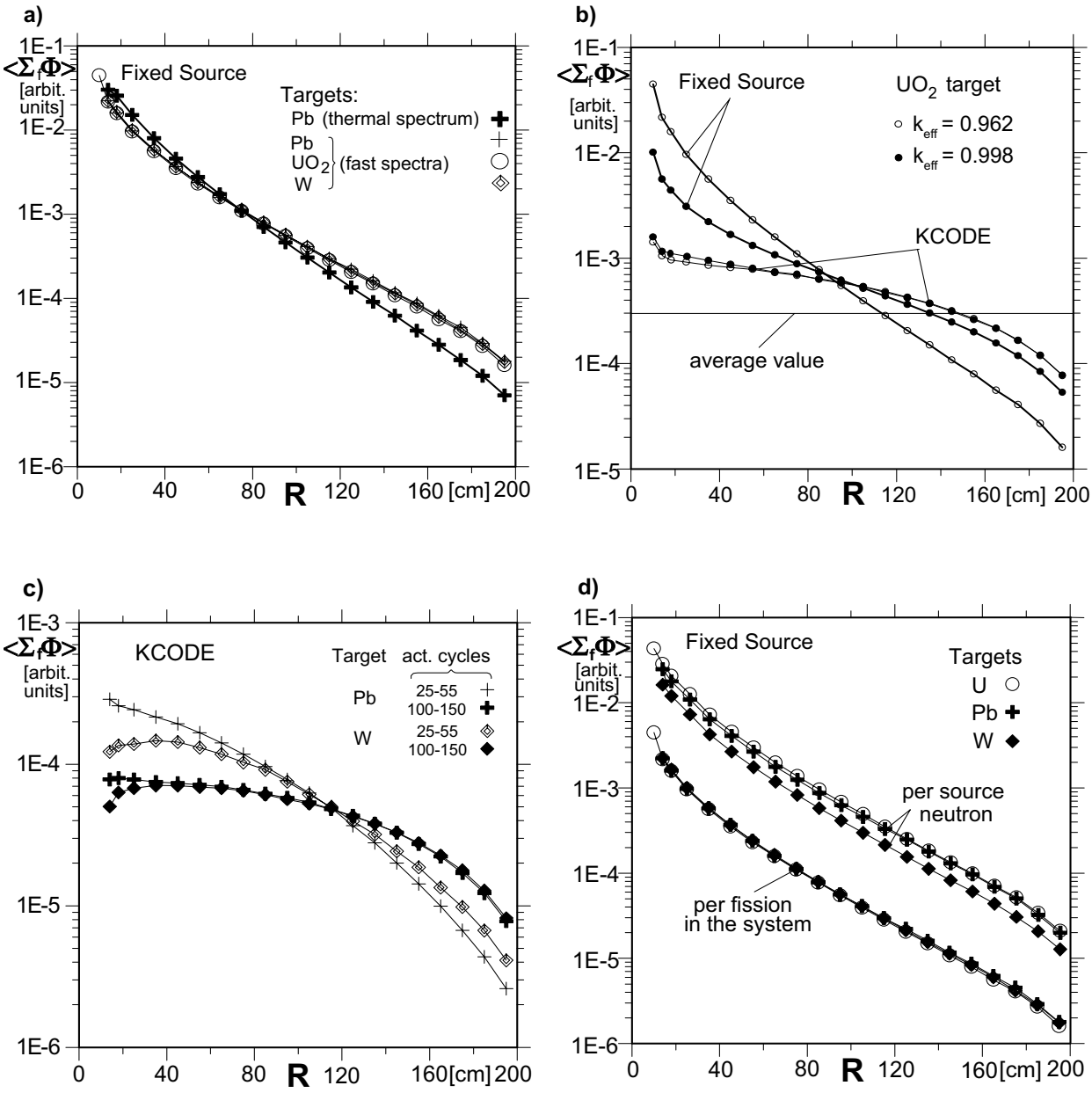

FIG. 7a-d. Radial distribution of specific fissioning in subcritical assembly for various targets and calculation modes with consideration of the external source (Fixed Source) and without (KCODE).

The presented pictures are well explainable. As the most important (Fig 7a,b), seems picturing the range in specific fissioning in large unshielded subcritical systems i.e. in heating, incineration rate, radiation damage etc. between the regions close to the neutron source and the outer ones. The span obtained in Fixed Source calculations (at $k_{eff} = 0.962$) prove up to three orders of magnitude higher than that obtained on the basis of asymptotic distribution (KCODE). The effect is still stronger (~3 times) for well-thermalised systems, moreover, it remains significant not solely at deeper subcriticalities, but also at k_{effs} amounting to 0.998 (Fig. 7b). On the other hand, one should note that the power peaking larger in uniform media even by factor of 10 than in eigenstate is mostly due to peak heating in the central zone of rather small volume. Yet, this is a disadvantage of subcritical systems since can draw behind difficulties in cooling and excessive burnup with all consequences. A trial of solution to this question, namely a distributed (shell) target, has been proposed in an earlier work of one of

the authors [5]. A more straightforward solution is varying the fissile material distribution, yet bringing also a complication of the system structure.

The negligible influence of the target on the shape of the effective heating distribution is also worth to notice. However, this influence manifests itself by the absolute values of fissioning, visible when is normalised to one source neutron. In this case, the material of the source zone directly affects the number of neutrons leaving the target. Thus, to the LEU target corresponds the highest level of fissioning, to the Pb one - slightly lower and to W target – the lowest level (Fig. 7c). Its asymptotic distribution is affected by the material of source zone. A LEU target increases the fissioning in its vicinity, while contrarily, a tungsten target – decreases it (Fig. 7c). Instead, for Pb target, because of some antagonistic tendencies (the target acts as a shield of the fissile material from one side but as a reflector from the opposite one) the distribution lies in between (Fig. 7c). Finally, it may be observed that the preponderant significance of the neutron source discourages to consider it as a mere perturbation of the eigenstate.

3.1. Time-dependent processes

The link to experimental validation of the computing tools and data is an important aspect of the present study. In particular the kinetic properties of subcritical reactors deserve more attention and are experimentally studied e.g., [2]. The interest in these properties of accelerator-driven systems is particularly justified in view of planned or accidental shutdowns of the beam making the source neutrons disappear and drawing behind a rapid drop in system power. The following descent of temperature may result, in turn, in a thermal shock.

Naturally, neutron's affiliation to individual generations cannot be verified experimentally, thus the knowledge of respective distributions is insufficient. In contrast to the indistinguishable, overlapping generations, the time distribution of neutron field can be object of experiments. Thus, fissioning distribution vs. time and space in spherical subcritical system is shown in the Fig. 8.

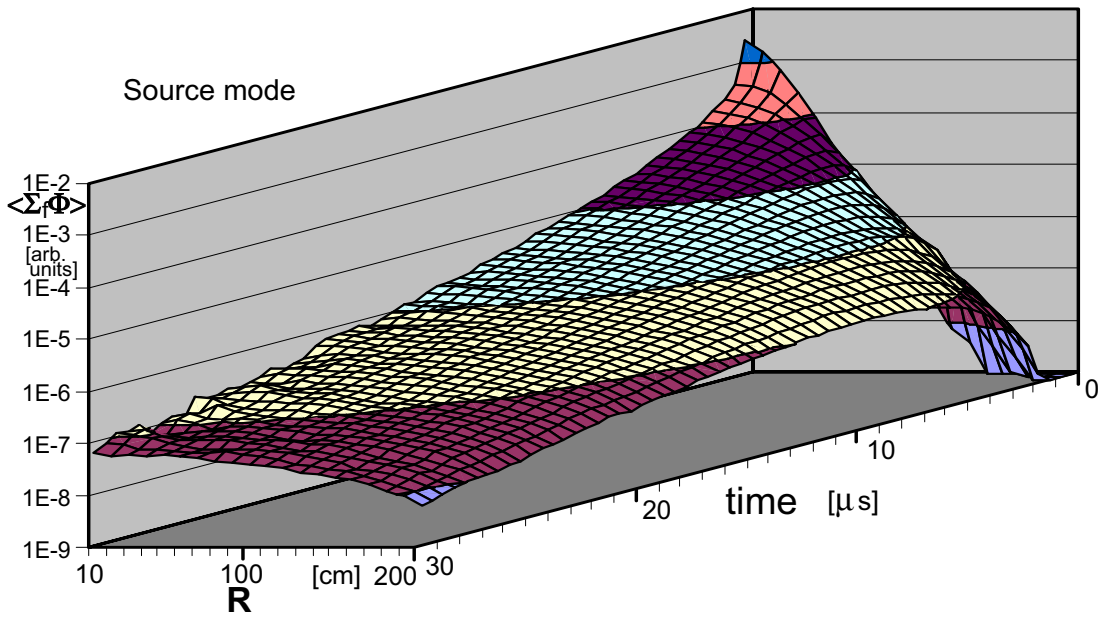

FIG. 8. Spatial distribution of fissioning vs. time in a subcritical system

In turn, the cross-sections (along time axis) of such 3-D distributions have been obtained for both assemblies considered in this study. The shown (Fig. 9a-d) trajectories regard not only the whole system, but are also local, seeing that fission chambers used in the respective measurements are usually quite small. In these calculations, when having assumed low repetition rates, for the given time intervals (0.3 μs–10 ms) the delayed neutron component is reduced to a negligible constant background and the k_{effs} are simply the prompt values.

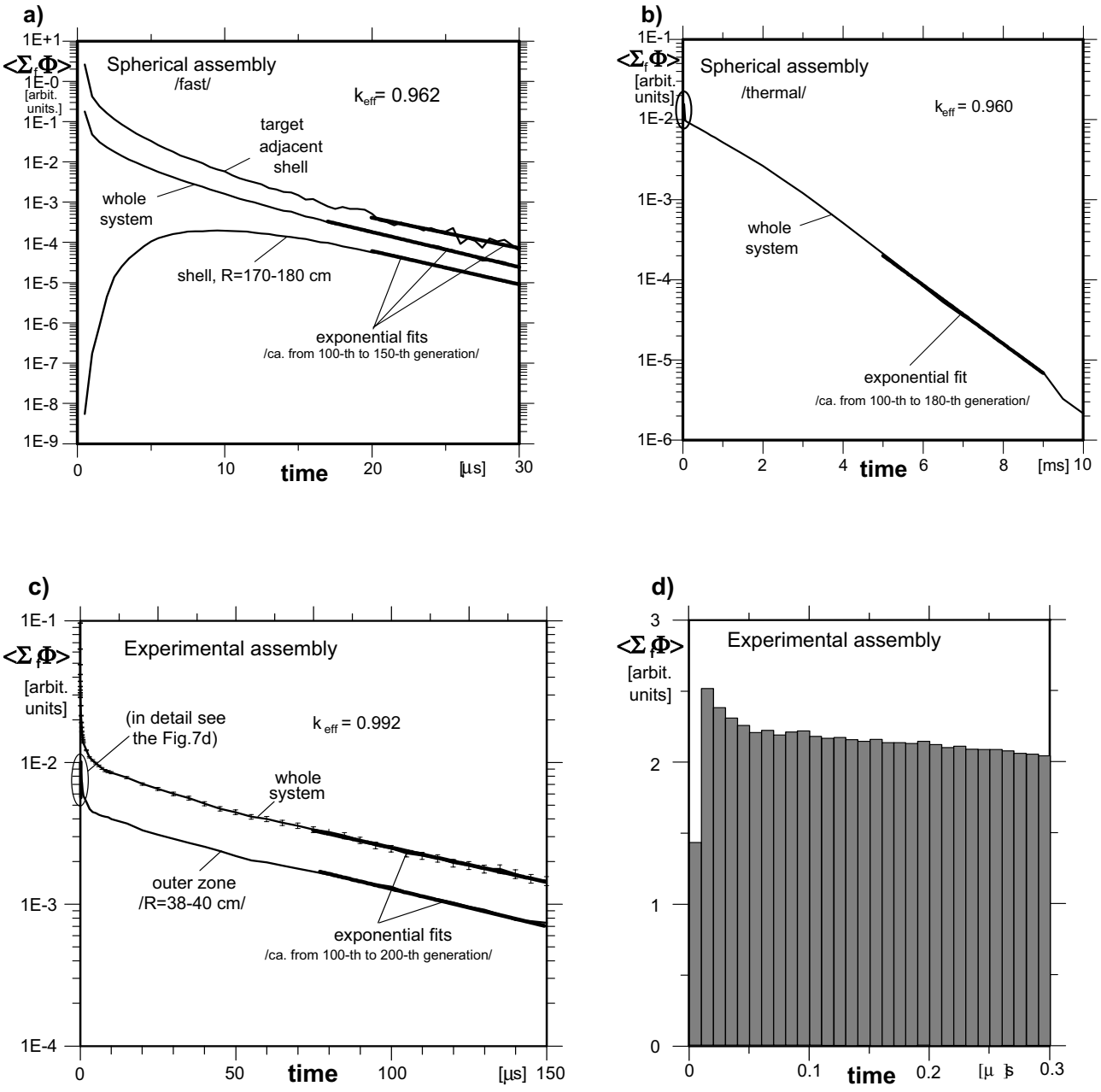

FIG. 9a-d. Distribution of fissioning in subcritical systems vs. time.

Yet, this component, as being amplified approximately by the factor $1/[1 - (k_{eff}-\beta_{eff})]$ may be a quite significant fraction of the total flux, in steady state, for continuous operation of the external source equal to $\beta_{eff}/[1 - (k_{eff}-\beta_{eff})]$. Thus, e.g., for β_{eff} = 0.5% and k_{eff} = 0.96 it constitutes as much as 1/9 of this flux, while for higher (0.995) k_{eff} even 1/2. Obviously, the

filling factors of the source are usually low ca. 10^{-3}. Nevertheless, this puts certain limits to the conditions in which the prompt neutrons decay can (if ever) be recognised as unaffected by the delayed ones. The diagrams shown above agree with intuition, also in details. For instance, a time lag of the fissioning in an outer zone of spherical system is well exposed in the Fig. 9a. Similar lag, but regarding a very short time scale, can be seen in Fig. 9d. In both cases, the effect results from the lapse of time needed for neutrons to reach the given region. In large assemblies, the source neutrons do not get that far, thus only the diffusion of "fission wave" from the centre of the system gradually reaches the outer regions. Instead, in a small assembly the source neutrons can arrive there. The route of 14 MeV neutrons, a direct one or with elastic scattering from the centre to the outermost fuel zone requires just some 10 ns.

The initial peak of fissioning, more or less distinct in all the Figs. 9a-d has also a basic physical explanation. However, not by higher importance of source neutrons and their closest descendants, since the mean probability of fissioning is not significantly changed until neutrons approach the system edge. Besides, the slowing-down of neutrons [taking some time (see Fig. 10)] might act in the opposite direction. The explanation lies in the build-up of generations, of which the early ones, obviously, have to be much less spread in time than the later ones (Fig. 11).

Yet, the neutron spectrum that anyway strongly affects fissioning is shown first (Fig. 10).

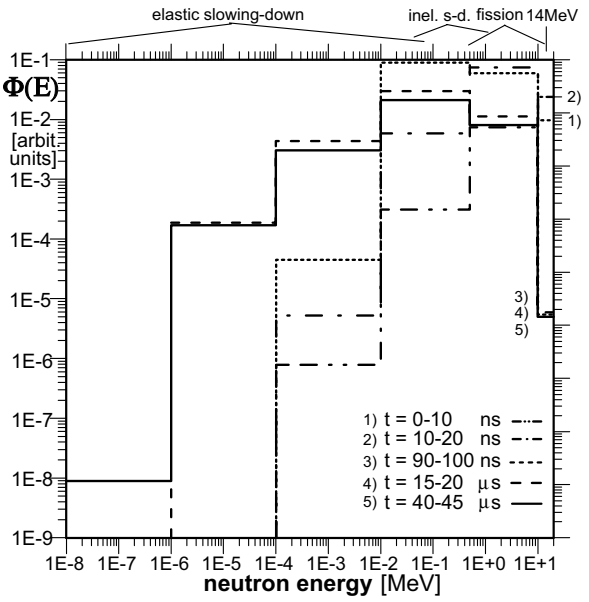

FIG. 10. Evolution of the neutron spectrum in the outer zone of subcritical system after 14 MeV neutron δ-shaped pulse.

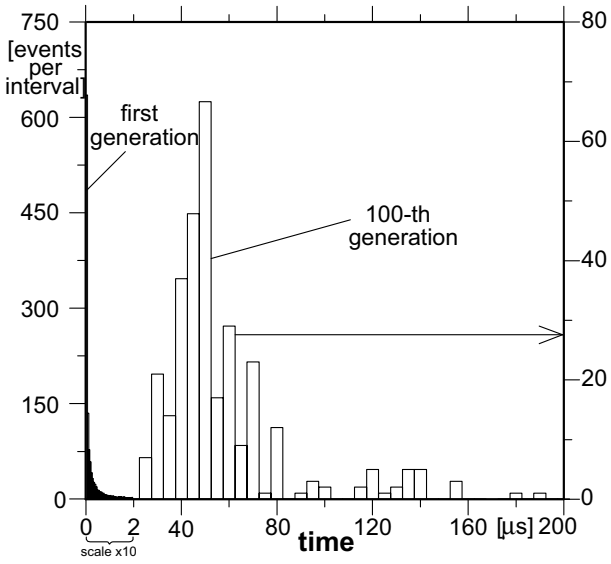

FIG. 11. Time distribution of fissions belonging to the first and to the 100-th neutron generation.

The increase in the flux component >10 MeV in the second shake (10-20 ns) as compared with the first one signifies that not all neutrons could reach the zone before 10 ns (Fig. 10.). The parallel rise in the interval 0.5-10 MeV indicates intense fissioning. The flux culmination, after nearly 0.1μs, in the adjacent energy region 0.01-0.5 MeV is a sign of slowing-down – mostly in inelastic processes. The slowing-down continues during next microseconds /through elastic scattering/ bringing neutrons from the above intervals down below 0.01 MeV. Summarising, in agreement with intuition, the spectra shown in the Fig. 10 indicate very fast and significant changes during first 100 ns, while quite negligible after 20 μs.

In connection with the kinetic parameters, the most interesting is the check of consistency of the results provided by the MCNP in different calculating modes. The values: the k_{eff}, /thus the reactivity ρ/ and the generation time τ /the neutron life span with regard to fission/, both obtained in the KCODE mode and the neutron field attenuation rate (Fixed Source) are mutually dependent thus should be consistent. The values of τ_s have been evaluated from the equation:

$$\exp(t\cdot\rho/\tau_s) = \exp(-at) \tag{1}$$

where *a* is the slope of decay curves obtained from the Fixed Source calculations (Fig. 9a-c).

Since measurements of the vanishing of neutrons in the system as a whole are more difficult (as requiring integration over its volume), the generation times are evaluated for selected regions too (Table 1).

TABLE 1. NEUTRON GENERATION TIMES

Assembly parameter	Spherical				Cylindrical experim.	
	fast			thermal	fast	
	out. zone	whole	inner zone	whole	out. zone	whole
k_{eff} (prompt)		0.962		0.960	0.9925	
τ [μs] (fission life span) KCODE		0.236		50.0	0.750	
τ_s [μs] (from decay slope) fixed source	0.214	0.209	0.236	50.5	0.670	0.740

As can be seen in the Table 1, consistency of the presented results is acceptable, though might be better (they should be accordant for systems consisted solely of fissioning zones, since in the KCODE the source distribution in each cycle is obviously confined to these regions).

Finally, seems purposeful to indicate some particularity of the MCNP concerning the neutron lifetimes provided in its standard outputs with regard to selected processes. The only intention of the respective calculations is to illustrate the problem (Table 2).

TABLE 2. EXAMPLES OF NEUTRON LIFETIMES OBTAINED WITH THE MCNP CODE

Process	escape		capture		capt. or escape		any termination	
k_{eff}	0.962	0.998	0.962	0.998	0.962	0.998	0.962	0.998
Calculation	(μs)							
KCODE	0.60	0.59	0.31	0.30	0.32	0.31	0.29	0.28
Fixed source	13.33	30.0	5.75	21.9	5.80	22.0	3.56	13.3

In Table 2 can be seen a very striking discrepancy between the values provided by the KCODE and the Fixed Source modes. Whereas the values obtained in the former mode do not seem to rise to some objections, the ones provided with the Fixed Source, larger even ca.

50 times, do not regard individual neutrons but, rather surprisingly - the *whole* neutron chain. Thus, these values do not correspond to the interval of exponential decay alone either and the observed extension of the lifetimes (ca. 4 times) cannot reflect the increase in the reciprocal of $(1 - k_{eff})$, i.e., 19. All this results from differences in program flow in both modes. In the KCODE mode, fission events terminate neutron histories, whereas in the Fixed Source mode they are regarded as the non-terminating inelastic scattering events only. In that case, the neutron history is not finished but the transport of the first emerging neutron continues. Since the neutrons cannot be killed by fission, their lifetime describe actually the whole chain of subsequent generations. Thus, in this case the results cannot be understood as previously in the KCODE and a reliable use of them seems doubtful without further studies.

4. CONCLUSIONS

The presented study allows for a number of remarks and statements. The attainment of the eigenstate in subcritical systems has proved a lengthy process lasting unexpectedly long time and many generations. Thus, in order to obtain a reliable evaluation of the asymptotic distribution the number of cycles to be skipped in the KCODE calculations should be quite high. Similarly, the span in heating density in large unshielded subcritical systems has proved much larger than might be anticipated. This effect shown in uniform systems, causes problems of cooling and fast burnup, gives rise to a need of counteraction. A varying of the fissile material distribution may be a solution, yet resulting in a complexity of the system structure & operation.

The details of time dependent processes are well simulated - in particular the early multiplication processes that leave consequences sometimes reflected in all the following generations. The obtained results have shown satisfactory consistence, thus confirming a possibility of MCNP use for validation in respective experiments. However, it should be noted, that the values of neutron lifetimes provided in the Fixed Source mode require further studies for correct interpretation. Summarising, the last remark notwithstanding, the MCNP code has proved a very useful universal tool for investigations of subcritical systems.

REFERENCES

[1] BRIESMEISTER, J.F., (Ed.), MCNP - A General Monte Carlo N-Particle Transport Code, LANL, Report 12625-M, Version 4B (1997).

[2] "MUSE Experiments for Subcritical Neutronics Validation", http://dbs.cordis.lu/EN_PROJI_search.html (2000).

[3] PEARLSTEIN, S., The Effective Delayed Neutron Fraction for Bare Metal Assemblies, Nucl. Tech. 128, (1999) 401.

[4] PRAEL R.D., LICHTENSTEIN, H., User Guide to LCS: the LAHET Code System, LANL Report, LA-UR-89-3014 (1989).

[5] TACZANOWSKI, S., Selected Properties of Accelerator-driven Subcritical Systems for Transmutations, Proc. IAEA Technical Committee Meeting on Advanced Fuels with Reduced Actinide Generation, Vienna, IAEA-TEC-DOC-985 (1997) 137-150.

[6] TACZANOWSKI, S., IAEA Techical Committee Meeting on Hybrid Concepts Nucl. Energy Generation & Transmutation 1997, Madrid, Spain, IAEA TC-903.3, Ciemat, Spain (1999) 409-424 and INT Report 270/I, Cracow (1997).

[7] TACZANOWSKI, S., KOPEĆ, M., Neutronic Study of Accelerator-driven Subcritical Systems for Transmutations; Proc. Int. Conf. on Future Nuclear Systems (Global'97), 5-10 October 1997, Yokohama, Japan, ECN Nucleaire Research/Facilities (NRG), ECN-RX- -97-022 (1997) 1301-1307.

[8] TACZANOWSKI, S., Neutronic Optimization of Accelerator-driven Subcritical Systems for Transmutation; Proc. Int. Conf. on Emerging Nuclear Systems (ICENES'98), 1998, Tel Aviv, Israel, Y. Ronen, L. Tepper, E. Elias (Eds), Knassim Ltd., Tel-Aviv, Israel (1998) 777-784.

[9] TAKAHASHI, H., YANG, Y., CETNAR, J., ZHANG, J., Monte Carlo calculation of burn up for an accelerator-driven reactor, ibid., Proc. CD ROM Tu-O-F18 (1999).

[10] TUCEK, K., WALLENIUS, J., GUDOWSKI, W., SOLTAN, A., IAEA Accelerator Driven System Neutronic Benchmark, Proc. IAEA Techical Committee Meeting on Hybrid Concepts Nuclear Energy Generation & Transmutation, 17-19 September 1997, Madrid, IAEA TC-903.3, Ciemat, Spain (1999) 535-551.

DESIGN CRITERIA AND MITIGATION OPTIONS FOR THERMAL FATIGUE EFFECTS IN ATW BLANKETS

F.E. DUNN
Argonne National Laboratory, Argonne, Illinois,United States of America

Abstract

Thermal fatigue due to beam interruptions is an issue that must be addressed in the design of an ATW blanket. Two different approaches can be taken to address this issue. One approach is to analyze current ATW blanket designs in order to set interrupt frequency design limits for the accelerator. The other approach is to assume that accelerator reliability can not be guaranteed before design and construction of the blanket. In this approach the blanket must be designed so as to accommodate an accelerator with a beam interruption frequency significantly higher than current high power accelerators in order to provide a margin of error. Both approaches are considered in this paper. Both a sodium cooled blanket design and a lead-bismuth cooled blanket design are considered. Thermal hydraulic analysis of the blanket for beam interruption transients is carried out with the SASSYS-1 systems analysis code to obtain the time histories of the coolant temperatures in contact with structural components. These coolant temperatures are then used in a detailed structure temperature calculation to obtain structure surface and structure average temperatures. The difference between the average temperature and the surface temperature is used to obtain thermal strains. Low cycle fatigue curves from the American Society of Mechanical Engineers Boiler and Pressure Vessel Code are used to determine the number of cycles that the structural components can endure, based on these strains. Calculations are made for base case designs and for a number of mitigation options. The mitigation options include using two separate accelerators to provide the beam, reducing the thickness of the above core load pads in the subassemblies, increasing the coolant flow rate or reducing power in order to reduce the core temperature rise, and reducing the superheat in the once-through steam generator.

1. INTRODUCTION

In the past, accelerator design was focused on maximum particle energy or maximum beam power, rather than on continuous reliable operation for long periods of time. Frequent beam interruptions were tolerated as a price to be paid for maximum particle energy or maximum beam energy. For instance, Table 1 lists the frequency of beam interruptions for the LANSCE accelerator [1]. In the past, power reactors were designed for constant power operation for long periods with no interruptions. The question that will be addressed in this paper is whether these two technologies can be mated successfully. A beam interruption in an accelerator driven system is similar to a reactor scram, but faster. The specific areas addressed in this paper are the thermal fatigue consequences of frequent beam interruptions in an accelerator driven system, and the mitigation options.

Calculations were made for both a sodium cooled blanket and a lead-bismuth cooled blanket. The sodium cooled design is based on the ALMR mod B design [2] with seven rows of subassemblies in the center of the core removed to make space for the beam and the target. The lead-bismuth cooled design analyzed here is similar except that the fuel pin diameter is smaller and the spacing between pins is larger in order to provide more coolant flow area and a lower core pressure drop. Other lead-bismuth designs use large pins with a large spacing between pins. In any case, a lead-bismuth cooled design will probably have a large coolant flow area per pin. Also, in the lead-bismuth cooled design the intermediate heat exchangers are removed and replaced by steam generators inside the primary vessel.

TABLE 1. FREQUENCY OF BEAM INTERRUPTIONS FOR THE LANSCE ACCELERATOR

Duration of interruption	Interruptions per day	Interruptions per year
10 s or more	39	14 200
1 min or more	9.5	3482
5 min or more	3.4	1237
15 min or more	1.7	617
1 h or more	0.6	214
5 hrs or more	0.09	34

Figure 1 shows a schematic of the coolant flow in the ALMR mod B design. The coolant flows upward through the core into an outlet plenum. From the outlet plenum the coolant flows directly into the shell side of the intermediate heat exchanger. In the intermediate heat exchanger the primary coolant flows downward and then out into a cold pool. From the cold pool the coolant is drawn into a pump and pumped back into the inlet plenum. The intermediate coolant flows upward through the tubes in the intermediate heat exchanger. It then flows through pipes to the steam generator and back to the intermediate heat exchanger. In the lead-bismuth cooled design the coolant flows are similar, but the intermediate heat exchangers are replaced by steam generators and there is no intermediate coolant loop.

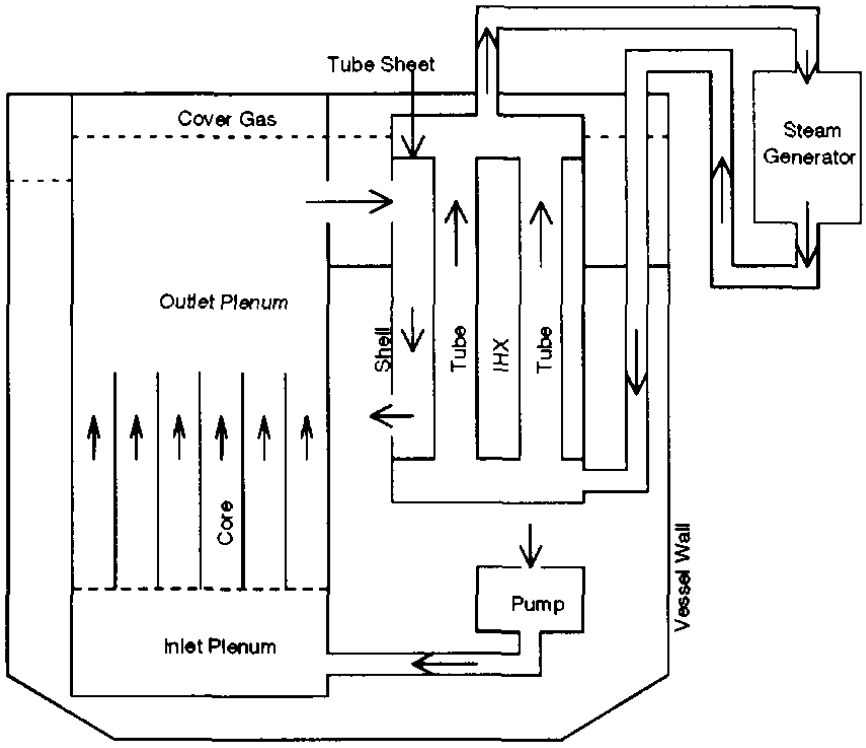

FIG. 1. Schematic of coolant flow in the ATW blanket.

2. ANALYSIS METHODS

2.1. The SASSYS-1 plant dynamics code

Temperature response in the primary coolant system, and in the intermediate coolant system in the case of sodium coolant, was calculated, using the SASSYS-1 systems analysis code [3], for an immediate drop in beam current from full power to zero. The SASSYS-1 plant dynamics code contains neutron kinetics coupled with a detailed thermal hydraulics treatment of the core, the primary and intermediate heat removal loops, and the steam generators. Both steady-state and transient calculations are done by the code. The neutron kinetics treatment contains point kinetics, with or without an external source. Also, the neutron kinetics treatment contains an optional 3-D time dependent neutron kinetics capability.

The thermal hydraulics in SASSYS-1 uses a multi-channel treatment for core subassemblies. Each channel represents one subassembly or a group of similar subassemblies. A channel models a fuel pin, its associated coolant, and structure. The subassembly duct wall is treated as structure, and wrapper wires around the fuel pins can be included in the structure. Coolant and structure above and below the fuel pin is also treated: the whole length of the subassembly from the inlet plenum to the outlet plenum is modeled. Beyond the core subassemblies the code calculates coolant pressures and flows, as well as temperatures for coolant and structure (walls). Calculations are made for inlet and outlet plenums, pipes, pumps, intermediate heat exchangers, and steam generators.

2.2. Programs Tslab and Tcylndr, one dimensional heat transfer in slab and cylindrical geometries

SASSYS-1 calculates structure temperatures, but SASSYS-1 uses only one or two radial nodes in the structure. One or two radial nodes are not sufficient to provide accurate transient temperatures in a transient as fast as those being considered in this work. Therefore, two small separate codes, Tslab and Tcylndr, were written to calculate accurate time-dependent structures given the coolant temperatures calculated by SASSYS-1. Up to 50 radial nodes can be used in these small codes. In Tslab the structure can consist of a number of separate materials in contact with each other. Thus, when calculating temperatures in the outlet plenum wall, one can include the vessel wall liner, the annulus of stagnant coolant between the wall liner and the vessel wall, and the vessel wall. In Tcylndr the region around a tube penetration through a tube sheet in an intermediate heat exchanger or a steam generator is modelled as a cylinder with an inner radius equal to the inner radius of the tube. The outer radius of the cylinder is chosen to conserve the tube sheet volume associated with one tube. The time-dependent temperatures of the coolant going through the inner hole in the cylinder is taken from the SASSYS-1 calculations. An adiabatic boundary is used at the outer radius of the cylinder. One dimensional radial heat transfer is calculated in the cylinder.

2.3. Evaluation of low cycle fatigue at elevated temperatures

The method used to evaluate low cycle fatigue at elevated temperatures uses an elastic analysis with corrections for creep and plasticity. This method is based on article T-1432 of Appendix T of Subsection NH of the ASME Boiler and Pressure Vessel Code [4]. This type of analysis is required when the temperatures exceed 700 or 800 EF. For a given peak strain and a given peak

temperature this method gives the maximum allowable number of cycles that the material can be subjected to.

One problem with the Appendix T treatment is that Appendix T only includes data for four materials: 304 stainless steel, 316 stainless steel, Ni-Fe-Cr alloy 800H, and 2 1/4 Cr-1 Mo steel. In the ALMR design, much of the primary and intermediate coolant loops are made of 304 stainless steel; and the steam generator is made from 2 1/4 Cr-1Mo steel. Any other material, such as the HT-9 used for fuel pin cladding and subassembly duct walls in the ALMR mod B design, is not covered by this treatment. The high silicon martensitic steel recommended by the Russians for use with lead-bismuth coolant is also not covered by this treatment. In contrast, the ASME low cycle fatigue treatment in Subsection NB of Section 3 is limited to temperatures below 700-800 EF; but it is applicable to broad classes of steels, including one category for ferritic steels, such as HT-9, and another category for austenitic steels, such as 304 and 316 stainless steel. The fatigue behavior of martensitic steels is probably similar to that of ferritic steels. To estimate fatigue limits for HT-9 at elevated temperatures, it was decided to analyze the load pads with the Appendix T treatment using 316 stainless steel properties and then to multiply the allowable number of cycles by a factor, f_{HT-9}, to get the allowable number of cycles for HT-9. To obtain a value for f_{HT-9} cases were evaluated for both HT-9 and 316 ss using the Section 3, Subsection NB treatment and no correction for elevated temperature operation. In these cases the allowable number of cycles for HT-9 tended to be about one sixth of the allowable number of cycles for 316 ss. Thus, the value used for f_{HT-9} is 1/6. The same factor is used for the high silicon martensitic steel used with lead-bismuth coolant.

3. RESULTS FOR CURRENT BLANKET DESIGNS

3.1. Loss of beam transient

Loss of beam transients were run for both the sodium cooled design and the lead-bismuth cooled design. In both cases the initial coolant temperature rise in the hottest core channel was 164 K, and the average coolant temperature rise was 139 K. In these transients, the external source from the beam dropped instantly from full power to zero. The pumps were not tripped. The detailed steam generator model in SAS4A was used in the analysis of these transients. The feed water flow and the turbine throttle valve were adjusted during the transient so as to maintain constant water level in the steam generator and so as to maintain constant steam pressure at the outlet of the steam generator.

Figure 2 shows the powers and flow for the loss of beam transient. At the beginning of a refuelling cycle k effective is about 0.975, but by the end of the cycle k effective can drop to 0.92 or lower. It can be seen from Figure 2 that the power drops almost instantly from nominal power to a much lower value after the loss of the beam. Then the power drops slowly toward decay heat levels. In the early part of the transient, the power drops significantly lower with a k effective of 0.92 rather than 0.975. The results presented in this section were all run with k effective equal 0.92. The impact of the degree of subcriticality is discussed in Section 3.2.

Figure 3 shows the coolant and structure temperatures at the position of the subassembly above core load pads in the hottest subassembly for the lead-bismuth cooled case. During much of the transient, the average structure temperature calculated with 20 radial nodes in TSLAB is about 10 K lower that the value calculated with two radial nodes in SASSYS-1.

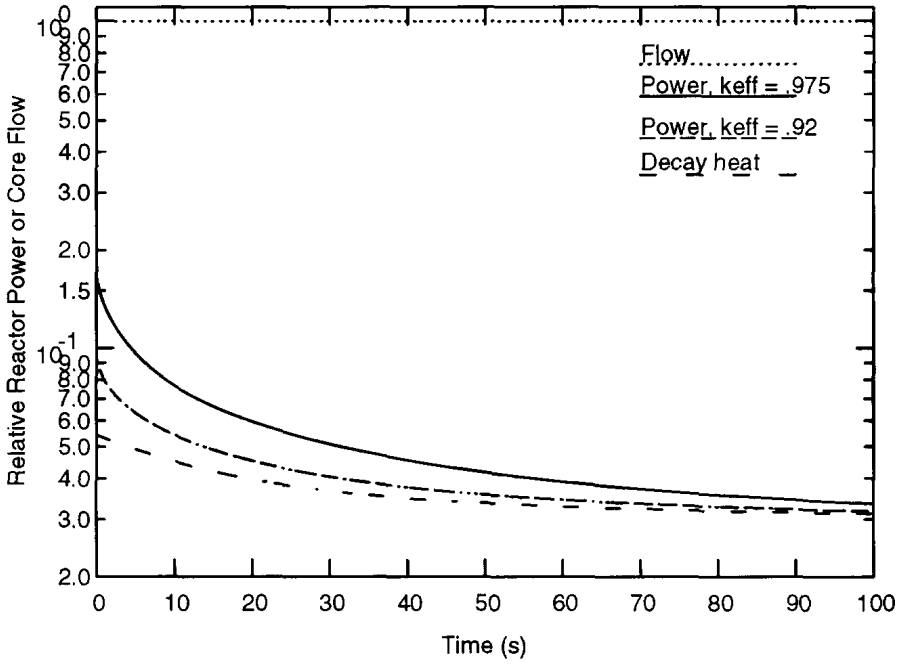

FIG. 2. Normalized power and flow for a beam loss.

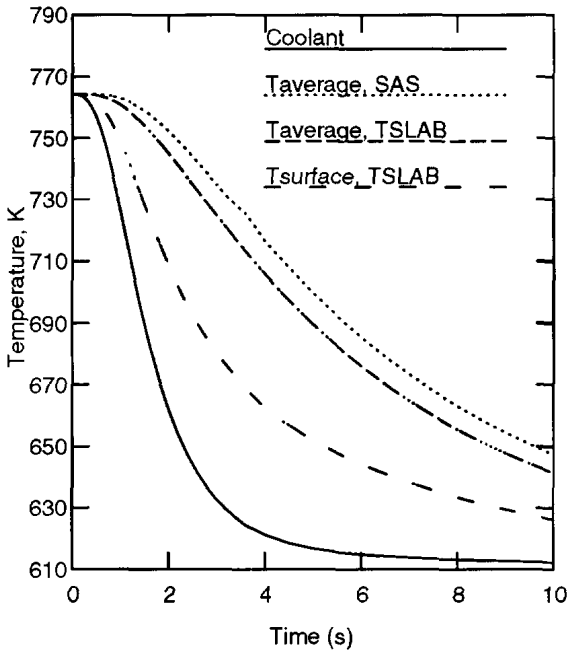

FIG. 3. Top of core coolant and structure temperatures, Pb-Bi.

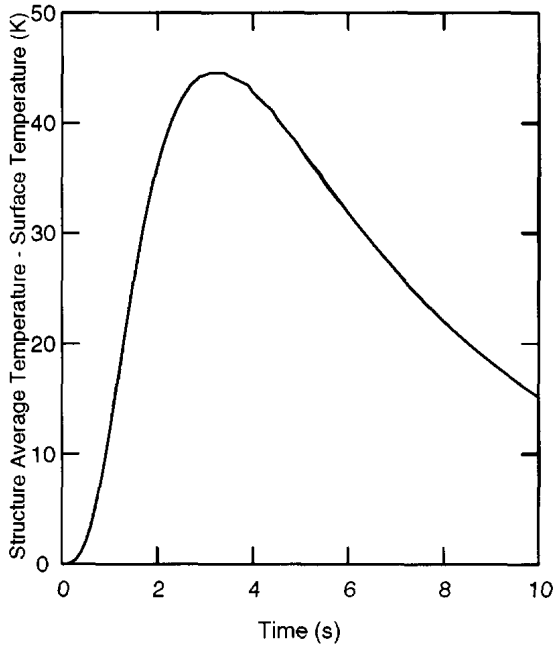

FIG. 4. Temperature difference at the top of the core, Pb-Bi.

Figure 4 shows the difference between the structure average temperature and the structure surface temperature at the position of the above core load pads. This difference peaks at 44.6 K at 3.2 s into the transient. Results for sodium coolant are similar, except the difference between the structure surface temperature and the coolant temperature is smaller because of the higher thermal conductivity of the sodium. This leads to a larger difference between the structure average temperature and the surface temperature.

Figure 5 shows the temperatures in the upper tube sheet of the steam generator in the lead-bismuth case. Because of the large diameter of the tubes and the large spacing between tubes, the average temperature in the tube sheet drops slowly even after the temperature of the steam going through the tubes has dropped significantly. The steam temperature drops from its initially superheated value to a temperature near saturation after about 200 s into the transient. The tube surface temperature drops to a minimum near 200 s then rises. The rise occurs because the steam flow rate drops during the transient, and the steam heat transfer coefficient drops as the flow rate drops. Figure 6 shows the difference between the average tube sheet temperature and the tube surface temperature. This difference peaks at 72.8 at 191 s into the transient.

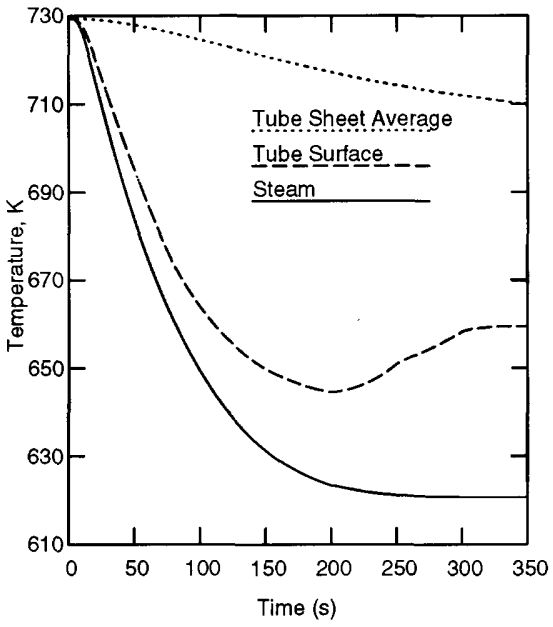

FIG. 5. Steam generator upper tube sheet temperatures, Pb-Bi.

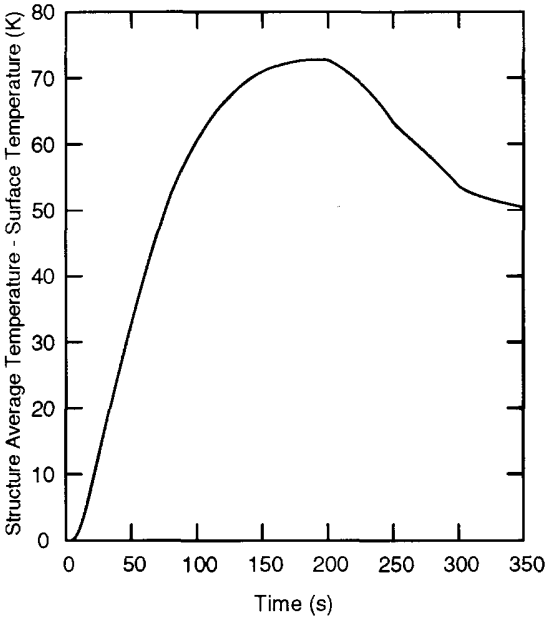

FIG. 6. Steam generator upper tube temperature differences, Pb-Bi.

Table 2 summarizes the peak structure temperature differences and gives the corresponding fatigue results for both sodium cooled and lead-bismuth cooled systems. Subassemblies are normally left in the core for three or four years, so with sodium coolant the fatigue damage to the above core load pads is not acceptable unless some mitigation action is taken. With the lead-bismuth design the above core load pads are okay if the frequency of beam interruptions is no worse than the LANSCE data. With either coolant the damage to the outlet plenum wall is within

acceptable bounds with the specified frequency of interruptions. If the plant is expected to operate for 30 years, then the fatigue damage to the intermediate heat exchanger tube sheet rim in the sodium cooled case, and to the steam generator tube sheet in the lead-bismuth cooled case, require mitigation action. The largest uncertainty in these calculations is the actual frequency of interruptions of the accelerator. The ATW accelerator has not been designed or built, so the actual reliability of the beam is unknown.

TABLE 2. ESTIMATES OF FATIGUE DAMAGE DUE TO BEAM INTERRUPTIONS

Structural element	Coolant	Material	Thickness (m)	Peak ΔT (K)	Time of Peak (s)	Allowable cycles	Interruptions/ Year	Tears of operation
Above core load pads	Pb-Bi	martensitic	0.0056495	44.6	3.2	6.8×10^{4}	14 200	4.8
	Na	HT-9	0.0056495	66.2	1.9	7517	14 200	0.53
Outlet plenum upper wall	Pb-Bi	martensitic	0.0254	27.0	127	1.7×10^{5}	2230	75+
	Na	304 ss	0.0254	40.7	121	10^{6}+	2230	450+
IHX tube sheet rim	Na	304 ss	0.0635	114.3	219	2475	1556	1.6
Steam generator tube sheet	Pb-Bi	martensitic	0.0753	72.8	191	8100	1648	4.9
	Na	2 1/4cr-1 Mo	0.0753	68.3	211	2.6×10^{5}	1556	167

It might appear from the results in Table 2 that from a thermal fatigue point of view lead-bismuth is a better coolant for the ATW design than sodium, but out of necessity the designs are different. In particular, in order to avoid a large coolant pressure drop in the core, the lead-bismuth design uses smaller pins with more space between pins. If the sodium cooled design used the same small pins and larger space between pins, then for the same pumping power the sodium cooled device could have a significantly higher coolant flow rate, leading to a smaller coolant temperature rise across the core and significantly lower thermal strains in the transient.

3.2. Impact of the degree of sub-criticality

As mentioned previously, the results in the previous section were run with a blanket k-effective of 0.92, which is typical of the value at the end of a re-fuelling cycle, whereas at the beginning of the cycle k effective might be 0.975. Therefore, one case was run with a k-effective of 0.975. This was a sodium-cooled case identical to the case previously described except for the value of k-effective. Figure 7 shows the influence of k effective on the difference between the above core load pad average temperature and the structure surface temperature at this location. With k-effective equal to 0.975, the peak temperature difference is 62.2 K instead of 66.2 K. This is not a large difference, but the fatigue curves are very non-linear. The difference of 4.0 K in peak temperature difference results in almost doubling the allowable number of cycles, from 7500 to 12 000. Downstream of the core subassemblies, in the outlet plenum and beyond, the transient temperature changes caused by changing k-effective from 0.92 to 0.975 are less than 1 K. Thus, the main fatigue consequence is in the subassemblies.

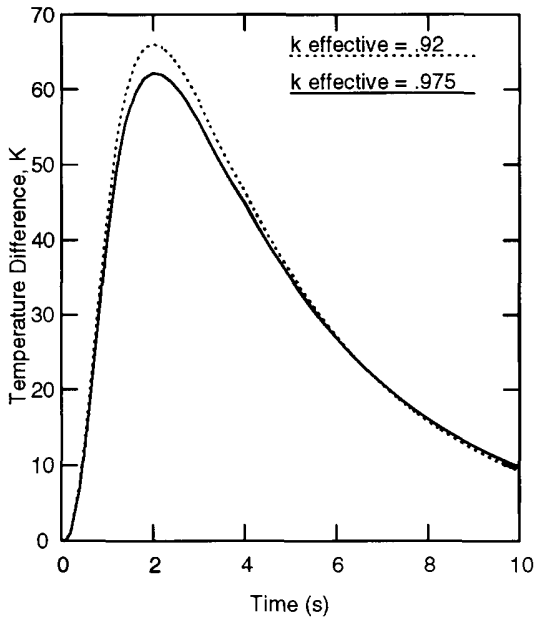

FIG. 7. Influence of k-effective on the structure temperature differences at the top of the core, Na coolant.

3.3. Beam interruption frequency design limits

Based on the results in Table 2, it is possible to obtain design limits for beam interruption frequencies. These limits are shown in Table 3, assuming a four-year lifetime in the blanket for subassemblies, and assuming a 30-year life for the intermediate heat exchangers and the steam generators.

4. MITIGATION OPTIONS

A number of mitigation options can be considered to solve thermal fatigue problems. These mitigation options tend to fall in one of two categories. One category is reducing the frequency of beam interruptions. The second category is to reduce the amplitude of the temperature perturbations. It is likely that a combination of options will be necessary.

TABLE 3. ALLOWABLE BEAM INTERRUPTION FREQUENCIES FOR CURRENT BLANKET DESIGNS

Interruption duration	Allowable interruptions per year, Pb-Bi coolant	Allowable interruptions per year, Na coolant
2 s or more	17 000	1900
3 min or more	270	80

4.1. Improving the reliability of the accelerator

Improving the reliability of the accelerator and reducing the frequency of beam interruptions would extend the lifetime of components subjected to thermal fatigue. Improving the reliability

of the accelerator would also improve the average effective utilization of the ATW, increasing the rate at which waste is transmuted and increasing the amount of electricity produced. Using multiple accelerators, with each providing a fraction of the required beam current is another solution. If two accelerators were used, with each providing half of the beam current, then losing one accelerator beam would only cut the blanket power in half. The amplitude of the thermal strain cycle would be cut in half. The frequency of interruptions might be doubled; but because of the non-linearity of the fatigue curves, the allowable number of cycles would be increased by an order of magnitude or more.

Figure 8 shows results of a beam interruption in one accelerator if two accelerators are used. These results are for the steam generator tube sheet in the lead-bismuth cooled case. Losing half of the beam current reduces the peak temperature difference from 73 K to 32 K and increases the tube sheet lifetime to more than 101 years.

4.2. Pump trip

In a liquid metal cooled critical reactor, the pumps are normally tripped when a scram occurs. This is to limit thermal shock in various structures. In an ATW the pumps and turbines could be tripped whenever a beam interruption occurs. This would largely eliminate thermal fatigue problems associated with beam interruptions.

There are two problems with tripping the pumps and turbines every time a beam interruption occurs in an ATW. One problem is a safety problem, and the other problem relates to the average load factor or utilization. If one trips the pumps a few hundred thousand times during the lifetime of a plant, then the probability is fairly high that sometime the beam will be lost, the pumps will be tripped, the beam will be restored, but the pumps will not be restarted. This results in an accident equivalent to a loss-of-flow accident. The ALMR reactor was designed to survive a loss-of-flow accident, with negative reactivity feedback reducing the power to a level that natural circulation flow could handle. In the ATW, negative reactivity feedback has little impact on the power level. Thus in a sodium cooled ATW, a loss-of-flow accident would lead to a core meltdown. For the lead-bismuth cooled reactor design considered here, there would be enough natural circulation flow that core melting would not occur.

The average load factor or utilization problem comes about because every time that the turbines are tripped, it takes many hours to bring them back on-line. If there is a beam interruption, followed by a pump trip and a turbine trip, every half hour or so of operation, followed by a number of hours restarting the turbines, then the device is not going to be operating very much of the time.

4.3. Reducing the core coolant temperature rise

If the frequency of beam interruptions can not be reduced sufficiently, and if a single accelerator is to be used, then probably the most feasible way to reduce the thermal fatigue to an acceptable level is to reduce the core coolant temperature rise by increasing the coolant flow rate or by reducing the power per fuel pin. It may also be necessary to limit the amount of superheat in the once-through steam generator. The temperature differences driving thermal fatigue effects in all structures from the core to the steam generator inlet are proportional to the core temperature rise. The temperature differences in the upper tube sheet of the steam generator are mainly

proportional to the steam superheat. Because of the highly non-linear nature of the fatigue curves, relatively small reductions in core coolant temperature rise and in steam generator superheat may be sufficient.

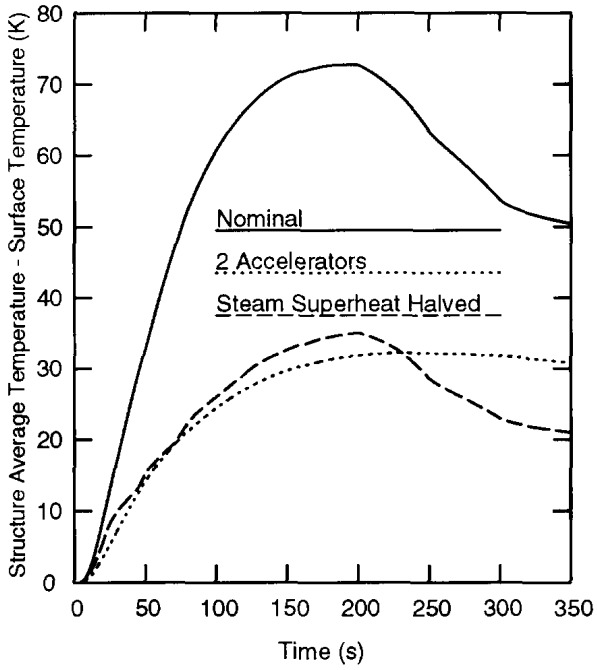

FIG. 8. Temperature differences in the steam generator tube sheet of a lead-bismuth cooled ATW, mitigation options.

One of the curves in Figure 8 shows the results of reducing the steam generator superheat from 103 to 52 K in the lead-bismuth cooled case. The peak temperature difference in the tube sheet is reduced from 73 to 35 K.

Figures 9 and 10 show temperature difference results when the coolant flow rate in the primary and intermediate coolant loops is doubled in the sodium cooled case. This cuts the steady-state core temperature rise in half. Doubling the coolant flow rates solves the thermal fatigue problems in both the above core load pads and the intermediate heat exchanger tube sheet rim.

4.4. Eliminating the above core load pads

In general, thermal fatigue is lower for thinner structures. Thus, subassembly duct wall thermal fatigue can be reduced by eliminating the above core load pads and using a free-flowering subassembly design with no clamping above the core. The subassembly wall thickness above the core would be reduced from the load pad thickness of 0.005652 m to the nominal subassembly wall thickness of 0.003937 m in the sodium cooled design. This reduces the peak temperature difference in the structure from 66.2 to 49.5 K. The allowable number of cycles is increased by about a factor of 5. If the LANSCE interruption frequency data of Table 1 is used, then the subassemblies will still not last in the core for three years, but only minor improvements in the accelerator reliability would be required to achieve an in-core lifetime of 3-4 years.

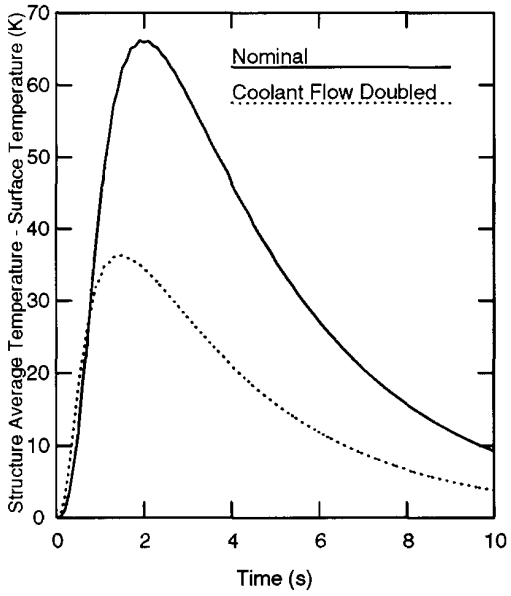

FIG. 9. Temperature differences in the above core load pads in the sodium cooled case, effect of doubling the coolant flow rate.

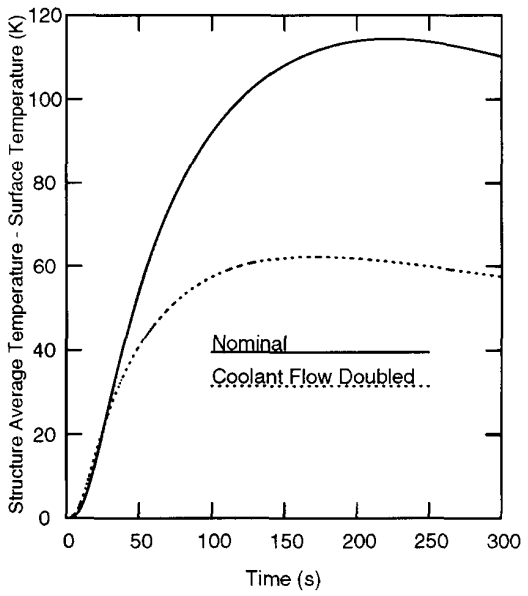

FIG. 10. Temperature differences in the IHX tube sheet rim in the sodium cooled case, effect of doubling the coolant flow rate.

5. SUMMARY AND CONCLUSIONS

Thermal fatigue in the blankets due to temperature transients caused by beam interruptions is a serious problem for current ATW blanket designs if beam interruption frequencies observed for the LANSCE accelerator are assumed. Allowable beam interruption frequencies are obtained for current sodium cooled and lead-bismuth cooled blanket designs. If the allowable beam interruption frequencies cannot be met, or if they can not be guaranteed before the design and construction of the blanket, then blanket design options exist that can accommodate higher beam interruption frequencies.

REFERENCES

[1] GUDOWSKI, W., DOE Expert Panel for the ATW, Washington DC (1999).

[2] MAGEE, P.M., DUBBERLEY, A.E., LIPPS, A.J., WU, T., Safety Performance of the Advanced Liquid Metal Reactor, Proc. Int. Top. Meeting on Advanced Reactors Safety (ARS'94), 17-21 April 1994, Pittsburgh, Pennsylvania, USA, ANS, ISBN: 0-89448-193-2,Vol. 2 (1994) 826-833.

[3] DUNN, F.E., PROHAMMER, F.G., WEBER, D.P., VILIM, R.B., The SASSYS-1 LMFBR Systems Analysis Code, Proc. Int. Top. Mtg. on Fast Reactor Safety, 1985, Knoxville, Tennessee, 999-1006 (21-25 April 1985).

[4] The American Society of Mechanical Engineers, ASME Boiler & Pressure Vessel Code, an International Code, Section III, Subsection NH, Appendix T, Article T-1432 (1998).

PRELIMINARY SAFETY ANALYSIS OF A SWEDISH ACCELERATOR DRIVEN SYSTEM EMPLOYING NITRIDE FUEL AND BURNABLE ABSORBERS

M. ERIKSSON, J. WALLENIUS, K. TUCEK, W. GUDOWSKI
Royal Institute of Technology, Stockholm, Sweden

J. CAHALAN
Argonne National Laboratory, Argonne, Illinois, United States of Amrerica

Abstract

Safety features of a heavy-metal cooled accelerator driven waste burning system (ADS) subject to a series of accident events have been investigated. The fuel consists of plutonium and minor actinides contained in a zirconium-nitride matrix. The SAS4A [1] computer code is applied to the analysis of transients imposed by a step increase in neutron source and to loss of coolant flow events. Special attention is paid to the maximum permissible temperature in the nitride fuel with regards to thermal dissociation mechanisms.
In general, it is found that the system copes with protected and unprotected loss of flow scenarios. Peak temperatures in fuel, cladding, and coolant are kept within postulated design criteria. The benign behavior is attributed to large pin pitches that allow for large coolant volume fractions, use of lead/bismuth as thermal bond between fuel and cladding, and a primary system designed to maintain large amounts of natural circulation flow.
It is found that the system is most sensitive to source transients. An increase in source intensity introduce high fuel temperatures and this may jeopardize the stability of nitride fuel. Safety consequences of source transients depend strongly on the particular assumptions involved in the analysis. Above all, the rate and magnitude of the source disturbance and the effectiveness of the heat removal equipment may significantly alter the accident scenario. The importance for early detection and successful termination of source transients is acknowledged.
Discussion is presented on the technique used in accelerators to fulfill emergency shut down of the proton beam. Key features are pointed out that distinguish accelerator beam shut off from the shut down mechanism used in critical reactors.

1. INTRODUCTION

The advantages of using nitride fuels in fast reactors have been described in detail in textbooks dedicated to this subject [2, 3]. Main incentives for using nitride fuel in an actinide burning transmuter reactor are in principle the same as those stated [4], for fast reactors. Benign properties of nitride fuel derive from its high thermal conductivity and compatibility with the PUREX reprocessing process.

An important safety issue in the use of nitride fuels is thermal dissociation. Nitride fuel has a tendency to dissociate into free metal atoms and nitrogen gas at a certain temperature. Evaporation and migration of nitrogen gas from the fuel matrix will lead to a reduction of the macroscopic capture cross-section. Thus, the possibility for a substantial positive reactivity insertion exists. Besides, yet mechanical in nature, the pressure increase in the cover gas space due to nitrogen evaporation imposes another difficulty [5].

In a paper [6], the reactivity consequence following escape of all nitrogen from the fuel pins was further investigated. It was shown that proper core and fuel design, i.e., using ^{15}N in the fabrication of nitride fuels and larger pin pitches, could maintain the nitrogen void worth within reasonable limits. In the present paper, fuel, cladding, and coolant temperatures following a series of accident scenarios are analyzed. The intention is to perform a safety analysis to identify the particular operating and safety characteristics of the present design with special attention to the limitations in nitride fuel temperatures.

In the present design we have adopted an eutectic lead/bismuth to serve as a thermal bond between the fuel and the cladding. While the use of sodium-bonded nitride fuel pins is well documented [4, 7] the use of lead/bismuth for the same purpose has been less examined.

Sodium is an excellent thermal bond (63 W/mK at 800 K) with little thermal resistance. But, sodium has a low boiling point (1155 K) and if the pin is sodium-bonded then damage will appear as bond vaporization with consequent insulation of the fuel. Although sodium boiling may or may not rupture the cladding, conditions are probably such that cladding failure is not far away. Eutectic lead/bismuth has lower thermal conductivity (15 W/mK at 800 K) than sodium but it compensates by offering higher boiling temperature (1943 K).

2. SYSTEM DESIGN

The SSC [8] (Sing-Sing Core) is a model of an ADS developed at the Royal Institute of Technology, Sweden. The model considered in the present accident analysis is rated at 800 MWth and it is cooled by an eutectic of liquid lead/bismuth. The fuel consists of plutonium and minor actinides contained in a zirconium-nitride based matrix. No fertile material is present in order to maximize transmutation rates and to avoid production of new transuranic nuclides. Separate pins of neutron absorbers, B_4C, are located within the core. Boron carbide pins are used to achieve a flat power profile at beginning of life and to compensate for reactivity losses during burnup. The use of B_4C also reduces the production of helium in the fuel [8]. The boron carbide is highly enriched in boron-10 due to its benign neutron capture properties which helps to increase fission to absorption probability in even neutron numbered nuclides. The design uses fixed absorber pins, separate from the fuel, that are radially zoned. Cross-section of the SSC layout is displayed in Fig. 1. The use of fixed absorber pins is advantageous since it does not necessitate fabricating pins of different composition. Pins are positioned in a triangular pin configuration. The fuel pins are hollow in order to reduce peak temperatures. Nitride fuel is employed to obtain high thermal conductivity and to allow for high linear ratings. The nitride fuel is highly enriched in ^{15}N to avoid the high capture cross section of ^{14}N and to minimize the accumulation of radioactive ^{14}C in the fuel. Major design parameters are displayed Tables 1 and 2, respectively.

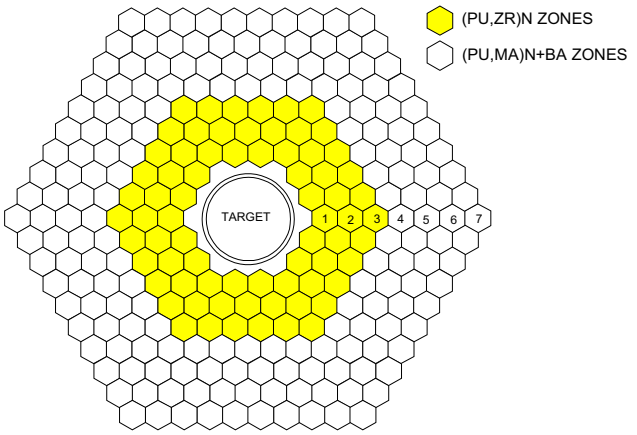

FIG. 1. Core map of the SSC.

TABLE 1.
SSC SUBASSEMBLY DATA

Subassembly data				
Zone	P/D	Fuel pins	BA pins	[kW/ pin]
1	2.19	61	0	52
2	2.19	61	0	52
3	2.19	61	0	52
4	1.75	41	50	51
5	1.75	64	27	49
6	1.75	70	21	48
7	1.75	84	7	45

TABLE 2. MAJOR SYSTEM DESIGN DATA OF THE SSC

Total reactor power	800 MWth
Beta effective	0.0017
Mean neutron generation time	1.0e-6
Initial k_eff (eigenvalue)	0.970
Active core height	1.00 m
Fuel porosity	15%
Pellet inner radius	1.00 mm
Pellet outer radius	2.40 mm
Cladding inner radius	2.49 mm
Cladding outer radius	2.94 mm
Inlet coolant temperature	573 K
Coolant flow velocity	2.5 m/s
Flat-to-flat distance	9.90 cm
Pitch between subassemblies	10.10 cm
Cladding	Ferritic steel
Thermal bond (fuel to cladding)	Pb/Bi
Direct heat deposition in coolant	9%
Direct heat deposition in cladding	1%

Integral reactor properties such as mean neutron generation time, effective delayed neutron fraction, and neutron flux distributions are obtained from MCNP calculations performed at steady-state condition. The transuranic fuel with a large fraction of minor actinides exhibits a low effective delayed neutron fraction. Plutonium 239, with a low yield of delayed neutron precursors, dominates the fission rate. Since the delayed neutrons are emitted at energies lower than that of prompt neutrons their importance with respect to leakage and fission is different. The average importance of the delayed neutrons is smaller than that of prompt neutrons in the SSC. The effective β value in the SSC is lower because delayed neutrons have a smaller chance of causing fission in even neutron numbered nuclei since most delayed neutrons have energies below the threshold energy for fast fission. Moreover, the prompt yield of ^{239}Pu, increases with energy, which also gives prompt neutrons higher importance than delayed neutrons. In addition, the existence of absorbers in the core increases the probability for capture of delayed neutrons in ^{10}B.The mean neutron lifetime in SSC, 1.0 μs, is 4-5 times the lifetime reported in other heavy-metal cooled subcritical designs, for example ~0.2 μs [9]. However, the coolant volume fractions in SSC is considerable larger (fuel/steel/coolant = 0.11/0.10/0.79) than in other similar designs (fuel/steel/coolan t = 0.32/0.18/0.50) [9].

A high pitch-to-diameter ratio reduces the coolant void worth [6] and increases the amount of natural circulation and reduces the potential for flow blockage. A large degree of natural circulation also has the benefit of self-distributing the flow radially to maintain relatively uniform coolant rise across all positions of the core. The SSC is designed to provide considerable natural circulation flow to ensure that heat removal capability is available even in complete pump failure events.

The core, heat exchanger, and primary pumps are immersed in a single pool of lead/bismuth. The primary heat exchangers are the steam generators. Four primary centrifugal pumps are located in the cold pool. An illustration of the primary system is displayed in Fig. 2.

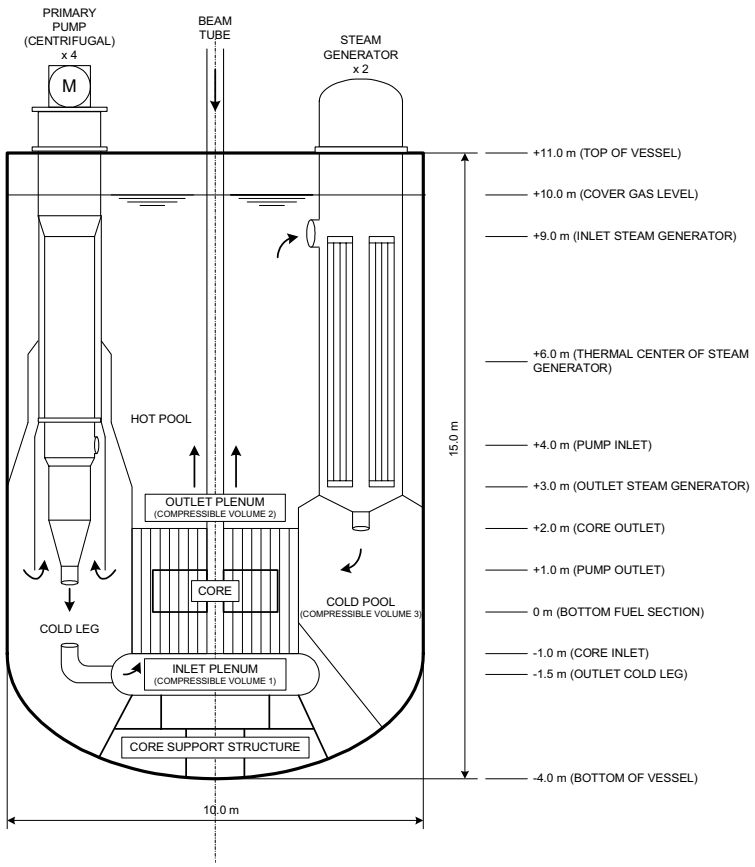

FIG. 2. SSC 800 MWth primary circuit (pool type system).

Temperatures in the coolant range from 573 K at inlet to 761 K at the outlet in steady-state. Because liquid lead/bismuth is nearly incompressible, a vapor volume is provided to accommodate thermal expansion of the fluid; otherwise expansion may rupture the primary system if the temperature increase is sufficiently large. The coolant is kept at a low pressure, slightly above 1 atmosphere. Since the saturation temperature of lead/bismuth is high, even at atmospheric pressure, there is no need to pressurize the primary system. Rather, as shown in Fig. 2 the reactor vessel is filled with lead/bismuth to a prescribed level, with the remainder of the vessel being occupied by an inert cover gas. The compressibility of this cover gas permits the lead/bismuth to expand with increasing temperatures.

Natural convection is promoted by a large separation distance between the heat exchanger and core mid-plane. Therefore, the steam generators are elevated well above the core. The drawback is that a large separation distance requires an increased vessel size which penalizes the economics of the plant and increases the seismic loading on the vessel in the event of an earthquake.

2.1. Model assumptions

For the present purposes the SAS4A code is set up to run in point kinetics mode. The SSC is a small, strongly coupled core with a very hard spectrum. Space-time effects in such cores are very small and point kinetics theory is known to predict transient power very well. The reason is mainly because of relatively large neutron mean free paths in SSC (~4 cm), which allow the spatial shape of the flux to be quickly established following a reactivity perturbation.

The effect of thermal feedbacks on the power generation and on the temperature of reactor components is negligible in the present accident analysis. Thus, reactivity feedbacks are not taken into account. There are two main reasons that justify this assumption. First of all, the reactivity of SSC is largely offset from critical condition (ρ = -18\$). The net result is a substantially reduced sensitivity to any reactivity disturbance. Thus, the impact of reactivity feedbacks (in a pre-disassembly accident) in an ADS is very small. Secondly, large contributors of reactivity feedback phenomena that typically are present in fast reactors, Doppler and coolant density changes, are small in the SSC. Since the core contains no fertile fuel and the energy spectrum is well above the resonance region [8], the Doppler effect is negligible. Coolant void reactivity has been calculated to be slightly negative [11] for the present design. The boiling point of liquid lead/bismuth is high (1943 K) and large departures in the coolant density from the steady-state value can be excluded in the pre-disassembly phase.

Constant steam generator boundary conditions are assumed, any influence from secondary circuit components is neglected. During all circumstances a constant inlet temperature of 573 K is assumed. This is equivalent of assuming that the steam generator removes heat at the same rate as it is produced, which is generally not the case. The result of introducing this simplification depends on the investigation being made. If, for example, a rapid power variation is the phenomenon under consideration, it would be adequate to assume constant inlet temperature. However, for "long" transients, in this case longer than the primary coolant loop time, an increase in coolant outlet temperatures will eventually raise the coolant inlet temperature. In a loss of flow accident this has low importance. In a source transient the assumption is not adequate in the long term and it must be taken into account in the safety evaluation.

3. ACCIDENT ANALYSIS

The present accident analysis investigates the dynamic response of SSC in a *pre-disassembly phase*. The purpose is to define failure mechanisms, possible ranges of safe operation and define where further studies ought to be performed. Considering the uncertainties involved in many of the parameters, the initial safety assessment calculations are rather crude. Once the design is more complete, it is suitable to carry out more elaborate calculations.

The analysis investigates the consequences of the following type of accident events:

- A *beam insertion* or a *source jerk* type of accident where the external neutron source is promptly increased by a factor of two. In an ADS this would correspond to inadvertent control of the proton beam. In the envisioned ADS design, transients may be caused by a relatively fast insertion or removal of the accelerator beam [12]. The ability to adjust beam power during operation is a design requirement in order to facilitate compensation for reactivity losses during burnup and maintain the ADS at constant power.
- A *protected Loss of Flow* (LOF) type of accident. In this case it is assumed that all centrifugal pumps fail to operate at the same time and coolant flow is driven by natural convection alone. It is supposed that the beam is shut off at the same instant when the pumps fail, which would be the normal response of the plant protection system. In that case total power rapidly drops to decay heat levels. Simultaneous failure of all the pumps because of power failure is not unlikely, common cause failure could cause failure of the supply of power to all primary pumps.
- An *unprotected Loss of Flow* (ULOF) type of accident. In a normal loss of flow event the plant protection system would automatically shut down the accelerator or at least divert

the beam from entering the core, however, in this case it is assumed that the accelerator continues to feed the core with protons. The ADS will remain at full power for the complete transient while the flow drops.

Peak temperatures in the fuel, cladding, and coolant are calculated. Possible safety consequences are considered with respect to a set of postulated design criteria, see Table 3, based on maximum allowable temperatures in reactor components. The decomposition temperature of nitride fuel depends strongly on the thermally dissociated nitrogen gas pressure. Experimental results indicate that dissociation of PuN is small for temperatures below 2150 K [2]. The dissociation behavior of minor actinide (Np, Am, Cm) nitrides is not well known [13]. However, it is known that stable AmN has been fabricated at 1573 K [14], but for higher temperatures the behavior is not known. Thus, a conservative approach is to suppose that partial nitrogen gas evaporation is assumed to occur when fuel temperature exceeds 1573 K and use this temperature as a safety limit.

TABLE 3. DESIGN CRITERIA FOR THE SSC

Component	Design criteria
Fuel, dissociation of PuN	2150 K (2800 K in N_2 environment)
Fuel, dissociation of AmN	1573 K
Cladding, steel melting point	1700 K
Cladding, corrosion	900 K (extended operation)

3.1. Loss of flow accident

In the event of failure of all primary coolant pumps, the pressure drop across the core decreases, causing decreased mass flow rate. It is assumed that the pump coast-down occurs in all pumps simultaneously. Pump failure due to loss of power does not result in an instantaneous loss of pressure head, since even if the pump motor suddenly fails, the rotational inertia of the pump impeller and possibly a fly wheel will cause the pump to coast down gradually over a period of time. Figure 3 shows the flow rundown in SSC due to loss of all electrical power to all four primary pumps. Figure 3 contains the flow reduction following a loss of flow accident in case a) the beam is shut off, b) the beam remains in operation.

Following failure of the power supply to the pumps, the pump torque immediately drops to zero. It is assumed that the SSC is designed with a fly wheel attached to the pumps, the pump then coasts down at a rate determined by the inertia of the fly wheel, the inertia within the pump, and the inertia of the coolant. It can be determined from Fig. 3 that the pump will continue to circulate the coolant for a substantial length of time (~100 s). In an unprotected loss of flow event (beam on), the mass flow rate is promoted by a larger fraction of natural convection. Since natural convection is driven by density differences in the liquid it is linked to the power generation and to the temperature of the coolant. The flow in SSC undergoes a minimum just as the pump impeller comes to rest. As we shall see, this generates peak temperatures in the core. This phenomena is physical, it typically occurs in any loss of flow event. The flow rate has a tendency to dip before establishing a natural circulation flow that is in equilibrium with the heat generation. Equilibrium flow rate is reached within 100 s in the SSC. An equilibrium mass flow rate corresponding to 30% of the initial flow is achieved in the SSC. This flow is sustained by natural convection alone.

Besides primary system design and nuclear and thermal properties of SSC, the course of the loss of flow accident depends strongly on the particular choice of assumptions defining the accident. In our case, the presence or absence of beam shut down greatly alters the outcome.

In the safety evaluation of the loss of flow accident, it must be ascertained whether natural convection on its own is adequate for heat removal, or else, other means for heat removal must be taken before excessive core heat-up takes place.

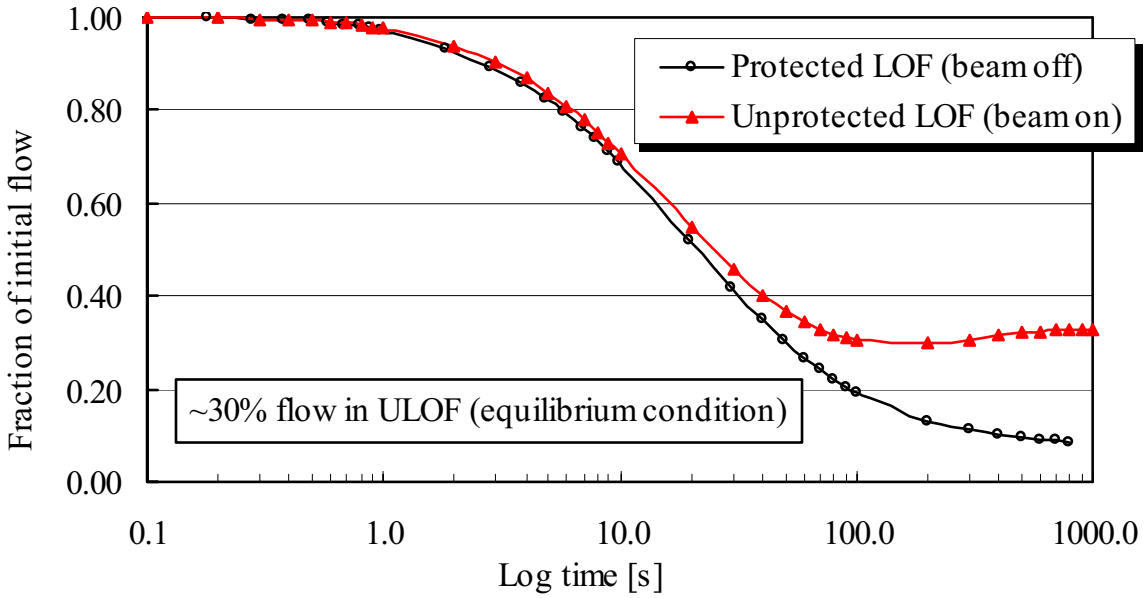

FIG. 3. Primary coolant flow reduction following pump failure.Loss of electrical power to all pumps. Flow is reduced to natural circulation only.

3.1.1. Protected loss of flow event (beam off)

Following beam shut-off the power will be generated by decay-heat alone. Figure 4 displays the normalized total reactor power of the SSC subjected to a *protected loss of flow* event. The decay heat amounts to approximately 7% of full power immediately following the shut down of the beam. After one hour the decay heat is produced at a rate of about 1% of full power. For the time period being analyzed (1000 s) the normalized flow substantially exceeds the normalized power. The resulting, maximum, core temperatures are shown in Fig. 5.

The favorable imbalance of normalized flow and power causes the overall temperature in the core to decrease. Redistribution of stored heat between fuel, cladding, and coolant causes the temperature of the fuel and cladding to drop immediately following beam shut down. The redistribution of heat from the fuel to cladding and coolant tends to dominate the early stages of any protected flow failure accident. The fuel temperature falls off at a rate determined by the fuel time constant (calculated to be 0.5 s for SSC fuel [15]) while the coolant requires the channel transit time (0.4 s) to elapse before any temperature changes occur.

Power decreases rapidly following beam shut down, while the pump inertia retains a considerable flow during the early phase. During the initial second, the flow coast down has a negligible influence on the transient, which is completely dominated by the power drop. The rapid temperature decrease continues in all components until an equilibrium is established between natural convection flow and decay heat generation. Subsequently, core temperatures are kept in balance as heat removal equalizes heat generation.

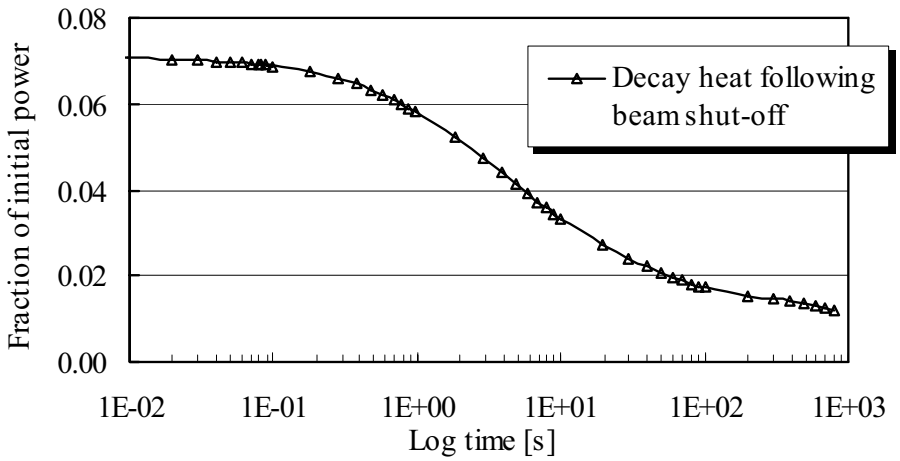

FIG. 4. Total reactor power of SSC following beam shut-off.

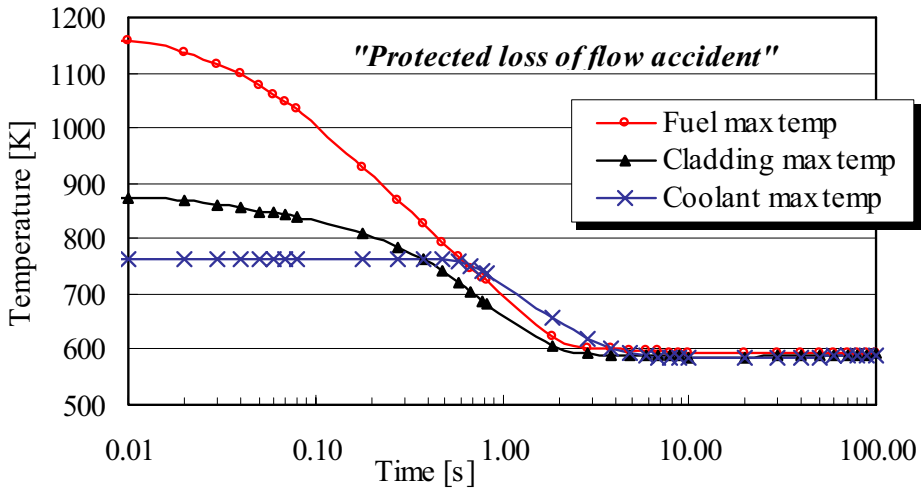

FIG. 5. Peak temperatures in fuel, cladding and coolant following protected loss of flow accident.

At a certain time, the maximum temperature of the coolant is higher than the maximum temperature of the cladding and the fuel. The reason is because maximum temperatures in fuel, cladding, and coolant occur at different axial locations. While maximum temperatures for the fuel and cladding show up close to core center, maximum temperatures for the coolant arise at core outlet. The coolant absorbs extra heat as it flows from core center to the outlet and it may temporarily obtain higher local temperatures at core outlet than the cladding and fuel at the midplane. In the equilibrium state, the production of decay heat results in the fuel temperature remaining slightly above that of the cladding and coolant.

From the above calculations we may conclude that the SSC responds in a benign way to a *protected loss of flow* event. Natural circulation flow effectively removes decay heat from the core.

3.1.2. Unprotected loss of flow event (beam on)

Typically the plant protection system is designed to automatically shut down the beam in a pump failure event. Thus, it is only when the plant protection system (PPS) malfunctions that an *unprotected loss of flow* (ULOF) event may occur. The term "unprotected" refers to the situation when the accident event is not protected by the PPS. Given the hypothesis of complete failure of the pumps and complete failure of the plant protection system the dynamic response of SSC is investigated. Since no reactivity feedbacks are present, power will remain at constant level throughout the transient. Figure 6 contains the calculated thermal response of the fuel, cladding, and coolant.

Reduction of flow reduces the core heat removal and coolant temperatures increase. The temperature of the coolant increases first and is a primary indication of flow reduction. As the coolant heats up, less heat is transferred from the fuel. The temperature of the fuel and cladding will gradually increase. Core heat-up occurs at a rate determined by the flow coast down. It is seen that minor core heat-up arises during the initial 10 s. Shut down of the beam within that period of time would effectively terminate the transient. When the pumps have come to a complete rest, mass flow rate is at a minimum. This enables core temperature to reach a critical point. As temperature peaks, it will give the buoyancy driven flow some extra boost.

From Fig. 6, it can be determined that the reactor can remain at full power without causing immediate excessive temperatures. Rapid shut down of the beam is not a necessary requirement to prevent core damage. In this case, peak fuel temperature is approximately 100 K below the fuel failure margin (set to 1573 K for the dissociation temperature of americium nitride). Peak fuel temperature occur in zone 1 and maximum cladding and coolant temperature occur in zone 7. The transient should result in little or no damage to the fuel. Both cladding and coolant temperatures exceed their recommended operational limits. The protective oxide film layer on the cladding may suffer some damage that potentially could harm the cladding in the long run.

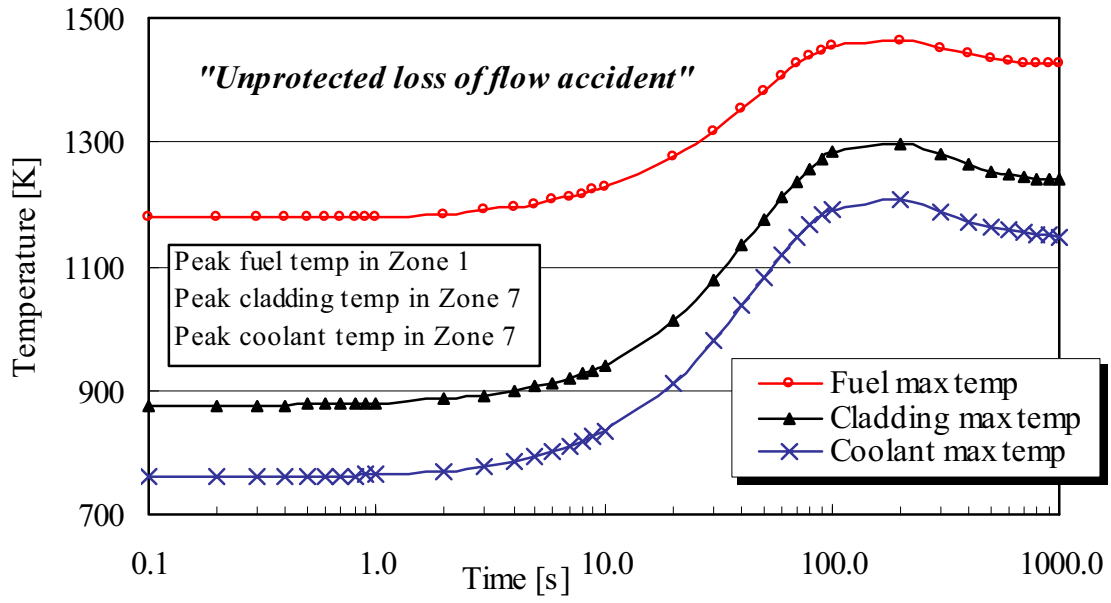

FIG. 6. Maximum temperatures in fuel, cladding and coolant following loss of flow with beam on.

3.2. Beam insertion accident

In a *beam insertion* accident the outcome of the transient is strongly dependent on the rate and magnitude of the beam insertion. In this case, the worst case scenario is assumed in which a step increase of source intensity is simulated. Source power is promptly increased by a factor of two and the reactor power will double at almost the same instant. Figure 7 displays peak fuel, cladding, and coolant temperatures calculated for the SSC with the assumption of constant coolant inlet temperature.

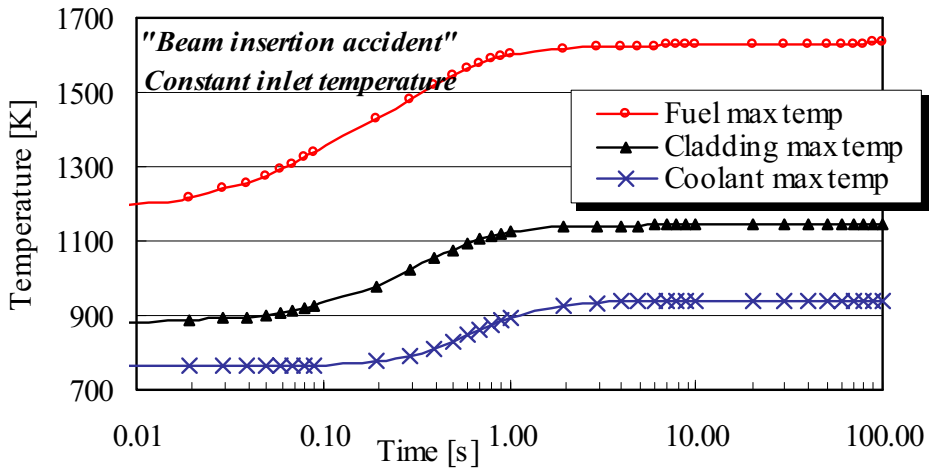

FIG. 7. Maximum temperatures in fuel, cladding, and coolant following a beam insertion transient. Constant inlet temperature is assumed.

The source disturbance is first noted as a rise in fuel temperatures and later by a rise in coolant temperatures. In any source disturbance the speed of the transient is characteristic. In a prompt increase of the source intensity, the reactor power reaches the asymptotic level before any temperature changes occur. It is seen that asymptotic thermal conditions are obtained within a few seconds. In fact, major parts of the transient are completed in the first second. Thus, early termination of source transients is desirable to diminish the safety implications.

The calculation indicates that temperatures following a prompt doubling of source power in the SSC may exceed the dissociation temperature of americium nitride. It should be taken into account that a constant coolant inlet temperature is assumed for the above case. This is a non-conservative assumption. Main concern in a source transient is that the power may increase to levels beyond the removal capabilities of the heat removal system. Normally the plant is designed to make full use of the heat removal system at steady-state in order to avoid oversized equipment. Some increase in heat removal may occur due to larger temperature gradients and slightly increased flow rates in the primary- and secondary loops. The net result, however is that coolant inlet temperature will increase steadily as the transient proceeds. A more conservative approach would be to assume a constant coolant temperature drop in the steam generator, see Fig. 8. This would necessarily generate continuously increasing coolant inlet temperatures as the transient extends for a longer period of time than the primary coolant loop time. As seen in Fig. 8, the cladding reaches its melting point in 700 s and coolant boiling is onset at approximately 1200 s. Peak fuel and cladding temperature is obtained in zone 1 and peak coolant temperature occur in zone 7.

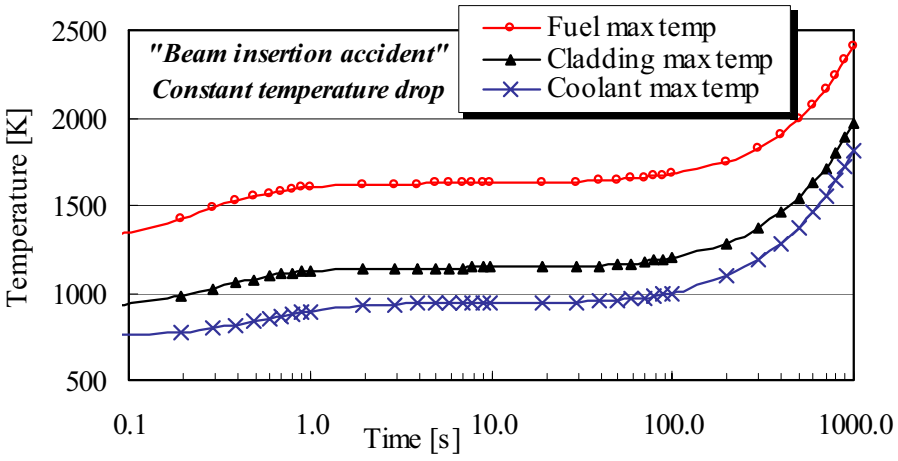

FIG. 8. Maximum temperatures in fuel, cladding, and coolant following a beam insertion transient. Constant temperature drop in the steam-generator is assumed.

Preferably the system should be designed to withstand, at all times, the instantaneous thermal transient following the maximum possible beam insertion capability of the accelerator. The initial thermal response that follows a prompt increase in source strength occurs so rapidly that it is unsafe to rely on a control system to detect and terminate the transient before (<1 s) excessive temperatures are obtained. This is especially important for nitride fuel. The temperature increase is most severe in the fuel pin. This imposes high demands on nitride fuel. If a beam insertion accident occurs, it is desirable to have the plant protection system shut off the beam before the coolant has completed a full loop through the primary system. The loop time depends on the coolant flow rate and on the primary system design, in the SSC it is approximately 30 s (which represents a typical loop time). Beam shut off would successfully terminate the transient.

4. BEAM SHUT DOWN VS. REACTOR SHUT DOWN

The outcome of a transient in an ADS depends strongly on the presence or absence of beam shut off. It is highly desirable to employ a fast and reliable beam shut off technique in an event that requires immediate shut down of the ADS. Following beam shut off the ADS would lose its generation of neutrons in the independent source. While the shut down procedure of a critical reactor is well known, the same task in an accelerator may not be as obvious.

Beam shut off is in principle more reliable and easier to accomplish than shut down in a critical reactor. In this case we refer to *beam shut off*, or rather “source shut off”, as the operation in which the generation of external source neutrons inside the core is terminated. This may be accomplished either by interrupting the transportation of protons at some point along the beam tunnel or by preventing the beam of protons from entering the core. We refer to *reactor shut down*, following the definition adopted by IAEA, as the process rendering a critical reactor subcritical and held in that state [16]. In both cases we limit the comparison to shut downs intended by the operator or control system. Intended reactor shut down is most commonly accomplished by introducing neutron absorbers in the core. As an example of accelerator shut down, the basic technique used in the envisioned APT accelerator is outlined [17 - 20]

In the APT accelerator protons are generated by ionizing hydrogen gas inside an ion source. The ion source uses microwave power to interact with hydrogen gas in the presence of a magnetic field to produce a plasma discharge, creating electrons, $^{1}H+$, $^{2}H+$, and $^{3}H+$ ions, as well as other ionic and atomic species. Hydrogen gas is fed to the plasma chamber by regulating the gas flow, with a conductance limiting aperture at the plasma chamber. This chamber is held at a positive potential with respect to a grounded extractor electrode. A continuous beam of protons is drawn by the electrostatic field from the chamber in a single high voltage extraction gap. Leaving the ion source the beam passes through a beam-kicker magnet (deflector) which may be used to shut off the beam, if necessary. In a response to immediate beam shut off, the fast kicker magnet will deflect the beam to a beamstop in 10-20 μs. Besides, a mechanical iris and a insertable beamstop may used to shut down the beam. Several other retractable beamstops are located along the beamline that each one is able to independently shut off the beam.

Key features that distinguish accelerator shut down from critical reactor shut down

- One important distinction is that reactor shut down relies on functioning of mechanical devices in one way or another while beam shut off may be accomplished through electrical, electromechanical, or mechanical activity. For example, either using the kicker magnet or switching of the power supporting the electrostatic field in the extraction gap would momentarily interrupt the beam. A more fail-safe system can hardly be designed than a switching device that requires no more than breaking an electronic circuit to accomplish the overall task. Control rod guide structures in a reactor may always have the possibility of being obstructed even though the simplest form of fail-safe design is used in which control rods are held above core by active means (current through a holding electromagnet) and dropped into the core by gravity. The limitation in reliability of devices that require mechanical movement is well known.
- The accelerator must be supplied with external power in order to operate whereas the critical reactor essentially is self-sustaining. Thus, while the shut down system in a critical reactor relies on a mechanism to function properly in order to render it subcritical, the accelerator in principle may be left in a passive condition and instead disconnect the external power supply.
- Reactor shut down requires continued functioning of the components in order to maintain the reactor in a subcritical state. This is not the case for an accelerator. For example, if the power is disconnected from the accelerator there is no way it will start-up unless active measures are taken to restore the supply of power. Subcritical conditions in a critical reactor design may discontinue at any time by removal or failure of some control rods or restructuring of core materials. Such events are intrinsic to the critical reactor and they do not necessarily require inadvertent action by personnel.
- Reactor shut down is limited by mechanical speeds such as control rod movement, motion of soluble absorbers in the coolant, hydraulic or pneumatic pressure injection, coolant velocity, etc. In an accelerator, successful beam shut off can be achieved within microseconds.
- The shut down system in a critical reactor is subject to long term exposure in a harsh environment. Devices that are vital for shutting down the reactor suffer from irradiation effects, temperature effects, chemical effects, and structural dimension changes.
- Active means for shutting down a critical reactor normally consist of two diverse systems, this is the requirement set by the IAEA [16]. The multitude of beam shut off options available in an accelerator significantly increases the redundancy.

5. CONCLUSIONS

Peak temperatures in the fuel, cladding, and coolant were calculated for a protected loss of flow accident, unprotected loss of flow accident, and beam insertion accident. The design uses large pin pitches, lead/bismuth as thermal bond between fuel and cladding, and it is designed to maintain a large degree of natural circulation flow even in pump failure accidents. Using sodium as bonding material appears to be less attractive because of the low boiling point. In both loss of flow events, maximum peak temperatures in the fuel are well within the range for safe operation. Thermal dissociation of nitride fuel (americium nitride compound) imposes the strongest operating limitations in the present design. Conditions may exist in which the dissociation temperature of nitride fuel is exceeded in a beam insertion accident. Prompt increase in source strength results in severe thermal transients, particularly in the fuel. The response is strongly dependent on the rate and magnitude of the beam insertion. It is recommended that an ADS is designed to withstand the instantaneous temperature swing following insertion of maximum beam output. This safety principle would provide the plant protection system with extra time to detect and terminate any inadvertent increase in source strength. Once a shut off signal is received, the technique to actually accomplish beam shut off is easier and more reliable compared to shut down of a critical reactor.

REFERENCES

[1] CAHALAN, J.E., TENTNER, A.M., MORRIS, E.E., Advanced LMR Safety Anlaysis Capabilities in the SASSYS-1 and SAS4A Computer Codes, Proc. Int. Top. Mtg. on Advanced Reactors Safety, 17-21 April 1994, Pittsburgh, USA, ANS, ISBN: 0-89448-190-8 (1994).

[2] MATZKE, H.J., Science of Advanced LMFBR Fuels, Amsterdam, North-Holland, (1986).

[3] BLANK, H., Materials Science and Technology, Nuclear Materials, Vol. 10A, Chapter Nonoxide Ceremic Nuclear Fuels, VCH, Weinheim (1994).

[4] MATTHEWS, B.R., Irradiation Performance of Nitride Fuels, Proc. Specialist Conf. on Space Nucl. Power and Propulsion Technologies – Materials and Fuels, 21-24 September 1993, Podolsk-Moscow, Los Alamos National Laboratory, LA-UR-23-2392.

[5] UMEOKA, T., et al., Study of CDA driven by ULOF for the nitride fuel core, Proc. Int. Conf. on Future Nuclear Systems (Global'99), 1999, Jackson Hole, Wyoming, USA, ANS, ISBN: 0-89448-641-1 (1999).

[6] WALLENIUS, J., TUCEK, K., GUDOWSKI, W., Safety Analysis of nitride fuels in cores dedicated to waste transmutation, paper presented in the 6th Information Meeting on Actinide and Fission Product Partitioning & Transmutation, 11-13 December 2000, Madrid, Spain, NEA, EUR 19783 EN (2001).

[7] LYON, W.F., BAKER, R.B., LEGGETT, R.D., MATTHEWS, R.B., Advancing Liquid Metal Reactor Technology with Nitride Fuels, Proc. Int. Conf. on Fast Reactors and Related Fuel Cycles, 28 October-1 November 1991, Kyoto, Japan, Prepared for the USDOE, Westinghouse Hanford Company, WHC-SA-1067, DE91 017807 (1991).

[8] WALLENIUS, J., TUCEK, K., CARLSSON, J., GUDOWSKI, W., Application of Burnable Absorbers in an Accelerator-Driven System, Nucl. Sci. Eng. 137 (2001) 96-106.

[9] MASCHEK, W., RINEISKI, A., MORITA, K., MUHLING, G., FLAD, M., Safety Analysis for ADS Cores with dedicated Fuel and Proposals for Safety Improvements, paper presented in the IAEA Technical Committee Meeting on Core Physics and Engineering Aspects of Emerging Nuclear Energy Systems for Energy Generation and Transmutation, 28 November-1 December 2000, Argonne, to be published as IAEA-TEDOC.

[10] WADE, D.C., Safety Considerations in Design of Fast Spectrum ADS for Transuranic or Minor Actinide Burning: A Status Report on Activities of the OECD-NEA Expert Group, paper presented in the 6th Information Meeting on Actinide and Fission Product Partitioning & Transmutation, 11-13 December 2000, Madrid, Spain, NEA, EUR 19783 EN (2001).

[11] WALLENIUS, J., private communication, 2001.

[12] ERIKSSON, M., Reliability Assessment of the LANSCE Accelerator System, M.Sc. thesis, Royal Institute of Technology, Stockholm (1998).

[13] SUZUKI, Y., ARAI, Y., Thermophysical and thermodynamic properties of actinide·mononitrides and their solid solutions, J. Alloys and Compounds, 271-273 (1998) 577-582

[14] TAKANO, M., et al., Synthesis of Americium Mononitride by Carbothermic Reduction Method, Proc. International Conf. on Future Nucl. Energy Systems, (Global'99), 1999, Jackson Hole, Wyoming, USA, ANS, ISBN: 0-89448-641-1 (1999).

[15] GUDOWSKI, W., WALLENIUS, J., TUCEK, K., CARLSSON, J., SELTBORG, P., ERIKSSON, M., Annual Report Dep. of Nuclear & Reactor Physics to the SKB AB (2001).

[16] INTERNATIONAL ATOMIC ENERGY AGENCY, Design for Reactor Core Safety in Nuclear Power Plants, IAEA Safety Series No. 50-SG-D14, IAEA Safety Guides, Vienna (1986).

[17] SHERMAN, J., et al., Development of a 110-mA, 75 keV Proton Injector for High-Current, CW Linacs, Proc. XVIII International Linac Conf. 26-30 August 1996, Geneva, Switzerland, CERN (1996).

[18] SCHNEIDER, J.D., MEYER, E., STEVENS, R.R, HANSBOROUGH, L., SHERMAN, J., Design and Testing of a DC Ion Injector Suitable for Accelerator-Driven Transmutation, Proc. 3rd Int. Conf. on Accelerator-Driven Transmutation Technologies and Applications (1994) 439.

[19] SHERMAN, J., STEVENS, R.R., SCHNEIDER, J.D., ZAUGG, T., Direct-Current Proton-Beam Measurements at Los Alamos, Proc. Int. Conf. on Accelerator-Driven Transmutation Technologies and Applications, Las Vegas, NV, 1994, (AIP Conference Proceedings 346), E.D. Arthur, A. Rodriguez, S.O. Schriber (Eds), Los Alamos National Laboratory, AIP Press, 432.

[20] SHERMAN, J., ARVIN, A., HANSBOROUGH, L., HODGKINS, D., MEYER, E., SCHNEIDER, J.D., SMITH, JR., H.V., STETTLER, M., STEVENS, JR., R.R., THUOT, M., ZAUGG, T., FERDINAND, R., Status Report on a dc 130 mA, 75 keV Proton Injector, 7th Int. Conf. of Ion Sources, 7-13 September 1997, Taormina, Italy, Los Alamos National Laboratory, LA-UR-97-3483.

SAFETY ANALYSES FOR ADS CORES WITH DEDICATED FUEL AND PROPOSALS FOR SAFETY IMPROVEMENTS

W. MASCHEK, A. RINEISKI, K. MORITA, G. MÜHLING, M. FLAD
Forschungszentrum Karlsruhe, Karlsruhe, Germany

R.J.M. KONINGS
European Commission, Institute of Transuranium Elements, Germany

Abstract

The efficiency of Accelerator Driven Systems (ADSs) for transmutation and incineration of nuclear waste is strongly related to the utilization of so-called dedicated fuels. In the ideal case these fuels should consist of pure TRUs without the classical fertile materials as U238 or Th232 for achieving highest incineration/transmutation rates. Dedicated fuels still have to be developed and programs are under way for their fabrication, irradiation and testing. These fertile-free fuels may suffer from deteriorated thermal-physical properties, as a reduced melting point, reduced thermal conductivity or even thermal instability. Safety analyses show, that the use of dedicated fuels may lead to a strong deterioration of the safety parameters of the reactor core as e.g. the void worth, the Doppler or the kinetics quantities as neutron generation time and β_{eff}. These quantities are of special importance in the case of severe accidents. In addition, a dedicated core may contain multiple 'critical' fuel masses, resulting in a considerable recriticality potential Current knowledge on these dedicated fuels suggests that 'critical' reactors may not be feasible, because of safety reasons. However, for ADSs, the subcriticality of the system should cope with these deteriorated safety parameters. First analyses are presented, which show potential safety problems for ADSs with such dedicated cores in the severe accident range. Inherent safety measures are proposed to obtain a balanced safety approach with special emphasis on severe accidents.

1. INTRODUCTION

The incineration/transmutation of plutonium (Pu) and minor actinides (MAs) can be performed with critical reactors and accelerator driven systems (ADS). Different scenarios exist how to handle the final destruction of these transuranics [6 - 9]. To achieve the highest transmutation/incineration rates the fuel in these transmuter/burner reactors should ideally consist of pure MAs plus varying amounts of plutonium, but without the fertile materials U238 or Th232. This so-called 'dedicated' fuel is still to be developed and programs have been initiated to fabricate, investigate and test these innovative fuels. The utilization of such fuels in a reactor core might lead to a strong deterioration of its safety relevant parameters as the coolant density/void effect and the Doppler feedback and to a significant reduction of the kinetics quantities, as the neutron generation time and β_{eff} [4]. In addition these fuels might possess high reactivity potentials resulting in an increased recriticality risk already under local core melt conditions. Besides the neutronics aspects, these fertile free fuels may also suffer from deteriorated thermal or thermo-mechanical properties, as a lowered melting point, reduced thermal conductivity or even thermal instabilities [5]. Based on the current knowledge on these dedicated fuels their use in critical reactors seems to be impossible, because of safety reasons. However, for ADSs the salient hope has been promoted that due to the subcriticality of the system the poor safety features of such fuels could be coped with.

In recent years a number of preliminary ADS safety analyses have been performed [6 - 9], which give some insight into the system behavior of an ADS and generally show its promising safety features. However, in these studies the ADS has been identified with a U233/Th232 system (energy amplifier), still having fertile material in the core and consequently with overall good safety parameters. The following investigations deal with the generic safety behavior of an ADS transmuter/burner with dedicated fuel. 'Dedicated core' is used synonymously for a core with the above mentioned deteriorated safety characteristics. Results

of these investigations are compared to a similar U233/Th232 system. These analyses will exhibit possible problems with innovative dedicated fuels, leading finally to the formulation of some requirements, which should be fulfilled to guarantee an adequate safety performance for an ADS transmutation system.

A general problem of these fuels is, that currently they only exist either in small quantities or even only on the 'drawing board' of the fuel designers. Naturally, both operational experience and experience under transient conditions is missing. Compared to the wealth of data and knowledge, especially gained by the TREAT [10] or the CABRI [11] programs, a safety related database for such new fuels does not exist. Therefore, extensive safety-related experimental programs have to be foreseen in the future for such innovative fuels. Current safety analyses suffer from lack of experimental knowledge. The investigations on dedicated cores focus on safety issues to be resolved and should help to formulate future research and development needs.

The analyses presented have been mainly performed with the SIMMER-III code [12], a safety code originally developed for liquid metal cooled critical reactors but recently extended to accelerator driven systems [13].

2. THE SIMMER-III CODE

The SIMMER-III code is developed by JNC (Japan Nuclear Cycle Development Institute, O-arai Engineering Center) [12] in cooperation with Forschungszentrum Karlsruhe and CEA (Commissariat à l'Energie Atomique, CEN Grenoble and CE Cadarache). The application of the SIMMER code to ADS is of special interest for the European partners in this cooperation. SIMMER-III is a two-dimensional (RZ,XY), three-velocity-field, multi-phase, multi-component, Eulerian, fluid-dynamics code coupled with a structure model (fuel pins etc.) and a space-, time- and energy-dependent neutron dynamics model. SIMMER-III uses an elaborate scheme of equation of state functions for fuels, steel, coolants (light and heavy liquid metals), absorber and simulation materials (e.g., alumina). In neutronics, the transient neutron flux distribution is calculated with the improved quasistatic method [14]. For the space dependent part, a TWODANT based flux shape calculation scheme has been implemented recently [15]. For ADS application, an external time- dependent neutron source has been implemented in the kinetics equations [16, 17]. For the calculation of the different kinetics quantities different weighting functions can be chosen. The source effectiveness, indicating the e.g., the position of the source relative to the bulk of fuel is transiently determined. Besides the SIMMER-III code, the 3D SIMMER-IV code (XYZ, RZ) is under development. One reason to develop this code is to analyze the ADS design proposal of FZK with 3 beams to achieve better power form factors. The fluid-dynamics part of SIMMER-IV has already been prepared by JNC and the neutronics part, based on the THREEDANT code [18] is currently integrated by FZK.

The key advantage of SIMMER-III/IV is its versatility and flexibility. The code can be used to investigate special effect problems (small scale) as e.g., freeze-out of locally molten fuel on colder structures, but it can also be used to investigate the complex coupled neutronics/thermal-hydraulics behavior of the whole core (medium scale) under transient conditions. Finally on the largest geometric scale the code can describe core material redistribution within the vessel and beyond e.g. after a fuel release from the core region. This includes both problems related to settling and cooling of fuel within the vessel, but also criticality questions in below core structures or core catcher can be treated.

3. SOME GENERAL REMARKS RELATED TO DEDICATED FUELS

Fuels for transmutation of minor actinides (MAs) and/or plutonium are often called ‘dedicated’ fuels as their composition, their chemical state and fuel form are optimised for this special purpose. They are characterised by a high content of transuranium elements, whereas the ratio of minor actinides and plutonium can vary over a large range depending on the underlying fuel cycle strategy [1 - 3]. The highest extent of actinide incineration/transmutation will be obtained when none of the ‘classical’ fertile isotopes U238 or Th232 is contained in the fuel. Though mixed transuranium fuel has been suggested (e.g., (Pu, MA)O_2), it is generally considered that the addition of a non-fissile (inert) support matrix is necessary to dilute the fissile phase and to give mechanical strength to the fuel. The matrix can also help to improve the properties of the fuel, as the omission of uranium (or thorium) as matrix has a penalty due to the fact that the properties of the actinides (melting point, thermal conductivity, chemical stability) gradually decrease along the actinide series going from Th to Am.

At present, a wide variety of concepts are considered for dedicated fuels as various combinations of chemical state, fuel state and fuel form are possible. The chemical state can be a metal, nitride or oxide, the fuel state can be a solid solution or a composite (a ceramic-ceramic CERCER, a ceramic metal CERMET or a metal-metal METMET), the fuel form can be a pellet or a (coated) particle. In addition, molten salts could be considered. In the US-ATW concept a METMET fuel composed of a (Pu,MA,Zr) phase dispersed in zirconium metal matrix has been suggested. In the Japanese ADS concept of JAERI a mixed nitride (solid solution) fuel is considered. In Europe, a specialist group has recommended that the European R&D for ADS fuel will concentrate on oxide fuel forms such as inert matrix mixed oxide (IMMOX), composites in which the oxide actinide phase is mixed with a metal matrix or thorium-based MA fuel [5].

As noted above, the omission of uranium from the fuel has a big impact on the fuel properties, even for oxides. For safety investigations mainly two issues are of importance and might influence the overall safety performance, especially for severe transients. Firstly, the dedicated fuel will have a lower melting point than U-based oxide fuel, and secondly, the thermal conductivity will be significantly lower. This will result in a smaller margin to melting which might have a severe impact on the behaviour under transients as the probability of fuel pin failure will become higher. In addition, actinide redistribution during irradiation (AmO_2), increased cladding corrosion, higher fission gas release and pressure built-up due to formation of relatively large amounts of helium (resulting from alpha-decay) deserve closer investigation. The latter aspect has been identified as a unique feature of MA-containing fuels, which has a big impact on the fuel behaviour. If helium is released from the fuel during normal operation, the internal pin-pressure will increase. If it is retained in the fuel, burst release can occur during temperature excursions. Both cases have to be analysed carefully for transient conditions.

4. SAFETY ANALYSES FOR ADSs WITH DIFFERENT FUELS

The safety investigations with SIMMER-III deal with generic features of an ADS. An ADS core with dedicated fuel with deteriorated safety parameters has been compared with a U233/Th232 fueled core with good safety parameters typical for a 'critical' core. It is investigated if dedicated cores are acceptable from the safety point of view relying on the ‘subcriticality’ level. As the composition of fuel (Pu and MA vector) depends on the envisioned fuel cycle, there does not exist a single 'dedicated' fuel. The important point for our

safety evaluation is the identification of a reactor with ‘dedicated’ fuel to be synonymous with a reactor having large inherent reactivity potentials, reduced prompt negative feedback effects (Doppler), a small β_{eff}, and a short prompt neutron lifetime.

A general target when developing new reactors as the ADS should be the integration of strong inherent and passive safety features. By this any escalation into severe accident scenarios should be prevented. This concept has already been introduced in a first step by a neutronically ‘subcritical’ core.

4.1 Dedicated core behavior under mild and severe transients

The behavior of a core with 'dedicated' nitride fuel (MAs+Pu/N) has been compared with an oxide core of the same power level containing Th232/U233 fuel. Within the neutronics of the SIMMER code the nitride fuel is simulated, but under severe transient thermal-hydraulic conditions an oxide fuel behavior (e.g., for pin disruption) is modeled. Thus possible dissociation process of the nitride under high temperatures are neglected. For our analyses an ADS with 1200 MW_{th} with lead as coolant has been chosen. The core height is 120 cm, the number of subassemblies, each with 397 pins, is 84 (see Fig. 1). The core volume fractions, fuel/steel/coolant = 0.32/0.18/0.50. For the dedicated core a TRU nitride fuel with 25% Pu (CAPRA type: 5.6/39.1/26.7/13.0/14.3/1.3) and 75% MAs (Np237/Am241/Am242m/Am243/ Cm243/Cm244/Cm245: 18.82/38.80/0.55/28.52/0.16/11.59/1.56) embedded in a ZrN matrix has been chosen. The U233/Th232 oxide core has an enrichment of about 10%. Both cores have a subcriticality level of k_{eff} = 0.97. The β_{eff} in the dedicated core is ~150 pcm and the neutron generation time $\Lambda \sim 2.0\times10^{-7}$ s. In the thorium core both values are higher by a factor of about 2 and 3 respectively. The core void is strongly positive in the case of the dedicated fuel, but negative for the U/Th core.

The comparison between a dedicated core and a core with fertile fuel covers operational transients within the design basis and severe transients with core melting. An example of the power-versus-time dependence for a particular kind of beam transient (operational beam transient) is given in Fig. 2 for the dedicated and the thorium cores. The neutron source strength is constant initially, than it is rapidly (within 1 ms) doubled, then almost shut off (to 1% of the original level) and then returned (within 1 ms) to its initial value. The standard weighting procedure (with k_{eff}-adjoint flux computed at t = 0) has been employed. These analyses demonstrate, that under intact core conditions (no fuel disruption has been allowed during the source transient), for the two ADS with rather different safety parameters, even strong source perturbations do lead to only minor differences in the power evolution. For the dedicated core a slight tendency for a positive feedback can be noted which is related to the coolant density effect. This effect also leads to some limited differences in the power evolution for reactivity transients within the subcriticality margin [6, 9, 16].

In the second step of calculations the core behavior under core disruptive accident conditions has been analyzed. The recriticality potential of the dedicated core has been first assessed by calculating the number of critical masses (in our case: fuel cylinder with H/D = 1 surrounded by lead + steel). For the core analyzed and with the conditions given, the dedicated core contains about 60 'critical' masses. Thus under core melt conditions with subsequent fuel compaction there would exist a potential to overcome the built-in subcriticality of the ADS, driving the reactor into a neutronically critical state.

Data for the U233/Th232 core are much more favorable and have already been given in [9] with about 2 critical masses. The safety parameters and the inherent 'criticality' potential of the fuel does not only determine a possible reactivity ramp rate under compactive fuel motion conditions but decisively influences the response of the core to a severe reactivity perturbation too. The core response has been investigated for a range of fuel disruption scenarios and subsequent compaction ramp rates. In the current set of calculations either external non-mechanistic reactivity-ramp rates have been inserted into the system, or these ramp rates were generated by gravity/pressure driven material motion. The absolute values of the power excursions are of lesser interest, but the different response of the cores to severe perturbations.

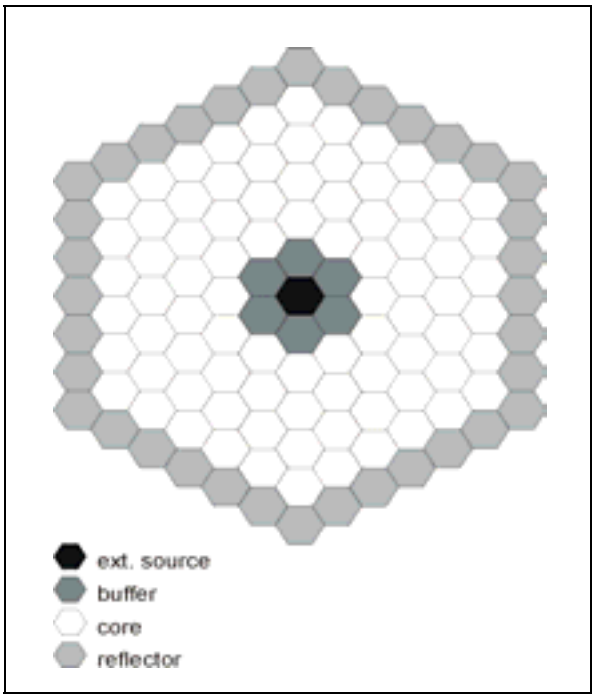

FIG. 1. Core layout in axial mid-plane.

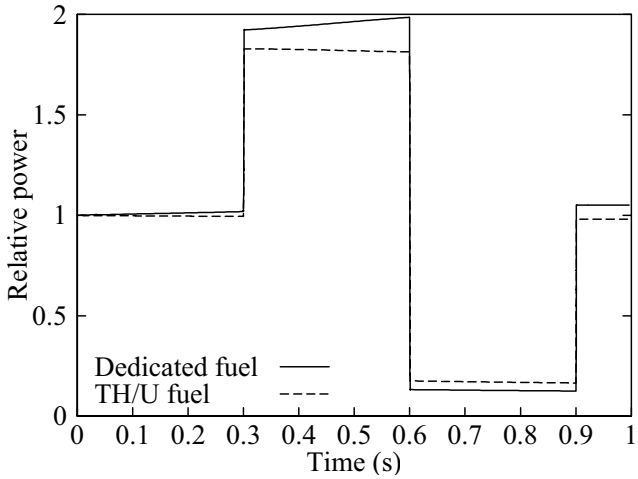

FIG. 2. Comparison of a beam trip transient in an ADS reactor core either with dedicated nitride fuel or U233/Th232 oxide fuel.

As SIMMER has been used for analyzing critical burner cores in the past, experience on the power excursions to be expected and their related accident energetics is available. As a general tendency, the power excursions for severe transients in the dedicated core are by an order of magnitude higher than those in the thorium core with its large Doppler effect. The excursion in the dedicated core is not hampered by a prompt negative reactivity feedback, but only by the delayed feedback coming from the core disassembly. The disassembly process itself might be further delayed by the heavy coolant in the core. The results for the thorium fueled core are in accordance with the results of analyses for the critical oxide cores of the EFR or CAPRA type [19, 20]. The high power excursions in the dedicated ADS core lead to a significant fuel vaporization and vapor pressure build-up that could imply a severe challenge for containment structures. A fuel vapor bubble generated within ms could accelerate the lead surrounding the core. The high lead density might cause significant impact shock pressures on vessel structures ($p = \rho \times c \times v$).

In the analyzed core with 'dedicated' fuel a pronounced 'cliff-edge' behavior can be noted. During 'normal operation' the influence of the deteriorated safety parameters is masked by the source dynamics. In the case of a severe accident leading to core disruption and melting, the phenomena in the accident event chain are enhancing the damage potential:

- A high recriticality potential exists;
- Deteriorated feedback effects and kinetics parameters ineffectively damp any excursion;
- Energetic power excursions with high pressure and temperature levels can be achieved;
- High shock impact pressures by the accelerated heavy coolant could result.

In Fig. 3 a typical expansion phase calculation is shown, where under a severe power transient fuel is vaporized and accelerates the coolant surrounding the core, leading to a final impact on vessel structures. The example shows a typical large scale application of the SIMMER code. In the current case only a simplified geometry has been chosen with steel reflectors surrounding the core and flow guide structures above. For a detailed ADS application all in-vessel structures including beam pipe, instrumentation trees and upper internal core structures could be modeled. In Fig. 3 one can observe an expected advantage of lead compared to sodium coolant. The lower vapor pressure contributes less to the coolant acceleration after heat transfer from the fuel and leads to lower quasi-static pressure levels in the vessel. However, single phase pressure spikes might be significantly higher with the lead coolant.

In summary the results of the analyses indicate that for a dedicated core without sufficient prompt negative feedback and deteriorated safety parameters the threat for severe accident consequences exists in case the subcriticality level is eliminated e.g., by fuel compaction.

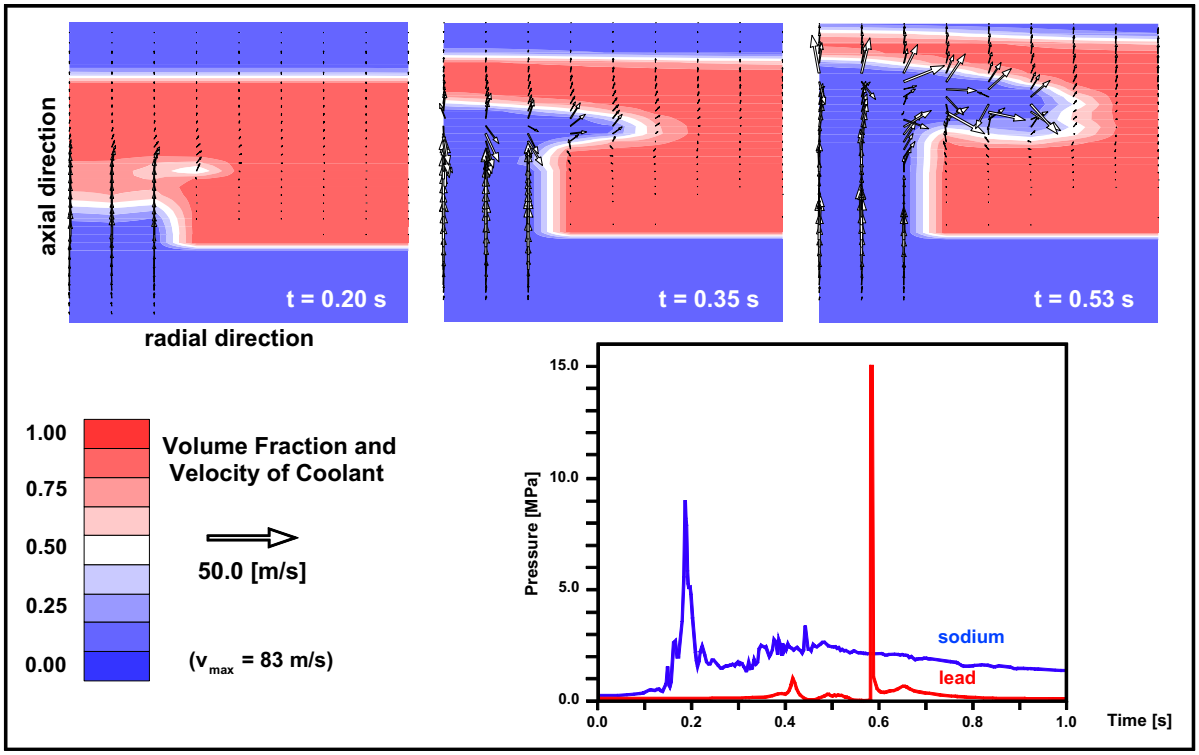

FIG. 3. Coolant volume fraction distribution and pressure trace in the upper plenum during the expansion phase of hot core material. Comparison of lead versus sodium for identical core conditions.

4.2. Influence of inherent reactivity potentials

In an ADS an essential inherent safety feature is the subcriticality level of the core. The subcriticality level is defined by normal operation requirements (e.g., accelerator conditions, burn-up behavior, structure effects), but also by safety requirements. One can speculate if and which reactivity potentials and material rearrangements could exist and cause the elimination of the subcriticality level under transient conditions; or how deep the 'subcriticality' level must be to cope with potential reactivity additions. Besides transient dimensional changes from heating up of structures or more severe, triggered by earthquakes, also other possibilities exist for reactivity addition e.g., by a selective removal of coolant and clad, which could take place before fuel involvement.

The coolant voiding problem is much relieved by the high boiling point of lead. However, voiding by gas release from breached pins or a massive gas blow-down from the fission gas plenum could introduce void into the core. The production of He by the Am and Cm decay could be a major source for plenum pressurization**.** The gas blow-down could start around core mid-plane at the maximum positive void worth location. The maximum positive void worth might therefore be an important safety indicator. Calculations show that the total core void could already be considerable in a dedicated core. The total void for the core analyzed was calculated with about 5000 pcm.

The gas release from the plena is calculated in a special model of the SIMMER-III code [21], originally used for sodium cooled reactors. In Fig. 4 the void front formation in an inner ring subassembly with a mid-plane breach location is shown after a gas blow-down from the upper plenum. This phenomenon has been analyzed comparing lead versus sodium and for fission gas and lighter helium. As one would expect, the axial extension of the void region in lead is smaller than in sodium. Additionally, the void fraction itself is lower in the lead coolant, and the gas bubble is swept out of the core. In Ref. [22] details are given on the SIMMER-III simulation of gas-liquid flows with large liquid densities.

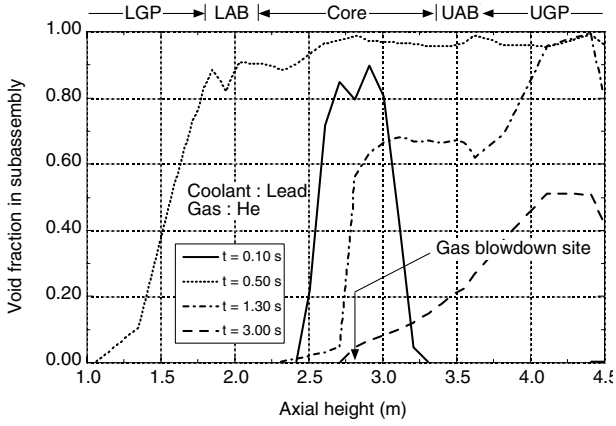

FIG. 4. Axial void front in an inner ring subassembly after gas-blow-down under loss of flow conditions.

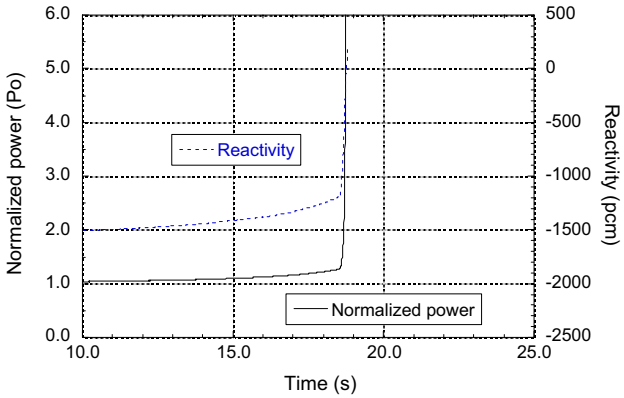

FIG. 5. Power transient under loss of flow conditions in a dedicated core after gas blow-down.

Besides the reactivity effects from lead, another requirement for the subcriticality level

may come from the clad steel worth. Transients could lead to clad melting and clad relocation [6, 9]. As the density ratio of liquid steel to lead is ~ 0.7, the clad will be swept upwards. The clad worth of the core analyzed is 2200 pcm. The steel floating upwards could block the exit regions above the core and cause severe cooling problems. There could exist a generic problem of enhanced blockage formation (caused e.g., by corrosion products, by PbO plate-out, up to the fore-mentioned steel blockages) related to the design of lead cooled systems. The large p/d ratio requires grid spacers in the core. As is known from former investigations [23] these grid spacers enhance the blockage formation problem significantly compared to wire wraps. Partial steel plate-out at the core exits leads to a further increase of reactivity by 600 pcm.

Currently, mechanistic calculations for different accident initiators as ULOF, ULOHS etc. are under way. These analyses show, that compared to the above scoping calculations (assessment of reactivity potentials) the core will only be partially voided and the clad steel will only be removed in some parts of the core. However, they also indicate that for the dedicated core investigated, coolant voiding, clad relocation and local fuel melting could finally develop into a severe accident (see example in Fig. 5). Results of these mechanistic analyses show the same trends for accident energetics as described before. Due to the mild reaction between fuel and lead (compared to fuel/sodium) autocatalytic processes (as e.g. LOF/TOP) are potentially less severe [9]. Nevertheless, the investigations show that for dedicated cores with a high recriticality potential - synonymous with high fuel and clad worth - the subcriticality level might have to be chosen very low to cope with the inherent reactivity effects.

5. REQUIREMENTS FOR DEDICATED CORES

A pronounced cliff-edge behavior, as observed in the safety analyses of the dedicated core, seems not to be tolerable. Therefore, some proposals are made by which this undesired behavior can be prevented. The main target is to assure a 'reasonable' core behavior also under hypothetical severe accident conditions and the removal of any cliff-edge effect. With these goals achieved, necessary mitigative measures, containment measures, can also be more reasonably defined. In addition, specific safety margins can be attributed to the built-in subcriticality directly related to accident prevention. The subcriticality level will thus will act as a strong line of defense against severe transients. In the following some proposals are made to be taken into account in the design of a core with dedicated fuel. They directly aim at the safety behavior under severe transient and accident conditions. The potential of passive engineered safety measures preventing severe accident scenarios are investigated currently.

- Fuel worth: The neutronic fuel worth of the dedicated core consisting of Pu and MAs will probably be high and the core will contain a high number of “critical” masses. By a local compactive fuel rearrangement the built-in subcriticality level of the ADS could thus be eliminated. With this condition accepted it is difficult to define a certain number of critical masses as a “safe” limit. As an orientation, one subassembly should not contain multiple critical masses.
- Fuel stability: The fuel worth and spectrum related neutronic quantities can change dramatically in a severe transient, if the fuel is not stable in its matrix under melting conditions. If the fissile component could separate and compact, more severe recriticalities must be expected.
- Coolant void worth: In the case of lead coolant, boiling processes will be of less importance, but voiding e.g. by a gas bubble passage caused by a gas blowdown from the plena (at core mid-plane) must be taken into account. The maximum positive void worth

must be significantly less than the subcriticality margin to cope with the additional clad worth contribution.

- Clad worth: Due to the high boiling point of lead; steel melting will occur first in most accident scenarios. The steel worth of the core should therefore additionally be covered by the subcriticality level. Reactivity effects related to the formation of reflective steel layers have to be taken into account.
- Feedback effects/kinetics quantities: For limiting any nuclear excursion in case the built-in subcriticality level might be consumed e.g., by local fuel compaction processes, a reasonable Doppler feedback effect should be available for oxide or nitride fuels (for metal fuels the expansion effect can replace the Doppler). As a rule from experience, the fast feedback as the Doppler, expressed by its constant should be around 1/3-1/4 (absolute value) of the core void worth. Note that by spectrum hardening effects (e.g., fuel/matrix separation) the Doppler might drop significantly. Information must be gained on the size of the Doppler effect of dedicated fuel and its reduction at higher temperatures. The kinetics parameters become more important for near critical or super critical conditions, in particular the neutron generation time. It is strongly desirable that it is not less than in conventional critical fast reactors.

A safety issue to solve is the high fuel reactivity potential (inherent number of critical masses), which might be so high, that any subcriticality level can be eliminated in case of local melting or compaction processes. In this case the quality of feedback effects and kinetics parameters plays a decisive role. In contrast, to cope with the coolant void worth or the clad worth the subcriticality level could theoretically be adjusted (note however problems of beam power, power form factors etc.). Introduction of moderating material into the core [24] could further improve the void worth and the Doppler. However, when dealing with core melt scenarios this measure may not be effective, due to possible separation processes of the fuel from the lighter moderator. Mechanistic accident analyses for the dedicated core reveal a problem intrinsic to source-powered systems. The increase in reactivity e.g. caused by coolant voiding, leads (besides the general power surge) to a significant change in the shape of the power profile (especially for systems with deep subcriticality). Approaching criticality results in higher power densities in the peripheral core regions away from the source. This could directly enhance propagation processes during a core disruptive accident.

Complying with the above proposals should guarantee a high safety potential for an ADS, even with a high recriticality potential. They devise a clear safety function to the subcriticality level, help to prevent accident escalation, limit any excursion energetics by inherent effects and facilitate the discussion of containment measures. Including additional passive/engineered measures will result in a well balanced safety approach for the ADS on all levels, from operational safety to hypothetical accidents.

To fulfill most of the above mentioned requirements the integration of U238 or Th232 would help. This would however mean a change in the transmutation strategy. Nevertheless it might be worthwhile to consider and investigate dedicated fuel alternatives with fertile fuel included for safety reasons.

6. CONCLUSIONS AND FINAL REMARKS

The safety behavior of a typical ADS dedicated core is investigated both under operational transient conditions and severe accident situations. The problems related to the status of dedicated fuel development are discussed which could strongly influence all levels from operational safety to severe transient and accident conditions. It is clear that a broad knowledge base (as for current oxide fuel) does not exist for such innovative fuels, especially under transient conditions. Such dedicated cores with fertile-free fuel could possess large inherent reactivity potentials and very poor safety coefficients, as a small Doppler, β_{eff} and neutron lifetime. Investigations show, that under normal operational conditions these safety coefficients have a limited influence on the dynamics in a source driven system. However, the situation changes drastically if any voiding, steel melting or pin disruption and fuel rearrangement should occur. The inherent reactivity potentials of the dedicated core are large and a threat from 'cliff-edge' effects with high energetics could exist under accident conditions. A dedicated core with such safety features and parameters does not comply with the requirement of high inherent safety. To assure a reasonable safety behavior of such dedicated cores, a number of proposals are made to obtain a balanced approach for safety on all levels from operational safety to severe accidents.

REFERENCES

[1] SALVATORES, M., SLESSAREV, I., RITTER, G., FOUGERAS, P., TCHISTIAKOV, A., YOUINOU, G., ZAETTA, A., Long-lived radioactive waste transmutation and the role of accelerator driven (hybrid) system, Nucl. Instr. And Methods in Phys. Research A 414, 1, 5 (1998).

[2] A Roadmap for Developing Accelerator Transmutation of Waste (ATW) Technology: A Report to Congress, DOE/RW-0519, US Department of Energy (1999).

[3] VASILE, A., VAMBENEPE, G., LEFEVRE, J.C., HESKETH, K., MASCHEK, W., DE RAEDT, Ch. HAAS, D., The New CAPRA-CADRA Program, paper presented in the 8th Int. Conf. on Nuclear Engineering (ICONE-8), 2000, Baltimore, USA, American Society of Mechanical Engineers (ASME), New York (2000).

[4] TOMMASI, J., MASSARA, S., LMFR Dedicated Cores for Transmutation, Critical versus Subcritical Comparison, Proc. Int. Conf. on Future Nuclear Systems (Global'99), 1999, Jackson Hole, Wyoming, USA, ANS, ISBN: 0-89448-641-1 (1999).

[5] Fuel Fabrication and Processing Subgroup of the Technical Working Group on ADS 2000, R.J.M. Konings (Ed.), Advanced fuel cycles for accelerator-driven systems: fuel fabrication and reprocessing, EUR 19928 (2001).

[6] WIDER, H.U., Severe Accident Studies in Fast Accelerator - Driven Systems, 2nd Int. Conf. on ADS Transmutation Technology and Application, (ADTT'96), Kalmar, Sweden (1996), H. Condé (Ed.), Uppsala University, Sweden (1997).

[7] WIDER, H.U., KARLSSON, J., JONES, A.V., Passive Safety Approaches in Lead/Bismuth-cooled Accelerator Driven Systems, JK'2000 Jahrestagung Kerntechnik, Bonn, Germany (2000).

[8] WIDER, H.U., KARLSSON, J., JONES, A.V., Lead/Bismuth – Cooled, Thorium Based ADS and Critical Systems Meet Sceptic's CriteriaProc. Int. Conf. on Emerging Nuclear Energy Systems (ICENES 2000), 2000, Bruxelles, Belgium, H. van Dam, J.C. Kuijper (Eds); Uitgave, NRG, Petten, Netherlands, ISBN: 90-805906-2-2 (2000).

[9] MASCHEK, W., MERK, B., WIDER, H.U., Some Safety Studies for Accelerator Driven Subcritical Systems, paper presented in the 2nd Int. Top. Mtg. on Nuclear Applications of Accelerator Technology (AccApp'98), 20-23 September 1998, Gatlinburg, USA, ANS, ISBN: 089448-633-0 (1998).

[10] KLICKMAN, A.E., THOMPSON, D.H., RAGLAND, W.A., WRIGHT, A.E., PALM, R.G., PAGE, R.J., Review of recent ANL experiments in SLSF and TREAT, Proc. LMFBR Safety Topical Meeting, Lyon, France, 1982, ENS-SFEN-ANS (1982).

[11] IMKE, U., STRUWE, D., NIWA, H., SATO, I., CAMOUS, F., MOXON, D., Transient Fuel-Pin Behavior and Failure Conditions in the CABRI-2 In-Pile Tests. Proc. Int. Top. Mtg. Sodium Cooled Fast Reactor Safety, 3-7 October 1994, Obninsk, Russia, IPPE, Obninsk (1994).

[13] MASCHEK, W., RINEISKI, A., MORITA, K., KIEFHABER, E., BUCKEL, G., FLAD, M., COSTE, P. PIGNY, S., RIMPAULT, G., LOUVET, J., CADIOU, T., KONDO, S., TOBITA, Y., SUZUKI, T., YAMANO, H., FUJITA, S., SIMMER-III, a Code for Analyzing Transients and Accidents in Accelerator Driven Systems (ADS), Proc. 4th Int. Top. Meeting on Nuclear Applications of Accelerator Technology (AccApp'00), Washington D.C., USA, ANS (2000).

[14] OTT, K.O., NEUHOLD, R.J., Nuclear Reactor Dynamics, ANS, La Grange Park, USA (1985).

[15] BUCKEL, G., HESSELSCHWERDT E., KIEFHABER, E., KLEINHEINS, S., MASCHEK, W., A new SIMMER-III version with improved neutronics solution algorithms, FZKA 6290 (1999).

[16] RINEISKI, R., MERK, B., MASCHEK, W., ADS Related Extension of the Neutronics Module in the Accident Analysis Code SIMMER-III, paper presented in the 3rd Int. Conf. on Accelerator-Driven Transmutation Technologies and Applications (ADDTA'99), 7-11 June 1999, Prague, Czech Republic, Eds: L M. Hron, V. Lelek (NRI Rez plc), M. Mikisek, M. Sinor, J. Uher, J. Zeman (FNSPE CTU, Prague), NRI Rez, Czech Republic (1999), Prague, Czech Republic.

[17] RINEISKI, R., KIEFHABER, E., MERK, B., MASCHEK, W., FLAD, M., Neutron Kinetics Developments of the SIMMER-III Safety Code for ADS Application, Proc. 2nd OECD/NEA Workshop on the Utilization and Reliability of High Power Proton Accelerators, Aix-en-Provence, France, 1999, NEA, ISBN: 92-64-18749-9 (1999).

[18] CODE COLLECTION, DANTSYS 3.0, One-, Two-, and Three-Dimensional, Multigroup, Discrete Ordinates Transport Code System, contributed by: Los Alamos National Laboratory, Los RSIC COMPUTER Alamos, New Mexico (1995).

[19] MASCHEK, W., THIEM, D., Energetic Potentials of Core Disruptive Accidents in Fast Reactors with Transmutation/Burning Capabilities, Proc. Int. Top. Meeting on Advanced Reactors Safety (ARS'94), Pittsburgh, USA, ANS (1994).

[20] MASCHEK, W., FLAD, M., LO PINTO, P., Core Disruptive Accident Analyses for Advanced CAPRA Cores, Proc. Int. Conf. on Nuclear Engineering (ICONE-4), 1996, New Orleans, USA, ASME & JSME (1996).

[21] TOBITA, Y., JNC, private communication (2000).

[22] SUZUKI, T., TOBITA, Y., KONDO, S.A., YAMANO, H., SIMMER-III Analysis of Gas-Liquid Flows with Large Liquid Densities, Proc. 2nd Japan-Korea Symposium in Nuclear Thermal Hydraulics and Safety (NTHAS2), 15-18 October 2000, Fukuoka, Japan, The Atomic Energy of Society of Japan/The Korean Nuclear Society (AESJ/KNS) (2000) 73-80.

[23] MINDEN, C.v., SCHULTHEISS, G.F., Upon local blockage formations in LMFBR fuel rod bundles with wire-wrapped spacers, GKSS 82/E/50 (1982).
[24] MASCHEK, W., THIEM, D., HEUSENER, G., Safety Features of a Reactor Core with Minor Actinide Transmutation and Burning Capabilities, Proc. Int. Conf. on Future Nuclear Systems (Global'99), 1999, Jackson Hole, Wyoming, USA, ANS, ISBN: 0-89448-641-1 (1999).

TARGET DEVELOPMENTS

(Session 5)

Chairperson

B.W. SPENCER

United States of America

MYRRHA: DESIGN OF A WINDOWLESS SPALLATION TARGET FOR A PROTOTYPE ACCELERATOR DRIVEN SYSTEM

K. VAN TICHELEN, P. KUPSCHUS, H. AÏT ABDERRAHIM
Belgian Nuclear Research Center (SCK•CEN), Mol, Belgium

J-M. SEYNHAEVE, G. WINCKELMANS, H. JEANMART
Université Catholique de Louvain, Louvain-la-Neuve, Belgium

F. ROELOFS, E. KOMEN
Nuclear Research and Consultancy Group, Petten, Netherlands

Abstract

The development of a new nuclear installation that is able to fulfil the economical, social, environmental and technological demands, is a cornerstone for the future provision of sustainable energy. Accelerator Driven Systems (ADS) can pave the way for a more environmentally safe and acceptable nuclear energy production. Fundamental and applied R&D are crucial in the development of ADS technologies and demand the availability of appropriate prototype installations. In answer to this need and in order to update its current irradiation potential, the Belgian Nuclear Research Centre (SCK•CEN), in partnership with Ion Beam Applications s.a. (IBA), is launching the MYRRHA project. It is focussed on the design, development and realisation of a modular and flexible irradiation facility based on the ADS concept. Currently the study and preliminary conceptual design of the MYRRHA system is going on and the basic engineering is being performed. This study will define the final choice of the characteristics of the facility depending on the selected fields of application to be achieved.
The MYRRHA concept, as it is today, is based on the coupling of a commercial proton accelerator with a spallation target surrounded by a subcritical neutron-multiplying medium. A 5 mA beam of accelerated protons of 350 MeV hits a liquid lead-bismuth spallation target and produces neutrons needed to deliver the primary neutrons for the neutron amplifier. During this process the beam deposits most of its energy into the Lead-Bismuth. The spallation target system consists of a flow loop designed to form a free surface with access to the downward directed beam and with contact to the beam line vacuum. No conventional window is foreseen between the free surface and the proton beam line vacuum in order to avoid engineering and operational difficulties. The windowless concept distinguishes MYRRHA from other ADS design activities and makes the design very challenging.
Indeed, the geometry of the spallation target and more specifically the form of the free surface determines to a large extent the neutronic and thermal-hydraulic characteristics and the technological feasibility of the spallation target. The creation of a stable and controllable free surface flow capable of removing the heat deposited by the beam within the neutronic constraints is of main importance. This paper describes the design activities, which have been and are being performed to study the flow behaviour and to obtain an adequate design. These activities include both experiments and Computational Fluid Dynamics (CFD) calculations and their interaction.

1. INTRODUCTION

At the heart of an Accelerator Driven System is the spallation target. It is a neutron source providing primary neutrons that are multiplied or amplified by the surrounding subcritical core. The primary source produces neutrons by the spallation reaction of heavy target nuclei under a high-energy (several 100 MeV) proton beam generated by a suitable particle accelerator.

During a first stage called ‘the intranuclear cascade’, the incident protons interact with the constituent nucleons (neutrons and protons) of the target individually, leading to the emission of very energetic secondary particles (neutrons and protons). In a second stage called ‘evaporation’, the target nuclei are left in very high excitation state after absorption of less energetic incident particles and de-excite by evaporating a large amount of "low" (few MeV) energy neutrons. As a result of these processes, one can obtain a large amount of spallation neutrons depending on the initial energy of the incident particle and on the atomic number of

the target nuclei. For instance a lead target bombarded with 1 GeV protons can yield ~ 25 n/p. At 350 MeV one expects 3 n/p [4].

Due to the high Z efficiency, a heavy metal is the most appropriate solution for the target. Moreover, due to very high power density one can reach, a liquid metal is most adequate, allowing to remove the heat by forced convection.

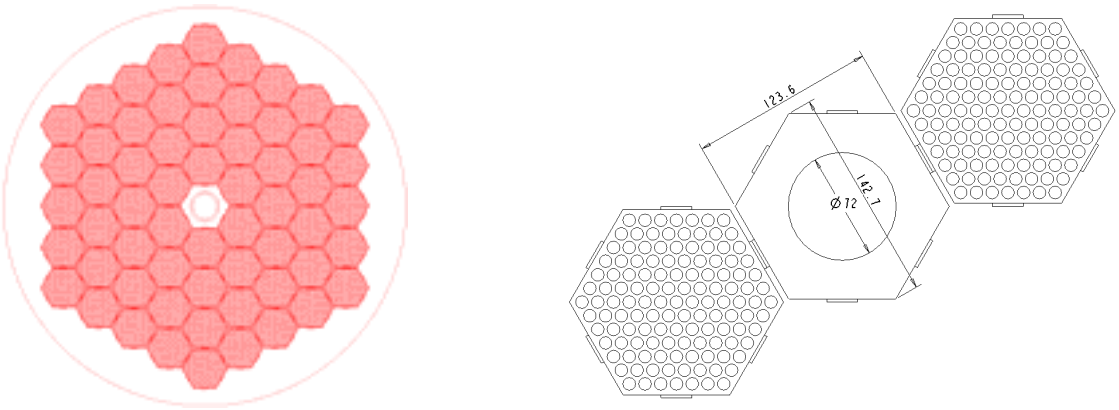

FIG. 1. Dimension of the central gap for the spallation target in the hexagonal core of MYRRHA.

The MYRRHA subcritical core consists of hexagonal assemblies of MOX Fast Reactor-type fuel pins with an active length of 500 mm placed centrally in a liquid Pb or Pb-Bi pool [1]. The central hexagon is removed, leaving a gap for the spallation target consisting of liquid Pb-Bi. The dimensions of this central gap are constrained by the neutronic performances of the core: in order to obtain the required fast neutron fluxes the central gap should be minimised to the dimensions shown in Fig. 1 [4]. At the position where the spallation process occurs, the diameter of the target loop is restricted to 72 mm. This allows irradiation samples to be introduced very close to the active target region where the fast neutron fluxes are at the highest. Above this position, a feeder and a nozzle taking the liquid to the centre position can use the full space between the central hexagon and the inner tube. The position of the target in the MYRRHA system is shown in Fig. 2.

The spallation target of MYRRHA will be bombarded with a (5 mA, 350 MeV)-proton beam. At this energy, the beam penetrates in the target over 130 mm. With a beam diameter slightly less than the inner tube diameter of Fig. 1, the current density at the target surface will amount to ~130 $\mu A/cm^2$ and the average energy deposited in the target region will be of the order of 3 kW/cm^3. A total of 1.75 Mw of beam power needs to be removed by neutrons (~20%) and by heat transport (~80%). The profile of the energy deposition as a function of the penetration depth at different radial positions is shown in Fig. 3.

In order to avoid engineering and operational problems with a target window between the liquid metal and the beam vacuum due to the high current density, the MYRRHA target will be windowless. The Pb-Bi surface will thus be in direct contact with the vacuum of the beam line. The vapour pressure is low enough to prevent excessive evaporation provided surface temperatures are sufficiently low.

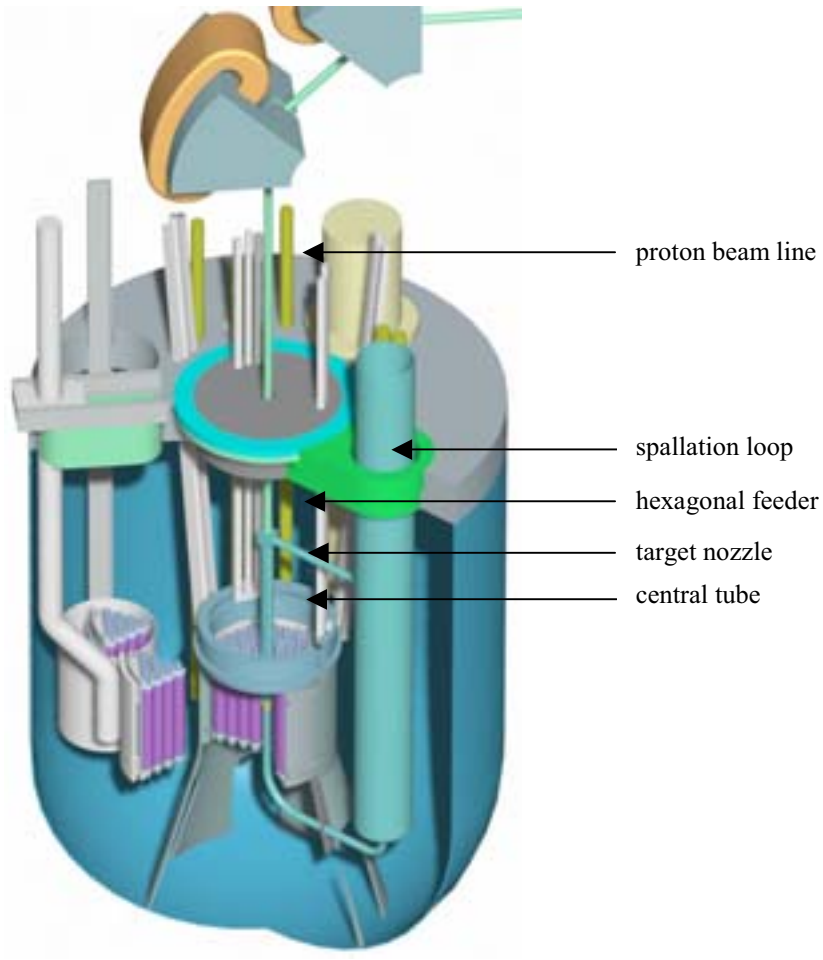

FIG. 2. The position of the spallation target in the MYRRHA system.

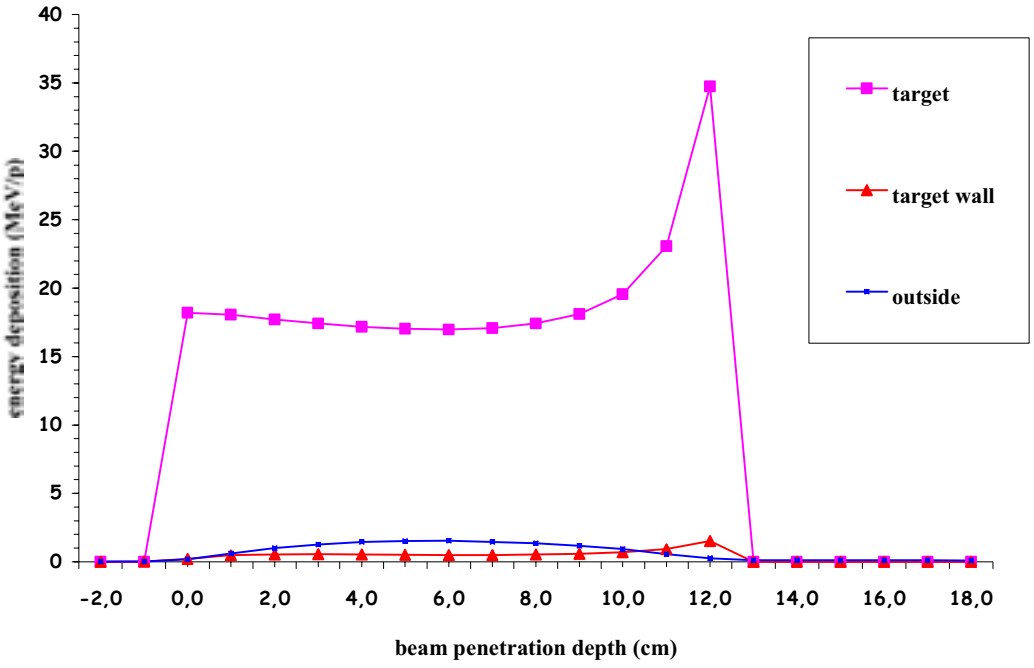

FIG. 3. The energy deposition in the spallation target at different radial positions [5].

To summarise, the challenge in the MYRRHA spallation target design is to create a Pb-Bi flow pattern with a free surface within the geometrical constraints, adequate to remove the heat deposited by the proton beam so that the thermal and vacuum requirements are met.

2. EXPERIMENTAL PROGRAM

To gain insight in the characteristics and expertise in the creation of an adequate free surface flow, SCK•CEN has developed a roadmap of experiments with increasing correspondence to the real situation.

2.1. Water experiments at UCL

In June 1999 an R&D program started in collaboration with the thermal-hydraulics department of Université Catholique Louvain-la-Neuve (UCL, Belgium). Within this R&D program, water experiments on a one-to-one scale under atmospheric pressure were performed. Water was used because of its easiness to handle and its good fluid-dynamic similarity with Pb-Bi [9]. All experiments were performed at a nominal flow rate of 5 L/s. Simplified thermal calculations have shown that this flow rate would be sufficient to remove by convective heat transport a beam with a current of 2 mA. More recent neutronic calculations have indicated the need for an increased beam current of 5 mA and a doubling of the flow rate for this current is foreseen.

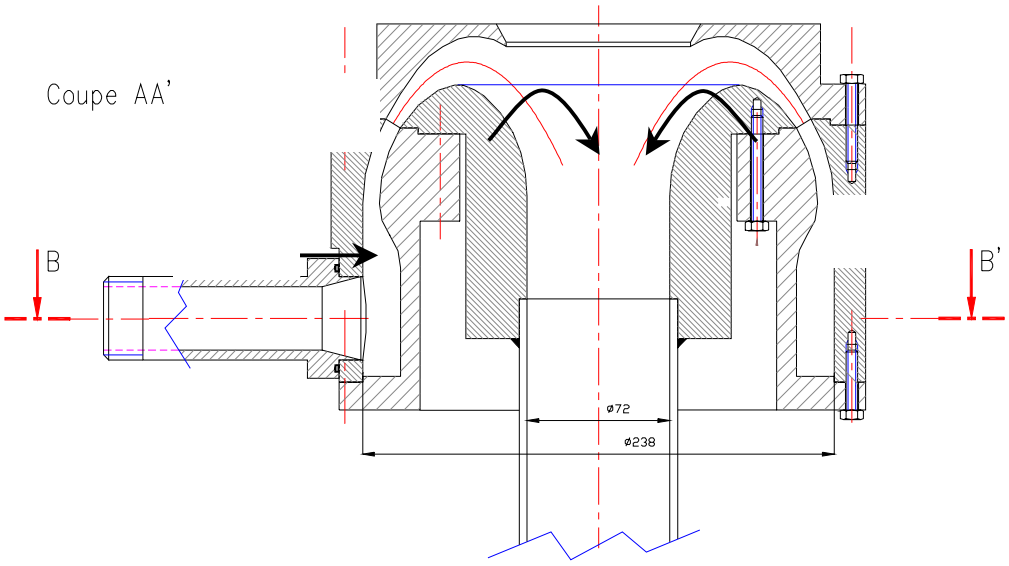

FIG. 4. The nozzle in the co-axial target experiment.

At the start of the experimental program, the full hexagonal space was available for the spallation target throughout the core. This led to a co-axial design in which the target could be inserted in the core from beneath, leaving the space above the core free for fuel manipulations. A first nozzle was shaped using simple analytical approach based on the continuity equation and a cross-section averaged Bernouilli equation. This nozzle is shown in Fig. 4. The feeder of the nozzle is also shown. It consists of an annular region fed at 5 L/s by four identical orthogonal tubes of which one is drawn. A pressure drop is inserted to distribute the flow equally over the circumference.

First experiments showed the creation of a strong and stable swirl in excess of one meter length in the central tube within a few seconds after the start of the pump. To avoid this swirl formation, an anti-swirl device with eight guiding vanes was designed (see Fig. 5). This anti-swirl has proven to be very effective in eliminating the swirl. CFD calculations by NRG (The Netherlands) have been able to demonstrate that the swirl is formed in the feeder. This will be discussed in the paragraph on the numerical program.

A stable free surface at different fluid levels could be established. The surface shape proved to be not very sensitive to a flow rate variation of 25%. A picture of the free surface at 5 L/s is also given in Fig. 5. The lower nozzle wall guides the main flow into the central tube. In the centre where the flow streams meet, a so-called recirculation zone or hydraulic jump is formed. In this zone, the streamlines are forming closed cells in which the fluid is going upward along the central axis, flows radially outwards and returns parallel with the main flow streamlines.

FIG. 5. The free surface in the co-axial target experiment with the anti-swirl device.

Experiments introducing dye in the flow have shown that the residence time of fluid particles in the recirculation zone is on the bridge of being critical. This has important implications on the fluid temperatures at the free surface when the beam heating will be present. The longer the residence times, the higher the temperature and the higher the vaporisation of the Pb-Bi into the beam line. Minimisation of the residence times by minimising the recirculation zone is seen as a major tool to handle the surface heating and is being addressed [7].

To characterise the velocity field in target, Hot Wire Anemometry measurements and more successful Ultrasonic Doppler Velocimetry (UDV) measurements have been performed in collaboration with Forschungszentrum Rossendorf (FZR, Germany). The UDV technique provides the mean axial velocity and its fluctuating component in the region from 15 to 110 mm under the free surface using two probes at different frequencies (2 & 4 MHz). Three radial scans have been performed. A result of these measurements for the 2 MHz probe is given in Fig. 6. The different curves are at different radial positions. A negative sign indicates an upward velocity. The mean velocity plot clearly shows the existence of a recirculation zone [2].

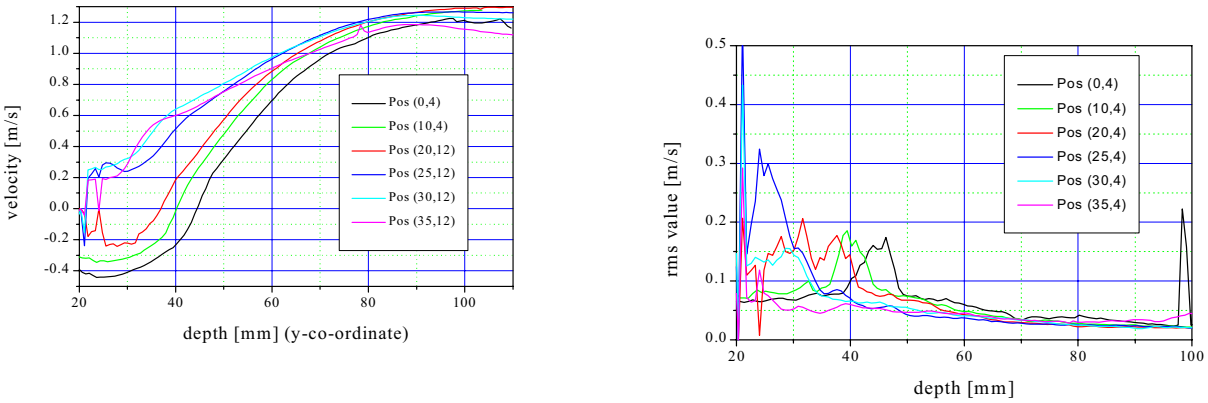

FIG. 6. The mean axial velocity and its r.m.s. value at different radial positions with UDV.

As the neutronic calculations proceeded, the necessity of reducing the target dimensions in the region of spallation became clear. The co-axial design had to be abandoned for reason of available space. A new design with the Pb-Bi descending through the space defined the hexagon and the central tube and fed to the central tube by a new kind of nozzle was developed. The design was tested experimentally at UCL adapting the existing configuration. The new configuration is shown in Fig. 7. The anti-swirl device is not drawn but is still present.

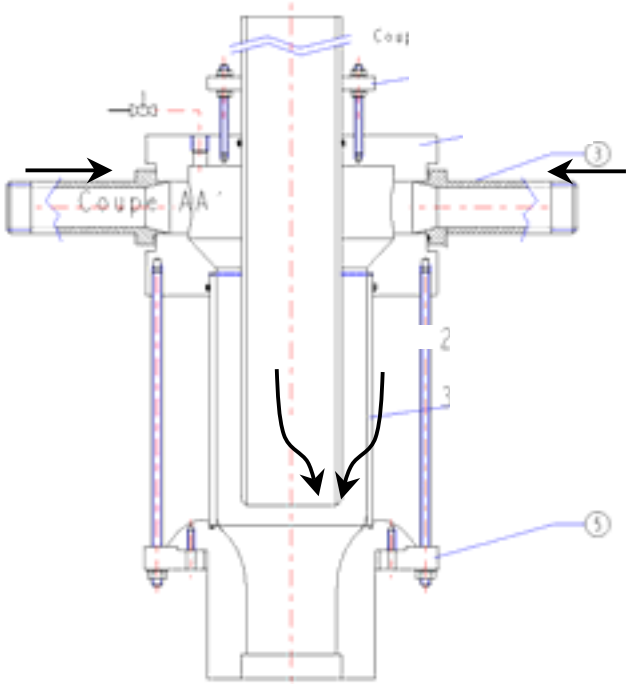

FIG. 7. The nozzle in the new target experiment.

A stable free surface of the same kind as in the 'old' configuration was established and the velocity field was measured using Laser Doppler Velocimetry (LDV) in an axial region limited by optical accessibility by UCL. As shown in Fig. 8, these measurements not only provided the mean axial velocity component and its fluctuation, but also the mean azimuthal component and its fluctuation. The comparison of the latter with the azimuthal velocity in a flow without anti-swirl device proved the effectiveness of the anti-swirl. Azimuthal velocities are reduced by one order of magnitude.

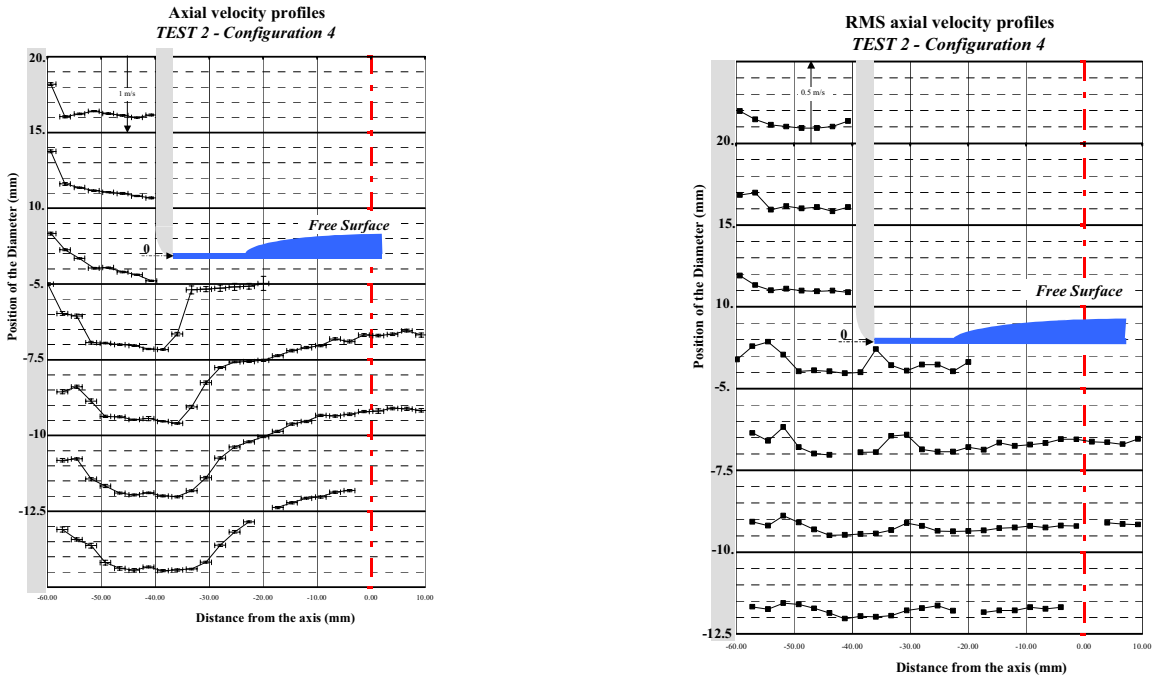

FIG. 8(1). The velocity profiles with anti-swirl device with LDV.

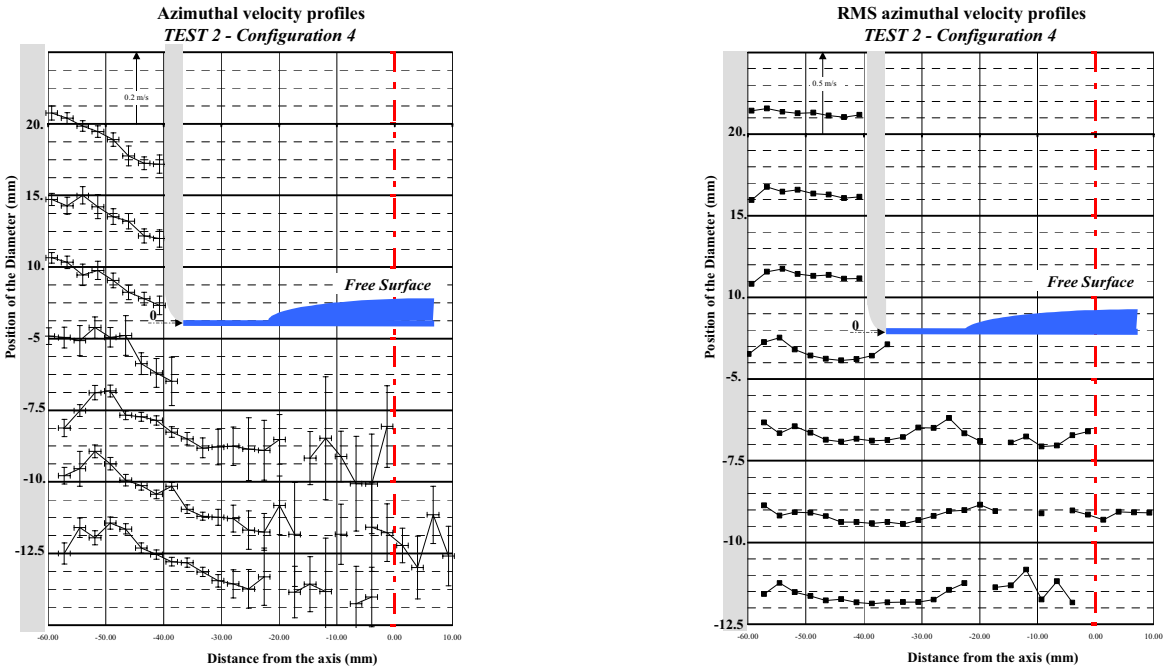

FIG. 8(2). The velocity profiles with anti-swirl device with LDV.

These experimental results were used to construct the streamline pattern of the axial velocity field, clearly showing the recirculation zone with the closed streamlines (see Fig. 9).

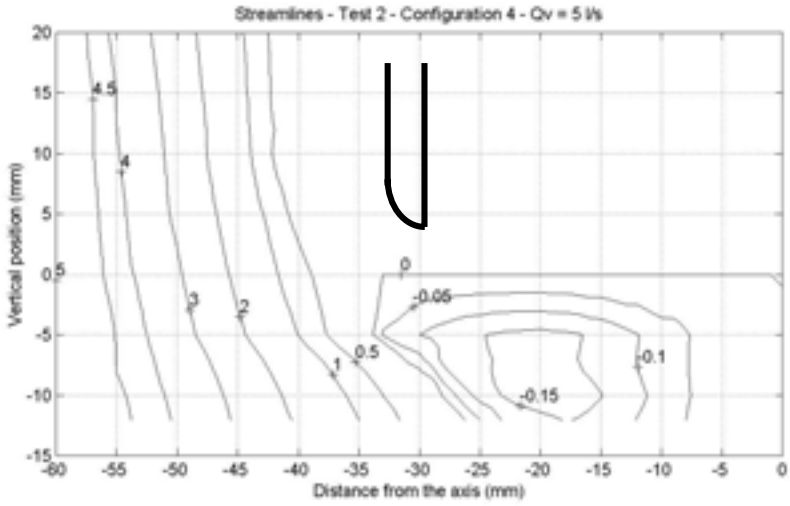

FIG. 9. The velocity profiles with anti-swirl device with LDV.

It also appeared that in the new experimental set-up the free surface level could be slightly (~10 mm) dropped under the top of the outlet of the feeding nozzle. This had never been possible in the old configuration because of immediate entrapment of air at the edge between main flow and the recirculation region disturbing the flow pattern. Figure 10 gives the results of LDV measurements in this case, indicating a decrease of the recirculation zone. Further minimisation of this zone was however not possible because of air entrapment. This entrapment creates a two-phase flow situation that drastically changes the flow behaviour. However, it gave a first glimpse of the possibility to minimise the recirculation zone and the corresponding residence times to keep fluid temperatures at an acceptable level in the presence of beam heating [2].

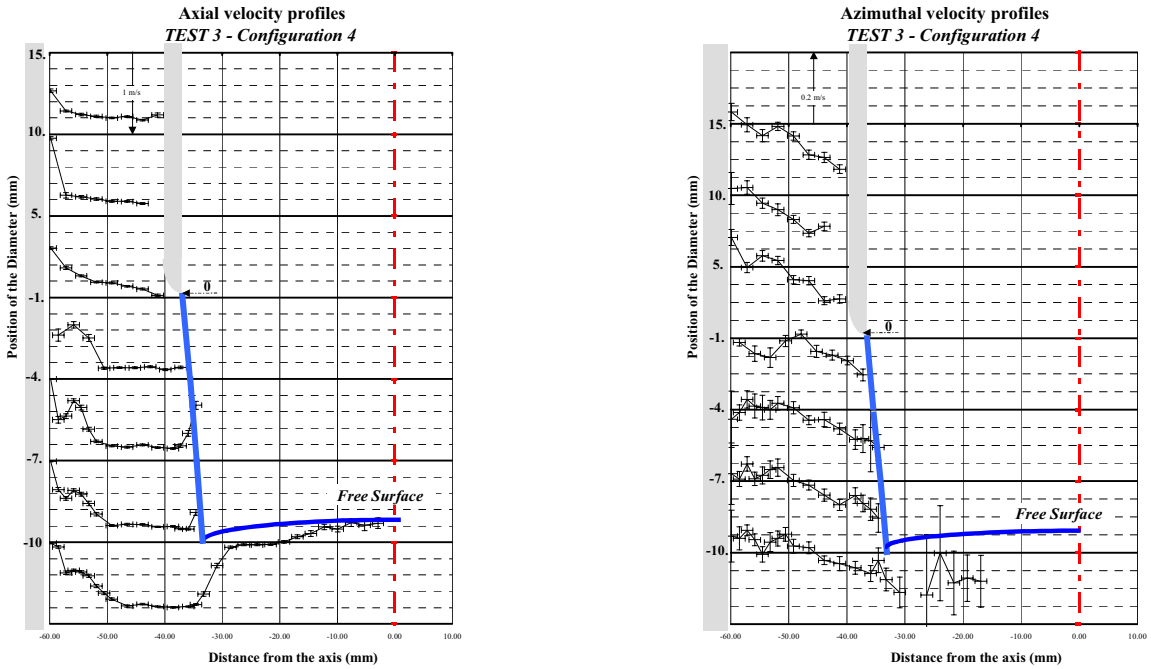

FIG. 10. The velocity profiles with a slightly dropped free surface.

2.2. Hg Experiments at IPUL

To eliminate the possibility of air entrapment and to create in that way the possibility to minimise the recirculation zone, a one-to-one experiment using liquid Hg under vacuum has been designed by SCK•CEN. The contract for performing the experiments at the Institute of Physics of the University of Latvia (IPUL, Latvia) is in the phase of finalization. A drawing of the target module is shown in Fig. 11. The experiments will be performed at the real flow rate of 10 L/s. For reasons of compactness a co-axial design has been used. However, measures will be taken to eliminate the flow history at the inlet of the nozzle.

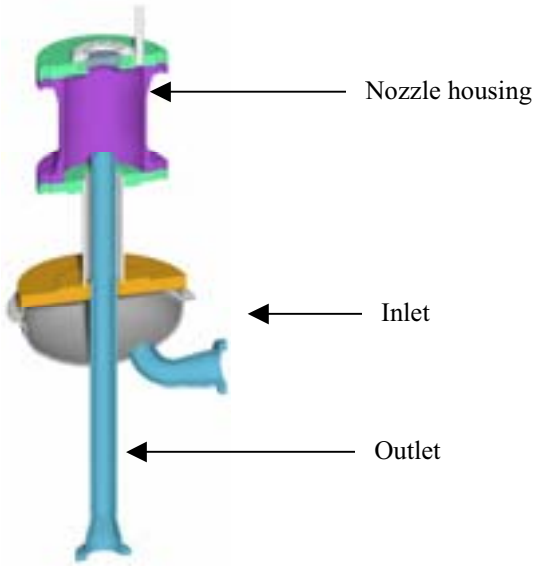

FIG. 11. The target module in the Hg experiment.

Different nozzle shapes will be investigated and different fluid levels will be established to minimise the recirculation zone. These fluid levels will be measured using contact probes. Potential probe and Ultrasonic Doppler Velocimetry measurements are foreseen to gain information about the velocity field. First results are expected around the time of the conference.

2.3. Pb-Bi experiments at FZK

As the spallation target design is a crucial point for the MYRRHA project, final confirmation experiments are foreseen to be performed with the real fluid at the actual temperatures. In view of this, the collaboration with Forschungszentrum Karlsruhe (FZK, Germany) has been negotiated aiming at inserting a one-to-one model of the MYRRHA spallation target similar to the one in Fig. 11 in their KALLA Pb-Bi loop that has a working temperature of about 250°C.

3. NUMERICAL PROGRAM

In parallel with the experiments, numerical simulations using CFD codes are performed aimed at reproducing the existing experimental results and giving input for the optimisation of the head geometry in the experiments. The CFD calculations are also used to investigate the flow pattern and temperature profile in the presence of the beam heating that cannot be simulated experimentally at this stage.

3.1. Simulation of the flow pattern

First CFD calculations have been performed at UCL with Fluent [7] and at SCK•CEN with FLOW-3D aimed at reproducing the results of the first UCL experiment. Later the same calculations were done with Star-CD in collaboration with NRG [6]. All three codes use the Volume of Fluid (VOF) method for simulation of the free surface [3].

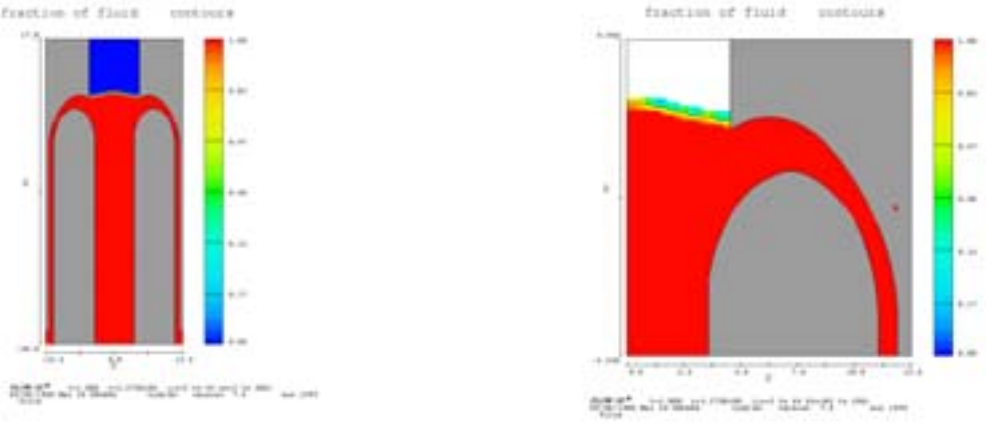

FLOW-3D

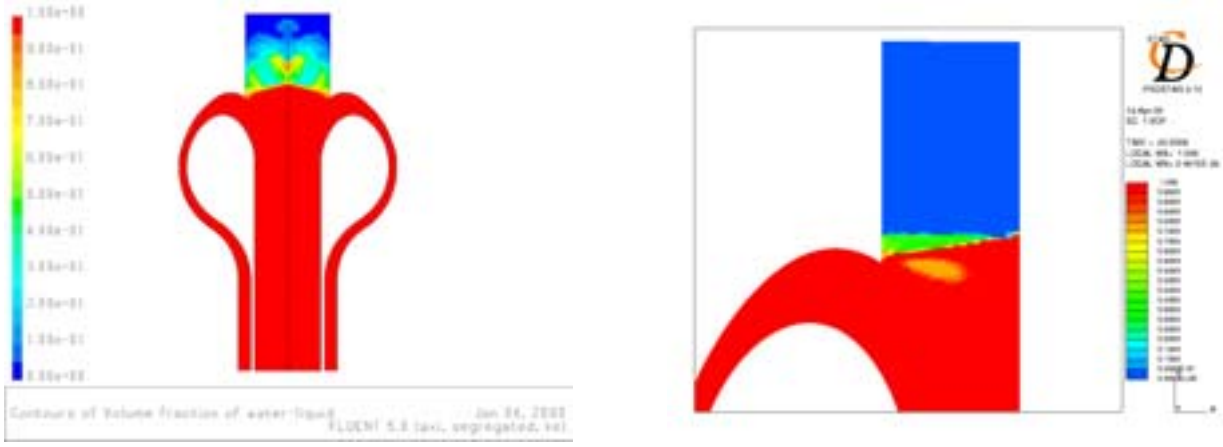

Fluent *Star-CD*

FIG. 12. The free surface and the recirculation zone with different CFD codes.

The codes were able to reproduce the recirculation zone and the hydraulic jump as shown in Fig. 12. However, as one can see, Fluent and Star-CD suffer from 'numerical diffusion' in a way thatisprohibitive for the heating calculations. The free surface region is a large diffuse zone and the surface shape cannot be defined. As the form of the free surface is crucial for the beam heating profile and the surface temperatures, a large amount of work was and is concentrated on the reduction of the diffusion.

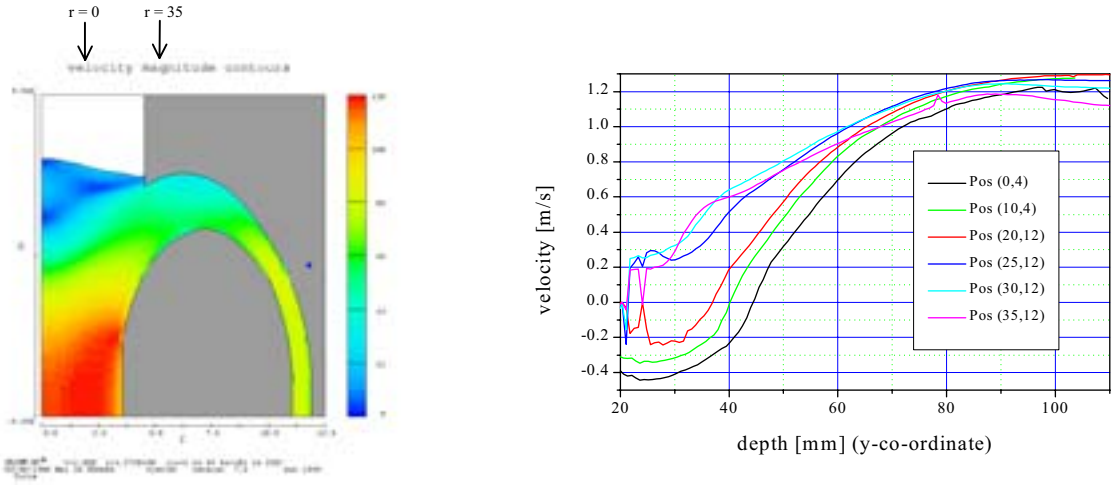

FIG. 13. The velocity profile with FLOW-3D.

The velocity profiles calculated by the codes are comparable to the measured profiles as is illustrated in Fig. 13 for FLOW-3D. A positive velocity in FLOW-3D [cm/s] corresponds to a negative velocity in the measurements [m/s].

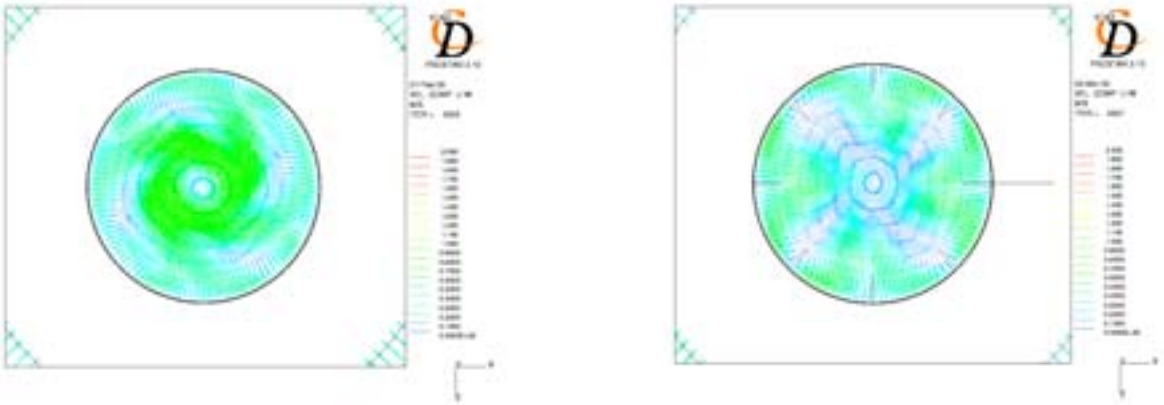

FIG. 14. The efficiency of the anti-swirl device with Star-CD.

As already mentioned in the previous paragraph, Star-CD calculations clearly demonstrated the formation of the swirl in the feeder section and the effectiveness of the anti-swirl device. Figure 14 pictures the reduction of the azimuthal velocities by one order of magnitude when the anti-swirl device is used.

The same code could also prove numerically the reduction of the residence times through the minimisation of the recirculation zone by plotting these times for different surface levels (see Fig. 15). In the right figure, the surface level is higher and residence times are larger. The red region corresponds to stagnant air.

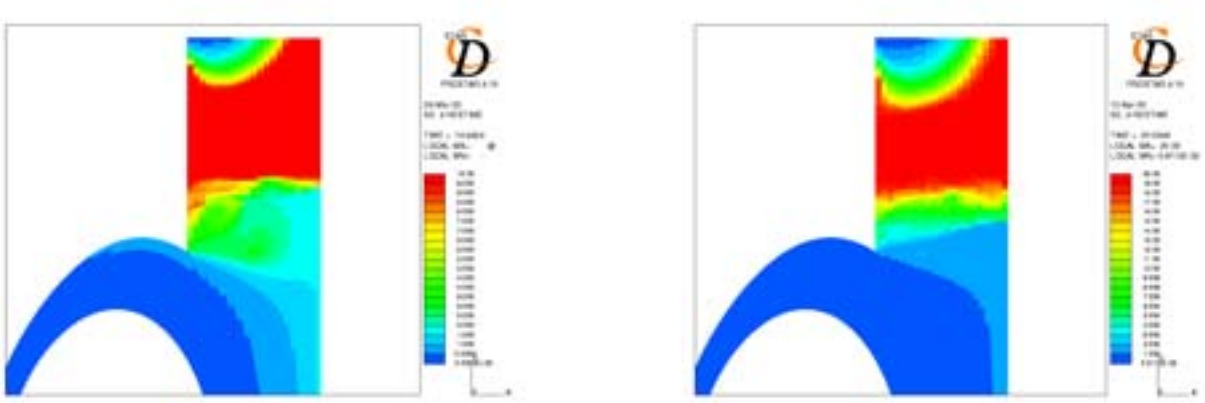

FIG. 15. The residence times for different free surface levels with Star-CD.

Flow-3D gave an indication to the possibility of minimisation of the recirculation zone by putting the free surface far under the top of the feeding nozzle as shown in Fig. 16.

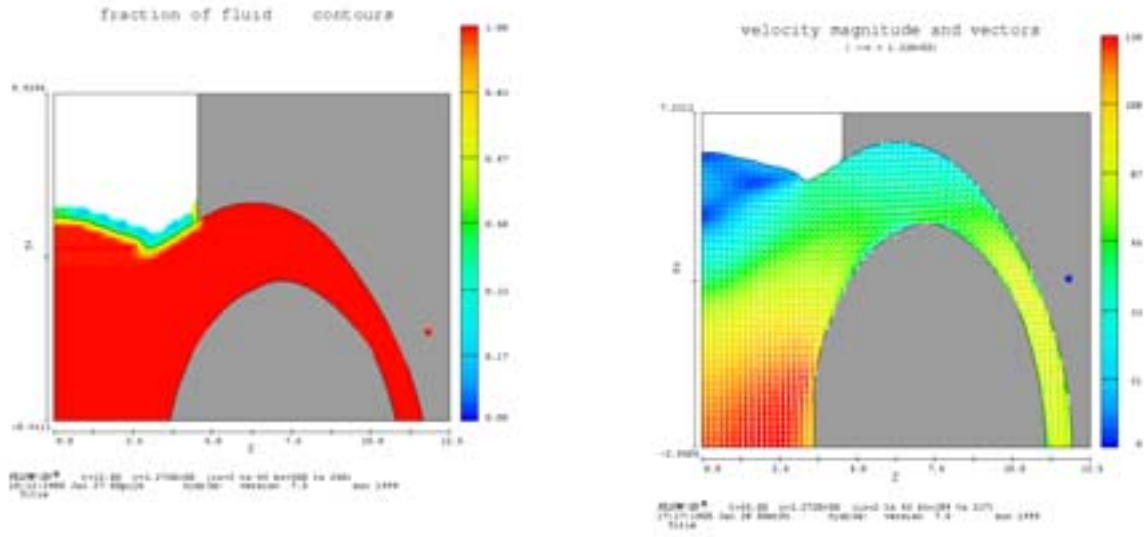

FIG. 16. The minimisation of the recirculation zone with FLOW-3D.

The FLOW-3D and Fluent code indicated the creation of a free surface in the second experimental set-up at UCL similar to the one in the first experiments before this second experiment was started (see Fig. 17). One can see that the numerical diffusion in Fluent is largely reduced in comparison with Fig. 12.

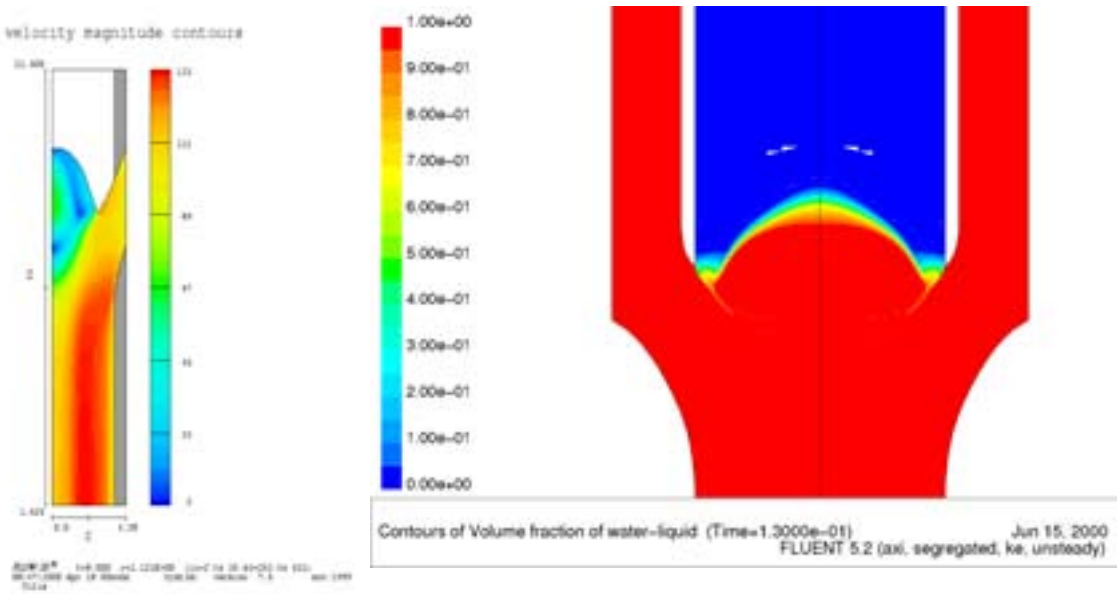

FIG. 17. The free surface and velocity profile in the new configuration with FLOW-3D and fluent.

3.2. Simulation of the temperature profile

Preliminary calculations of the temperature profiles in the presence of the proton beam heating have indicated the presence of hot spots in the recirculation zone. This is illustrated in Fig. 18 for a flow rate of 5 L/s and a beam current of 5 mA. One sees a pronounced hot spot along the centre axis in the recirculation region.

To eliminate this hot spot, a central hole was cut in the proton beam profile resulting in reduced temperatures and a movement of the hot spot from the central axis to the centre of the recirculation cells under the surface as shown in Fig. 18. This has of course a positive influence on the vaporisation at the surface. It is expected that this beam tailoring will be an effective tool for shaping the temperature profile. The results of the calculations will be fed back to the accelerator designers who gave their consent in a first approximation to the required shaping.

Further temperature decrease is expected by increase of flow rate, residence time reduction by recirculation zone minimisation and turbulent heat transfer enhancement. The effects of these measures are currently investigated.

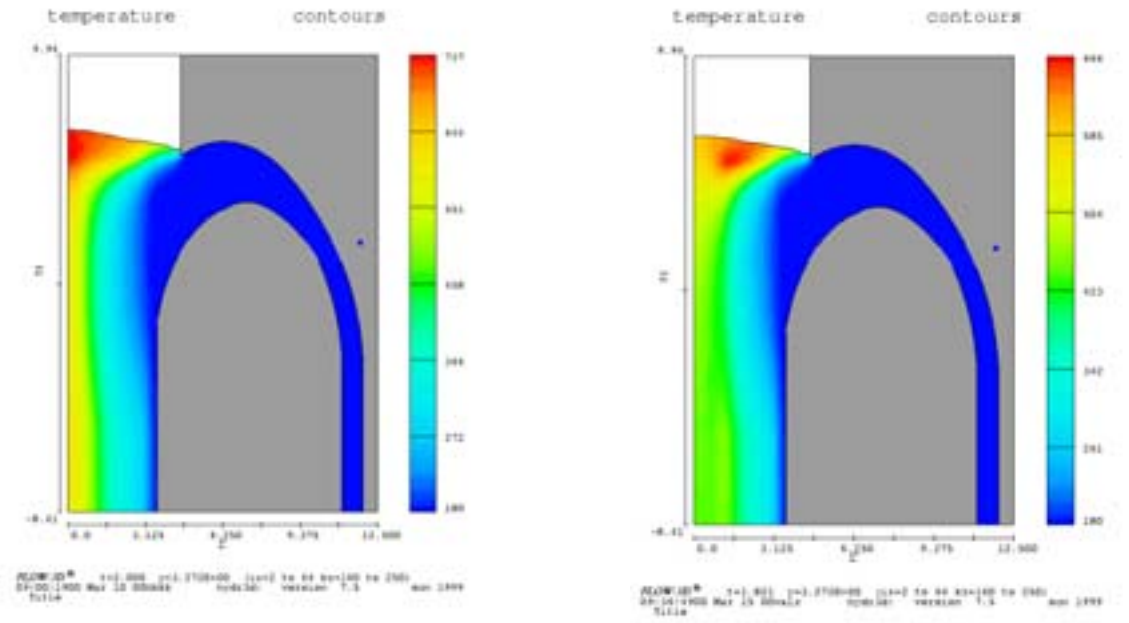

FIG. 18. The temperature profile without and with beam tailoring with FLOW-3D.

4. CONCLUSION

The design of the MYRRHA spallation is very challenging: a Pb-Bi flow pattern with a free surface needs to be established within the geometrical constraints, adequate to remove the heat deposited by the proton beam so that the thermal and vacuum requirements are met. A number of the design activities have been and are being performed to study the flow behaviour and to obtain an adequate design. These design activities include both experiments and CFD calculations and their interaction. In summary, the results of these activities, although not yet conclusive, look encouraging.

REFERENCES

[1] AÏT ABDERRAHIM, H., KUPSCHUS, P., JONGEN, Y., TERNIER, S., MYRRHA, A multipurpose Accelerator Driven System for R&D, first step towards waste transmutation, SCK•CEN, Mol, BLG 841 (2000).

[2] ECKERT, S., WEIER, T., Report about the velocity measurements at the MYRRHA water model, Forzungszentrum Rossendorf, Dresden (2000).

[3] HIRT, C.W., NICHOLLS, B.D., Volume of Fluid (VOF) Method for Dynamical Free Boundaries, J. Comput. Phys. 39 (1981) 201-225.

[4] MALAMBU, E., Neutronic Performance Assessment of the MYRRHA ADS Facility, SCK•CEN, Mol, R3438 (2000).

[5] MALAMBU, E., Sensitivity of the spallation source performance to the FWHM-to diameter ratio, SCK•CEN, Mol (2000).

[6] ROELOFS, F., KOMEN, E.M.J., CFD Analysis of the co-axial MYRRHA Windowless Spallation Target Design, NRG 20289/00.33126/C, Petten, Netherlands (2000).

[7] SEYNHAEVE, J.-M., WINCKELMANS, G., BOLLE, L., JEANMART, H., MYRRHA project: R&D collaboration between SCK•CEN and UCL/TERM: Phase 1 and 2, Université Catholique de Louvain, Louvain-la-Neuve (2000).

[8] SEYNHAEVE, J.-M., MYRRHA project: R&D collaboration between SCK•CEN and UCL/TERM: Phase 3, Université Catholique de Louvain, Louvain-la-Neuve (2000).
[9] VAN TICHELEN, K., BELLEFONTAINE, J.-L., MALAMBU, E., AÏT ABDERRAHIM, H., Proc. 3rd Int. Conf. on Accelerator Driven Transmutation Technologies and Applications (ADTTA'99), 7-11 June 1999, Prague, Czech Republic, Eds: L M. Hron, V. Lelek (NRI Rez plc), M. Mikisek, M. Sinor, J. Uher, J. Zeman (FNSPE CTU, Prague), NRI Rez, Czech Republic (1999), Prague, Czech Republic.

ANALYSIS OF DIFFERENT DESIGN OPTIONS FOR THE BEAM TARGET OF THE ENERGY AMPLIFIER DEMONSTRATION FACILITY

S. BUONO, C. ARAGONESE, L. MACIOCCO, V. MOREAU, L. SORRENTINO
Center for Advanced Studies, Research and Development in (CRS4), Sardinia, Italy

Abstract

A thermal fluid dynamic analysis of different design options of a high intensity proton beam target has been performed for the 80 MW Demonstration Facility of the Energy Amplifier proposed by C. Rubbia (EADF), presently under development in Italy by Ansaldo, CRS4, ENEA and INFN. The present machine is driven by a 600 MeV proton accelerator at a current varying from about 2 to 6 mA during the fuel cycle. Two options have been considered: (i) a "windowless" design, where the free surface of the spallation material (liquid Pb-Bi eutectic) is the interface with the void of the beam transport line, and (ii) a "window" design, where a physical separation is made by means of a 9Cr 1Mo V Nb martensitic steel hemispherical window. Both designs have advantages and drawbacks. The beam window is a delicate element whose lifetime is at present moment difficult to assess, since it is affected by the combined action of liquid metal corrosion, radiation damage (induced by protons and high energy neutrons interactions) and thermal fatigue (induced by stress cycling due to beam trips and beam interruptions). The windowless option is less sensible to radiation damage, but its design is more complex for the presence of a free surface flow and of Pb-Bi vapours in the beam pipe.

1. INTRODUCTION

The spallation target represents one of the main technological problems related not only to the design of the Energy Amplifier Demonstration Facility (EADF) [1, 2] but to all High Power Spallation Sources (HPSS) currently under study or in construction worldwide [3, 4]. In fact, the spallation process produces a large quantity of heat (typically some MW) concentrated in a small volume, and induces an intense radiation damage in the structural materials [5]. For these power densities, the best way to remove efficiently the spallation heat is to use the spallation material also as coolant, namely to use an Heavy Liquid Metal (HLM) for the target cooling. This introduces a further problem related to the erosion and corrosion caused by the HLM flow on the target structures [6, 7]. The HLM chosen for the EADF is a Lead-Bismuth Eutectic (LBE). The motivations of this choice can be found in [2].

Two types of spallation targets have been selected: the "window" target, where the spallation material is separated from the beam pipe by a solid window, and the "windowless" target, where the free surface of the LBE is directly exposed to the vacuum pipe and the proton beam hits directly the target eutectic.

Configurations using a beam window have the additional problem of the beam window cooling and of the radiation damage induced in the beam window material, which is of a slight different nature of the one induced in the other structures. Both options have been proposed and developed for the EADF; considerations about the advantages and disadvantages of these two options are discussed elsewhere [5, 8].

2. WINDOW TARGET DESIGN

This window target configuration is completely independent from the core operating conditions and has many advantages in terms of operation flexibility, giving also the possibility of operating with the sole natural convection. The version considered here is based on the design and optimization work described in [9], carried out through extensive Computational Fluid Dynamics (CFD) simulations and finite-element structural analysis [10, 11] joined with the results of the design of a bayonet heat exchanger [12].

The target, sketched in Fig. 1 is an axisymmetric device consisting of a vertical pipe (beam pipe) closed at the bottom by a hemisphere of variable thickness (window); the beam pipe is enclosed in a vertical coaxial cylinder with a hemispherical bottom (container). The region between the beam pipe and the container is filled with the spallation/cooling fluid. High vacuum is maintained inside the beam pipe.

The coolant flow is guided by a flow guide, placed between the beam pipe and the container, which separates the hot rising flow coming from the spallation region from the cold down-coming flow cooled in the heat exchanger, located at the top of the down-coming duct.

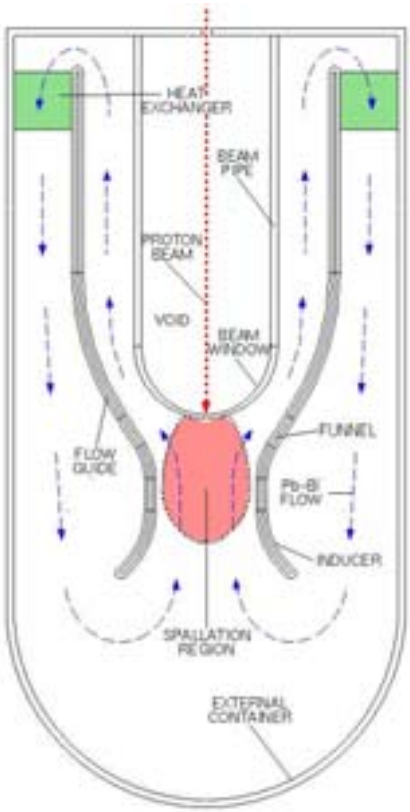

FIG. 1. Spallation target scheme.

In the spallation zone, the flow guide is shaped like a funnel in order to enhance the cooling of the window and the spallation region. The funnel is made of a converging duct, which reverses the flow from the downcomer channel into a narrow pipe where the spallation takes place. The funnel and the rising channel are connected by a divergent.

2.1. Target materials

The structural materials used in the target device must be able to work in severe condition. The main requirements are:

- Capability of sustaining conventional loads such as temperature and mechanical stresses. Such loads can be quite high;
- Compatibility with the radiation environment: materials are exposed to a neutron flux which is at least equal in intensity and harder in spectrum than the one experienced by the closest pins of the EADF core;
- Compatibility with the LBE environment (corrosion, erosion).

This is especially true for the beam window, which is subject to the highest temperatures and stresses, and which has to cope also with the effect of the high-energy proton flux on the material structure. For a detailed discussion on the choice of the material for the EADF beam window see [5, 7].

The type of steel chosen for the beam window and for the other critical structures of the target is a Low-Activation Martensitic Steel (LAMS) and in particular the 9Cr 1Mo V Nb steel [6, 7].

2.2. Computational model

2.2.1. Description

The computational domain has been built using the IDEAS CAD [13]. All CFD simulations have been performed with the Adapco STAR-CD commercial code [14]. All the main target components have been simulated, including all the solid structures relevant from a thermal-fluid-dynamic point of view, whose thermal field is solved coupled with the fluid-dynamic equations.

A computational model for the heat exchanger, able to give a realistic simulation of both thermal exchanges and pressure losses, has been also introduced (see Section 2.2.4). This allows the estimation of the efficiency of the natural convection circulation, which is the only pumping force for the target. Moreover, the heat exchanger model can simulate the dynamics of the coupling between the primary (LBE) and the secondary (oil) cooling circuit, allowing the detailed simulation of transient and accidental conditions.

2.2.2. Computational mesh

Due to the axial symmetry, only 1/72 of the target has been considered in the simulation, equivalent to an angle of 5 degrees out of 360. The IDEAS mesh generator was used to create a parametric mixed structured-unstructured mesh. An unstructured mesh is used in zones with irregular geometry and whose shape was optimized, like the funnel zone, shown in Fig. 2. The fluid regions near the walls are meshed with structured grids, easier to handle and more suitable for the application of the turbulent near-wall algorithms.

Structured grids are also used for the meshing of the solids. In order to make possible the use of meshes with different coarseness in the rising and down-coming sides, a non-matching mesh approach is adopted for the flow guide. The total number of cells is about 25 000. The discretisation is very accurate in the funnel zone, especially close to the window stagnation point. Cells with high aspect ratio are used in the rising and downcoming duct, where the flow is supposed to be regular.

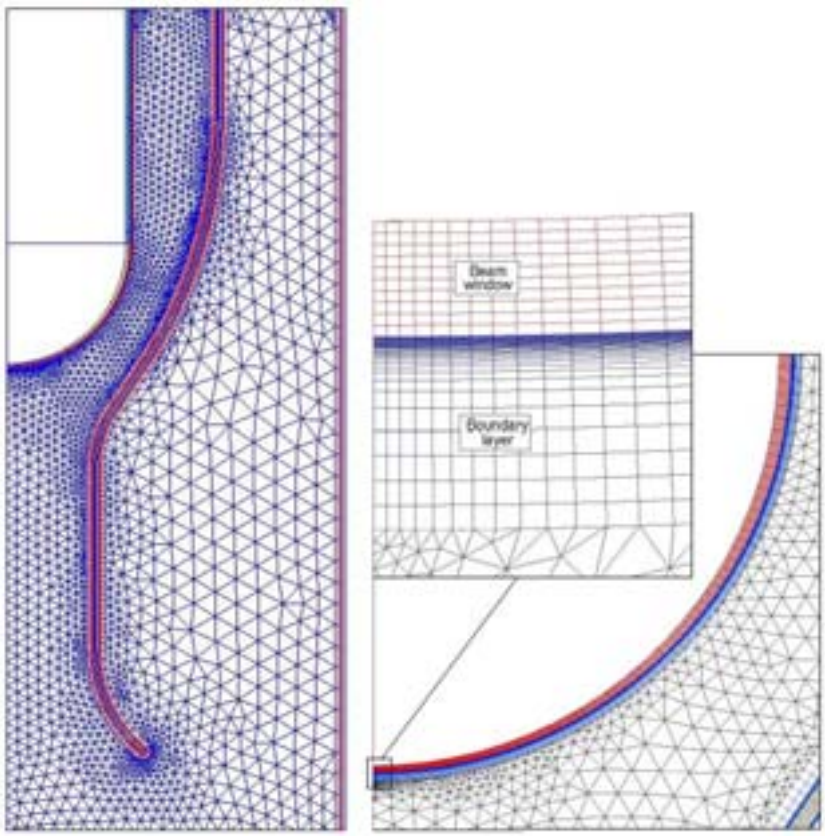

FIG. 2. The unstructured mesh in the funnel zone and the structured mesh in the window and in the near-wall region.

2.2.3. Spallation heat source

The proton beam of the EADF is a circular spot of 75 mm radius, with energy of 600 MeV and with the proton intensity distributed as a paraboloid (see Ref. [5] for further details). The interactions of the proton beam with the window and with the coolant have been simulated with the FLUKA code [15]. The result of this calculation, a Montecarlo simulation using 1 000 000 protons, is the volumetric heat source distribution shown in Fig. 3.

The heat source distribution in the window is assigned through an analytical curve as a function of the distance from the beam axis. The curves for the 9Cr 1Mo V Nb steel window are given below and reported in Fig. 4.

For $0 < r < 7.5$ cm $\quad q = -1.020457\, r^2 + 4.124325\, r + 27.42338 \quad [W/cm^3/mA]$

For $7.5 < r < 10$ cm $\quad q = -0.3341885\, r + 3.983076 \quad [W/cm^3/mA]$

where

r is the distance from the beam axis (in cm). The spallation heat distribution described above is assigned as a heat source term in the CFD simulation.

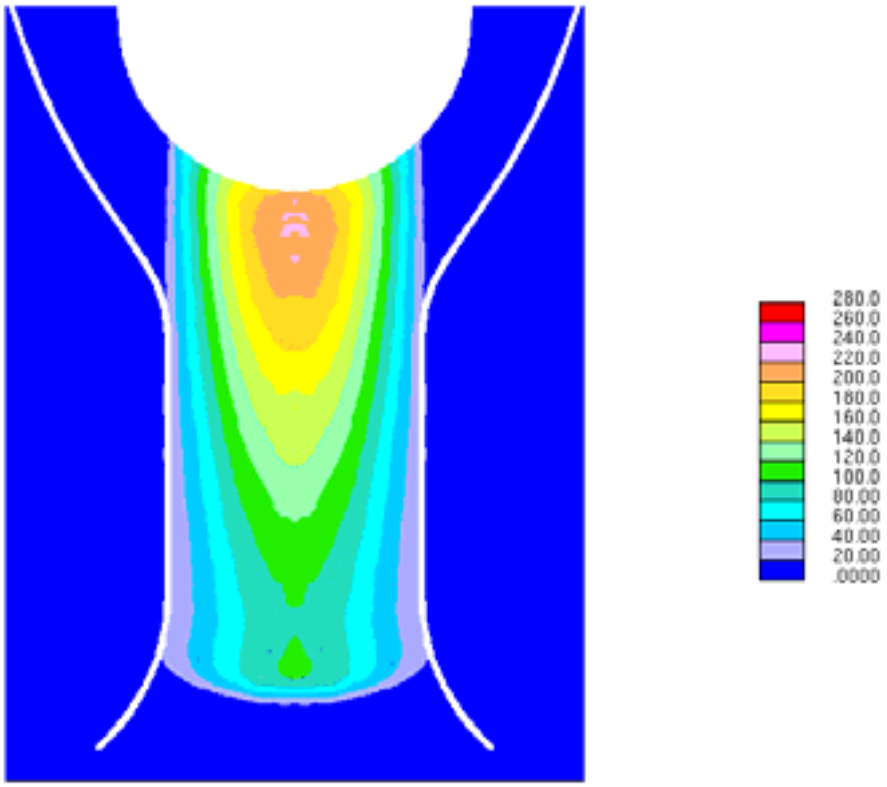

FIG. 3. FLUKA heat source distribution in the Pb-Bi eutectic [W/cm^3/mA].

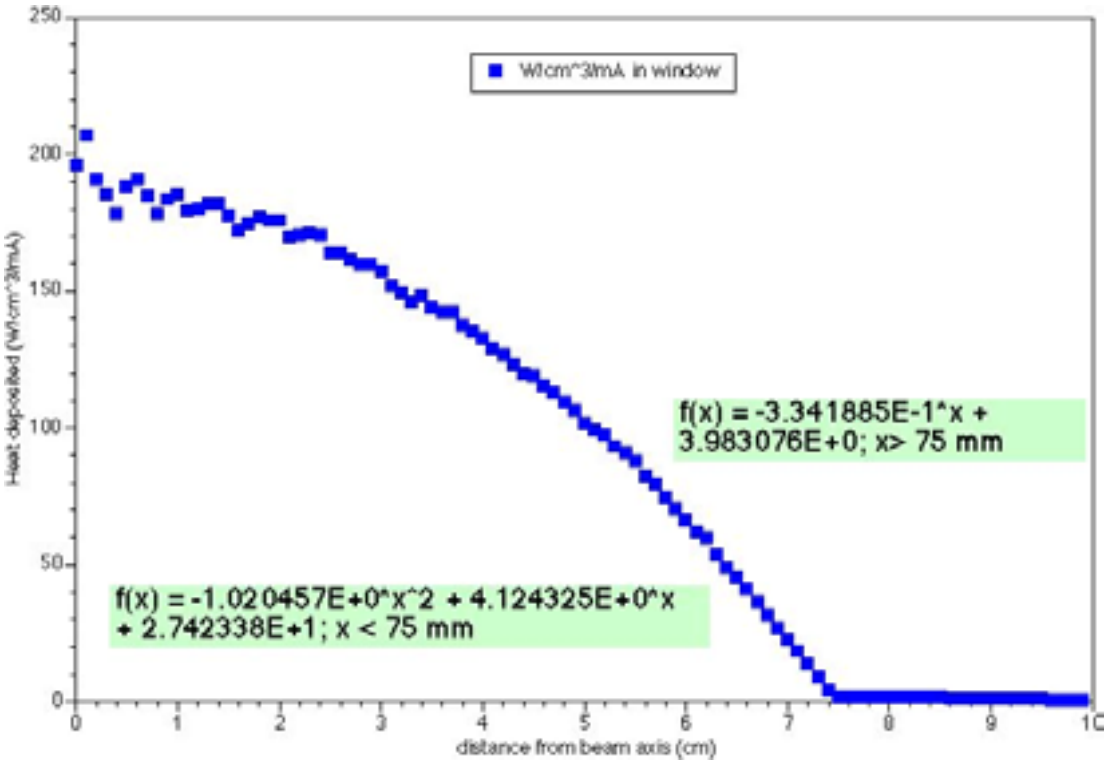

FIG. 4. FLUKA heat source distribution in the beam window.

2.2.4. Heat exchanger

A Bayonet Heat Exchanger (BHE) for the target has been designed [12], using diathermic oil as secondary coolant [2]. The target BHE consists of a bundle of tubes immersed in the upper part of the downcomer channel. The scheme of a single tube-element is reported in Fig. 5.

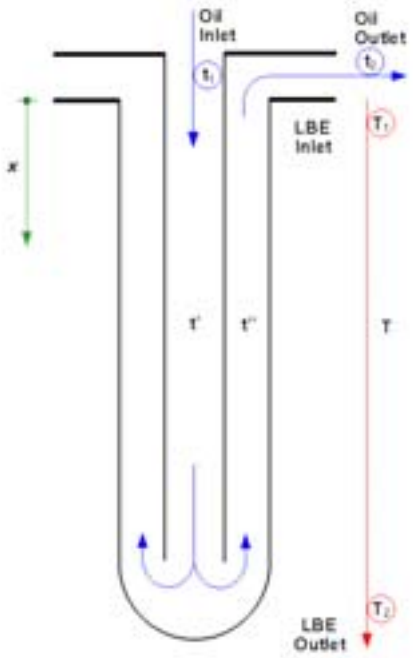

FIG. 5. Scheme of a single tube of the bayonet heat exchanger.

The main design requirements are to keep both the tubes length and the pressure drop as low as possible, in order to allow the use of natural circulation for the cooling of the target in standard operating conditions. The BHE was designed to remove a power of 2.6 MW, corresponding to the spallation heat generated in the target coolant at the maximum power, with a beam current of 6 mA The main characteristics of the LBE are listed in Table 1.

TABLE 1. THE MAIN CHARACTERISTICS

Internal diameter of the target container (mm)	592
Tube length (m)	1.5
Bundle pitch (mm)	19.8
Tubes external diameter (mm)	15.88

A model of the heat exchanger has been implemented in the target CFD model as shown in Fig. 6, where the top part of the target computational domain is illustrated. Two image-meshes of the heat exchanger domain (HE1, colored in green) have been created: one for the internal part of the tubes of the BHE, where the down-coming oil flows (HE3, colored in red), and one for the annular ducts, where the rising oil flows (HE2, colored in violet).

It is assumed that each cell of the HE domains contains a number of BHE tubes such as to be considered as a little heat exchanger. This makes possible to apply cell-by-cell, in the Pb-Bi side (HE1), the empirical relations for the heat exchange coefficients and pressure drops valid for bundle of tubes.

Heat exchanges take place between HE1 and HE2, and between HE2 and HE3. The heat exchange coefficients are calculated cell-by-cell for each HE domain through empirical relationships based on the local flow characteristics. Global heat exchange coefficients between the corresponding cells of the HE domains are calculated, taking into account the contributions of convection in the two sides of the interface and conduction across the interface wall. Then, the heat transferred is calculated on the basis of the temperature difference between the corresponding cells, and applied to each cell as a source/sink term. Pressure losses are also calculated for each cell of the three domains, and applied as momentum source terms. The relations used for heat transfer and pressure drops calculation are listed in Table 2.

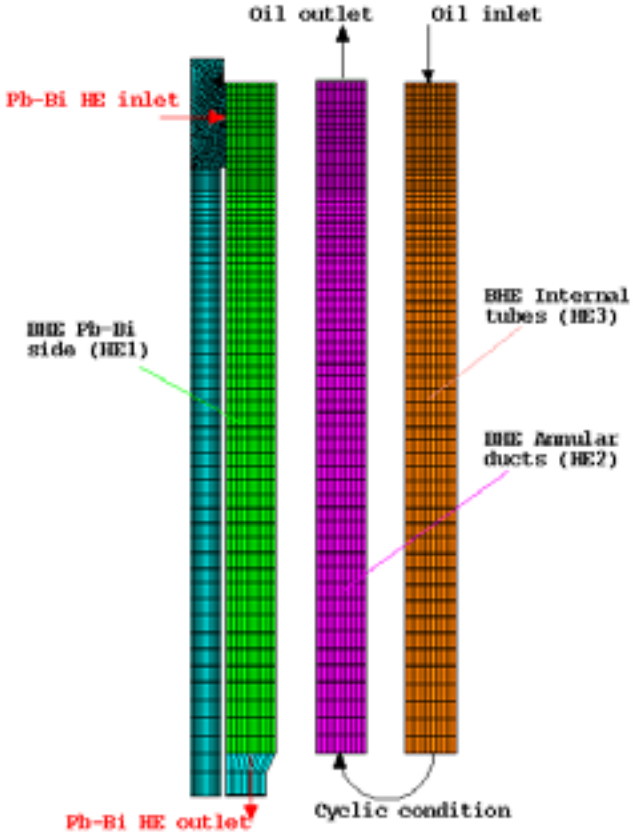

FIG. 6. CFD model of the heat exchanger.

TABLE 2. EMPIRICAL RELATIONSHIPS FOR HEAT EXCHANGE COEFFICIENTS AND PRESSURE DROPS IN THE THREE SIDES OF THE BAYONET HEAT EXCHANGER

Quantity	Relationship	Ref. [16]
Nusselt oil internal pipe	$0.023\ Re^{0.8}Pr^{0.333}$	Sieder-Tade eqs. for tubes
Nusselt oil annuli	$0.02\ Re^{0.8}Pr^{0.333}(d_e/D_i)^{0.53}$	Monrad and Pelton equation for annuli
Nusselt LBE longitudinal	$7+ 0.025\ Re^{0.8}Pr^{0.8}$	Martinelli equation for liquid metals
Nusselt LBE transversal	$4.03+0.0228\ (Re_{max}Pr)^{0.67}$	Brookhaven Laboratory equation for liquid metals
Friction factor oil internal pipe	$0.079\ Re^{-0.25}$	
Friction factor annuli	$0.087\ Re^{-0.25}$	
Friction factor LBE longitudinal	$0.079\ Re^{-0.25}$	
Friction factor LBE transversal	$0.0675+0.03186/R_f)Re^{-0.16}$	$R_f = [S_T-D_e)/D_e]^{1.08}$

2.2.5. Numerical schemes and turbulence model

The SIMPLE integration algorithm was used for all the simulations. The QUICK third order convective scheme was used for the spatial discretisation of momentum and energy equations, while an Upwind first order scheme was used for the k-ε equations. References of these algorithms can be found [13, 14].

Turbulence were simulated through the Chen k-ε model, coupled with a Norris & Reynolds two-layer model for the simulation of low-Reynolds number near-wall effects [14].

2.2.6. Boundary conditions

The boundary conditions of the system are the following:

- Thermal conduction with zero resistance for all fluid-solid interfaces;
- Adiabatic wall for the external side of the container;
- Adiabatic wall for the internal side of the beam pipe;
- Cyclic boundaries on the lateral surfaces of the sector.

Concerning the oil side of the BHE, the following conditions were applied:

- Inlet (imposed temperature and mass flow rate);
- Periodicity condition between the outlet of the down-coming ducts (HE3) and the inlet of the rising ducts (HE2). This means that the HE3 outlet profile is simply turned of 180◦ and applied to the HE2 inlet.
- Outlet (conservation of the mass flow rate);
- Cyclic boundaries on the lateral surfaces of the sector.

2.3. Results

An optimized configuration has been found following the requirements of having low window temperatures and thermal stresses, while keeping the LBE temperature in the downcomer channel as high as possible in order to avoid too strong temperature difference between the target container and the LBE in the EADF core.

TABLE 3. GLOBAL RESULTS

Total spallation heat generated within the target (kW)	2648
Spallation heat generated within the window (kW)	16.4
LBE mass flow rate (kg/s)	227
Mean LBE temp. in the riser (◦C)	325
Mean LBE temp. in the downcomer (◦C)	250
Maximum LBE temperature (◦C)	483
Maximum window temperature (◦C)	502
Max. radial temp. diff. across the window (◦C)	24
Mean LBE temp. in the HE inlet (◦C)	320
Mean LBE temp. in the HE outlet (◦C)	238
Oil temp. in the HE outlet (◦C)	246
Mean LBE velocity in the riser (m/s)	0.372
Mean LBE velocity in the downcomer (m/s)	0.159
Maximum LBE velocity (in the funnel) (m/s)	1.52

This result has been achieved with a window thickness varying from 3 to 1 mm, and with an inlet temperature of the secondary coolant (diathermic oil) of 200°C and a mass flow rate of 31.2 kg/s. The most relevant parameters of the simulation are reported in Table 3.

The complete profile of window temperatures is shown in Fig. 7. Velocity and temperature fields in the spallation region are Figs 8 and 9, respectively.

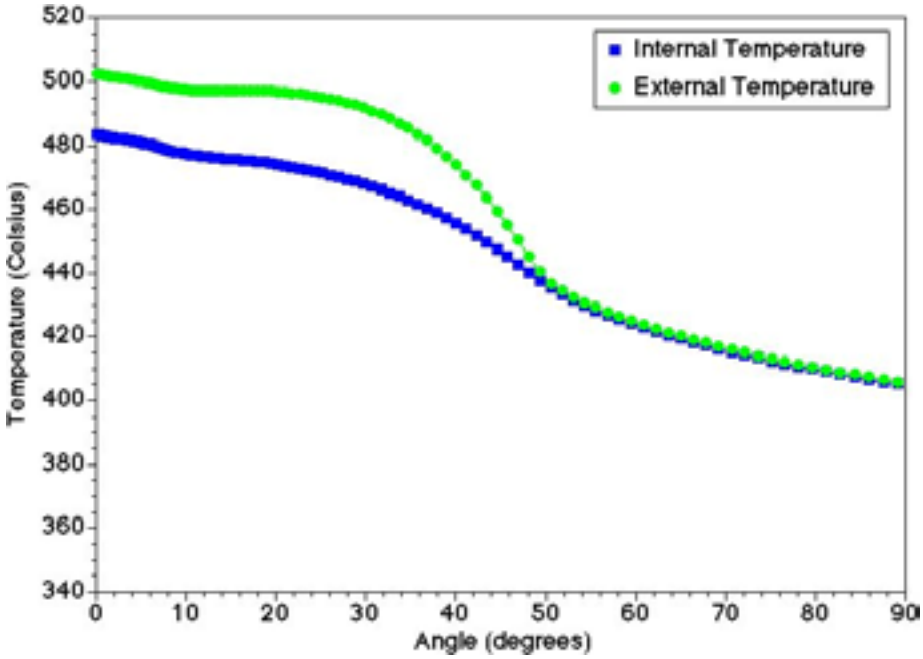

FIG. 7. Beam window temperature profile in steady state conditions.

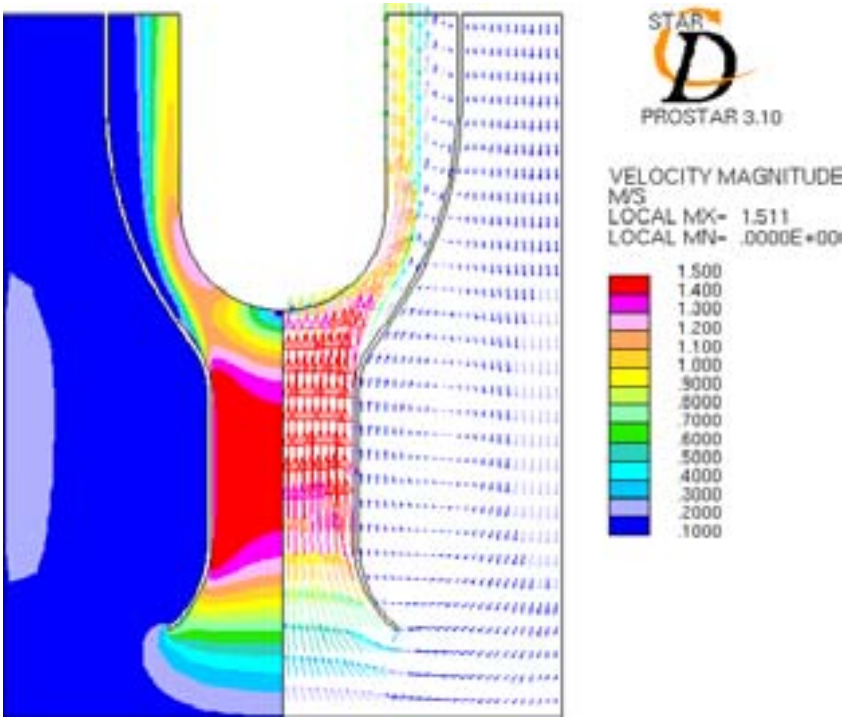

FIG. 8. Velocity field in the spallation zone of the window target.

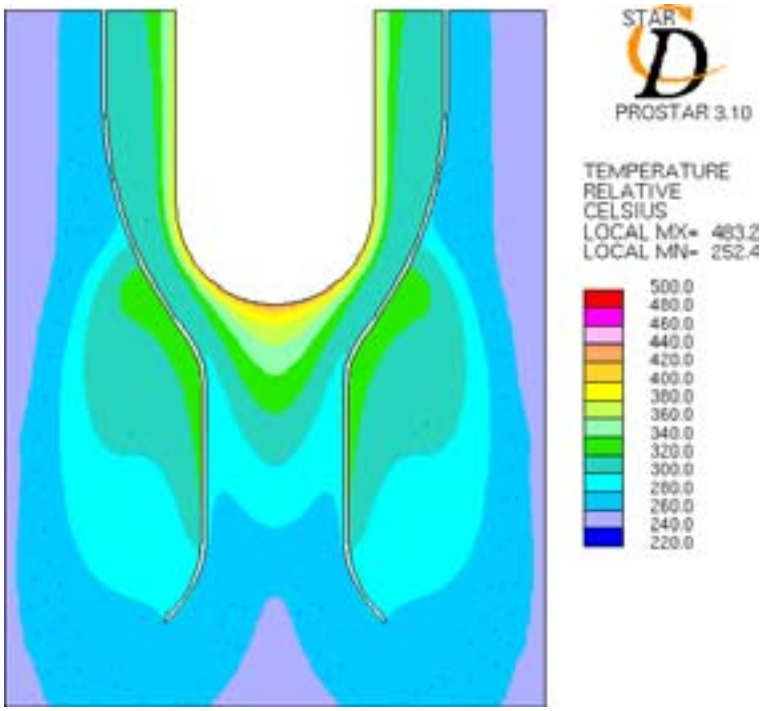

FIG. 9. LBE temperature distribution in the spallation zone of the window target.

2.4. Flow inverter

Recently, a further variant of this design has been proposed, with the insertion of a flow-inverter [18], which deviates the rising flow to the external target flow-section and the down-coming flow to the internal one. A sketch of this principle is shown in Fig. 10.

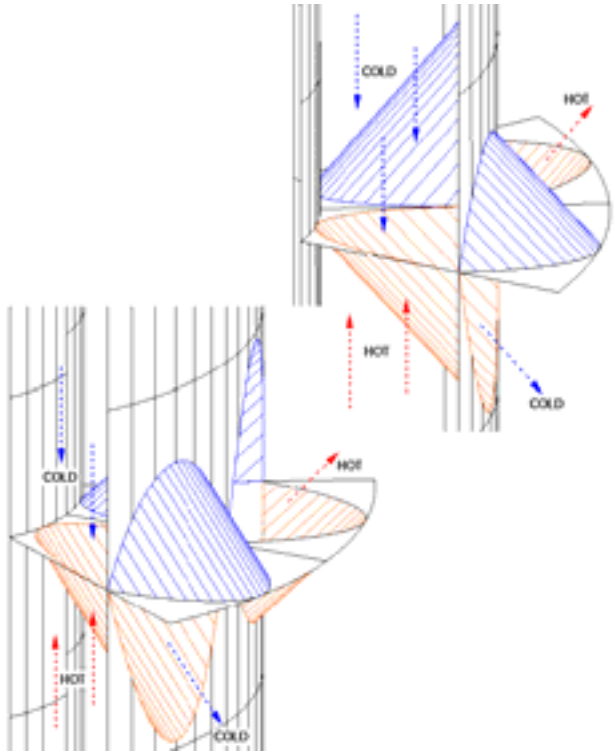

FIG. 10. Two different views of the flow inverter principle.

This solution gives the possibility to use the heat transferred from the EADF primary LBE across the target container for the natural circulation of the target coolant, which is guaranteed even in beam-shutdown conditions. This allows the operation of the target in start-up and stand-by conditions using only natural convection.

3. WINDOWLESS TARGET DESIGN

The second option for the target is a "windowless" configuration where the free surface of the LBE has a direct interface with the vacuum pipe, so that the proton beam from the accelerator hits directly the target eutectic. In the windowless target configuration, the structural materials are not exposed to the direct proton irradiation, so reducing the problems of material damage. However, this configuration requires a careful control of the LBE free surface level, temperature and shape.

A research activity on this subject is going on in the framework of the Belgian Myrrha project [19], devoted to the development of a windowless axial-symmetrical target. Since the Italian ADS group and the Myrrha project are collaborating on this design activity, it was decided to investigate the feasibility of an alternative windowless design with a non axial-symmetric flow configuration. The principle of this design is shown in Fig. 11. The liquid eutectic flows in a direction perpendicular to the beam in a horizontal channel, which has to be sufficiently deep to contain the entire beam. In the case of a 600 MeV beam 30 cm are enough to contain all the heat produced. In the Figure the LBE rises from the left channel and comes down through the channel on the right. Some baffles are added in this case to avoid major recirculations in the interaction zone, which could create hot spots.

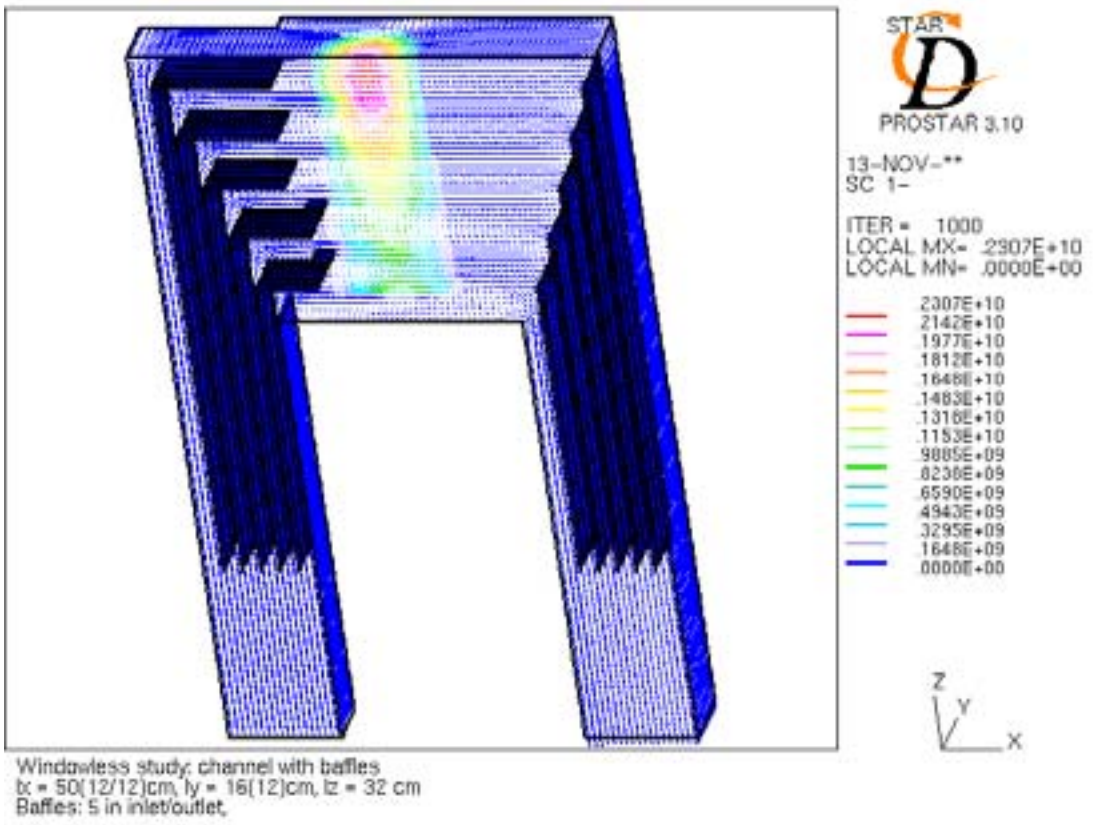

FIG. 11. Non axial-symmetric windowless scheme. The beam energy deposit in GeV/cm^{3}p is shown.

An example of temperature distribution in such configuration is shown in Fig. 12. One can observe that temperatures are acceptable, especially near the free surface, where temperature values have to be kept as low as possible to limit the eutectic evaporation. Nevertheless, the flow can still be strongly optimized to limit pressure losses and flow recirculations, and to shape the velocity distribution in the interaction zone in order to obtain a more uniform temperature distribution.

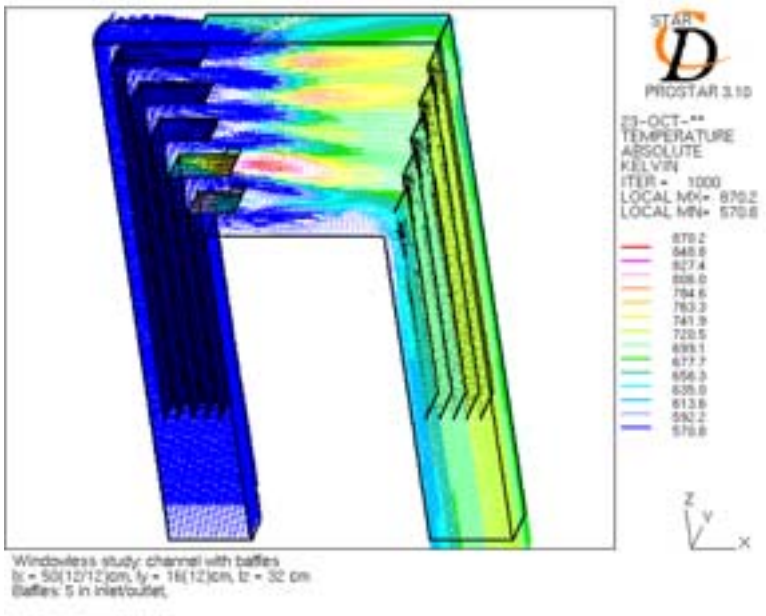

FIG. 12. Temperature distribution in the windowless configuration.

A heavy work is undergoing (see Ref. [20]) to optimize this solution in the constraints of the EADF design.

4. CONCLUSIONS

The cooling of the EADF target can be achieved in a "window" configuration through the natural circulation of the LBE. An optimized configuration has been found following the requirements of having low window temperatures and thermal stresses, while keeping the LBE temperature in the downcomer channel as high as possible in order to avoid too strong temperature difference between the target container and the LBE in the EADF core.

This result has been achieved with a window thickness varying from 3 to 1 mm, and with an inlet temperature of the secondary coolant (diathermic oil) of 200◦C. In this configuration, the LBE mass flow-rate is 227 kg/s, corresponding to a maximum LBE temperature of 483◦C and a maximum window temperature of 502◦C. The maximum LBE velocity is 1.5 m/s. The LBE thermal cycle in the heat exchanger goes from 320 to 238◦C, with the oil being heated from 200 to 246◦C.

The introduction of a flow inverter in this configuration gives the possibility to use the heat transferred from the EADF primary LBE across the target container for the natural circulation of the target coolant, which is guaranteed even in beam-shutdown conditions. This allows the operation of the target in start-up and stand-by conditions using only natural convection.

A concept of a non axial-symmetric windowless target has been introduced, giving promising results. Work is undergoing to optimize this solution in the constraints of the EADF design.

REFERENCES

[1] RUBBIA, C., et al., Conceptual Design for Fast Neutron Operated High Power Energy Amplifier, CERN Report, CERN/AT/95-44 (ET) Geneva (1995).

[2] Energy Amplifier Demonstration Facility Reference Configuration, Summary Report, Ansaldo Nucleare, EA B0.00 1 200 (1999).

[3] PAUL SCHERRER INSTITURE, Proc. of the Meetings ICANS-XIII and ESS-PM4, BAUER, G., BERCHER, R., (Eds), PSI Proceedings 95-02, Villigen (1995).

[4] Proceedings of the International Workshop on the Technology and Thermal Hydraulics of Heavy Liquid Metals (IWSMT4), 25-28 March 1996, Schruns, Austria, compiled by APPLETON, B.R., BAUER, G.S. (1996).

[5] BELLUCCI, V., BUONO, S., FOTIA, G., MACIOCCO, L., MOREAU, V., MULAS, M., SIDDI, G., SORRENTINO, L., Requirements of the beam target of the Energy Amplifier prototype, CRS4-TECH-REP 98/38.

[6] DAI, Y., Martensitic/Ferritic Steels as Container Material for Liquid Mercury Target of ESS, Proc. International Workshop on the Technology and Thermal Hydraulic of Heavy Liquid Metals (IWSMT4), 25-28 March 1996, Schruns, Austria, compiled by APPLETON, B.R., BAUER, G.S. (1996).

[7] BENAMATI, G., BUTTOL, P., Material Selection for reactor components of an ADS Demonstrator, ENEA Report HS-A-R-002 (1998).

[8] Energy Amplifier Project web page, http://www.crs4.it/~cfdea, CRS4, Centre for Advanced Studies, Research and Development in Sardinia, Cagliari, Italy, 1993-2000.

[9] BELLUCCI, V., BUONO, S., FOTIA, G., MACIOCCO, L., MOREAU, V., MULAS, M., SIDDI, G., SORRENTINO, L., Preliminary sizing of the window-type target of the Energy Amplifier, CRS4-TECH-REP 98/36.

[10] BELLUCCI, V., BUONO, S., FOTIA, G., MACIOCCO, L., MOREAU, V., MULAS, M., SIDDI, G., SORRENTINO, L., Thermo Mechanical Stresses on the Beam Window, Proc. NEA Workshop on Utilization and Reliability of High Power Accelerators, 13-15 October 1998, Mito, Japan, NEA, ISBN: 92-64-17068-5 (1999).

[11] FOTIA, G., ARAGONESE, C., BELLUCCI, V., BUONO, S., MACIOCCO, L., MOREAU, V., SIDDI, G., SORRENTINO, L., Structural Response of the EADF target Beam Window to Beam Interruptions: Transient Thermo-Mechanical Computations, paper presented in Second Workshop on Utilization and Reliability of High Power Accelerators, 22-24 November 1999, Aix-en-Provence, France, NEA, ISBN: 92-64-18749-9 (2001).

[12] ARAGONESE, C., BUONO, S., FOTIA, G., MACIOCCO, L., MOREAU, V., SORRENTINO, L., A heat exchanger design for the separated window target of the EADF, CRS4-TECH-REP 00/08.

[13] IDEAS web page: http://www.scdc.com/ideas/index.shtml

[14] Star-CD, Version 3.10 manual, Computational Dynamics, London (1999).

[15] FERRARI, A., SALA, P.R., Intermediate and High Energy Models in FLUKA: Improvements, Benchmarks and Applications, invited talk in Proc. Int. Conf. on Nuclear Data for Science and Technology, NDST-97, International Centre for Theoretical Physics, Miramare-Trieste, Italy, 19-24 May 1997, published by Italian Physical Society, G. Reffo, A. Ventura and C. Grandi (Eds), ISBN: 88-7794-114-6, Bologna, Part I (1997) 247-253.

[16] PERRY, R.H., GREEN, D.W., (Eds.), Perry's Chemical Engineers' Handbook, sixth edition, Mc Graw Hill (1984).

[17] BELLUCCI, V., BUONO, S., FOTIA, G., MACIOCCO, L., MOREAU, V., MULAS, M., SIDDI, G., SORRENTINO, L., Integration of numerical tools for the combined thermal-hydraulics and structural analysis of Energy Amplifier components, CRS4-TECH-REP 99/14.
[18] SORRENTINO, L., MACIOCCO, L., MOREAU, V., A proposal for the flow inverter of the EADF Beam Target, CRS4/EA/ Internal Note 00-03 (2000).
[19] http://www.sckcen.be/research/reactorsafety/fuel/myrrha/myrrha_home.html
[20] BUONO, S., MACIOCCO, L., MOREAU, V., SORRENTINO, L., A windowless design for the target of the EADF, CRS4-TECH-REP 01/44.

EXPERIMENTAL AND NUMERICAL STUDIES ON THERMAL-HYDRAULICS OF SPALLATION TARGETS

X. CHENG, C. PETTAN, J.U. KNEBEL, T. SCHULENBERG, G. HEUSENER
Forschungszentrum Karlsruhe, Karlsruhe, Germany

Abstract

Transmutation of actinides and other high level nuclear waste offers the possibility of increasing the public acceptance for nuclear energy. In this aspect accelerator driven systems (ADS) are promised to play an important role [1, 2]. The target where neutrons are generated by a proton beam is one of the most important units of an ADS. To achieve high thermal-hydraulic performance, different target concepts have been proposed in the past. One of the most favorable concepts is the liquid-metal target. In a liquid metal target the beam window is exposed to a high radiation and thermal flux. The coolability of the beam window is considered as one of the most critical items in designing a spallation target. It has been agreed that detailed thermal-hydraulic R&D works are needed for designing liquid metal targets. To gather practical experience on a liquid metal target, two pilot liquid lead-bismuth targets of 1 MW are now under design or under construction. The first one was designed and fabricated at the Institute of Physics and Power Engineering in the framework of the ISTC 559 project. This target will be tested at the LANSCE accelerator of Los Alamos National Laboratory. The second target will be designed and fabricated in Western Europe and be tested at the SINQ accelerator at Paul Scherrer Institut. The Forschungszentrum Karlsruhe (FZK) is actively involved in both projects, especially in thermal-hydraulic design of both targets. A three steps strategy is being proposed for the research activities accompanying the target design, i.e.:

- Numerical analysis with the aim to provide the first knowledge about the thermal-hydraulic behavior in a spallation target and to achieve a preliminary design of the target;
- Model experiments to achieve basic information for the target design, to provide experimental data base for model development and code validation;
- Prototypic experiments in Pb-Bi for the final design of a spallation target.

A comprehensive experimental and numerical research program is underway at FZK. Table 1 summarizes the research activities undertaken at FZK relating to the target thermal-hydraulics. At present, three different target systems are taken into consideration, i.e. two pilot targets and an ADS-target system that can be used in an ADS-demonstrator or in the ADS reactor of the three-beam concept [7]. Test facilities suitable for different fluids, e.g. water and Pb-Bi, have been set up or are being under construction. Computer codes of different purposes, e.g. 1-D system analysis or 3-D CFD codes, have been used for the overall layout of the target system and for the detailed assessment of local thermal-hydraulic phenomena.

The results obtained up to now confirm the necessity of the model experiment and the suitability of the HYTAS test facility for studying the hydraulic behavior of spallation targets. Numerical simulation with both the 1-D system code and the CFD code has provided useful information for design of the targets. The experimental studies at both the HYTAS test facility and in KALLA will provide important test data for the final target design, for model improvement and for validation of computer codes.

In the present paper, an overview is given about the research programme at FZK relating to the target thermal-hydraulics. Main results obtained up to now are presented and discussed.

1. INTRODUCTION

Plutonium and other minor actinides are known to be responsible for long decay times up to a million of years of radioactive waste of nuclear power plants. Following a proposal by Rubbia [2], these nuclides can be transmuted to shorter living fission products with an accelerator driven system (ADS). One of the main components in an ADS is the spallation target where a large number of fast neutrons are produced. Heavy liquid metal, e.g. lead or lead-bismuth eutectic, is preferred to be used as target material and as coolant as well, due to its high production rate of neutrons and its efficient heat removal properties [1].

The beam window of a liquid metal target is exposed to a high radiation and thermal flux. Thus, the coolability of the beam window is considered as one of the most critical items in designing a spallation target. To gather practical experience relating to liquid metal targets, two pilot targets are being designed or constructed. The first one was designed and fabricated in Russia in the framework of the ISTC 559 project [3]. The second target (MEGAPIE target) will be designed and fabricated in Western Europe [4, 5]. Forschungszentrum Karlsruhe is actively involved in both projects, especially in thermal-hydraulic design of both targets.

A three-step strategy is being proposed for the research activities accompanying the target design. In the *first step*, numerical analysis is carried out with available CFD codes, to provide the first knowledge about the thermal-hydraulic behaviour in a spallation target. Based on these numerical studies, a preliminary design of a target can be achieved.

Due to the deficiency in the modeling of turbulent flow and heat transfer under the prototypic conditions of a spallation target, experimental studies are inevitable. They provide information for the target design and form an experimental database for model development and code validation. At the present stage where large deficiencies in practical experience exist, experimental investigations with a model fluid, e.g., water, are recommended first. Such a model experiment enables a systematical study into the physical phenomena involved and allows a much more sophisticated measurement than in the case with the original fluid. Therefore, before performing experiments in Pb-Bi, model experiments with water are considered as the *second step*. For this purpose the HYTAS test facility has been set up with water as the working fluid. Experimental studies are being performed for both the ISCT-559 target and the MEGAPIE target. If the buoyancy effects are negligible, the hydraulic results obtained in the model experiment can well be transferred to the prototype.

On the other hand, it is well known that the results obtained in a water experiment can not be transferred directly to the prototype, as long as heat transfer is concerned. Therefore, as the *third step,* experimental studies in liquid metal should be carried out for the final design of a spallation target. The thermal-hydraulic loop of the KALLA laboratory at Forschungszentrum Karlsurhe, which is now under construction, can be used for this purpose.

The present paper gives an overview about the research programme at Forschungszentrum Karlsruhe relating to the target thermal-hydraulics. Examples of results obtained up to now are presented and discussed.

2. RESEARCH ACTIVITIES

Table 1 summarizes the research activities undertaken at Forschungszentrum Karlsruhe relating to the target thermal-hydraulics. At present, three different target systems are taken into consideration. Both pilot targets, i.e., the ISTC-target and the MEGAPIE target, will be put into test in the accelerator LANSCE of Los Alamos National Laboratory (LANL) and in the accelerator SINQ of Paul Scherrer Instutut (PSI) in Switzerland, respectively [3, 5]. The third target system, indicated as ADS-target in Table 1, can be used in an ADS-demonstrator or in the ADS reactor of the three-beam concept of Forschungszentrum Karlsruhe [6, 7]. All the research activities are being performed under a tight international cooperation.

TABLE 1. RESEARCH ACTIVITIES AT FZK/IKET

Target systems	Research activities			Int. partners
	Numerical codes	Experimental facilities		
		HYTAS	KALLA	
ISTC	FIDAP, CFX	completed	---	Europe, Russia, USA
MEGAPIE	CFX, HETRAF	running	planned	Europe, Japan, Korea
ADS-target	FIDAP, CFX, HETRAF	running at CEA	planned	Europe (Benchmark working group)

2.1. ISTC target

A detailed description of the target has been given in Ref. [3]. The proton energy and the beam power is 0.8 GeV and 1.0 MW, respectively. The diameter of the beam is 6.5 cm. Liquid Pb-Bi is used as target and as coolant. Design of the active part is one of the main tasks in the design phase. Different designs have been proposed. Figures 1 and 2 show schematically two examples. The first one (Fig. 1) has a semi-spherical window surface, with a diameter of 110 mm. The active part consists of two coaxial cylinders with inner diameters of 130 and 185 mm, respectively. The coolant flows into the annular gap between the cylinders, makes a U-turn at the top, cools the window surface, and then exits the active part via the central cylinder. In order to reduce the flow stagnation zone near the window center, a perforated plate, made of steel with distributed holes, is mounted beneath the window. This way, coolant flow and heat transfer near the window center will significantly be enhanced.

The second design (Fig. 2), proposed by the Institute of Physics and Power Engineering (IPPE) in Russia, is similar to the first one and consists of two coaxial cylinders with the same diameter as in the first proposal. The beam window is a surface of two different curvature radii, i.e., 80 mm for the center part and 37 mm for the outer part. The main advantage of this proposal is the short height of the beam window and the U-turn part. The location of the perforated plate, the size and the distribution of holes on the plate should be optimized referring to thermal-hydraulic performance.

The target material is liquid lead-bismuth eutectic which also serves as coolant. It cools down the beam window and removes the heat deposited in the active part of the target. The temperature of the liquid metal coolant, entering the active part of the target, is 220°C. The design value of the flow rate is 15 m^3/h. In average, the coolant heats up to about 315°C at the outlet of the target active part. To keep the coolant temperature as low as possible before it cools the beam window, the coolant should enter into the target active part through the region far away from the beam axis.

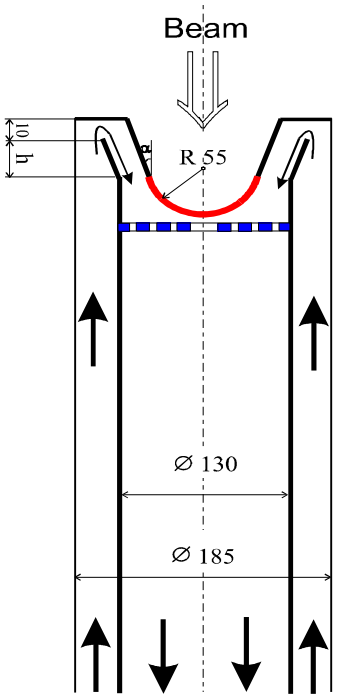

FIG. 1. ISTC target – 1st design proposal.

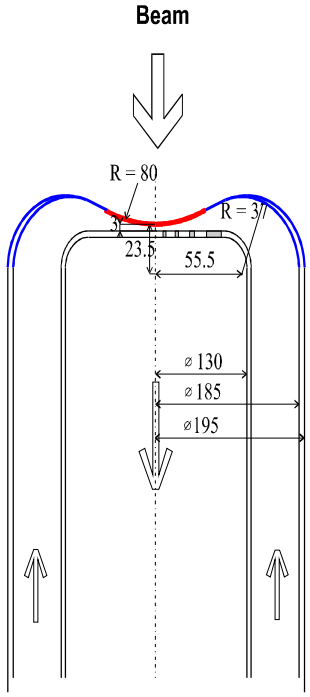

FIG. 2. ISTC target – 2nd design proposal.

2.2. MEGAPIE target

MEGAPIE (MEGAwatt PIlot Experiment) is a collaborative project of PSI Switzerland, CEA and CNRS France, FZK Germany, ENEA Italy, SCK-CEN Belgium, JAERI Japan and KAERI Korea. The final goal of the MEGAPIE project is to design, build, operate, examine and decommission a liquid lead-bismuth spallation target of 1MW beam power, making use of the existing accelerator facility SINQ at PSI [5]. A sketch of the MEGAPIE target is given in Fig. 3.

The major objectives are:

- A full feasibility demonstration of a spallation target system,
- Study of radiation and damage effects of structures and window in a realistic spallation spectrum,
- Effectiveness of the window cooling under realistic conditions,
- Liquid metal/metal interactions under radiation and stress.

The MEGAPIE project will also demonstrate the feasibility of coupling a high power accelerator, a spallation target and a subcritical blanket for future use in an ADS. The MEGAPIE experiment will provide an important database for validating and improving neutronic and thermal-hydraulic computer codes. In addition, it allows experience to be gained in the safe handling and decommissioning of irradiated components that have been in contact with lead-bismuth. The MEGAPIE project has been running since May 1999. Right now, it is in the engineering design phase.

A reference design of the active part of the target is indicated in Fig. 3. The semi-spherical beam window has an inner diameter of 174 mm. The diameter of the inner cylinder is about 130 mm. To improve the window cooling, especially in the region of the window center, two different measures are considered. The first method is to cut the lower end of the inner cylinder with an inclination angle of about 10° to the horizontal. In this way the axial-symmetry of the flow is destroyed and the flow stagnation zone near the window center can be reduced. By the second method an injection bypass is introduced, as indicated in Fig. 3. The details of the injection pipe have to be optimized based on numerical and experimental results.

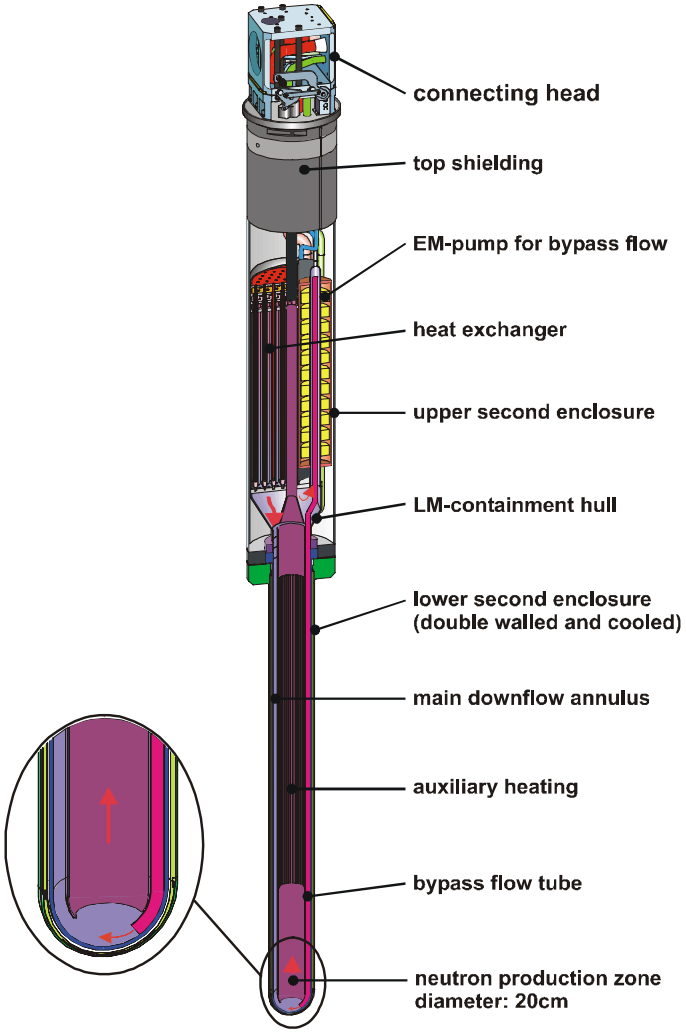

FIG. 3. Sketch of the 1MW liquid lead-bismuth spallation target MEGAPIE.

2.3. ADS-target

Recently, FZK has proposed a three-beam concept of an ADS [6, 7]. Design of the target for the three-beam concept is now underway. It is expected that the target geometry will be similar to that of the Energy Amplifier concept [2]. Based on the studies performed at CERN and CRS4 [8] a reference geometry of the spallation target has been proposed, as shown in Fig. 4. The main characteristics of this spallation target are summarized as follows:

proton energy:	= 1 GeV
beam current:	= 4 mA
beam power:	= 4 MW
beam diameter:	= 15 cm
window diameter:	= 20 cm
target material/coolant:	= Pb or Pb-Bi
coolant circulation:	= natural or forced convection
window thickness:	= 1.5-3.0 mm

This target design is currently being optimised by the Benchmark Working Group [9]. At the present stage it is not yet decided, whether the heat can be removed by natural convection or by forced convection. Numeric studies have been carried out for both natural and forced convection. Under natural convection conditions, a sufficiently large convection height should be chosen to achieve a high coolant flow rate and, subsequently, to provide a safe heat removal from the spallation volume and from the beam window [7]. In the frame of the BWG activities, model experiments are being carried out at the COULI test facility of CEA/Grenoble [9]. Main objectives of the COULI experiment will be to study hydraulic behavior in the spallation target and to provide necessary information for designing a test section for the next experiment in Pb-Bi (KALLA-laboratory).

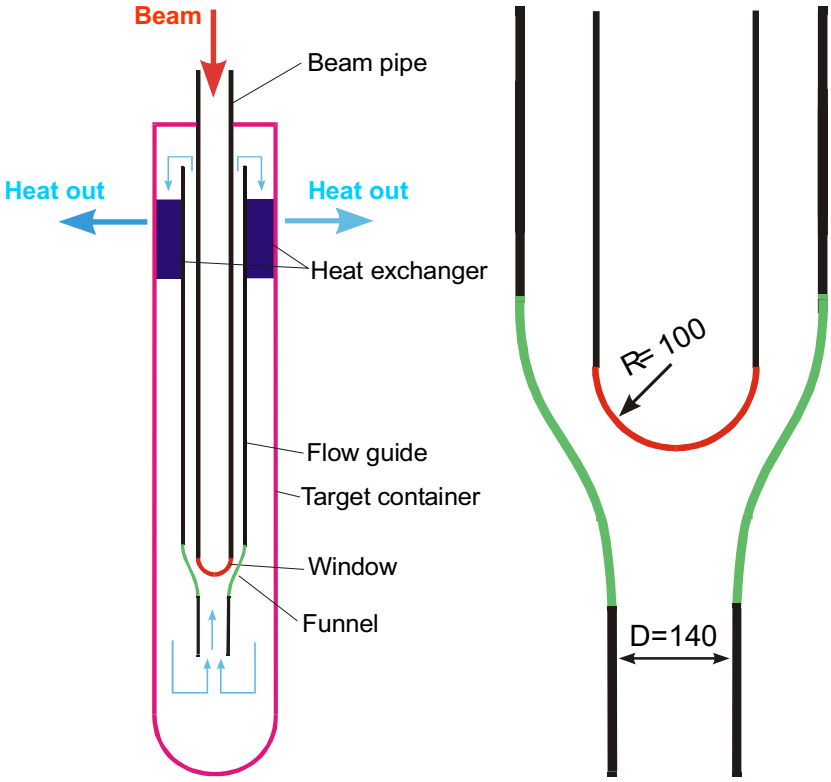

(a) target system (b) active part of the target

FIG. 4. Sketch of the ADS target.

2.4. HYTAS test facility

Figure 5 shows schematically the HYTAS test facility. The loop is capable of circulating a maximum volumetric flow rate of 100 m^3/h with a maximum pressure drop of 0.4 MPa. Test sections with a length up to 3.5 m can be integrated in the test facility. A laser light sheet technique is used to visualize the flow field. The local velocity of fluid is measured with a 2-D Laser-Doppler Anemometry (LDA).

The main purpose of the HYTAS experiment is to study the hydraulic behaviour. The hydraulic behaviour in a target can be exactly simulated in the model experiment, if the Reynolds numbers in both the prototype and the model experiment are identical. Using the thermal-physical properties of the model fluid (water) and the original fluid (Pb-Bi), The volumetric flow rate and the pressure drop in the model experiment is expressed as

$$V_M = 6.0 \frac{l_{0,M}}{l_{0,P}} \cdot V_P$$

and

$$\Delta P_M = 3.5 \left(\frac{l_{0,P}}{l_{0,M}} \right)^2 \cdot \Delta P_P \text{ , respectively.}$$

Here, l is the characteristic length of the test channel. The subscripts M and P stand for model and prototype, respectively. It is seen that for a geometric scaling of 1:1, the volumetric flow rate and the pressure drop in water are about 6 times and 3.5 times, respectively, of that in Pb-Bi. A reduction in the geometric scaling leads to a reduction in volumetric flow rate and an increase in the pressure drop. Therefore, design optimisation is required for test sections used in the HYTAS facility.

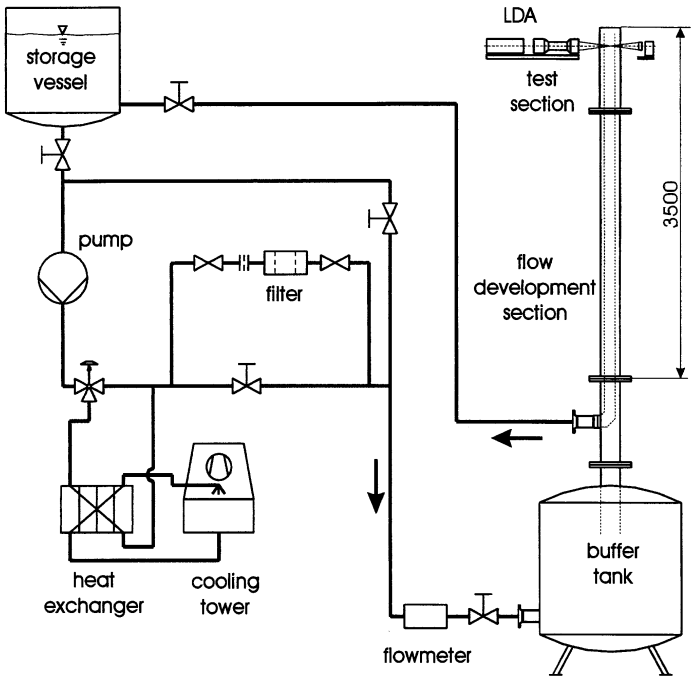

FIG. 5. Scheme of the HYTAS test facility.

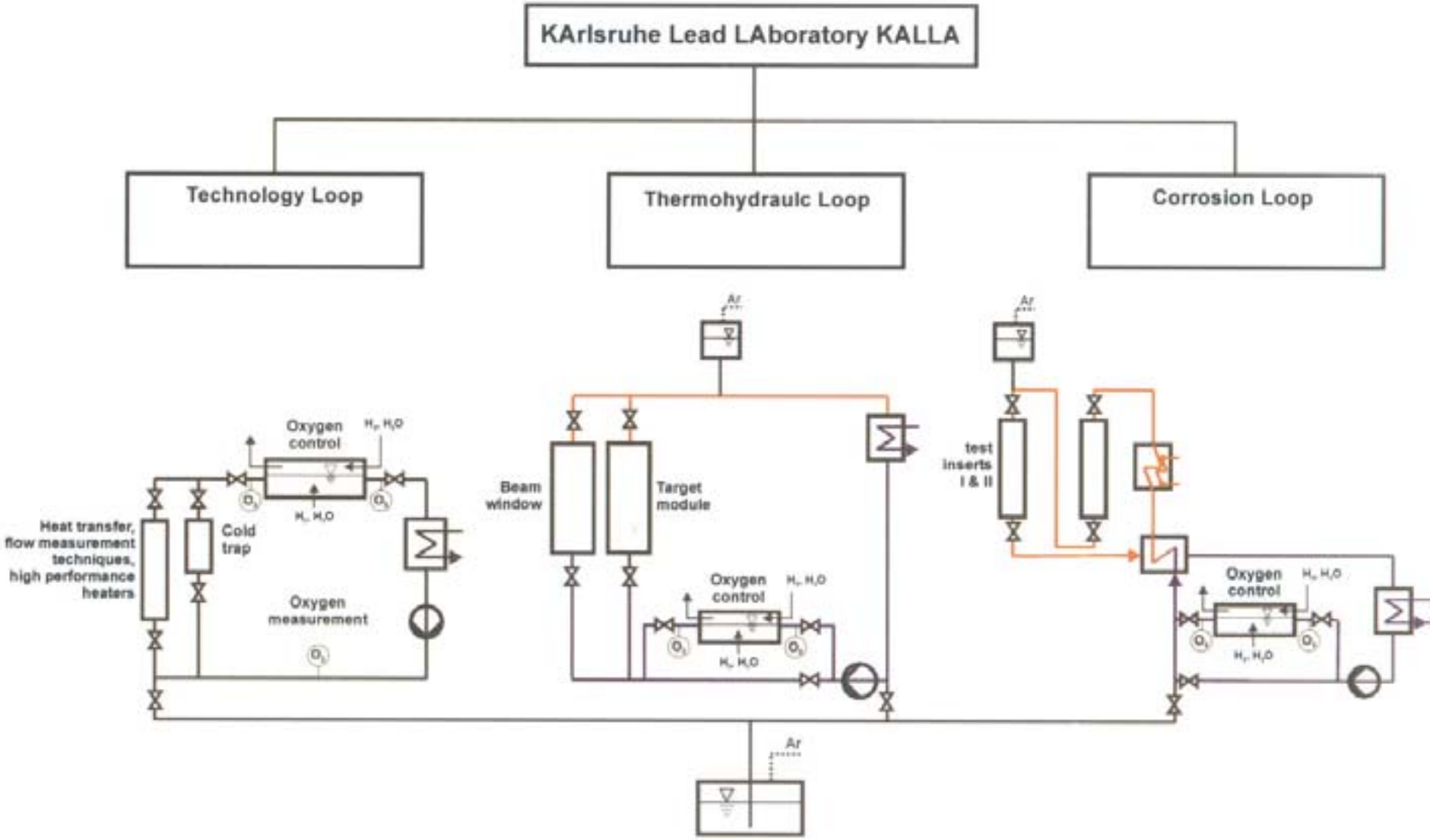

FIG. 6. Test loops of the KALLA.

2.5. Test facilities in KALLA

The KArlsruhe Lead LAboratory KALLA is being constructed at FZK. KALLA comprises three different experimental loops, as shown in Fig. 6. The research subjects and the technical specification of each loop are summarised in Table 2.

TABLE 2. THE KARLSRUHE LEAD LABORATORY KALLA

Technology loop	Thermalhydraulic loop	Corrosion loop
	Research subjects	
Oxygen measurement Oxygen control Measurement techniques Heat transfer High-performance heaters	Beam window Target module Fuel element Heat exchanger	Corrosion mechanisms Protection layers Mechanical tests Dynamic conditions
	Technical specification	
Fluid volume: 0.1 m³ Temperature: max 550°C Flow rate: max 5 m³/h	Fluid volume: 4.0 m³ Temperature: max 550°C Flow rate: max 100 m³/h Power: max. 4.0 MW	Fluid volume: 0.03 m³ Temperature: max 550°C Flow rate: max 3.5 m³/h

The *Technology Loop* concentrates on the establishment of an oxygen measurement and control technique. Measurement techniques are adapted to or specially developed for Pb and Pb-Bi. In addition, basic heat transfer experiments will be performed.

The *Thermal-hydraulic Loop* is designed for single-effect investigations of the thermally high-loaded beam window, the heat removal from a target module, thermal-hydraulic behaviour of fuel elements and heat exchangers.

The *Corrosion Loop* allows for fundamental investigations of corrosion mechanisms, the formation and the stability of protection layers and the performance of mechanical tests.

3. RESULTS EXAMPLES

3.1. Numerical studies on the ISTC target

For numerical calculations the CFD code FIDAP has been applied, which is a general purpose computer program that uses the finite element method (FEM) to simulate many classes of fluid flows [11]. The standard k-ε model with wall functions has been used for turbulence modeling. For simplicity, the flow is treated as a 2-D problem under the following simplifications [10]:

- Flow entering the target is axial symmetric.
- The buoyancy effect is negligibly small.
- The perforated plate is simplified by an axial symmetric object using two different approaches, i.e., (a) porous body approach, and, (b) annular gap approach.

The effect of different parameters on the thermal-hydraulic performance of the target has been analysed. Figure 7 shows the temperature distribution in the coolant of the first target design (Fig. 1, h = 35 mm, $\alpha = 0°$). The hot spot is located on the symmetric line, about 45 cm from the window. The maximum fluid temperature is 364°C.

Figure 8 shows the distribution of the temperature on the window outer surface. A hot spot is clearly observed in the center of the window surface. The surface temperature decreases rapidly with the distance from the window center. The maximum temperature on the window outer surface is about 340°C, i.e., lower than the maximum temperature in the coolant (364°C).

Figures 9 shows the temperature distribution of the coolant in the second target design (Fig. 2). The maximum window temperature, the maximum coolant temperature and the maximum coolant velocity are comparable to the first target design. However, for the second design flow recirculation appears in the outer region of the inner cylinder. This will result in a high coolant temperature in case the proton beam deviates from its original axis.

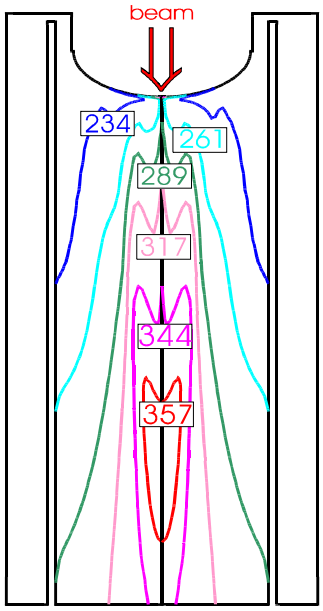

FIG. 7. Fluid temperature distribution 1st design proposal.

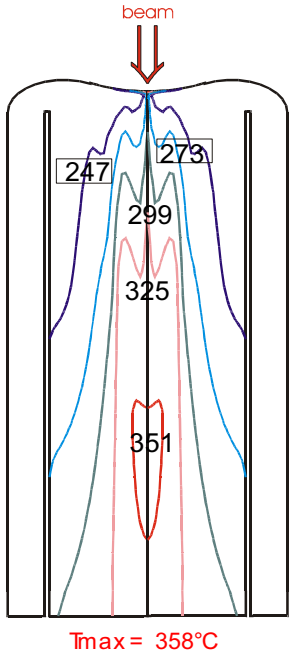

FIG. 9. Fluid temperature distribution 2nd design proposal.

Figure 10 shows the temperature distribution along the symmetric line for the first design without a perforated plate compared to that with a perforated plate. Near the window a sharp temperature increase is observed. This is due to the heat transfer from the window surface to the coolant. In the case without a perforated plate, a temperature increase of about 350°C is obtained, much larger than in the case with a perforated plate (≈ 50°C). Obviously, introduction of the perforated plate improves the heat transfer near the window center significantly. Because of the heat release in the coolant, the coolant temperature increases with the distance to the window. A local maximum temperature appears about 45 cm from the window in the case with a perforated plate and 20 cm from the window in the case without perforated plate. After then, the coolant temperature decreases due to transversal energy exchange in the coolant. At the outlet cross section, nearly the same coolant temperature for both cases is found.

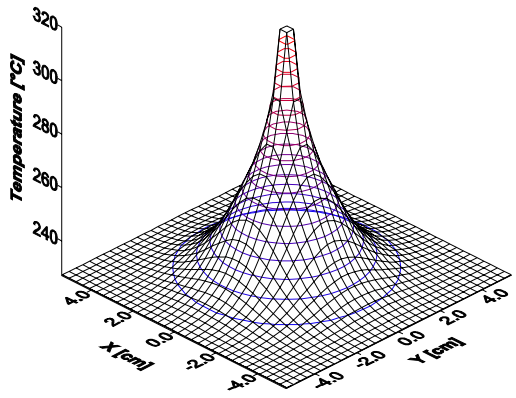

FIG. 8. Temperature distribution on the window surface - first design proposal.

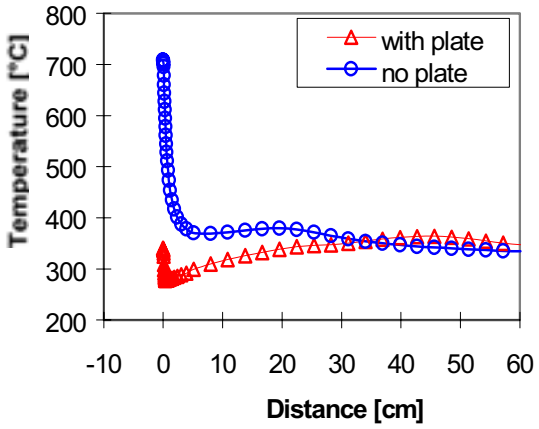

FIG. 10. Temperature distribution along the symmetric line.

3.2. Numerical studies on the MEGAPIE target

One of the proposals for heat removal from the active part of the MEGAPIE target is a combined mode of natural and forced convection [5]. Forced convection is only restricted to the injection bypass with a mass flow rate of about 5 kg/s, whereas the 'main flow' is initiated by natural convection. Under natural convection mode, the start-up phase (or the onset of the convection) is of crucial importance. Any unaceptable hot spot in the fluid as well as in the beam window has to be avoided. The 1-D code HETRAF [12] has been applied to analyse the transient behavior of the target under beam start-up and beam interrupt condition. Figures 11 and 12 show an example of the mass flow rate and the fluid temperature after switching the beam power on. The beam power in the reference case is increased suddenly from zero to its final value.

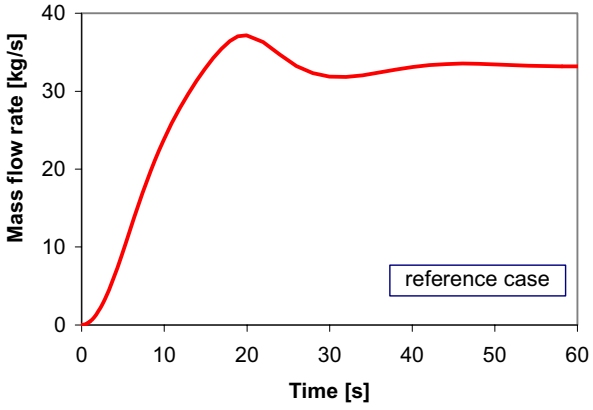

FIG. 11. Transient behavior of mass flow rate after switching on the beam power.

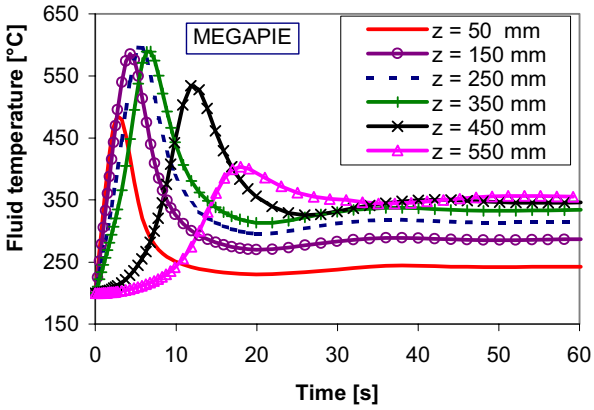

FIG. 12. Transient behavior of fluid temperature after switching on the beam power.

After switching on the beam power, the mass flow rate of Pb-Bi increases continuously and reaches its maximum after about 20 s. A steady state is reached after about 40 s. For the system considered the mass flow rate at steady state is about 33 kg/s. The hot spot in the fluid is located about 200 mm from the beam window (z = 200 mm). This temperature maximum (600°C) is reached after about 5 s after the onset of the beam power. The fluid temperature near the beam window reaches a maximum value of about 480°C. Taking into account the

high heat flux on the window surface, an extremly high temperature of the beam window is expected. Therefore, for the system considered here, a start-up mode with a sudden power increase has to be avoided.

Figure 13 indicates the effect of a finite ramp time of the start-up phase on the fluid temperature transient. For the reference case, the ramp time of the start-up phase is zero and the wall of the inner cylinder is thermal-insulating. For the other calculations, a linear increase of the beam power is taken. The ramp time of the start-up phase means that during this time period the beam power is increased from zero to its final value. For comparison, the results for the case with a thermal-conducting wall of the inner cylinder are also presented in the same figure. It is seen that the maximum fluid temperature decreases with increasing ramp time of the start-up phase. With a ramp time of 30 s the maximum fluid temperature is reduced from 600 down to 400°C.

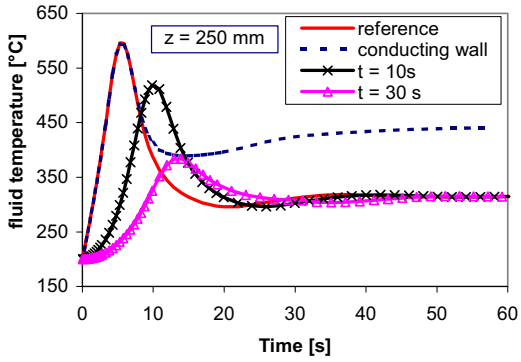

FIG. 13. Effect of the time duration of the start-up phase and the conducting wall.

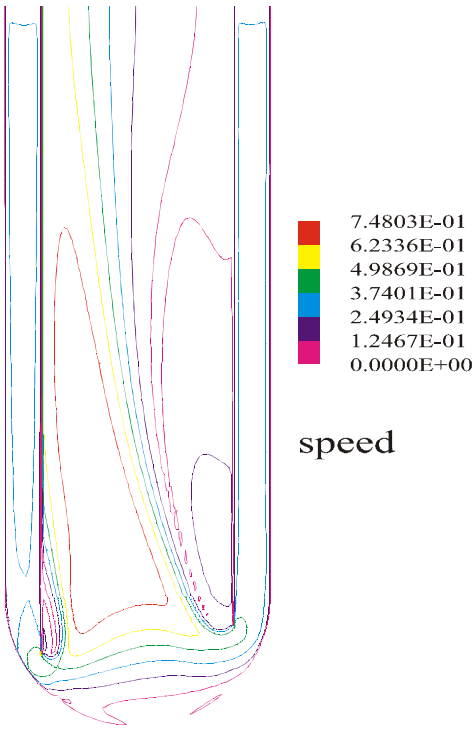

FIG. 14. Velocity distribution in the active part of the MEGAPIE target.

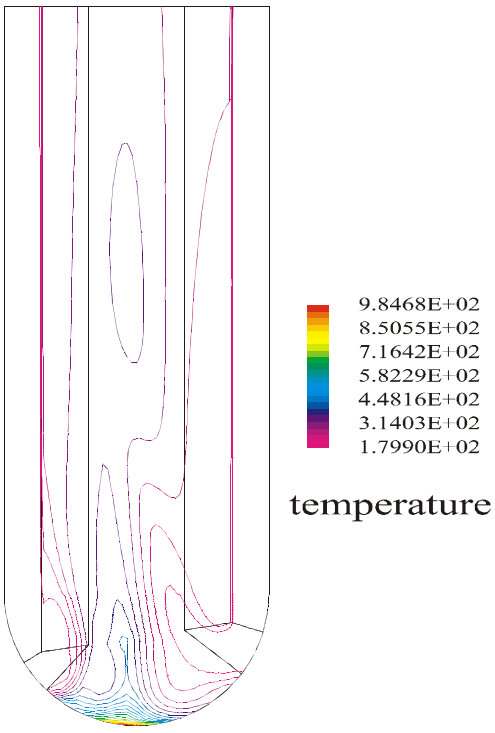

FIG. 15. Temperature distribution in the active part of the MEGAPIE target.

The effect of the conducting wall of the inner cylinder on the maximum fluid temperature is negligibly small. However, a conducting wall leads to a significant increase in the fluid temperature at steady state condition. Therefore, the inner cylinder wall should be thermally insulated.

Figures 14 and 15 present the velocity and temperature distribution in the MEGAPIE target without the injection bypass. The results are obtained with the CFX-4.3 code [13]. Due to the non-symmetric geometry, a high velocity region is observed in the left part of the inner cylinder. A large flow recirculation occurs in the right part, where the gap size is larger. However, flow is stagnant near the window center. This leads to an unacceptable high temperature of the window surface. Obviously, in case without an injection bypass, the beam window can not be cooled down sufficiently. A Further detailed numerical analyses combined with model experiments will make a crucial contribution to the design of the MEGAPIE target.

3.3. Numerical studies on the ADS-Target

Studies have been carried out for both natural and forced convection. Under natural convection a sufficiently large convection height should be taken, to achieve high coolant flow rate and subsequently to remove heat from the target and to cool down the window safely.

Figure 16 shows the relationship between the coolant flow rate and the circulation height under natural convection condition. At a convection height of 10 m, a volume flow rate of about 70 m³/h is obtained. Increasing the convection height up to 20 m leads to an increasing in the coolant flow rate of about 30%. Figure 17 shows the distribution of the temperature rise on the window outer surface. The temperature rise is defined as the difference between the window local temperature and the coolant temperature at the target inlet. The results are obtained at a volume flow rate of 70 m³/h. The maximum temperature rise is as high as 315°C at the window center. The dependence of the maximum temperature rise on the coolant flow rate is presented in Fig. 18. Increasing the coolant flow rate from 70 to 200 m³/h leads to a reduction in the maximum window temperature of about 200°C.

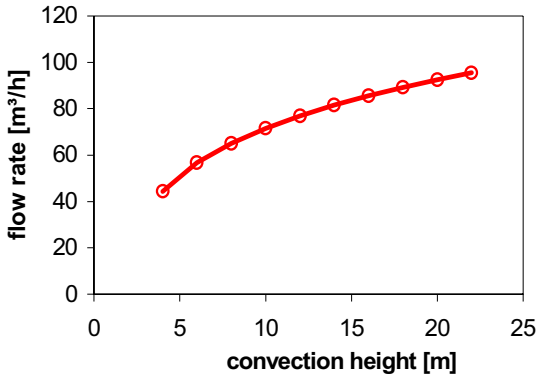

FIG. 16. Coolant flow rate in the target under natural convection.

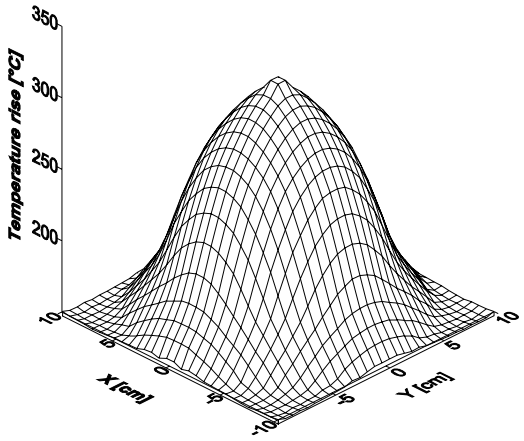

FIG. 17. Temperature distribution on the window outer surface.

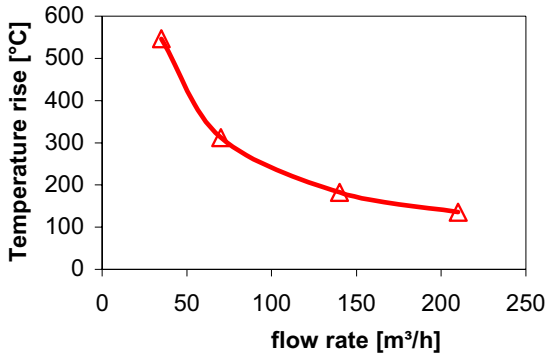

FIG. 18. Temperature rise on the window versus the coolant flow rate.

3.4. Experimental studies on the ISTC target

Experiments for the ISTC target have been performed at the HYTAS test loop using water as working fluid. The test section, shown in Fig. 19, is geometrically similar to the 1st proposed target (see Fig. 1). Tests were performed both with and without a perforated plate. Two different flow directions, i.e., either flowing upwards or downwards through the central channel, have been realised to study the effect of the flow direction. The local velocity and velocity fluctuation of the fluid was measured with a 2-D Laser-Doppler Anemometry (LDA). Moreover, the flow field has been visualized by using the laser light sheet method.

Figure 20 shows the flow pattern around the beam window for water flowing upwards through the central channel without perforated plate. The picture shows that water flows upwards in the central channel, diverges in the vicinity of the beam window. Flow stagnation was observed at the central surface of the beam window. Figure 21 shows the flow pattern around the beam window for water flowing downwards through the central channel without a perforated plate. The fluid flows nearly vertically downwards along the wall (left boundary) after entering the central channel from the top. After travelling certain distance flow reverses its direction and goes upwards in the central region of the channel. Large vortices are symmetrically formed below the window. It is well known that flow stagnation as well as flow recirculation near the window results in a reduction in the window cooling efficiency. Additional measures, e.g., by introducing a perforated plate, had to be taken to reduce the flow stagnation zone and the recirculation zone.

Figure 22 shows the measured axial velocity distributions along the x-axis (radial direction) at different elevations (y-values). The origin of the coordinate system is the middle point on the window surface. X and y are the radial and axial co-ordinates, respectively. The axial velocity u is positive, if the fluid flows upwards. As expected, the plotted data show two distinct flow regions below the beam window (negative y values): the downward flow close to the wall and the upward flow in the central region of the channel. A fast incoming stream can be seen very close to the wall (at $x \approx 60$ mm). The fluid flowing in the central region turns its direction from downward to upward at certain distance below the window. At $y = 10$ mm, the velocity is positive near the window surface. This indicates a separation of the boundary layer. Qualitatively, the velocity measurements show a good agreement with the flow visualization (Fig. 21).

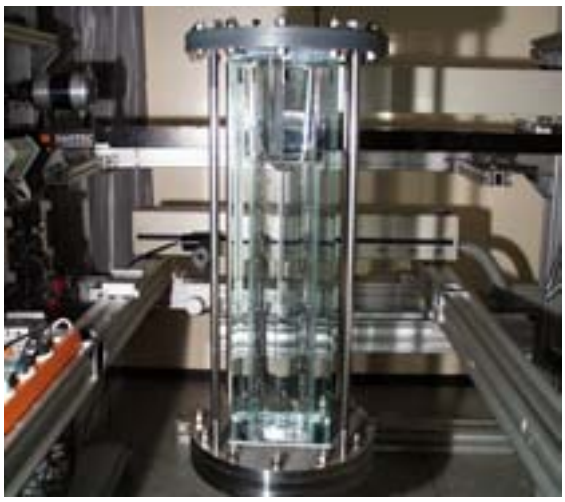

FIG. 19. Test section ISTC target.

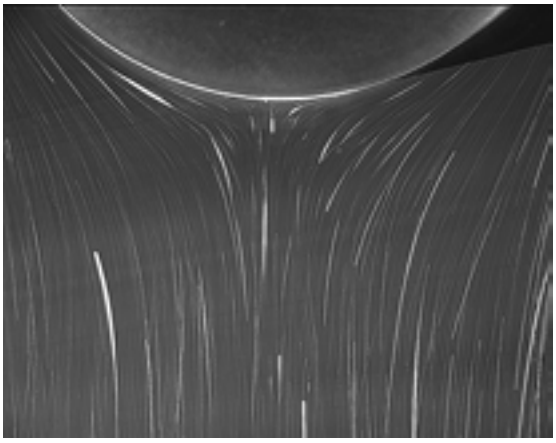

FIG. 20. Flow pattern for upward flow.

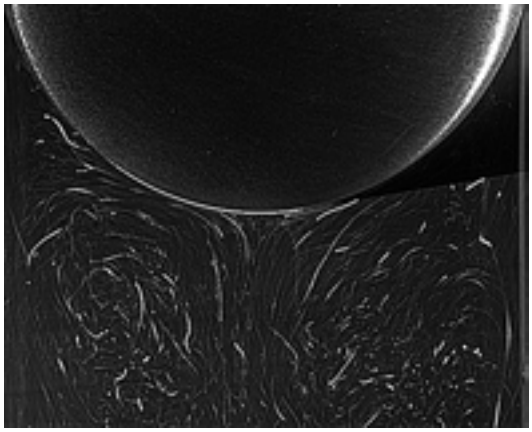

FIG. 21. Flow pattern for downward flow.

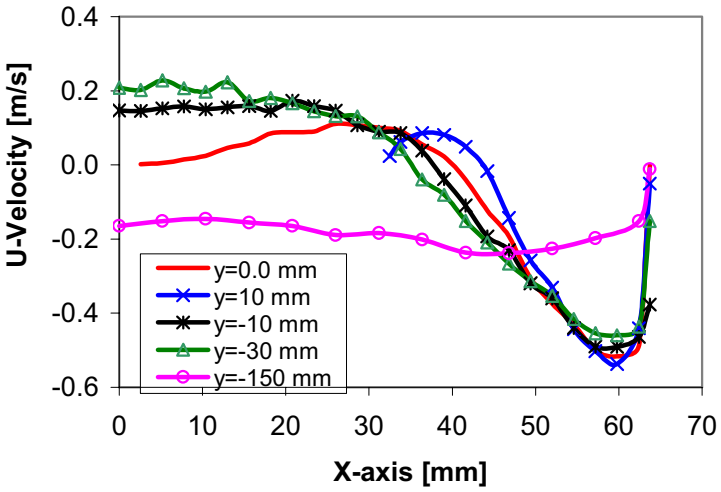

FIG. 22. Velocity profiles with downward flow through the central channel without perforated plate, V = 10 m³/h.

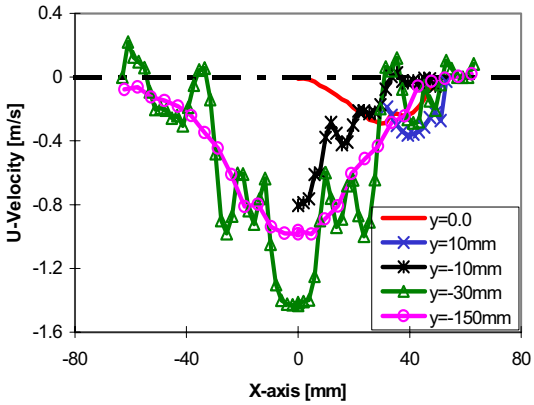

FIG. 23. Velocity profiles with downward flow through the central channel with a perforated plate, V = 10 m³/h.

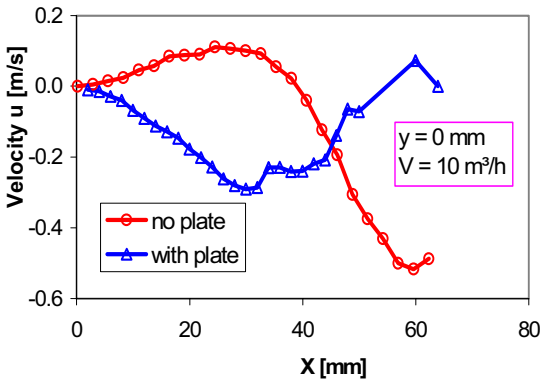

FIG. 24. Axial velocity along the line y = 0 comparison of the results with and without perforated plate.

Figure 23 shows the distribution of the axial velocity along the radial direction in the test channel with a perforated plate. The distance between the perforated plate and the window center is 15 mm. There is no boundary separation on the window surface: at both elevations (y = 0 and 10 mm) the axial velocity is negative along the whole radial axis. Close to the perforated plate a strong increase in the axial velocity is obtained. As indicated in Fig. 23, the axial velocity on the central line (x = 0) is about -0.8 m/s at 5 mm upward from the plate and -1.5 m/s at 10 mm downward from the plate. Obviously, a flow recirculation occurs beneath the plate and between the holes.

Figure 24 compares the axial velocity distributions along the radial line at y = 0 for both cases with and without the perforated plate. It is seen that the introduction of a perforated plate leads to a strong increase in the axial velocity near the window. The stagnation zone close to the window is reduced significantly. In the outer region, i.e., x ≥ 40 mm, flow recirculates. The hot spot in the fluid in case of proton beam shift can be avoided, if the holes in the perforated plate are optimized.

Figures 25 and 26 compare the experimental data in the test channel without perforated plate with the numerical results obtained by two different CFD codes, i.e., FIDAP and CFX-4.3. A good agreement between the numerical results and the experimental data is obtained. Both, the flow recirculation beneath the window (Fig. 25) and the boundary separation on the window surface (Fig. 26) are well reproduced by the codes.

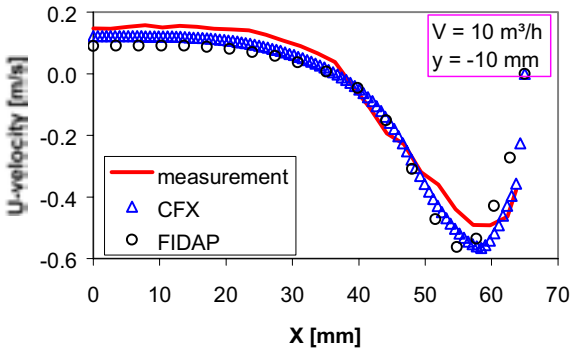

FIG. 25. Axial velocity at y = -10 mm: comparison of numerical results with experimental data.

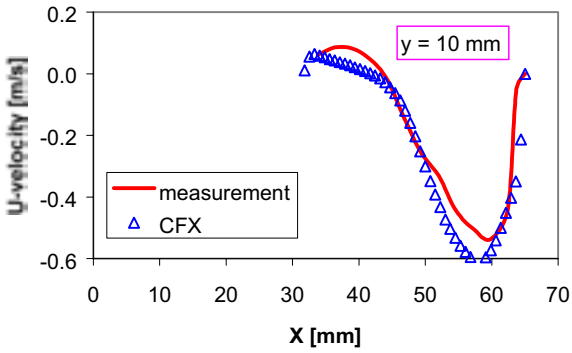

FIG. 26. Axial velocity at y = 10 mm: comparison of numerical results with experimental data.

4. CONCLUSIONS

The Forschungszentrum Karlsruhe is involved in the thermal-hydraulic design of spallation targets and has proposed a three step strategy for the research activities accompanying the target design, i.e.,

- Numerical analysis with the aim to provide the first knowledge about the thermal-hydraulic behavior in a spallation target and to achieve a preliminary design of the target.
- Model experiments in water to achieve basic information for the target design, to provide experimental database for model development and code validation.
- Prototypic experiments in Pb-Bi for the final design of a spallation target.

Computer codes of different purposes are used for the target design, i.e., 1-D system code HETRAF and CFD codes CFX-4.3 and FIDAP-7. Model experiments at the HYTAS test facility with water as the working fluid are carried out for different target designs. Laser measurement techniques have been applied to visualize the flow and to measure the fluid velocity. The thermal-hydraulic loop of the KALLA laboratory will be used for the prototypic experiment in lead-bismuth. Based on the results obtained up to now, the following specific main conclusions can be drawn:

- In the ISTC target, introduction of a perforated plate reduces the flow stagnation zone, minimizes flow recirculation and enhances the coolability of the beam window. An optimization of the perforated plate can well be achieved by numerical analysis.
- Under natural convection conditions, the ramp time of the start-up phase has to be large enough to avoid any unacceptable hot spot in the coolant as well as in the beam window. For the MEGAPIE target a ramp time of about 30 s should be chosen. Moreover, a thermally insulating wall of the inner cylinder will lead to a reduction in the window temperature of about 100°C.
- For the reference proposal of the MEGAPIE target, a bypass jet is inevitable to cool down the beam window sufficiently. Numerical studies as well as water experiments have to be carried out to optimize the bypass jet.
- For the spallation target of an ADS, forced convection seems to be a more promising way to cool down the bean window and to remove heat from the target.
- Water experiments at the HYTAS test facility are proven to be suitable to provide basic information for target design and experimental database for code validation.
- Relating to the average velocity, both CFD codes (CFX-4.3 & FIDAP-7) show a good agreement with the experimental data. Further validation is necessary by considering turbulence parameters and heat transfer data as well.

REFERENCES

[1] HEUSENER, G., SALVATORES, M., Use of heavy liquid metal: A perspective for critical/subcritical fast neutron concepts, paper presented in the Conf. on Heavy Liquid Metal Coolant in Nuclear Technology (HLMC'98), 1998, Obninsk, Russia, CRS4, TECH-REP-00/50 (1999).

[2] RUBBIA, C., et al., Conceptual design of a fast neutron operated high power energy amplifier CERN/AT/95-44(ET), Geneva (1995).

[3] YEFIMOV, E., The main results of feasibility study of liquid metal targets and the working plan on the project #559, Kick-off meeting on the ISTC project #559, 1998, Obninsk, Russia.

[4] SALVATORES, M., BAUER, G., HEUSENER, G., The MEGAPIE Initiative – Executive Outline and Status as per November 1999, Paul Scherrer Institut, Villigen, Switzerland, internal document MPO-1-GB-6/0-GB, Paul Scherrer Institut, Villigen, Switzerland (1999).
[5] BAUER, G., et al., Description of SINQ and Boundary Conditions for MEGAPIE, paper presented in the 1st MEGAPIE General Meeting, CEA, Cadarache, 14-15 June 2000, Cadarache, France, paper not published (distributed during the meeting).
[6] KNEBEL, J.U., CHENG, X., BROEDERS, C.H.M., The FZK Three-Beam Concept for an ADS Jahrestagung Kerntechnik, Forschungszentrum Karlsruhe, Karlsruhe (1999) 639-643.
[7] CHENG, X., KNEBEL, J.U., HOFMANN, F., Thermalhydraulic design of an ADS with three spallation targets, Proc. 3rd Int. Conf. on Accelarator-Driven Transmutation Technologies and Applications (ADTTA'99), 7-11 June 1999, Prague, Czech Republic, Eds: L M. Hron, V. Lelek (NRI Rez plc), M. Mikisek, M. Sinor, J. Uher, J. Zeman (FNSPE CTU, Prague), NRI Rez, Czech Republic (1999), Prague, Czech Republic.
[8] MACIOCCO, L., et al., Design and Optimisation of a Liquid Metal Spallation Target for the Energy Amplifier Prototype, paper presented in the Int. Top. Mtg. on Nuclear Applications of Accelerator Technology (AccApp'98), 1998, Gatlinburg, TN, USA, ANS, ISBN: 089448-633-0 (1998).
[9] BUONO, S., (Ed.), Proc. First Meeting of the Benchmark Working Group on Heavy Liquid Metal Thermalhydraulics, CERN, Geneva (1999).
[10] CHENG, X., SLESSAREV, I., Thermalhydraulic Investigations on Liquid Metal Target Systems, accepted to be published in Nuclear Engineering & Design (2000).
[11] FIDAP User Manuel, Revision 7.0, Fluid Dynamics International, Inc., (1993)
[12] CHENG, X., Numerical analysis of thermally induced transients in forced flow of supercritical helium cryogenics, Vol. 34, No.3 (1994) 195-201.
[13] CFX 4.3 User Guide, AEA Technology (1998).

EXPERIMENTAL STUDIES

(Session 6)

Chairperson

Y.H. KIM

Republic of Korea

CORROSION OF STRUCTURAL MATERIALS BY LEAD BASED REACTOR COOLANTS

D.P. ABRAHAM, L. LEIBOWITZ, V.A. MARONI, S.M. McDEAVITT, A.G. RARAZ
Argonne National Laboratory, Argonne, Illinois, United States of America

Abstract

Advanced nuclear reactor design has, in recent years, focused increasingly on the use of heavy-liquid-metal coolants, such as lead and lead-bismuth eutectic. Similarly, programs on accelerator-based transmutation systems have also considered the use of such coolants. Russian experience with heavy-metal coolants for nuclear reactors has lent credence to the validity of this approach. Of significant concern is the compatibility of structural materials with these coolants. We have used a thermal convection-based test method to allow exposure of candidate materials to molten lead and lead-bismuth flowing under a temperature gradient. The gradient was deemed essential in evaluating the behavior of the test materials in that should preferential dissolution of components of the test material occur we would expect dissolution in the hotter regions and deposition in the colder regions, thus promoting material transport. Results from the interactions of a Si-rich mild steel alloy, AISI S5, and a ferritic-martensitic stainless steel, HT-9, with the molten lead-bismuth are presented.

1. INTRODUCTION

Advanced nuclear reactor design has, in recent years, focused increasingly on the use of heavy-metal coolants, such as lead and lead-bismuth eutectic [1]. Similarly, programs on accelerator-based transmutation systems [2] have also considered the use of such coolants. Russian experience with heavy-metal coolants for nuclear reactors has lent credence to the validity of this approach [3]. The advantages and disadvantages of such coolants have been previously reviewed [4] and will not be discussed here.

Interest in the use of lead and lead alloys as coolants in nuclear reactors has a long history going back to the 1950s. In the United States, however, sodium became the coolant of choice in fast reactors because of some superior properties. An extensive development program was undertaken on sodium cooling and work on lead-cooled reactors was given considerably less attention. In contrast, researchers in the Soviet Union continued work on lead-based coolants and according to their reports had considerable success. In spite of the earlier choice of sodium there are significant advantages to the use of lead and lead-based alloys. Substituting lead for sodium eliminates a significant combustion hazard. In addition, the high boiling point of lead allows for potentially much higher operating temperatures. Prominent among the disadvantages of using lead as a reactor coolant are uncertainties regarding corrosion and liquid-metal embrittlement.

The compatibility of structural materials with lead-based coolants is of pivotal concern in nuclear reactor technology and several studies have been reported in the literature. Early work at Argonne National Laboratory [5] reported in 1955 (actually performed in 1949) involved static immersion tests of the compatibility of a number of materials with molten lead at 1000°C. Sintered beryllia, fused silica, tantalum, and niobium were reported to have good resistance to lead. However, the results of static tests can be misleading because they do not account for material transport under a temperature gradient. Thermal convection loops were constructed and operated at Brookhaven National Laboratory [6] with the hot leg at roughly 500°C and the cold leg at about 400°C. Relatively low liquid velocities, averaging around 0.05 ft/s were obtained, but more importantly, the potential for material transport existed. Material testing in thermal convection loops has also been reported by researchers in Russia [3], the United Kingdom [7] and Germany [8].

This article presents corrosion results for alloys exposed to molten lead-bismuth flowing under a temperature gradient. The gradient was deemed essential in evaluating alloy behavior because it allowed for the possibility of material transport. Preferential dissolution was expected in the hotter regions of the test assembly and material deposition was expected in the colder regions. A test system used successfully by researchers at Oak Ridge National Laboratory [9] was adapted for our experiments. Iron-based alloys containing alloying elements expected to form stable protective oxides were selected for testing. These were AISI S-5, a 2wt% Si mild steel and HT-9, a Cr-bearing ferritic-martensitic stainless steel, chosen because it approximates the composition of a Russian steel, EP-823, claimed to be very resistant to lead corrosion. Nominal alloy compositions are shown in Table 1. A comparison of alloy corrosion characteristics demonstrates the crucial role of chromium in the passivation behavior of iron-based alloys.

TABLE 1. COMPOSITION (wt%) of HT-9, AISI S-5, AND EP-823

	Ni	Cr	Mn	Mo	Si	W	V	C
HT-9	0.5	12.0	0.2	1.0	0.25	0.5	0.5	0.2
AISI S-5	0.06	0.35	0.81	0.75	1.79	-	0.26	0.55
EP-823	0.8	12.0	0.6	1.0	1.3	0.8	0.4	0.2

2. EXPERIMENTAL

A schematic of the quartz convection harp installed in a furnace assembly is shown in Fig. 1. Tubular samples of AISI S-5 (test H-2) and X-shaped samples of HT-9 were fabricated from available stock. Test samples were placed in the center of the two vertical legs of the harp and held in place with dimples above and below the samples. The quantity of granular Pb-Bi eutectic needed to fill the harp was placed in the large bulb (see Fig. 1) for treatment prior to introduction into the harp. A porous quartz frit below the bulb prevented the metal from running into the harp prematurely. The harp-furnace enclosure assembly was mounted in a ventilated hood containing a specially designed gas-handling system. The harp was evacuated and flushed several times with He-4% H_2 (He-H_2) sweep gas then heated to ~350°C with sweep gas flowing through it. Heating tape was wrapped around the large bulb and the Pb-Bi eutectic was melted. Sweep gas was allowed to bubble through the molten Pb-Bi and the moisture content of the exit gas was measure using a Panametrics Series 3 moisture monitor. When the moisture level reached ~25 ppm the arm below the frit (see Fig. 1) was evacuated and pressure (He-H_2) was applied above the molten eutectic, forcing the liquid metal into the harp. Sweep gas was continually passed over the molten Pb-Bi for the entire duration of the experiment.

Temperature controllers were provided on the two vertical legs and Variacs supplied power, as needed to the upper and lower slanted branches of the harp. Following filling, the hot leg temperature was raised to 550°C. Temperatures were monitored using a National Instruments data logger. The cold leg controller was set at 350°C; however, heat transport from the hot leg was sufficient to raise the cold-leg temperature above the cold leg set point by about 50-75°C. Attempts were made to determine the flow rate of the eutectic by introducing a brief cold pulse of air to the top branch of the harp and observing the appearance of a brief thermal dip on the cold leg. From the signals obtained we were able to estimate a flow rate of ~30.5 cm/min (1 ft/min), similar to that reported in [9].

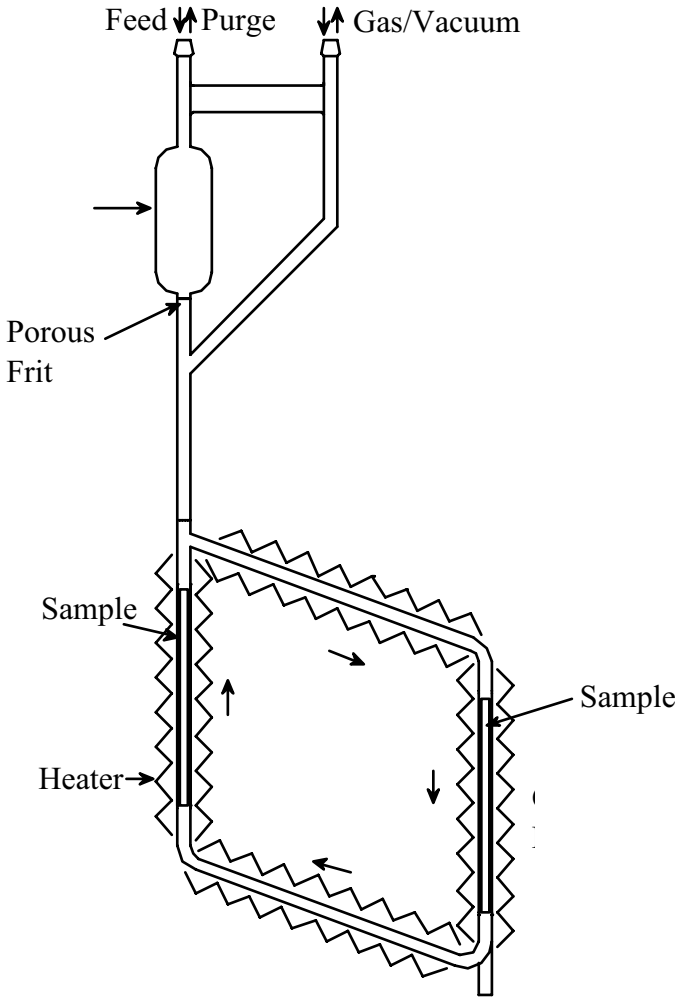

FIG. 1. Schematic drawing of a quartz convection harp installed in a furnace assembly.

The harp systems operated with excellent thermal and flow stability for 4500 hours, after which they were shut down for examination. Each harp was disassembled and the sections containing the test pieces were placed in separate filtering tubes, shown in Fig. 2, to remove as much adhering Pb-Bi as possible.

These filtering tubes operated like the harp filling system. Heating tape was wrapped around the upper section to melt the eutectic. Evacuation and pressurization, conducted as for the fill operation, forced the molten metal into the lower chamber leaving the test alloy with a thin coating of Pb-Bi in the upper section. In separate procedures, a sample of Pb-Bi was treated with He-H_2 and filtered to provide a control sample that was not exposed to the alloys tested.

Samples of lead-bismuth from the control, and from the harp containing the HT-9 specimens were analyzed by ICP/AES. The HT-9 was examined using Raman spectroscopy, Auger electron spectroscopy (AES), scanning electron microscopy (SEM), transmission electron microscopy (TEM), and X-ray diffraction (XRD). The AISI S-5 sample has, to date, been examined only by SEM. Results of these examinations are given below.

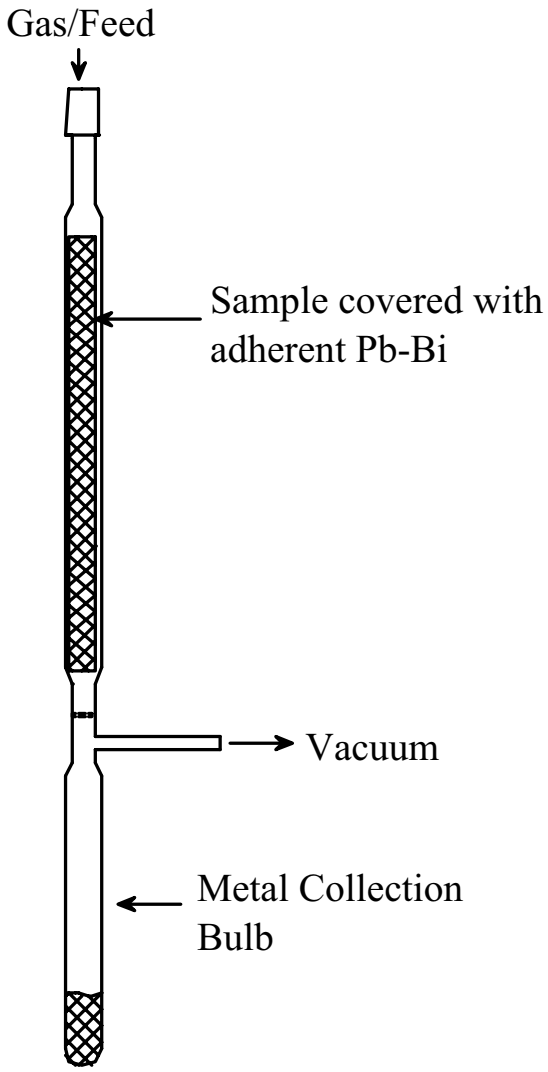

FIG. 2. *Schematic drawing of filter tube.*

3. RESULTS

3.1. Examination of the AISI S-5 samples

Visual examination of the test samples showed a black discoloration under the adhering lead-bismuth alloy. Sections of the exposed samples were examined by scanning electron microscopy (SEM). Micrographs from a sample in the hot leg (~550°C) are shown in Figs 3a and 3b.

Intergranular penetration of lead-bismuth into the sample is plainly evident in Fig. 3a, making this material a poor candidate for structural applications. The depth of penetration ranged from 10 to 40 μm. A non-adherent scale, rich in Si, Fe and O, was found on the sample surface; the nature of this scale is being determined by X-ray diffraction. This scale is evident in Fig. 3b, which clearly shows the debris left behind after the sample was attacked. Samples from the cold leg (~350-425°C) also showed some attack. However, the depth of penetration in these samples ranged from 1-5 μm. The difference in attack in the hot and cold legs clearly demonstrates the influence of temperature on alloy corrosion.

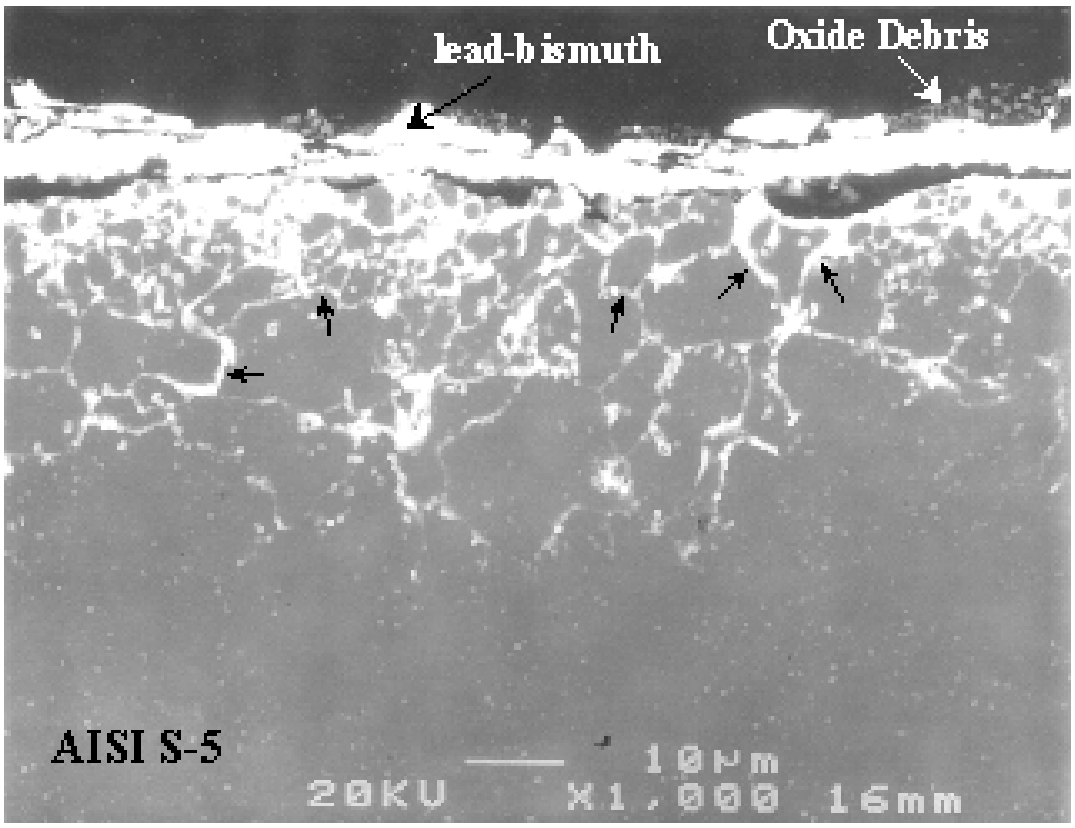

FIG. 3a. Micrograph of an AISI S-5 sample exposed to molten lead-bismuth in the hot leg of the convection harp. Penetration of the lead-bismuth into the sample (marked by arrows) is evident.

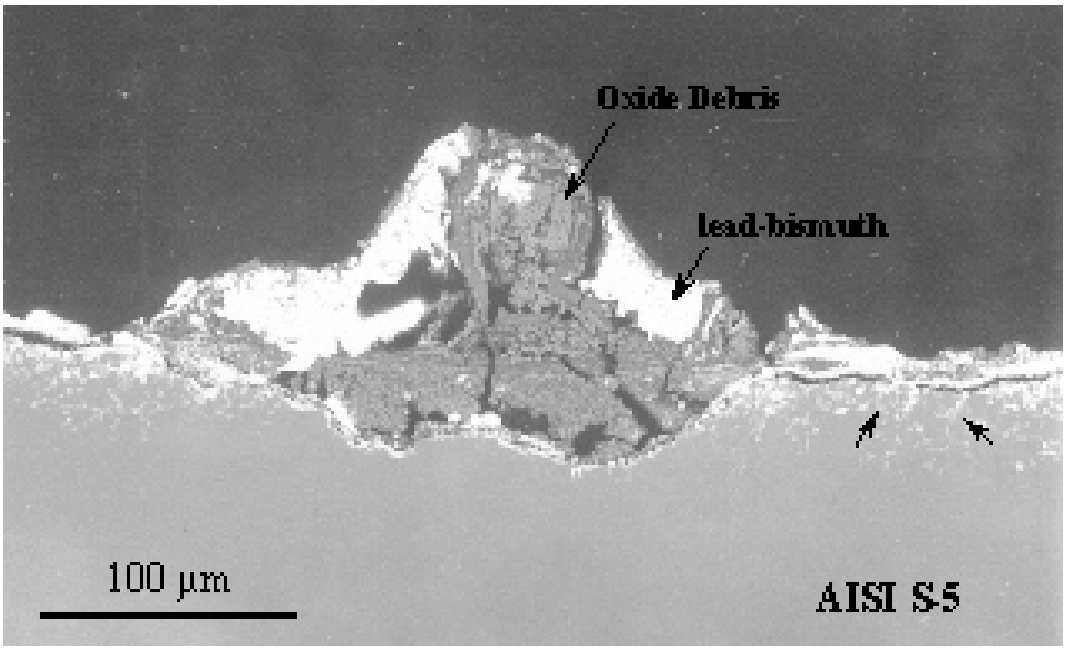

FIG. 3b. Same sample as in Fig. 3a, but showing the "debris" left behind by the attack. The arrow in the metal show the intergranular penetration.

3.2. Examination of the HT-9 samples

The appearance of harp H-1 (containing the HT-9 samples) after the test is shown in Fig. 4.

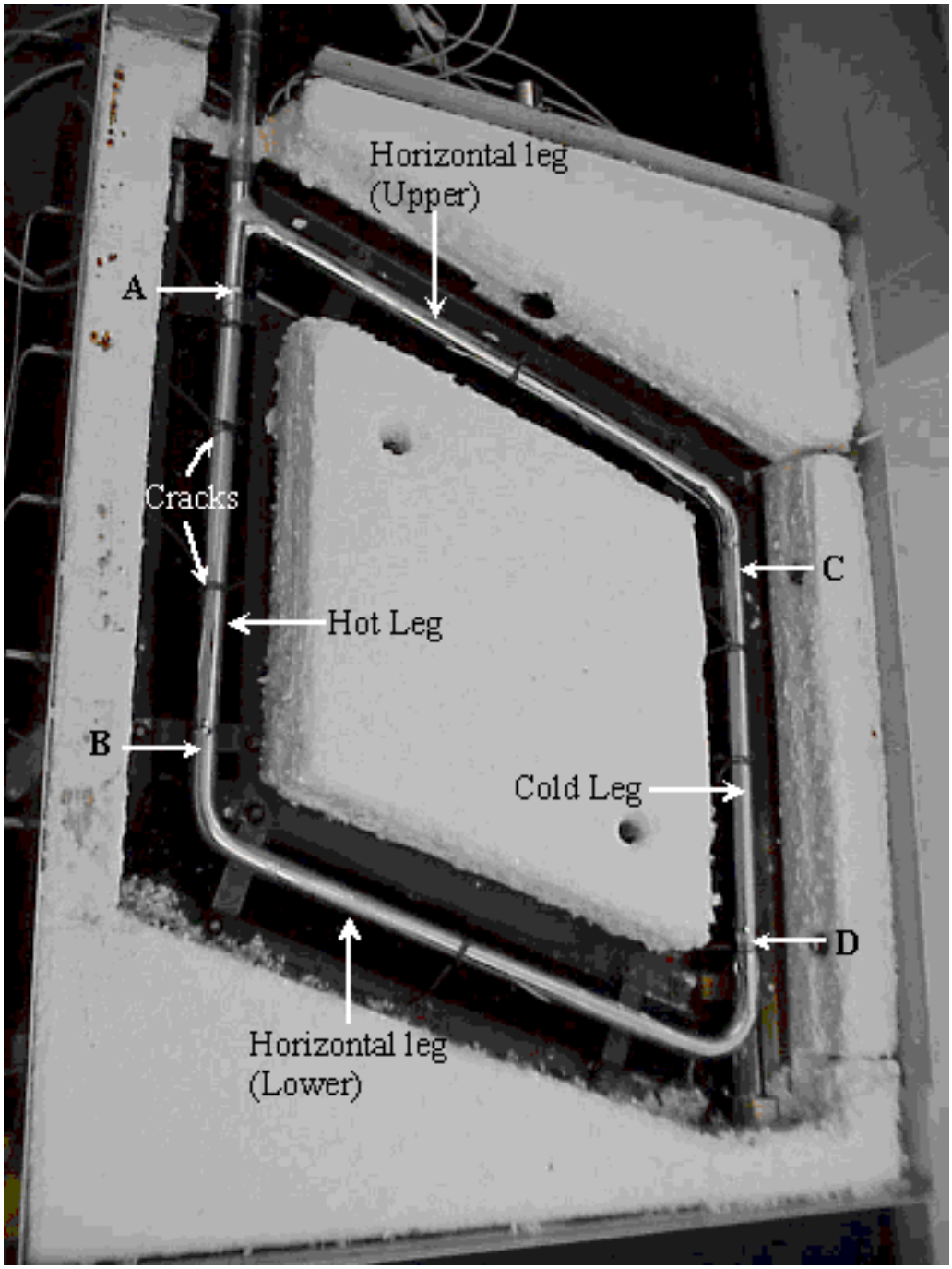

FIG. 4. Quartz convection harp after termination of the test showing sample locations. The quartz cracked after the assembly was cooled to room temperature.

Note that the quartz cracked on cooling. The lead-bismuth, however, was quite shiny and showed no obvious signs of contamination. The elemental analyses of the Pb-Bi samples are shown in Table 2.

TABLE 2. COMPOSITION (ppm) OF Pb-Bi SAMPLES FROM THE CONTROL, HOT LEG (HOT) AND THE COLD LEG (COLD)
(Estimated accuracy is ± 10%)

	Cd	Cu	Fe	Ni	Sn	Zn	Si	Bi wt%	Pb wt%
Control	42.5	8.71	52.0	16.1	3280	31.6	247	49.5	49.3
Hot	42.5	16.8	32.7	10.5	3416	35.2	300	50.0	48.9
Cold	41.5	14.6	30.8	12.2	3414	29.6	259	50.4	46.9

Although some of the changes appear to be outside the reported analytical uncertainty, no major differences are seen between the exposed samples and the control sample. However, decreases in Fe and Ni and increases in Cu and Sn in the exposed Pb-Bi samples are noteworthy. Visual observation of the HT-9 samples revealed a black coating under an adherent lead-bismuth layer (see Fig. 5).

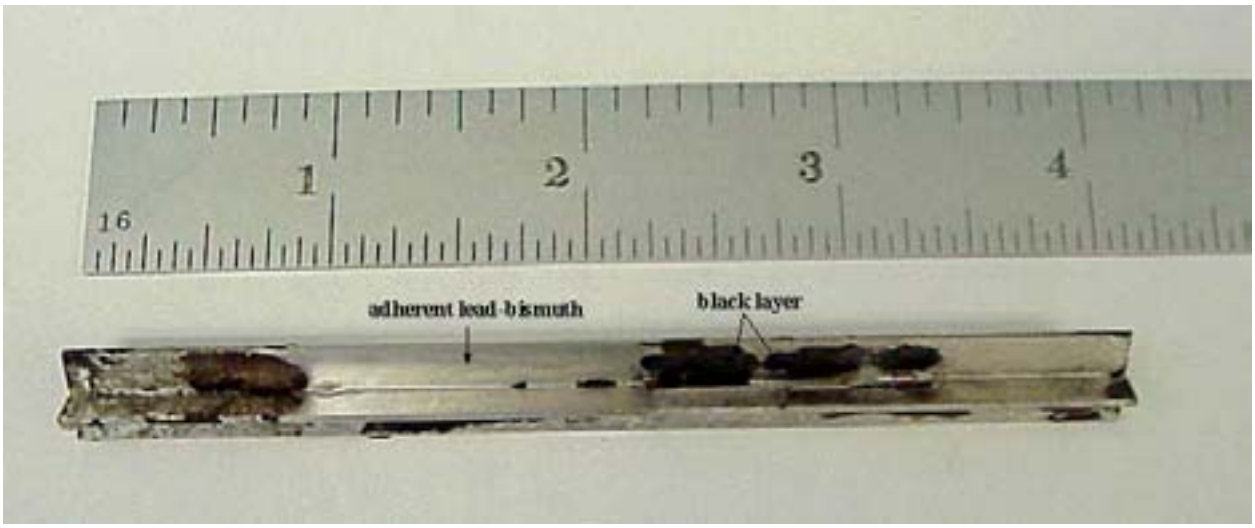

FIG. 5. HT-9 sample from hot leg (~550°C) of convection harp. Note the black layer under the adherent lead-bismuth.

This black coating was not present on the original HT-9. Considerable effort was devoted to the characterization of this layer.

Samples from both the hot and cold legs were examined by SEM. The studies showed that the Pb-Bi did not penetrate the samples. A thin surface layer (see Fig. 6), ranging from 0.1 to 0.2 μm was observed on samples in the hot leg (~550°C).

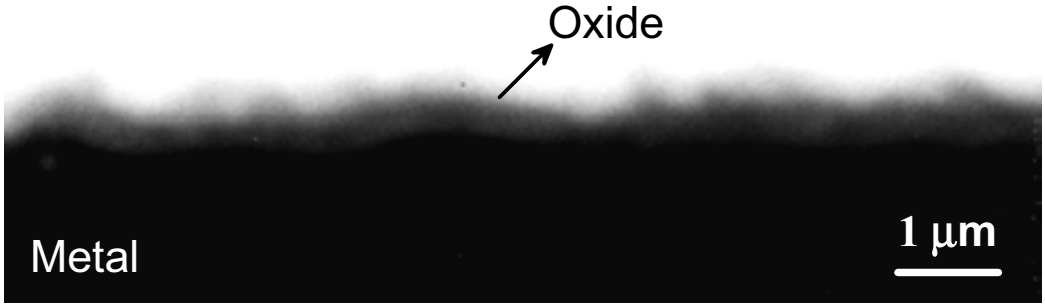

FIG. 6. SEM image of HT-9 after exposure to Pb-Bi. at ~550°C. Note thin surface layer.

Detailed SEM-EDS analysis could not be conducted because the surface layer was too thin. However, cursory analysis indicated that the layer was enriched in chromium. Examination of samples in the cold leg revealed no obvious surface film; any layer present was apparently too thin to be seen under the SEM.

The corrosion product on one hot leg sample was examined by Auger Electron Spectroscopy (AES). The samples were sputtered with argon (Ar^+) ions to measure elemental composition as a function of depth. A ~10 nm lead-bismuth layer present on the top surface was initially removed by sputtering. A typical AES depth profile is shown in Fig. 7; other areas examined on the sample showed essentially the same result.

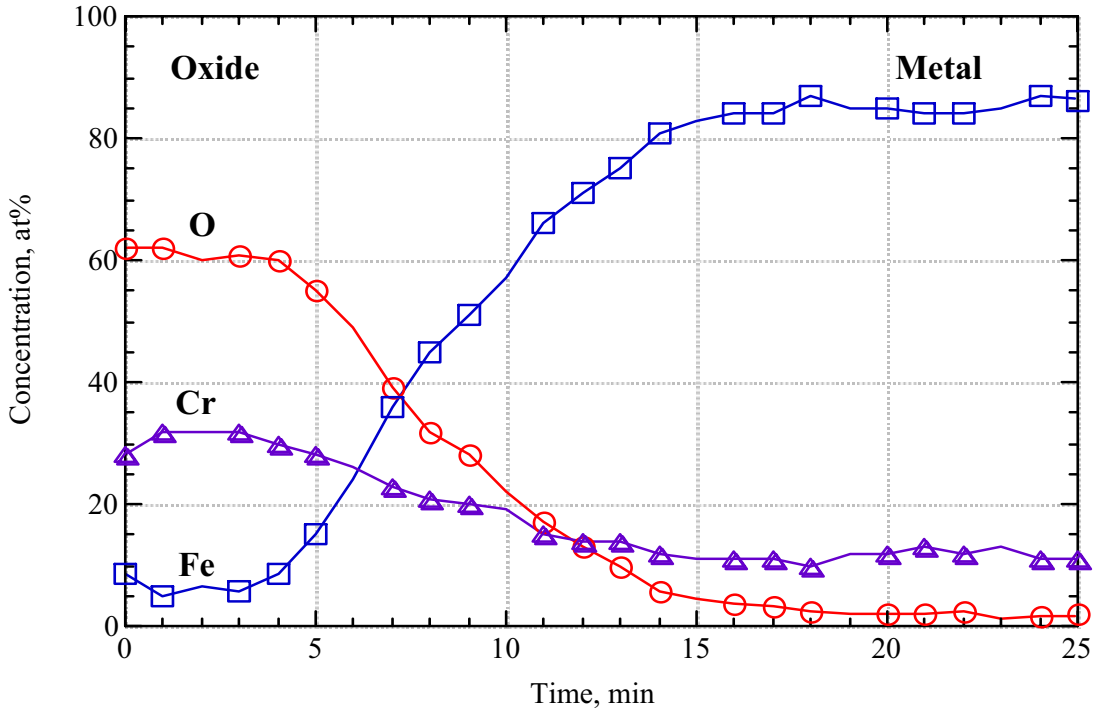

FIG. 7. AES depth profile from HT-9 samples exposed to ~550°C lead-bismuth.

Only Fe, Cr and O were observed in the corrosion layer. Furthermore, the data clearly showed chromium-enrichment in areas near the oxide-molten metal interface.

Raman spectra of the surface of a hot leg sample were recorded using a Renishaw System 2000 Imaging Raman Microscope. The spectra were obtained with the specimen surface perpendicular to the excitation/observation directions. The spectra obtained were similar to those observed previously for mildly oxidized iron-chromium alloys [10]. The oxide film was identified as being of the $Fe_{3-x}Cr_xO_4$-type. From the specific band shape and peak frequencies we inferred that x was substantially greater than zero, i.e., the oxide film was rich in chromium.

Low angle X-ray diffraction (XRD) patterns were obtained on the samples at the Advanced Photon Source (APS) at Argonne National Laboratory (ANL). A sample with the black layer exposed was mounted in a diffractometer at the MRCAT beam line. Diffraction patterns were obtained with the sample at a constant angle of 3.5° or 6.5° to the beam. A conventional θ-2θ scan, in which the beam penetration varies with incident angle, was also obtained with a beam energy of 11 keV (wavelength = 0.11271 nm). Analysis of the diffraction peaks indicated the existence of a $FeCr_2O_4$ -type spinel on the sample.

Preliminary transmission electron microscopy (TEM) results have confirmed the existence of an adherent $FeCr_2O_4$ -type spinel on the sample surface. The analysis has shown that the spinel layer is ~100-150 nm (0.1-0.15 μm thick). Crystalline particles with $BiPb_3$- or $BiPb_4$- type structure containing Fe and Cr have also been observed on the sample surface. The TEM observations are consistent with the results of XRD, Raman spectroscopy and AES.

4. DISCUSSION

The formation of an oxide film on an alloy surface is determined by temperature, oxide stability and oxygen activity in the system. The relationships involved can be illustrated for the case of Cr_2O_3. For one mole of oxygen, the relevant equation for Cr_2O_3 formation is:

$$4/3\ Cr + O_2 = 2/3\ Cr_2O_3 \quad (1)$$

The equilibrium constant for this reaction is

$$K = (a_{Cr2O3})^{2/3} / (a_{Cr})^{4/3}\ P_{O2}$$

where

a_{Cr} and a_{Cr2O3} are the activities of Cr and Cr_2O_3, respectively and P_{O2} is the oxygen pressure. If the activities of the solids are assumed to be unity, then the oxygen pressure is the reciprocal of the equilibrium constant.

At 550°C the Gibbs energy change for reaction (1) is -146.7 kcal yielding an equilibrium constant of 9.06×10^{38} and the equilibrium oxygen pressure will be $\sim10^{-39}$ atm. Thus at 550°C, Cr_2O_3 will only form at pressures higher than $\sim10^{-39}$ atm. Similar calculations can be carried out for other oxides by using reference data available in literature. Table 3 summarizes the equilibrium oxygen pressures for various oxides assuming condensed phases at unit activity.

TABLE 3. COMPARISON OF OXYGEN PARTIAL PRESSURES IN EQUILIBRIUM WITH VARIOUS OXIDES AT 550°C

Oxide	Oxygen pressure (atm.)
Bi_2O_3	2.4×10^{-15}
PbO	4.3×10^{-18}
Fe_3O_4	1.6×10^{-27}
$FeCr_2O_4$	3.8×10^{-38}
Cr_2O_3	1.1×10^{-39}
SiO_2	4.9×10^{-49}

The oxygen partial pressure in our system can be roughly estimated from the measured moisture content (about 10 ppm) and the hydrogen concentration in the He-H_2 cover gas (about 4%). From the known Gibbs energy of formation of water we estimate PO_2 in our system at 550°C to be about 1×10^{-33}, much larger than needed to form Cr_2O_3 or $FeCr_2O_4$, but very much lower than that needed to form PbO. Clearly the existing oxygen partial pressure in

our system permits formation of the Cr-containing oxides but not PbO or Bi_2O_3. Table 3 shows that the oxygen partial pressure for formation of Cr_2O_3 and the spinel $FeCr_2O_4$ are very close. The spinel structure may be favored on HT-9 because of the high iron content of the samples.

5. SUMMARY AND CONCLUSIONS

An experimental setup was designed and used to test iron-based alloys alloys exposed to molten lead-bismuth flowing under a temperature gradient. The temperature in the hot leg of the convection harp was ~550°C and the temperature in the cold leg was ~350-425°C. The alloys chosen for the test were AISI S-5, a 2wt% Si mild steel, and HT-9, a ferritic-martensitic stainless steel. The tests were terminated after sample exposure for ~4500 hours. The results of our studies may be summarized as follows:

i. The AISI S-5 alloy was attacked by the molten lead-bismuth. The depth of intergranular penetration ranged up to 40 μm in the hot leg and up to 5 μm in the cold leg. The test showed that AISI S-5 would not be suitable as a structural material for nuclear reactors using lead-based alloy coolants.

ii. The HT-9 samples were not attacked by the molten lead-bismuth. The samples appear to have been protected by a stable, adherent, $FeCr_2O_4$-type spinel layer. Close control of oxygen activity was not necessary to form the protective spinel. As long as the oxygen activity is well below that needed to form PbO and above that needed to form the spinel, ample leeway exists to form a protective layer on HT-9.

iii. A comparison of AISI S-5 and HT-9 corrosion behavior clearly demonstrates the important role of chromium in the passivation of HT-9 and EP-823 alloys exposed to molten Pb-Bi.

REFERENCES

[1] SPENCER, B.W., HILL, R.N., WADE, D.C., HILL, D.J., SIENICKI, J.J., KHALIL, H.S., CAHALAN, J.E., FARMER, M.T., MARONI, V.A., LEIBOWITZ, L., An Advanced Modular HLMC Reactor Concept Featuring Economy, Safety, and Proliferation Resistance, Proc. 8th Int. Conf. on Nuclear Engineering (ICONE-8), 2000, Baltimore, MD, American Society of Mechanical Engineers (ASME), New York (2000).

[2] PARK, J.J., BUKSA, J.J., Selection of Flowing Lead Target Structural Materials for Accelerator Driven Transmutation Applications, Proc. Int. Conf. on Accelerator-Driven Transmutation Technologies and Applications, Las Vegas, NV, AIP Press, Woodbury, New York (1995).

[3] GROMOV, B.F., ORLOV, YU.I., MARTYNOV, P.N, IVANOV, K.D., GULEVSKY, V.A., Physical-Chemical Principles of Lead-Bismuth Coolant Technology in "Liquid Metal Systems", H.U. Borgstedt, (Ed.), Plenum, New York (1995) 339-343.

[4] SPENCER, B.W., The Rush to Heavy Liquid Metal Reactor Coolants - Gimmick or Reasoned, Proc. 8th Int. Conf. on Nuclear Engineering (ICONE-8), 2000, Baltimore, MD, American Society of Mechanical Engineering (ASME), New York (2000).

[5] WILKINSON, W.D., HOYT, E.W., RHUDE, H.V., Attack on materials by lead at 1000°C, Argonne National Laboratory Report, ANL-5449 (1955).

[6] ROMANO, A.J., KLAMUT, C.J., GURINSKY, D.H., The investigation of container materials for Bi and Pb alloys, Part I, Thermal convection loops, Brookhaven National Laboratory Report, BNL 811 (T-313) (1963).

[7] ASHER, R.C., DAVIES, D., BEETHAM, S.A., Some observations on the compatibility of structural materials with molten lead, Corr. Sci., 17 (1977) 545-557.

[8] MULLER, G., SCHUMACHER, G., ZIMMERMANN, F., Investigation on oxygen controlled liquid lead corrosion of surface treated steels, J. Nucl. Mater., 278 (2000) 85-95.

[9] CATHCART, J.V., MANLEY, W.D., A Technique for Corrosion Testing in Liquid Lead, Corrosion, Vol. 10, 432 (1954).

[10] MARONI, V.A., MELENDRES, C.A., KASSNER, T.F., KUMAR, R., SIEGEL, S., Spectroscopic Characterization of Oxide Films on Type 304 SS Exposed to Water at 289°C: Correlation with the Fe-Cr-H_2O Pourbaix Diagram, J. Nucl. Mater., 172, 13 (1990).

[11] ROBIE, R.A., HEMINGWAY, B.S., FISHER, J.R., Thermodynamic Properties of Minerals and Related Substances at 298.15 K and 1 Bar (10^5 Pascals) Pressure and at Higher Temperatures, Geological Survey Bulletin 1452, United States Government Printing Office, Washington (1978).

[12] BARIN, I., Thermochemcial Data of Pure substances, Third Ed., VCH Publishers, New York (1995).

A KINETIC MODEL FOR CORROSION AND PRECIPITATION IN NON-ISOTHERMAL LBE FLOW LOOP

X. HE, N. LI, M. MINEEV
Los Alamos National Laboratory, Los Alamos, New Mexico, United States of America

Abstract

A kinetic model was developed to estimate the corrosion/precipitation rate in a nonisothermal liquid lead-bismuth eutectic (LBE) flow loop. The model was based on solving the mass transport equation with the assumptions that convective transport dominates in the longitudinal flow direction and diffusion dominates in the transverse direction. The species concentration at wall is assumed to be determined either by the solubility of species in LBE in the absence of oxygen or by the reduction reaction of the protective oxide film when active oxygen control is applied. Analyses show that the corrosion/precipitation rate depends on the flow velocity, the species diffusion rate, the oxygen concentration in LBE, as well as the temperature distribution along a loop. Active oxygen control can significantly reduce the corrosion/precipitation of the structural materials. It is shown that the highest corrosion/precipitation does not necessarily locate at places with the highest/lowest temperature. For a material testing loop being constructed at the Los Alamos National Laboratory (LANL), the highest corrosion occurs at the end of the heater zone, while the highest precipitation occurs in the return flow in the recuperator.

1. INTRODUCTION

Using liquid lead-bismuth eutectic (LBE) as coolant in nuclear systems has been studied for more than fifty years. LBE has many unique nuclear, thermophysical and chemical attributes that are attractive for nuclear coolant applications [1, 2]. In addition, lead and bismuth can produce copious of spallation neutrons when bombarded with energetic protons. This makes LBE one of the top candidates for high power spallation target in an Accelerator-driven Transmutation of Waste (ATW) system [3].

One of the key obstacles to applying LBE in an ATW system or any other nuclear facilities is the corrosiveness of LBE to structural materials. The corrosion is primarily due to the relatively high solubility of the base and major alloying components of steels, such as Ni, Fe, Cr, etc., in lead-bismuth. Without some protective means, containment structures would be rapidly corroded via dissolution and mass transfer. Considerable efforts were devoted to finding ways of maintaining effective protective films on structural materials in the West before mid 1960s, without much success. This problem was first solved in the Russian nuclear submarine program using an active oxygen control technique [1].

The active oxygen control technique [1, 4] exploits the fact that lead and bismuth are chemically less active than the major components of steels, such as Fe, Ni, and Cr. By carefully controlling the oxygen concentration in LBE, it is possible to maintain an iron and chrome oxide based film on the surfaces of structural steels, while keeping lead and bismuth from excessive oxidization that can lead to precipitation contamination. The oxide film, especially the compact portion rich in Cr effectively separates the substrates from LBE. Once this oxide film is formed on the structure surface, the direct dissolution of the structural materials becomes negligible because the diffusion rates of the alloying components are very small in the oxides. In this circumstance, the only effective mean of transferring structural materials into LBE is through the reduction of the oxide film at the interface of the film and LBE.

The reduction of the oxide film will reach a local equilibrium and the Fe concentration near the interface equals an equilibrium value. This equilibrium Fe concentration depends highly on the oxygen concentration in LBE. When the oxygen level is controlled within a certain

range, this Fe concentration can be several orders of magnitude smaller than the Fe solubility in LBE. Subsequently, the depletion or corrosion of the structural material can be reduced to a tolerable level for long-term applications. This is the working mechanism behind the active oxygen control technique.

The concentrations of steel elements near surfaces, with the oxygen control or without any oxygen, are functions of temperature [4]. A sustained corrosion process can only happen in a non-isothermal system. Without temperature variation, species concentration would eventually reaches a homogeneous distribution and no further corrosion would occur. With a temperature variation, steel elements will be depleted from hot structural wall, transfer to locations with lower temperatures, and precipitate there. It should be pointed out that the precipitation at cold walls is often more important because severe precipitation may lead to clog of piping and degradation of heat transfer. Both diffusion and convection are important in a corrosion/precipitation process. Diffusion is usually the limiting process for transferring species from the wall surface to the bulk fluid; while convection effectively transfers the species from hot places to cold places. Clearly, a systematic study including convection and diffusion is necessary for a full understanding of the complete corrosion/precipitation process.

It is the purpose of this study to carry out such an analysis on corrosion/precipitation in a non-isothermal LBE flow loop. We will derive an analytic model for estimating the corrosion/precipitation rate on the loop wall. From this non-local analysis, we can determine what the maximum corrosion and precipitation rates are and where they locate. This information will be useful for helping design and operate LBE cooled systems. The rest of the paper is organized as follows: in Section 2, we present the derivation of the model. The model is applied in Section 3 to analyze two non-isothermal LBE flow loops. Some discussions are presented in Section 4, with conclusions in Section 5.

2. THEORY

As discussed in the last section, the corrosion of molten lead-bismuth eutectic (LBE) to structural materials, steels in particular, usually occurs in two different ways. No matter in which way the corrosion proceeds, it is usually sufficiently fast that the component concentrations are always at their saturated or equilibrium levels. For a dissolution process, the surface component concentrations equal to their saturated concentration [4]:

$$\log(c) = \log(c_s) = A + \frac{B}{T} \tag{1}$$

where T is the absolute temperature in Kelvin. Unless otherwise mentioned, all the concentrations are measured in wt ppm in this report. The values of parameters A and B vary for species and some of them are listed in Table 1 for common components in steels.

TABLE 1. SOLUBILITY DATA

C_s	Ni	Fe	Cr	O
A	5.53	6.01	3.98	5.2
B	-843	-4380	-2280	-3400

In the reduction process, the protective Fe_3O_4 -based film can be reduced by Pb via the following chemical reaction:

$$\frac{1}{4}Fe_3O_4 + Pb = \frac{3}{4}Fe + PbO$$

The equilibrium concentration of Fe is [4]:

$$\log(c_{Fe}) = 11.35 - \frac{12844}{T} - \frac{4}{3}\log(c_o) \tag{2}$$

where c_o is the oxygen concentration in LBE.

Eq. (2) should be used with cautions. For a given temperature, it has an intersection with Eq. (1) in the $c_{Fe}v_S \sim c_o$ plot (Fig. 1). This intersection determines the minimum oxygen level required for retaining a protective oxygen film. Below that oxygen level, no iron oxide based film can exist and the Fe concentration at the surface is given by Eq. (1). Above that oxygen level, a continuous iron oxide film can form and the Fe concentration is given by Eq. (2). It is not clear how these two regions connect to each other, but in practice we can assume that the species concentration at surfaces is given by the minimum of the saturation concentration and the chemical equilibrium concentration.

For Fe, we have:

$$c_{Fe} = \min(c_o^{\frac{3}{4}} 10^{11.35-\frac{12844}{T}}, 10^{6.01-\frac{4380}{T}}) \tag{3}$$

which is the thick solid line in Fig. 1. Notice that there is an upper limit for operating oxygen level in LBE beyond that Pb and Bi could be oxidized to contaminate the coolant. For further information on the upper limit of operating oxygen level, see Ref. [4].

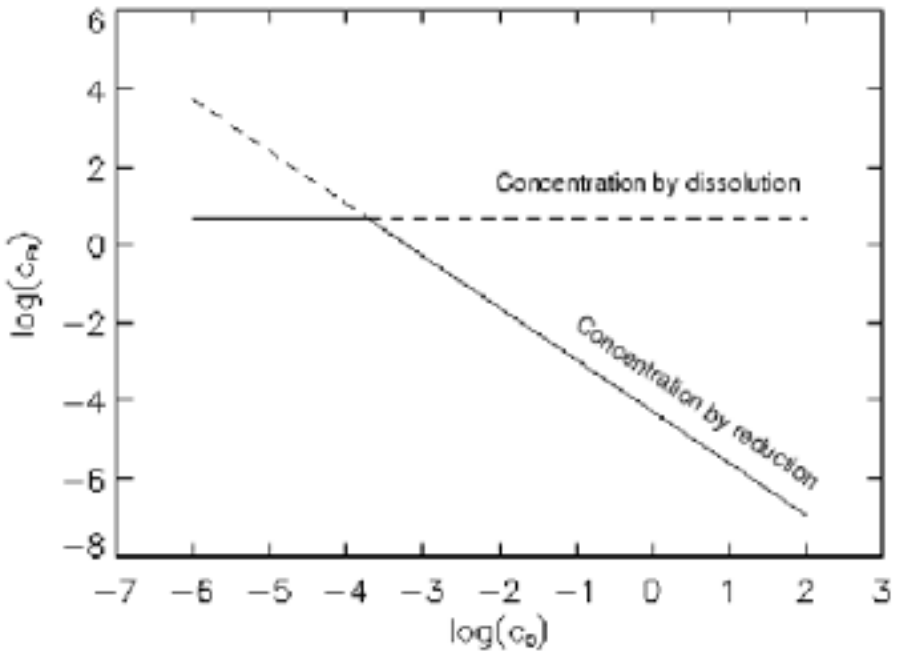

FIG. 1. Fe concentration at wall surfaces (T = 400°C).

In general, the transport of species in LBE satisfies the convection-diffusion equation:

$$\frac{\partial c}{\partial t} + (u \cdot \nabla)c = D\nabla^2 c + q \tag{4}$$

where c is the concentration, u the flow field of the fluid, D the diffusion coefficient, and q is the net mass production/depletion rate due to chemical reactions. In this study, we assume that the chemical reaction is much slower than the characteristic times of diffusion and convection. So chemical reaction contributes little to mass transfer in bulk fluids. The average time for coolant to complete a cycle in a typical testing loop is less than 1 minute (loop length/average velocity), and the characteristic boundary layer diffusion time is on the order of minutes. To justify the above assumption, the characteristic time for the chemical reaction must be longer than tens of minutes, which appears to be reasonable. We are planning to carry out experiments to verify this.

For a loop flow, it is reasonable to assume that the convection is dominant in the longitudinal direction and the diffusion is dominant in the transverse direction. In addition, we assume the diffusion is confined in a thin layer near vessel walls. We will only focus on steady flow in this study. With these considerations, the governing equation for species transport can be simplified as:

$$\gamma y \frac{\partial c}{\partial x} = D\frac{\partial^2 c}{\partial y^2} \tag{5}$$

where x and y are coordinates in the axial and transverse directions, respectively; γ is the shear rate at the wall (y is measured from walls). Introducing

$$\xi = \frac{x}{L}, \eta = (\frac{\gamma}{DL})^{\frac{1}{3}} y$$

where L is the length of a loop, Eq. (5) becomes:

$$\eta \frac{\partial c}{\partial \xi} = \frac{\partial^2 c}{\partial \eta^2} \tag{6}$$

Now we expand the concentration field in a Fourier series:

$$c(\xi, \eta) = \sum_k Y_k(\eta) e^{2\pi i k \xi} \tag{7}$$

Each Fourier harmonics, $Y_k(\eta)$, satisfies the following ODE:

$$2\pi i k \eta Y_k(\eta) = \frac{d^2 Y_k(\eta)}{d\eta^2} \tag{8}$$

which has the general solution:

$$Y_k(\eta) = a_k Ai[(2\pi ik)^{\frac{1}{2}}\eta] + b_k Bi[(2\pi ik)^{\frac{1}{2}}\eta] \tag{9}$$

where *Ai* and *Bi* are Airy functions. As for the boundary conditions, the concentration at the walls is given by Eq. (3) and the concentration in the bulk fluid is limited. Applying these boundary conditions yields:

$$Y_k(\eta) = c_k \frac{Ai[(2\pi ik)^3\eta]}{Ai(0)} \tag{10}$$

where c_k is the harmonics of the Fourier transform of the species concentration at the wall:

$$c(y=0) = \sum_k c_k e^{2\pi ik\xi} \tag{11}$$

The species flux at the vessel wall, or the corrosion/precipitation rate, can be subsequently calculated as:

$$q = D\frac{\partial c}{\partial y} = 0.730(\frac{2\pi\gamma D^2}{L})^{\frac{1}{3}}\sum_k c_k k^{\frac{1}{3}} e^{2\pi ik\xi + i\frac{\pi}{6}} \tag{12}$$

where we have used Ai(0) = 0.355 and Ai'(0) = 0.259.

Eq. (12) can be easily implemented in a computer program.

3. ANALYSIS RESULTS

The above model is applied to an ideal loop and a test loop under construction in our laboratory.

3.1. Loop with sinusoidal concentration profile

The corrosion/precipitation rate can be exactly calculated when the species concentration varied sinusoidally along a loop. Suppose that the species concentration has the following distribution:

$$c(y=0) = c_0 + c_1\cos(2\pi x + \phi_0) \tag{13}$$

The corrosion/precipitation rate can be readily derived from Eq. (12):

$$q = D\frac{\partial c}{\partial y} = 0.730(\frac{2\pi\gamma D^2}{L})^{\frac{1}{3}} c_1 \cos(2\pi x + \phi_0 + \frac{\pi}{6}) \tag{14}$$

This result indicates that the corrosion/precipitation rate also varies sinusoidally along the loop. However, it is important to note that the highest corrosion/precipitation do not occur at the highest/lowest temperature. Instead, there is a phase shift of one-twelfth of the loop length between the highest corrosion/precipitation rate and the highest/lowest temperature. Although this phase shift value is not generally applicable for all concentration distributions, as indicated in the later analysis, it shows that the highest corrosion/precipitation does not necessarily occur at places with the highest/lowest concentration or temperature.

Numerical simulations verify the above analytical result. The simulations are based on solving the full mass transport equations using a lattice Boltzmann method [5].

Figure 2 shows a sample concentration distribution and the consequent mass flux from the analytical solution, Eq. (14), and from the numerical simulation. The results agree with each other well.

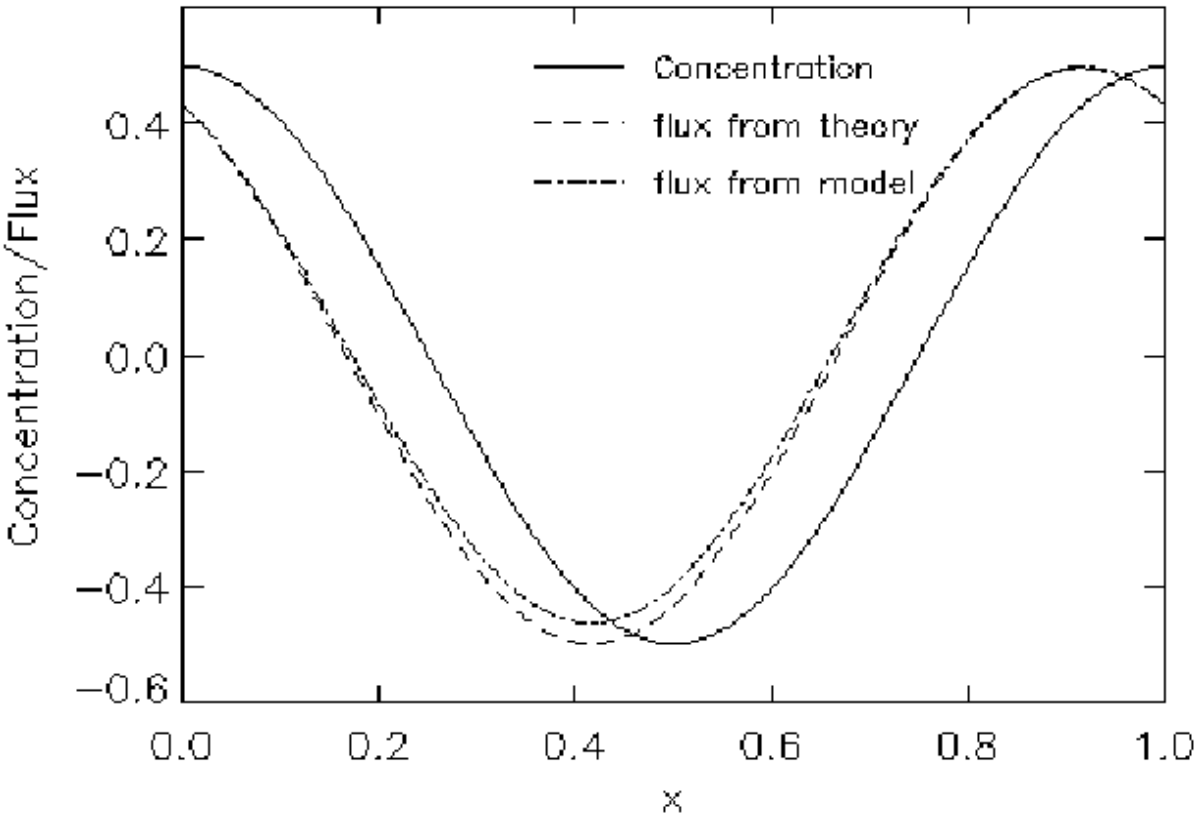

FIG. 2. Corrosion/precipitation rate for a sinusoidal concentration distribution.
The concentration is scaled as $(c - c_{\min})/(c_{\max} - c_{\min})$ (*c-cmin*)/(*cmax-cmin*);
While the flux is scaled as $q/[\beta(c - c_{\min})]$ where $\beta = 0.730(2\pi\gamma D^2 / L)^{0.333}$.

3.2. LANL materials test loop

To study the corrosion/precipitation phenomenon in LBE flow systems, a material testing loop is being constructed at the Los Alamos National Laboratory (LANL). The loop is designed to test corrosion/precipitation of various structural materials in LBE in a nonisothermal circulation system. It uses a heater, a recuperator, and a heat exchanger to set and control the temperature variations. LBE comes out of a pump at about 350°C. It is partially warmed up to 450°C when flowing through a recuperator and absorbing heat from LBE returning from the test section (hot leg of the loop). After that, a series of heaters bring the temperature to 550°C before LBE reaches the test section. In the course of returning, LBE first passes the recuperator that reduces the LBE's temperature to 450°C. A heat exchanger further reduces the temperature to 350°C. This temperature variation along the LANL material testing loop is shown in Fig. 3.

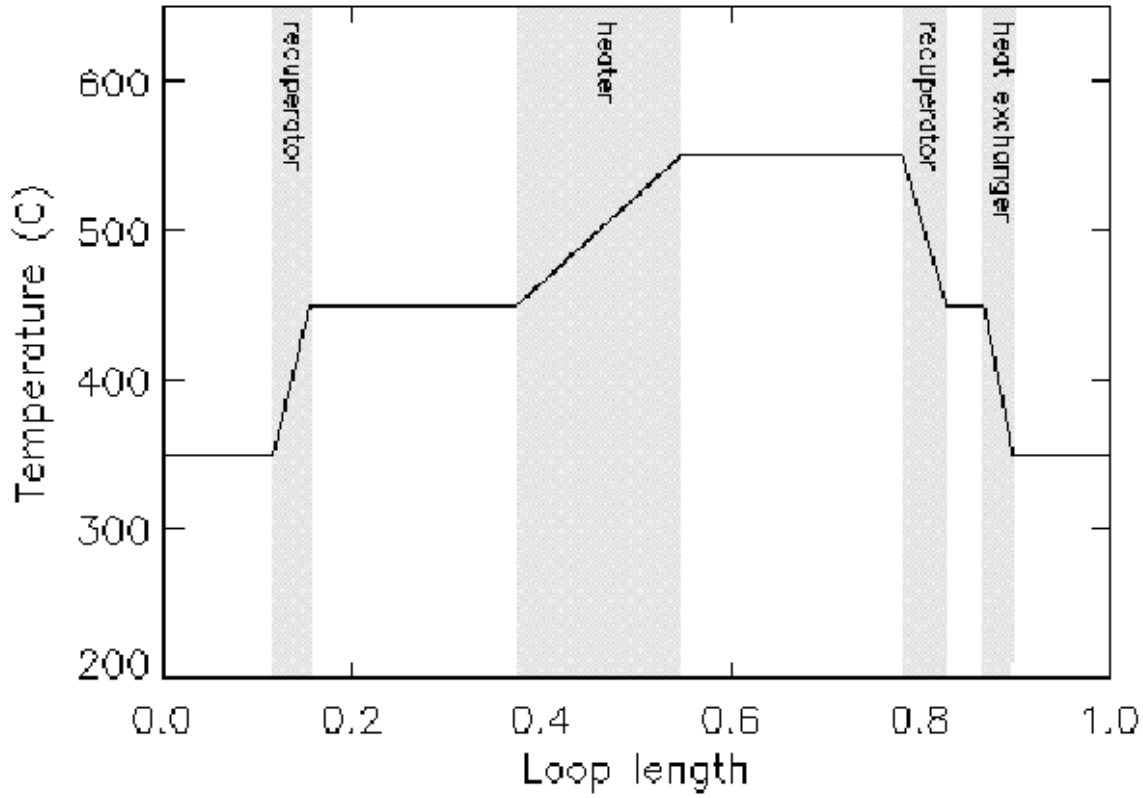

FIG. 3. Temperature distribution in the LANL material testing loop.

From the temperature distribution, we can calculated the species concentration at the wall along the testing loop based on Eq. (3). Figure 4 shows such variations of Fe under various operating conditions. With proper oxygen control, the Fe concentration at the wall can be reduced several orders of magnitude. For example, by controlling the oxygen concentration at 0.01 ppm level in LBE, the highest Fe concentration is about 0.03 ppm, which is more than 100 time smaller than that without oxygen. With a further increase of the oxygen concentration to 0.1 ppm, the Fe concentration can be reduced to 0.001 ppm, which is more than 1000 time smaller than that without oxygen.

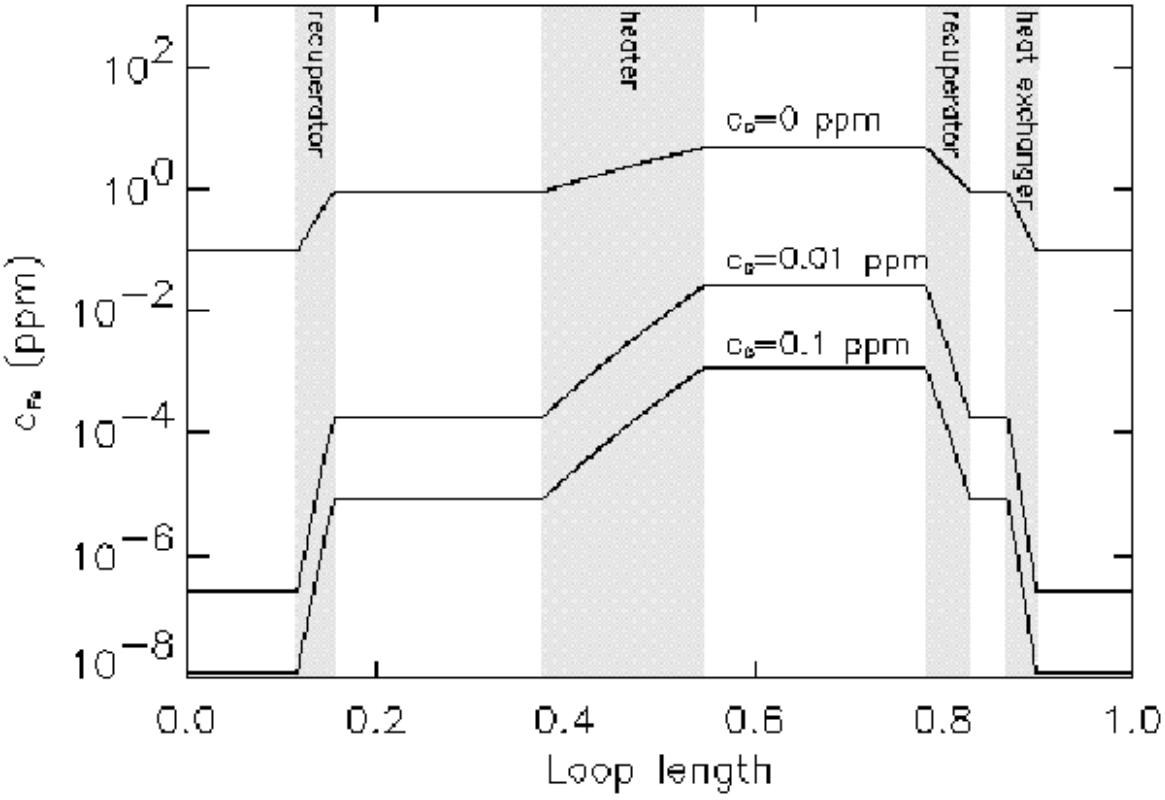

FIG. 4. Fe concentration at wall surface with different operation conditions.

Before proceeding to calculate the corrosion/precipitation rate, it is useful to estimate the parameter:

$$\beta = 0.730(\frac{2\pi\gamma D^2}{L})^{\frac{1}{3}} \tag{15}$$

This parameter, in the unit of m/s, depends on the shear rate γ, the loop length, L, and the diffusion rate, D. The loop is designed to run at an average flow velocity of 0.6 m/s and most of the vessels' diameter is d = 0.05 m. This yields a Reynolds number ($\mathrm{Re} = Vd/v$) around 200 000, which is well within the full turbulent regime. Thus the shear rate can be calculated by:

$$\gamma = \frac{\lambda\rho V^2}{2\mu} \tag{16}$$

where the coefficient of resistance, λ, is given by [6]:

$$\frac{1}{\sqrt{\lambda}} = 2.0\log(\mathrm{Re}\sqrt{\lambda}) - 0.8 \tag{17}$$

For $\mathrm{Re} = 200{,}000, \lambda = 0.0156$ and subsequently, $\gamma = 1.9\times10^4 s^{-1}$

We are unaware of any direct measurements of the diffusion coefficient of iron in LBE. However, there exists an extensive body of data suggesting that it is in the range of [7]:

$$1\times10^{-10} m^2/s \le D \le 1\times10^{-8} m^2/s$$

In this study, we choose $D = 1\times10^{-9} m^2/s$. Combining these data of γ and D with the loop length of 27.8 m, we obtain $\beta = 1.2\times10^{-5} m/s$.

The calculated corrosion/precipitation rates in the loop are shown in Fig. 5 for different operating conditions. Without any oxygen, the corrosion/precipitation can reach as high as several millimeters per year. This rate is not acceptable. Active oxygen control can significantly reduce the corrosion/precipitation. With the oxygen level maintained at a level of 0.01 ppm, the maximum corrosion/precipitation rate is about 0.015 mm/yr, which is more than 100 time less than that without oxygen. When the oxygen level is increased to 0.1 ppm, the corrosion/precipitation rate can be further reduced to 0.0007 mm/yr. These rates appear to be consistent with the preliminary corrosion tests currently carried out by LANL and IPPE [8].

The highest corrosion occurs at the end of the heater zone where the temperature reaches the maximum. The highest precipitation, however, does not occur at the end of heat exchanger where the temperature is the lowest. Instead, it occurs at the return end of the recuperator where the temperature is at the middle range. The reason is that the corrosion/precipitation depends more on the gradient of surface concentration rather than on the concentration itself.

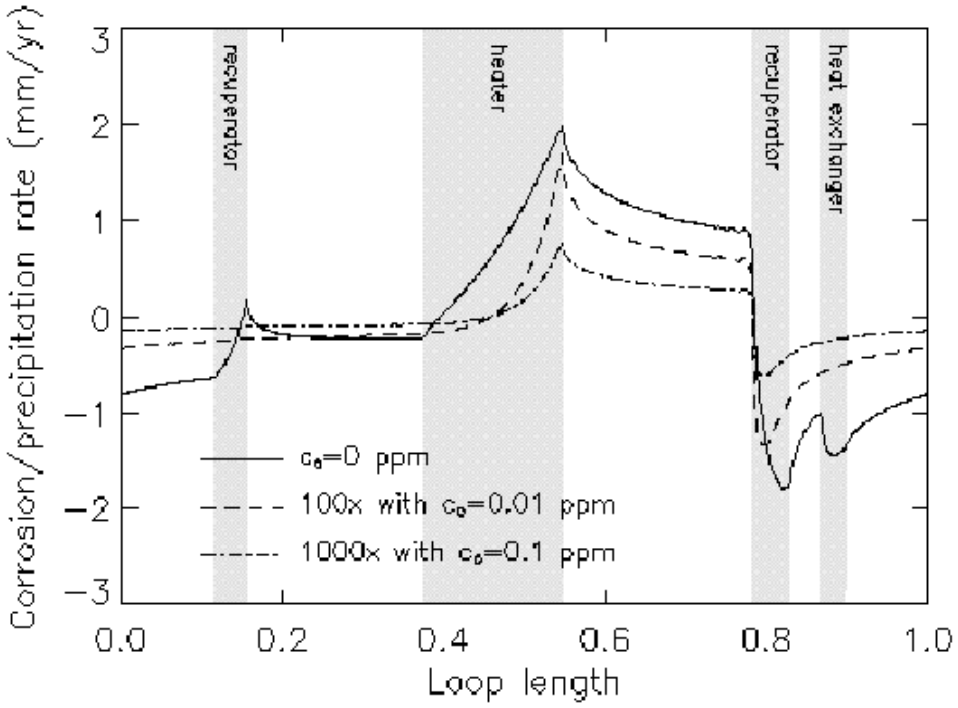

FIG. 5. Corrosion/precipitation rates in LANL material testing loop under three operating conditions.

The corrosion/precipitation in the testing loop can be better understood from the concentration distribution near the structural walls. Figure 6 shows the Fe concentration distribution in the near-wall region with the oxygen level maintained at 0.1 ppm. The concentration along the wall has a considerable variation due to the temperature changes. In the bulk fluid, however,

the Fe concentration is quite uniform. Adjacent to the wall exists clearly a concentration boundary layer where the Fe concentration changes sharply from its wall value to the bulk value. The thickness of the concentration boundary is about 0.2 mm. Corrosion occurs when the concentration at the wall is higher than that in the bulk fluids. Precipitation occurs when the concentration at the wall is lower than that in the bulk fluids.

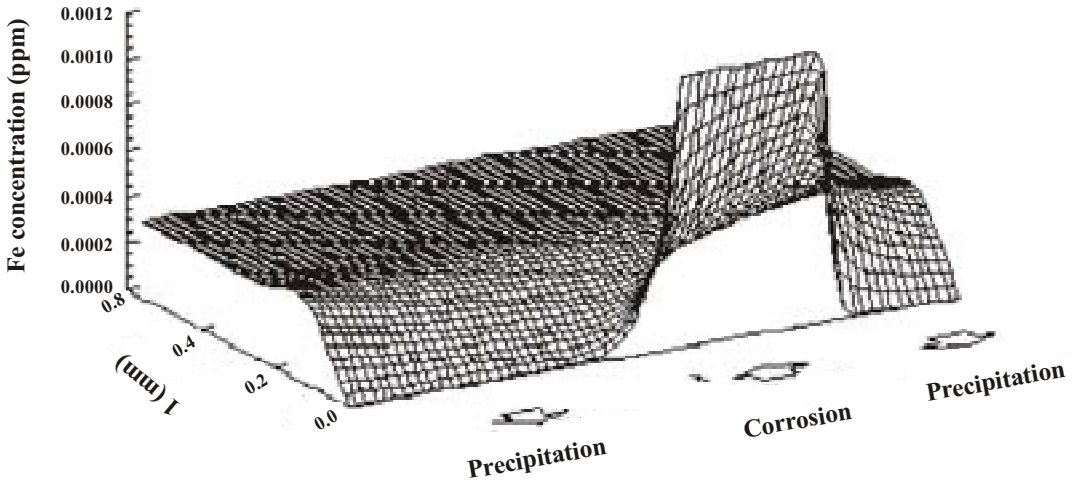

FIG. 6. Fe concentration distribution in the near-wall regions (the oxygen level is maintained at 0.1 ppm).

4. DISCUSSIONS

First, if we use $\lambda = 0.184\,\mathrm{Re}^{-0.2}$ to replace Eq.(17) [9], we have:

$$q = D\frac{\partial c}{\partial y} = 0.608(D/d)\,\mathrm{Re}^{0.6}\,Sc^{\frac{1}{3}}(d/L)^{\frac{1}{3}}\sum_{k} c_k k^{\frac{1}{3}} e^{2\pi i k\xi + i\frac{\pi}{6}}$$

where

$Sc = v/D$ is the Schmidt number. This equation can be compared with the formula proposed by Epstein [7]:

$$q = 0.023(D/d)\,\mathrm{Re}^{0.8}\,Sc^{0.4}\,\frac{dS}{dT}\Delta T$$

Epstein's equation only gives the average corrosion rate while our model gives the local corrosion/precipitation rate along the whole loop. Nevertheless, the dependence of the corrosion rate on the Reynolds number $\mathrm{Re}^{0.8}$ *vs* $\mathrm{Re}^{0.6}$ and Schmidt number $Sc^{0.4}$ *vs* $Sc^{0.33}$ are reasonably consistent for both models. Notice that the Epstein's formula is based on a heat-transfer analogy, while in our analysis we solve the full convection diffusion equation.

In terms of physical quantities, our model predicts that the corrosion/precipitation rate is proportional to $V^{0.6}, d^{-0.067}$ *and* $L^{-0.33}$ $V_{0.6}$, $d_{-0.067}$ and $L_{-0.33}$. This implies that the corrosion/precipitation increases with flow velocity, decreases with the length of flow path, but depends little on the tube dimension. These predictions are consistent with the experimental observations.

One of the important assumptions in deriving the current model is that the velocity profile is linear in the concentration boundary layer. This is valid only when the thickness of the concentration boundary layer is very small. In addition, since we neglect the effect of the turbulence on the diffusion coefficient, the model is valid only when the concentration boundary layer is submerged in the laminar sub-layer of the turbulent channel flow. In the last section, we have seen that the thickness of the concentration boundary is about 0.2 mm. According to turbulence theory, the thickness of the laminar sub-layer in a smooth tube can be estimated by:

$$\delta = \frac{70d}{\mathrm{Re}}\sqrt{\frac{8}{\lambda}} \approx 0.4 \ mm$$

Hence, the concentration boundary layer is indeed submerged in the hydraulic boundary layer. This condition, of course, will change in more complicated geometric configurations such as elbows, gauge, etc. More sophisticated models are necessary for analyzing corrosion/precipitation in those configurations.

In case the chemical reaction (Fe and oxygen in LBE forming oxide that is insoluble) in the bulk, then the mass transport equation must be expanded to include the additional species and reaction kinetics. We will investigate this possibility in the near future.

5. CONCLUSIONS

We have developed a kinetic model for analyzing corrosion/precipitation in a nonisothermal LBE convection loop. It was found that the highest corrosion/precipitation does not necessarily occur at places with the highest/lowest temperature. In the LANL materials test loop, the highest corrosion occurs at the end of the heater zone and the highest precipitation occurs at the low temperature end of the return flow in the recuperator. The active oxygen control technique can significantly reduce the corrosion rate. The current model provides a useful tool for designing and operating LBE cooling systems.

REFERENCES

[1] GROMOV, B.F., et al., Use of lead-bismuth coolant in nuclear reactors and accelerator driven systems, Nuclear Engineering and Design, Vol. 173 (1997) 207.

[2] SPENCER, B., The rush to heavy liquid metal reactor coolants - Gimmick or Reasoned, Proc. 8th Int. Conf. on Nuclear Engineering (ICONE-8) 2000, Baltimore, MD, USA, American Society of Mechanical Engineers (ASME), New York (2000).

[3] A Roadmap for Developing Accelerator Transmutation of Waste (ATW) Technology: A Report to Congress, DOE/RW-0519, US Department of Energy (1999).

[4] LI, N., Active Control of Oxygen in Molten Lead-Bismuth Eutectic Systems to Prevent Steel Corrosion and Coolant Contamination, Technical report, Los Alamos National Laboratory, LA-UR-99-4696 (1999).

[5] HE, X.Y., LI, N., Lattice Boltzmann Simulation of Electrochemical Systems, Comp. Phys. Comm., Vol. 129 (2000) 158.

[6] SCHLICHTING, H., Boundary-layer Theory, McGraw-Hill Book Company (1979).

[7] EPSTEIN, L.F., Static and dynamic corrosion and mass transfer in liquid metal systems, Liquid Metals Technology, Vol. 20 (1957) 67.

[8] LI, N., HE, X., RUSANOV, A., DEMISHONNKOV, A.P., Results of Corrosion Tests of 316, 316L, T-410, HT-9 and D-9 Steels, Corrosion Test of US Steels in Lead-Bismuth Eutectic (LBE) and Kinetic Modelling of Corrosion in LBE Systems, Proc. AccApp/ADTTA'01, Reno, NV, USA, NRG, Petten, Netherlands, ISBN: 0-98448-666-7 (2000).

[9] DEWITT, Fundamentals of Heat and Mass Transfer, John Wiley & Sons, Inc. (1996).

LIST OF PARTICIPANTS

BELARUS	S.E. CHIGRINOV SOSNY, 220109 Minsk
BELGIUM	H. AIT-ABDERRAHIM Belgian Nuclear Research Center SCK•CEN, B-2400 Mol
	B. LANCE Belgonucleaire, B-1200 Brusselles
CHINA	XU Mi China Atomic Energy Institute, 102413 Beijing
CZECH REPUBLIC	P. HEJZLAR Czech Technical University, CZ-16607 Prague
	M.J. HRON Nuclear Research Institute Rez plc, CZ-250 68 Rez
GERMANY	C.H.M. BROEDERS Forschungszentrum Karlsruhe, D-76021 Karlsruhe
	G. HEUSENER Forschungszentrum Karlsruhe, D-76021 Karlsruhe
	W. MASCHEK Forschungszentrum Karlsruhe, D-76021 Karlsruhe
ITALY	S. BUONO CRS4, Center for Advanced Studies, Sardinia, I-09010 C.P. 94 Uta (CA)
	M. CARTA ENEA C.R. CASACCIA, Rome
	G. GHERARDI ADS Project, ENEA-CRP-E. Clementel, I-40129 Bologna
JAPAN	M. SAITO Tokyo Institute of Technology, Tokyo 152-8550
	T. TAKIZUKA Japan Atomic Energy Research Institute (JAERI), 319-1195
POLAND	S. TACZANOWSKI Academy of Mining & Metallurgy, 30-059 Krakow
SWEDEN	M. ERIKSSON The Royal Institute of Technology, S-100 44 Stockholm

UNITED STATES OF AMERICA

D.P. ABRAHAM
Argonne National Laboratory, Argonne, IL 60439

D.R. BENNETT
Los Alamos National Laboratory, Los Alamos, NM 87545

H. BLISS
Argonne National Laboratory, Argonne, IL 60439

J.E. CAHALAN
Argonne National Laboratory, Argonne, IL 60439

D.C. CRAWFORD
Argonne National Laboratory, Idaho Falls, ID 83403

F.E. DUNN
Argonne National Laboratory, Argonne, IL 60439

P.J. FINCK
Argonne National Laboratory, Argonne, IL 60439

Y. GOHAR
Argonne National Laboratory, Argonne, IL 60439

F.J. GOLDNER
US Department of Energy, Washington D.C. 20585

D.J. HILL
Argonne National Laboratory, Argonne, IL 60439

R.N. HILL
Argonne National Laboratory, Argonne, IL 60439

M.S. KAZIMI
Massachusetts Institute of Technology, Cambridge, MA 02139

H.S. KHALIL
Argonne National Laboratory, Argonne, IL 60439

J.J. LAIDLER
Argonne National Laboratory, Argonne, IL 60439

N. LI
Los Alamos National Laboratory, Los Alamos, NM 87545

M.K. MEYER
Los Alamos National Laboratory, Idaho Falls, ID 83403

P.J. PERSIANI
Argonne National Laboratory, Argonne, IL 60439

E. PITCHER
Los Alamos National Laboratory, Los Alamos, NM 8754

B.W. SPENCER
Argonne National Laboratory, Argonne, IL 60439

T.A. TAIWO
Argonne National Laboratory, Argonne, IL 60439

M. TODOSOW
Brookhaven National Laboratory, Upton, NY 11973-5000

G.J. VAN TUYLE
Los Alamos National Laboratory, Los Alamos, NM 87545

F. VENNERI
Los Alamos National Laboratory, Los Alamos, NM 87545

D.C. WADE
Argonne National Laboratory, Argonne, IL 60439

L.C. WALTERS
Argonne National Laboratory, Idaho Falls, ID 83403

M.A. WILIAMSON
Argonne National Laboratory, Argonne, IL 60439

W.S. YANG,
Argonne National Laboratory, Argonne, IL 60439

IAEA

A. STANCULESCU
International Atomic Energy Agency, A-1400 Vienna, Austria